

UNCLASSIFIED

AD NUMBER
AD840582
NEW LIMITATION CHANGE
TO Approved for public release, distribution unlimited
FROM Distribution authorized to U.S. Gov't. agencies and their contractors; Critical Technology; JUL 1968. Other requests shall be referred to Army Materiel Command, Attn: AMCRD-TV, Washington, DC 20315.
AUTHORITY
usamc ltr, 14 jan 1972

THIS PAGE IS UNCLASSIFIED

UNCLASSIFIED

AD NUMBER
AD840582
NEW LIMITATION CHANGE
TO Distribution authorized to U.S. Gov't. agencies and their contractors; Specific Authority; JUL 1968. Other requests shall be referred to Army Materiel Command, Attn: AMCRD-TV, Washington, DC 20315.
FROM Distribution: Further dissemination only as directed by Army Materiel Command, Attn: AMCRD-TV, Washington, DC 20315, JUL 1968, or higher DoD authority.
AUTHORITY
amc per dtic form 55

THIS PAGE IS UNCLASSIFIED

AMC PAMPHLET

AMCP 706-280

AID 840582

ENGINEERING DESIGN HANDBOOK

DESIGN OF AERODYNAMICALLY STABILIZED FREE ROCKETS

STATEMENT #2 UNCLASSIFIED

This document is subject to special export controls and each transmittal to foreign governments or foreign nationals may be made only with prior approval of: Army Materiel Command, Attn: AMCRD-TV, Washington, D.C. 20315

DDC
RECEIVED
OCT 8 1968
RECEIVED
C

HEADQUARTERS, U.S. ARMY MATERIEL COMMAND

JULY 1968

DISCLAIMER NOTICE

THIS DOCUMENT IS BEST QUALITY PRACTICABLE. THE COPY FURNISHED TO DTIC CONTAINED A SIGNIFICANT NUMBER OF PAGES WHICH DO NOT REPRODUCE LEGIBLY.

PREFACE

The Engineering Design Handbook Series of the Army Materiel Command is a coordinated series of handbooks containing basic information and fundamental data useful in the design and development of Army materiel and systems. The handbooks are authoritative reference books of practical information and quantitative facts helpful in the design and development of Army materiel so that it will meet the tactical and technical needs of the Armed Forces.

This handbook provides extremely useful data for the engineer primarily interested in the preliminary design of aerodynamically stabilized free rockets. The data are arranged in a convenient format—tables, graphs, and solution guides—which permits ready access and easy application in order to make possible the rapid response required of preliminary design activities. As a bonus, the chapter arrangement provides each technical area having responsibilities in the preliminary design phase with an appreciation for the data requirements and applications of the supporting technical areas.

The preparation of this handbook was initially an in-house effort of the U. S. Army Missile Command. The organization of the text, data, and much of the written material originated with that agency. The Chrysler Corporation Space Division, Huntsville, Alabama, under subcontract to the Engineering Handbook Office of Duke University, prime contractor to the Army Research Office-Durham for the Engineering Design Handbook Series—with the continued assistance of the U. S. Army Missile Command—completed the handbook.

The Handbooks are readily available to all elements of AMC including personnel and contractors having a need and or requirement. The Army Materiel Command policy is to release these Engineering Design Handbooks to other DOD activities and their contractors, and other Government agencies in accordance with current Army Regulation 70-31, dated 9 September 1966. Procedures for acquiring these Handbooks follow

a. Activities within AMC and other DOD agencies should direct their request on an official form to:

Publications Distribution Branch
Letterkenny Army Depot
ATTN: AMXLE-ATD
Chambersburg, Pennsylvania 17201

b. Contractors who have Department of Defense contracts should submit their request, through their contracting officer with proper justification, to:

AMSP 703-200

Director
Defense Documentation Center
(for Scientific and Technical Information)
Cameron Station
Alexandria, Virginia 22314

c. Government agencies other than DOD may submit their request directly to:

Commanding General
U. S. Army Materiel Command
ATTN: AMCAD-PP
Washington, D. C. 20315

or

Director
Defense Documentation Center
(for Scientific and Technical Information)
Cameron Station
Alexandria, Virginia 22314

d. Industry not having a Government contract (this includes Universities) must forward their requests to:

Commanding General
U. S. Army Materiel Command
ATTN: AMCRD-TV
Washington, D. C. 20315

e. All foreign requests must be submitted through the Washington, D. C. Embassy to:

Office of the Assistant Chief of Staff for Intelligence
ATTN: Foreign Liaison Office
Department of the Army
Washington, D. C. 20310

All requests, other than those originating within the DOD, must be accompanied by a valid justification.

Comments and suggestions on this handbook are welcome and should be addressed to Army Research Office-Durham, Box CM, Duke Station, North Carolina 27706.

TABLE OF CONTENTS

PREFACE	i
LIST OF ILLUSTRATIONS	ix
LIST OF TABLES	xvi

CHAPTER 1. INTRODUCTION

CHAPTER 2. ATMOSPHERIC DATA

<i>Paragraph</i>		<i>Page</i>
2-1	Introduction	2-1
2-2	Atmospheric Properties	2-1
2-2.1	Atmospheric Density, Temperature and Pressure	2-1
2-2.2	Winds, Upper Level	2-1
2-2.3	Winds, Lower Level	2-2
2-2.4	Regional Annual and Seasonal Density Models	2-2
	References	2-4

CHAPTER 3. SYSTEM DESIGN

3-1	General	3-1
3-2	Classes of Rockets	3-1
3-2.1	Military Rocket Systems	3-1
3-2.1.1	Artillery	3-1
3-2.1.2	Infantry	3-1
3-2.1.3	Air Defense	3-1
3-2.1.4	Armor	3-2
3-2.1.5	Aviation	3-2
3-2.1.6	Logistic	3-2
3-2.1.7	Support	3-2
3-2.2	Research Rocket Systems	3-2
3-2.2.1	General	3-2
3-2.2.2	Meteorological	3-3
3-2.2.3	High Altitude Sounding	3-3
3-2.2.4	Satellites	3-3
3-2.2.5	Dispensing	3-3
3-3	Operational Modes	3-3
3-3.1	General	3-5
3-3.2	Ground-to-Ground	3-3
3-3.3	Ground-to-Air	3-4
3-3.4	Air-to-Air	3-4
3-3.5	Air-to-Ground	3-4
3-3.6	Underwater-to-Air	3-4
3-3.7	Surface/Air-to-Underwater	3-4
3-4	Launching Methods	3-4
3-4.1	General	3-4
3-4.2	Rail Launchers	3-4
3-4.2.1	Single	3-5

AMCP 703-200

TABLE OF CONTENTS (cont)

<i>Paragraph</i>		<i>Page</i>
3-4.2.2	Multiple	3-5
3-4.2.3	Helical	3-5
3-4.3	Tube Launchers	3-5
3-4.3.1	Single	3-5
3-4.3.2	Multiple	3-5
3-4.3.3	Open Breech	3-5
3-4.3.4	Closed Breech	3-6
3-4.3.5	Restricted Breech	3-6
3-4.3.6	Gatling	3-6
3-4.4	Other Launcher Types	3-6
3-4.5	Variations	3-6
3-4.5.1	Autospin	3-6
3-4.5.2	Prespin, Automatic Dynamic-Alignment (PADA)	3-7
3-4.5.3	Spin-on-Straight-Rail (SOSR)	3-7
3-4.6	Methods of Transport	3-7
3-5	System Elements	3-8
3-5.1	General	3-8
3-5.2	Rocket	3-8
3-5.2.1	Warhead	3-8
3-5.2.2	Motor	3-9
3-5.2.3	Structure	3-11
3-5.3	Launcher	3-13
3-5.4	Ancillary Equipment	3-13
3-6	Concept Selection	3-13
3-6.1	Requirements	3-13
3-6.2	Constraints	3-14
3-6.3	Parametrics	3-14
3-6.4	System Selection	3-14
3-7	Preliminary Design	3-14
3-7.1	Payload	3-15
3-7.2	Propulsion	3-15
3-7.3	Aerodynamics	3-15
3-7.4	Dynamics	3-15
3-7.5	Structure	3-15
3-7.6	Performance Estimates	3-15
3-7.7	Auxiliary Devices	3-15
3-8	Design Optimization	3-16
3-9	System Integration	3-16
3-10	Testing Methods	3-17
3-10.1	Static Testing	3-17
3-10.2	Flight Testing	3-17
3-10.3	Structural Testing	3-17
3-10.4	Aerodynamic Testing	3-18
3-10.5	Environmental Testing	3-18
3-11	Cost Effectiveness	3-18

TABLE OF CONTENTS (cont)

<i>Paragraph</i>		<i>Page</i>
CHAPTER 4. PERFORMANCE PARAMETRICS		
	Symbols	4-1
4-1	Introduction	4-2
4-2	Performance Parameters	4-2
4-2.1	Performance Factors	4-2
4-2.2	Propulsion System Factors	4-2
4-2.3	Aerodynamic Considerations	4-2
4-3	Approximation Techniques and Applicable Equations	4-3
4-3.1	Estimation of Velocity Requirement	4-3
4-3.1.1	Indirect-Fire Systems	4-3
4-3.1.2	Direct-Fire Rockets	4-3
4-3.1.3	Sounding Rockets	4-5
4-3.2	Estimation of Rocket Motor Requirements	4-5
4-3.2.1	Specific Impulse and Booster-Mass Ratio	4-5
4-3.2.2	Propellant-Weight Fraction	4-5
4-3.2.3	Growth Factor	4-5
4-3.3	Summary	4-5
4-4	Parametric Performance Data for Indirect-Fire Systems	4-8
4-4.1	Delivery Techniques	4-8
4-4.1.1	Trajectory Profile	4-8
4-4.1.2	Energy Management Techniques	4-8
4-4.2	Parametric Performance Data	4-8
4-5	Parametric Performance Data for Direct-Fire Systems	4-12
4-5.1	Delivery Techniques	4-15
4-5.1.1	Trajectory Profiles	4-12
4-5.1.2	Energy-Management Techniques	4-12
4-5.2	Parametric Performance Data	4-13
4-6	Parametric Performance Data for Sounding Rockets	4-15
4-6.1	Delivery Techniques	4-15
4-6.1.1	Trajectory Profile	4-15
4-6.1.2	Energy-Management Techniques	4-15
4-6.2	Parametric Performance Data	4-15
4-7	Parametric Performance Data for Surface-to-Air Rockets	4-16
4-7.1	Delivery Techniques	4-16
4-7.1.1	Trajectory Profile	4-16
4-7.1.2	Energy-Management Techniques	4-16
4-7.2	Parametric Performance Data	4-18
4-8	Numerical Example	4-19
CHAPTER 5. PROPELLSION		
	Symbols	5-1
5-1	General	5-2
5-2	Nozzle	5-3
5-2.1	Thermodynamic Relations	5-4
5-2.1.1	Ideal Flow	5-4

AMCP 703-2C0

TABLE OF CONTENTS (cont)

<i>Paragraph</i>		<i>Page</i>
5-2.1.2	Real Flow	5-7
5-2.2	Nozzle Contours	5-7
5-2.3	Nozzle Erosion	5-7
5-3	Propellants	5-7
5-3.1	Grain	5-7
5-3.1.1	Chemical Compositions	5-10
5-3.1.2	Configuration Geometry	5-10
5-3.1.3	Burning Rate	5-11
5-3.1.4	Erosion	5-12
5-3.2	Ignition	5-12
5-3.3	Handling	5-13
5-4	Internal Ballistics	5-13
5-5	Scaling of Solid Propellant Motors	5-13
5-6	Testing	5-15
	References	5-15

CHAPTER 6. STRUCTURES

	Symbols	6-1
6-1	General	6-2
6-2	Weight and Balance	6-2
6-2.1	Mass and Center of Gravity Estimation	6-2
6-2.2	Pitch Inertia	6-2
6-2.3	Roll Inertia	6-7
6-3	Loads	6-10
6-3.1	Transport and Handling Loads	6-10
6-3.2	Flight Loads	6-11
6-4	Stress	6-13
6-4.1	Beams	6-13
6-4.2	Columns	6-15
6-4.3	Pressure Vessels	6-15
6-4.4	Plates	6-15
6-4.5	Joints	6-15
6-5	Safety Factors	6-19
6-6	Heating	6-19
6-6.1	General	6-19
6-6.1.1	Conduction Heat Transfer	6-19
6-6.1.2	Radiation Heat Transfer	6-20
6-6.1.3	Convection Heat Transfer	6-21
6-6.1.4	Combined Heat Transfer	6-21
6-6.1.5	Transient Heat Transfer	6-21
6-6.2	Combustion Chamber Heating	6-22
6-6.3	Exhaust Plume Heating	6-22
6-6.4	Aerodynamic Friction Heating	6-22
6-7	Testing	6-24
	References	6-24

TABLE OF CONTENTS (cont)

<i>Paragraph</i>		<i>Page</i>
CHAPTER 7. ACCURACY		
	Symbols	7-1
7-1	Introduction	7-2
7-2	Definitions of Error Sources	7-2
7-3	Design Considerations Influencing Accuracy	7-2
7-3.1	Design Considerations Associated With Speed Change Errors	7-2
7-3.2	Design Considerations Associated With Angular Errors	7-3
7-3.2.1	The Effect of Aerodynamic Stability	7-3
7-3.2.2	The Effect of Wind	7-3
7-3.2.3	The Effect of Thrust Malalignment	7-3
7-3.2.4	The Effect of a Slow Spin	7-5
7-3.2.5	The Effect of Dispersion Reduction on the Optimum σ	7-7
7-4	Prelaunch Errors	7-7
7-4.1	Aiming Errors	7-7
7-4.2	Errors Due to Variations in Meteorological Conditions	7-8
7-5	Calculation of Angular Errors	7-8
7-6	Launch Phase Errors	7-10
7-6.1	Angular Velocity	7-10
7-6.2	Translational Velocity	7-10
7-6.3	Dynamic Unbalance	7-14
7-7	Propulsion Phase Errors	7-14
7-7.1	Nonrotating Rocket	7-14
7-7.2	Dispersion Reduction Techniques	7-18
7-7.2.1	Constant Spin Rate	7-18
7-7.2.2	Constant Spin Acceleration	7-20
7-7.2.3	Slowly Uniformly Decreasing Spin (SUDS)	7-20
7-7.2.4	Spin-Buck	7-20
7-7.2.5	Prespin Automatic Dynamic Alignment (PADA)	7-24
7-7.2.6	Variable Acceleration	7-24
7-8	Ballistic Phase Errors	7-25
7-8.1	Forces Acting on the Projectile	7-25
7-8.2	Sources of Error	7-25
7-8.2.1	Errors Due to Winds	7-26
7-8.2.2	Change in Drag	7-27
7-8.2.3	Nonstandard Conditions	7-27
7-8.2.4	Malalignment of Fins	7-27
7-8.2.5	Static Unbalance	7-27
7-8.2.6	Dynamic Unbalance	7-27
7-8.2.7	Curvature of the Trajectory	7-27
7-8.2.8	Fuzing Errors	7-27
7-8.3	Calculation of Dispersion	7-27
7-8.3.1	Launch Errors	7-28
7-8.3.1.1	Malaim	7-28
7-8.3.1.2	Mallaunch	7-29
7-8.3.2	Propulsion Errors	7-30
7-8.3.2.1	Wind	7-30

TABLE OF CONTENTS (cont)

<i>Paragraph</i>		<i>Page</i>
7-8.3.2.2	Thrust Malalignment	7-30
7-8.3.2.3	Impulse Variation	7-30
7-8.3.3	Ballistic Errors	7-30
7-8.3.3.1	Density	7-30
7-8.3.3.2	Ballistic Wind	7-31
7-8.3.3.3	Ballistic Coefficient	7-31
7-8.3.4	Tabulation of Results	7-31
7-8.3.5	Additional Reference Graphs	7-31
7-9	Statistical Methods	7-31
7-9.1	Measures of Dispersion for One Error Source	7-32
7-9.1.1	Variance	7-32
7-9.1.2	Standard Deviation	7-32
7-9.1.3	Probable Error	7-32
7-9.2	Measures of Dispersion for Several Error Sources	7-34
7-9.3	Use of Figures 7-42 and 7-43	7-34
7-10	Computation of Accuracy	7-34
7-10.1	Range Probable Error (RPE)	7-35
7-10.2	Deflection Probable Error (DPE)	7-35
7-10.3	Circular Probable Error (CPE)	7-35
	References	7-92

CHAPTER 8. AERODYNAMICS

	Symbols	8-1
8-1	General Design Considerations	8-3
8-2	Stability Characteristics of Rockets	8-4
8-2.1	Bodies of Revolution	8-4
8-2.1.1	Nose Cylinder	8-4
8-2.1.2	Boattail	8-5
8-2.1.3	Conical-Flare Afterbody	8-5
8-2.1.4	Oversize Head Configurations	8-16
8-2.2	Fins	8-17
8-2.3	Ring Tail	8-22
8-2.4	Stability of Complete Configuration	8-22
8-2.4.1	General	8-22
8-2.4.2	Fin-Body Interference	8-34
8-2.4.3	Fin-Fin Interference	8-37
8-2.4.4	Sample Calculation Sheet	8-42
8-3	Drag	8-44
8-3.1	Wave Drag	8-44
8-3.1.1	Nose Wave Drag	8-44
8-3.1.2	Boattail Wave Drag	8-45
8-3.1.3	Flare Wave Drag	8-46
8-3.1.4	Fin Wave Drag	8-48
8-3.1.5	Ring Tail Wave Drag	8-48
8-3.2	Friction Drag	8-51
8-3.3	Base Drag	8-51
8-3.3.1	Body-of-Revolution Base Drag, Rocket Jet Off	8-51

TABLE OF CONTENTS (cont)

<i>Paragraph</i>		<i>Page</i>
8-3.3.2	Body-of-Revolution Base Drag, Rocket Jet On	8-63
8-3.3.3	Fin Base Drag	8-65
8-3.4	Drag Characteristics of Complete Configurations	8-65
8-3.4.1	Interference Effects—Fin on Base	8-65
8-3.4.2	Computational Table	8-66
8-4	Aerodynamic Testing	8-67
	References	8-71
	Index	i-1

LIST OF ILLUSTRATIONS

<i>Fig. No.</i>	<i>Title</i>	<i>Page</i>
2-1	Maximum Speed and Associated Shear	2-3
2-2	Strongest Wind for Temperature Range	2-12
2-3	Density Deviation Versus Altitude—Worldwide, Annual	2-13
2-4(A)	Subtropics and Tropics—Annual Density Model	2-19
2-4(B)	Temperate Zone—Annual Density Model	2-20
2-4(C)	Polar Zone—Annual Density Model	2-21
2-4(D)	Subtropics—Seasonal Density Models	2-22
2-4(E)	Tropics—Seasonal Density Models	2-23
2-4(F)	Temperate Zone—Seasonal Density Models	2-24
2-4(G)	Polar Zone—Seasonal Density Models	2-25, 2-26
4-1	Effect of Ballistic Coefficient on Burnout Velocity	4-4
4-2	Effect of Ideal Burnout Velocity on Booster-Mass Ratio	4-6
4-3	Effect of Growth Factor on Ideal Burnout Velocity	4-7
4-4	Indirect Fire—All-Boost; Effect of Thrust-to-Weight Ratio on Optimum Launch Quadrant Elevation	4-9
4-5	Indirect Fire—Boost/Sustain; Effect of Impulse Ratio on Optimum Launch Quadrant Elevation	4-9
4-6	Indirect Fire—All-Boost; Effect of Range on Growth Factor	4-10
4-7	Boost/Sustain Engine; Variation of Specific Impulse With Thrust	4-10
4-8	Indirect Fire—Boost/Sustain; Effect of Range on Impulse Ratio	4-11
4-9	Indirect Fire—Boost/Sustain; Effect of Range on Growth Factor	4-11
4-10	Indirect Fire—All-Boost; Effect of Propellant Weight Fraction on Growth Factor	4-12
4-11	Indirect Fire—All-Boost; Effect of Ballistic Coefficient on Growth Factor	4-12
4-12	Direct Fire—Boost/Sustain; Effect of Impulse Ratio on Time to Target	4-13
4-13	Direct Fire—All-Boost; Effect of Growth Factor on Minimum Time to Target	4-14

AMCP 783-280

LIST OF ILLUSTRATIONS (cont)

<i>Fig. No.</i>	<i>Title</i>	<i>Page</i>
4-14	Direct Fire—All-Boost; Effect of Ballistic Coefficient on Growth Factor	4-14
4-15	Direct Fire—All-Boost; Effect of Propellant Weight Fraction on Growth Factor	4-15
4-16	Sounding Rocket—All-Boost and Boost/Sustain; Effect of Growth Factor on Summit Altitude	4-16
4-17	Sounding Rocket—All-Boost; Effect of Propellant Weight Fraction on Growth Factor	4-17
4-18	Sounding Rocket—All-Boost; Effect of Ballistic Coefficient on Growth Factor	4-17
4-19	Surface-to-Air—All-Boost; Effect of Time to Altitude on Growth Factor	4-18
4-20	Surface-to-Air—All-Boost; Effect of Propellant Weight Fraction on Growth Factor	4-18
4-21	Surface-to-Air—All-Boost; Effect of Ballistic Coefficient on Growth Factor	4-19
4-22	Flow Diagram	4-20
5-1	Schematic of a Case-Bonded, Unrestricted-Burning Solid-Propellant Rocket Motor	5-2
5-2	Subsonic Flow Through a Converging Nozzle	5-3
5-3	Flow Through a Supersonic (DeLaval) Nozzle	5-5
5-4	Supersonic Nozzle Area Expansion Ratios	5-6
5-5(A)	Thrust Coefficient Versus Area Ratio for $\gamma = 1.3$	5-8
5-5(B)	Thrust Coefficient Versus Area Ratio for $\gamma = 1.2$	5-9
5-6	Examples of Grain Cross-Sections	5-11
5-7	Typical Grain Installations	5-11
5-8	Typical Igniter	5-12
6-1	Volumes of Cones	6-5
6-2(A)	Ratio of Volume of Ogive to Cone Versus l/r at Various l/d 's	6-6
6-2(B)	Ratio of Volume of Ogive to Cone Versus l/r at Various l/d 's	6-6
6-2(C)	Ratio of Volume of Tangent Ogive to Cone With Identical l/d	6-7
6-3	Surface Area of Cones	6-3
6-4(A)	Ratio of Area of Ogive to Cone With Identical l/d Versus l/r at Various l/d 's Less Than or Equal To 0.5	6-9
6-4(B)	Ratio of Area of Ogive to Cone With Identical l/d Versus l/r at Various l/d 's Greater Than 0.5	6-9
6-4(C)	Ratio of Area of Tangent Ogive to Cone With Identical l/d	6-10
6-5	Axial Loads on Free Flight Rocket	6-11
6-6	Concentrated Bending Loads on Free Rocket	6-12
6-7	Circumferential Loads on Combustion Chamber	6-13
6-8	Beam-Section Load Distribution	6-14
6-9	Flat Plate Stress Width-to-Length Ratio Parameter	6-17
6-10	Riveted and Bolted Joints	6-17
6-11	Welded Joints	6-18
6-12	Bolted Joints	6-19
6-13	Plane Conduction Heat Transfer Medium	6-20
6-14	Cylindrical Conduction of Heat Transfer Medium	6-20

LIST OF ILLUSTRATIONS (cont)

<i>Fig. No.</i>	<i>Title</i>	<i>Page</i>
6-15	General Geometry of Rocket Exhaust Plumes	6-23
7-1	Variation of Angular Dispersion and Wavelength of Yaw During Flight	7-4
7-2	Effect of Wind on an Aerodynamically Stable Rocket	7-4
7-3	Effect of Wavelength of Yaw on Angular Dispersion Due to Wind	7-4
7-4	Effect of a Thrust Malalignment on an Aerodynamically Stable Rocket	7-5
7-5	Effect of Wavelength of Yaw on Angular Dispersion Due to Thrust Malalignment	7-5
7-6	Optimum Wavelength of Yaw for Minimum Total Dispersion	7-5
7-7	Growth of Angular Dispersion for a Rocket With a Thrust Malalignment and No Spin	7-5
7-8	Growth of Angular Dispersion for a Rocket With a Thrust Malalignment and a Slow Spin	7-5
7-9	Effect of Spin on the Build-Up of Angular Dispersion Due to Thrust Malalignment	7-6
7-10	Aiming Errors	7-8
7-11	Definitions of Sign Conventions for the Rocket Equations of Motion	7-8
7-12(A)	Angular Dispersion Due to Mallaunch—Initial Angular Rate	7-11
7-12(B)	Angular Dispersion Due to Mallaunch—Initial Angular Rate	7-11
7-12(C)	Angular Dispersion Due to Mallaunch—Initial Angular Rate	7-12
7-13(A)	Angular Dispersion Due to Mallaunch—Initial Translational Velocity	7-12
7-13(B)	Angular Dispersion Due to Mallaunch—Initial Translational Velocity	7-13
7-13(C)	Angular Dispersion Due to Mallaunch—Initial Translational Velocity	7-13
7-14(A)	Angular Dispersion Due to Wind	7-15
7-14(B)	Angular Dispersion Due to Wind	7-15
7-14(C)	Angular Dispersion Due to Wind—Initial Translational Velocity	7-16
7-15(A)	Angular Dispersion Due to Thrust Malalignment—Zero Spin	7-16
7-15(B)	Angular Dispersion Due to Thrust Malalignment—Zero Spin	7-17
7-15(C)	Angular Dispersion Due to Thrust Malalignment—Zero Spin	7-17
7-16	Effect of Constant Spin on Angular Dispersion	7-18
7-17(A)	Constant Spin	7-19
7-17(B)	Constant Spin	7-19
7-17(C)	Constant Spin	7-20
7-18(A)	Constant Spin Acceleration	7-21
7-18(B)	Constant Spin Acceleration	7-21
7-18(C)	Constant Spin Acceleration	7-22
7-19(A)	Slowly Uniformly Decreasing Spin (SUDS)	7-22
7-19(B)	Slowly Uniformly Decreasing Spin (SUDS)	7-23
7-19(C)	Slowly Uniformly Decreasing Spin (SUDS)	7-23

LIST OF ILLUSTRATIONS (cont)

<i>Fig. No.</i>	<i>Title</i>	<i>Page</i>
7-20	Effect of Wavelength of Yaw on Buck Distance for Zero Angular Dispersion	7-24
7-21	Effect of Buck Distance on Dispersion Reduction	7-25
7-22	Action of Winds on a Free Rocket	7-26
7-23	Initial Velocity Versus Maximum Range	7-29
7-24(A)	Unit Effect, Range/Departure Angle Versus R/R _{max} —Impact Fuze	7-36
7-24(B)	Unit Effect, Range/Departure Angle Versus R/R _{max} —Impact Fuze	7-37
7-24(C)	Unit Effect, Range/Departure Angle Versus R/R _{max} —Impact Fuze	7-38
7-25(A)	Unit Effect, Range/Velocity Versus R/R _{max} —Impact Fuze	7-39
7-25(B)	Unit Effect, Range/Velocity Versus R/R _{max} —Impact Fuze	7-40
7-25(C)	Unit Effect, Range/Velocity Versus R/R _{max} —Impact Fuze	7-41
7-26(A)	Unit Effect, Range/Density Versus R/R _{max} —Impact Fuze	7-42
7-26(B)	Unit Effect, Range/Density Versus R/R _{max} —Impact Fuze	7-43
7-26(C)	Unit Effect, Range/Density Versus R/R _{max} —Impact Fuze	7-44
7-27(A)	Unit Effect, Range/Wind Versus R/R _{max} —Impact Fuze	7-45
7-27(B)	Unit Effect, Range/Wind Versus R/R _{max} —Impact Fuze	7-46
7-27(C)	Unit Effect, Range/Wind Versus R/R _{max} —Impact Fuze	7-47
7-28(A)	Unit Effect, Deflection/Wind Versus R/R _{max} —Impact Fuze	7-48
7-28(B)	Unit Effect, Deflection/Wind Versus R/R _{max} —Impact Fuze	7-49
7-28(C)	Unit Effect, Deflection/Wind Versus R/R _{max} —Impact Fuze	7-50
7-29(A)	QE Versus R/R _{max} —Impact Fuze	7-51
7-29(B)	QE Versus R/R _{max} —Impact Fuze	7-52
7-29(C)	QE Versus R/R _{max} —Impact Fuze	7-53
7-30(A)	Time of Flight Versus R/R _{max} —Impact Fuze	7-54
7-30(B)	Time of Flight Versus R/R _{max} —Impact Fuze	7-55
7-30(C)	Time of Flight Versus R/R _{max} —Impact Fuze	7-56
7-31(A)	QE Versus R/R _{max} —Time Fuze	7-57
7-31(B)	QE Versus R/R _{max} —Time Fuze	7-58
7-31(C)	QE Versus R/R _{max} —Time Fuze	7-59
7-32(A)	Time of Flight Versus R/R _{max} —Time Fuze	7-60
7-32(B)	Time of Flight Versus R/R _{max} —Time Fuze	7-61
7-32(C)	Time of Flight Versus R/R _{max} —Time Fuze	7-62
7-33(A)	Unit Effect, Range/Density Versus R/R _{max} —Time Fuze	7-63
7-33(B)	Unit Effect, Range/Density Versus R/R _{max} —Time Fuze	7-64
7-33(C)	Unit Effect, Range/Density Versus R/R _{max} —Time Fuze	7-65
7-34(A)	Unit Effect, Range/Velocity Versus R/R _{max} —Time Fuze	7-66
7-34(B)	Unit Effect, Range/Velocity Versus R/R _{max} —Time Fuze	7-67
7-34(C)	Unit Effect, Range/Velocity Versus R/R _{max} —Time Fuze	7-68
7-35(A)	Unit Effect, Range/Wind Versus R/R _{max} —Time Fuze	7-69
7-35(B)	Unit Effect, Range/Wind Versus R/R _{max} —Time Fuze	7-70
7-35(C)	Unit Effect, Range/Wind Versus R/R _{max} —Time Fuze	7-71
7-36(A)	Unit Effect, Range/Departure Angle Versus R/R _{max} —Time Fuze	7-72

LIST OF ILLUSTRATIONS (cont)

<i>Fig. No.</i>	<i>Title</i>	<i>Page</i>
7-36(B)	Unit Effect, Range/Departure Angle Versus R/R _{max} --Time Fuze	7-73
7-36(C)	Unit Effect, Range/Departure Angle Versus R/R _{max} --Time Fuze	7-74
7-37(A)	Unit Effect, Deflection/Wind Versus R/R _{max} --Time Fuze	7-75
7-37(B)	Unit Effect, Deflection/Wind Versus R/R _{max} --Time Fuze	7-76
7-37(C)	Unit Effect, Deflection/Wind Versus R/R _{max} --Time Fuze	7-77
7-38(A)	Unit Effect, Altitude/Density Versus R/R _{max} --Time Fuze	7-78
7-38(B)	Unit Effect, Altitude/Density Versus R/R _{max} --Time Fuze	7-79
7-38(C)	Unit Effect, Altitude/Density Versus R/R _{max} --Time Fuze	7-80
7-39(A)	Unit Effect, Altitude/Velocity Versus R/R _{max} --Time Fuze	7-81
7-39(B)	Unit Effect, Altitude/Velocity Versus R/R _{max} --Time Fuze	7-82
7-39(C)	Unit Effect, Altitude/Velocity Versus R/R _{max} --Time Fuze	7-83
7-40(A)	Unit Effect, Range/Time Versus R/R _{max} --Time Fuze	7-84
7-40(B)	Unit Effect, Range/Time Versus R/R _{max} --Time Fuze	7-85
7-40(C)	Unit Effect, Range/Time Versus R/R _{max} --Time Fuze	7-86
7-41(A)	Unit Effect, Altitude/Time Versus R/R _{max} --Time Fuze	7-87
7-41(B)	Unit Effect, Altitude/Time Versus R/R _{max} --Time Fuze	7-88
7-41(C)	Unit Effect, Altitude/Time Versus R/R _{max} --Time Fuze	7-89
7-42	Ratio of CPE to σ_x/σ_y for Elliptical Distribution	7-90
7-43	Chart for Determination of Circular Probable Error	7-91
7-44	Variation of Range Probable Error With Range--Impact Fuze	7-91
7-45	Variation of Deflection Accuracy With Range--Impact Fuze	7-91
7-46	Variation of CPE With Range--Impact Fuze	7-91
8-1	Apparent Mass Factor	8-4
8-2	Normal Force Coefficient Gradient for Tangent Ogive-Cylinder Configurations	8-6
8-3	Center of Pressure for Tangent Ogive-Cylinder Configurations	8-7
8-4	Normal Force Coefficient Gradient for Cone-Cylinder Configurations	8-8
8-5	Center of Pressure for Cone-Cylinder Configurations	8-9
8-6(A)	Normal Force Coefficient Gradient and Center of Pressure--4-Caliber Tangent Ogive With Varying Afterbody Length	8-10
8-6(B)	Normal Force Coefficient Gradient and Center of Pressure--7.125° Cone With Varying Afterbody Length	8-11
8-6(C)	Normal Force Coefficient Gradient and Center of Pressure--1/2-Power Nose With Varying Afterbody Length	8-12
8-7(A)	Normal Force Coefficient Gradient and Center of Pressure--Varying Tangent Ogive Nose Length With Constant Afterbody Length of 6 Calibers	8-13
8-7(B)	Normal Force Coefficient Gradient and Center of Pressure--Varying Conical Nose Angle With Constant Afterbody Length of 6 Calibers	8-14
8-7(C)	Normal Force Coefficient Gradient and Center of Pressure--Varying n-Power Nose Shape With Constant Afterbody Length of 6 Calibers	8-15
8-8	Normal Force Coefficient Gradient for a Boattail	8-16

LIST OF ILLUSTRATIONS (cont)

<i>Fig. No.</i>	<i>Title</i>	<i>Page</i>
8-9	Center of Pressure for a Boattail	8-17
8-10(A)	Incremental Normal-Force Coefficient Gradient for a Flare	8-17
8-10(B)	Incremental Normal-Force Coefficient Gradient for a Flare	8-18
8-10(C)	Incremental Normal-Force Coefficient Gradient for a Flare	8-18
8-10(D)	Incremental Normal-Force Coefficient Gradient for a Flare	8-19
8-10(E)	Incremental Normal-Force Coefficient Gradient for a Flare	8-19
8-11	Subsonic Fin Normal-Force Coefficient Gradient	8-20
8-12(A)	Normal-Force Coefficient Gradient for Rectangular Fins	8-21
8-12(B)	Center of Pressure for Rectangular Fins	8-21
8-13(A)	Fin Normal Force Coefficient Gradient at Supersonic Mach Numbers	8-23
8-13(B)	Fin Normal Force Coefficient Gradient at Supersonic Mach Numbers	8-24
8-13(C)	Fin Normal Force Coefficient Gradient at Supersonic Mach Numbers	8-25
8-14(A)	Fin Center of Pressure	8-25
8-14(B)	Fin Center of Pressure	8-27
8-14(C)	Fin Center of Pressure	8-28
8-15	Fin Normal Force Coefficient Gradient Correction Factor for Sonic Leading Edge Region	8-29
8-16	Normal Force Coefficient Gradient and Center of Pressure for Rectangular Fins	8-29
8-17(A)	Incremental Normal Force Coefficient Gradient for a Ring Tail Mounted on a Cylindrical Afterbody	8-30
8-17(B)	Incremental Normal Force Coefficient Gradient for a Ring Tail Mounted on a Cylindrical Afterbody	8-30
8-17(C)	Incremental Normal Force Coefficient Gradient for a Ring Tail Mounted on a Cylindrical Afterbody	8-31
8-17(D)	Incremental Normal Force Coefficient Gradient for a Ring Tail Mounted on a Cylindrical Afterbody	8-31
8-17(E)	Incremental Normal Force Coefficient Gradient for a Ring Tail Mounted on a Cylindrical Afterbody	8-32
8-17(F)	Incremental Normal Force Coefficient Gradient for a Ring Tail Mounted on a Cylindrical Afterbody	8-32
8-18	Values of Lift Ratios Based on Slender-Body Theory	8-35
8-19	Interference Effects of Fin on Body	8-35
8-20	Lift Factors—Influence of Fin on Body	8-36
8-21(A)	Lift of Fin (Body) for $a_t/m = 0$ (Rectangular Fin)	8-38
8-21(B)	Lift of Fin (Body) for $a_t/m = 0.2$ (Clipped Delta Fin)	8-38
8-21(C)	Lift of Fin (Body) for $a_t/m = 0.4$ (Clipped Delta Fin)	8-39
8-21(D)	Lift of Fin (Body) for $a_t/m = 0.6$ (Clipped Delta Fin)	8-39
8-21(E)	Lift of Fin (Body) for $a_t/m = 0.8$ (Clipped Delta Fin)	8-40
8-21(F)	Lift of Fin (Body) for $a_t/m = 1.0$ (Delta Fin)	8-40
8-22	Normal Force Coefficient Gradient of Multiple Fins at Supersonic Speeds	8-41
8-23	Fin Geometry	8-42
8-24	Body Geometry	8-42

LIST OF ILLUSTRATIONS (cont)

<i>Fig. No.</i>	<i>Title</i>	<i>Page</i>
8-25	Configuration and Design Data for Numerical Example	8-43
8-26(A)	Effects of Mach Number and Nose Fineness Ratio on Wave Drag	8-44
8-26(B)	Effects of Mach Number and Nose Fineness Ratio on Wave Drag	8-44
8-27	Wave Drag Coefficient of Optimum Secant Ogive Cylinder at Transonic Speed	8-45
8-28	Wave Drag Coefficient of Slender Ogives at Transonic Speeds	8-46
8-29	Wave Drag Coefficient of Cones and Ogives at Supersonic Speeds	8-46
8-30	Wave Drag Coefficient of Conical Boattails at Supersonic Speeds	8-47
8-31	Wave Drag Coefficient of Parabolic Boattails at Supersonic Speeds	8-47
8-32	Wave Drag Coefficient of a Boattail at Transonic Speeds	8-48
8-33(A)	Wave Drag Coefficient of Conical Flare	8-49
8-33(B)	Wave Drag Coefficient of Conical Flare	8-49
8-33(C)	Wave Drag Coefficient of Conical Flare	8-49
8-33(D)	Wave Drag Coefficient of Conical Flare	8-49
8-33(E)	Wave Drag Coefficient of Conical Flare	8-50
8-33(F)	Wave Drag Coefficient of Conical Flare	8-50
8-33(G)	Wave Drag Coefficient of Conical Flare	8-50
8-33(H)	Wave Drag Coefficient of Conical Flare	8-50
8-33(I)	Wave Drag Coefficient of Conical Flare	8-51
8-34(A)	Wave Drag Coefficient of Fins at Supersonic Speeds	8-52
8-34(B)	Wave Drag Coefficient of Fins at Supersonic Speeds	8-53
8-34(C)	Wave Drag Coefficient of Fins at Supersonic Speeds	8-54
8-34(D)	Wave Drag Coefficient of Fins at Supersonic Speeds	8-55
8-34(E)	Wave Drag Coefficient of Fins at Supersonic Speeds	8-56
8-34(F)	Wave Drag Coefficient of Fins at Supersonic Speeds	8-57
8-34(G)	Wave Drag Coefficient of Fins at Supersonic Speeds	8-58
8-34(H)	Wave Drag Coefficient of Fins at Supersonic Speeds	8-59
8-35	Wave Drag Coefficient of Fins of Various Sectional Shapes	8-60
8-36	Wave Drag Coefficient of Rectangular Fins at Subsonic and Transonic Speeds	8-61
8-37	Wave Drag Coefficient of Delta Fins at Subsonic and Transonic Speeds	8-61
8-38	Wave Drag Coefficient of a Double Wedge Fin at Transonic Speeds	8-62
8-39	Flat Plate Average Skin Friction Coefficient	8-62
8-40	Reynolds Number as a Function of Flight Mach Number and Altitude	8-63
8-41	Base Pressure Coefficient of Cylinders, Boattails, and Flares With Rocket Jet Off	8-64
8-42	Effect of Rocket Jet on Base Pressure	8-64
8-43	Base Pressure Correction for Boattail and Flared Air-bodies	8-65
8-44	Base Pressure on Cylindrical Bodies	8-66

LIST OF ILLUSTRATIONS (cont.)

<i>Fig. No.</i>	<i>Title</i>	<i>Page</i>
8-45	Base Pressure Coefficient of Fins at Supersonic Speeds	8-66
8-46	Base Pressure Coefficient of Fins at Transonic Speeds	8-67
8-47	Comparison of Test Results on Full Size and Scale Model Artillery Missile	8-69
8-48	Relationship Between Maximum Allowable Model Dimensions and Test Section Dimension in a Specific Wind Tunnel Facility	8-70
8-49	Aerodynamic Force Components	8-71

LIST OF TABLES

<i>Table No.</i>	<i>Title</i>	<i>Page</i>
2-1	U. S. Standard Atmosphere 1962	2-2
2-2	Resultant Wind Conditions in the Northern Hemisphere	2-5
2-3	Extreme Annual Wind Speeds	2-11
2-4	Density and Temperature Profiles	2-14
	A. Key to Code Numbers of Density and Temperature Profiles	2-14
	B. Density Profiles for Tropics and Subtropics (kg/m ³)	2-14
	C. Density Profiles for Temperate Zone (kg/m ³)	2-15
	D. Density Profiles for Polar Zone (kg/m ³)	2-15
	E. Density Profiles for Tropics and Subtropics (% Dev. SA)	2-16
	F. Density Profiles for Temperate Zone (% Dev. SA)	2-16
	G. Density Profiles for Polar Zone (% Dev. SA)	2-17
	H. Density Profiles for Tropics and Subtropics (°K)	2-17
	I. Density Profiles for Temperate Zone (°K)	2-18
	J. Density Profiles for Polar Zone (°K)	2-18
6-1	Geometrical Properties of Typical Rocket Sections	6-3
6-2	Geometric Properties of Airfoil Sections	6-16
7-1	Error Budget for Indirect Fire Rocket With Impact Fuze, Launch Quadrant Elevation 45 Degrees	7-28
8-1	Computational Table	8-74
8-2	Drag Force Calculation Sheet	8-96

CHAPTER 1

INTRODUCTION

This handbook, written for the engineer interested in the preliminary design of aerodynamically stabilized free rockets, has a twofold purpose:

- a. To provide the preliminary design engineer with specific, "best available" design information and data devised to allow the rapid response required of preliminary design activities, and
- b. To provide each technical area having responsibilities in the preliminary design phase an appreciation or "feel" for the data requirements and data applications of other specific technical areas.

The term free-flight rocket implies the absence of an active guidance system. Such a rocket is guided or aimed by a launching rail or tube and can be classified into one of two categories:

- a. Spin-stabilized
- b. Aerodynamically stabilized

The spin-stabilized rocket, as the name implies, depends upon a high rate of spin and resulting gyroscopic moments to oppose disturbing moments and forces. Conversely, the aerodynamically stabilized rocket depends upon the moments generated by a flare or fins placed aft of the center of gravity to oppose disturbing moments and forces. The aerodynamically stabilized rocket generally employs some spin history to minimize dispersion due to nonstandard conditions (body malalignment, fin malalignment, etc.). The data and concepts presented by this handbook are limited to aerodynamically stabilized free-flight rockets.

The rocket is assumed to be a rigid body, i.e., the elastic properties of the structure have been neglected. However, for some configurations (primarily long, slender bodies) the dynamic modes of oscillation may be of sufficient amplitude to warrant detailed investigations.

Finally, there are three major propulsion systems that could be applicable:

- a. liquid propellants
- b. solid propellants
- c. hybrid propellants (combination of liquid and solid)

The applications of this handbook are limited to solid-propellant motors, used almost exclusively in free-flight aerodynamically stabilized rockets.

The basic handbook is organized into chapters, each self-contained and applicable to a particular technical area with which preliminary design is concerned. These areas are: Atmospheric Data, Systems Design, Parametric Performance, Propulsion, Structures, Accuracy, and Aerodynamics.

Chapter 2, Atmospheric Data, presents climatological data pertinent to free rocket design. Chapter 3, Systems Design, discusses the factors affecting design, considering each technical area from preliminary design to actual hardware. Chapter 4, Parametric Performance, presents data describing the performance of various design concepts, with variations that permit consideration of trade-offs to maximize range for given mass or mass for given range. Chapter 5, Propulsion, presents concepts and data necessary to predict propulsion system performance, as well as important aspects to consider in conceptual and preliminary design. Chapter 6, Structures, presents data and methods pertinent to structural design. Chapter 7, Accuracy, considers both burning-phase and ballistic-phase errors, the effect of these errors on rocket accuracy, and techniques necessary to estimate accuracy. Finally, Chapter 8, Aerodynamics, presents design curves and formulas that will permit the prediction of stability (force and moment) and drag characteristics for practically any conceivable aerodynamic body or combinations of bodies.

CHAPTER 2

ATMOSPHERIC DATA

2-1 INTRODUCTION

Atmospheric information is a very important consideration in the preliminary design of rockets, particularly those that are free-flight or uncontrolled after launch. Since atmospheric data are time- and space-dependent, and therefore widely variable, statistical processes are normally used for their presentation, analysis, and utilization.

Because some types of statistical data are subject to considerable controversy, one can hardly hope to develop standardized actual climatological data profiles, and perturbations to them, that will receive universal acceptance. Instead, meteorologists have developed synthetic standard profiles, independent of physical location. Means and extremes of these profiles were then developed, dependent upon rather general geographic location. Finally, models of microclimatological (localized) conditions can be accomplished to meet specific conditions.

In rocket design, the preliminary design phase is concerned primarily with macroclimatology (large-scale conditions). Density, temperature, and pressure profiles (variation of these factors with altitude) must be presented to the trajectory analyst so that configuration performance can be determined. Wind profiles and wind shear information are necessary for structural design as well as for accuracy studies. Finally, consideration of extreme conditions is necessary to ensure complete system integration and operation.

2-2 ATMOSPHERIC PROPERTIES

2-2.1 ATMOSPHERIC DENSITY, TEMPERATURE AND PRESSURE

The U. S. Standard Atmosphere (USSA) is based upon the International Civil Aviation Organization (ICAO) Standard Atmosphere to 20 km altitude, and upon the proposed ICAO extension from 20 km to 32 km. Data for the first 20 km are in agreement with the Air Research and Development Command (ARDC) 1959 Stand-

ard Atmosphere. The major reason for revising standard atmospheres in recent years has been the observed orbit perturbations of artificial satellites due to atmospheric drag. This subject is beyond the present scope of interest. See Reference 2 for complete tables.

Table 2-1 presents a useful summary of atmospheric properties taken from Reference 2.

2-2.2 WINDS, UPPER LEVEL

The problem of selecting wind profile information for use as design criteria led to development of an estimated synthetic profile which presented the 1 percent probable wind speed and associated shear at the most critical altitude, and speeds of other altitudes typical for such wind fields. Subsequent investigation revealed that, if accuracy in the calculated risk is desired, the use of synthetic wind profiles is hazardous. However, logically developed synthetic profiles are useful in preliminary design. Fig. 2-1 is a synthetic wind profile that was developed in 1954 to determine vehicle responses that would be exceeded during only 1 percent of the windiest season of the year in that area of the U. S. where tropospheric wind streams were considered the strongest. It is reasonable to shift the curve upward or downward by as much as 5000 ft to make the peak wind speed coincide with the altitude of maximum wind influence.

Ideally, in missile design and accuracy studies, the designer must know mean wind velocity and standard deviation for both hemispheres. Table 2-2 gives the resultant wind direction, vector mean wind velocity and the standard vector deviation for the Northern hemisphere between 20°N and 80°N at altitudes from 10,000 to 100,000 ft for winter and summer.

See Reference 4, the *Handbook of Geophysics and Space Environments*, 1965, Chapter 4, for the mean wind speed, standard deviation, and correlation between levels for a series of altitudes for each vector component at specific stations during the winter season.

AMCP 763-200

TABLE 2-1. U. S. STANDARD ATMOSPHERE, 1952

Geometric Altitude, km	Density, kg/m ³	Temperature, °K	Pressure, N/m ²	Accel. of Gravity, m/sec ²	Speed of Sound, m/sec
0	1.2250	288.150	10325	9.8066	340.294
1	1.1117	281.651	89376.2	9.8036	336.435
2	1.0006	275.154	79501.4	9.8055	332.532
3	0.90225	268.659	70121.1	9.7974	328.583
4	0.81835	262.163	61650.4	9.7943	324.589
5	0.73843	255.676	54048.2	9.7912	320.545
6	0.66211	249.187	47217.6	9.7882	316.452
7	0.59002	242.700	41105.2	9.7851	312.306
8	0.52579	236.215	35651.6	9.7820	308.105
9	0.46706	229.733	30300.7	9.7789	303.848
10	0.41351	223.252	26499.9	9.7759	299.532
11	0.36490	216.774	22699.9	9.7728	295.154
12	0.31194	216.650	19399.4	9.7697	295.069
13	0.26500	216.650	16479.6	9.7667	295.059
14	0.22768	216.650	14170.4	9.7636	295.069
15	0.19475	216.650	12111.8	9.7605	295.069
16	0.16647	216.650	10352.8	9.7575	295.069
17	0.14230	216.650	8849.71	9.7544	295.069
18	0.12165	216.650	7565.22	9.7513	295.069
19	0.10400	216.650	6487.28	9.7483	295.069
20	0.089310	216.650	5529.30	9.7452	295.069
21	0.075715	217.581	4728.93	9.7422	295.703
22	0.064510	218.574	4047.49	9.7391	296.377
23	0.055006	219.567	3466.86	9.7361	297.049
24	0.047933	220.560	2971.74	9.7330	297.720
25	0.040034	221.552	2549.22	9.7300	298.389

2-2.3 WINDS, LOWER LEVEL

Chapter 4, Section 4.1 of Reference 4 contains information concerning mean wind as a function of height. This section gives approximate equations to compute the mean wind speed. It also gives information and tabulated data concerning wind-direction shifts and directional variation, and low-level jet streams.

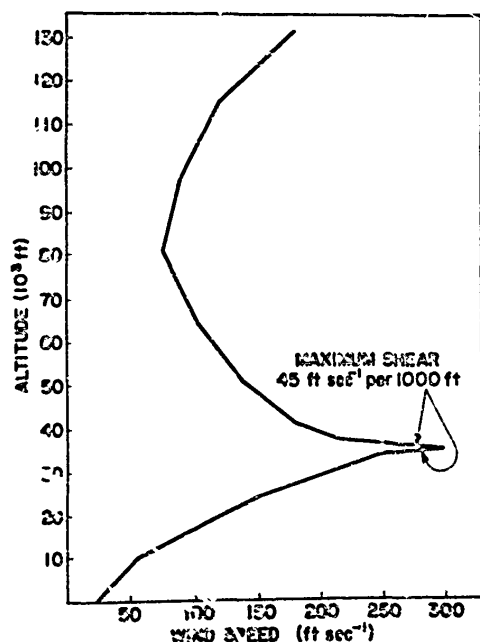
Table 2-3 gives the number of years of record, mean, and standard deviation of the extreme wind speed at 50 ft above the ground for various stations in the northern hemisphere.

Fig. 2-2 shows the strongest wind for temperature range observed during a five-year period. Wind speeds are, in general, for 40 to 100 ft above the surface. Speeds at 10 feet are approximately 80 percent of the values given, except for

the coldest temperatures, where winds are 50 percent of the indicated values.

2-2.4 REGIONAL ANNUAL AND SEASONAL DENSITY MODELS

Evaluation of flight performance and rocket design necessarily includes the consideration of vertical distribution of atmospheric environment parameters. Our knowledge in this field has rapidly expanded beyond the status of a "Standard Atmospheric Model", which can only describe the atmospheric environment as a first approximation, under limited circumstances. In recognition of these limitations, the Committee on the Extension of the Standard Atmosphere (COESA) has recently adopted supplementary atmospheres (Reference 2).



Maximum speed (300 ft sec⁻¹) and associated maximum shear (45 ft sec⁻¹ per 1000 ft) are likely to be exceeded only 1% of the wintertime over the northeastern USA. Wind speeds and shears at levels above and below the levels of maximum speed and shear are typical of those likely to be encountered for this 1% probability condition.

Figure 2-1. Maximum Speed and Associated Shear

From *Handbook of Geophysics and Space Environments*, by Shea L. Valley, Air Force Cambridge Research Laboratories. Used by permission of copyright owner, McGraw-Hill Book Co., Inc.

These supplements to the standard atmosphere, although welcomed by the design engineer, still cannot fully describe the status of the atmosphere and are not intended to do so. Besides having reference models of mean conditions, the designer needs information to describe the deviations from these preset models, usually in the form of some error function or standard deviations.

It has been customary to assume a certain deviation, e.g., the plus-one-sigma threshold, at every height level, and then to connect these points from one level to the next. The resulting synthetic altitude relationship will be called here the plus-one-sigma envelope (to be distinguished from profiles). Also, constants, such as a 3 percent deviation for density, have been utilized.

Such an approach is very attractive because it compresses a large amount of statistical information into a few altitude curves. However, it completely ignores the altitude relationship of meteorological elements, which is admittedly complex and cannot be expressed in simple terms. Although it is logical to establish any probability threshold separately at any altitude level, the curves that result when these threshold values are combined to form a single vertical profile deviate totally from realistic profiles, particularly for density. Fig. 2-3 illustrates this point. Improper design of the rocket system may result as a consequence of this negligence.

Although the introduction of more realistic profiles may increase some of the engineers' computational work by adding a few profiles or by making his computations more complex, hopefully the engineer will thereby realize a gain for his system by avoiding improper design. Ideally, investigations would employ sample profiles. The disadvantage of this approach is the tremendous amount of calculations that result if individual atmospheric conditions are used as inputs from random data selections. Some of the advantages of realistic data can be retained, with a reasonable amount of computation, by using carefully selected, small but representative samples.

One such selection has been prepared by Dr. O. M. Essenwanger, Chief, Aerophysics Branch, Physical Science Laboratory, Army Missile Command, Redstone Arsenal. His collection consists of 800 representative individual profiles, arranged in eight sets of 100 profiles; two sets for each of four stations represent summer and winter conditions. Fig. 2-3 is a selection from this collection. The entire collection, on punched cards, may be obtained from Dr. Essenwanger.

The next best, and also simpler, approach would be to use a representative profile. Their use will keep computational effort relatively simple, but will provide realistic estimates of actual atmospheric conditions. Data obtained through use of these profiles will provide information on missile behavior adequate for preliminary design.

Such a set of representative profiles is the 20 sets of air density and associated temperatures presented in Table 2-4 and Fig. 2-4. These profiles may be used to represent mean and one-sigma conditions for four zones, by summer, winter, and annual reference periods. The proper profile for each condition is presented on the first page of Table 2-4, where the numbers refer

AMCP 700-280

to the subscripts in subsequent column headings and the various curves of Fig. 2-4.

Mr. H. P. Dudel of the Aerophysics Branch, Physical Sciences Lab, R&DD, U. S. Army Missile Command, has published a report (Reference 7) giving the mean, minus-one sigma, and plus-one sigma density profiles for the midseason months of January and July at latitudes of 15°N, 30°N, 45°N, 50°N and 75°N. The associated temperatures are not yet available, but will be included in a forthcoming report. In the meantime, the Committee on Extension of the Standard Atmosphere (COESA) has announced adoption and proposed republication of the Air Force Interim Supplemental Atmospheres as published by Cole and Kentar (Reference 3). These supplementary atmospheres to the U. S. Standard Atmosphere, 1962, approximate mean conditions at the same geographic latitudes and months as does H. P. Dudel's report, Ref. 7.

REFERENCES

1. AMCP 706-283, Engineering Design Handbook, *Aerodynamics*.
2. U. S. Standard Atmosphere, 1962 COESA, NASA, USAF, U. S. Weather Bureau, U. S. Government Printing Office, Dec 1962.
3. Air Force Interim Supplemental Atmosphere to 30 Kilometers, Air Force Surveys in Geophysics No. 153, 1963.
4. Handbook of Geophysics and Space Environments, AFCRL, McGraw-Hill, April 65.
5. AR 705-15, Change 1. Operation of Material Under Extreme Conditions of Environment.
6. MIL-STD-210A, Climatic Extremes in Military Equipment.
7. H. P. Dudel, Regional Seasonal One-Sigma Density Profiles, Aerophysics Branch, Physical Sciences Lab, R&DD, USAMICOM.

TABLE 2. RESULTANT WIND CONDITIONS IN THE NORTHERN HEMISPHERE

Resultant wind direction (d in degrees), vector mean wind velocity (V in knots), and standard vector deviation (δ in knots) at various altitudes (H) for various latitudes and longitudes in the Northern Hemisphere, summer and winter seasons.

H 10 ³ ft	Summer																																			
	180° W			160° W			140° W			120° W			100° W			80° W			60° W			40° W			20° W											
	d	V	δ	d	V	δ	d	V	δ	d	V	δ	d	V	δ	d	V	δ	d	V	δ	d	V	δ	d	V	δ	d	V	δ	d	V	δ			
LATITUDE 20° N																																				
10	80	09	13	80	07	09	115	05	09	115	05	08				120	11	11	130	12	12	65	10	14	90	12	16									
20	35	04	14	150	02	13	250	06	12	150	10	12	105	10	10	100	07	12	150	05	12	10	05	14	120	05	14									
30	300	04	19	255	12	20	250	16	18	150	14	17	100	08	15	65	05	16	245	05	16	220	08	16	180	10	14									
40	300	10	26	270	25	27	245	20	26	140	14	20	95	10	20	30	06	22	270	10	22	225	13	23	160	12	20									
50	30	03	20	230	10	20	230	10	20	120	10	15	80	10	20	25	08	18	50	05	20	170	10	20	130	10	20									
60	100	15		100	20	10	110	15	10	100	20	10	95	20	10	85	20	10	90	20	10	100	15		90	15										
70	90	30		90	30	10	90	30	10	90	30	10	90	30	10	90	30	10	90	30	10	90	25		90	30										
80	90	35		90	35	10	90	35	10	90	35	10	90	35	15	90	35	15	90	35	15	90	35	15	90	30										
90	90	35		90	40	10	90	40	10	95	40	15	95	40	15	95	40	15	90	35	15	90	30		90	30										
100	90	45		90	45	12	90	45	12	95	45	15	95	45	15	95	45	15	90	35	15	90	30		90	30										
LATITUDE 30° N																																				
10	150	02	15	60	04	13	50	05	13	205	05	12	150	05	14	220	04	13	220	05	14	305	04	16	310	04	16									
20	330	08	18	290	05	18	200	04	15	230	10	16	150	02	15	240	04	15	240	06	16	220	05	17	275	08	17									
30	325	10	20	275	12	24	260	13	24	240	20	25	360	06	20	300	05	23	280	07	22	280	08	22	255	15	20									
40	335	12	20	280	18	30	255	23	30	225	25	30	325	06	30	325	07	28	290	08	25	280	14	28	255	20	25									
50	360	08	20	270	10	25	245	20	25	190	10	20	360	06	25	340	08	25	315	05	25	360	10	25	240	10	20									
60	40	08		40	10	10	170	10	10	130	05	10	85	10	10	80	10	10	80	10	10	80	10	10	40	10										
70	90	20		90	20	10	90	20	10	90	20	10	90	20	10	90	20	10	90	20	10	90	20	10	90	20										
80	90	25		90	25	10	90	25	10	90	25	10	90	25	10	90	25	10	90	25	10	90	25	10	90	25										
90	90	30		90	30	10	90	30	10	90	30	10	90	30	10	90	30	10	90	25	10	90	25	10	90	25										
100	90	30		90	35	15	90	35	15	90	35	15	90	35	15	90	35	15	90	30	10	90	25	10	90	25										
LATITUDE 40° N																																				
10	245	18	18	240	13	18	315	10	18	240	07	14	270	10	16	275	16	17	260	16	18	270	14	18	285	10	17									
20	270	24	24	265	21	24	300	14	22	250	18	22	270	19	20	275	23	21	265	24	22	270	17	24	280	16	22									
30	270	32	30	265	24	32	280	18	30	255	26	34	270	31	28	275	30	29	270	30	29	280	21	32	275	19	28									
40	285	35	35	275	23	34	270	22	35	250	32	36	265	40	34	280	35	35	270	30	33	280	25	35	275	24	30									
50	295	20	25	270	15	25	260	20	25	245	20	24	250	20	24	280	18	25	280	20	25	275	20	25	250	20	25									
60	210	10		190	07	10	180	10	10	180	10	10	190	10	10	220	10	15	200	10	10	200	10	10	200	10										
70	90	10		90	10	10	90	10	10	95	10	10	90	10	10	85	10	10	80	10	10	80	10	10	90	10										
80	90	20		90	20	10	90	20	10	90	20	10	90	20	10	90	15	10	90	15	08	90	20	08	90	15										
90	90	20		90	20	10	90	20	10	90	20	10	90	20	10	90	20	10	90	20	10	90	20	10	90	20										
100	90	25		90	25	10	90	25	10	90	25	10	90	25	10	90	20	10	90	20	10	90	20	10	90	20										
LATITUDE 50° N																																				
10	260	17	23	245	18	23	260	14	23	275	10	15	285	14	18	285	18	18	270	16	22	260	20	20	265	17	23									
20	265	23	29	255	26	30	275	21	29	265	18	25	275	24	23	285	28	25	270	27	29	265	29	30	270	15	30									
30	270	31	38	260	32	38	280	30	40	265	25	37	275	36	34	285	38	33	265	46	40	265	40	42	270	31	40									
40	270	36	38	260	32	38	275	30	35	270	28	35	270	40	34	280	38	34	265	45	38	265	40	37	265	32	38									
50	265	15	25	260	15	25	260	15	25	260	20	25	265	25	20	280	25	25	265	25	25	270	25	25	265	20	25									
60	210	10		190	10	10	190	10	10	210	05	10	220	10	15	230	10	10	190	10	10	190	10	10	200	10										
70	90	05		95	05	10	95	10	10	100	05	10	90	05	10	80	05	10	80	05	10	80	05	10	90	05										
80	90	10		90	10	10	90	10	10	90	10	10	90	10	10	90	10	10	90	10	10	90	10	10	90	10										
90	90	15		90	15	10	90	15	10	90	15	10	90	15	08	90	15	08	90	15	08	90	15	08	90	15										
100	90	15		90	15	10	90	15	10	90	20	10	90	15	08	90	15	08	90	15	08	90	15	08	90	15										
LATITUDE 60° N																																				
10	240	08	20	210	08	20	230	05	18	295	06	14	310	12	18	290	10	20	230	06	20	260	05	21	250	08	24									
20	260	10	30	235	11	30	250	10	25	290	12	22	300	17	22	290	18	26	50	10	29	270	13	30	260	14	32									
30	260	20	38	245	16	38	260	15	40	280	10	30	295	22	33	290	24	32	255	15	37	260	19	39	265	22	45									
40	255	14	34	245	17	33	265	15	32	275	10	23	290	22	30	290	24	29	255	19	30	260	22	35	260	21	35									
50	275	05	20	260	10	20	260	10	20	275	10	20	290	15	20	290	15	20	255	10	20	260	15	25	240	15	25									
60	220	05		180	05	10	180	05	10	190	05	10	210	10	10	220	08		200	08		200	10		190	08										
70	90	05		90	05	10	95	05	10	100	05	10	90	05	10	80	05	10	80	05	10	80	05	10	90	05										
80	90	10		90	10	10	90	10	10	90	10	10	90	10	10	90	10	10	90	10	10	90	10	10	90	10										
90	90	10		90	10	08	90	10	08	90	10	10	90	10	10	90	10	10	90	10	10	90	10	10	90	10										
100	90	10		90	15	08	90	15	08	90	15	08	90	15	08	90	15	08	90	15	08	90	15	08	90	15										

From Handbook of Geophysics and Space Environments, by Shea L. Valley, Air Force Cambridge Research Laboratories. Used by permission of copyright owner, McGraw-Hill Book Co., Inc.

AMCP 700-200

TABLE 2-2. RESULTANT WIND CONDITIONS IN THE NORTHERN HEMISPHERE (cont)

Resultant wind direction (d in degrees), vector mean wind velocity (\bar{v} in knots), and standard vector deviation (δ in knots) at various altitudes (H) for various latitudes and longitudes in the Northern Hemisphere, summer and winter seasons. (Continued)

Summer																													
H 10 ³ ft	100° W			160° W			140° W			120° W			100° W			80° W			60° W			40° W			20° W				
	d	\bar{v}	δ	d	\bar{v}	δ	d	\bar{v}	δ	d	\bar{v}	δ	d	\bar{v}	δ	d	\bar{v}	δ	d	\bar{v}	δ	d	\bar{v}	δ	d	\bar{v}	δ	d	\bar{v}
LATITUDE 70° N																													
10	240	10	12	210	07	17	250	07	16	300	09	13	330	08	18	270	04	18	140	03	17	65	03	16	330	04	18		
20	250	12	27	240	11	26	260	11	21	300	15	18	320	13	24	280	07	26	210	06	25	270	04	24	270	04	27		
30	240	13	35	230	12	36	266	14	29	290	17	24	320	15	29	280	08	32	235	08	32	250	08	33	270	05	38		
40	250	10	28	230	12	28	250	13	24	285	13	22	315	16	24	270	10	23	230	07	25	255	07	25	265	08	25		
50	255	05	15	255	05	15	270	05	15	290	10	15	310	10	15	285	05	15	245	05	15	210	03	10	210	05	20		
60	210	05		190	03	10	180	03	10	190	03	10	210	03		230	05		230	03		140	02		150	02			
70	90	05		90	05	10	90	05	10	90	05	10	90	05		90	05		90	05		90	05		100	05			
80	90	08		90	03	10	90	08	10	90	03	10	90	08		90	08		90	08		90	08		90	08			
90	90	08		90	03	10	90	10	08	90	03	08	90	08		90	08		90	08		90	08		90	08			
100	90	10		90	10	08	90	10	08	90	10	08	90	10		90	10		90	10		90	10		90	10			
LATITUDE 80° N																													
10	250	07	16	255	06	17	265	06	17	285	06	17	280	04	16	195	03	16	205	04	14	315	04	15	310	04	15		
20	250	11	24	260	12	24	280	10	24	290	08	23	285	04	25	235	04	26	230	05	24	265	07	23	285	05	24		
30	270	07	32	275	10	32	300	10	30	320	10	30	280	04	30	265	04	30	215	06	30	270	06	34	300	09	32		
40	270	10	23	285	10	22	300	10	20	325	10	20	315	05	19	240	04	20	195	04	20	245	04	20	280	05	20		
50	220	05	10	270	05	10	305	05	10	310	05	10	280	05	15	260	02	10	170	02	10	180	02	10	240	03	15		
60	200	05		200	05		190	05		190	05		30	02		40	02		40	02		150	02		150	02			
70	90	05		90	05		80	05		60	05		70	05		80	05		90	05		100	05		110	05			
80	90	05		90	05		90	05		80	05		90	05		90	05		100	05		90	05		100	05			
90	90	05		90	05		90	05		90	05		90	05		90	05		90	05		90	05		90	05			
100	90	05		99	03		90	08		90	08		90	05		90	05		90	05		90	05		90	05			

Summer																													
H 10 ³ ft	0°			20° E			40° E			60° E			80° E			100° E			120° E			140° E			160° E				
	d	\bar{v}	δ	d	\bar{v}	δ	d	\bar{v}	δ	d	\bar{v}	δ	d	\bar{v}	δ	d	\bar{v}	δ	d	\bar{v}	δ	d	\bar{v}	δ	d	\bar{v}	δ	d	\bar{v}
LATITUDE 20° N																													
10	115	15	15	30	10	12	05	10	13	330	03	12	240	05	15	280	07	17	210	05	15	160	05	15	150	08	10		
20	115	03	15	25	08	14	05	07	15	70	07	12	110	05	15	115	05	14	165	05	15	170	03	15	130	05	13		
30	165	05	15	20	05	17	05	12	15	70	12	12	80	15	15	90	15	15	90	05	15	25	03	15	350	03	18		
40	150	10	20	30	05	22	110	22	18	70	28	18	80	25	20	85	25	70	85	10	25	30	05	25	355	05	25		
50	120	15	20	110	25	25	110	30	20	90	40	25	80	45	25	75	40	25	75	20	25	65	15	25	60	10	20		
60	100	20		100	25		100	35		90	35		90	40		90	40		80	40		90	30		90	20			
70	90	30		90	30		90	30		90	30		90	30		90	30		90	40		90	40		90	30			
80	90	35		90	35		90	35		90	35		90	35		90	35		90	40		90	40		90	40			
90	90	35		90	35		90	35		90	35		90	35		90	35		90	45		90	45		90	40			
100	90	35		90	35		90	35		90	35		90	35		90	35		90	50		90	50		90	50			
LATITUDE 30° N																													
10	130	03	16	330	10	15	295	08	16	345	04	15							245	05	18	230	07	15	245	10	15		
20	200	07	18	315	13	18	270	12	17	360	07	15	175	05	15				245	10	20	250	15	20	250	10	18		
30	250	18	19	270	17	20	240	10	21	345	03	18	225	05	20	170	10	25	220	15	30	270	17	27	290	12	23		
40	270	20	25	255	25	25	220	17	23	320	07	25	260	08	25	190	15	30	225	15	35	305	20	35	310	15	30		
50	245	15	30	220	15	25	195	10	20	180	07	25	30	05	25	60	15	30	340	10	35	340	10	30	345	10	30		
60	170	15		150	10		150	15		90	10		90	10		90	20		60	20		70	15		40	10			
70	90	20		90	20		100	20		100	20		90	20		90	20		90	25		90	20		90	20			
80	90	25		90	25		90	25		90	30		90	30		90	30		90	30		90	25		90	25			
90	90	25		90	25		90	25		90	30		90	30		90	30		90	30		90	30		90	30			
100	90	30		90	30		90	30		90	30		90	30		90	35		90	35		90	40		90	40			

TABLE 2-2. RESULTANT WIND CONDITIONS IN THE NORTHERN HEMISPHERE (cont)

Resultant wind direction (d in degrees), vector mean wind velocity (\bar{v} in knots), and standard vector deviation (δ in knots) at various altitudes (H) for various latitudes and longitudes in the Northern Hemisphere, summer and winter seasons. (Continued)

H		Summer																											
		0°			20° E			40° E			60° E			80° E			100° E			120° E			140° E			160° E			
10·ft	d	\bar{v}	δ	d	\bar{v}	δ	d	\bar{v}	δ	d	\bar{v}	δ	d	\bar{v}	δ	d	\bar{v}	δ	d	\bar{v}	δ	d	\bar{v}	δ	d	\bar{v}	δ		
LATITUDE 40° N																													
10	265	13	16	315	14	18	255	08	17	330	08	16	250	05	09	290	06	16	285	07	18	260	11	18	265	16	18		
20	265	22	20	290	22	23	240	17	20	295	15	20	255	12	20	270	13	20	260	14	25	265	20	25	275	24	24		
30	265	30	28	280	32	30	270	38	30	280	33	30	260	34	25	255	20	26	270	23	35	260	37	37	280	34	32		
40	265	32	30	265	40	30	255	38	35	275	38	30	260	43	35	275	35	35	275	40	35	265	40	45	280	39	38		
50	265	25	25	260	30	25	260	35	25	260	30	25	265	30	30	290	25	25	280	30	30	235	25	35	285	20	30		
60	190	15		200	15		200	20		200	20		200	20		200	20		210	20		220	15		220	10			
70	90	10		100	10		160	15		100	10		100	10		90	10		90	10		90	10		90	10			
80	90	20		90	20		90	20		90	20		90	20		90	20		90	20		90	20		90	20			
90	90	20		90	20		90	20		90	20		90	20		90	20		90	20		90	20		90	20			
100	90	25		90	25		90	25		90	25		90	25		90	25		90	25		90	25		90	25			
LATITUDE 50° N																													
10	260	14	20	285	10	20	260	06	19	310	08	18	280	08	17	285	07	16	315	06	17	280	05	19	290	08	20		
20	265	20	28	275	14	27	260	08	24	295	13	24	280	14	25	280	13	21	290	13	25	280	12	27	285	16	28		
30	270	27	40	270	20	35	260	14	32	290	27	33	275	20	31	275	20	27	275	18	35	285	23	35	285	25	37		
40	270	27	35	265	24	35	260	20	35	280	27	35	270	34	32	275	30	30	270	25	36	290	27	35	290	30	40		
50	270	15	25	260	20	25	255	25	20	275	25	25	270	25	25	280	20	25	275	20	25	290	20	25	290	20	30		
60	200	10		200	10		200	10		200	10		200	10		200	15		200	10		200	10		220	10			
70	100	05		100	05		100	10		100	05		100	05		90	05		90	05		80	05		90	05			
80	90	10		90	10		90	10		90	12		90	12		90	12		90	10		90	10		90	10			
90	90	15		90	15		90	15		90	15		90	15		90	15		90	15		90	15		90	15			
100	90	20		90	20		90	20		90	20		90	20		90	20		90	20		90	20		90	20			
LATITUDE 60° N																													
10	245	12	20	260	08	20	270	07	20	285	08	21	250	07	19	250	05	15	280	05	16	280	05	18	280	05	19		
20	250	16	30	260	13	27	275	10	27	290	09	27	270	09	26	270	08	22	280	08	24	275	08	24	280	08	27		
30	255	22	45	260	20	40	280	15	32	290	14	34	270	10	35	265	10	30	270	12	27	275	14	30	275	17	34		
40	255	22	35	260	20	32	275	20	27	280	17	28	270	18	26	270	15	25	265	16	26	280	16	28	280	12	33		
50	255	10	20	260	10	20	270	15	20	270	15	20	270	15	15	270	10	15	270	12	20	290	10	20	300	10	25		
60	190	05		200	05		200	05		200	05		200	05		190	05		200	05		200	05		220	05			
70	100	05		100	05		100	05		100	05		90	05		90	05		90	05		90	05		90	05			
80	90	10		90	10		90	10		90	10		90	08		90	08		90	10		90	10		90	10			
90	90	15		90	15		90	15		90	15		90	15		90	15		90	15		90	15		90	15			
100	90	15		90	15		90	15		90	15		90	15		90	15		90	15		90	15		90	15			
LATITUDE 70° N																													
10	255	05	18	225	07	15	235	05	17	225	05	17	210	05	19	210	05	14	240	07	15	250	09	16	250	11	18		
20	240	08	26	240	11	22	265	08	23	275	05	23	260	05	24	260	05	22	270	09	24	265	12	23	260	13	25		
30	210	14	37	230	16	28	260	08	27	265	05	30	260	04	30	260	04	26	260	08	24	260	12	26	260	14	32		
40	245	13	26	240	12	24	260	12	22	265	11	22	260	11	20	255	11	21	255	09	22	255	09	23	255	09	25		
50	240	08	15	245	08	15	255	08	15	255	08	15	250	07	15	240	08	13	250	08	15	250	07	15	245	05	15		
60	170	05		180	05		200	05		210	05		210	05		190	05		200	05		200	05		210	05			
70	100	05		100	05		100	05		100	05		90	05		90	05		90	05		90	05		90	05			
80	90	08		90	08		90	08		90	08		90	08		90	08		90	08		90	08		90	08			
90	90	08		90	08		90	08		90	08		90	08		90	08		90	08		90	08		90	08			
100	90	08		90	08		90	08		90	08		90	08		90	08		90	08		90	08		90	08			
LATITUDE 80° N																													
10	270	05	15	265	07	14	260	05	15	245	05	15	245	06	15	245	05	14	250	07	15	250	08	14	255	08	16		
20	270	05	23	270	06	22	255	05	21	255	05	20	255	08	22	255	05	23	260	09	24	260	10	24	255	11	24		
30	270	03	30	235	07	25	240	05	25	245	05	25	250	03	26	250	03	26	260	04	26	265	05	28	265	07	30		
40	255	07	20	240	07	19	240	07	18	245	07	18	250	06	18	255	05	18	265	06	20	270	06	20	270	07	20		
50	245	05	15	270	05	15	240	05	12	230	05	10	220	04	10	220	05	10	210	03	10	210	03	10	210	03	10		
60	160	05		180	05		210	05		210	05		210	02		210	05		210	05		210	05		210	05			
70	110	05		110	05		110	05		110	05		100	05		100	05		90	05		90	05		90	05			
80	100	05		90	05		90	05		90	05		90	05		90	05		80	05		80	05		90	05			
90	90	05		90	05		90	05		90	05		90	05		90	05		90	05		90	05		90	05			
100	90	05		90	05		90	05		90	05		90	05		90	05		90	05		90	05		90	05			

AMCP 703-200

TABLE 2.2. RESULTANT WIND CONDITIONS IN THE NORTHERN HEMISPHERE (cont)

Resultant wind direction (d in degrees), vector mean wind velocity (V in knots), and standard vector deviation (s in knots) at various altitudes (H) for various latitudes and longitudes in the Northern Hemisphere, summer and winter seasons. (Continued)

Winter																													
H 10 ³ ft	160° W			140° W			120° W			100° W			80° W			60° W			40° W			20° W							
	d	V	s	d	V	s	d	V	s	d	V	s	d	V	s	d	V	s	d	V	s	d	V	s					
LATITUDE 20° N																													
10	30	03	18	140	03	17	170	04	15	210	04	15	70	05	14	105	04	17	245	04	18	270	06	17					
20	300	16	27	290	08	25	225	05	21	245	14	20	240	13	18	325	05	20	340	09	23	315	05	22	280	18	19		
30	290	33	35	290	25	35	260	15	30	255	30	28	250	27	25	275	23	27	295	27	30	290	20	25	280	45	28		
40	235	35	35	285	40	35	280	33	35	265	38	30	255	37	28	265	35	30	285	43	33	280	45	30	275	55	32		
50	295	25	30	295	30	35	285	30	30	260	30	25	250	33	25	270	30	25	285	30	30	275	30	30	270	40	30		
60	190	15		265	15	15	270	15	20	270	15	20	265	15	20	265	15	20	280	15	20	270	15		270	15			
70	80	08		150	08	15	70	05	15	250	08	15	220	05	15	210	05	15	240	03	15	240	03		240	03			
80	90	05		60	08	15	80	05	15	80	08	15	90	02	15	90	03	15	80	05	15	110	03		110	03			
90	90	05		90	05		90	05		90	05		90	05		240	03		90	05		90	05		90	05		90	05
100	90	02		90	02		90	10		90	10		90	03		240	05		90	03		90	10		90	10		90	10
LATITUDE 30° N																													
10	270	20	24	245	12	24	265	07	23	290	11	19	255	20	18	250	17	20	280	13	23	260	08	22	315	07	19		
20	270	40	33	270	25	32	275	15	30	280	24	30	260	38	28	275	36	28	290	25	32	285	13	28	300	17	24		
30	270	60	40	275	40	42	280	25	40	275	38	40	260	57	40	275	55	35	285	38	40	280	23	35	290	27	33		
40	275	70	40	275	55	42	290	37	45	275	48	40	240	70	40	275	65	35	285	48	40	275	35	38	285	35	37		
50	250	50	35	285	35	35	290	35	35	270	35	30	260	55	30	270	60	30	285	45	35	280	30	30	280	30	30		
60	250	25		265	20	20	270	20	20	285	20	20	265	30	20	270	35	20	270	30	20	280	20		280	20			
70	200	03		150	08	15	30	08	15	300	08	15	270	15	15	270	20	20	270	20	15	270	15		270	15			
80	110	05		90	05	15	60	05	15	330	05	20	280	10	15	270	15	20	250	15	20	260	15		270	10			
90	90	05		85	05	20	90	03		320	08	20	280	10	20	270	15	20	270	20		270	10		270	10		270	10
100	270	10		270	08		270	03		300	10	30	270	15	25	270	20	25	270	25		270	10		270	15		270	15
LATITUDE 40° N																													
10	260	30	25	260	24	28	270	21	29	280	15	23	285	20	23	270	35	25	275	28	27	260	15	28	275	12	24		
20	250	47	37	260	37	39	275	32	39	280	29	37	275	37	37	270	53	37	265	47	37	260	30	38	282	16	32		
30	260	65	45	265	53	45	275	43	50	285	42	48	270	53	45	270	75	47	265	57	46	260	35	45	280	22	38		
40	260	74	45	265	60	45	280	47	45	285	47	43	270	60	45	270	80	40	265	55	48	260	40	43	280	25	38		
50	255	55	40	275	40	40	285	35	35	290	35	30	270	45	35	270	60	30	265	50	35	265	35	35	280	25	30		
60	250	50		265	20	20	290	20	20	290	25	20	280	30	20	270	35	25	270	35	25	270	35		270	30			
70	210	10		260	20	20	270	15	20	300	15	20	290	20	20	260	50	25	270	30	25	260	30		270	30			
80	240	05		240	10	10	270	10	15	330	10	20	300	20	25	270	25	30	270	30	25	260	30		270	25			
90	270	10		270	10		270	10		330	10	25	300	15	30	270	25	30	270	25	30	270	20		270	20			
100	270	25		270	25		270	20		310	15	30	300	20	35	270	30	35	270	30	35	270	20		270	25			
LATITUDE 50° N																													
10	240	20	23	260	20	30	260	21	31	265	18	20	295	20	20	275	22	25	265	23	27	250	28	33	260	24	32		
20	240	26	33	255	32	40	270	32	43	280	31	35	290	33	32	275	37	35	260	40	38	245	43	43	265	34	44		
30	240	35	45	255	40	45	270	42	50	285	38	45	285	42	38	270	50	40	255	48	45	250	55	55	265	44	50		
40	240	42	45	260	40	40	280	42	40	285	38	35	285	42	33	270	45	35	255	52	40	250	50	45	270	40	45		
50	245	30	35	265	30	35	280	30	35	285	30	30	285	35	25	270	45	30	255	45	35	250	35	35	275	30	35		
60	230	25		270	25	30	290	20	25	290	25	25	290	35	30	280	40	30	270	40	30	250	40		270	35			
70	230	15		260	20	25	300	15	25	300	25	25	290	30	30	280	35	30	270	40	30	260	40		270	35			
80	230	10		270	15	25	290	20	25	300	20	30	300	30	30	280	30	30	270	40	35	260	35		260	40			
90	260	15		270	15		290	20	30	300	25	30	295	25	35	280	30	35	270	40	35	270	40		270	35			
100	270	30		270	25		290	25	35	300	30	35	295	30	40	280	35	40	270	45		270	40		270	35			
LATITUDE 60° N																													
10	240	07	27	285	08	27	235	08	25	290	13	20	310	14	18	285	13	20	250	12	24	220	14	28	245	20	32		
20	240	12	36	260	15	40	270	20	35	290	22	27	305	23	27	275	19	28	245	19	35	230	23	41	250	28	43		
30	235	20	40	260	23	42	275	27	42	295	25	33	305	30	32	270	25	33	240	27	40	240	33	47	255	37	55		
40	235	26	35	260	27	35	280	30	35	295	25	30	300	30	28	270	25	30	235	30	35	240	38	38	260	40	45		
50	240	20	30	255	30	30	290	30	30	295	25	25	300	30	25	270	25	25	240	30	30	240	35	35	270	35	35		
60	240	30		270	30	30	290	30	30	290	30	30	300	35		290	35		270	35		250	40		260	40			
70	220	35		270	35	35	290	35	30	280	35	30	300	40		290	40		270	40		250	45		260	40			
80	250	30		270	35	35	280	35	35	290	35	35	270	35		270	45		270	45		250	45		270	45			
90	270	30		270	40	40	275	40	40	275	40	40	275	40		270	45		270	45		270	45		270	45			
100	270	35		270	40	45	275	40	40	285	40	40	270	40		270	45		270	50		270	55		370	55			

TABLE 2-2. RESULTANT WIND CONDITIONS IN THE NORTHERN HEMISPHERE (cont)

Resultant wind direction (d in degrees), vector mean wind velocity (V in knots), and standard vector deviation (δ in knots) at various altitudes (H) for various latitudes and longitudes in the Northern Hemisphere, summer and winter seasons. (Continued)

H		Winter																																			
		180° W			160° W			140° W			120° W			100° W			80° W			60° W			40° W			20° W											
10 ³ ft		d	V	δ	d	V	δ	d	V	δ	d	V	δ	d	V	δ	d	V	δ	d	V	δ	d	V	δ	d	V	δ	d	V	δ	d	V	δ			
LATITUDE 70° N																																					
10		330	03	26	300	04	24	285	07	20	310	08	20	330	08	18	110	02	18	195	07	21	165	08	24	270	09	25									
20		280	06	30	290	09	30	290	15	27	310	14	24	325	13	24	190	03	27	195	13	33	215	13	36	245	17	36									
30		265	13	34	275	17	35	285	19	33	310	17	27	325	17	20	250	05	29	200	15	35	225	15	40	250	23	46									
40		240	17	30	265	23	28	290	20	28	315	18	25	320	17	25	260	15	25	205	15	30	225	20	30	255	25	32									
50		240	25	25	260	25	25	285	25	25	305	25	25	310	20	25	275	15	25	225	15	25	230	25	30	260	25	30									
60		250	35		270	35	35	290	35	30	300	35	30	310	30		310	20		270	20		250	30		260	30										
70		250	40		270	35	35	290	35	35	310	40	35	310	35		320	30		280	25		250	35		260	35										
80		270	40		270	40	35	280	40	35	290	40	35	290	35		300	35		270	30		270	35		270	40										
90		270	40		270	40	40	275	40	40	280	40	40	280	40		280	40		280	40		270	40		270	40										
100		270	40		270	45	45	275	45	45	280	40	40	270	45		270	45		270	40		270	45		270	50										
LATITUDE 80° N																																					
10		330	03	20	330	03	20	330	04	20	355	05	20	30	03	18	95	03	19	155	06	19	180	06	20	220	07	23									
20		310	04	25	320	05	25	325	06	25	355	04	25	45	02	25	120	05	25	160	10	29	210	10	32	225	13	30									
30		300	08	25	320	10	25	320	10	25	345	07	25	60	03	25	140	05	25	190	10	30	215	10	33	230	15	37									
40		265	12	23	295	13	25	325	12	25	360	10	25	60	03	25	160	05	25	180	10	25	210	10	27	240	15	25									
50		260	20	20	260	20	25	280	15	25	300	15	25	285	10	25	275	08	25	230	10	25	235	10	25	250	15	25									
60		250	20		270	25		280	20		310	20		320	15		340	15		320	15		290	10		260	10										
70		250	25		270	35		280	25		310	20		320	20		330	15		330	15		310	15		260	15										
80		270	30		270	35		270	30		290	25		300	20		300	15		300	20		290	20		260	20										
90		270	30		270	35		270	35		280	25		280	20		290	20		290	20		280	25		270	25										
100		270	35		270	35		270	35		270	30		270	25		270	25		270	25		270	30		270	30										
Winter																																					
H		0°												20° E			40° E			60° E			80° E			100° E			120° E			140° E			160° E		
		d	V	δ	d	V	δ	d	V	δ	d	V	δ	d	V	δ	d	V	δ	d	V	δ	d	V	δ	d	V	δ	d	V	δ	d	V	δ	d	V	δ
LATITUDE 20° N																																					
10		240	06	16	265	08	15	290	13	15	250	09	15	270	12	15	290	08	15	200	12	14	210	11	17	210	07	17									
20		265	27	21	245	15	25	260	22	22	285	23	23	285	22	20	265	24	20	230	20	17	225	25	20	285	17	20									
30		265	55	32	260	35	27	275	40	30	270	45	28	260	40	25	250	45	25	255	40	22	245	32	25	295	30	25									
40		265	62	35	260	50	30	275	50	30	255	65	33	250	65	30	250	52	25	250	45	25	240	30	28	280	35	30									
50		265	50	25	260	45	30	270	45	25	260	55	30	250	55	32	250	45	25	240	40	25	230	25	25	280	30	25									
60		270	40		270	35		270	35		270	35		270	40		270	35		260	30		260	20		150	20										
70		250	10		250	15		210	15		210	15		210	25		220	20		250	10		220	10		90	05										
80		160	05		160	05		30	05		30	05		30	05		30	05		230	05		110	05		70	10										
90		90	05		90	05		90	05											90	10		90	10		90	10										
100		90	10																	90	10		90	10		90	10										
LATITUDE 30° N																																					
10		290	14	20	280	16	20	265	20	19	250	18	15						285	28	17	275	30	20	270	30	20										
20		280	36	30	270	32	33	255	38	28	265	35	25	270	35	25			270	55	25	270	65	30	265	60	30										
30		280	50	45	270	60	45	270	65	40	270	55	35	275	58	35	270	70	35	270	65	35	265	90	35	270	80	40									
40		280	55	45	270	65	40	270	75	40	265	75	40	260	80	40	270	80	35	270	90	35	270	10	40	270	95	40									
50		280	50	35	270	55	30	270	65	30	265	70	35	260	75	35	265	80	35	265	85	35	265	85	35	275	70	35									
60		280	39		280	35		265	35		270	35		270	40		270	50		270	55		270	50		260	35										
70		290	20		290	20		260	25		270	30		270	20		280	30		260	25		240	20		200	15										
80		290	15		280	20		270	20		280	20		280	20		270	15		240	20		220	15		250	05										
90		270	15		270	25		270	20											250	20		260	20		270	08										
100		270	20		270	30														270	25		270	25		270	15										

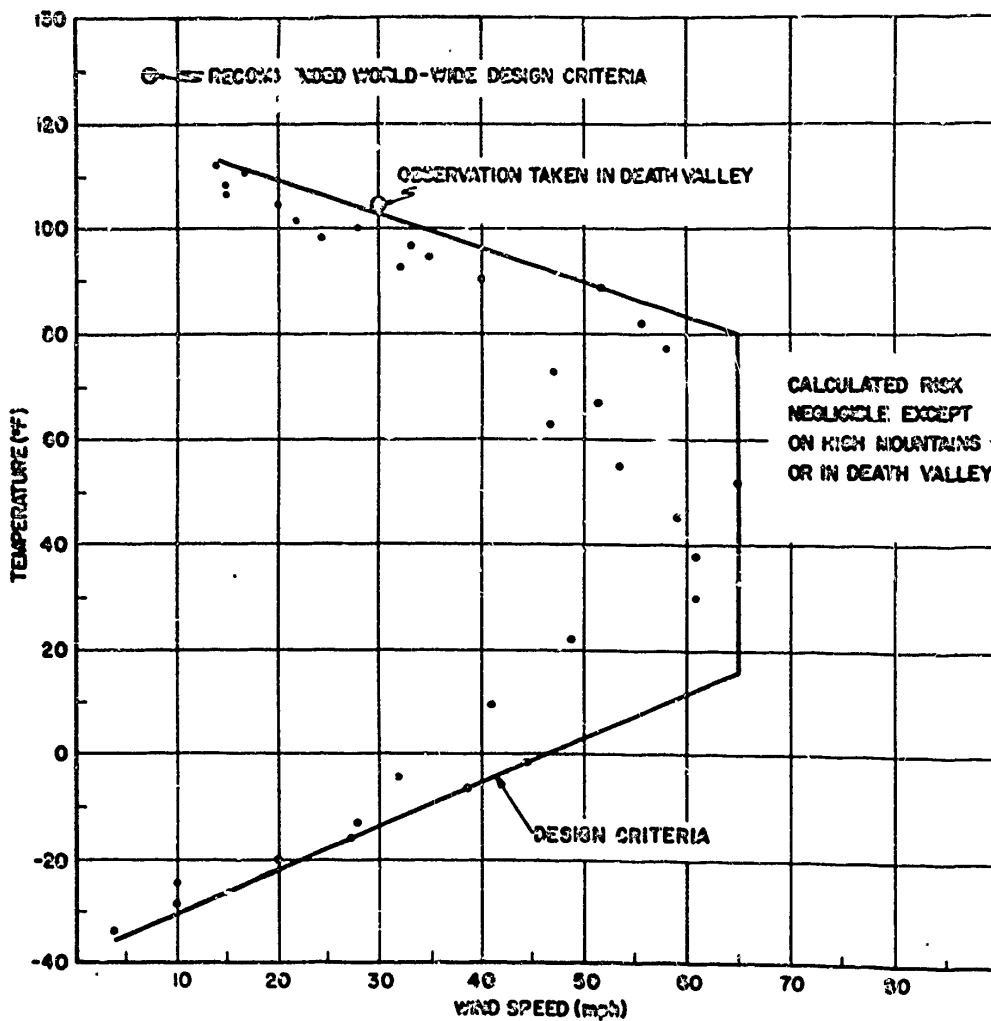
TABLE 2-3. EXTREME ANNUAL WIND SPEEDS

Extreme annual wind speed (fastest mile) at 50 ft above ground at the given stations;
(A) denotes airport station.

Station	Years of Record	Mean (mile h ⁻¹)	S.D. (mile h ⁻¹)	1% Risk in 10 yr (mile h ⁻¹)
Tampa, Fla. (A)	1941-56	52	8.8	95
Miami, Fla.	1943-58	54	18.0	143
Wilmington, N. C. (A)	1951-58	67	15.9	146
Hatteras, N. C.	1912-57	62	13.4	129
Dallas, Tex. (A)	1941-58	52	6.5	84
Washington, D. C. (A)	1949-58	50	8.5	92
Dayton, Ohio (A)	1944-58	60	8.6	103
Atlanta, Ga. (A)	1953-58	50	7.4	87
Abilene, Tex. (A)	1945-58	63	13.6	131
Columbia, Mo. (A)	1949-58	56	6.2	87
Kansas City, Mo.	1934-58	55	7.0	90
Buffalo, N. Y. (A)	1944-58	58	8.3	99
Albany, N. Y. (A)	1936-58	52	8.4	94
Boston, Mass. (A)	1936-50	59	12.1	119
Chicago, Ill. (A)	1943-58	51	5.6	79
Cleveland, Ohio (A)	1941-58	59	5.8	83
Detroit, Mich. (A)	1934-58	49	5.7	77
Minneapolis, Minn. (A)	1938-58	52	11.1	107
Omaha, Nebraska (A)	1936-58	59	13.1	124
El Paso, Tex. (A)	1943-58	58	4.5	80
Albuquerque, N. M. (A)	1933-58	61	10.2	112
Tucson, Ariz.	1948-58	50	7.1	85
San Diego, Calif.	1940-58	36	6.0	66
Cheyenne, Wyo.	1935-58	63	6.9	97
Rapid City, S. D.	1942-58	66	6.7	99
Bismarck, N. D.	1940-58	66	5.2	92
Great Falls, Mont.	1944-54	65	3.5	82
Portland, Ore.	1950-58	57	6.2	91
New York, N. Y.	1949-58	58	4.8	82
Pittsburgh, Pa.	1935-52	52	6.2	83
	Number of Years of Data			
Fairbanks, Alaska	9	37	8.3	78
Nome, Alaska	11	61	9.1	106
Elmendorf AFB, Alaska	14	45	7.1	81
Shemya Island, Alaska	10	70	6.2	101
Hickam AFB, Hawaii	17	45	8.4	86
Clark AB, Philippines	13	39	12.2	100
Lajes Field, Azores	13	62	16.9	146
Albrook AFB, Canal Zone	18	26	4.1	47
San Pablo, Spain	11	77	15.3	153
Wheelus AB, Libya	14	49	11.8	108
Stuttgart, Germany	15	40	4.8	65
Keflavik, Iceland	9	84	10.8	138
Thule, Greenland	14	80	12.4	142
Tainan, Formosa	39	53	21.2	158
Taipei, Formosa	39	59	21.9	167
Itazuke AB, Japan	14	43	10.0	93
Misawa AB, Japan	11	47	7.2	83
Tokyo Intl. Airport, Japan	15	52	12.2	103
Kimpo AB, Korea	8	43	8.0	82
Bombay, India	1	50	14.2	120
Calcutta, India	6	57	7.4	93
Caya, India	6	52	6.8	85
Madras, India	6	45	7.5	82
New Delhi, India	6	52	3.8	70
Poona, India	6	39	6.1	69
Central AB, Iwo Jima	17	78	37.9	266
Kadena AB, Okinawa	14	82	25.3	208

From *Handbook of Geophysics and Space Environments*, by Shea L. Valley, Air Force Cambridge Research Laboratories.
Used by permission of copyright owner, McGraw-Hill Book Co., Inc.

AMCP 703-200



Strongest wind (five-min average) for temperature range observed during a five-yr period. Wind speeds are, in general, for 40 to 100 ft above the surface. Speeds at 10 ft are approximately 80% of the values given, except for the coldest temperatures, where winds are 50% of the indicated values. Stations used for this study are:

Caribou, Me.
Burlington, Vt.
Boston, Mass.
New York, N. Y.
Washington, D. C.
Hatteras, N. C.

Jacksonville, Fla.
Miami, Fla.
Galveston, Tex.
Oklahoma City, Okla.
Phoenix, Ariz.
Los Angeles, Calif.

San Francisco, Calif.
Tatoosh I., Wash.
Great Falls, Mont.
Salt Lake City, Utah
Wichita, Kansas

Minneapolis, Minn.
Chicago, Ill.
Buffalo, N. Y.
Pittsburgh, Pa.
Columbus, Ohio

Figure 2-2. Strongest Wind for Temperature Range

From *Handbook of Geophysics and Space Environments*, by Shea L. Valley, Air Force Cambridge Research Laboratories. Used by permission of copyright owner, McGraw-Hill Book Co., Inc.

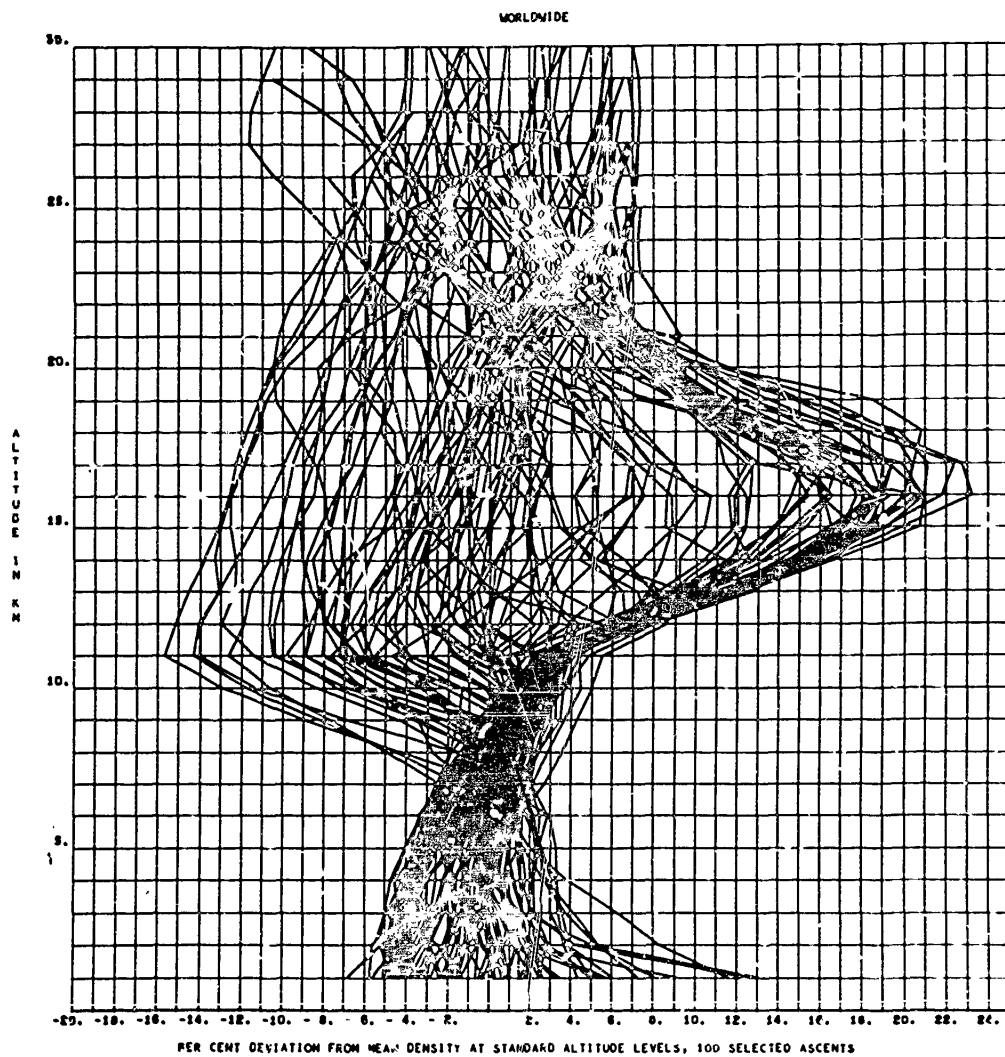


Figure 2-3. Density Deviation Versus Altitude - Worldwide, Annual

AMCP 703-200

TABLE 2-4. DENSITY AND TEMPERATURE PROFILES

A. Key to Code Numbers of Density and Temperature Profiles
(Figs. 2-4 (A) through (F))

Zone	Season	Mean Profile	" +0" Profile	" +0" Profile
Annual Models				
Tropics	Annual	#1	(a)	(a)
Subtropics	Annual	#3	#2	#5
Temperate Z.	Annual	#10	#3	#12
Polar Z.	Annual	#17	#15	#19
Seasonal Models				
Tropics	Summer	#1	(b)	(b)
Tropics	Winter	#1	(b)	(b)
Subtropics	Summer	#2	(b)	(b)
Subtropics	Winter	#5	#4	#6
Temperate Z.	Summer	#8	#7	#9
Temperate Z.	Winter	#12	#11	#13
Polar Z.	Summer	#15	#14	#16
Polar Z.	Winter	#17	#18	#20

(a) Annual variation negligible

(b) Variation negligible

B. Density Profiles for Tropics and Subtropics

(Unit: kg/m³)

Altitude (km)	Profile Number					
	D ₁	D ₂	D ₃	D ₄	D ₅	D ₆
0	1.18375	1.17579	1.19353	1.21632	1.22022	1.24352
1	1.08165	1.06355	1.06676	1.10178	1.11493	1.12318
2	.98629	.96387	.96523	.99730	1.00910	1.02090
3	.89470	.87702	.88321	.91613	.92849	.94785
4	.80203	.78707	.79783	.81057	.81786	.82115
5	.71129	.70232	.72355	.73067	.73636	.74205
6	.64183	.63227	.65750	.65950	.66223	.66596
7	.57822	.57116	.59127	.59320	.59433	.59556
8	.51963	.52747	.53045	.53326	.53195	.53064
9	.45706	.47241	.47494	.47792	.47376	.46360
10	.41247	.42163	.42116	.42423	.41862	.41296
11	.37372	.37450	.37112	.37245	.36567	.35885
12	.33652	.33050	.32443	.32032	.31662	.30962
13	.29959	.29084	.28100	.27810	.27142	.26474
14	.26317	.25403	.24250	.23355	.23317	.22779
15	.22601	.22049	.20900	.20469	.20054	.19639
16	.18910	.18509	.17903	.17545	.17209	.16373
17	.15255	.16175	.15253	.14953	.14656	.14419
18	.12442	.13033	.12923	.12634	.12450	.12276
19	.11150	.11403	.10900	.10716	.10565	.10414
20	.09385	.09353	.09201	.09057	.08944	.08831
21	.07912	.07657	.07763	.07663	.07576	.07489
22	.06477	.06325	.06000	.06496	.06424	.06342
23	.05485	.05765	.05063	.05514	.05456	.05398
24	.04792	.04929	.04770	.04639	.04637	.04535
25	.04063	.04190	.04062	.03991	.03946	.03891

AMCP 705-200

TABLE 2-4. DENSITY AND TEMPERATURE PROFILES (cont)

C. Density Profiles for Temperate Zone
(Unit: kg/r³)

Altitude (km)	Profile Number						
	D ₇	D ₈	D ₉	D ₁₀	D ₁₁	D ₁₂	D ₁₃
0	1.21521	1.22279	1.23037	1.23795	1.24553	1.25311	1.26069
1	1.19610	1.10530	1.11550	1.13046	1.14557	1.15177	1.16797
2	1.145	.89965	1.00784	1.01610	1.01591	1.03061	1.04531
3	.84356	.89990	.90624	.91249	.91174	.92344	.93514
4	.80425	.80927	.81429	.81934	.81871	.82801	.83731
5	.72371	.72775	.73179	.73584	.73496	.74233	.74970
6	.65067	.65396	.65725	.66013	.65911	.66430	.66949
7	.58444	.58715	.58986	.59141	.58954	.59356	.59758
8	.52824	.52824	.52824	.52801	.52781	.52781	.52781
9	.47157	.47052	.46947	.46942	.46906	.46634	.46362
10	.42211	.41769	.41327	.41294	.41652	.40692	.39732
11	.37284	.36522	.35760	.35820	.36140	.35030	.33920
12	.32160	.31327	.30494	.30643	.30877	.29837	.28797
13	.27048	.26730	.26112	.26110	.26132	.25376	.24620
14	.23382	.22913	.22444	.22327	.22219	.21650	.21081
15	.20024	.19643	.19302	.19129	.18572	.18533	.18094
16	.1736	.16865	.16594	.16385	.16232	.15872	.15512
17	.14667	.14458	.14249	.14020	.13859	.13563	.13267
18	.12547	.12391	.12235	.11995	.11850	.11605	.11360
19	.10730	.10612	.10494	.10256	.10138	.09932	.09726
20	.09161	.09091	.09001	.08775	.08673	.08504	.08335
21	.07860	.07760	.07720	.07511	.07465	.07257	.07109
22	.06736	.06680	.06624	.06425	.06330	.06199	.06068
23	.05770	.05725	.05680	.05495	.05410	.05297	.05184
24	.04940	.04904	.04868	.04701	.04628	.04527	.04426
25	.04231	.04199	.04167	.04020	.03962	.03872	.03782

D. Density Profiles for Polar Zone
(Unit: kg/m³)

Altitude (km)	Profile Number						
	D ₁₄	D ₁₅	D ₁₆	D ₁₇	D ₁₈	D ₁₉	D ₂₀
0	1.22769	1.24200	1.25631	1.33520	1.41360	1.43400	1.45440
1	1.09063	1.11235	1.12907	1.17170	1.20340	1.22460	1.24580
2	.89077	1.00261	1.01435	1.03904	1.05278	1.06968	1.08658
3	.89396	.90223	.91050	.92897	.94777	.94697	.95917
4	.80508	.81134	.81760	.82668	.83384	.84194	.85004
5	.72466	.72816	.73366	.74063	.74410	.74860	.75310
6	.65195	.65493	.65791	.66121	.66332	.66424	.66516
7	.58607	.58742	.58877	.58970	.59061	.59701	.59341
8	.52636	.52527	.52418	.52123	.52244	.51479	.50714
9	.47079	.46740	.46401	.45739	.45635	.44617	.43549
10	.41753	.41043	.40333	.39630	.39425	.38265	.37105
11	.36349	.35478	.34607	.33928	.33544	.32564	.31624
12	.31245	.30375	.29505	.29019	.28573	.27831	.27039
13	.26804	.26000	.25336	.24866	.24422	.23950	.23278
14	.22818	.22364	.21910	.21364	.20938	.20466	.19994
15	.19322	.19263	.18993	.18380	.17972	.17570	.17168
16	.16354	.16563	.16272	.15760	.15434	.15095	.14754
17	.14460	.14231	.14002	.13560	.13263	.12979	.12690
18	.12404	.12224	.12044	.11640	.11381	.11139	.10897
19	.10323	.10487	.10351	.10000	.09773	.09563	.09333
20	.09106	.09003	.08933	.08580	.08386	.08216	.08046
21	.07818	.07733	.07658	.07404	.07193	.07049	.06905
22	.06709	.06641	.06579	.06357	.06178	.06045	.05912
23	.05740	.05700	.05659	.05441	.05297	.05183	.05079
24	.04935	.04934	.04933	.04856	.04842	.04442	.04342
25	.04233	.04201	.04169	.03996	.03899	.03803	.03717

AMCP 783-200

TABLE 2-4. DENSITY AND TEMPERATURE PROFILES (cont)

E. Density Profiles for Tropics and Subtropics
(Unit: Percent Deviations from U. S. Standard Atmosphere, 1962)

Altitude (km)	Profile Number					
	D ₁	D ₂	D ₃	D ₄	D ₅	D ₆
0	-5.0	-4.0	-2.1	-7	4	1.5
1	-4.5	-6	-2.2	-9	3	1.5
2	-4.0	-4.3	-2.0	-9	2	1.4
3	-3.8	-3.5	-1.8	-1.1	-1	.9
4	-3.7	-2.7	-1.4	-1.1	-2	.7
5	-3.4	-1.9	-9	-8	0	.8
6	-2.8	-1.2	-4	-2	3	.9
7	-2.3	-5	2	5	.7	.9
8	-1.2	3	.9	1.4	1.2	.9
9	0.0	1.1	1.5	2.3	1.4	.5
10	1.2	1.9	1.8	2.6	1.2	-.1
11	4.1	2.3	1.7	2.1	.2	-1.6
12	8.0	6.0	4.0	3.7	1.5	-.7
13	12.0	9.1	5.4	4.3	1.8	-.7
14	15.5	11.5	6.4	4.7	2.3	-.0
15	18.0	13.2	7.3	5.1	3.0	.8
16	19.0	13.9	7.6	5.4	3.4	1.3
17	15.0	13.7	7.2	5.1	3.2	1.3
18	10.5	12.1	6.2	4.3	2.6	.9
19	7.5	9.7	4.8	3.0	1.6	.1
20	5.0	7.5	3.5	1.9	.6	-.7
21	4.2	6.1	2.5	.9	-.2	-1.3
22	3.5	5.8	2.3	.7	-.4	-1.5
23	3.0	5.3	1.9	.2	-.8	-1.9
24	2.1	5.0	1.6	-.1	-1.2	-2.3
25	1.5	4.8	1.3	-.4	-1.5	-2.7

F. Density Profiles for Temperate Zone
(Unit: Percent Deviations from U. S. Standard Atmosphere, 1962)

Altitude (km)	Profile Number						
	D ₇	D ₈	D ₉	D ₁₀	D ₁₁	D ₁₂	D ₁₃
0	-.8	-.2	.4	2.9	4.1	5.6	7.1
1	-1.4	-.5	.3	1.7	2.1	3.6	5.1
2	-1.5	-.7	.1	.9	.9	2.4	3.8
3	-1.7	-1.0	-.3	.3	.3	1.6	2.8
4	-1.8	-1.2	-.6	-.0	-.1	1.0	2.2
5	-1.7	-1.2	-.6	-.1	-.2	.8	1.8
6	-1.4	-.9	-.4	.0	-.1	.6	1.4
7	-.9	-.5	-.0	.2	-.1	.6	1.3
8	.1	.1	.1	.4	.4	.4	.4
9	1.0	.7	.5	.5	.4	-.1	-.7
10	2.1	1.0	-.0	-.1	-.7	-1.6	-3.9
11	2.2	.1	-2.0	-1.8	-.9	-4.3	-7.6
12	3.1	.4	-2.2	-1.8	-1.0	-4.3	-7.7
13	2.6	.3	-2.0	-2.1	-2.0	-4.8	-7.6
14	2.6	.5	-1.5	-2.0	-2.5	-5.0	-7.5
15	2.8	1.0	-.9	-1.8	-2.6	-4.8	-7.1
16	2.9	1.3	-.3	-1.6	-2.5	-4.6	-6.8
17	3.1	1.6	.1	-1.5	-2.5	-4.7	-6.8
18	3.1	1.8	.6	-1.4	-2.6	-4.6	-6.6
19	3.2	2.0	.9	-1.4	-2.5	-4.5	-6.5
20	3.5	2.2	1.2	-1.3	-2.4	-4.3	-6.2
21	3.5	2.6	1.7	-1.1	-2.5	-4.4	-6.4
22	4.4	3.5	2.7	-.4	-1.9	-3.3	-5.9
23	4.9	4.1	3.2	-.1	-1.6	-3.7	-5.8
24	5.2	4.5	3.7	.1	-1.4	-3.5	-5.7
25	5.6	4.9	4.9	.3	-1.1	-3.4	-5.6

AMCF 706-280

TABLE 2-4. DENSITY AND TEMPERATURE PROFILES (cont)

G. Density Profiles for Polar Zone
(Unit: Percent Deviations from U. S. Standard Atmosphere, 1962)

Altitude (km)	Profile Number						
	D ₁₄	D ₁₅	D ₁₆	D ₁₇	D ₁₈	D ₁₉	D ₂₀
0	.2	1.4	2.5	9.0	15.4	17.1	18.7
1	-1.3	.0	1.5	5.4	8.2	10.1	12.1
2	-1.6	-4	.8	3.2	4.6	6.3	7.9
3	-1.7	-8	.1	1.9	2.8	4.1	5.5
4	-1.7	-1.0	-2	1.1	1.8	2.7	3.7
5	-1.6	-1.0	-4	.6	1.0	1.6	2.3
6	-1.2	-8	-3	.2	.5	.6	.8
7	-.7	-4	-2	-.2	.1	-.5	-1.1
8	.1	-1	-3	-.9	-.6	-2.1	-3.5
9	.8	.1	-.6	-2.1	-2.2	-4.5	-6.7
10	1.0	-.7	-2.5	-4.2	-4.6	-7.5	-10.5
11	-.3	-2.7	-5.1	-7.0	-8.0	-10.7	-13.3
12	.2	-2.6	-5.4	-7.0	-8.4	-10.8	-13.1
13	-.2	-2.5	-4.7	-6.7	-8.4	-10.5	-12.7
14	.1	-1.8	-3.8	-6.2	-8.1	-10.2	-12.2
15	.8	-1.1	-3.0	-5.7	-7.7	-9.8	-11.8
16	1.2	-.5	-2.2	-5.2	-7.3	-9.3	-11.4
17	1.6	.0	-1.6	-4.7	-6.8	-8.8	-10.8
18	2.0	.5	-1.0	-4.3	-6.4	-8.4	-10.4
19	2.1	.8	-.5	-3.8	-6.0	-8.0	-10.0
20	2.4	1.2	.1	-3.4	-5.7	-7.6	-9.5
21	3.0	1.9	.9	-2.5	-5.2	-7.1	-9.0
22	3.9	2.9	2.0	-1.4	-4.2	-6.3	-8.3
23	4.5	3.6	2.7	-1.1	-3.7	-5.7	-7.7
24	5.1	4.3	3.4	-.8	-3.2	-5.4	-7.5
25	5.6	4.8	4.0	-.3	-2.7	-5.0	-7.3

H. Temperature Profiles for Tropics and Subtropics
(Unit: Degrees Kelvin)

Altitude (km)	Profile Number					
	T ₁	T ₂	T ₃	T ₄	T ₅	T ₆
0	299.5	298.2	293.1	290.5	287.3	284.1
1	293.2	296.4	299.0	285.1	281.6	278.7
2	288.5	290.8	283.0	279.6	275.6	271.1
3	287.8	283.9	276.8	274.0	270.3	266.8
4	278.5	276.6	270.3	268.1	264.5	261.9
5	272.9	269.9	263.6	261.6	257.9	254.4
6	267.1	267.1	258.6	254.6	250.8	247.2
7	260.9	256.4	249.4	247.2	243.5	239.3
8	254.3	249.5	242.0	239.6	236.1	232.5
9	247.2	242.6	234.6	232.2	228.6	225.2
10	239.5	235.9	228.1	225.0	222.8	222.8
11	231.6	229.5	222.6	218.4	216.7	222.0
12	223.4	223.4	213.2	213.0	213.1	221.1
13	215.4	217.9	215.4	209.8	215.3	219.6
14	207.7	213.1	213.0	203.4	213.9	217.8
15	200.9	209.0	210.7	207.2	212.0	215.9
16	193.0	206.3	209.0	206.2	210.4	214.2
17	194.6	205.2	203.5	205.6	209.7	213.0
18	195.2	205.4	209.2	207.3	209.9	213.0
19	201.7	209.6	211.1	209.0	211.1	213.5
20	206.5	212.9	213.0	210.7	212.4	214.3
21	210.2	215.6	214.9	212.2	213.9	215.5
22	213.1	217.7	216.7	213.7	215.4	217.0
23	215.6	219.6	218.2	215.1	216.9	218.6
24	218.0	221.4	219.8	216.5	218.4	220.3
25	220.4	223.2	221.4	217.8	219.9	222.1

AMCP 703-100

TABLE 2-4. DENSITY AND TEMPERATURE PROFILES (cont)

I. Temperature Profiles for Temperate Zone
(Unit: Degrees Kelvin)

Altitude (km)	Profile Number						
	T ₇	T ₈	T ₉	T ₁₀	T ₁₁	T ₁₂	T ₁₃
0	290.0	283.7	287.4	280.3	276.6	272.8	269.0
1	285.8	283.6	281.4	278.9	273.8	270.6	267.4
2	279.7	277.7	275.7	272.0	269.2	266.3	263.4
3	274.5	272.5	270.5	266.8	263.8	261.0	258.2
4	269.9	267.9	264.9	261.0	257.8	255.0	252.2
5	262.6	260.8	259.0	254.5	251.1	248.3	245.5
6	265.9	264.2	262.5	247.6	244.1	241.3	238.5
7	249.7	247.1	245.5	240.3	236.7	234.0	231.3
8	240.1	239.5	237.9	232.9	229.3	226.8	224.3
9	232.4	231.9	230.6	225.9	222.0	220.5	219.0
10	225.9	224.9	224.2	220.4	214.9	216.2	216.3
11	219.8	220.9	222.7	217.5	211.7	214.5	216.6
12	217.5	220.8	224.3	217.5	211.5	214.9	217.0
13	219.3	221.8	224.7	218.2	212.5	215.6	217.7
14	219.5	221.8	224.3	218.3	212.9	215.2	217.5
15	219.7	221.7	223.7	218.1	212.5	214.9	217.1
16	220.2	221.7	223.2	217.0	212.1	214.5	216.8
17	220.8	221.8	222.8	217.6	211.8	214.0	216.3
18	221.4	222.2	223.0	217.5	211.4	213.6	215.8
19	221.8	222.6	223.4	217.4	211.1	213.3	215.6
20	222.3	223.1	223.9	217.5	210.7	213.1	215.4
21	222.8	223.8	224.4	217.8	210.2	212.9	215.3
22	223.1	224.1	225.1	217.9	209.9	212.7	215.4
23	223.7	224.7	225.7	218.2	209.6	212.5	215.4
24	224.5	225.6	226.7	218.6	209.2	212.3	215.4
25	225.5	226.7	227.9	219.1	208.8	212.1	215.3

J. Temperature Profiles for Polar Zone
(Unit: Degrees Kelvin)

Altitude (km)	Profile Number						
	T ₁₄	T ₁₅	T ₁₆	T ₁₇	T ₁₈	T ₁₉	T ₂₀
0	289.1	282.9	276.7	265.2	254.8	247.8	240.8
1	283.3	280.3	274.3	263.0	251.0	243.8	236.6
2	280.3	275.1	269.9	263.4	260.6	253.6	246.6
3	274.5	269.7	264.9	259.9	256.6	249.8	243.0
4	269.8	264.0	259.2	253.4	251.0	244.5	238.0
5	262.7	257.8	252.9	248.1	244.3	238.3	232.3
6	254.0	251.0	246.0	240.8	237.2	232.0	226.8
7	249.8	243.8	238.8	234.2	229.7	226.0	222.3
8	241.1	235.5	231.9	228.1	223.2	221.3	218.6
9	233.5	229.5	227.4	223.5	217.3	218.5	219.7
10	229.3	225.1	224.0	221.3	215.1	218.0	221.3
11	229.2	224.0	227.0	221.6	216.5	219.2	223.1
12	219.9	224.5	226.5	222.3	217.1	220.0	223.6
13	221.8	225.5	228.3	222.7	216.7	220.0	223.8
14	222.4	225.3	227.8	222.5	216.2	219.5	223.2
15	222.2	224.2	227.5	222.1	215.6	219.2	223.4
16	222.1	224.5	226.9	221.8	215.6	218.8	223.2
17	222.3	224.5	226.7	221.6	214.4	218.5	223.0
18	222.7	224.8	226.7	221.3	213.8	218.2	222.8
19	223.1	225.0	226.9	221.2	213.2	217.9	222.6
20	223.6	225.5	227.4	221.2	212.6	217.6	222.4
21	224.1	226.0	227.9	221.1	212.0	217.4	222.2
22	224.6	226.5	228.4	220.9	211.4	217.0	222.0
23	225.1	227.0	228.9	220.7	210.8	216.6	221.8
24	225.9	227.8	229.7	220.9	210.2	216.2	221.6
25	223.7	226.6	230.5	221.1	209.6	215.8	221.4

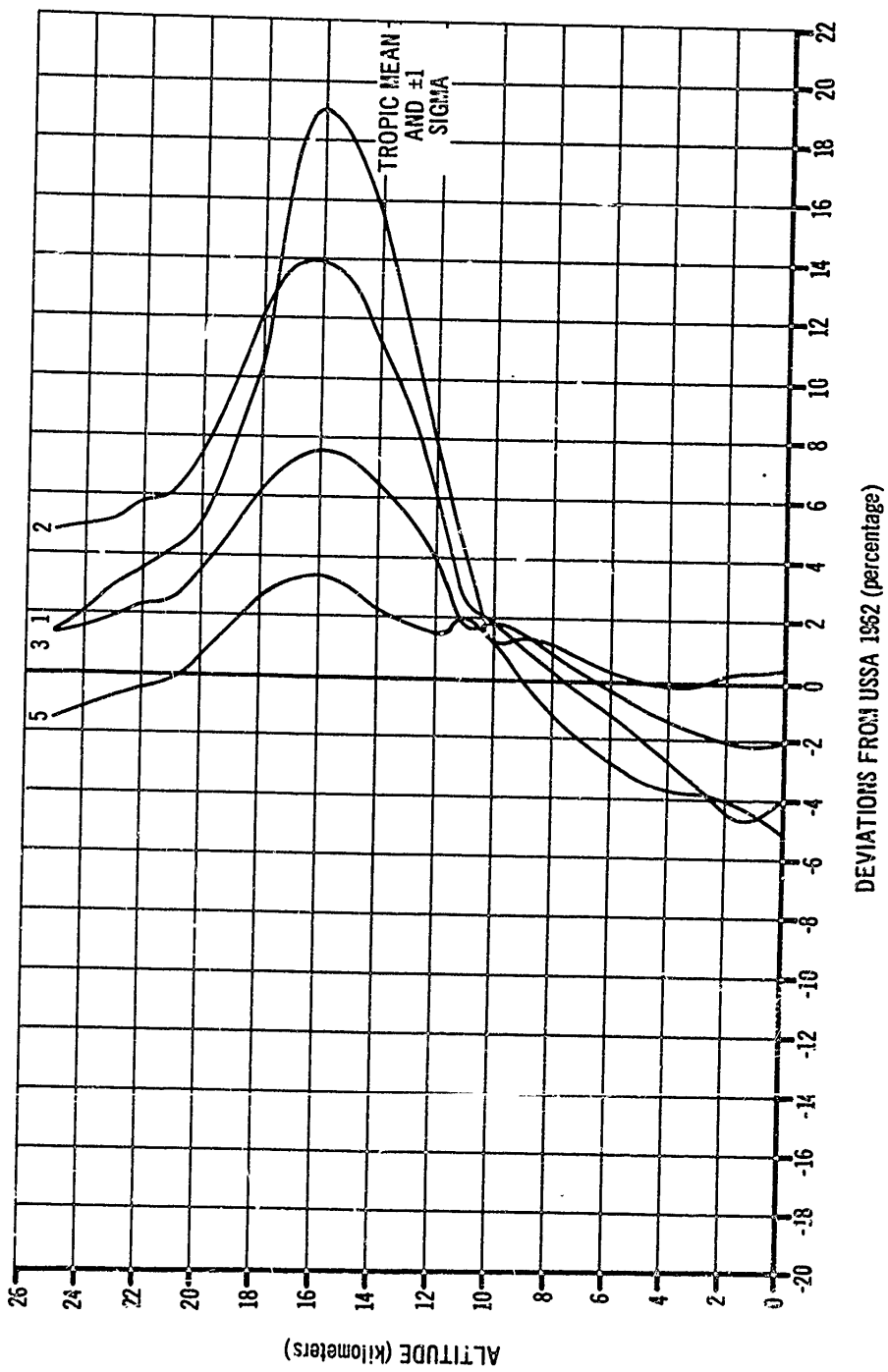


Figure 2-4(A). Subtropics and Tropics -- Annual Density Model

ARJCP 703-200

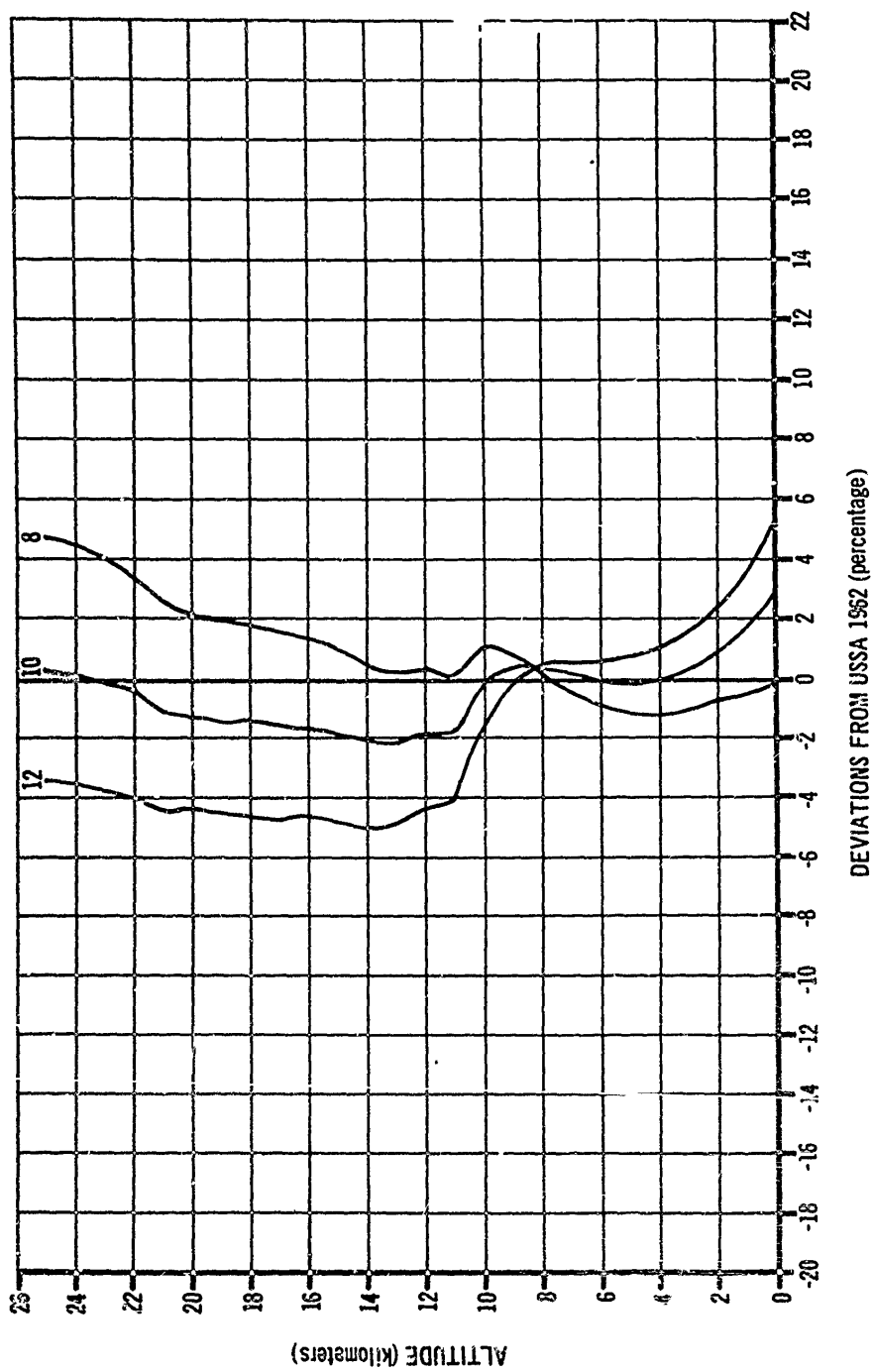


Figure 2-4(B). Temperate Zone - Annual Density Model

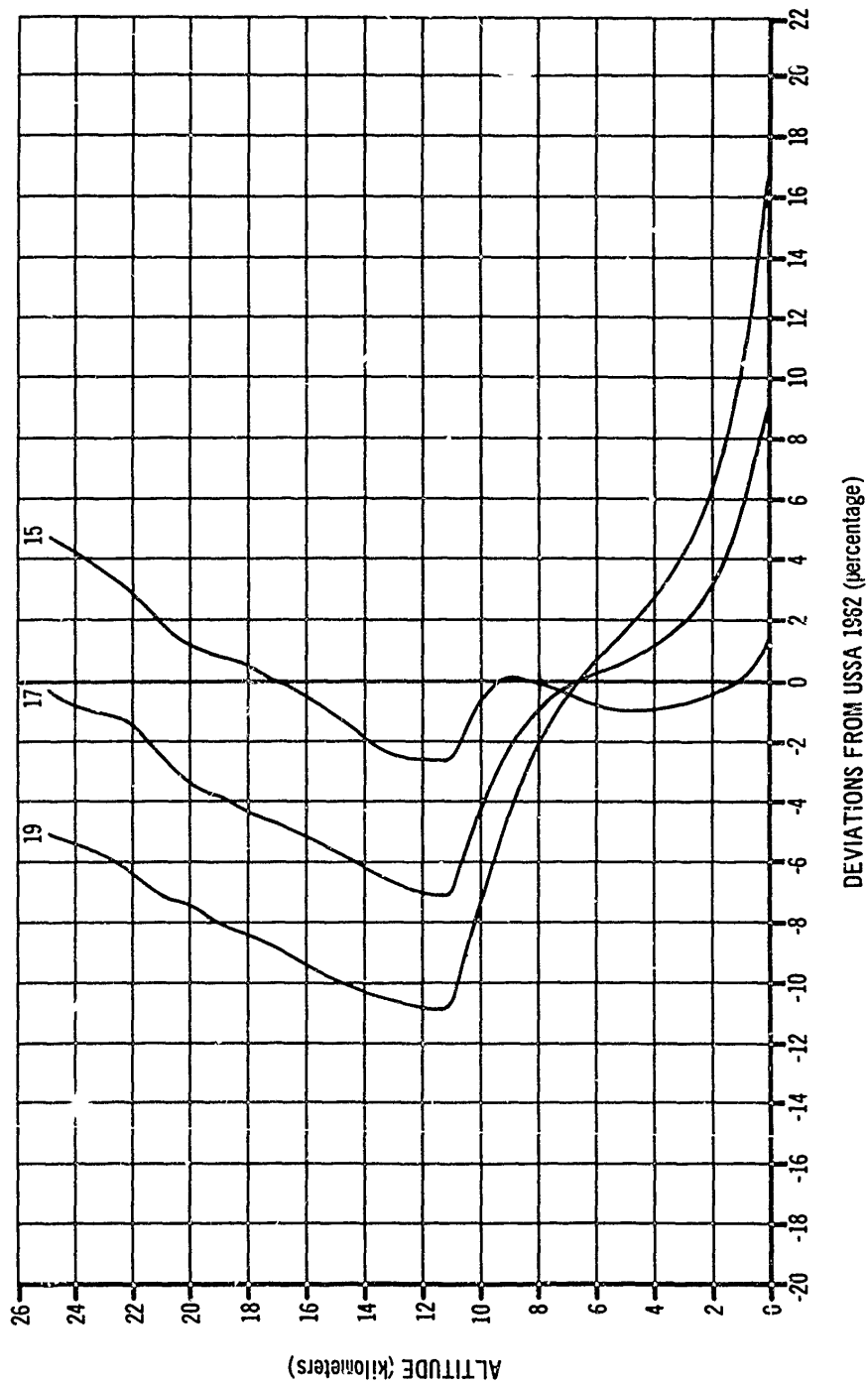


Figure 2-4(C). Polar Zone - Annual Density Model

AMCP 703-200

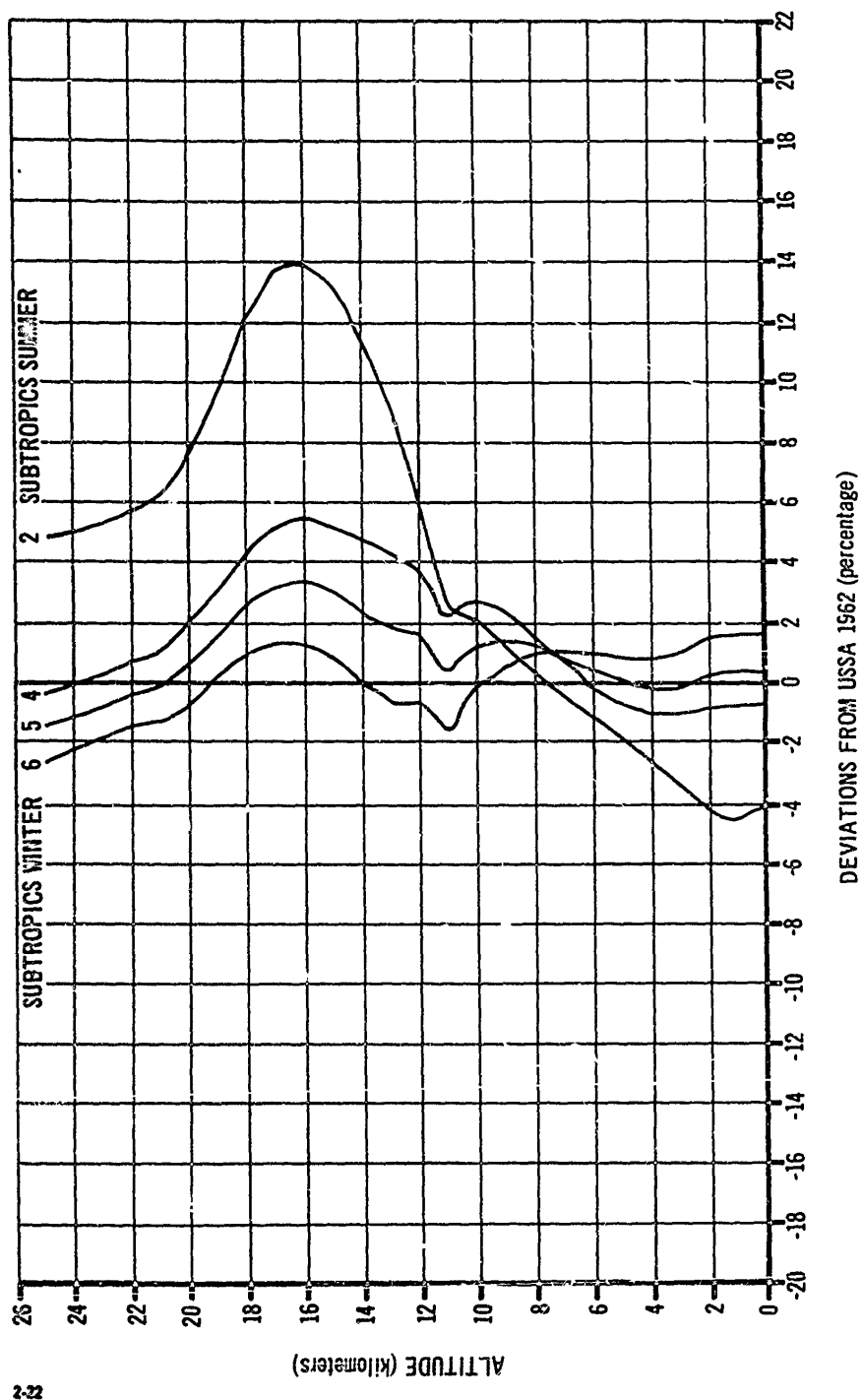


Figure 2-4(D). Subtropics - Seasonal Density Models

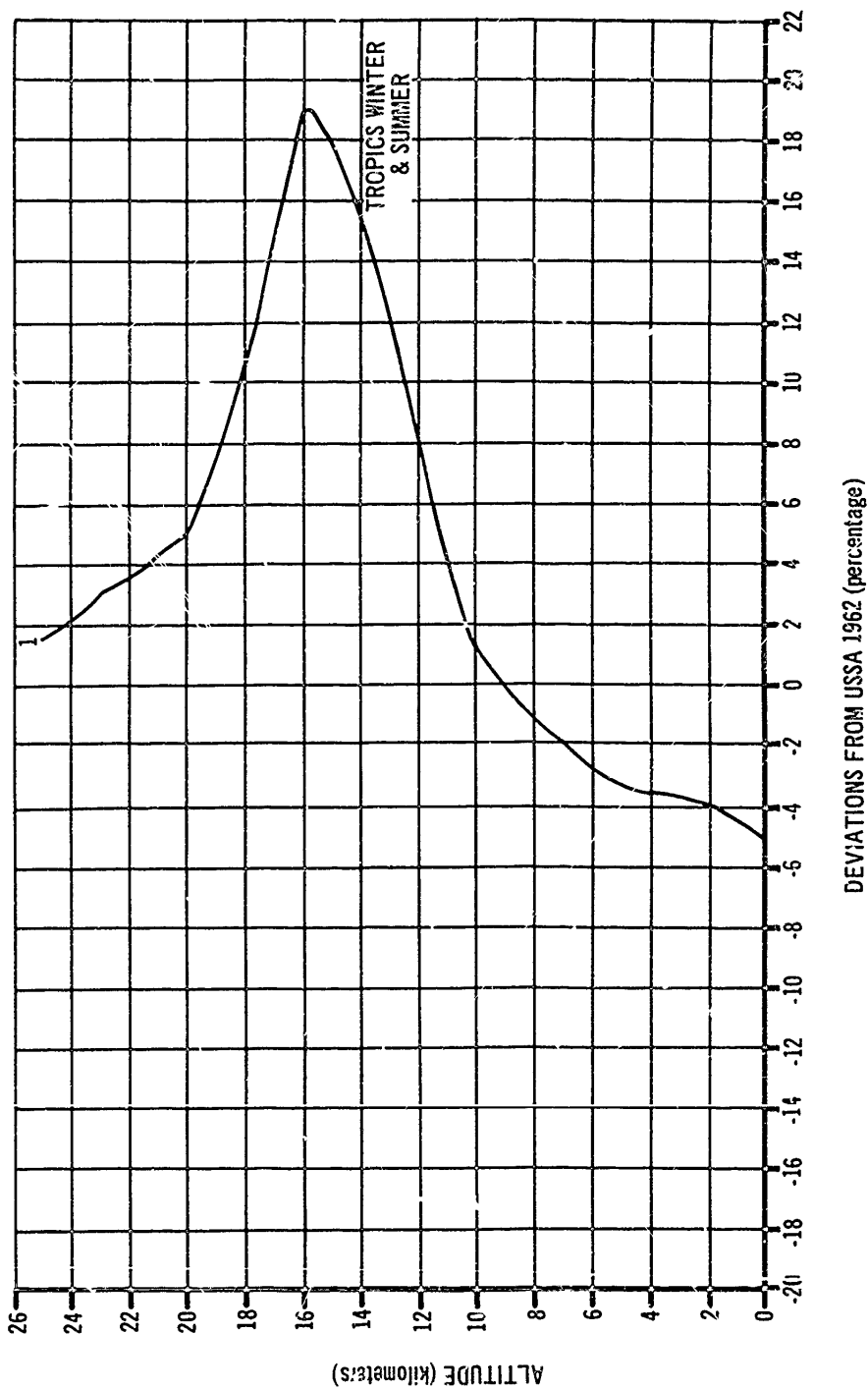


Figure 2-4(E). Tropics - Seasonal Density Models

AMCP 703-200

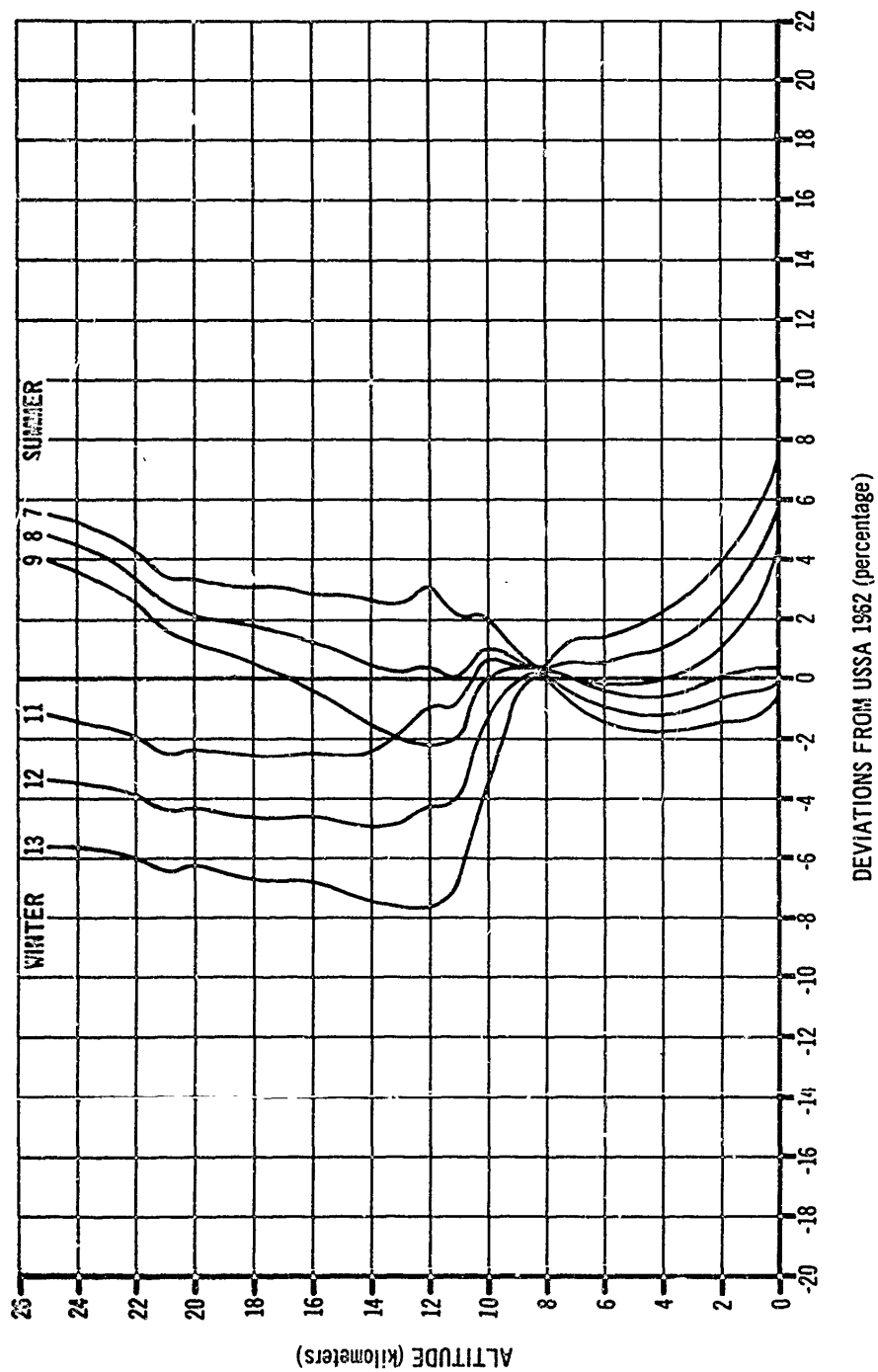


Figure 2-4(F). Temperate Zone -- Seasonal Density Models

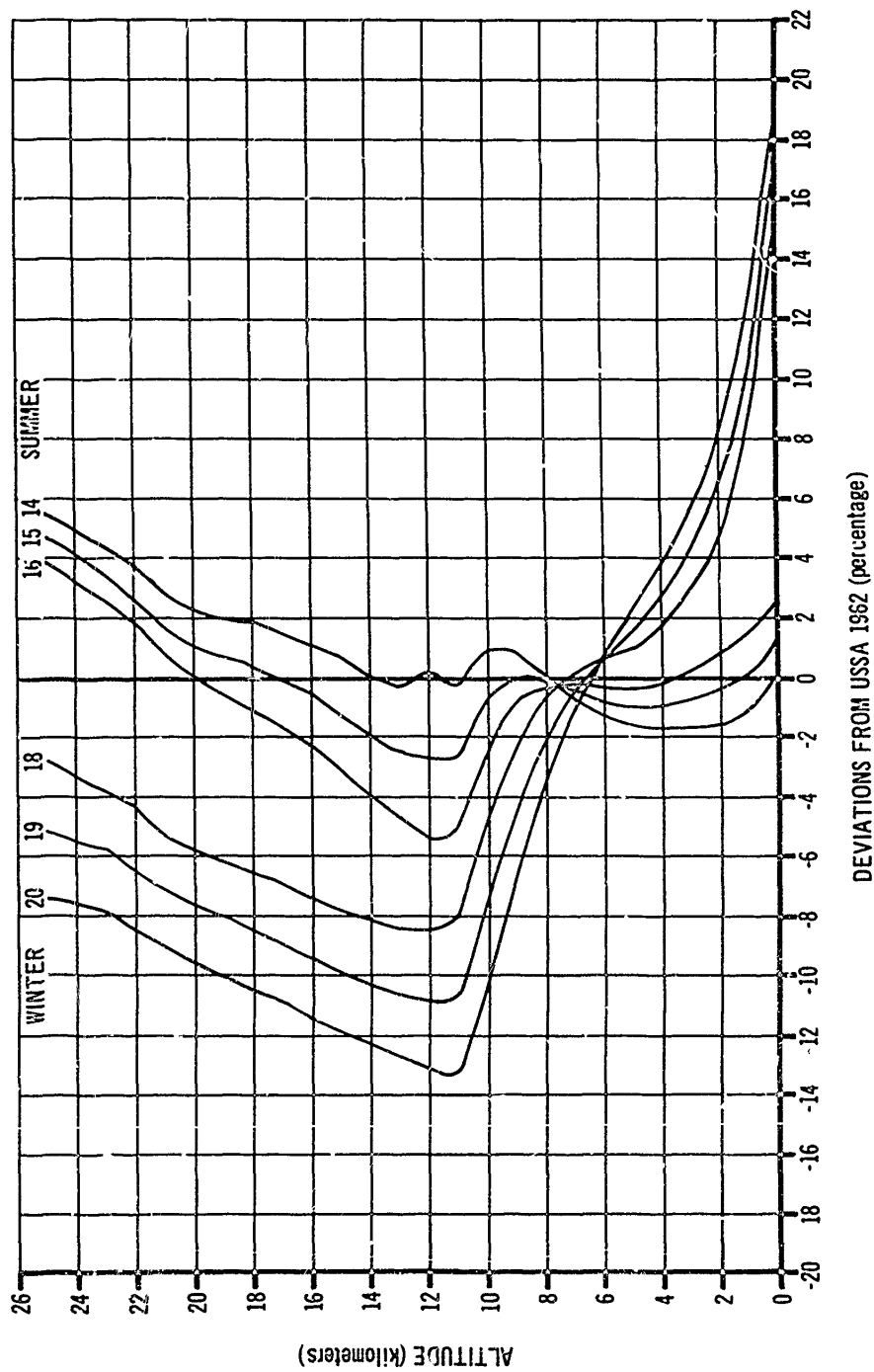


Figure 2-4(G). Polar Zone - Seasonal Density Models

CHAPTER 3 SYSTEM DESIGN

3-1 GENERAL

The first point to be considered in the design of a rocket system is the purpose of the system. We shall attempt to answer the first questions usually asked: To what use will the system be put; who will use it, and how will it be used? Next will be a more precise and detailed examination of the requirements to provide a basis for developing, first, the conceptual approach and, then, the detailed design. Rocket system requirements can be documented in various forms, as will be explained in more detail later, or they can be orally expressed statements in anticipation of later, formally documented statements. Regardless of form, requirements based on real or anticipated needs should precede any system design in order for the design to be meaningful. With the requirements as a basis, an orderly and systematic procedure leading to a successful conclusion can then be established.

Before discussing the systematic procedure for the design of a rocket system, however, a brief survey of classes of rockets, operational modes, and launching methods will give us a common background and terminology for the discussion.

3-2 CLASSES OF ROCKETS

3-2.1 MILITARY ROCKET SYSTEMS

In general, rocket systems used by the several branches of the armed forces are classed as military systems. They are used, except in several instances which will be noted later, to deliver some form of destructive warhead on an enemy target. The types used most frequently by the Army are briefly described in the paragraphs which follow.

3-2.1.1 Artillery

Artillery rocket systems are used in the same manner as artillery gun systems--to support personnel in contact with the enemy in forward areas

They have long range capability and vary in size from small, man-handled rockets to very large rockets requiring heavy equipment for handling and loading. The primary function of an artillery rocket system is support by indirect fire, but most systems have some capability for direct fire. System accuracy is probably the most important consideration in artillery rocket systems.

3-2.1.2 Infantry

Infantry rocket systems are used by personnel in forward areas, in direct contact with the opposing forces. Infantry systems are generally direct-fire-type weapons, usually smaller than artillery systems, and, frequently, man-carried and -fired. The most notable type of infantry system is the antitank weapon, carried by the individual soldier and designed to be fired from the shoulder. Many special factors must be considered in such systems since the rocket and man are in such close contact. The weapon must be effective, yet safe to be handled and fired without endangering the user. Infantry systems are light, easily transported by men, and simple to facilitate fast reaction to changing battlefield conditions.

3-2.1.3 Air Defense

Air defense rocket systems are used to protect the ground soldier from enemy aircraft. They range in size from small, individually carried and fired systems to large, complicated systems capable of attaining very high altitudes. Many of these employ some type of guidance system to enable the rocket to maneuver and counteract the aircraft evasive tactics. The free rocket systems are generally fired in number into an area where the aircraft is or is expected to be. This results in a pattern in the target area similar to a pattern of shotgun pellets fired at a flying bird. The rockets in these systems are usually small and simple in design to permit large numbers to be used economically.

AMCP 703-289**3-2.1.4 Armor**

Rocket systems used by the armored forces are, in many instances, the same as those used by the infantry and artillery. The tank, armed with a direct-firing gun or rocket system, is the primary weapon of the armored forces. The primary target of tanks is enemy tanks; consequently, the antitank type of rocket is generally employed. However, tank weapons are also used against many types of ground targets. For this reason, they carry ammunition mixes suitable to the more prevalent targets expected.

3-2.1.5 Aviation

Rocket systems to be mounted on, and fired from, Army fixed and rotary wing aircraft have been of increasing interest. The need for these small aircraft to have some type of defense, and to be able to perform an attack function in close support of the ground soldier, has been shown to be of considerable importance, as evident in brush-fire activity in several parts of the world. When this need for aerial rocket weapons first became urgent, attention was turned to adapting an appropriate rocket system originally developed to fill other requirements. Since aircraft are used by the individual branches of the Army ground forces, rocket systems are used to accomplish the missions assigned the using branch. In addition, airborne rockets are used for the defense against aircraft of the opposing forces. The notable difference in these systems is that they are fired from an elevated platform that is unstable and in many instances rapidly moving. Rotary wing aircraft can stop and hover but, unlike a tank, they have no firm ground base as a steady firing point. Many additional factors must be considered in the design of aircraft systems to permit attainment of the tactical performance desired without endangering the aircraft or its crew.

3-2.1.6 Logistic

Although no significant development of logistic rocket systems has occurred up to this time in this class of rocket, it will undoubtedly play an important role in future large scale warfare. The logistic rocket is proposed as an extremely fast

direct method of delivering to ground forces all types of supplies needed on the battlefield. In this concept the payload, instead of being a destructive mechanism, is composed of food, clothing, ammunition, medical items, or any other items of supply needed by personnel, and can be any single item or any desired mixture of items. At the destination, the payload is separated and parachuted to the ground. Rapid movement of men to forward areas and distant points by means of rocket transport has been proposed; however, much more elaborate techniques must be developed and utilized before this method of transport becomes practical.

3-2.1.7 Support

Rocket systems can also be used to support other operations. Examples of such systems are flare rockets for night operations in the battle area, tactical meteorological rockets for obtaining data necessary in artillery fire operations, rockets for delivery of some type of electronic equipment to a specified point for place-marking or transmittal of intelligence, and rockets that will produce smoke or other visual means of spotting on a target. The uses to which rocket systems can be put in their support role seem to have no particular limit. The same design approach is used for support rocket systems as for any other rocket system; the designer is limited only by the particular dictates of the specific requirement.

3-2.2 RESEARCH ROCKET SYSTEMS**3-2.2.1 General**

Research rocket systems have, in common with military rockets systems, the general characteristic of delivering a payload to some designated point. Research rockets are also made up of the same general group of components. Their prime function, however, is different. They are designed to accomplish a mission from which useful technological data will be obtained to further a scientific understanding of a specific discipline. In this role, the payload becomes a device to gather data for later evaluation. Such a payload obviously necessitates a means for payload recovery and a means to prevent payload damage or de-

struction that would negate mission completion. In a sense, many military rockets serve as research rockets during their developmental phase. In this phase, the payload is a ballast weight or data gathering device; equipment exterior to the system also is used to gather information on the rocket flight. The knowledge obtained is used to further the understanding of rockets and their behavior as powered airborne vehicles.

3-2.2.2 Meteorological

Rocket systems have been used to place sensing devices at various altitudes in and out of the earth's atmosphere. These have the purpose of providing information about the earth's air, the winds, temperature, radiation, moisture, and other phenomena. Because these systems utilize a vertical or near-vertical trajectory, the objective is the attainment of altitude.

3-2.2.3 High Altitude Sounding

Rocket systems for sounding at high altitudes are used for obtaining some specific bit of information at altitudes ranging to several hundred miles above the earth's surface. These, like the meteorological rockets, utilize a vertical or near-vertical trajectory.

3-2.2.4 Satellites

Unguided, aerodynamically stabilized rocket systems can be used to place a payload into earth orbit. The payloads of these systems are usually small sensing devices for gathering information and transmitting it back to earth. These systems are usually multistage, with the first, and perhaps a second, stage operating in the unguided or free-flight mode. In later stages, it is necessary to provide some type of guidance to permit maneuvering into an attitude to attain the desired orbital path. In these stages, the purpose of the unguided phase is to place the vehicle at some appropriate altitude from which the orbital phase can be initiated. For small payloads, this system approach results in considerable saving in guidance hardware, particularly where precise orbital mechanics are not required.

3-2.2.5 Dispensing

Dispensing rocket systems can be either research or military. The purpose of such a rocket system is to dispense a material, or materials, at some point in the rocket's trajectory. Examples are chaff-dispensing rockets, leaflet-dispensing rockets, smoke screen rockets, and rockets to disseminate crystals of various substances for cloud seeding to induce rain. The chaff dispensers are used to put large quantities of very small metallic wires into an area at some height above the ground. These wires, or dipoles, are then tracked by ground radar to determine the nature of wind currents at various altitudes. Leaflet rockets are used to deliver propaganda leaflets over areas not accessible from the ground. The payload is released at a specific altitude and the leaflets flutter, spread, and are carried over large ground areas by the wind. Although not in general use, cloud-seeding rockets have been proposed, e.g., a rocket to dispense small pellets of dry ice into fog banks for fog removal over airports and similar areas. It appears practical to use rocket delivery methods for dispensing materials such as those described above, particularly where other means requiring human presence are not practical or are denied. The rocket's presence is almost unknown until after it has accomplished its mission.

3-3 OPERATIONAL MODES

3-3.1 General

Rockets may be designed and used in an almost unlimited number of ways. They have been used not only to serve military and research purposes, as discussed in the foregoing paragraphs, but also to propel aircraft and land-based vehicles, and for other similar purposes. It is not the purpose of this handbook to discuss the many facets of rocket uses, but only to present the uses most commonly employed in military systems. The paragraphs which follow will briefly describe the modes normally used for military rocket systems.

3-3.2 GROUND-TO-GROUND

In the ground-to-ground mode the rocket is launched from a point on the ground to a target

AMCP 706-280

on the ground. Most artillery, infantry, and armor systems are used in this mode.

3-3.3 GROUND-TO-AIR

In the ground-to-air mode the rocket is launched from the ground against an airborne target. The target may be a manned airplane, an unmanned drone, another rocket or missile, or simply a point in space. The air defense, meteorological, high altitude sounding, and dispensing rocket systems operate in this mode.

3-3.4 AIR-TO-AIR

The air-to-air rocket systems are used in defensive and offensive operations from aircraft against other airborne targets. Some of the aviation rocket systems for use on fixed and rotary wing aircraft are in this category.

3-3.5 AIR-TO-GROUND

Air-to-ground rocket systems are used in suppressive fire over areas of ground, for point targets on the ground, and to deny an enemy a ground position. They are fired from fixed wing and rotary wing aircraft, usually at relatively low altitudes. It is extremely difficult, except in unusual circumstances, to recognize and identify ground targets from an aircraft, and the higher the viewing position, the more difficult this becomes. For this reason most air-to-ground rockets do not need extremely long range capability; however, they do need to be as accurate as possible to permit effective fire from the unstable aircraft firing platform.

3-3.6 UNDERWATER-TO-AIR

Rocket systems have been designed and built to be fired from under the surface of a body of water and to continue flight after emerging into the atmosphere. At present, the submarine-launched POLARIS missile system is the most notable example. Although the POLARIS is a guided missile of considerable complexity, there is nothing inherent in rocket technology to prevent any rocket system, guided or unguided, from

functioning in this mode. The critical factor is accuracy since the purpose of firing this type of rocket is to hit a target.

3-3.7 SURFACE/AIR-TO-UNDERWATER

These systems are the reverse of those described in the preceding paragraph. In these systems, the rocket is fired from a surface or air launching point, enters a body of water, and continues its trajectory in that medium. One current example is the SUBROC, or submarine rocket, used by the Navy to attack underwater targets from surface ships.

3-4 LAUNCHING METHODS**3-4.1 GENERAL**

A rocket is primarily a powered, airborne vehicle. As such, it must have some point of departure, or launching point. Rocket launchers have assumed many varied shapes and sizes, depending on system requirements and intended uses. The launcher supports the rocket and points it in the desired direction before launching. During the launch operation, the launcher guides the rocket in its first motion and prevents small disturbances from diverting it from the desired path. The launcher can also be used for other purposes, such as a packaging and shipping case, as a transporter, and for imparting other desired motions (such as spin) to the rocket during the launch phase. The paragraphs which follow describe the more common launchers and launching systems.

3-4.2 RAIL LAUNCHERS

Rail launchers derive their name from their similarity to the rail of a railroad track. The rocket is supported on the rail with shoes which slide along the rail as the rocket moves forward. The launching shoes are usually a part of the rocket and can be fixed, retractable, or jettisoned after leaving the launcher. Since the sliding motion occurs only over a few feet of travel, friction is usually not of critical concern. Rail launchers may have a number of variations, the most common of which are described below.

3-4.2.1 Single

Single-rail launchers have one rail along which the rocket moves. The rail must have sufficient width, and the launching shoes must be so designed that lateral, or rocking, motion is prevented or held to a minimum as the rocket moves over the rail.

3-4.2.2 Multiple

Multiple-rail launchers may be interpreted in two ways. One concept is a launcher having two or more rails, each of which serves as the launch guidance for a rocket. The barrage-type rocket systems, which launch a number of rockets simultaneously, often use this launching scheme. On the other hand, a launcher with two or more rails can be used to launch one rocket. Such schemes are used to provide a more rigid launching support and, in some instances, to dispense with launching shoes. The rocket slides through the rail structure the same as it would through a tube.

3-4.2.3 Helical

For this launcher concept, the rail is twisted through a helical angle in order to impart spin to the rocket. Generally, the helical rail launcher has two or more rails to provide a torsional couple to the rocket because it is impractical to impart a torsional couple with one rail. The technique is analogous to the rifling grooves in the bore of a gun or rifle. Unlike the gun, however, helical-rail launchers are not used for spin rates of sufficient magnitude to provide spin, or gyroscopic, stabilization. The spin produced is low in magnitude for the purpose of reducing errors resulting from some of the rocket imperfections. This is discussed more fully in Chapter 7.

3-4.3 TUBE LAUNCHERS

Rockets may be launched from tubes in much the same way as gun projectiles. The length of the tube can vary from about one rocket length to several rocket lengths, depending on the characteristics of the rocket, its intended use, the environment in which it will be used, and accuracy considerations. This tube can have a smooth

bore or may be grooved in some manner to provide or prevent rotational motion during the launching. No launching shoes are required on a tube-launched rocket, although devices known as bore-riders may be used to support a portion of the rocket that is smaller than the tube. The bore-riders prevent the rocket from wobbling, or balloting, as it moves through the tube, and assure its continuing in the desired direction. Tube launchers may be designed to be reusable or may be designed to be disposable after the firing of one rocket. The latter is found quite often as a part of small rocket systems, particularly the small infantry antitank systems. This allows the individual soldier to discard unnecessary encumbrances on the battlefield. For similar reasons, disposable launchers are also incorporated in aviation rocket systems to permit the launcher to be jettisoned after use. The most common types of tube launcher are briefly discussed in the paragraphs which follow.

3-4.3.1 Single

Single-tube launchers are generally used in hand-held or single-man-operated rocket systems and in some systems with automatic feed mechanisms. As with any rocket system, the choice of a single tube results from considerations of the system requirements and rocket characteristics.

3-4.3.2 Multiple

Multiple-tube launchers are used to provide a fast firing rate where the complexity of automatic feed mechanisms in conjunction with a single tube is either undesirable or is prohibitive. With the employment of a multiple-tube launcher, the rockets can be fired all at once, in salvo, or in fast ripples. The ability to fire one rocket at a time is also inherent and can save considerable time by not requiring reloading after each firing. Multiple-tube launchers are frequently employed as barrage weapons, replacing a number of guns concentrated in a small area.

3-4.3.3 Open Breech

An open-breech launcher is one where the rear end of the tube is completely open and is the

AMCP 706-200

full diameter of the tube. This is the most common form of tube launcher. The gases exiting from the rocket are unrestricted in passing through and out the rear of the tube, and the tube experiences little if any reaction force.

3-4.3.4 Closed Breech

A closed-breech launcher is one in which the rear end of the tube is completely closed. The gases from the rocket cannot escape, and pressure builds up between the closed tube-end and the rocket. This type of tube launcher experiences a reaction force, or recoil, similar to that of a gun. Tubes of this type are generally used in places where the rocket exhaust gases would be undesirable or dangerous if allowed to exhaust rearward. The tube launcher of a tank-mounted system is an example of the closed-breech launcher. In this instance, the rocket is loaded into the tube from within the tank but the rocket exhaust gases, for obvious reasons, cannot be tolerated inside the tank.

3-4.3.5 Restricted Breech

A restricted-breech tube launcher is one in which the rear end of the launcher has been reduced to some diameter less than the bore diameter, but not sealed off completely. This form of tube launcher is used only in instances where some particular effect is desired. If the restriction is made in the form of a rocket nozzle, some useful forward thrust may be obtained that will counteract to some degree the recoil resulting from the restriction. The higher pressures resulting in the tube may be utilized to afford a higher muzzle velocity to the rocket without changing the rocket or increasing its size.

3-4.3.6 Gatling

As this name implies, the gatling launcher is derived from the old Gatling gun concept. It is a form of automatic feeding launcher since, as one or several rockets are firing, one or several are being fed into empty tubes. The tube cluster rotates so that those tubes firing are always at a fixed position, as are those being loaded. Several rocket systems have been designed around this

type of launcher, using the closed-breech type of tube mentioned above.

3-4.4 OTHER LAUNCHER TYPES

In many instances the simple approach to a launcher design is not adequate. It then becomes necessary to examine techniques and designs that will provide a necessary function, a particular motion or effect, or will impart to the rocket some required characteristic. The result may be a modification of one of the types described in the preceding paragraphs, a combination of several types, or a completely new approach. It may be necessary to add varying degrees of sophistication, or to provide additional equipment or devices for a particular effect or function. One of the more notable types is the zero-length launcher.

This launcher is, as its name implies, one that supports the rocket but releases it from constraints immediately, or with zero guidance upon first rocket motion. It is not too practical in most instances to achieve a true zero-length guidance; however, guidance lengths of a fraction of an inch have been achieved for small rocket systems and several inches for large systems. The rocket must be adequately supported on the launcher and must maintain its aim alignment until it is launched. Mechanical considerations generally will dictate the size and length of the attaching devices and, consequently, the guidance length in zero-length launchers.

3-4.5 VARIATIONS**3-4.5.1 Autospin**

As has already been stated, it is sometimes desirable to impart a slow spin to rockets in order to reduce or eliminate some types of error during the flight phase. One method of imparting spin that has been analyzed and tested uses in the rocket a device that spins the rocket warhead in one direction; the reaction spins the propulsion motor in the opposite direction. Spinning during the flight phase, or even before rocket motion occurs is desirable. Since simplicity is also important, the rocket is made to spin after it has traveled approximately one inch. In this case, the zero-length launcher is necessary, because the rocket

must be free of launcher constraints at the time spinning begins. It must be borne in mind that the thrust and acceleration characteristics of the rocket motor must be suitable to maintain the rocket in an acceptable flight attitude at this time, otherwise, the rocket may drop or deviate in such a manner as to make its flight meaningless.

3-4.5.2 Prespin, Automatic Dynamic-Alignment (PADA)

One effect of spinning a rocket is to cause the accrual of errors from dynamic unbalance. No rocket is perfectly balanced, and the center of mass will not lie exactly on the longitudinal axis. Even the longitudinal axis cannot be expected to be perfectly aligned since the rocket is usually made of components joined together. Consequently, the rocket will not spin these components around the longitudinal axis of symmetry, but will seek to spin about some other axis which is the dynamic axis. The rocket, if spun on a rigid launcher and attached to the launcher by rigid mounts, will be constrained to rotate around the longitudinal axis of symmetry purely from mechanical aspects. Once released from the launcher constraints, however, the rocket will seek immediately to spin around its dynamic axis, which results in errors along the flight path. The dynamics and errors resulting from this phenomenon are discussed in more detail in Chapter 7. The zero-length launcher with flexible arms supporting the rocket is one approach to gaining the beneficial effects of spinning the rocket before launching without the undesirable effects of jump at release of launcher constraints. This is more practical than attempting to design flexible shoes for the rocket. Zero length is the logical launch approach since it would be very difficult to provide flexible rails that would function in the desired manner during the guidance phase. The flexible launcher arms permit the rocket to find and align itself along its dynamic axis as it spins, and when launched, to maintain the attitude attained during the spin-up period. The critical consideration in this scheme is to make sure that the spin rate of the rocket does not couple with the resonant frequency of the launcher arms. This can cause violent perturbations of the rocket and possible failure of the launcher structure. It

is desirable to stay below the critical rate or, if it is necessary to go above, to provide a spin acceleration sufficient to carry through the resonant point as rapidly as possible. The name ascribed to this launcher concept is prespin, automatic dynamic alignment launcher, or PADA (pronounced "Payday").

3-4.5.3 Spin-On-Straight-Rail (SOSR)

Although the effects of shifting axes produce undesirable results, prespinning a rocket before launch on a rigid launcher is nevertheless sometimes beneficial. The benefits derived overshadow the ill effects of dynamic unbalance sufficiently to justify the inflexible launcher. The rocket is thus provided with bearing systems in which it can rotate while on the launcher and then be launched along a rail in the usual manner. This technique has been termed spin-on-straight-rail, or SOSR. Although helical rails could be used, they may be undesirable because of length, weight, or other factors. Also, the spin rate desired may not be attainable with any reasonable rail length and helix angle. In the SOSR system almost any desired spin rate can be obtained. The method of spinning can be an integral part of either the rocket or launcher. The spin mechanism, if it is a part of the rocket, is usually a system of small rocket motors exhausting tangentially to the longitudinal axis. If the spin mechanism is a part of the launcher, it may be electrical, hydraulic, mechanical, or it may use whatever power source is most applicable. Power transmission to the rocket may be by belt, gears, or other appropriate means. The dynamic treatment of this technique is also covered in Chapter 7.

3-4.6 METHODS OF TRANSPORT

Rocket launchers can be transported in many different ways, with or without rocket loads. The small infantry launchers designed for the individual soldier are usually hand-carried and strap-suspended, much the same as a rifle. Larger types may still be man-transportable by dividing the system into man-load components, although the assembled launcher when it is fired may have to be supported on a tripod or other appropriate

AMCP 706-280

base. The larger, heavier, artillery rocket launchers are mounted on wheels and towed behind a vehicle as a trailer, or are mounted on a vehicle that is then an integral part of the launcher system. The largest of these systems are frequently mounted on self-propelled, tracked vehicles to provide a maximum cross-country capability. The mobility characteristics of the rocket-and-launcher system are dictated by the system requirements and the rocket characteristics. Many of the medium and large rocket systems are required to be air transportable. Here the designer must be conscious of both weight and size if he is to achieve a system small enough to fit into modern transport aircraft and light enough to be carried. The aviation rocket systems are mounted on, and are an integral part of, the aircraft. Size, weight, and aerodynamic characteristics of the configuration are paramount. A high-drag design can slow an aircraft to the point where its vulnerability to enemy air and ground fire becomes acute. Rocket armament for a tank is also an integral part of its transporter. The factors for serious consideration with these systems are that of space in the tank and that of the burned gases from the rocket. The launcher designer must provide means of exhausting the gases, must provide adequate room for the tank crew to operate, and must provide means for handling and loading the rockets from within the tank. Considerable ingenuity is required to achieve an acceptable balance of space, weight, and safety for systems that are to be operated in such closely confined spaces.

3-5 SYSTEM ELEMENTS**3-5.1 GENERAL**

A rocket system is made up of a number of elements, or subsystems, each of which performs a function necessary to the successful performance of the system. In general the system is composed of three main elements: (a) the rocket, (b) the launcher, and (c) the fire control device. Each of these in turn is composed of subelements, or components, each of which has a necessary function to permit successful operation of the whole.

In keeping with the intent and purpose of this handbook, only the rocket will be discussed in

detail. This is not to imply that the other elements are any less important, but they are more properly considered in other handbooks dealing with their particular disciplines. The launcher and fire control elements will be described sufficiently to permit an evaluation and appreciation of the particular problems attendant upon these elements. This approach is also taken with the payload, or warhead, of the rocket, which is covered in considerable detail in other handbooks.

3-5.2 ROCKET

The rocket is composed of a payload, or warhead, a propulsion motor, and an airframe to provide structural rigidity. In the smaller, simpler rockets the warhead and propulsion motor serve also as the airframe, and no additional structure is required other than the fins or other device to provide aerodynamic stabilization.

3-5.2.1 Warhead

The rocket warhead has a shell, or casing, which is hollow, and which may be aerodynamically shaped to serve as the nose of the rocket. An appropriate high explosive is loaded into the casing. Actuation of the explosive is performed by the fuze. The fuze may be located in a number of positions in the warhead structure, depending on its type and method of operation, and on the type of detonation desired. For high explosive warheads, the fuze may be placed at the forward tip of the warhead and may be actuated by striking the ground or another object. The shape of the warhead may take a number of forms, the selection usually being determined by the type of warhead, the aerodynamic characteristics and requirements for the rocket, the fuze type, and structural considerations. The warhead has two general parts, the shaped nose portion, or ogive, and a body, usually a cylindrical portion. The cylindrical portion may or may not be present, depending on the design requirements, but the nose or ogival portion is always used. The ogive may have a number of shapes. It may be conical; it may have curvature and be termed a tangent or secant ogive, or it may be hemispherical. Ogival shapes and their aerodynamic characteristics are covered in more detail in Chapter 8.

The material for the warhead casing is also selected according to requirements. It may be cast iron, steel, aluminum, or a combination of these or other materials. The material, in combination with the high explosive, is the destructive mechanism, and thus must have characteristics that will produce the maximum desired effect on the target.

Fuzes, as mentioned above, can be of several types. The point-detonating fuze initiates the explosive charge immediately upon striking an object. The delay fuze initiates a powder train that delays the actual explosion for a period of time ranging from several seconds to minutes, and in some cases to hours and days. The air-burst fuze is timed to actuate at some desired point in the air above or in the proximity of the target. Fuzes may also be located at the aft end of the explosive charge with an actuating device in the nose. On impact with an object, the actuating device generates an electrical impulse to initiate action of the fuze. For some aircraft rockets the warhead should penetrate and enter the aircraft structure before detonation. These warheads may use a coil-type actuator, located behind the warhead, which will generate an electrical impulse on passing through the metal structure. Fuzes for actuating the explosive charge may be simple, or may be intricate devices requiring the technical competence of a watchmaker to design, build, and assemble. These mechanisms, though precise, must be rugged and must perform well under the most trying conditions.

A necessary aspect of fuze design and functioning is that of safing and arming. The rocket warhead must be kept safe to handle, even to drop, without endangering personnel to accidental explosion. For this reason fuzes have built-in safety devices that must be actuated in some manner before the fuze can function. These safety devices range from simple pull wires, which are removed by hand just prior to firing the rocket, to intricate mechanical and electrical mechanisms that are actuated by the forward acceleration of the rocket. In many instances, for safety reasons, the fuze should not be fully armed until the rocket has moved for some distance away from its launch point. For these cases the safing and arming device may be a small escapement mechanism (similar to that of a watch) that is actuated by the forward acceleration of the rocket, removing

a blocking device between the fuze detonator and the high explosive.

For a full and comprehensive treatment of explosives, warhead design, and fuze types and design, the reader is referred to other handbooks in this series.

3-5.2.2 Motor

The rocket motor is the engine that propels the rocket from the launch point to the target. For present purposes a general description of its components will suffice. A more detailed coverage of its design is presented in Chapter 5.

The motor is an internal combustion engine with a combustion chamber, an orifice through which the burning gases are expelled at high velocity, and the propellant charge that produces the high-temperature high-pressure gases as products of the combustion process. Also included is the igniter which starts the combustion process in the chamber.

The propellant charge, or grain, is a mixture of a suitable fuel and an oxidizer. Thus, unlike most air-breathing internal combustion engines, a rocket motor does not utilize or need the surrounding air to operate. In fact, it can and does function equally as well in a vacuum or in outer space. When the propellant charge is ignited, the heat generated causes a decomposition of the chemical compounds in its structure to produce combustible gases on the grain surface. The gases are burned, and the process proceeds in an orderly and predictable fashion. The products of the combustion process are high temperature gases and, in some cases, solids in suspension in the gases.

Propellant grains may be obtained in a large variety of compositions and shapes. Each is designed to operate in a specified manner and environment, the particular manner of operation is selected to fit the performance requirements. The grains may be cast directly into the motor combustion chamber, or may be molded or cast into a separate container that is loaded into the chamber as a cartridge. A grain may be end-burning, as a cigarette burns, or it may have perforations in which the burning occurs. Some motors, called multi-grain motors, may be loaded with a number of small grains. Generally the end-burning grains operate at low pressure over relatively long

AMCP 706-280

periods of time, whereas the perforated grains operate at medium and high pressures for relatively short periods of time. Multi-grain motors are usually employed to provide extremely short burning periods at very high temperatures.

Grain compositions vary in operational characteristics. The more general types of fuel mixtures are single base, double base, triple base, and composite propellants. To the fuel is added the chemical oxidizer. Other chemical agents are added to the mixture to obtain desired performance characteristics. These agents act to inhibit or slow down the burning, to speed up burning, to stabilize the burning, to counteract or minimize temperature and pressure effects on the burning, and to produce other desirable effects.

Propellant compositions are in many instances developed to provide desirable physical characteristics. The propellant strength should be fairly uniform over wide temperature ranges, and its density and specific volume remain as constant as possible despite temperature change. Powdered metals are added to some propellants to raise the combustion temperature and the usable energy. The designer is concerned with obtaining the propellant with the highest possible density and energy per unit weight since these factors will provide the least weight and size of motor to do the required job.

The motor combustion chamber is a pressure vessel to contain the propellant and the high-temperature, high-pressure gases during burning. An opening is provided at one end through which the gases are expelled. The size of the orifice relative to the physical dimensions and burning characteristics of the propellant grain is governed by precise mathematical relationships and differs with types of propellant and operating conditions. The motor case may be constructed of any material capable of withstanding the pressure generated, but it is of primary interest to keep the weight to a minimum. For this reason, the very high-strength steels, high-strength aluminum, and the glass-reinforced plastics are most often used. Other metals, such as titanium and magnesium, have been used, usually to obtain some particular characteristic not afforded by the more common materials.

The motor exit-orifice, or nozzle, is designed to have precise geometric and mathematical relationships, both with the propellant grain and

with the properties of the exhaust gases. The design usually is in the form of the De Laval nozzle with converging-diverging sections. The converging section, located before the throat orifice, is commonly called the expansion cone. Materials used in nozzle construction are generally the same as those used for the motor chamber. However, it is not unusual to employ a reinforced plastic nozzle with a steel or aluminum motor case. Sometimes the nozzle throat is lined with graphite. This material resists the erosive characteristics of the exhaust gases much better than most materials and it changes dimensions very little with changes of temperature. Because it is brittle and has little physical strength, this material must be adequately supported in the nozzle throat to prevent disintegration. Protective coatings of other types also are used to cover the entire inside surface. Particularly applicable to nozzles made of aluminum, the coatings provide a very hard, erosion-resistant surface. These coatings, too, are very brittle in nature and must be adequately supported to prevent disintegration.

Variations of the De Laval nozzle have been employed on rockets. They are designed to provide a particular effect on, or enhancement of, the motor thrust characteristics. The production costs for some of these variations may be appreciably higher than for the simple conical-section De Laval nozzle. Therefore, the effect to be gained must be weighed carefully against the added cost. One variation that has been of considerable interest and study is the plug nozzle. This is essentially an inside-out De Laval nozzle which has the characteristic of providing optimum or near-optimum expansion characteristics for the exhaust gases at all altitudes, or, more properly stated, at all ambient pressures. Thus, this nozzle has the potential of performing equally as well at sea level as it does in the vacuum of outer space. It is not too difficult to build and should compare favorably with the conventional nozzle in cost and weight.

A necessary consideration for some types of rocket motors is that of insulating the case wall. For the long-time, end-burner type of propellant grains, and for cartridge-type grains where the gases may impinge directly on the case wall, the loss of strength in the material can cause rupture and failure of the system. To prevent this occurrence, an insulating lining that will prevent over-

heating and loss of strength should be applied to the wall. The material selected for insulation may be applied directly to the wall by painting, casting and curing it in place, or by other suitable means. Insulation may also be fabricated and inserted into the motor case. The liner must be bonded to the wall with an adhesive since it will not function properly if the hot gases flow between the insulation liner and the wall. Insulating materials may be of several types. Some are charring in nature, others ablative. No one type is superior, some work best in one type of environment, others best in another environment. The best guide to selection is past experience and experiment. The primary consideration is maximum effect for minimum thickness and weight since insulation reduces space available in a given chamber for propellant.

Some device is necessary to initiate propellant combustion in the chamber. The device that performs this function is called the igniter. Although it may take a number of forms, they all have the same general characteristics. The squib, a device that receives the firing signal, may be electrical or mechanical, the latter usually being of the percussion type. The electrical squib is in essence an electric match. The current passes through a resistance wire that becomes very hot, much as the cooking element of an electric stove. The hot wire ignites a small powder charge that generates hot gases. The hot igniter gases are directed against the propellant grain surface that is in turn ignited. The small container in which the igniter is housed is usually of a brittle or very flexible material, plastic in most cases, so that it may be easily ejected through the nozzle after propellant ignition. The igniter cup must not be permitted to block the nozzle throat as this would cause an extremely fast pressure rise in the motor chamber, resulting in chamber rupture.

Most propellants exhibit better ignition characteristics under pressures considerably higher than atmospheric. The surface of the grain ignites faster, and the flame front covers the entire burning surface much faster under elevated pressure. To provide this pressure condition a closure, called the nozzle closure, is placed in the nozzle throat. It is designed so that the igniter gases are not permitted to escape, but build up pressure in the combustion chamber. It is also designed to blow out of the nozzle at some predetermined

pressure, usually lower than the operating pressure of the motor. The igniter cup may function also as the nozzle closure, or a separate closure may be provided. The closure may be of any suitable material, usually plastic or metal. It must exit at the desired pressure level and must be constructed in such a manner that the nozzle or expansion cone will be undamaged as it leaves. For some aircraft rockets, the nozzle closure may be ejected at a fairly high velocity. If it were to strike a vital part of the aircraft, it could endanger both aircraft and crew. In such instances the nozzle closure should be made of a material that is very light and that preferably will disintegrate into a powder when ejection occurs. Other problems and environmental requirements may dictate that different materials and techniques be used in designing the nozzle closure.

3-5.2.3 Structure

The rocket must have a frame of some sort to tie the parts together and to provide the desired aerodynamic shape. For the smaller and simpler rockets, the components themselves frequently constitute the airframe, being joined together by threaded sections, by bolts or screws, or by a simple crimping process. The components, warhead and motor, are shaped so that the desired aerodynamic configuration is obtained when they are joined. As size and/or complexity increase, it may be desirable or necessary to provide a properly configured frame that will enclose the functional components. The warhead need be shaped only from a maximum effectiveness standpoint, and the motor for maximum performance. One or both may be enclosed in the airframe, depending on the particular system requirements.

The skin of the airframe is made of a lightweight material, usually aluminum or reinforced plastic. It may be shaped by drawing, hot or cold, by rolling and welding, by stretch forming, or by any other appropriate process. The particular forming process used is the result of considerations of requirements, materials, and economics. The skin is supported on a framework consisting of bulkheads and, in some cases, stringers. The more elaborate the structure becomes, the more stringent become the requirements for close tolerances, alignments, positioning, and shaping. For a fully enclosed system, the components are tied to sev-

AMCP 706-260

eral key bulkheads; where only part of the components are enclosed, they may be attached to bulkheads and/or the nonenclosed member.

For some types of rockets, several propulsion motors are used in a cluster. This arrangement provides the capability for obtaining different thrust levels by firing varying numbers of the motors to meet varying operational conditions. The clustered motor configuration is one that is usually fully enclosed within the airframe.

The rockets of immediate concern in this handbook are the free-flight aerodynamically stabilized rockets. The component that provides the aerodynamic stabilization is most often a set of fins located at the aft end of the airframe. Other means of aerodynamically stabilizing a rocket have been used and a number of proposed methods have been studied. The functional action of fins and other aerodynamic stabilization methods are covered in considerable detail in Chapters 7 and 8.

In order to stabilize a rocket along the flight path, a minimum of three fins, equally spaced circumferentially around the body, is required. The more usual configuration has four fins; however, as many as six and eight have been used to satisfy a particular set of environmental requirements. Generally the fins are either rectangular or triangular, with any number of variations of these. They may be mounted normal to the rocket centerline, or tangential to the airframe. They may be fixed or, if necessary, folded, in which case they open after the rocket is launched. They may open due to rocket acceleration or may be opened by some mechanical device such as springs, pistons and cylinders, or other appropriate means. Folding may be radial or longitudinal; for the latter, they are either forward folding or rearward folding. For some rockets it may be necessary to curve the fins to the same curvature as the airframe to provide a smooth contour prior to launch. This is especially true for some tube-launched rockets where restrictions of size and weight are imposed and where there is insufficient space to mount other types of fins.

The size and configuration of the fin are determined from a comprehensive study by the aerodynamicist of the flight path environment, the performance characteristics, and the configuration of the body of the rocket. As mentioned,

the available space, launching technique, and weight restrictions also play important roles in designing the fin planform.

The method of attaching the fins to the airframe is again determined from physical and mechanical considerations of the particular system. They may be welded, riveted, bolted, screwed, or cemented on. It is often desirable to mount them with a small cant angle to the rocket centerline so that the aerodynamic reactions on the canted fins will produce a roll in the rocket.

The rocket must be attached to the launcher, except in the tube launcher, where the rocket merely slides through the tube and no special attachment devices are required. Other types of launchers such as rail launchers use a connecting device, or launching shoe, to constrain the rocket to move in a precise and predetermined manner during the launch operation. The number of shoes required is determined by the size of the rocket and the degree of complexity of launching motion imparted by the launcher to the rocket. For most rockets a minimum of two shoes is usually adequate, particularly where the motion is simply a straight, nonrotating movement along the rail. The shoes may be fixed permanently to the rocket, may be folding or retractable, or may be of an ejection type.

Other devices are at times included in a free rocket system to provide some desirable or necessary function. One frequently employed is a mechanism to produce slow spin to the rocket prior to or immediately after launching. This mechanism ranges from the small canted vanes in the exhaust nozzle of the rocket that react to the exhaust gases, to complex devices such as gear trains, drive shafts, pistons operated pneumatically through helices, and other similar systems. Other devices for providing spin may be a component that (a) must be tied into the rocket system by the airframe, (b) may be a part of the airframe, or (c) may be a simple attachment—whatever the device, it must have proper consideration and emphasis in the overall structural assembly. In addition, the effect of the spin produced must be considered along with the aerodynamic and acceleration forces when analyzing the structural integrity of the airframe and component assembly.

3-5.3 LAUNCHER

The launcher, like the rocket, consists of several components each of which performs a function to provide the total required performance (see par. 3-4 above). Many of the terms used for launcher components have been carried over from artillery practice since much of the design and development work has been done by gun designers. The similarity between a rocket launcher and an artillery field piece is in many instances quite evident, the gun tube being replaced by the launcher rail. Only a brief description of the three basic launcher components will be given since this subject is more properly covered in other texts and handbooks.

The *launcher rail* is the component on which the rocket rests and which guides it in its first motion of travel. The rail may take any number of forms and may also be a tube through which the rocket slides. It must have sufficient strength to support the rocket and must be sufficiently rigid to prevent successive deflections and oscillations that could cause mallaunch of the rocket.

The launcher rail is supported on an *upper carriage* through a trunnion connection. This is the joint that provides for the angular elevation and depression of the rail, or change in quadrant elevation, necessary to achieve varying ranges for the rocket. If the rocket system is large, a means of assisting the elevation change—through gear trains, hydraulic pistons, or other suitable means—may be necessary. The assist mechanisms may be manually operated or may be mechanized for remote control, faster operation, or for lessening the burden on the launcher crew.

The launcher rail and upper carriage assembly is mounted on a *lower carriage* through a vertical pin connection around which it can rotate. This provides the change in azimuth, or direction of fire. Manual operations or mechanized means of assisting the motion may be provided. The lower carriage also forms the base of the launcher. It may have wheels mounted to it for towing behind a vehicle; it may be mounted on a wheeled or tracked vehicle as a self-propelled unit; or it may, for small rocket systems, have legs or a base to stand directly on the ground.

Other equipment that may be a part of the launcher to provide a specific function or capability includes devices for imparting spin to the

rocket; the firing mechanism, either electrical or mechanical; and cranes or hoists to assist loading the rocket on the rail for the larger systems.

Launchers may consist of less than the three basic components—rail, upper carriage, and lower carriage—but, of course, must always have the rail or other device for supporting or guiding the rocket. For the antitank rocket systems of the bazooka type, where the launcher is a tube supported on the man's shoulder, the other components do not exist; the flexibility of the man provides the necessary motion capability for changing azimuth and quadrant elevation. In other systems the carriages may not exist as such, being reduced to nothing more than pinned joints or very simple support members. When the system is self-propelled, the vehicle on which it is mounted may constitute the lower carriage; however, it would not be identifiable as such if the launcher were removed. The particular system and the dictates of the system requirements will determine how the launcher rail is to be supported and how the required motions are to be provided.

3-5.4 ANCILLARY EQUIPMENT

Many rocket systems require items of specialized equipment necessary to effect total operation. Military systems are required to have the capability of functioning in all types of weather and terrain conditions anywhere in the world. Some rocket components, such as propellant grains, may be limited in their operational characteristics by temperature or some other factor. In order to provide total capability, it is at times necessary to provide some piece of equipment to aid, facilitate, or accomplish some function to offset the restrictions. In the case of the propellant grains that are temperature-limited, a heating blanket is provided that can be wrapped around the outside of the motor case. This blanket has electric resistance heating elements very similar to those found in commercial electric blankets for home use.

3-6 CONCEPT SELECTION

3-6.1 REQUIREMENTS

The need for a new weapon system becomes established when a situation that cannot be

AMCP 706-230

handled by existing weapons is encountered either in actual battle or by projection of what is expected to occur in future conflicts. When the need for a weapon becomes apparent, a set of general requirements can be established that will satisfy the needs. The requirements might be in the form of the amount of explosive force required to destroy the objectives as well as the mobility of the weapon and any adverse condition that might hinder its use. For instance, a requirement might exist for a weapon system that could destroy a target of defined size and hardness in a mountainous environment.

These general requirements for weapon systems are usually documented and made available to various groups for conceptual studies. At this point parametric studies are made of a wide range of concepts that might meet the requirements. The purpose of these studies is to determine whether the weapon should be a gun, mortar, rocket, etc., and whether the concept lies in the present or foreseeable state-of-the-art.

The end results of the conceptual studies are: the definition of the weapon system; specification of acceptable limits in range, weight, accuracy, etc.; and establishment of problem areas. These requirements are documented and used as the basis for the preliminary design of the weapon system.

3-5.2 CONSTRAINTS

It is not usually possible to proceed directly into the selection of the weapon concept. Circumstances beyond the control of the designer always exist that prevent him from achieving the weapon performance he desires. Inevitably, there are components of each system concept whose performance is limited by the state-of-the-art to something less than required. Therefore, constraints are imposed within which the analyst must work.

There are two alternatives. The time allowable for the development of the weapon may permit components to be included that are outside the present capability of these components but are considered feasible within the development time of the weapon. This, a prediction of future component availability is made that is based on present research and expected results. In this case, the analyst is taking the chance of having to ex-

tend the time required to put the weapon in the field should unforeseen problems appear in developing the component. In fact, it is possible that the required performance cannot be achieved, and the weapon system may suffer more than it would have if existing components had been specified at the beginning.

The second alternative is to restrict the selection of components to those that are immediately available. In this situation the analyst is attempting to reduce development time at the cost of system performance. Naturally, considerable thought must be given to either approach so that the best possible weapon can be obtained in the time available.

3-6.3 PARAMETRICS

The requirements and components having been specified, a range of weapon concepts is considered that will satisfy them. The performance of each system is studied in terms of parametric variations of the important system variables. In this way it is possible further to identify problem areas and to understand the sensitivity of the overall system performance to changes in the performance of critical items. These studies pave the way for detailed trade-offs and the selection of the concept that best meets the requirements.

3-6.4 SYSTEM SELECTION

The results of the parametric studies allow each weapon concept to be compared to all others. Weighting factors can be applied to the advantages and disadvantages of each concept. Finally, a concept is selected; the system is then defined as a rocket, gun, etc.; and its acceptable performance is specified. These specifications are documented and released for the preliminary design of the weapon system.

3-7 PRELIMINARY DESIGN

The preliminary design phase, like all the other stages of the development of a weapon system, is simply a more detailed refinement of the work that preceded it. The overall process consists of

a continuous review and rework of the design. The depth of the refinements increases, until the final phase when the requirements for each rivet have been established.

We will assume for the remainder of the chapter that the weapon system is a free rocket.

3-7.1 PAYLOAD

The conceptual design phase establishes the function of the payload and the limits of its size and weight. During the preliminary phase, more detailed questions are studied such as the nature of the device to accomplish the objective (anti-personnel, hardened site construction, armor penetration, etc.) as well as more exact determination of the size, shape, and weight.

3-7.2 PROPULSION

In the preliminary design of the propulsion system, parametric studies are made to determine the required thrust of the rocket motor, its specific impulse, total impulse, burning rate, etc. Studies are made of available propellants and grain cross sections. In this process problem areas may be uncovered that require further study.

Detailed accounts of the methods used to determine the required motor performance and the design of the motor elements are presented in Chapters 4 and 5.

3-7.3 AERODYNAMICS

Aerodynamic shapes must be developed that will contain the payload and motor while keeping drag to a minimum. In addition, the amount of aerodynamic stability required by the mode of operation of the weapon must be established. The amount of stability required is affected by any dispersion reduction techniques that may be employed. These subjects are discussed in Chapters 7 and 8.

In addition to drag and stability considerations, the preliminary aerodynamic analysis must consider the aerodynamic heating that is encountered in high speed flight. The results of these studies determine the requirements for insulation and ablative materials.

3-7.4 DYNAMICS

Estimates of the accuracy must be made. Parametric studies are made of the accuracy available with different launcher lengths and levels of stability, as well as spin or other dispersion reduction techniques. Problems associated with launcher requirements and spin methods are identified. In addition, manufacturing tolerances on static and dynamic balances are established.

Computations are made of the dynamic loads under all conditions to which the rocket is expected to be subjected.

3-7.5 STRUCTURES

A tabulation of the weight and balance characteristics of all the preliminary design configurations under consideration must be constantly kept up to date. In addition, the information from the dynamics analysis must be used to define the proper sizing of all the structural elements.

The preliminary aerodynamics analysis will place requirements on any insulation material that must be considered in the structural analysis. Problems in weight and balance must be identified as early as possible so that a wide range of structural materials may be considered.

3-7.6 PERFORMANCE ESTIMATES

Each preliminary design configuration must be evaluated for performance. Comparisons are made between the systems, and changes are defined. The preliminary performance estimates are the basis for important design modifications.

3-7.7 AUXILIARY DEVICES

The preliminary design phase defines the requirements for devices that are not considered a part of the primary rocket system but are necessary for its operation. Such devices are: heating blankets for propellant temperature control, anemometers for field wind measurements, and firing equipment and other devices that might be required to perform functions unique to a given system.

AMCP 733-280

3-8 DESIGN OPTIMIZATION

It was mentioned above that the design process is repetitive. The conceptual and preliminary design phases involve similar computation, the only difference is the amount of detail that is included. However, the consideration of some of these details may invalidate or at least modify some of the preceding results. These detailed considerations are possible because the gross factors have previously been identified. This allows individual areas to be studied in depth. The optimization process is the consideration of the design details and the combination of these details in such a way that cost, performance, and reliability are optimum.

3-9 SYSTEM INTEGRATION

System integration is first accomplished during the concept phase design. Estimates of the design and performance characteristics of various elements of a total system are integrated to make up a hypothetical design. An infinite number of design options are available. Components or elements in a range of sizes may be assembled in combinations to make up various configurations. The design and performance characteristics of each selected component or element affect the design and performance characteristics of each of the components or elements of the overall rocket. The selection and integration of these elements, therefore, involve the resolution of numerous design compromises and the formulation of numerous design decisions. The objective is to select and integrate those elements that provide the best promise of achieving system performance requirements, with high reliability and minimum cost by some specified availability date.*

As design and development progress, the design of each subsystem becomes more specific.

*The manufacturing, operations, maintenance, and logistics problems and costs associated with each candidate design must also be considered, and can easily be controlling factors in the selection of design options. Fixed and variable costs for anticipated launch rates etc. must be considered. However, this handbook is concerned primarily with the integration of the rocket system, particularly with respect to design and performance characteristics and design and development costs and schedules of rocket systems. Therefore no extensive discussion of manufacturing, operations, maintenance, and logistics factors is included.

Throughout this period, coordination must be accomplished among the design groups to assure compatibility and to resolve design compromises. A propulsion design group may desire a high chamber pressure to provide higher engine performance. The structural design group may desire lower pressure to save structural weight. These are the obvious considerations of the problem and do not represent all considerations that must be made. The total range of possible chamber pressure must be investigated with respect to effects on all systems and total rocket performance. The objective is to determine the pressure that results in maximum overall rocket performance within cost and schedule limitations. Similar compromises must be resolved in all areas of rocket design. Each must be made on the basis of performance of all elements and the total rocket, and must include considerations of cost, schedule, performance, and reliability.

As the design becomes more refined, the design and performance estimates must be altered. Mission requirements, and the design and performance characteristics of various elements change. Payload weight may increase; mission profiles may change. A problem may occur during the development of an engine, resulting in lower than anticipated thrust. Structural weight, rigidity, etc. may vary from that originally planned. Product improvement proposals may be presented that alter the design and performance characteristics of various systems. Since the design and performance characteristics of each element affect or interact with the design and performance characteristics of each of the other elements, each alteration of original estimates requires reintegration of the rocket system. As in the problem of integrating the original rocket design, numerous solutions to each integration problem are possible. Any of several approaches can be employed to meet increased mission requirements. Numerous redesigns can be initiated to regain a performance loss due to failure of a system to meet expectations. Evaluation of a produced improvement proposal may present several design alternatives. Once again, the objective is to select that approach that best meets project objectives of performance, cost, reliability, and schedules.

Any of numerous design changes may be employed to meet increased mission requirements.

Upon development of a design problem, such as an engine that will not produce desired thrust, several redesign alternatives must be considered. The alternative that offers the best promise of restoring the original performance with minimum cost and schedule impact must be established. Each proposed product improvement change must be evaluated on the basis of effect on all rocket systems, overall vehicle performance, cost and schedule impact of the change, etc. System integration, therefore, must be accomplished constantly throughout design and development.

In summary, system integration is first accomplished during conceptual design. Throughout the remainder of design and development, design compromises must be resolved and design options must be selected. Mission requirements change, and design and performance characteristics of various elements of the rocket change. Each of these changes may require reintegration of the total design. For each reintegration problem, there are numerous alternate solutions or approaches to reintegrating the system. The objective is to ensure that the selected approach best meets performance and reliability requirements with a minimum cost by a delivery date.

3-10 TESTING METHODS

Before a rocket system can be released for use in the field, it must undergo a series of rigorous tests that verify its performance and integrity. Testing, therefore, is also a part of the development process. Aerodynamic testing of scale models, as well as characteristics, structures, and materials, help to establish the rocket configuration by supplementing theoretical analyses.

This paragraph discusses the role of testing in the development of the rocket system. More detailed coverages of testing methods are available in other parts of this handbook and in the cited reference material.

3-10.1 STATIC TESTING

Static testing is primarily a check of the rocket motor performance that is accomplished by tying down the rocket so that it cannot move. The

test rocket may be actual flight hardware or a boilerplate model that has a structure designed to permit firing the rocket motors without the danger of damage.

Static testing permits the use of extensive instrumentation. The testing can be carried out under closely controlled conditions. For these reasons static testing reveals much about the detail characteristics of many of the rocket system components. However, many of the conditions countered in flight, such as aerodynamic and dynamic loads, are not present.

3-10.2 FLIGHT TESTING

Final evaluation of the rocket system performance, as well as some phases of development, can only be accomplished by actual flight.

Development flight testing consists of making final adjustments of the aerodynamic configuration to provide the required stability. Study of the rocket on the launcher determines if the releasing mechanism and rocket clearances provide satisfactory initial conditions for the flight. Spin systems require extensive development testing, especially those whose ignition timing is critical, such as the Spin-Buck concept.

The final phase of testing is the performance testing where range and accuracy are compared against the expected values. Range testing is straightforward and consists of firing rounds at various quadrant elevations and propellant grain temperatures. However, a precise knowledge of atmospheric conditions is required. Extensive meteorological data are collected over the entire flight trajectory. Measurements of winds, temperature, and density are made on the ground and at altitudes along the path of the rocket.

Accuracy testing requires many rockets to be fired so that the impact points can be combined statistically to determine operational accuracy. Atmospheric effects are eliminated by firing the rockets in pairs.

3-10.3 STRUCTURAL TESTING

The complexity of rocket structures makes it difficult to predict the structural strength of a design with sufficient confidence. The available analytical methods are inadequate to consider

AMCP 706-260

the effects of stress concentrations, fasteners, bonding materials, etc. The heavy loss in performance caused by excess structural weight makes it important to keep the structure as light as possible. Therefore, the design process for rocket structures is a combination of predictions, based on results of theory and past experience with similar structures, and of verification by testing.

Chapter 6 presents a more complete discussion of structural testing methods.

3-10.4 AERODYNAMIC TESTING

The design of the aerodynamic configuration requires the development of a shape that will provide adequate volume for the payload while obtaining minimum drag. In addition, the accuracy requirements determine a specific level of aerodynamic stability. Aerodynamic testing, like structural testing, is a process of theoretical prediction and verification. Aerodynamic testing is thus an integral part of the development process.

A more complete discussion of aerodynamic testing methods is presented in Chapter 6.

3-10.5 ENVIRONMENTAL TESTING

Military rockets must be able to operate under a wide range of climatic conditions. Investigation of the effects of temperature, humidity, and other environmental influences, such as sand and rain, on the deployment and firing of the rocket system plays a very important role in determining its value as a field weapon. Some propellants smoke excessively under humid conditions. Most solid propellants must be heated by special blankets in cold climates. Factors such as these must be identified before a weapon is ready for use in any given area of the world.

3-11 COST EFFECTIVENESS

Cost effectiveness might be thought of as getting the most performance for the money spent on a rocket system. However, the concept is much more complex. There are many factors that must be considered before a value can be at-

tached to performance. The cost of developing higher levels of performance must be considered in relation to time and money. Often performance becomes all-important. For example, the need for a rocket of a given capability might be so great that any cost is justified. Other situations may justify sacrificing performance potential to meet an urgent time requirement. Another possibility is that the highest level of performance possible is not needed to satisfy the existing requirement. The framework within which these cost-performance trade-offs are made is called the design economy. Under war conditions, time and performance are of utmost importance; cost plays a relatively minor role.

It should be emphasized that cost effectiveness is not so much a design method as an awareness of the relationship between cost, performance, and reliability. Cost effectiveness is the conscious evaluation of the trade-offs between these items according to a set of established ground rules throughout the design of a rocket system.

Increased performance capability does not necessarily indicate greater probability of destroying a target. The reliability of weapon systems usually decreases with increased performance since performance is usually gained at the cost of complexity.

Another consideration is the evaluation of the importance to be given the accuracy of the system. From a cost effectiveness standpoint it may be more desirable to fire several rounds of a less accurate weapon than to pay the increased cost of developing a more accurate weapon that may require only one round.

The cost and reliability of a weapon system can be significantly affected by the concentrated effort of the people involved in the design and manufacturing process to avoid mistakes and waste. The Army has called attention to this fact in its Zero Defects program. The time and money saved by avoiding the repetition of work because of errors reflect directly in the cost of the weapon and its availability for use against an enemy.

CHAPTER 4

PERFORMANCE PARAMETRICS

LIST OF SYMBOLS

Symbol	Meaning	Symbol	Meaning
C	Ballistic coefficient parameter $\left(\frac{W}{id^2}\right)$, psi	Q	Growth factor, the ratio of gross weight to payload weight $\left(\frac{W_0}{W_{PL}}\right)$, nondimensional
C'	Modified form of ballistic coefficient $\left(\frac{W_{PL}}{id^2}\right)$, psi	QE	Quadrant elevation, or launch angle measured from horizontal, deg
C_D	Drag coefficient of projectile, nondimensional	r_B	Booster mass ratio, the ratio of gross rocket weight to total weight without propellant $\left(\frac{W_0}{W_0 - W_P}\right)$, nondimensional
$C_{D_{STD}}$	Drag coefficient of a standard projectile, nondimensional	R	Range, km
d	Maximum diameter of projectile, in.	R_T	Range to target, km
$\frac{\pi}{4} d^2$	Reference area for aerodynamic coefficients, in. ²	t_B	Booster burning time, sec
F_B	Thrust of booster motor, lb	t_t	Time to target, sec
F_S	Thrust of sustainer motor, lb	V_B	Velocity increment imparted by booster, (burnout velocity) fps
g	Gravitational acceleration constant, ft/sec ²	V_{IDEAL}	Velocity increment by booster in absence of drag and gravity, fps
i	Drag form factor $\left(\frac{C_D}{C_{D_{STD}}}\right)$, nondimensional	W	Weight, lb
I_B	Total impulse of booster motor, lb-sec	W_B	Weight of rocket at burnout, lb
I_S	Total impulse of sustainer motor, lb-sec	W_0	Initial or gross weight of rocket, lb
I_{sp}	Specific impulse delivered by rocket motor, sec	W_P	Propellant weight, lb
$\ln; \ln$	Natural logarithm	W_{PL}	Payload weight, lb
PWF	Propellant weight fraction, the ratio of propellant weight to loaded motor weight $\left(\frac{W_P}{W_0 - W_{PL}}\right)$, nondimensional	Y_{MAX}	Summit altitude, ft

AMCP 709-260

4-1 INTRODUCTION

In the design of any rocket system, the determination of performance parameters is a necessary first step since these define the relationship between the performance requirement and physical characteristics. Performance parameters not only serve as the basis for trade-off considerations among competing requirements and characteristics, but they also serve to show the sensitivity of the rocket's physical characteristics to variations in performance requirement, propulsion system efficiency, aerodynamic characteristics (primarily drag), and energy management technique.

It is not possible, in a handbook of this scope, to present parametric performance data which will cover every conceivable situation. The purposes of this discussion, therefore, will be to call attention to those parameters which affect the performance of a rocket; to illustrate various approximation techniques; and to present a limited amount of parametric performance information.

The discussion will be limited to items necessary to define the relationships between performance and physical characteristics for the following types of rocket:

- a. Indirect-fire, or surface-to-surface artillery rockets
- b. Direct-fire rockets of the type normally employed in antitank or similar roles
- c. Sounding rockets which are launched vertically for the purpose of reaching extreme altitudes
- d. Surface-to-air rockets for an interceptor role

4-2 PERFORMANCE PARAMETERS

The parameters, or variables, that are considered in the evaluation of the rocket's performance can be divided into three major categories:

- a. Those factors associated with performance such as payload, velocity, range, altitude, time of flight, and launch angle
- b. Factors associated with the propulsion system such as energy management technique, specific impulse, thrust, burning time, and propellant-weight fraction

- c. Aerodynamic considerations such as shape, means of stabilization, drag characteristics, and diameter

4-2.1 PERFORMANCE FACTORS

Generally speaking, those factors associated with performance will be specified as fixed conditions for the solution of a given problem, with the possible exception of launch angle (in the case of indirect-fire artillery rockets) and time of flight.

4-2.2 PROPULSION SYSTEM FACTORS

With regard to the propulsion-system variables, it is necessary to examine the effects of variations in the following:

- a. I_{sp} : specific impulse delivered by the rocket motor
- b. F_R/W_0 : ratio of booster thrust to rocket takeoff weight (a measure of boost phase acceleration)
- c. F_S/F_B : ratio of sustainer thrust to booster thrust
- d. I_S/I_B : ratio of sustainer total impulse to booster total impulse
- e. PWF : propellant weight fraction (ratio of usable propellant weight to loaded motor weight)
- f. Time and duration of propulsive force application

Determination or selection of optimum values of the propulsion-system variables for a rocket system is called energy-management. Energy-management determines the magnitude of the boost and sustainer thrusts, and their duration. It also considers the duration of coast periods. The objective of energy-management is to deposit the payload at the target with a minimum expenditure of propulsive energy while meeting performance, cost, and reliability requirements.

4-2.3 AERODYNAMIC CONSIDERATIONS

With regard to the aerodynamic considerations, it is generally assumed that, for the types of rockets being discussed, drag is of paramount concern. Discussions of the effects of drag on projectile trajectories are given in Reference 1. It shall suffice here to say that the effects of drag

on the trajectory are the functions of the drag coefficient i , the mass of the projectile W , and the diameter of the projectile d . The ballistic coefficient parameter given in Reference 1 is $C = W/id^2$ and is useful in describing the effects of drag on the rocket during the post-burnout flight phase.

Although the ballistic coefficient is a useful parameter for the determination of drag effects for the post-burnout trajectory phase, it is not useful for the propulsive phase of the trajectory because of the effects of thrust and weight changes. In the compilation of parametric performance data, it is more convenient to work with a modified form of the ballistic coefficient C , defined as $C' = W_{PL}/id^2$, where W_{PL} is the payload weight in pounds. This form of the ballistic-coefficient parameter is more convenient to use because the rocket payload is usually specified as an initial condition, as opposed to the situation for artillery projectiles where the weight of the complete projectile is specified.

Performance parametrics provide data relating performance to physical characteristics. Weight is the principal physical characteristic with which the rocket designer is usually concerned. This discussion will therefore be limited to the weight consideration, although other physical characteristics—such as length, diameter, or volume—may sometimes also be limiting factors. The weight parameter for a rocket design may be stated in a nondimensional form, as the ratio of rocket gross weight to payload weight. This ratio is designated the growth factor Q because it indicates to the designer how much his rocket must weigh in relation to the payload, or how much the overall weight must "grow" to account for unit increases in payload. The growth factor is useful, not only as a nondimensional measure of the weight of the rocket, but also as an indicator of the efficiency of the chosen method of delivery; a low growth factor indicates high efficiency.

4-3 APPROXIMATION TECHNIQUES AND APPLICABLE EQUATIONS

4-3.1 ESTIMATION OF VELOCITY REQUIREMENT

Where the effects of drag can be estimated accurately or neglected without undue effect,

it is possible to estimate the velocity increment that the propulsion system must impart to the payload. It is then a simple matter to calculate the size of the propulsion system required. There are various methods for estimating the velocity requirement, depending upon the application, and the degree of accuracy desired. These are discussed in the paragraphs which follow.

4-3.1.1 Indirect-Fire Systems

A crude approximation of the velocity requirement for the indirect-fire rocket is given by the drag-free range equation

$$R = \frac{V_B^2 \sin(2QE)}{g} \quad (4-1)$$

which, for the optimum launch angle of 45° , yields the required velocity increment

$$V_B = \sqrt{Rg} \quad (4-2)$$

In the above equations, R is the range; V_B is the velocity increment imparted by the booster; QE is the quadrant elevation, or launch angle, measured from the horizontal, in degrees; and g is the gravitational acceleration constant. Any consistent set of units may be used.

While the drag-free approximations are adequate for preliminary work on most rocket systems, the relatively greater effect of drag on the indirect-fire system often requires a more accurate calculation. This can be obtained through use of ballistic range tables (Reference 1), which introduce the effect of drag in the form of the ballistic coefficient W/id^2 . Fig. 4-1 presents the relationship between range, burnout velocity and ballistic coefficient, taken from Reference 1. Since the ballistic coefficient is not independent of burnout velocity, the use of Fig. 4-1 requires an iterative procedure for any given payload and diameter. However, these data are extremely useful for rapid, accurate estimation of performance parametrics for high acceleration, surface-to-surface rockets.

4-3.1.2 Direct-Fire Rockets

If we assume that the effects of drag can be accounted for, it is usually a simple matter to determine the velocity requirement for a direct-

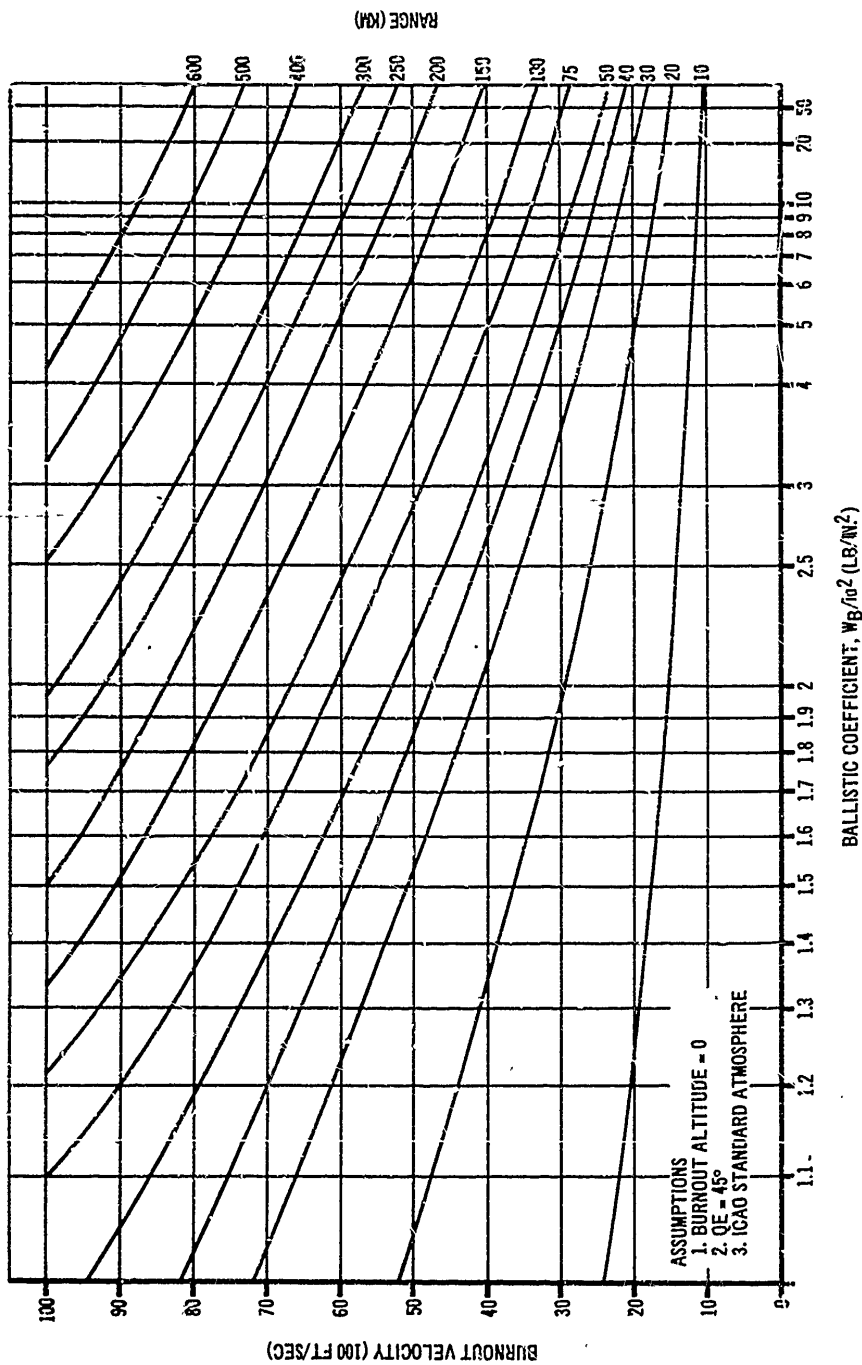


Figure 4-1. Effect of Ballistic Coefficient on Burnout Velocity

fire rocket, based on the range to the target R_T , the desired time of flight t_1 , and the desired burning distance or time t_3 . In the absence of drag, the velocity requirement for a constant-acceleration boost phase is

$$V_B = \frac{R_T}{t_1 - \frac{1}{2} t_B} \quad (4-3)$$

Although this equation neglects the effects of drag and gravity, it is useful for approximation.

4-3.1.3 Sounding Rockets

In the absence of drag, the summit altitude Y_{MAX} reached by a vertically launched projectile is given as

$$Y_{MAX} = \frac{V_B^2}{2g} \quad (4-4)$$

Therefore, an approximation of the required velocity would be

$$V_B = \sqrt{2g Y_{MAX}} \quad (4-5)$$

4-3.2 ESTIMATION OF ROCKET MOTOR REQUIREMENTS

If we can assume that a sufficiently accurate estimate of the velocity requirement is achieved by use of any of the methods described above, we can calculate the weight of the rocket using the relationships defined below.

4-3.2.1 Specific Impulse and Booster-Mass Ratio

The relationship between rocket weight, specific impulse, and propellant weight is given by the "ideal" velocity equation

$$V_{IDEAL} = gI_{sp} \ln \left(\frac{W_0}{W_0 - W_p} \right) = gI_{sp} \ln (r_B) \quad (4-6)$$

where I_{sp} is the specific impulse delivered by the rocket motor in seconds, W_0 is the initial or gross weight of the rocket in pounds, W_p is the propellant weight in pounds, and \ln is the natural logarithm. The ratio $W_0/(W_0 - W_p)$ is commonly

referred to as the booster-mass ratio r_B . This relationship is illustrated graphically in Figure 4-2.

4-3.2.2 Propellant-Weight Fraction

If we consider the rocket to consist of two major components—the payload and the rocket motor—we can define the gross weight as

$$W_0 = W_{PL} + \frac{W_p}{PWF} \quad (4-7)$$

where PWF is the propellant weight fraction $W_p/(W_0 - W_{PL})$, nondimensional, and the burn-out weight as

$$W_B = W_{PL} + \frac{W_p}{PWF} - W_p \quad (4-8)$$

The booster-mass ratio can then be expressed as

$$r_B = \frac{W_0}{W_0 - W_p} = \frac{W_0}{W_B} = \frac{W_{PL} + \left(\frac{W_p}{PWF} \right)}{W_{PL} + \left(\frac{W_p}{PWF} \right) - W_p} \quad (4-9)$$

4-3.2.3 Growth Factor

Eq. 4-9 can be reduced to a form which expresses the weight of the rocket in a nondimensional form (growth factor Q) as follows:

$$Q = \frac{W_0}{W_{PL}} = \frac{r_B (PWF)}{1 - r_B (1 - PWF)} \quad (4-10)$$

4-3.3 SUMMARY

The relationship among growth factor, propellant-weight fraction, specific impulse, and velocity requirement is illustrated in Figure 4-3. Information of this type is useful since it illustrates the sensitivity of the rocket weight (for any given performance level) to variations in specific impulse and propellant-weight fraction.

It should be remembered that the equations developed in paragraph 4-3 are only crude approximations of the representations of rocket performance described in the paragraphs which

AMCP 706-280

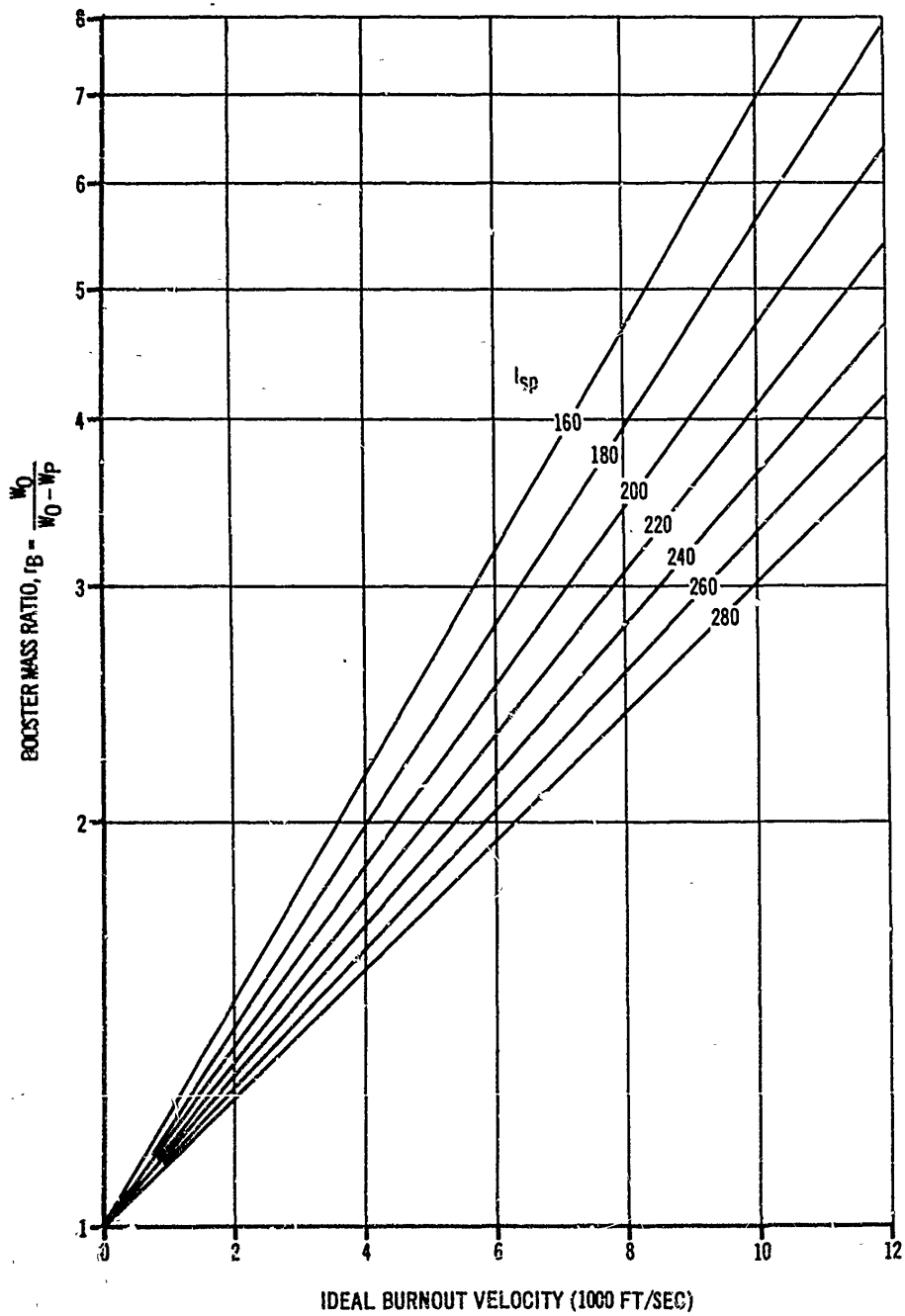


Figure 4-2. Effect of Ideal Burnout Velocity on Booster-Mass Ratio

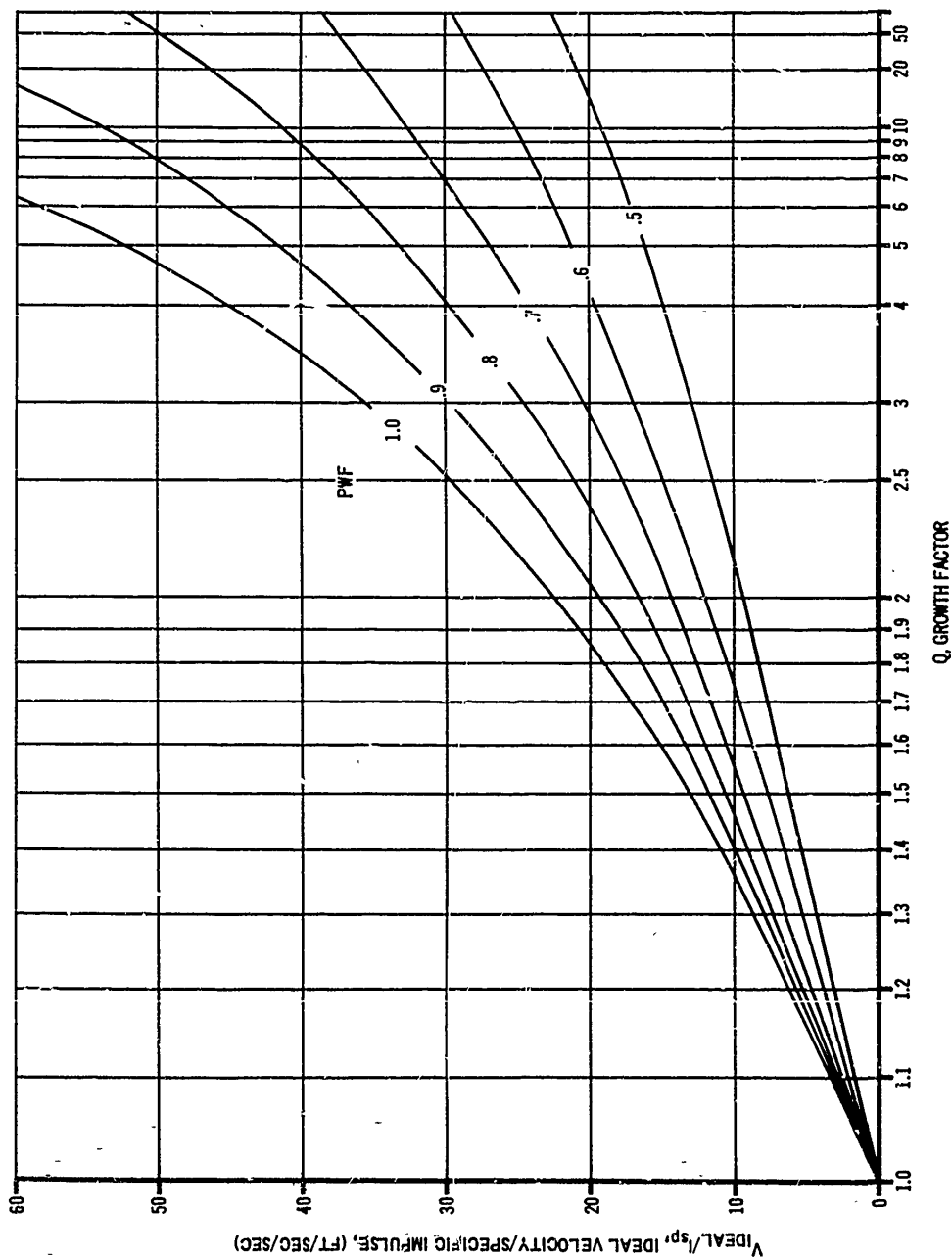


Figure 4-3. Effect of Growth Factor on Ideal Burnout Velocity

AMCP 706-280

follow. Nevertheless, they are extremely valuable in the preliminary design of any rocket. As demonstrated in the example problem at the end of this chapter, these relationships are used in the early phases of design to establish the approximate values of the important rocket variables such as I_{sp} and growth factor. These values will determine if the design requirements are inconsistent with the state of the art. In addition, the approximate numbers will establish the region of interest for the more detailed analysis of the variables.

4-4 PARAMETRIC PERFORMANCE DATA FOR INDIRECT-FIRE SYSTEMS

4-4.1 DELIVERY TECHNIQUES

4-4.1.1 Trajectory Profile

The trajectory profile for an unguided surface-to-surface rocket (ballistic rocket) is shaped generally like a parabola, with an initial departure angle of between 45° and 60° for maximum range. Some large ballistic rockets are launched vertically; however, these require a maneuver to tilt the rocket onto a ballistic path. The discussion that follows will be limited to the non-maneuvering type of rocket.

4-4.1.2 Energy-Management Techniques

Among the methods that have been used to impart propulsive energy to indirect-fire rocket systems are:

- a. Boost
- b. Boost/sustain
- c. Staged boost

In the *boost* method, the booster motor fires continuously throughout the flight of the rocket, or until fuel is depleted. This approach is by far the least complex of the above and has found use generally in the field of simple, unguided, ballistic rockets.

The *boost/sustain* approach consists of an initial thrust of the booster motor, followed by a constant sustaining thrust of lesser magnitude. While this approach offers performance advan-

tages over the *boost* approach for some applications, it requires a more complex and costly motor construction.

In the *staged boost* approach, the total thrust is delivered by a series of booster motors, each jettisoned upon burnout. This is the most efficient means of energy-management but its use is limited to those cases where weight considerations override the cost and reliability penalties of staging, and where the hazards of falling motor cases can be permitted. Since very few rockets within the scope of this handbook meet these limitations, this discussion will not include the *staged boost* approach.

4-4.2 PARAMETRIC PERFORMANCE DATA

The relationship between growth factor (ratio of gross rocket weight to payload weight) and range for an indirect-fire rocket system is a function of the following items:

- a. QE : launch elevation angle
- b. I_{sp} : propellant specific impulse
- c. PWF : motor propellant weight fraction
- d. W_{PL}/d^2 : ratio of payload weight to diameter squared
- e. i : drag-form factor, ratio of drag coefficient of rocket under consideration to drag coefficient of standard rocket shape for which range tables have been computed
- f. F_B/W_0 : initial-thrust-to-weight ratio (boost acceleration)
- g. F_S/F_B : ratio of sustain thrust to boost thrust
- h. I_S/I_B : ratio of sustain impulse to boost impulse

The angle at which the rocket must be launched in order to achieve maximum range is of initial interest to the designer. Fig. 4-4 presents the effect of boost acceleration F_B/W_0 and growth factor Q on the optimum launch angle for an all-boost system, with fixed values of I_{sp} , PWF , and W_{PL}/id^2 . Although the data would be different if these parameters (I_{sp} , PWF , W_{PL}/id^2) were varied, the trends of the curve are worth noting. Low accelerations require the highest launch angles, with the dependence of launch angle on acceleration being strongest at low accelerations. Higher growth factors indicate higher launch

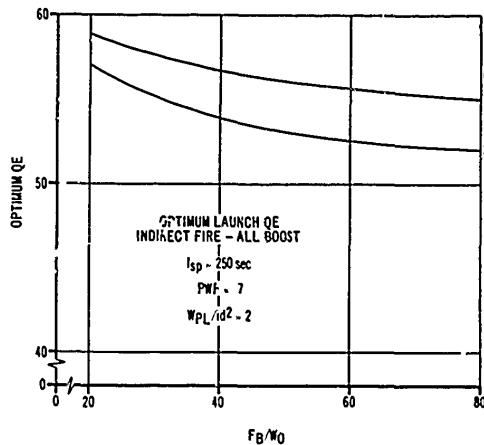


Figure 4-4. Indirect Fire - All-Boost; Effect of Thrust-to-Weight Ratio on Optimum Launch Quadrant Elevation

angles because they are equivalent to longer boost burning times at any given level of acceleration.

For a boost/sustain system, the optimum launch angle will be a little greater than for an all-boost system, as shown in Fig. 4-5. As the ratio of sustainer thrust to booster thrust is decreased and/or the ratio of sustainer impulse to booster impulse is increased, an increase in optimum launch angle is indicated.

Fig. 4-6 presents the relationship between growth factor and range for an all-boost system, with QE optimized and PWF, I_{sp} , and W_{PL}/id^2 held constant. It is seen that the lower accelerations permit more efficient energy-management schemes since they yield a lower growth factor for any specified range. Although this curve is constructed for only one value each of I_{sp} , PWF, and W_{PL}/id^2 , it is indicative of trends; we may therefore say that the growth factor (for a given range) will be inversely proportional to I_{sp} , PWF, and W_{PL}/id^2 . The designer would, of course, examine trade-offs between these parameters, as discussed later on in this chapter. Before leaving Fig. 4-6, however, we should note another trend of significance to the designer or to the requirements originator. Examination of the curve shows that significant range increases can be obtained for relatively minor rocket-weight increases. For example, whereas a growth factor

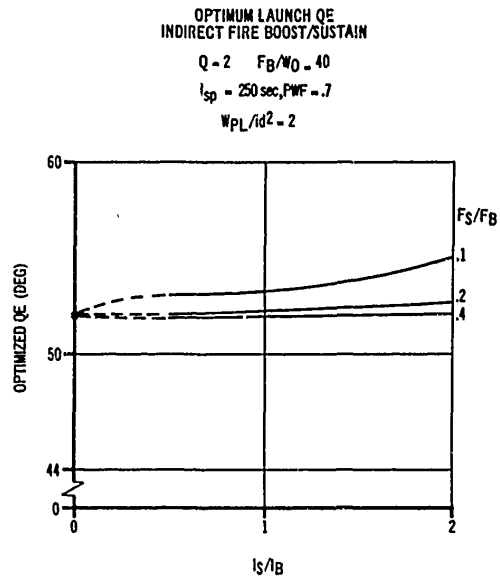


Figure 4-5. Indirect Fire - Boost/Sustain; Effect of Impulse Ratio on Optimum Launch Quadrant Elevation

of about 2 is required for a range of 30 kilometers, a 25 percent increase in missile weight (an increase of Q from 2.0 to 2.5) doubles the range (to 60 km).

The relationship between growth factor and range for a boost/sustain system will be dependent upon the choice of sustainer parameters in addition to the parameters discussed above for the all-boost system. There is no unique method for determining optimum sustainer parameters since the choice will depend upon which characteristics of the rocket the designer is attempting to optimize; for example, weight or accuracy. The designer has a choice of methods for providing the sustainer impulse. This can be done with separate booster and sustainer motors, or by one motor with two thrust levels. In the case of separate motors, it is possible to achieve high specific impulse with each motor, but the propellant weight fraction of the combination is usually lower than for a single motor. In the case of a single motor with two thrust levels, the specific impulse of the sustainer will be less than for the booster (due to decreased chamber pressure during the sustainer phase) if a constant-

AMCP 706-280

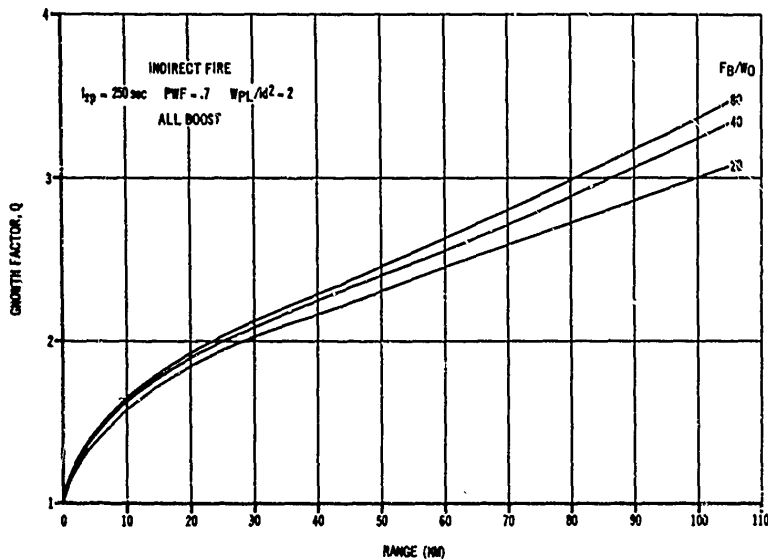


Figure 4-6. Indirect Fire - All-Boost; Effect of Range on Growth Factor

geometry nozzle is used. For this discussion it will be assumed that a single motor with two thrust levels and fixed nozzle geometry is used. The relationship between the ratio of sustainer thrust to booster thrust and the resulting ratio of specific impulse is presented in Fig. 4-7.

Fig. 4-8 indicates the type of parametric data which should be generated for optimization of sustainer parameters in situations where minimizing weight is the primary concern.

Fig. 4-9 presents the relationship between growth factor and range for a boost-sustain system, where the sustainer parameters are assumed to have been fixed by considerations other than minimum weight. A comparison of these data with the data for the all-boost system will show that there are conditions for which the boost/sustain system is heavier than an all-boost system. This results from the reduction in sustainer specific impulse as discussed earlier.

The data above have been presented for only one value each of I_{sp} , PWF , and W_{pL}/id^2 . The designer will be interested in knowing the sensitivity of the missile weight to variations in these parameters also. Fig. 4-10 presents the effects of I_{sp} and PWF on the growth factor for a specific range, acceleration level, and ballistic coefficient. Fig. 4-11 presents a similar trade-

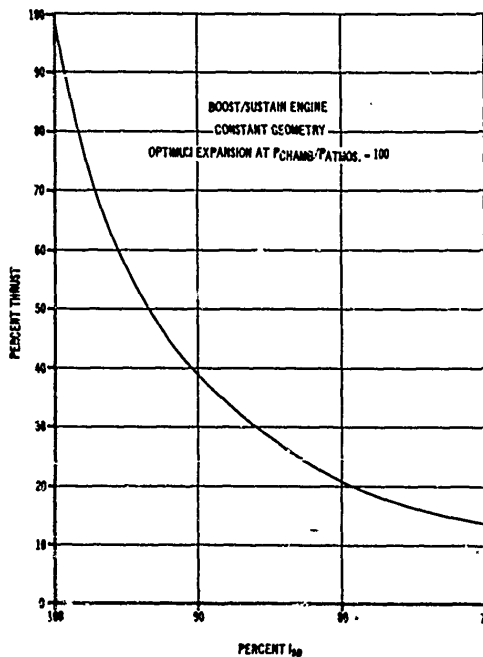


Figure 4-7. Boost/Sustain Engine; Variation of Specific Impulse With Thrust

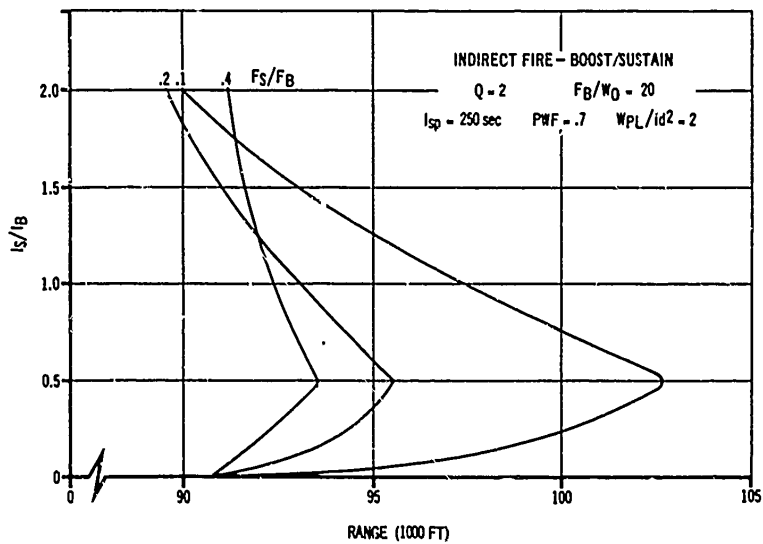


Figure 4-8. Indirect Fire - Boost/Sustain; Effect of Range on Impulse Ratio

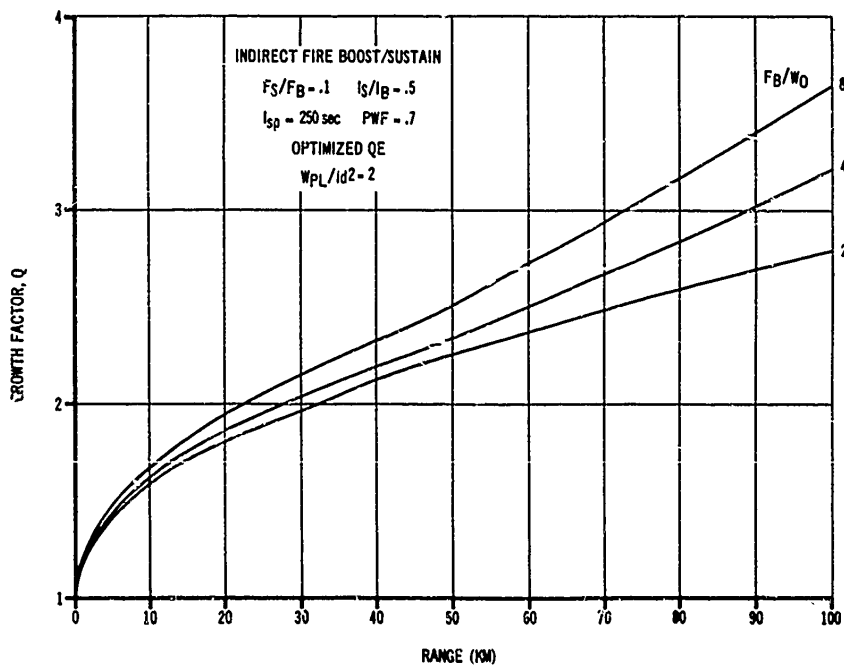


Figure 4-9. Indirect Fire - Boost/Sustain; Effect of Range on Growth Factor

AMCP 706-280

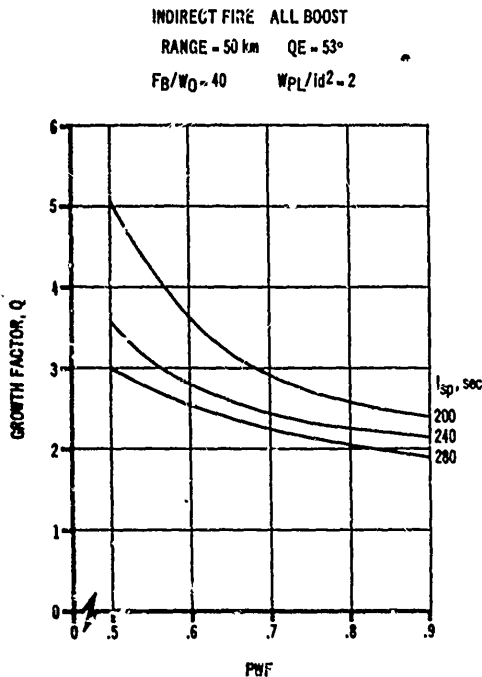


Figure 4-10. Indirect Fire - All-Boost; Effect of Propellant Weight Fraction on Growth Factor

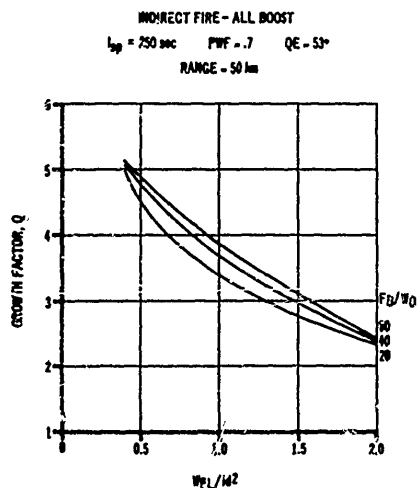


Figure 4-11. Indirect Fire - All-Boost; Effect of Ballistic Coefficient on Growth Factor

4-12

off with acceleration and ballistic coefficient as variables.

The data presented above have not been intended to cover every situation. They are an indication of trends and serve to illustrate the various trade-offs which the designer must consider.

4-5 PARAMETRIC PERFORMANCE DATA FOR DIRECT-FIRE SYSTEMS

4-5.1 DELIVERY TECHNIQUES

4-5.1.1 Trajectory Profiles

Both ballistic and maneuvering types of trajectories have been used for direct-fire systems. Either of these is essentially flat, however, and the degree of maneuver, if used, is generally limited. Therefore, for purposes of parameterization, no distinction is made between the two types. Generally speaking, it is sufficient for performance calculations to assume a constant-altitude, line-of-sight trajectory.

4-5.1.2 Energy-Management Techniques

Among the commonly employed energy-management techniques for direct fire rockets are:

- Boost
- Boost/sustain
- Boost/coast/sustain

The choice here will depend to some extent on the level of performance required and on the intended method of use. Considering the method of use, we must determine whether burning outside the launch tube can be permitted. In the case of direct-fire infantry weapons, this cannot usually be permitted; whereas for weapons to be employed on armored vehicles, there is no problem (aside from accuracy considerations) involved in burning outside the launch tube. If burning outside the launch tube is permitted, either the *boost* or the *boost/sustain* approaches will apply. Where burning outside the tube is not permitted, the choice is between the *boost* and the *boost/coast/sustain* approaches, with the *boost* approach generally limited to low performance systems by the maximum velocity

which can be attained within the limitations of the tube length and the rocket acceleration.

4.5.2 PARAMETRIC PERFORMANCE DATA

In defining the relationship between performance and physical characteristics for direct-fire rockets, it is not necessary to separate those rockets which must have a coast phase from those that do not. The reason for this is that, in the usual case, the additional time of flight will be negligible, on the order of 1/10 sec.

The relationships between growth factor (ratio of rocket weight to payload weight), range, and time of flight are determined by:

- a. I_{sp} : propellant specific impulse
- b. PWF : motor propellant weight fraction
- c. W_{PL}/d^2 : ratio of payload weight to diameter squared
- d. i : drag-form factor
- e. F_B/W_0 : ratio of initial thrust to weight
- f. F_S/F_B : ratio of sustain thrust to boost thrust
- g. I_S/I_B : ratio of sustain impulse to boost impulse

For initial considerations, the first four of these parameters (I_{sp} , PWF , W_{PL}/d^2 , i) can usually be estimated with adequate accuracy; however, it is desirable also to examine variations of these parameters if the situation permits.

Fig. 4-12 presents the relationship between target range, time of flight, and energy-management scheme for a given set of missile characteristics. The best energy-management scheme is seen to be the *boost* (no sustainer) in cases where a minimum time of flight is desired. This is usually the case for systems in which the gunner has no control over the projectile after launch. However, in cases where command guidance is used, time of flight is a secondary consideration, with the velocity of the projectile being limited by considerations of gunner capabilities, command data rates, type of command link, etc. Since the considerations involved in the determination of time of flight (or average velocity) for the command-guided case are many and varied, it is desirable to concentrate for the remainder of this discussion on the system which

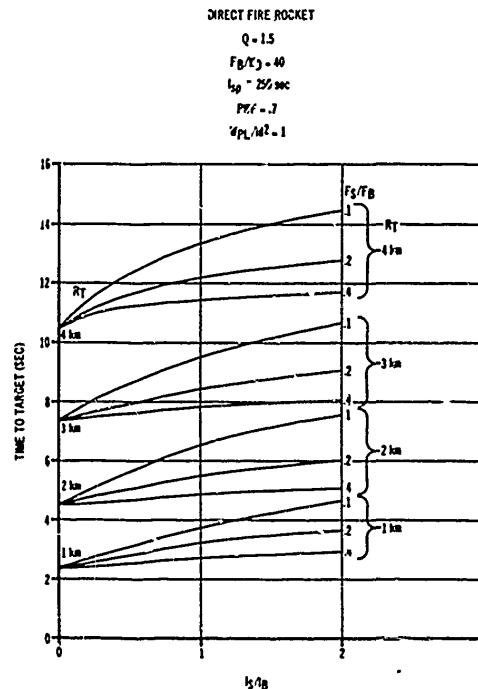


Figure 4-12. Direct Fire - Boost/Sustain; Effect of Impulse Ratio on Time to Target

yields minimum time of flight, namely, the *boost* system.

Fig. 4-13 presents trade-offs with respect to growth factor, time of flight, range, and boost acceleration. A performance limit appears to be reached at a growth factor of about 3.0 because increases beyond this point reduce the time of flight an insignificant amount. Increasing the boost acceleration reduces the time of flight, but decreases the percentage of powered flight. For example, at a growth factor of 1.7 and $F_B/W_0 = 20$ the burning distance is about 3 km, and we reach 4 km in 9.7 sec. If we increase F_B/W_0 to 80, the burning distance is reduced to about 1 km and we reach 4 km in 8.5 sec. This illustration points out another of the choices facing the designer, namely, the trade-off between time to target and percentage of powered flight.

Once the designer has examined the trade-offs between range and time of flight, he may wish to

AMCP 706-280

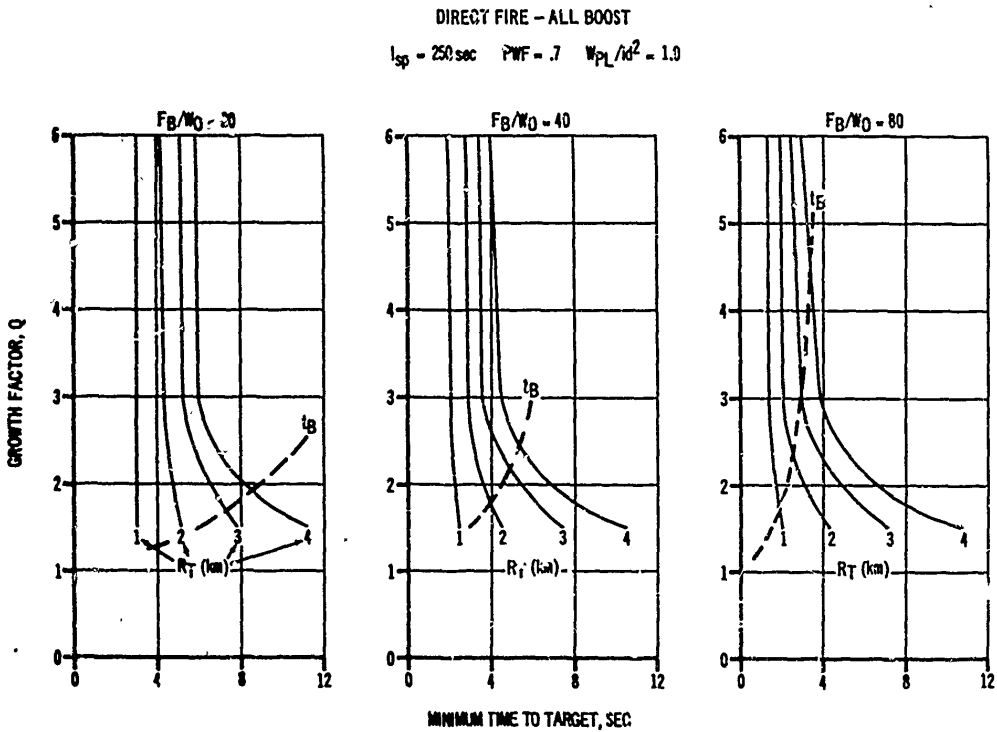


Figure 4-13. Direct Fire - All-Boost; Effect of Growth Factor on Minimum Time to Target

determining the effects of various design parameters on the missile weight (or growth factor) for a specified performance level. For example, Fig. 4-14 shows the trade-off between W_{PL}/d^2 , F_B/W_0 , and growth factor for a specified performance level of 2 km in 3 sec. Fig. 4-15 illustrates the trade-off between PWF, I_{sp} , and growth factor for the same performance level.

In the preceding paragraphs an attempt has been made merely to illustrate the types of trade-offs with which the designer of direct-fire rockets must be concerned. From this discussion, the following conclusions can be drawn:

- a. For minimum time to target, the boost system is superior to the boost/sustain system.
- b. The choice of boost acceleration must result from a consideration of the trade-off between time to target and percentage of powered flight desired.

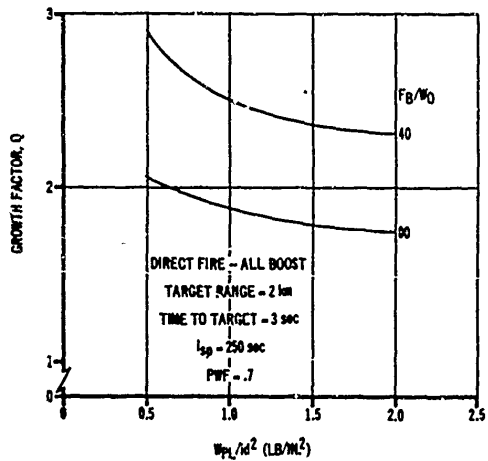


Figure 4-14. Direct Fire - All-Boost; Effect of Ballistic Coefficient on Growth Factor

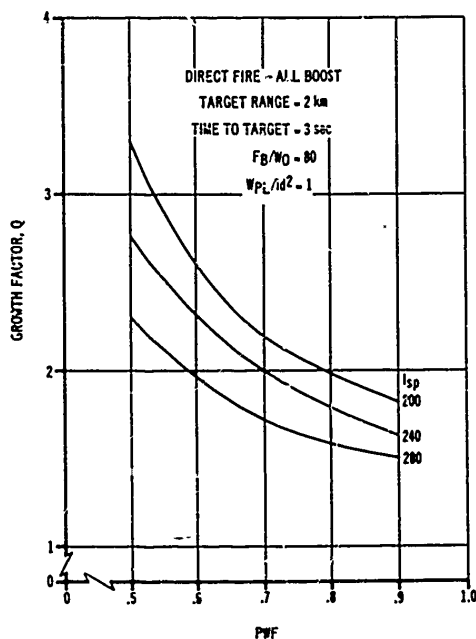


Figure 4-15. Direct Fire - All-Boost; Effect of Propellant Weight Fraction on Growth Factor

c. Increasing PWF , I_{sp} , W_{PL}/id^2 , or F_B/W_0 results in decreased missile weight for a given payload weight and specified performance (time to target).

d. Increasing the growth factor beyond about 3.0 results in negligible performance increase for the range of parameters studied.

4-6 PARAMETRIC PERFORMANCE DATA FOR SOUNDING ROCKETS

4-6.1 DELIVERY TECHNIQUES

4-6.1.1 Trajectory Profiles

The only trajectory profile to be considered here for the sounding rocket is the vertical ascent. In some cases it may be desirable to launch a sounding rocket away from the vertical to insure impact within a given area, but for pur-

poses of performance parameterization, the vertical ascent is sufficient.

4-6.1.2 Energy-Management Techniques

The energy-management techniques which are used with sounding rockets are the same types as listed for the indirect fire rocket systems, namely:

- Boost
- Boost/sustain
- Staged boost

As stated earlier, the choice between these approaches must be the result of a trade-off, considering the *boost* system to be the simplest, cheapest, most reliable, and least efficient; whereas the *staged boost* would be the most efficient, most expensive, and least reliable. The *boost/sustain* approach would be intermediate in all of the above considerations.

4-6.2 PARAMETRIC PERFORMANCE DATA

The relationship between growth factor and peak altitude for a sounding rocket is determined by the following parameters:

- I_{sp} : specific impulse
- PWF : propellant weight fraction
- W_{PL}/id^2 : ballistic parameter
- i : drag form factor
- F_B/W_0 : ratio of boost thrust to takeoff weight
- F_S/F_B : ratio of sustain thrust to boost thrust
- I_S/I_B : ratio of sustain impulse to boost impulse

In Fig. 4-16 the relationship between growth factor, energy-management scheme, boost acceleration, and peak altitude is presented. It can be seen here that the boost/sustain approach would provide the lowest missile weight for a given altitude. This relationship is shown for only one value each of I_{sp} , PWF , and W_{PL}/id^2 , some shifting of data would occur if these parameters were changed.

For any given maximum altitude, the growth factor will be inversely proportional to PWF , I_{sp} ,

AMCP 706-200

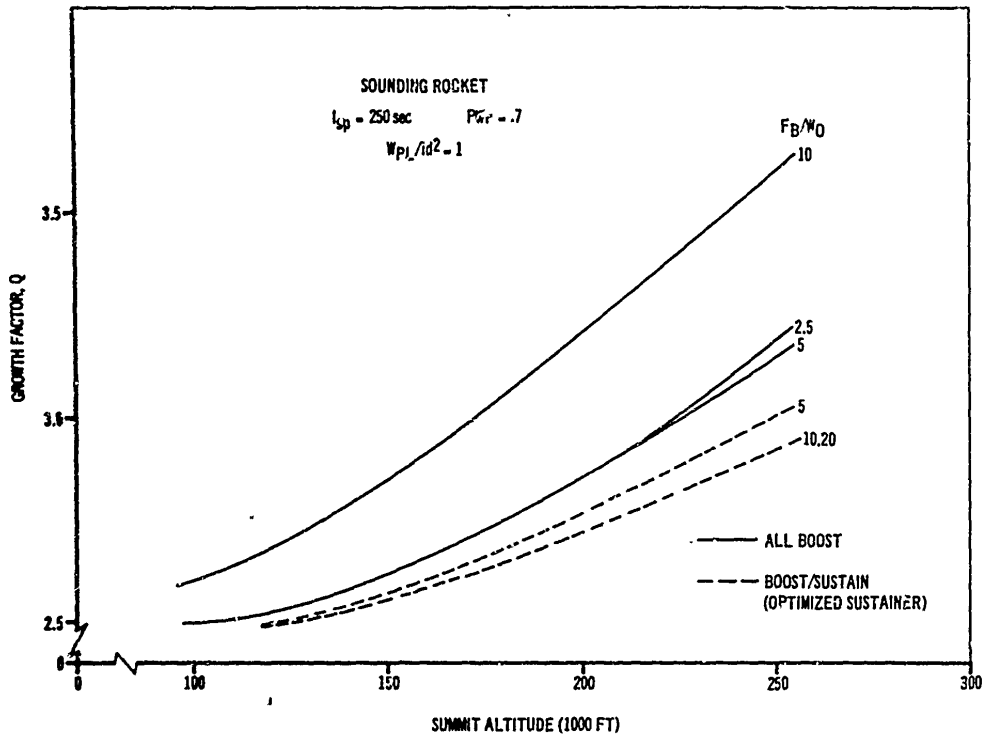


Figure 4-16. Sounding Rocket - All-Boost and Boost/Sustain; Effect of Growth Factor on Summit Altitude

and W_{pl}/id^2 . This is shown in Figs. 4-17 and 4-18 for summit altitudes of 150,000 ft and 250,000 ft. These curves are for the all-boost case; however, the boost/sustain curves would be similar. From these curves, we see that the lightest missile results from a high performance motor (high PWF and I_{sp}) and a large payload-to-diameter ratio.

rant-elevation angle necessary for intercept of the target. Usually, the rocket will be designed to reach a given altitude in a given time and, therefore, the vertical ascent is of primary concern. For this reason the vertical trajectory is normally used to size the rocket, although it must be kept in mind that the distance traveled in a given time will be slightly less for trajectories other than the vertical.

4-7 PARAMETRIC PERFORMANCE DATA FOR SURFACE-TO-AIR ROCKETS

4-7.1 DELIVERY TECHNIQUES

4-7.1.1 Trajectory Profile

The unguided surface-to-air-rocket flies a ballistic trajectory and may be launched at any quad-

4-7.1.2 Energy-Management Techniques

Energy-management techniques applicable to surface-to-air rockets are:

- a. Boost
- b. Boost/sustain
- c. Staged boost

If we consider that minimum time to target will be desired for the surface-to-air rocket, and that

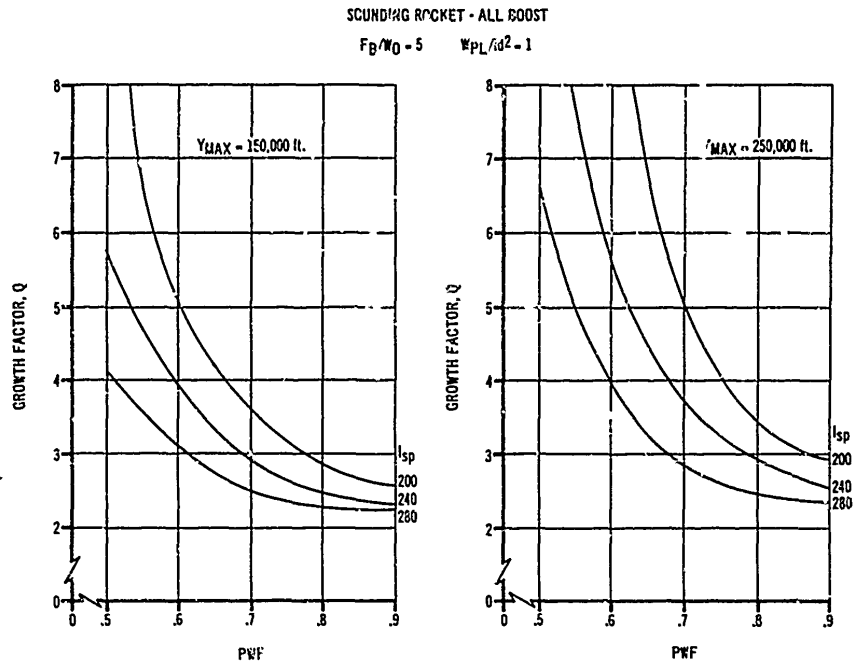


Figure 4-17. Sounding Rocket - All-Boost; Effect of Propellant Weight Fraction on Growth Factor

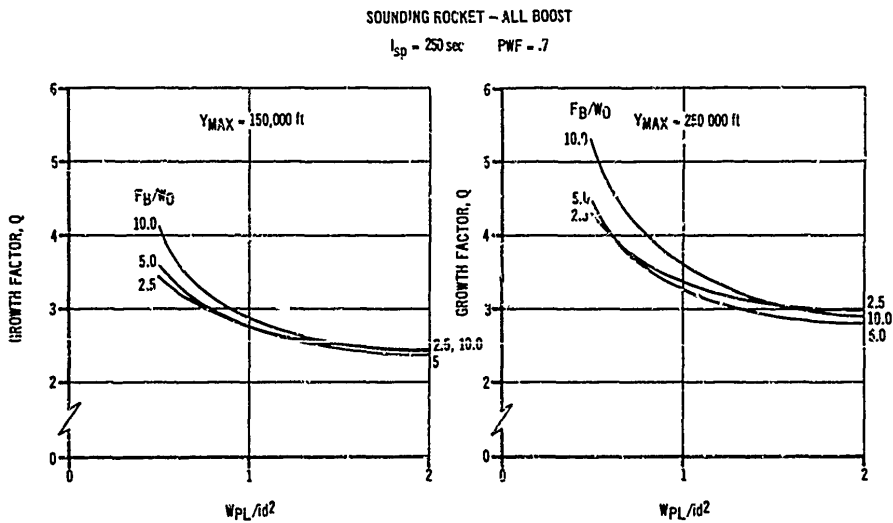


Figure 4-18. Sounding Rocket - All-Boost; Effect of Ballistic Coefficient on Growth Factor

AMCP 708-280

achievable accuracy will limit this type of rocket to low altitude application (under 30,000 ft), the *boost* approach will usually be found to be the most attractive. For this reason, the discussion will be limited to the *boost* approach.

4-7.2 PARAMETRIC PERFORMANCE DATA

The relationship between growth factor and performance requirement (specified as time to a given altitude) is determined by the following parameters:

- I_{sp} : specific impulse
- PWF : propellant weight fraction
- W_{PL}/id^2 : ballistic parameter
- i : drag-form factor
- F_B/W_0 : ratio of boost thrust to takeoff weight

Fig. 4-19 presents the relationship between growth factor, boost acceleration, and time to al-

titude for target altitude of 20,000 ft. As seen in these curves, an increase in boost acceleration reduces the time to altitude. An increase in growth factor above 5 would decrease time to altitude very little.

The trade-off between I_{sp} , PWF , and growth factor for a specified performance level of 20,000 ft in 5 sec is given in Fig. 4-20. Fig. 4-21 illustrates the trade-off between PWF , I_{sp} , and growth factor for the same performance level.

From the previous discussion, the following conclusions may be drawn:

- increasing growth factor above 5 results in negligible performance increase for the range of parameters studied.
- Increasing PWF , I_{sp} , and W_{PL}/id^2 results in decreased missile weight for a given payload weight.

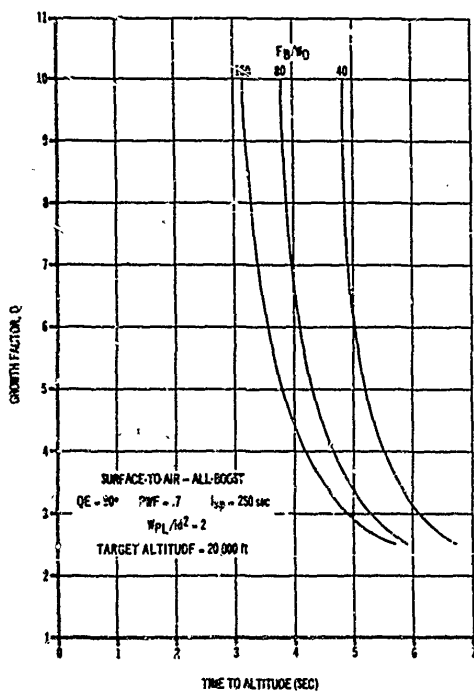


Figure 4-19. Surface-to-Air - All-Boost; Effect of Time to Altitude on Growth Factor

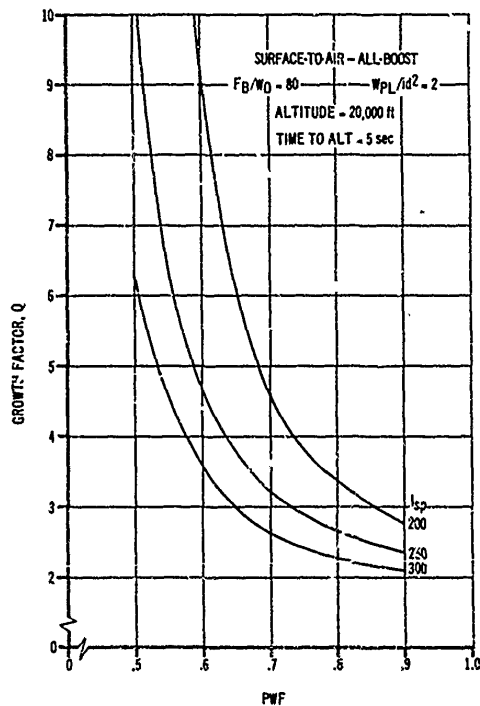


Figure 4-20. Surface-to-Air - All-Boost; Effect of Propellant Weight Fraction on Growth Factor

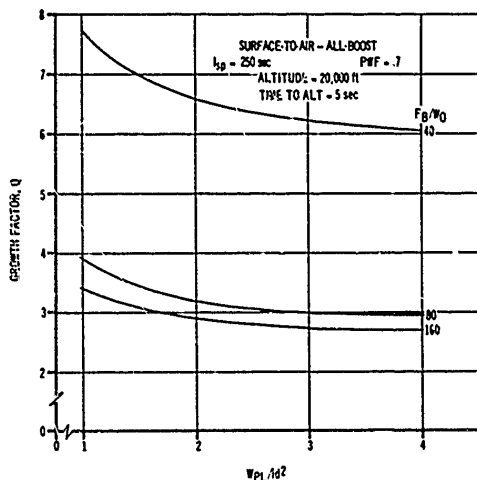


Figure 4-21. Surface-to-Air - All-Boost; Effect of Ballistic Coefficient on Growth Factor

4-8 NUMERICAL EXAMPLE

An indirect fire surface-to-surface missile design problem is presented here to illustrate the steps to be followed in designing a missile when the required performance is specified. The problem is to determine the propulsion system characteristics, the weight breakdown, and the dimensions of the vehicle that will transfer a given payload over a desired range.

The graphs presented in the preceding paragraphs of this chapter indicate the complexity of the relationships between the performance parameters. Because of these complex relationships, there is no easy way to arrive at a rocket configuration which will satisfy all the required relationships and still meet the performance requirements. The only alternative is to assume some of the important rocket or motor parameters, such as body diameter and specific impulse, and calculate the performance for these assumed conditions. The calculated performance data are compared with the desired values; then the original assumptions are modified and the procedure is repeated until the desired results are obtained. It is easily seen that the accuracy of the original assumptions determine the

amount of work required to reach the final solution. This is the reason that experience with the design of rocket systems is so important during the preliminary design stage.

Fig. 4-22 is a flow diagram illustrating the steps of the design procedure. Block 1 indicates the design performance specification. In this case the rocket range and payload are specified. Blocks 2 and 3 show the parameters whose values are being assumed - - that is, the first guess at the design configuration. The next sequence of blocks (4 through 8) illustrates the iterative procedure which must be followed until the initial assumptions are verified. After the iterative process is complete, enough is known about the system to define its performance parameters. This is done in the final Block 11, headed CALCULATE.

A ballistic coefficient is assumed in the first block of the iterative loop (Block 3). This fixes the burnout velocity, the booster-mass ratio, the burnout-to-payload-weight ratio, and the payload ballistic coefficient. Notice that the value of the payload ballistic coefficient was assumed in Block 3 and it is necessary that this value be duplicated. If this has been satisfied, there are no contradictions and the example can proceed to the defining of values.

If the payload ballistic coefficient value cannot be duplicated and/or the resulting values are not realistic, it will be necessary to make a trade-off study of the parameters in the second block until all criteria are satisfied.

The numerical example which follows utilizes the logic shown in the flow diagram.

1. We shall start with a specified range R of 30.0 km and a payload weight of 890.0 lb.
2. From a knowledge of similar rockets, assume a propellant weight fraction PWF of 0.77, a specific impulse I_{sp} of 250 sec and a payload ballistic coefficient W_{pL}/id^2 of 4.0 lb/in.
3. For the required range, assume a ballistic coefficient W_B/id^2 of 4.5 lb/in. Therefore, a burnout velocity V_B of 2700 ft/sec is necessary as shown in Fig. 4-1.
4. For an I_{sp} of 250 sec, the booster mass ratio r_B is determined from Fig. 4-2 to be 1.4.

AMCP 706-280

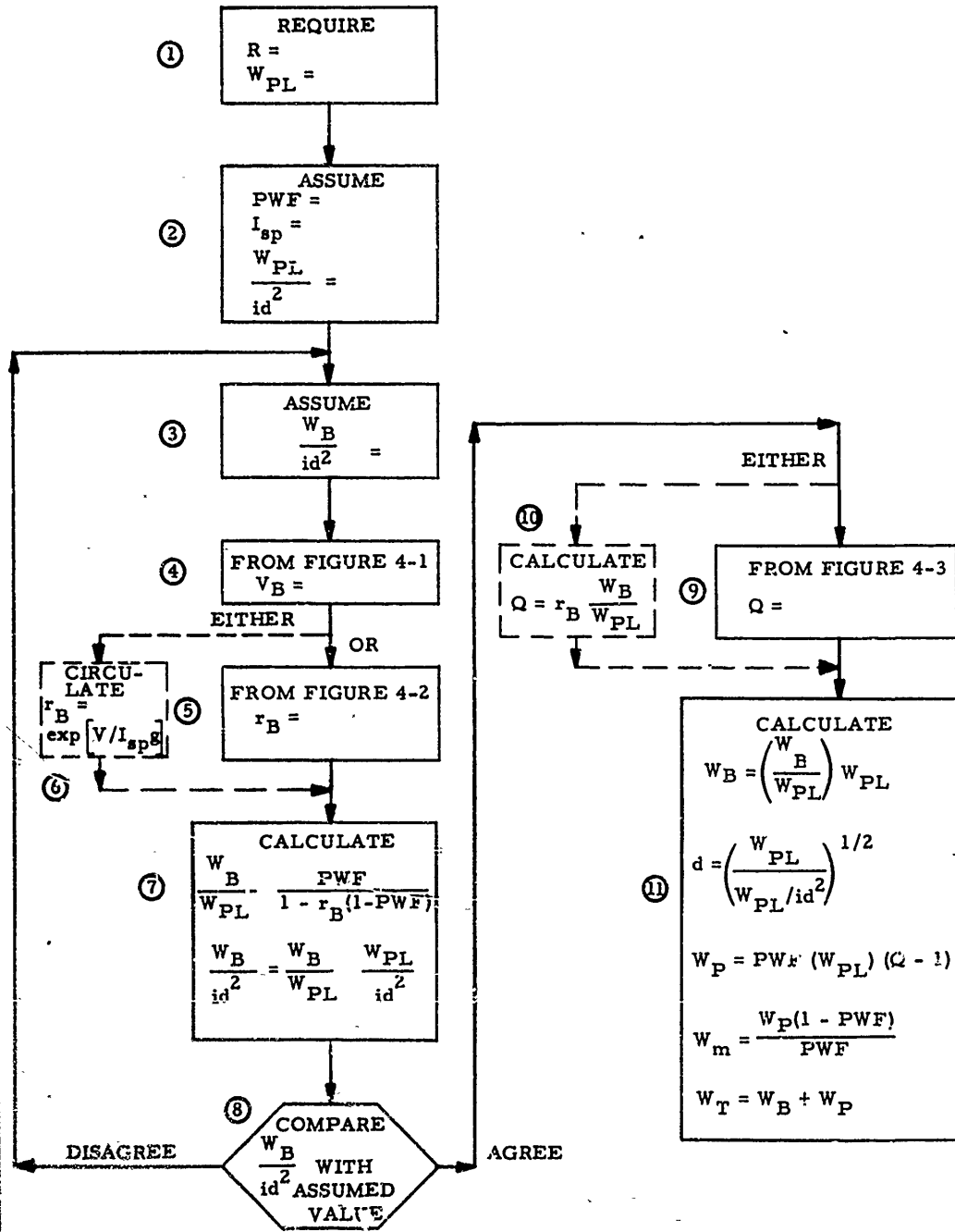


Figure 4-22. Flow Diagram

5. For a given PWF of 0.77, calculate the ratio of burnout weight to payload weight:

$$\frac{W_B}{W_{PL}} = \frac{PWF}{1 - r_B(1 - PWF)}$$

$$= \frac{0.77}{1.0 - 1.4(0.23)} = 1.138.$$

6. Calculate the ballistic coefficient:

$$\frac{W_B}{id^2} = \frac{W_B}{W_{PL}} \left(\frac{W_{PL}}{id^2} \right) = 1.138 (4)$$

$$= 4.552 \text{ lb/in}^2$$

7. A value of W_B/id^2 was assumed in Step 3. Match this value with the value calculated in Step 6. They are the same. If they were not the same, then another value of W_B/id^2 should be selected and Steps 3 through 7 repeated until they agree.

8. After satisfying Step 7, either calculate the growth factor Q or read it from Fig 4-3.

$$Q = r_B \left(\frac{W_B}{W_{PL}} \right) = 1.4(1.138) = 1.59$$

9. The burnout weight W_B is calculated

$$W_B = \left(\frac{W_B}{W_{PL}} \right) W_{PL} = 1.138(890) = 1014 \text{ lb}$$

10. The rocket diameter d can be calculated

$$d = \left(\frac{W_{PL}}{W_{PL}/id^2} \right)^{1/2} = \left(\frac{890}{4} \right)^{1/2} = 15 \text{ in.}$$

11. Propellant weight W_p is found by

$$W_p = PWF(W_{PL})(Q - 1)$$

$$= 0.77(890)(0.59) = 405 \text{ lb}$$

12. Motor weight W_m is

$$W_m = \frac{W_p(1 - PWF)}{PWF}$$

$$= \frac{890(0.23)}{0.77} = 120 \text{ lb}$$

13. Total weight W_T is

$$W_T = W_{BO} + W_p = 1014 + 405$$

$$= 1419 \text{ lb}$$

CHAPTER 5 PROPULSION

LIST OF SYMBOLS

Symbol	Meaning	Symbol	Meaning
a_1	Constant (see Eq. 5-19a)	V	Velocity, ft/sec
a_2	Constant (see Eq. 5-19b)	W	Weight, lb
A	Area, ft ²	ϵ	Erosion factor (see Eq. 5-21)
b	Constant (see Eq. 5-19b)	γ	Ratio of specific heats (C_p/C_v)
c	Effective exhaust velocity, ft/sec; speed of sound, ft/sec	ζ_d	Discharge correction factor
C_F	Thrust coefficient	ζ_f	Thrust correction factor
C_p	Specific heat at constant pressure, BTU/lb °R	ζ_v	Velocity correction factor
C_v	Specific heat at constant volume, BTU/lb °R	θ	Propellant burning time, sec
f	Scale factor	ρ	Density, slug/ft ³
F	Rocket thrust, lb	Σ	Summation
g	Gravitational acceleration, ft/sec ²		
I_{total}	Total motor impulse, lb-sec	Subscripts:	
I_{sp}	Motor specific impulse, sec	<i>atmosphere</i>	Ambient (or atmospheric) conditions
K	Erosion burning constant (see Eq. 5-21); ratio of grain burning surface area to nozzle throat area	b	Burn-out condition; burning surface (see Eq. 5-20)
m	Mass of propellant, slug	<i>basic</i>	Basic (or original) configuration
\dot{m}	Mass flow rate, slug/sec	B	Back pressure
\dot{m}^*	Mass flow rate that will produce a velocity equal to the speed of sound, slug/sec	c	Combustion or stagnation conditions
\bar{m}	Molecular weight of gas, R_u/\bar{R}	e	Erosion condition; exit conditions
M	Mach number	<i>exhaust</i>	Exhaust (or exit) condition
n	Exponent (see Eq. 5-19a); number of moles	g	Propellant grain
P	Combustion chamber pressure parameter (see Eq. 5-23b)	i	Inlet (or entrance) condition
P	Pressure, lb/ft ²	m	Molal value (see Eq. 5-25)
Q_R	Heat of reaction at reference temperature, BTU/lb	<i>max</i>	Conditions for optimum expansion (see Eq. 5-9)
r	Grain burning rate, in./sec	<i>motor</i>	Motor condition
R_u	Universal gas constant, 1545 ft-lb/lb-mole °R	<i>scaled</i>	Scaled (from basic) configuration
\bar{R}	Gas constant, R_u/\bar{m}	t	Throat (or minimum area) conditions
T	Temperature, °R	x	Axial distance (along the nozzle centerline)

AMCP 706-200

5-1 GENERAL

A rocket is propelled by an internal combustion engine that burns either liquid or solid fuel. The primary function of rocket propulsion is to move the warhead and airframe from the launcher to the target with prescribed accuracy. Since the oxidizer is carried internally, rocket engines can operate in the atmosphere, above the atmosphere, or under water. As previously indicated, this handbook will discuss only solid propellant rocket engines.

Unlike other combustion engines, a rocket motor does not contain cylinders, pistons, or turbine blades, nor does it need a supply of air to mix with the fuel. Because its oxygen supply is carried within the propellant, a rocket engine has a number of advantages over other types of power plants:

- Thrust is practically independent of its environment and flight speed.
- There is no altitude ceiling.
- It functions in a vacuum.
- Thrust per unit of frontal area is the largest of any known propulsion engine.

The basic rocket motor consists of an igniter, a propellant charge, and a chamber that is strong enough to withstand the combustion of the propellant and the pressures thus generated. The chamber has a nozzle through which the propellant gases escape in the form of a jet. Igniter types, propellant composition, and chamber ma-

terials vary from system to system, depending on the individual requirements. A schematic of a typical rocket motor is shown in Fig. 5-1.

Rocket propulsion involves the study of the burning rate of propellant in the motor chamber and the discharge rate of gas through the nozzle. The pressure in the motor is the result of a delicate balance between the burning of the propellant and the escape of gases through the nozzle.

For the operation of a solid propellant motor, the chamber is loaded with a propellant charge and an igniter. Motor operation is initiated when the igniter ignites the propellant. The burning propellant furnishes at high pressure a continuous supply of gas that expands and is ejected from the chamber nozzle at high velocity.

The thrust of the rocket motor is produced by the change in momentum of the combustion gas expelled through the nozzle and the pressure forces acting on the rocket body, so that

$$F = \dot{m}V_{\text{exhaust}} + (P_{\text{exhaust}} - P_{\text{atmosphere}}) A_{\text{exhaust}} \quad (5-1)$$

where F is the rocket thrust, \dot{m} is the flow rate of the combustion gas, V_{exhaust} is the velocity of the exhaust gas, P_{exhaust} is the pressure of the exhaust gas, $P_{\text{atmosphere}}$ is the atmospheric pressure, and A_{exhaust} is the exhaust gas flow area. If the flow is ideally expanded in the nozzle

$$P_{\text{exhaust}} = P_{\text{atmosphere}}$$

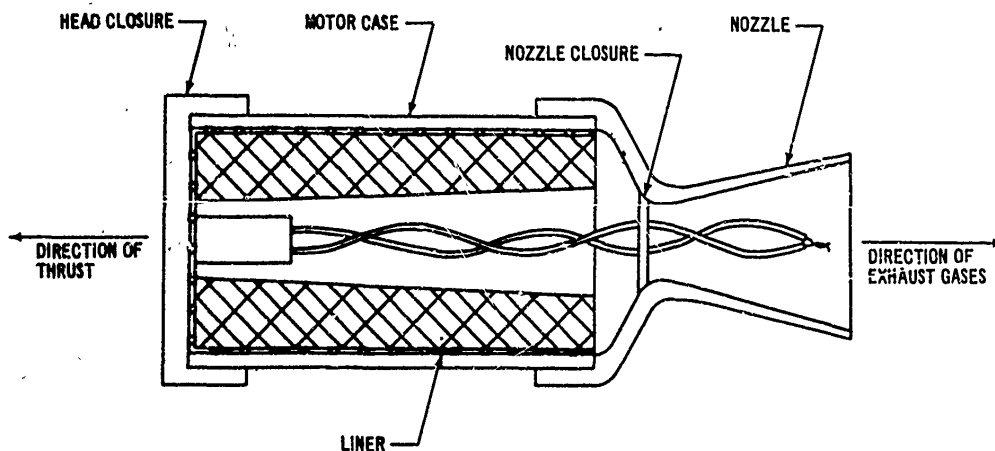


Figure 5-1. Schematic of a Case-Bonded, Unrestricted-Burning Solid-Propellant Rocket Motor

and

$$F = \dot{m}V_{\text{exhaust}} \quad (5-2)$$

For convenience, an effective exhaust velocity c is defined as

$$c = V_{\text{exhaust}} + \frac{(P_{\text{exhaust}} - P_{\text{atmosphere}}) A_{\text{exhaust}}}{\dot{m}} \quad (5-3)$$

thus

$$F = \dot{m}c \text{ if } P_{\text{exhaust}} = P_{\text{atmosphere}} \quad (5-4)$$

Two useful performance indicators are the specific and total impulses. The specific impulse I_{sp} is the thrust per unit weight rate of consumption of the propellant; thus

$$I_{sp} = \frac{F}{\dot{m}g} = \frac{c}{g} \quad (5-5)$$

where g is local gravitational acceleration (32.2 ft per sec²), and all other symbols are as defined previously. The total impulse I_{total} is the integral of the thrust over the time that the propellant burns. Thus,

$$I_{\text{total}} = \int_0^{\theta_b} F d\theta = \int_0^{\theta_b} I_{sp} \dot{m} g d\theta \quad (5-6)$$

or for constant thrust,

$$I_{\text{total}} = F\theta_b = I_{sp} m g \quad (5-7)$$

where θ_b is the time during which the propellant burns, m is the total mass of propellant consumed, and all other symbols are as defined previously.

For additional information on rocket motors see Ref. 9.

5-2. NOZZLE

The rocket nozzle expands the combustion chamber gas from the chamber pressure to atmospheric pressure. The gas is accelerated by converting internal energy into kinetic energy. Subsonic gas flow (i.e., velocity less than the speed of sound) is expanded and accelerated by decreasing the flow area (e.g., a convergent nozzle). Supersonic gas flow (i.e., velocity greater than the speed of sound) is expanded and accelerated by increasing the flow area (e.g., a divergent nozzle).

The velocity of a gas exhausting from a convergent nozzle increases as the ratio of upstream to downstream pressure increases but will not exceed the speed of sound. To illustrate, let us consider a convergent nozzle with a constant upstream pressure and a variable downstream pressure, such as that shown in Fig. 5-2. When the upstream and downstream pressures are equal, there will be no flow. As the downstream pressure is reduced, the gas will begin to flow and the velocity and mass flow exhausting from the nozzle will increase until the exhaust velocity is equal to the speed of sound. Further reduction in the downstream pressure will have no effect on the velocity or mass flow. The minimum pressure ratio across the nozzle that will yield a sonic velocity is termed the critical pressure ratio, and is a function of the flow conditions and gas properties. At pressure ratios greater than the critical, the velocity will remain sonic and the mass flow can only be increased by increasing the upstream pressure. The sonic velocity will always occur (if it occurs) at the minimum area section. The ratio of velocity to the speed of sound is termed the Mach number M .

The above discussion indicates that a subsonic gas may be accelerated to the speed of sound in a convergent section. It may then be further accelerated to supersonic velocities in a divergent

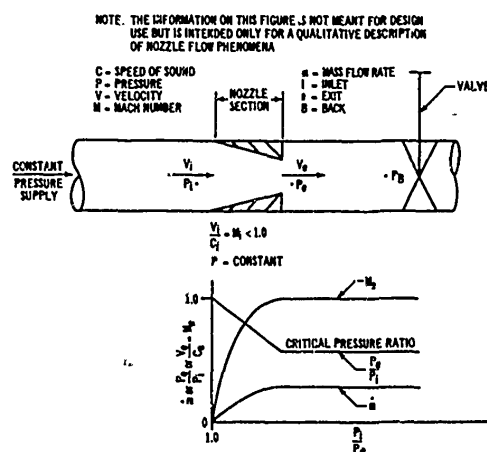


Figure 5-2. Subsonic Flow Through a Converging Nozzle

AMCP 706-280

section. Such a nozzle with convergent and divergent sections is called a supersonic or De Laval nozzle. The velocity at the section of minimum area (throat) will always be less than or equal to the speed of sound, depending upon the pressure ratio across the nozzle. To illustrate the flow phenomena, let us consider a supersonic nozzle with a constant upstream pressure and a variable downstream pressure as shown in Fig. 5-3. When the upstream and downstream pressures are equal, there will be no flow. As the downstream pressure is reduced, the gas will begin to flow, and the exhaust velocity and mass flow will increase until the velocity at the throat is equal to the speed of sound. As the downstream pressure is further reduced, the mass flow will remain constant and the velocity at the throat will remain at the speed of sound. A downstream pressure will be reached at which the gas is completely expanded ideally within the nozzle and the exhaust velocity is supersonic. At downstream pressures lower than this, the exhaust flow remains supersonic but the gas is underexpanded within the nozzle; therefore, additional expansion takes place outside the nozzle. At higher downstream pressures the gas is overexpanded in the divergent section of the nozzle, resulting in pressure shock waves and in flow separation from the nozzle wall. Pressure shock waves are distinguished by abrupt pressure rises and a velocity change from supersonic to subsonic.

As internal energy is converted to kinetic energy throughout the nozzle, the gas temperature decreases. The gas pressure and density also decrease as the gas expands through the nozzle.

The above discussion presents a qualitative description of nozzle flow phenomena. The discussion which follows will present methods of defining the flow phenomena quantitatively.

5-2.1 THERMODYNAMIC RELATIONS

To design and evaluate the performance of a rocket, it is necessary to define the thermodynamic relations of the gas flow through the nozzle. The normal approach is to evaluate the thermodynamic relations based on the ideal flow of an ideal gas and then modify these relations for the real flow of the real gas. Generally, the actual rocket motor performance is within 10 percent of the performance calculated for ideal conditions.

5-2.1.1 Ideal Flow

Flow through nozzles is considered to be ideal when: (a) there is no friction, (b) there is no heat transfer (adiabatic), (c) flow is steady, (d) flow is uniform across sections normal to the nozzle longitudinal axis, (e) flow exhausting to the atmosphere is parallel to the nozzle longitudinal axis, (f) the gas (products of propellant combustion) is homogeneous, (g) the gas is in chemical equilibrium and does not shift, and (h) the gas obeys the perfect gas laws. The above assumptions allow the definition of flow through the nozzle to be based on the isentropic thermodynamic relations and the perfect gas laws. Flow across pressure shocks cannot be considered as ideal.

If we apply the principle of the conservation of energy and consider the isentropic flow of a perfect gas, the nozzle exhaust velocity is

$$V_{\text{exhaust}} = \sqrt{\frac{2g\gamma}{\gamma-1} \frac{\bar{R}}{RT_c} \left[1 - \frac{P_{\text{exhaust}}}{P_c} \right]^{(\gamma-1)/\gamma}} \quad (5-8)$$

where g is gravitational acceleration (32.2 ft/sec²), γ is the ratio of the gas constant pressure specific heat to constant volume specific heat, \bar{R} is the gas constant (R_u/\bar{m}), T_c is the temperature of the gas in the combustion chamber, P_c is the pressure of the gas in the combustion chamber, and P_{exhaust} is the pressure of the exhaust gas. For optimum expansion, the pressure of the exhaust gas will be equal to the atmospheric pressure. If the exhaust gas pressure is greater than atmospheric, the gas will be underexpanded (because the exhaust flow area is too small) and expansion will continue to take place outside the nozzle. The relationship between the area ratio (exhaust to throat) and pressure ratio (chamber to exhaust) for ideal expansion in the divergent section of a supersonic nozzle is shown in Fig. 5-4. If, for a given area ratio, the exhaust pressure (determined from Fig. 5-4) is less than atmospheric, the gas will be overexpanded (as the exhaust flow area is too large) resulting in shock waves and flow separation within the divergent section of the nozzle. When the gas is overexpanded, a portion of the divergent section of the nozzle is unused and, therefore, is unnecessary weight. The decrease of atmospheric pressure with altitude

NOTE: THE INFORMATION ON THIS FIGURE IS NOT MEANT FOR DESIGN USE BUT IS INTENDED ONLY FOR A QUALITATIVE DESCRIPTION OF NOZZLE FLOW PHENOMENA

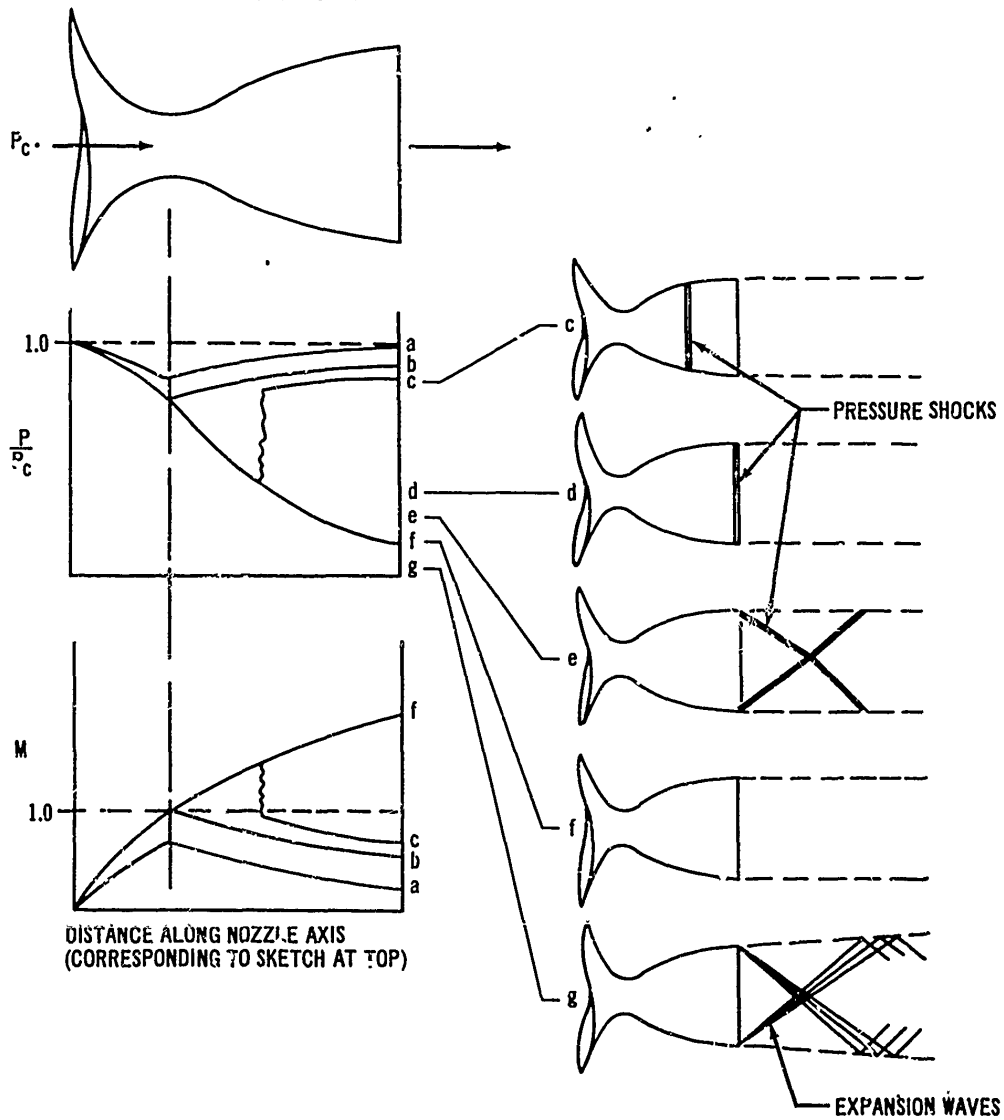


Figure 5-3. Flow Through a Supersonic (DeLaval) Nozzle

AMCP 706-280

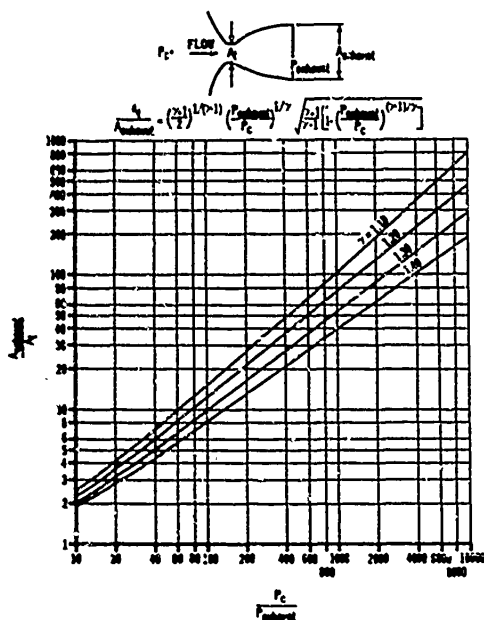


Figure 5-4. Supersonic Nozzle Area Expansion Ratios

makes impossible the design of a nozzle that will always operate at optimum expansion. Consequently, the nozzle is generally designed to operate at optimum expansion at sea-level (or at a relatively low altitude) and thus to operate over-expanded at higher altitudes. A maximum exhaust velocity exists for a given combustion gas and combustion temperature. When the ratio of P_{exhaust} / P_c is zero ($P_{\text{exhaust}} = 0$), as would be the case for optimum expansion in a vacuum, the velocity is:

$$(V_{\text{exhaust}})_{\text{max}} = \sqrt{\frac{2\gamma}{\gamma-1} \bar{R} T_c} \quad (5-9)$$

Nozzle pressure ratios, for rockets of the class discussed in this handbook, are sufficient to produce a sonic velocity in the throat. The sonic velocity is equal to

$$V_t = \sqrt{\frac{2\gamma}{\gamma+1} \bar{R} T_c} \quad (5-10)$$

If we use the continuity equation, then, for steady flow, the mass flow rate through the nozzle is

$$\dot{m} = \frac{A_t P_c \gamma \sqrt{\frac{2}{\gamma+1}}^{(\gamma+1)/(\gamma-1)}}{\sqrt{\gamma \bar{R} T_c}} \quad (5-11)$$

where A_t is the throat area and all other symbols are as defined previously.

Under the conditions of adiabatic isentropic flow, the temperature at any axial location x in the nozzle is

$$T_x = T_c - \frac{V_x^2}{1556gC_p} \quad (5-12)$$

where V_x is the velocity at location x , and C_p is the constant-pressure specific heat of the gas. The relationships between the pressure, temperature, and density in the combustion chamber and location x are

$$\frac{T_c}{T_x} = \left(\frac{P_c}{P_x}\right)^{\frac{\gamma-1}{\gamma}} = \left(\frac{\rho_c}{\rho_x}\right)^{\gamma-1} \quad (5-13)$$

The pressure, temperature, and density at any location x are related according to the perfect gas law as

$$P_x = \rho_x \bar{R} T_x \quad (5-14)$$

Substituting Eqs. 5-8 and 5-11 into Eq. 5-1 yields the following expression for rocket thrust:

$$F = A_t P_c \sqrt{\frac{2\gamma^2}{\gamma-1} \left(\frac{2}{\gamma+1}\right)^{(\gamma-1)/(\gamma-1)}} \left[1 - \left(\frac{P_{\text{exhaust}}}{P_c}\right)^{(\gamma-1)/\gamma} \right] + (P_{\text{exhaust}} - P_{\text{atmosphere}}) A_{\text{exhaust}} \quad (5-15)$$

The thrust coefficient C_F is defined as:

$$C_F = \frac{A_t P_c \sqrt{\frac{2\gamma^2}{\gamma-1} \left(\frac{2}{\gamma+1}\right)^{(\gamma-1)/(\gamma-1)}} \left[1 - \left(\frac{P_{\text{exhaust}}}{P_c}\right)^{(\gamma-1)/\gamma} \right] + \frac{(P_{\text{exhaust}} - P_{\text{atmosphere}}) A_{\text{exhaust}}}{A_t}}{P_c} \quad (5-16)$$

Thus,

$$F = C_F A_t P_c \quad (5-17)$$

The thrust coefficient is shown graphically in Fig. 5-5 (A) and (B).

5-2.1.2 Real Flow

In real nozzles, friction is present, heat is transferred; flow may be unsteady; flow and gas properties across sections of the nozzle are nonuniform; flow is nonaxial, equilibrium shifts in the nozzle; and the gas is nonhomogeneous and imperfect. An empirically derived correction factor is generally used to account for all deviations from the ideal flow performance.

Reference 1 presents indications of the magnitude of the deviations from ideal conditions. The velocity, discharge, and thrust correction factors account for friction effects, heat transfer, imperfect gases, nonaxial flow, nonuniformity of the gases, and nonuniformity of the flow distribution. The velocity correction factor ζ_v is the ratio of actual exhaust velocity to ideal exhaust velocity, and ranges between 0.85 and 0.98, with an average of 0.92. The discharge correction factor ζ_d is the ratio of the actual mass flow rate to the ideal mass flow rate, and ranges between 0.98 and 1.15, with an average of 1.04. The thrust correction factor ζ_f is the ratio of actual thrust to ideal thrust, and ranges between 0.92 and 1.0, with an average of 0.96. The correction factors are related as follows:

$$\zeta_f = \zeta_v \zeta_d \quad (5-18)$$

The average values of the correction factors indicated above are recommended for preliminary design. In advanced design, it will be necessary to consider chemical equilibrium shifts through the nozzle, gas property variations across sections of the nozzle, and other effects treated only as averages in this handbook.

For a more detailed study of flow in nozzles, consult References 1 and 2.

5-2.2 NOZZLE CONTOURS

The design of the optimum nozzle contour requires complex analyses utilizing high-speed digi-

tal computers as outlined in Reference 3. In general, the contour of the divergent section is critical. The primary requirement on the convergent and throat sections is that they be well rounded to avoid disturbances in the flow.

For ease of manufacture and design, the use of a conical divergent section is often desirable. The cone half angle of such a section, according to Reference 4, should be approximately 9 deg to obtain maximum thrust. Since the nozzle should be as short as possible to reduce weight, a cone half angle as large as 19 deg can be used with only a 2 percent reduction in thrust. To prevent flow separation, angles greater than 18 deg should be avoided. The nozzle exit should be manufactured with a sharp edge to prevent overexpansion and flow separation.

The thrust may be increased by roughly 1 percent by using a parabolic instead of a conical divergent section. A method of approximating the optimum parabolic contour is presented in Reference 4.

5-2.3 NOZZLE EROSION

The high-velocity gases passing through the nozzle contain solid particles that erode the inner surfaces of the nozzle. Erosion at the nozzle throat is particularly serious since the flow area is increased, which alters the combustion chamber pressure, mass flow rate, velocities, and, consequently, the rocket performance. Erosion may be controlled for short durations through use of protective coatings such as chrome plating, or for longer durations by using ceramic or graphite inserts.

5-3 PROPELLANTS

5-3.1 GRAIN

The body or mass of the solid propellant, which is formed by casting, molding, or extrusion, is called the grain. It is a specific chemical composition that sustains combustion. The grain, when it is properly designed, burns at a uniform rate in a direction normal to the burning surface. Burning may be prevented on surfaces by employing inhibitors that are chemically inert substances.

AMCP 106-280

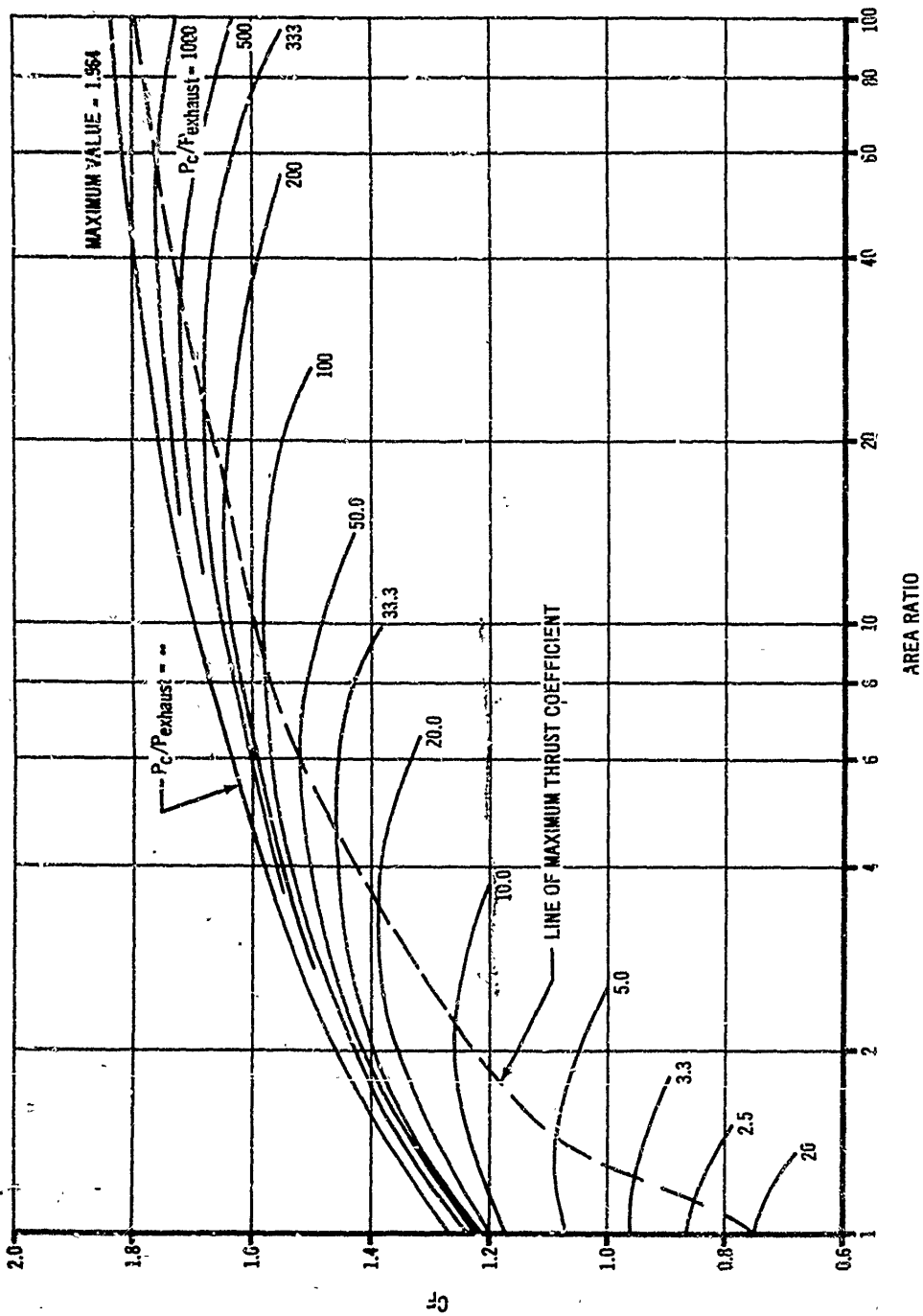


Figure 5-5(A). Thrust Coefficient Versus Area Ratio for $\gamma = 1.3$

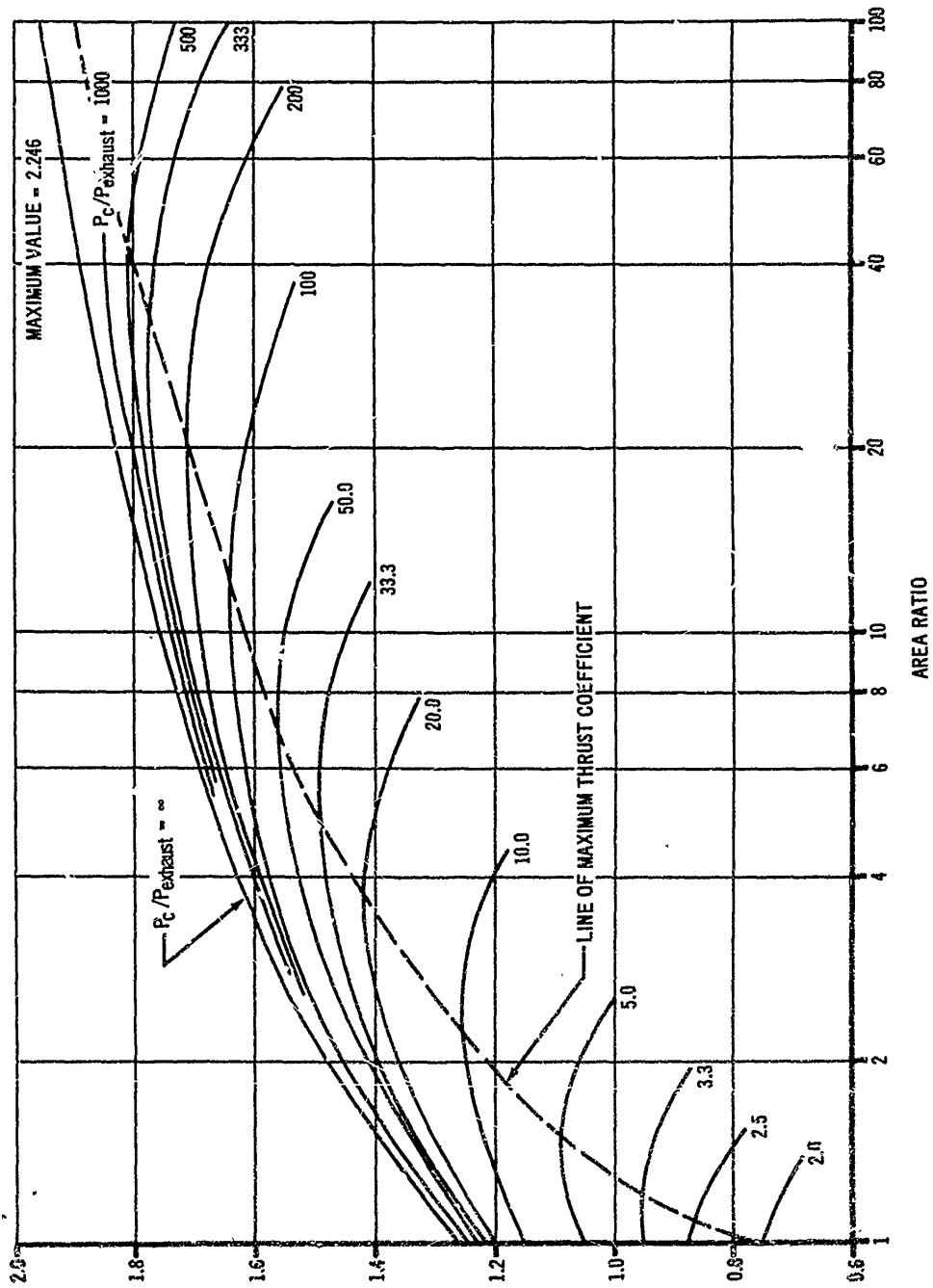


Figure 5-5(B). Thrust Coefficient Versus Area Ratio for $\gamma = 1.2$

AMCP 706-280

The burning is termed restricted or unrestricted, depending upon whether inhibitors are used or not. The geometric configuration of the grain determines the burning area and, thus, the chamber pressure and thrust for a given chamber and nozzle design. The burning characteristics are termed progressive, neutral, or regressive, depending upon whether the burning area increases, remains constant, or decreases with time, respectively.

3-3.1.1 Chemical Compositions

Solid propellants are classified as composite when made up of an oxidizer and fuel, or as double-base when made up of unstable chemical compounds, each a self-sufficient combustible. The term double-base refers to the common approach of combining two of the unstable compounds in a colloid. Additional ingredients may be added to the grain for strength, heat transfer characteristics, catalysis, chemical stability, reduction in temperature sensitivity, and ease of processing.

The oxidizers generally employed in composite propellants are the perchlorates and inorganic nitrates. Sodium, potassium, magnesium, and ammonium perchlorates, and sodium, potassium, and ammonium nitrates are the most common. The reaction of the perchlorates with the fuel produces chlorine products that are toxic and corrosive, such as hydrogen chloride. Ammonium and potassium perchlorate are useful in situations where the propellant is exposed to moisture since these perchlorates are only slightly soluble in water. Potassium and sodium nitrates produce smoke, whereas ammonium nitrate is smokeless and nontoxic but has a low oxidizing potential.

The organic fuels generally employed in composite propellants are asphalt, synthetic rubbers, and plastics. Oil must be added to asphalt fuels to make them less brittle. The addition of oil, however, makes the asphalt soft and subject to deformations at higher storage temperatures. The plastics used are thermosetting (such as phenol formaldehyde) or non-thermosetting (such as styrene). The rubber fuels are especially useful where the propellant is subjected to an environment with a wide temperature range.

The compounds generally employed in double-base propellants are the organic nitrates and aromatic

nitro compounds. The most common nitrates are glycerol trinitrate (nitroglycerin), diethyleneglycol dinitrate (DEGN), and cellulose nitrate (nitrocellulose). The most common nitro compounds are ammonium picrate and trinitrotoluene (TNT).

The preceding discussion is only a cursory review of some of the propellants employed in solid rockets and some of their salient characteristics. For a more detailed discussion of solid propellants, see References 4, 5, 9, 10, and 11.

3-3.1.2 Configuration Geometry

The design of the grain configuration must be based primarily on the required thrust history but must also consider strength, heat transfer, erosion, and missile size requirements. An infinite series of thrust histories can be attained by variations in propellant compositions, grain geometries, inhibitor locations, and grain combinations (when using more than one grain). Complex thrust histories require solution on digital computers. Examples of some typical grain cross sections are shown in Fig. 5-6.

For simple cylindrical grain configurations, the burning will be progressive, if restricted to internal cylindrical surfaces (i.e.; longitudinal ports or port); neutral, if restricted to the cylinder end or allowed on both internal and external cylindrical surfaces; and regressive, if restricted to external cylindrical surfaces. Other simple geometries are the cruciform which burns regressively, and the rod and tube (burning on inside of tube and outside of rod) which burn neutrally. Burning will also be neutral if restricted to a star-shaped port with a periphery equal to the circumference of the outside of the cylindrical grain. Examples of the installations of some typical grains are shown in Fig. 5-7.

For some configurations, especially the internal star design mentioned above, not all of the grain will be burned. That portion remaining is known as "slivers" and represents added weight to the rocket.

It is desirable to bond the grain to the combustion chamber case; this acts as thermal insulation, allowing thinner and lighter case walls. Burning on external surfaces subjects the case walls to severe heating, requiring use of insulation or heavier walls.

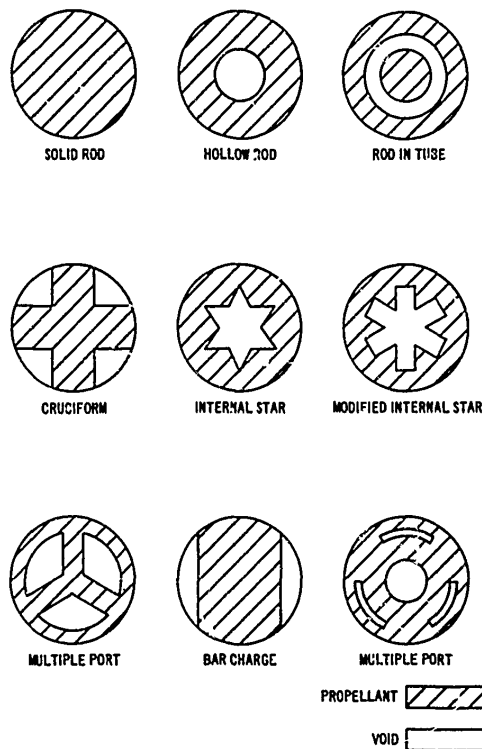


Figure 5-6. Examples of Grain Cross-Sections

Combustion gases formed at the forward sections of perforated grains must pass across the aft grain surfaces to reach the nozzle. It is desirable to keep passages through the grain large enough so that gas velocities will be low and erosion effects on the grain surface will be reduced. Erosion will be discussed further in Par. 5-3.1.4.

For a more complete discussion of grain configuration design, see References 6, 7, 9, 10, and 11.

5-3.1.3 Burning Rate

The burning rate is the velocity at which the grain is consumed in the direction normal to the burning surface. The burning rate is generally determined empirically and presented in literature supplied by the rocket motor manufacturer.

The following two equations approximate the burning rate:

$$r = a_1 P_c^n \quad (5-19a)$$

or

$$r = a_2 + bP_c \quad (5-19b)$$

where r is the burning rate; P_c is the combustion chamber pressure; and a_1, a_2, b , and n are empirically determined constants whose values depend on the propellant composition and initial temperature. The burning rate increases with increasing chamber pressure and grain initial temperature. Typical burning rates for the most common propellants vary between approximately 0.025 and 2.5 inches/second. The flow of high velocity gases across the grain burning surfaces increases the burning rate. This phenomenon is defined as erosion and is discussed in Par. 5-3.1.4.

The mass flow rate of propellant is related to the burning rate as follows:

$$\dot{m} = A_b \rho_g r \quad (5-20)$$

where \dot{m} is the mass flow rate, A_b is the grain burning surface area at the particular time in question, and ρ_g is the grain density.

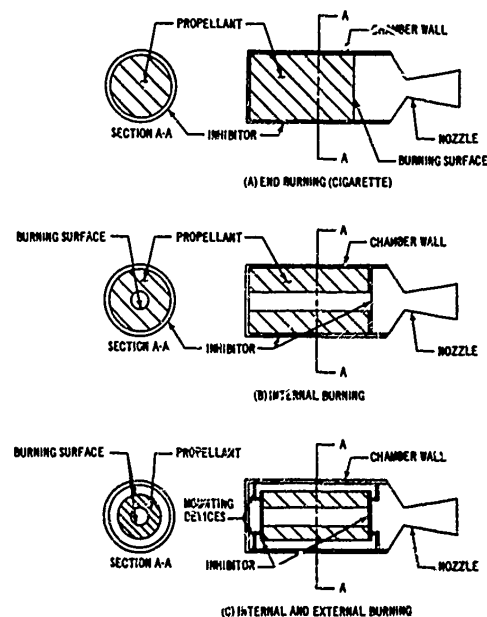


Figure 5-7. Typical Grain Installations

AMCP 706-280

5-3.1.4 Erosion

Although only the effects, and not the nature, of erosion are understood, erosion seems to be a result of the increased convection heat transfer rate from the combustion chamber gas to the grain surfaces.

Erosion must be determined experimentally. The effects on the burning rate can be evaluated from the following equation:

$$\epsilon = \frac{r_e}{r} = 1 + K \frac{\dot{m}}{\dot{m}^*} \quad (5-21)$$

where ϵ is the erosion factor, r is the burning rate without erosion, r_e is the burning rate with erosion, K is the erosion burning constant (determined experimentally), \dot{m} is the mass flow rate through the grain, and \dot{m}^* is the mass flow rate that will produce a velocity through the grain equal to the speed of sound (Mach number = 1.0).

The erosion effects may be eliminated by designing flow passages large enough to maintain low gas velocities. The effects will be greatest in the early phases of rocket engine operation and will decrease as the grain burns away and the flow passages become larger. Erosion is greater in slow burning propellants than in faster burning grains.

For a further study of erosion, see References 1 and 8.

5-3.2 IGNITION

The ignition of the solid propellant is effected by heating the propellant to its ignition temperature while maintaining the chamber pressure at a sufficient level to sustain combustion. The propellant is usually heated by hot gases produced by a pyrotechnic igniter containing a solid charge that is detonated electrically. A schematic of a typical igniter is shown in Figure 5-8. To build up the pressure in the chamber during ignition, it is sometimes necessary to install a nozzle closure that will rupture when the desired pressure is reached.

The igniter should be positioned to expose the maximum amount of grain surface to the direct impingement of the ignition gases. The most common locations for the igniter are in the forward end of the chamber, in the nozzle, or embedded in the propellants.

The exact nature of ignition is not understood and no adequate ignition theory exists. Therefore, design of ignition systems for solid propellants is based primarily on empirical data and experience.

Propellants employing ammonium nitrate are the most difficult to ignite while double-base propellants and propellants employing ammonium perchlorate as the oxidizer are the easiest to ignite. Propellant manufacturer's specifications are the best source of information for ignition data.

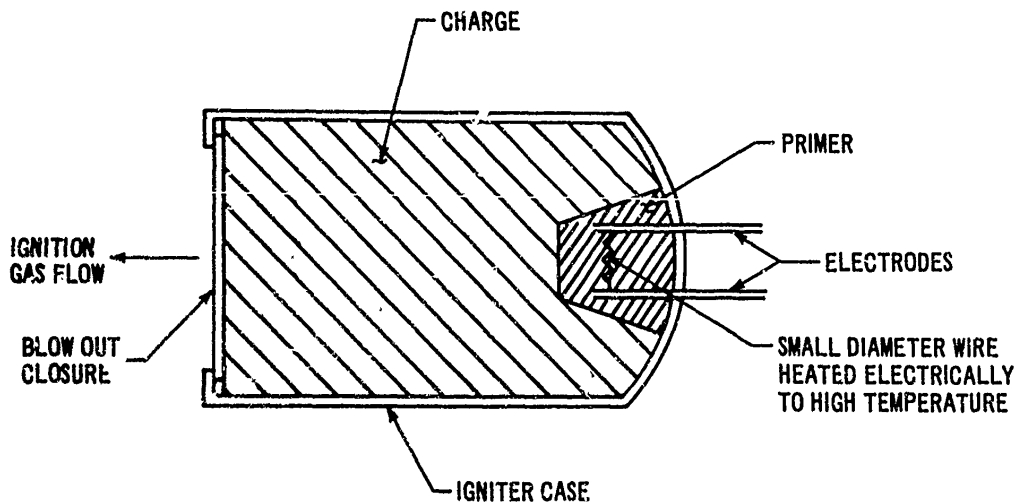


Figure 5-8. Typical Igniter

5-3.3 HANDLING

Because they are susceptible to cracking, solid propellant grains must be handled carefully. Cracks increase the burning surface area, altering the rocket performance. Chapter 6 discusses handling procedures that can be applied to the grains.

5-4 INTERNAL BALLISTICS

The combustion chamber pressure, for a given propellant composition, is a function of the ratio of the grain burning area to the nozzle throat area. Equating the mass generation rate for steady flow (Eq. 5-20) with the nozzle mass flow rate (Eq. 5-11), utilizing the burning rate equation (Eq. 5-19), and rearranging the terms, yields

$$P_c = \left(\frac{A_b}{A_t} \right)^{\frac{1}{1-n}} \left(\frac{\rho_g a_t \sqrt{g RT_c}}{\sqrt{\gamma \left(\frac{2}{\gamma+1} \right)^{(\gamma+1)/(\gamma-1)}}} \right)^{\frac{1}{1-n}} \quad (5-22)$$

when

$$k = \frac{A_b}{A_t} \quad (5-23a)$$

and

$$p = \left(\frac{\rho_g a_t \sqrt{g RT_c}}{\sqrt{\gamma \left(\frac{2}{\gamma+1} \right)^{(\gamma+1)/(\gamma-1)}}} \right)^{\frac{1}{1-n}} \quad (5-23b)$$

then

$$P_c = p k^{\frac{1}{1-n}} \quad (5-24)$$

where P_c is the combustion chamber pressure, A_b is the grain burning area, A_t is the nozzle throat area, ρ_g is the density of the grain, a_t and n are constants from the burning rate equation (Eq. 5-19), R is the gas constant, T_c is the temperature of the gas in the combustion chamber, g is the gravitational constant, and γ is the ratio of the constant-pressure specific heat of the gas to its constant-volume specific heat.

The evaluation of the combustion chamber gas temperature requires a detailed analysis of the chemical reaction, product composition, and product quantities. Equating the heat of reaction and the summation of the change of each of the combustion chamber products yields

$$Q_R = \sum \left[n \int_{T_o}^T (C_p)_n dT \right] \quad (5-25)$$

where Q_R is the heat of reaction at reference temperature T_o , n is the number of moles of each product formed, $(C_p)_n$ is the constant-pressure molal specific heat of each product formed, and $\int_{T_o}^T (C_p)_n dT$ is the enthalpy change of the product formed associated with the enthalpy change from reference temperature T_o to combustion chamber gas temperature T . The heat of reaction is the algebraic difference between the heat of formation of the products and the heat of formation of the reactants. The heat of formation and the constant-pressure molal specific heat of the various compounds are available in standard chemical handbooks. A more detailed discussion of the evaluation of chamber gas temperatures is presented in Reference 1. Rocket motor manufacturer's specifications and performance reports should be consulted to estimate gas temperatures.

Other factors associated with internal ballistics (such as burning rate, erosion, grain configuration, and ignition) were discussed under Paragraph 5-3. Consult Reference 8 for a further discussion of internal ballistics.

5-5 SCALING OF SOLID PROPELLANT MOTORS

The performance characteristics of solid propellant rocket motors may be scaled within certain limitations. This means that performance data available for a basic motor may be modified and applied to a similar motor that differs from the basic in size, thrust level, total impulse, and propellant composition.

When all dimensions are varied from the basic motor dimensions by the same scale factor

$$F_{scaled} = f^2 F_{basic} \quad (5-26)$$

AMCP 706-280

$$\left(\frac{F}{W_{\text{motor}}}\right)_{\text{scaled}} = \frac{1}{f} \left(\frac{F}{W_{\text{motor}}}\right)_{\text{basic}} \quad (5-27)$$

$$(I_{\text{total}})_{\text{scaled}} = f^3 (I_{\text{total}})_{\text{basic}} \quad (5-28)$$

and

$$(\theta_b)_{\text{scaled}} = f(\theta_b)_{\text{basic}} \quad (5-29)$$

where F is the thrust, W_{motor} is the weight of the rocket motor, I_{total} is the total impulse, f is a scale factor, and θ_b is the time required for the propellant to be consumed. In evaluating the rocket motor weight, it is assumed that the same materials and structural criteria are applied to the basic and scaled motors.

When only the length of the grain (with ends restricted) is varied from the basic by the scale factor f , and when the nozzle flow areas are adjusted to maintain the same chamber pressure as in the basic motor,

$$F_{\text{scaled}} = fF_{\text{basic}} \quad (5-30)$$

$$(A_t)_{\text{scaled}} = f(A_t)_{\text{basic}} \quad (5-31)$$

$$(A_{\text{exhaust}})_{\text{scaled}} = f(A_{\text{exhaust}})_{\text{basic}} \quad (5-32)$$

and

$$(W_{\text{motor}})_{\text{scaled}} = f(W_{\text{motor}})_{\text{basic}} \quad (5-33)$$

where A_t is the nozzle throat area, A_{exhaust} is the nozzle exhaust flow area, and all other symbols are as defined previously. If it is desirable to change the nozzle throat area by utilizing inserts while maintaining the same exhaust area as the basic nozzle,

$$F_{\text{scaled}} = f \frac{(C_F)_{\text{scaled}}}{(C_F)_{\text{basic}}} F_{\text{basic}} \quad (5-34)$$

$$(I_{\text{sp}})_{\text{scaled}} = \frac{(C_F)_{\text{scaled}}}{(C_F)_{\text{basic}}} (I_{\text{sp}})_{\text{basic}} \quad (5-35)$$

and

$$(I_{\text{total}})_{\text{scaled}} = \frac{(C_F)_{\text{scaled}}}{(C_F)_{\text{basic}}} (I_{\text{total}})_{\text{basic}} \quad (5-36)$$

where C_F is the thrust coefficient, I_{sp} is specific impulse, and all other symbols are as defined previously. The above technique is not applicable if the grain erosion effects are altered significantly.

The motor thrust level may be changed by scaling the nozzle throat area by the factor f so that

$$F_{\text{scaled}} = f^{-\frac{n}{1-n}} \frac{(C_F)_{\text{scaled}}}{(C_F)_{\text{basic}}} F_{\text{basic}} \quad (5-37)$$

$$(P_c)_{\text{scaled}} = f^{-\frac{1}{1-n}} (P_c)_{\text{basic}} \quad (5-38)$$

$$r_{\text{scaled}} = f^{-\frac{n}{1-n}} r_{\text{basic}} \quad (5-39)$$

$$(\theta_b)_{\text{scaled}} = f^{-\frac{n}{1-n}} (\theta_b)_{\text{basic}} \quad (5-40)$$

$$(I_{\text{total}})_{\text{scaled}} = \frac{(C_F)_{\text{scaled}}}{(C_F)_{\text{basic}}} (I_{\text{total}})_{\text{basic}} \quad (5-41)$$

and

$$(I_{\text{sp}})_{\text{scaled}} = \frac{(C_F)_{\text{scaled}}}{(C_F)_{\text{basic}}} (I_{\text{sp}})_{\text{basic}} \quad (5-42)$$

where P_c is the combustion chamber pressure, r is the grain burning rate, n is the exponent in the burning rate equation (Eq. 5-19), and all other symbols are as defined previously. If the grain erosion effects are significantly altered, or if the chamber pressure during burning is not constant, this technique is not applicable. The above technique requires an iterative solution because the thrust coefficient is a function of the nozzle throat area and combustion chamber pressure.

The total impulse may be changed by scaling the nozzle exhaust flow area, thus changing the expansion ratio so that

$$F_{\text{scaled}} = \frac{(C_F)_{\text{scaled}}}{(C_F)_{\text{basic}}} F_{\text{basic}} \quad (5-43)$$

$$(I_{sp})_{scaled} = \frac{(C_F)_{scaled}}{(C_F)_{basic}} (I_{sp})_{basic} \quad (5-44)$$

and

$$(I_{total})_{scaled} = \frac{(C_F)_{scaled}}{(C_F)_{basic}} (I_{total})_{basic} \quad (5-45)$$

where all symbols are as defined previously.

When the propellant composition is changed, and when it is desirable to maintain the same chamber pressure as the basic motor by changing the nozzle configuration

$$(A_t)_{scaled} = \left[\frac{P_{scaled}}{P_c} \right]^{1-n_{scaled}} \left[\frac{P_c}{P_{basic}} \right]^{1-n_{basic}} (A_t)_{basic} \quad (5-46)$$

$$(A_{exhaust})_{scaled} = \frac{(A_t)_{scaled}}{(A_t)_{basic}} (A_{exhaust})_{basic} \quad (5-47)$$

$$F_{scaled} = \frac{(A_t)_{scaled}}{(A_t)_{basic}} F_{basic} \quad (5-48)$$

$$(\theta_b)_{scaled} = \left[\frac{(a_t)_{basic}}{(a_t)_{scaled}} \right] \left[P_c \right]^{(n_{basic} - n_{scaled})} (\theta_b)_{basic} \quad (5-49)$$

where P is the constant (combustion chamber pressure parameter) in Eq. 5-23, a_t is the constant in Eq. 5-19, n_{scaled} is the new propellant exponent in Eq. 5-19, n_{basic} is the old propellant exponent in Eq. 5-19, and all other symbols are as defined previously. The above technique is only applicable if the erosion characteristics are not altered significantly and the chamber pressure does not vary significantly during burning.

When changes in the basic motor require more than one of the techniques described above, the scaling should be performed in steps. One scaling technique should be completed and all scaled characteristics computed. This new information is used to complete the next scaling technique, and so on.

Care must be exercised in scaling motors in which erosion is significant. Erosion characteristics may not scale well even when the ratio of grain internal flow area to nozzle throat area is preserved in the scaling.

5-6 TESTING

Tests must be conducted on rocket propulsion systems during the periods of development, manufacture, and qualification. These tests are usually of the following types, although additional tests may be required depending on the peculiarities of the particular system:

- Pressure proof and leak checks
- Component functional and operational checks
- Static firings
- Flight performance

In some cases it may be desirable and necessary to test only statistical samples, while in other cases every item produced must be tested. Often it is possible to test scale models—utilizing scaling techniques discussed in Par. 5-5—thus reducing the cost, the size of the test item, and the size of the test facility. Rather than formulate rigid rules for designing test programs, the test designer should exercise freedom in establishing test criteria, basing his parameters upon the information required from the test and utilizing the most economical and expeditious testing methods.

Propulsion testing will be discussed in the paragraphs which follow. For a more complete presentation and an excellent bibliography, see Reference 1.

Instrumentation is required to measure forces, flows, temperatures, pressures, structural stresses, time sequences, and all other parameters—such as acceleration and vibrations—that are of interest. Instrumentation consists basically of a pickup, a sensing element, and an indicator. Auxiliary equipment, such as electronic amplifiers or telemetering devices to transmit flight measurements to ground stations, may also be needed. The pickup is installed at the location where the value of a particular parameter is to be measured and transmits the magnitude of the parameter to the sensing elements. The sensing element, which often is integral part of the pickup, gauges the magnitude of the parameter under consideration by mechanical, electrical, or other means. The

AMCP 706-280

indicator then displays the measurements of the sensing element. The American Society of Mechanical Engineers' Power Test Codes describe various forms of instrumentation and present recommendations for their use.

Extensive and elaborate safety precautions are required, especially during the rocket development period. Although solid propellants do not present the explosive hazard exhibited by liquid propellants, personnel must be located remotely when the rocket is launched, in case of explosion or an uncontrolled flight. The ignition must be

initiated from a remote location, and the instruments must be capable of remote indication, to allow personnel to monitor and control the test in safety. Photography and television are employed extensively to observe the rocket closely during the test. For flight tests, a range must be constructed that is instrumented and is located away from inhabited areas. For long-range flight tests, it is necessary to build into the rocket a destruction system that can be activated from the ground if the trajectory should present a hazard to personnel or property.

REFERENCES

1. G. P. Sutton, *Rocket Propulsion Elements*, John Wiley and Sons, Inc., New York, 1956.
2. H. W. Liepman and A. Roshko, *Elements of Gasdynamics*, John Wiley and Sons, Inc., New York, 1957.
3. G. V. R. Rao, "Exhaust Nozzle Contour for Optimum Thrust", *Jet Propulsion* **28**, (June 1958).
4. H. H. Koelle, *Handbook of Astronautical Engineering*, McGraw-Hill Book Company, Inc., New York, 1961.
5. F. A. Warren, *Rocket Propellants*, Reinhold Publishing Corporation, New York, 1958.
6. J. M. Vogel, "A Quasi-morphological Approach to the Geometry of Changes for Solid Propellant Rockets: The Family Tree of Change Designs". *Jet Propulsion* **26**, 102, (1956).
7. L. I. Epstein, "The Design of Cylindrical Propellant Grains", *Jet Propulsion* **28**, 757, (1956).
8. R. N. Wimpers, *Internal Ballistics of Solid Fuel Rockets*, McGraw-Hill Book Company, Inc., New York, 1950.
9. AMCP 706-282, *Engineering Design Handbook, Propulsion and Propellants*.
10. AMCP 706-175, *Engineering Design Handbook, Solid Propellants, Part One*.
11. AMCP 706-176 (C), *Engineering Design Handbook, Solid Propellants, Part Two (U)*.

CHAPTER 6 STRUCTURES

LIST OF SYMBOLS

Symbol	Meaning	Symbol	Meaning
a	Linear acceleration, ft/sec ²	M_∞	Free stream Mach number, dimensionless
A	Area, ft ²	$M.S.$	Margin of Safety, dimensionless
A_r	Cross sectional area of fin at exposed root chord (Table 6-1), ft ²	n	Number of rivets
b	Fin span, ft	N	Aerodynamic normal force, lb
c	Airfoil chord length, ft	N_{Nu}	Nusselt number, dimensionless
c	Perpendicular distance from beam neutral surface, ft	N_{Pr}	Prandtl number, dimensionless
C_D	Aerodynamic drag coefficient, dimensionless	N_{Re}	Reynolds number, dimensionless
C_f	Skin friction coefficient (see Chapter 8), dimensionless	p	Pressure, lb/ft ²
$C_{N\alpha}$	Aerodynamic normal force coefficient gradient, per degree	P	Structural load (force), lb
C_p	Constant pressure specific heat, BTU/lb °R	q	Dynamic pressure, lb/ft ² ; heat transfer rate, BTU/sec
cg	Center of gravity	r	Recovery factor, dimensionless; radius, ft
cp	Center of pressure	S_{ref}	Rocket reference area, ft ²
d	Diameter, ft	t	Thickness, ft
D	Aerodynamic drag force, lb	T	Temperature, °R
E	Modulus of elasticity (Young's Modulus), lb/ft ²	U	Overall heat transfer coefficient, BTU/(sec) (ft ²) (°R)
F	Rocket thrust, lb	V	Velocity, fps
F_{12}	Radiation combined emissivity, absorptivity, and orientation factor, dimensionless	w	Width, ft
h_{is}	Inside surface heat transfer coefficient, BTU/(sec) (ft ²) (°R)	W	Weight, lb
h_{os}	Outside surface heat transfer coefficient, BTU/(sec) (ft ²) (°R)	y	Height, ft
I	Mass moment of inertia, slug-ft ² ; area moment of inertia, ft ⁴	α	Thermal radiation absorptivity, dimensionless; angle of attack, deg
k	Thermal conductivity, BTU/(sec) (ft ²) (°R/ft)	β	Angle between the rocket longitudinal axis and the vertical, deg
K	Coefficient of plate stress, dimensionless	γ	Ratio of specific heat at constant pressure to specific heat at constant volume, dimensionless
l, ℓ	Length or distance, ft	ϵ	Thermal radiation emissivity, dimensionless
ln	Natural logarithm	θ	Time, sec
m	Mass, slug	μ	Dynamic viscosity, slug/ft-sec
M	Mach number, dimensionless; bending moment in structure, ft-lb	ρ	Density, slug/ft ³ ; internal gage pressure
		σ	Stress, lb/ft ² ; Stephan-Boltzmann radiation constant, BTU/(sec) (ft ²) (°R ⁴)
		τ	Shearing stress, lb/ft ²

AMCP 706-280

6-1 GENERAL

The rocket structure provides a specific external shape, a protective envelope, and a platform for the delivery of a payload to a target. This chapter will present methods of designing a structure with minimum weight and sufficient strength to withstand ground handling and flight loads.

The strength of a structure depends on the physical and mechanical properties of the materials, and the geometric configurations of the structural members. The proportional limit, elastic limit, yield point, ultimate strength, modulus of elasticity, ductility, and hardness are the significant properties of materials for preliminary design. These properties are defined as follows:

a. Proportional limit is the maximum stress that a material can resist without deviating from the law of proportionality of stress to strain (Hooke's law).

b. Elastic limit is the maximum stress that a material can resist without permanent deformation. The proportional limit and elastic limit are often taken as the same value.

c. Yield point is the minimum stress at which the material will deform without an increase in load, and also often will deform with an abrupt decrease in load.

d. Ultimate strength is the maximum stress in a material before fracture.

e. Modulus of elasticity is the ratio of stress to strain, at stresses below the proportional limit.

f. Ductility of a material is the percent of elongation at the time of fracture in tension.

g. Hardness of a material is a measure of the resistance to scratching, abrasion, and indentation.

The physical dimensions, moment of inertia, and cross-sectional area are the significant geometric factors of the structural members.

6-2 WEIGHT AND BALANCE

6-2.1 MASS AND CENTER OF GRAVITY ESTIMATION

The mass of much of the rocket structure and many of the rocket components will not be known and must be estimated. For analysis, the rocket should be divided into sections made up of homo-

geneous materials and volumes that are easily defined. The mass of the sections may be estimated by multiplying the section volume by the material density. The volume of thin-skin sections is easily approximated by multiplying the surface area by the skin thickness.

The equations for evaluating the volumes of some typical rocket sections are presented in Table 6-1. The volume of an ogive nose cannot be so easily determined. A method of approximating the volume of an ogive was developed in Reference 1, based on the relationship between the ogive volume and volume of a cone with the same length and diameter. The equivalent cone volume can be evaluated from the nomograph in Fig. 6-1, and the ratio of ogive volume to cone volume can be obtained from Fig. 6-2. The equivalent cone surface area can be evaluated from the nomograph in Fig. 6-3, and the ratio of ogive surface area to cone surface area can be obtained from Fig. 6-4.

The location of the center of gravity of some typical rocket sections is presented in Table 6-1. For convenience these locations should be identified as rocket station numbers, i.e., distances from the nose tip. The location of the center of gravity of the complete configuration can be estimated by summing moments of the section masses about the nose tip and dividing by the total rocket mass, making sure that consistent units are used.

6-2.2 PITCH INERTIA

The rocket pitch inertia is the mass moment of inertia of the complete configuration with respect to the pitch axis, which passes through the center of gravity and is perpendicular to the longitudinal axis of symmetry. For analysis the rocket should be divided, as before, into sections made up of homogeneous materials and easily defined geometries. Then the pitch inertia of the complete configuration is the algebraic sum of the individual section moments of inertia with respect to the pitch axis. For convenience, the section moments of inertia may be evaluated with respect to an axis through the section center of gravity and transferred to the parallel pitch axis by the following formula:

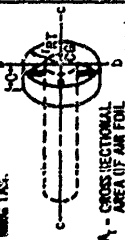
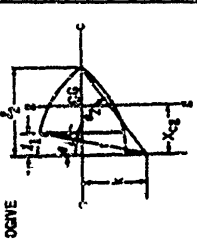
$$I_{CG} = \bar{I} + ml^2 \quad (6-1)$$

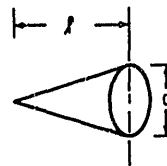
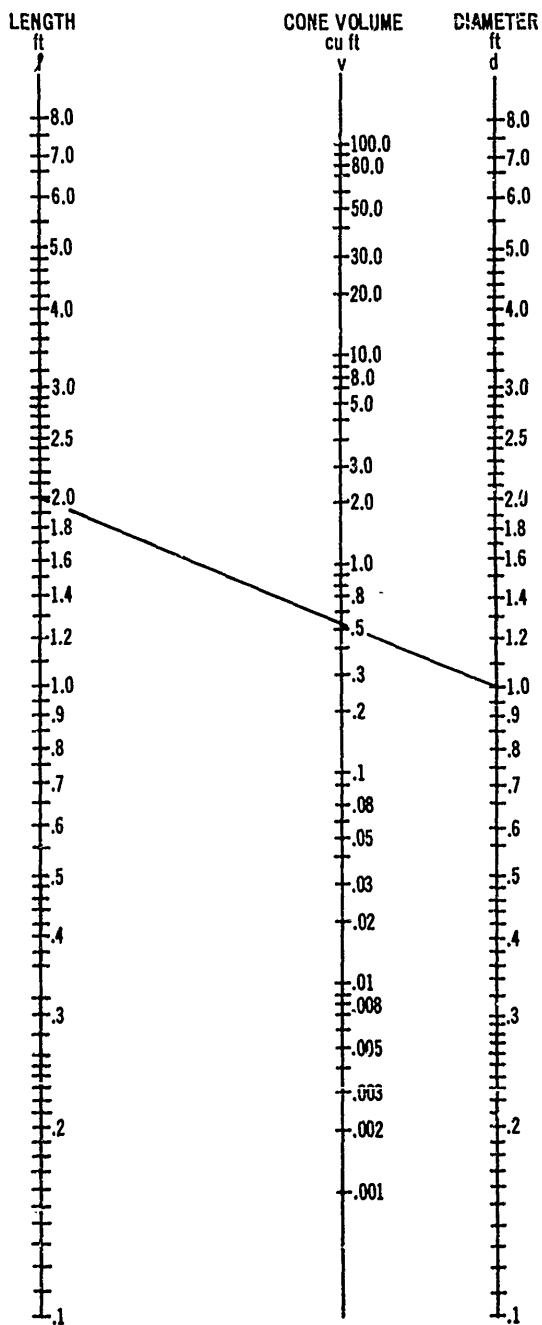
TABLE G-1. GEOMETRICAL PROPERTIES OF TYPICAL ROCKET SECTIONS

FIGURE	VOLUME & SURFACE AREA	CENTER OF GRAVITY	MOMENT OF INERTIA
<p>CONE</p>	<p>SURFACE AREA = $\pi r_B \sqrt{r_B^2 + h^2}$</p> <p>VOLUME = $\frac{\pi r_B^2 h}{3}$</p>	<p>$X_{CG} = \frac{h}{4}$</p>	<p>$I_g = \frac{2\pi}{20} (r_B^2 + \frac{r_B^4}{4})$</p> <p>$I_c = \frac{3\pi r_B^2}{10}$</p>
<p>CONE FRUSTUM</p>	<p>SURFACE AREA = $\pi(r_B + r_{B1}) \sqrt{h^2 + (r_B - r_{B1})^2}$</p> <p>VOLUME = $\frac{\pi h}{3} (r_B^2 + r_B r_{B1} + r_{B1}^2)$</p>	<p>$X_{CG} = \frac{h}{4} \frac{(r_B^2 + 2r_B r_{B1} + 3r_{B1}^2)}{(r_B^2 + r_B r_{B1} + r_{B1}^2)}$</p>	<p>I_g' Treat as the difference between two cones</p> <p>$I_g = \frac{3\pi}{10} (r_B^5 - r_{B1}^5)$</p> <p>$I_c = \frac{3\pi}{10} (r_B^3 - r_{B1}^3)$</p>
<p>PARABOLOID OF REVOLUTION</p>	<p>SURFACE AREA = $\frac{4\pi h}{3} \left[\left(\frac{r_B^2 + r_{B1}^2}{2} \right)^{3/2} - \left(\frac{r_B r_{B1}}{2} \right)^{3/2} \right]$</p> <p>VOLUME = $\frac{\pi h r_{B1}^2}{2}$</p>	<p>$X_{CG} = \frac{h}{3}$</p>	<p>$I_g = \frac{\pi}{18} (3r_2^2 + r_1^2)$</p> <p>$I_c = \frac{\pi r_1^2}{3}$</p>
<p>FRUSTUM OF PARABOLOID OF REVOLUTION</p>	<p>SURFACE AREA: Treat as the difference between two paraboloids</p> <p>VOLUME = $\frac{\pi h}{2} (r_2^2 + r_{B1}^2)$</p>	<p>$X_{CG} = \frac{h}{3} \frac{(r_1^2(r_1^4 - r_2^4) - r_2^4)}{(r_1^2 - r_2^2)(r_1^4 - r_2^4)}$</p>	<p>I_g' Treat as the difference between two paraboloids</p> <p>$I_c = \frac{\pi}{3} \left(\frac{r_1^4 + r_1^2 r_2^2 + r_2^4}{r_1^2 + r_2^2} \right)$</p>
<p>CYLINDER</p>	<p>SURFACE AREA (OUTSIDE) = $2\pi r l$</p> <p>VOLUME = $(\pi r^2 - \pi r_2^2) l$</p>	<p>$X_{CG} = \frac{l}{2}$</p>	<p>$I_g = \frac{\pi}{12} (3r_1^2 + 3r_2^2 + l^2)$</p> <p>$I_c = \frac{\pi}{2} (r_1^2 + r_2^4)$</p>
<p>FINS</p>	<p>SURFACE AREA = Function of fin cross section</p> <p>VOLUME = $\frac{A \cdot b}{4} \left(1 + \frac{c}{c_1} \right)$ constant thickness along span</p>	<p>$X_{CG} = \frac{b}{6} \left(\frac{1 + 2 \frac{c}{c_1}}{1 + \frac{c}{c_1}} + \frac{d}{c} \right)$</p> <p>At Centroid of Sectional Area</p>	<p>$I_g \approx 0$ (when compared to fin pitch inertia)</p> <p>$I_c = \frac{\pi}{4} \left[\frac{b^2}{6} \left(\frac{1 + 3 \frac{c}{c_1}}{1 + \frac{c}{c_1}} + d^2 \right) + \frac{c^2}{c_1} \right]$</p>

AMCP 706-290

TABLE 6-1. GEOMETRICAL PROPERTIES OF TYPICAL ROCKET SECTIONS (CON)

<p>FIGURE 6-1 </p> <p>A_1 - CROSS SECTIONAL AREA OF AIR FOIL</p>	<p>VOLUME & SURFACE AREA SURFACE AREA $\approx 4\pi R^2$ VOLUME $\approx 2A_1 L$</p>	<p>CENTERS OF GRAVITY SECTIONAL AREA CENTROID PROJECTED ON LONGITUDINAL AXIS OF SYMMETRY (C-C)</p>	<p>MOMENT OF INERTIA $I_x \approx 0$ $I_y \approx \pi R^4$</p>
<p>FIGURE 6-2 </p> <p>P - MATERIAL DENSITY</p>	<p>SURFACE AREA \approx See Figures 6-4 & 6-5 VOLUME \approx See Figures 6-2 & 6-3</p>	$x_{CG} = \frac{\frac{1}{2} (r_1^2 + r_2^2) (L_2 - L_1) - \frac{(L_2^3 - L_1^3)}{3}}{(L_2^2 - L_1^2) (L_2 - L_1) - \frac{L_2^3 - L_1^3}{3}}$ $+ \frac{2k}{3} \left[\frac{(L_2^3 - L_1^3)^{3/2}}{2} - (L_2 - L_1)^{3/2} \right]$ $- k \left[\frac{(L_2^2 - L_1^2)^{3/2}}{2} - \frac{(L_2 - L_1)^{3/2}}{2} \right] \left[\frac{L_2 + L_1}{2} - \theta_1 \right]$	$I_x = \pi R^4 \left\{ \frac{1}{6} (L_2^4 + 6kL_2^2 + k^2) (L_2 - L_1) \right.$ $+ \frac{1}{6} (L_2^4 - 6kL_2^2 + k^2) (L_2^3 - L_1^3) - \frac{2}{20} (L_2^5 - L_1^5)$ $+ k(L_2(L_2^2 - L_1^2))^{3/2} - L_1(L_2^2 - L_1^2)^{3/2}$ $- (L_2 - L_1) \left[\frac{1}{2} (L_2^2 - L_1^2)^{3/2} + \frac{L_2^2}{2} \theta_2 \right.$ $\left. - \frac{3}{2} (L_2^2 - L_1^2)^{3/2} \theta_1 \right\} - \pi R^2 \theta_2^2$
			$I_y = \frac{\pi R^2}{2} \left\{ (L_2^4 + 6kL_2^2 + k^2) (L_2 - L_1) \right.$ $- \frac{1}{3} (L_2^4 + 6kL_2^2 + k^2) (L_2^3 - L_1^3) + \frac{1}{3} (L_2^5 - L_1^5)$ $- k(L_2(L_2^2 - L_1^2))^{3/2} - L_1(L_2^2 - L_1^2)^{3/2}$ $- (6k^2 - 3\pi R^2) \left[\frac{L_2}{2} (L_2^2 - L_1^2)^{1/2} + \frac{L_2^2}{2} \theta_2 \right.$ $\left. - \frac{1}{2} (L_2 - L_1)^{1/2} - \frac{L_2^2}{2} \theta_1 \right\}$



EXAMPLE

l - LENGTH - 2.0 ft
 d - DIAMETER - 1.0 ft
 ∴ VOLUME - .524 cu ft

NOTE: IF CONE DIMENSIONS ARE OUTSIDE THE RANGE OF THIS FIGURE, CALCULATE VOLUME AS:

$$V = \frac{\pi d^2 l}{12}$$

Figure 6-1. Volumes of Cones

AMCP 708-280

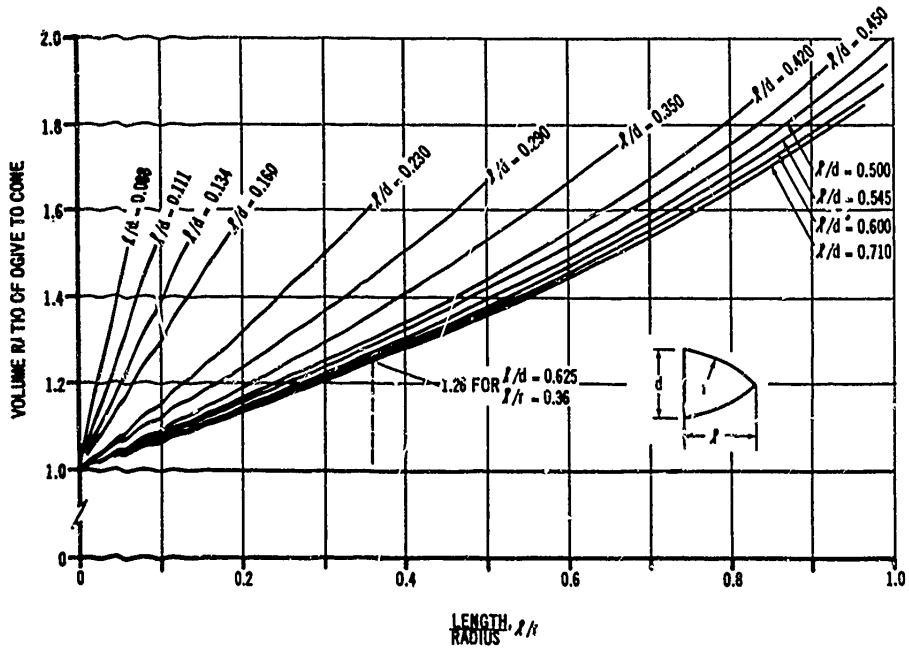


Figure 6-2(A). Ratio of Volume of Ogive to Cone Versus l/r at Various l/d 's

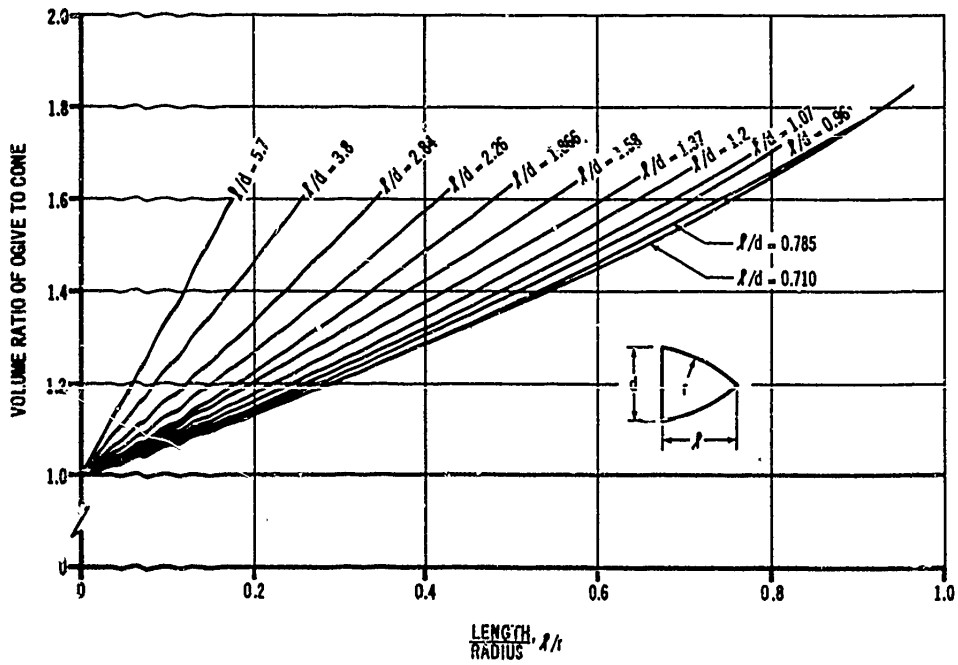


Figure 6-2(B). Ratio of Volume of Ogive to Cone Versus l/r at Various l/d 's

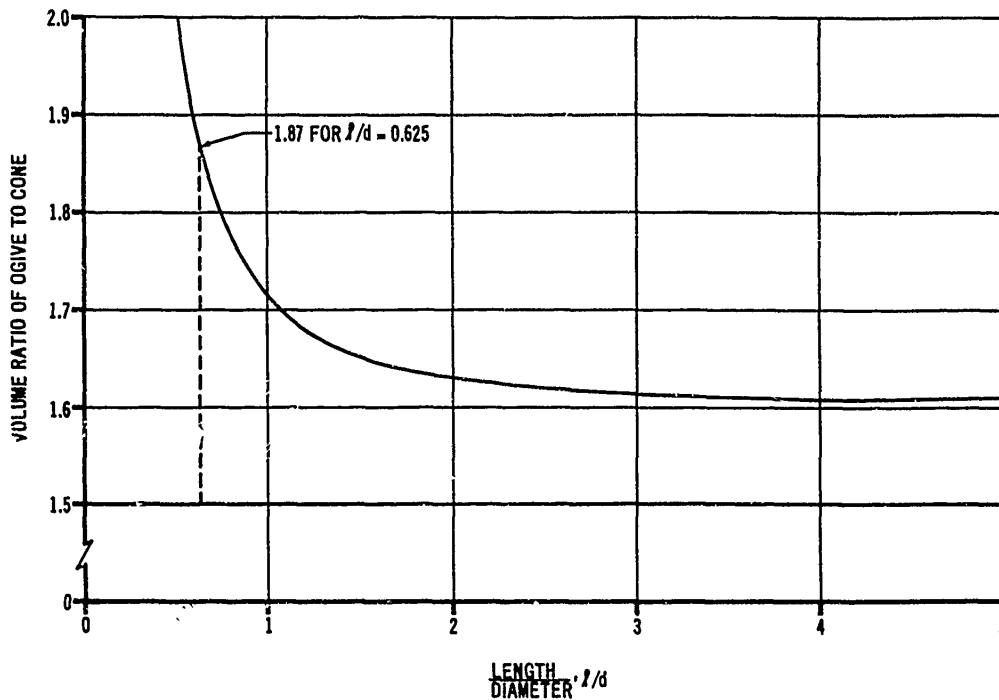


Figure 6-2(C). Ratio of Volume of Tangent Ogive to Cone With Identical l/d

where I_{CG} is the section moment of inertia with respect to the pitch axis, \bar{I} is the section moment of inertia with respect to the local axis that is parallel to the pitch axis, m is the mass of the section, and l is the distance between axes.

The moments of inertia of typical rocket sections can be determined from Table 6-1. The pitch moments of inertia of fins and ring tails may be approximated for preliminary design by considering the fin mass to be concentrated at the rocket base. Then,

$$I_{CG} = ml^2 \quad (6-2)$$

where m is the mass of the fins and l is the distance between the rocket center of gravity and the base. The error due to this approximation will be less than 4 percent if the fin root chord is less than one-third, and the span less than two-thirds, of the distance between the rocket base and the rocket center of gravity.

The moments of inertia are not explicitly defined in Table 6-1 for rocket sections that are partially hollow and/or made up of composite

materials. The moments of inertia of these sections can be evaluated by employing the principle that, with respect to a common axis, the total moment of inertia is equal to the algebraic sum of the moments of inertia of the parts. For example, the total moment of inertia of a cone with a hollow cylindrical center is equal to the moment of inertia of the solid cone less the moment of inertia of the cylindrical portion.

6-2.3 ROLL INERTIA

The rocket roll inertia is the mass moment of inertia of the complete rocket configuration with respect to the longitudinal axis of symmetry. For analysis, the rocket should be divided, as before, into sections made up of homogeneous materials and easily defined geometries. Then the roll inertia of the complete configuration is the algebraic sum of the individual section moments of inertia with respect to the longitudinal axis.

AI-CP 708-280

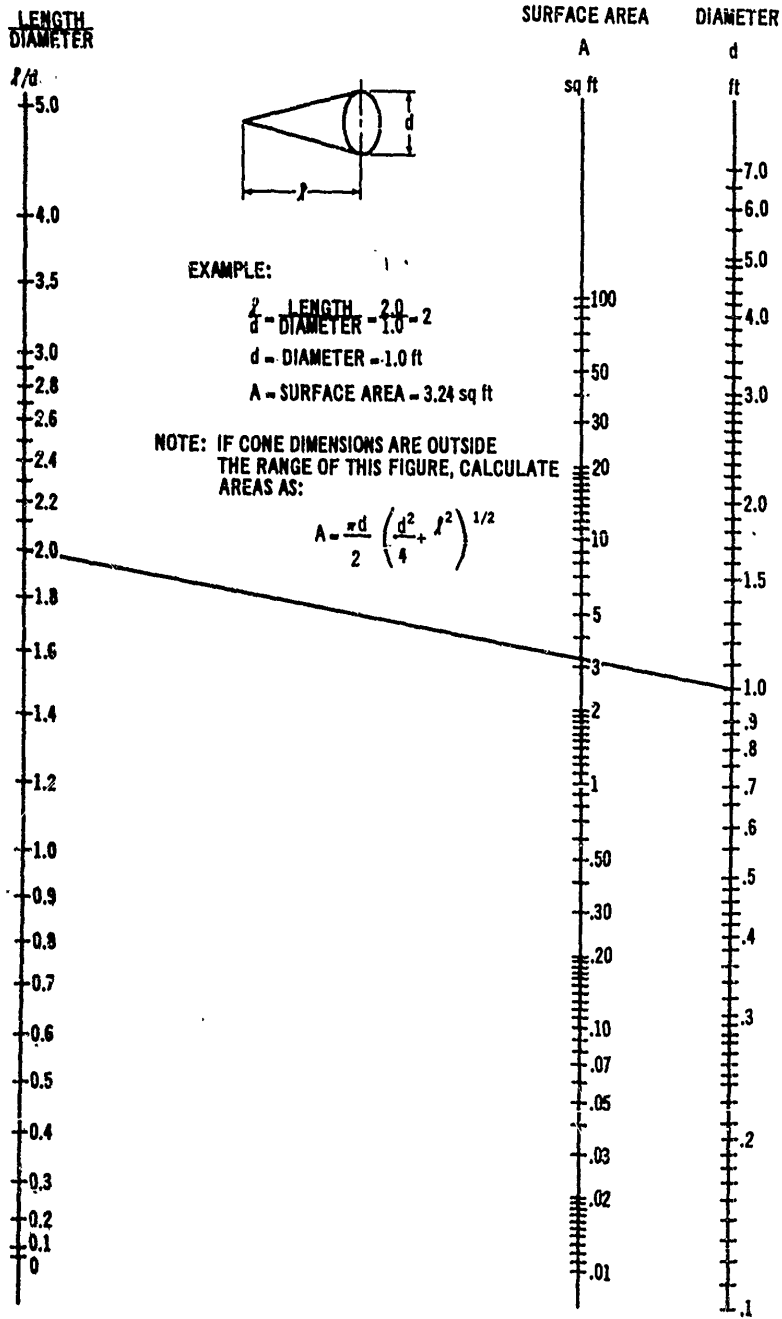


Figure 6-3. Surface Area of Cones

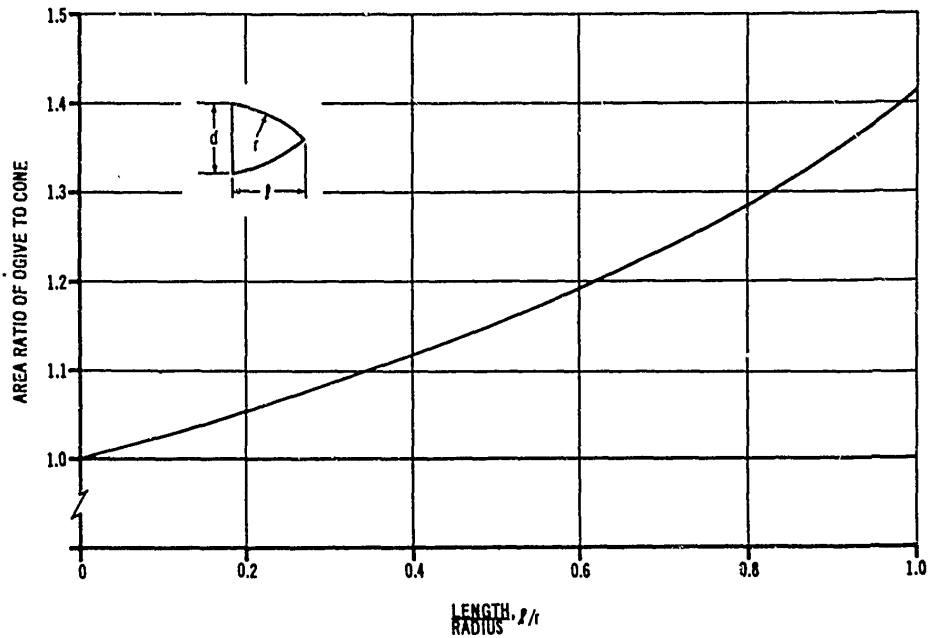


Figure 6-4(A). Ratio of Area of Ogive to Cone With Identical Q/d Versus Q/r for Q/d Less Than or Equal to 0.5

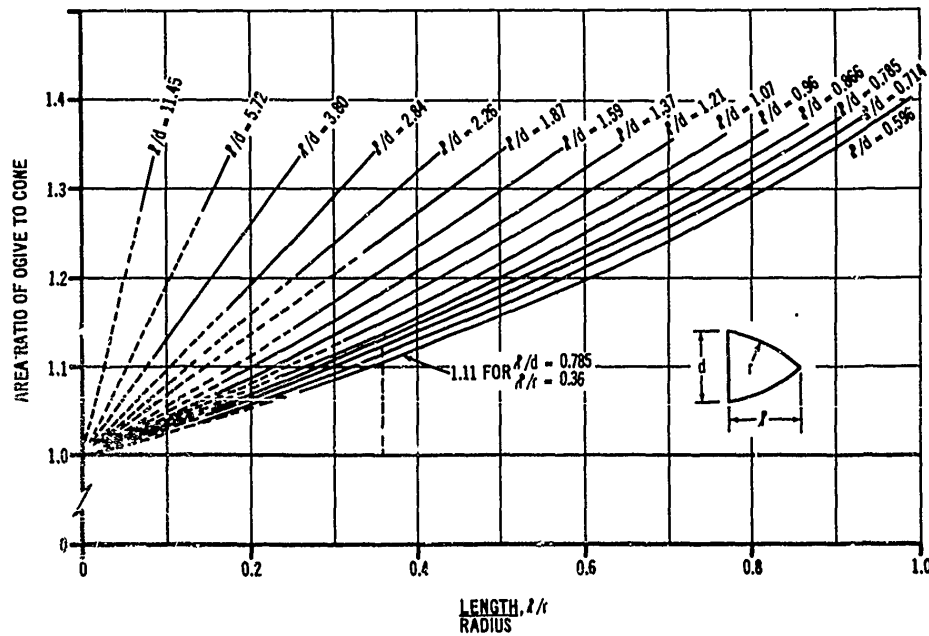


Figure 6-4(B). Ratio of Area of Ogive to Cone Versus Q/r at Various Q/d 's

AMCP 708-280

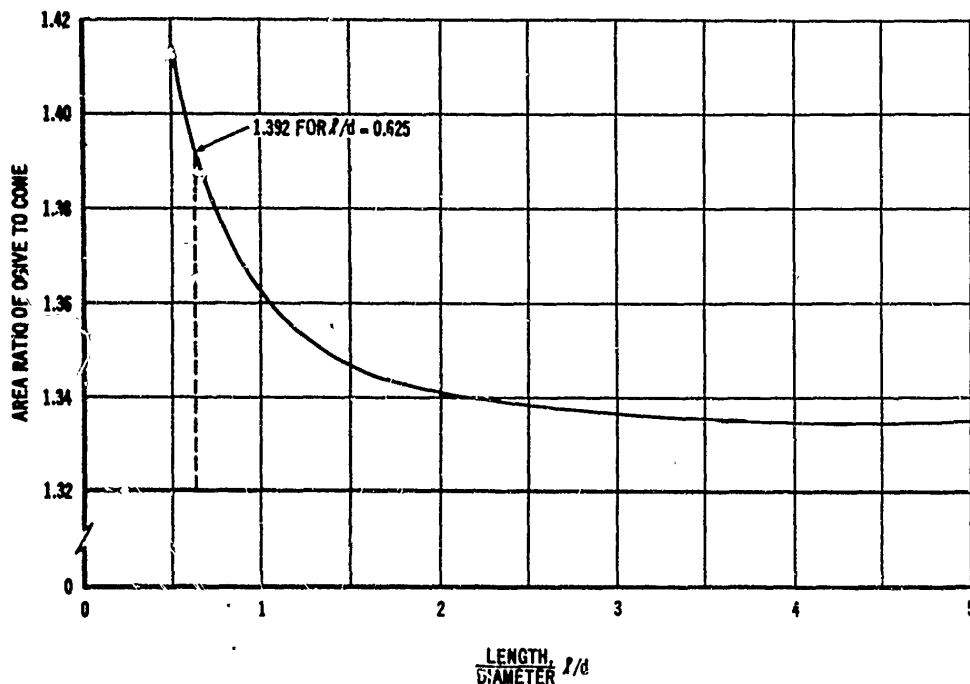


Figure 6-4(C). Ratio of Area of Tangent Ogive to Cone With Identical Q/d

The moments of inertia of typical rocket sections can be determined from Fig. 6-1. The moments of inertia are not explicitly defined in Table 6-1 for rocket sections that are partially hollow and/or made up of a composite of materials but may be evaluated as outlined in Par. 6-2.2 by algebraic summation of the moments of inertia of the parts.

6-3 LOADS

6-3.1 TRANSPORT AND HANDLING LOADS

The preliminary design phase must consider flight loads in conjunction with transportation loads to insure that one does not predominate the other. However, flight loads are generally the most severe since adequate containers containing shock mounts can be designed to account for expected or unexpected transportation loads.

During transportation the rocket package will be subjected to vibrations, shocks, variable temperature environments, and moisture. Reference

2 presents packaging techniques for shipment. The loads during shipment by truck, ship, railway, or airplane are specified in References 3, 4, 5, 6, 7, 8, and 17. Truck transportation subjects the rocket to the most severe vibration and shock loads, and airplane transportation to the least severe, under normal conditions.

The human factor involved in handling makes the problem of specifying loads very difficult. In general, realistic field conditions are simulated by drop tests. Heights used for these tests vary, from three and one-half feet for twenty pound articles, to one foot for articles weighing more than one hundred pounds.

Rockets launched from air vehicles may be subjected to severe vibrations. These loads should be determined from manufacturer's performance reports for the particular vehicle involved.

In general, military specifications are available to define the design environmental conditions for a particular class of rockets. These specifications should be consulted in evaluating design loads.

6-3.2 FLIGHT LOADS

During flight the rocket will be subjected to loads from engine thrust, aerodynamic lift, aerodynamic drag, inertia of rocket mass, structural weight, and internal pressures. For structural stress analysis, the loads may be divided into axial components acting along the body longitudinal axis, bending components acting perpendicular to the body axis, and internal pressure forces acting circumferentially.

The axial load component is made up of forces from the engine thrust, aerodynamic drag, inertia of the rocket mass in the axial direction, structural weight component acting along the body axis, and internal pressures. Fig. 6-5 shows a free-body diagram of the axial forces acting on a rocket in flight. The sum of these forces is zero. Therefore,

$$-am_x + F - D - W \cos \beta = 0 \quad (6-3)$$

where a is the rocket acceleration along the longitudinal axis, m_x is the rocket mass, F is the engine thrust, D is the total drag, W is the rocket weight, and β is the angle between the body longitudinal axis and the vertical. Likewise, the axial load (P_{xx}) at any plane $x-x$ is found by the formula

$$P_{xx} = am_x + D_x + W_x \cos \beta - \rho A \quad (6-4)$$

where m_x is the rocket mass forward of plane $x-x$, D_x is the total drag on the rocket forward of plane $x-x$, W_x is the weight of the rocket forward of plane $x-x$, ρ is the internal gage pressure, and A is the area of the plane perpendicular to the longitudinal axis on which the internal pressure acts.

The drag coefficient on the rocket sections can be evaluated as indicated in par. 8-3. The drag force D can then be determined as follows:

$$D = C_D q S_{ref} \quad (6-5)$$

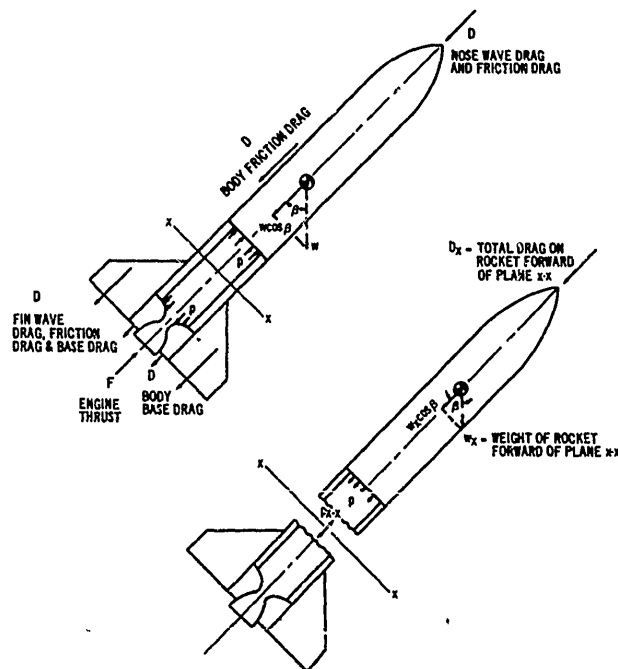


Figure 6-5. Axial Loads on Free Flight Rocket

AMCP 786-200

where C_D is the drag coefficient, q is the dynamic pressure, and S_{ref} is the rocket reference area.

The bending load components are made up of forces from aerodynamic lift and inertia of the rocket mass in the direction perpendicular to the body axis. Manufacturing techniques permit thrust alignment to within approximately 10 sec of longitudinal axis, resulting in negligible bending loads. For preliminary design, the rocket section masses can be considered concentrated at the section centers of gravity, and the section lift forces concentrated at the section centers of pressure.

Fig. 6-6 shows the bending loads acting on a rocket in flight. The inertia loads are equal to

the mass m of the section, multiplied by acceleration a , acting in a direction perpendicular to the longitudinal axis, and

$$ma = N - W \sin \beta \quad (6-6)$$

where N is the total lift on the rocket, W is the total weight, and β is the angle between the body longitudinal axis and the vertical.

The normal-force coefficient gradients on the rocket sections can be evaluated as indicated in par. 8-2. The normal force N can be determined as follows:

$$N = C_{N\alpha} \alpha q S_{ref} \quad (6-7)$$

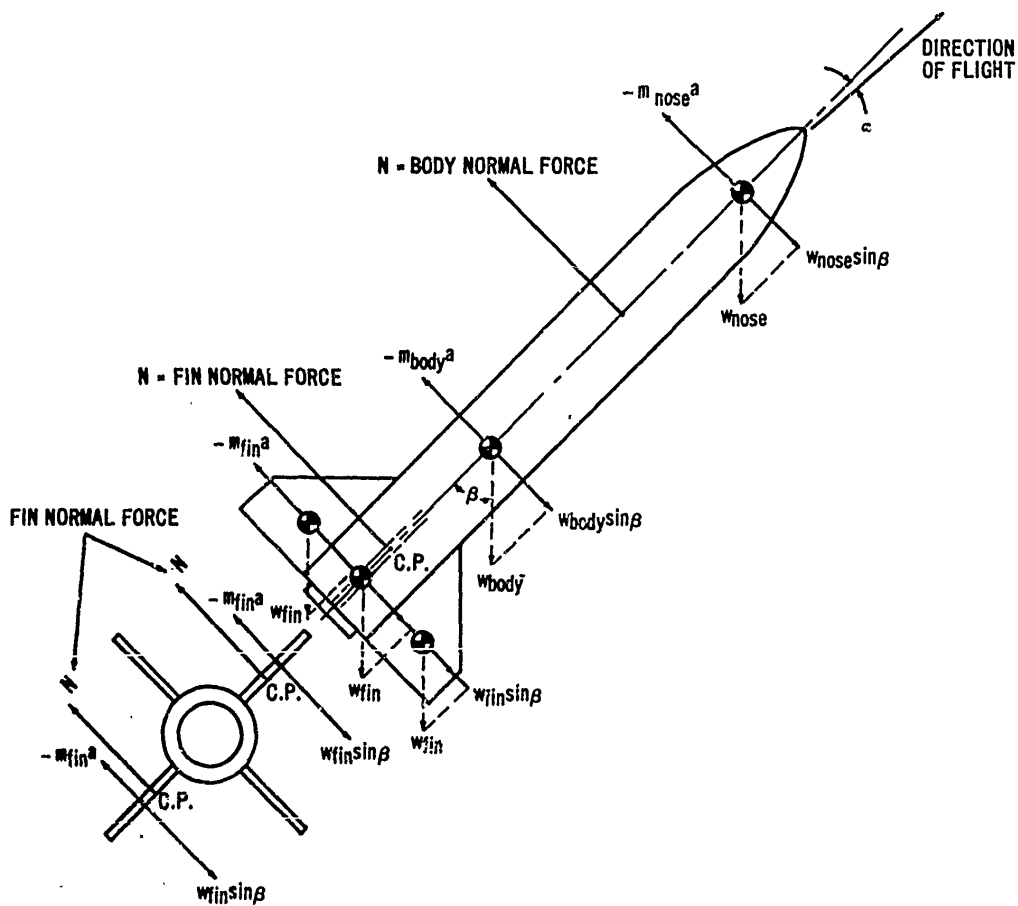


Figure 6-6. Concentrated Bending Loads on Free Rocket

where q is the dynamic pressure, S_{ref} is the rocket reference area, α is the angle of attack, and $C_{N\alpha}$ is the normal force coefficient gradient. The bending moment at any section of the rocket is equal to the algebraic sum of the moments of the forces acting on either side of the section.

The circumferential load in the combustion chamber cylinder walls, as shown in Fig. 6-7, is caused by the internal pressure acting radially along the cylinder length. The circumferential load at plane A-A (P_{A-A}) is

$$P_{A-A} = pA_{A-A} \quad (6-8)$$

where p is the combustion chamber internal gage pressure, and A_{A-A} is the area on which the pressure acts, projected on plane A-A.

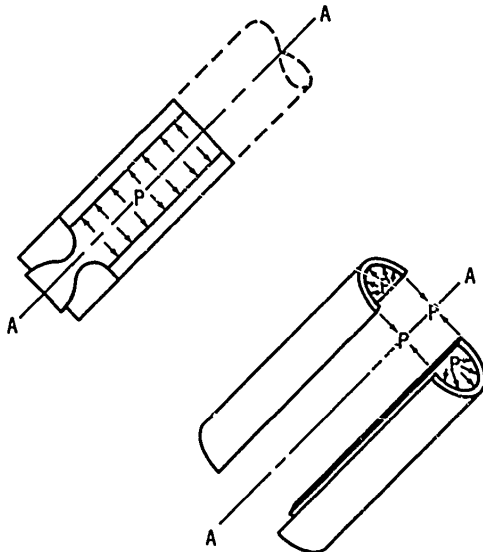


Figure 6-7. Circumferential Loads on Combustion Chamber

6-4 STRESS

6-4.1 BEAMS

A beam is defined as a structural member subjected principally to transverse loads that tend to bend it. The convex side of a loaded beam is in tension and the concave side is in compression. Between the convex and concave surfaces,

there exists a plane called the neutral surface, where the tensile and compressive stresses are zero. The stress distributions across the section of a typical beam are shown in Fig. 6-8. The stress, due to bending loads only, on any element, is

$$\sigma = \frac{Mc}{I} \quad (6-9)$$

where σ is the tensile or compressive stress, M is the bending moment, c is the distance (positive in the direction of the concave surface and negative in the direction of the convex surface) from the neutral surface to the element in which the stress is to be computed, and I is the section area moment of inertia with respect to an axis through the area centroid and perpendicular to the plane of the loads. When a beam is subjected to axial loads in addition to the transverse bending loads, the total stress on any element across a section of a beam is the algebraic sum of the loads acting independently. Therefore,

$$\sigma = \frac{Mc}{I} + \frac{P}{A} \quad (6-10)$$

where P is the axial load, positive if compressive and negative if tensile; A is the area of the beam section; and all other symbols are as defined above. This equation is only true if the beam deflection is negligible and the beam is subjected principally to transverse loads. If the principal loads are axial, the structure must be treated as a column (see par. 6-4.2).

The body and fins of a rocket may act as beams. For preliminary design, the rocket body may be considered as a simple hollow cylinder. Then the maximum stress (positive at the concave surface and negative at the convex surface) at any section due to bending is

$$\sigma = \frac{4M}{\pi d_c^2 t} \quad (6-11)$$

where d_c is the cylinder diameter, t is the wall thickness, and all other symbols are as defined above. If the cylinder is also subjected to an axial load, the maximum stress is

$$\sigma = \frac{4M}{\pi d_c^2 t} + \frac{P}{\pi d_c t} \quad (6-12)$$

AMCP 705-200

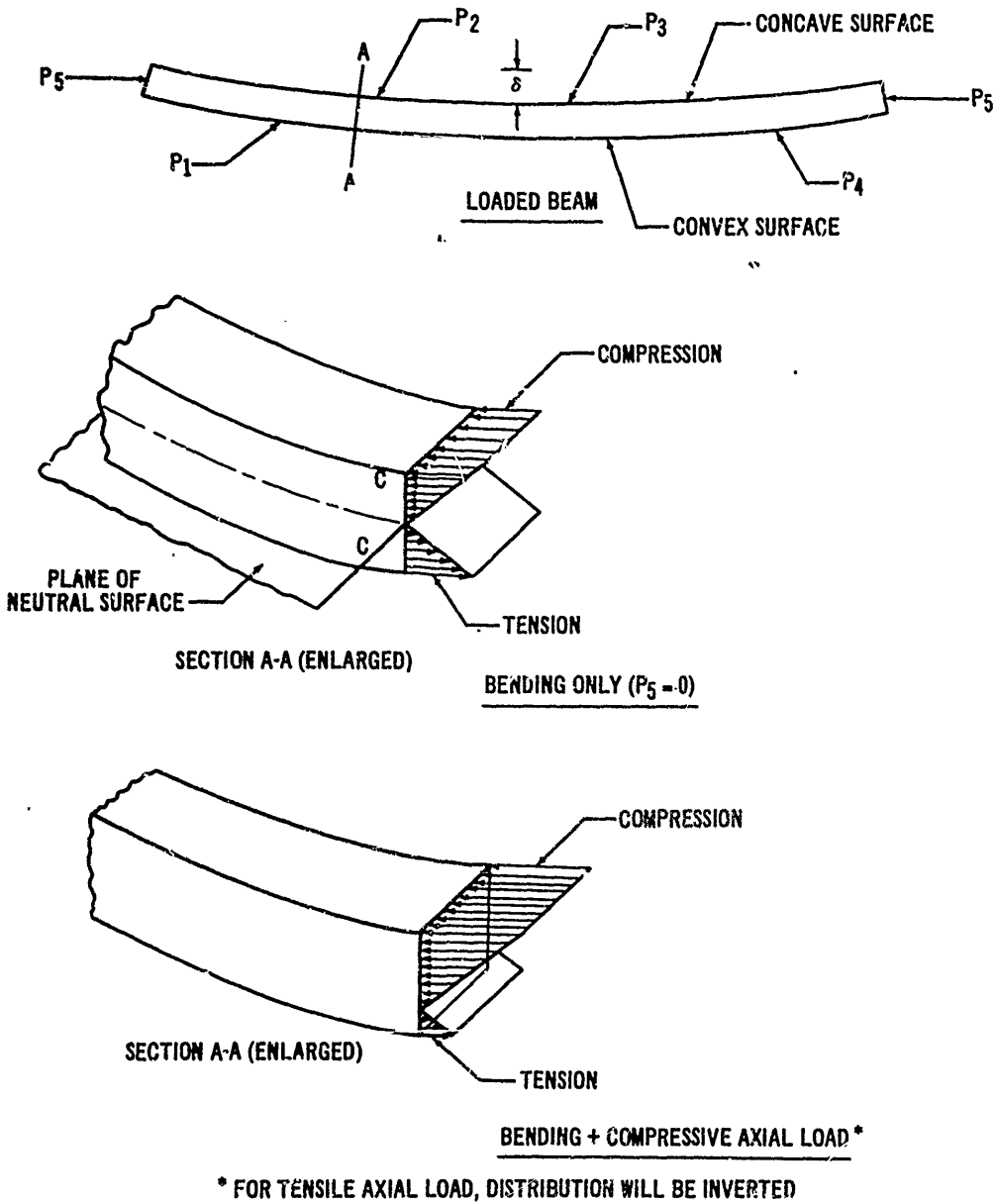


Figure 6-8. Beam-Section Load Distribution

where P is the axial load (positive if compressive and negative if tensile), and other symbols are as shown above. The rocket fins act as cantilever beams (one end fixed), with the maximum bending moment occurring at the point of attachment to the rocket body. The maximum stress due to bending at any section of the fin is

$$\sigma = \frac{Mt}{2I} \quad (6-13)$$

where t is the airfoil thickness. The methods of calculating the area moments of inertia of various airfoil sections are presented in Table 6-2.

6-4.2 COLUMNS

A column is defined as a structural member principally loaded axially in compression and of sufficient length that failure tends to occur by buckling at compressive stresses below the elastic limit. The classical formula for buckling is that developed by Euler as

$$P = \frac{\pi^2 EI}{l^2} \quad (6-14)$$

where P is the buckling load, E is the material modulus of elasticity (Young's Modulus), I is the minimum centroidal moment of inertia of the cross section, and l is the column length. Euler's formula is only applicable to very long columns. Generally, columns must be designed on the basis of empirically-derived relationships.

The rocket body may be a column susceptible to buckling. A method of evaluating the critical buckling stress in thin-walled cylindrical columns, such as rocket bodies, was developed in Reference 9 as

$$\sigma_{cr} = 9E \left(\frac{2t}{d_c} \right)^{1.6} \quad (6-15)$$

where σ_{cr} is the unit compressive stress in the cylinder wall at which buckling will commence, E is the material modulus of elasticity, t is the cylinder wall thickness, and d_c is the cylinder diameter. If the cylinder is also subjected to transverse loads, the critical buckling stress due to the axial load is

$$\sigma_{cr} = 9E \left(\frac{2t}{d_c} \right)^{1.6} - \frac{4M}{\pi d_c^2 t} \quad (6-16)$$

where M is the bending moment due to transverse loads.

6-4.3 PRESSURE VESSELS

For the classes of solid propellant rockets discussed in this handbook, the combustion chamber structure is the primary pressure vessel. This structure is generally cylindrical and is subject to circumferential tensile (or hoop) stresses in the walls due to the loads discussed in par. 6-3.2 and shown in Fig. 6-7. This tensile stress is

$$\sigma = \frac{pr}{t} \quad (6-17)$$

where σ is the unit tensile stress, p is the internal pressure, r is the cylinder inside radius, and t is the wall thickness.

The internal pressure, acting on the ends of the cylindrical vessel, applies in the walls a longitudinal tensile stress that helps support the weight, drag, and inertia compressive stresses.

6-4.4 PLATES

Some of the rocket structure—such as access doors or fin panels—may be considered as flat plates, uniformly loaded and fixed around the edges. For such a rectangular plate, the unit stress is



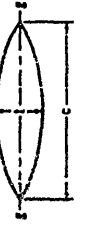
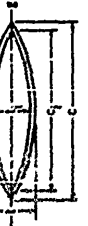


$$\sigma = 6K \frac{Pw}{lt^2} \quad (6-18)$$

where σ is the unit stress, w is the plate width, l is the plate length, P is the total load on the plate, t is the plate thickness, and K is a function of the width-to-length ratio, as shown in Fig. 6-9. Reference 10 presents methods of calculating the unit stress in plates of other geometries and edge conditions.

6-4.5 JOINTS

Riveted, welded, and bolted joints are used in rockets of the class discussed in this handbook.

TABLE 6-2. GEOMETRIC PROPERTIES OF AIRFOIL SECTIONS

FIGURE	MOMENT OF INERTIA	AREA OF CROSS SECTION
 <p>DOUBLE WEDGE</p>	$I_x = \frac{ct^3}{48}$	$A = \frac{ct}{2}$
 <p>MODIFIED DOUBLE WEDGE</p>	$I_x = \frac{ct^3}{24} (2 - 3a)$	$A = ct (1 - a)$
 <p>BICONVEX</p>	$I_x = \frac{4ct^3}{26}$	$A = \frac{(c^2 + ct^2)^2}{8t^2} \left(\frac{c}{2} - \sin^{-1} \frac{c^2 - t^2}{c^2 + t^2} \right) - \frac{c}{4t} (c^2 - t^2)$
 <p>HOLLOW BICONVEX</p>	$I_x = \frac{4ct^3}{26} \cdot \frac{4c_1 t_1^3}{26}$	$A = \frac{(c^2 + ct^2)^2}{8t^2} \left(\frac{c}{2} - \sin^{-1} \frac{c^2 - t^2}{c^2 + t^2} \right) - \frac{c}{4t} (c^2 - t^2) - \frac{(c_1^2 + ct_1^2)^2}{8t_1^2} \left(\frac{c_1}{2} - \sin^{-1} \frac{c_1^2 - t_1^2}{c_1^2 + t_1^2} \right) - \frac{c_1}{4t_1} (c_1^2 - t_1^2)$
 <p>HOLLOW DOUBLE WEDGE</p>	$I_x = \frac{ct^3}{48} - \frac{ct_1 t_1^3}{48}$	$A = \frac{1}{2} (ct - ct_1 t)$
 <p>HOLLOW MODIFIED DOUBLE WEDGE</p>	$I_x = \frac{ct^3}{24} (2 - 3a) - \frac{ct_1^3}{24} (2 - 3a_1)$	$A = ct (1 - a) - ct_1 t (1 - a_1)$

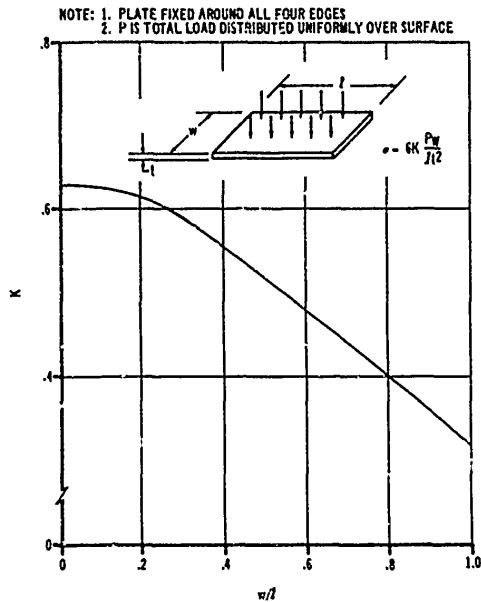


Figure 6-9. Flat Plate Stress Width-to-Length Ratio Parameter

Riveted joints are classified as butt plates and butt straps, and are shown in Fig. 6-10. The stresses in these joints are of three kinds:

- a. Tension in the connected members
- b. Shearing in the rivets
- c. Bearing stresses in rivets and connected members at the surface of contact

Each rivet in a joint will carry an equal shearing stress for rivets of constant cross-sectional area. Therefore, the load across any section of the connected members is equal to the total load on the joint multiplied by the number of rivets between the section being analyzed and the applied load, and divided by the total number of rivets in the joint. The stress in the section then is

$$\sigma = \frac{\left(\frac{n'}{n_t}\right)P}{(w - nd)t} \quad (6-19)$$

where σ is the stress in the connected member, n' is the number of rivets between the applied load and the section under consideration, n_t is the total number of rivets in the joint, P is the applied load, w is the width of the section, n is the number of rivet holes that may be present across

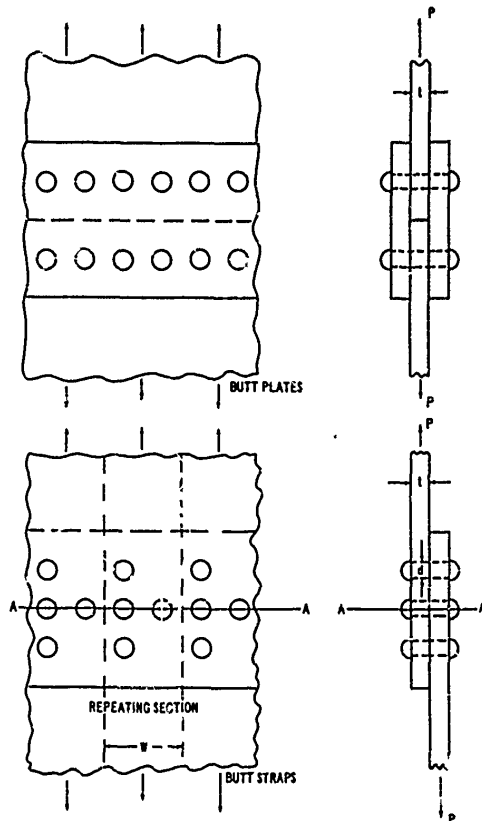


Figure 6-10. Riveted and Bolted Joints

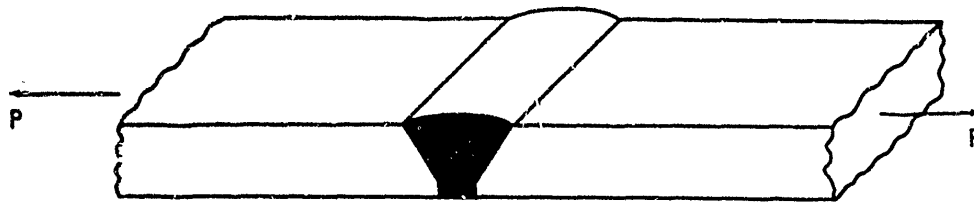
the section under consideration, d is the diameter of the rivets, and t is the thickness of the connected member. Where rivet patterns are repeating, it is only necessary to evaluate the stress in a single repeating section since the stress in all other sections will be equal. For example, the stress in the connecting member shown in Fig. 6-12 across the section A-A will be

$$\sigma = \frac{1/4 P}{(w - 2d)t} \quad (6-20)$$

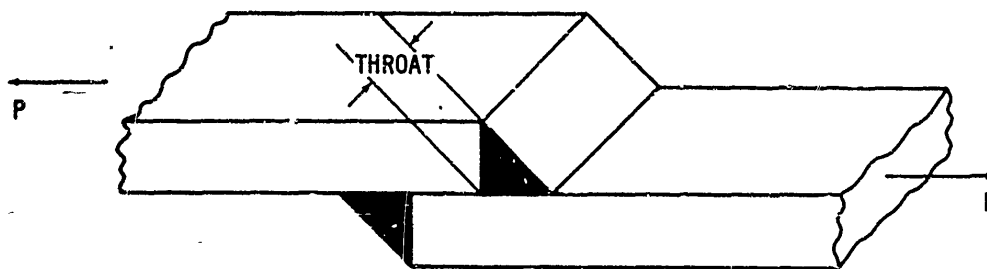
The shearing stress in the rivets is equal to the load on the rivet divided by the cross sectional area of the rivet. Therefore, the unit shearing stress τ is

$$\tau = \frac{4P}{n_t \pi d^2} \quad (6-21)$$

AMCP 706-230



VEE TYPE



FILLET TYPE

Figure 6-11. Welded Joints

where all symbols are as defined previously.

The bearing stress in the rivets or connected members at each rivet location is equal to the load on the rivet divided by the bearing area. Therefore, the bearing stress σ_b is

$$\sigma_b = \frac{P}{ndt} \quad (6-22)$$

where all symbols are as defined previously.

Welded joints may be used in conjunction with or as a replacement for riveted and bolted joints. Although there exists many types of welds, in many combinations and configurations, only the vee-type and fillet-type shown in Fig. 6-11 will be discussed as the most general and common. Welded joints are subjected to shearing, tensile, and compression stresses. The compression or tensile stress in a vee-type joint is equal

to the applied load divided by the cross sectional area, at the weld, or the thinnest member connected. Shearing is the significant stress in a fillet-type weld and is equal to the load, divided by the length of all welds in the joint, multiplied by the weld throat thickness.

Bolts may be subjected to the stresses discussed above for rivets and/or a tensile load along the longitudinal axis as shown in Fig. 6-12. Each bolt may be considered to carry an equal portion of the tensile load. Then the unit tensile stress in each bolt is:

$$\sigma = \frac{P}{nA} \quad (6-23)$$

where P is the tensile load, n is the total number of bolts in the joint, and A is the cross sectional area of the bolt.

For a more extensive treatment of joints, see Reference 11.

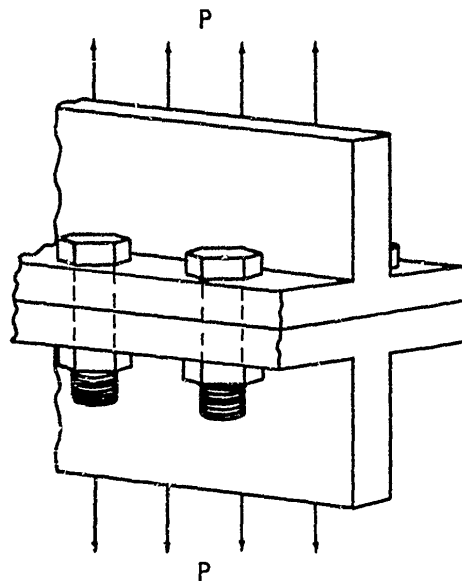


Figure 6-12. Bolted Joints

6-5 SAFETY FACTORS

The factor of safety is defined as the ratio of ultimate strength or yield strength of the material to the allowable stress. The ultimate strength is used for brittle materials and the yield strength for ductile materials. The factor of safety is employed to account for differences between design and actual load conditions, and for statistical variations in the structure. Large factors of safety are desirable for reliability but must be balanced against the associated increase in structural weight.

When possible, it is advisable to base the allowable stress on test results and eliminate the use of the factor of safety. When test data are not available, a factor of safety of 1.15 should be used for the structure in general. For pressure vessels and other structures that may be a hazard to personnel, a factor of safety of 2.0 should be used.

The margin of safety is defined as the ratio of excess strength to the required strength or:

$$M.S. = \left(\frac{\sigma_{\text{allowable}}}{\sigma} \right) - 1 \quad (6-24)$$

where $M.S.$ is the margin of safety, $\sigma_{\text{allowable}}$ is the allowable stress, and σ is the actual maximum stress. The margin of safety gives an indication of permissible load increases or structural strength decreases in design modification.

6-6 HEATING

6-6.1 GENERAL

Heat is transferred by the processes of conduction, radiation, and convection. In general, heat is conducted through a medium by the transport of the kinetic energy of both free electrons and molecules; heat is radiated by the transport of electromagnetic energy, requiring no transport medium; heat is convected by a combination of conduction, radiation, and the motion of a fluid mass. The heat transfer is considered to be transient if heat is being stored or released within the media involved and the temperatures of the media are varying with time. The heat transfer is considered to be steady-state if the temperatures of the media do not vary with time. During steady-state conditions the one-dimensional heat transfer across any one section of a medium is equal to the heat transferred across any other parallel section.

6-6.1.1 Conduction Heat Transfer

The one-dimensional, steady-state conduction heat transfer through a homogeneous medium with a constant thermal conductivity is

$$q = \frac{k}{t} A (T_1 - T_2) \quad (6-25)$$

where q is the heat transfer rate, k is the thermal conductivity of the medium (obtained from material property data), A is the section area of the medium through which the heat is transferred, $(T_1 - T_2)$ is the temperature difference across the medium, and t is the medium thickness. For a composite of plane media such as shown in Fig. 6-13, the one-dimensional steady-state conduction heat transfer is equal to

$$q_{4-2} = \frac{yw(T_4 - T_2)}{\frac{t_1}{k_1} + \frac{t_2}{k_2} + \frac{t_3}{k_3} + \dots + \frac{t_n}{k_n}} \quad (6-26)$$

AMCP 708-280

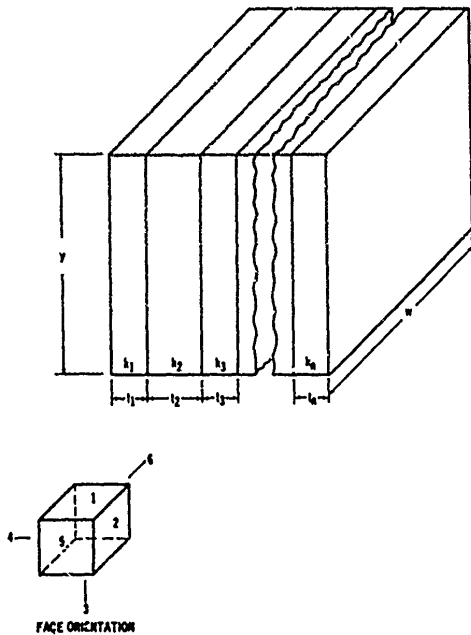


Figure 6-13. Plane Conduction Heat Transfer Medium

or in another direction is equal to

$$q_{5-6} = \frac{(k_1 t_1 + k_2 t_2 + k_3 t_3 + \dots + k_n t_n) y (T_5 - T_6)}{w} \quad (6-27)$$

where q_{4-2} and q_{5-6} are the one-dimensional conduction heat transfer rates from face 4 to 2 and face 5 to 6, respectively, with the other four faces insulated; T_4 , T_2 , T_5 , and T_6 are the uniform surface temperatures on faces 4, 2, 5, and 6, respectively; and all other symbols are as shown in Fig. 6-13. For a composite of cylindrical mediums such as shown in Fig. 6-14, the steady-state conduction heat transfer is equal to

$$q = \frac{l(T_{is} - T_{os})}{\frac{\ln(r_2/r_1)}{2\pi k_1} + \frac{\ln(r_3/r_2)}{2\pi k_2} + \dots + \frac{\ln(r_n/r_{n-1})}{2\pi k_n}} \quad (6-28)$$

6-28

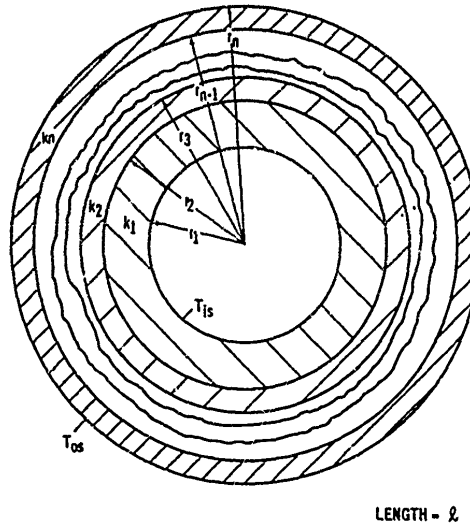


Figure 6-14. Cylindrical Conduction of Heat Transfer Medium

where q is the conduction heat transfer rate, T_{is} and T_{os} are the uniform surface temperatures on the inside and outside of the cylinder, respectively, and all other symbols are as shown in Fig. 6-14.

6-6.1.2 Radiation Heat Transfer

All substances above the temperature of absolute zero emit thermal electromagnetic energy. A body that emits and absorbs the maximum amount of heat is defined as a black body and the heat it emits is equal to

$$q = \sigma AT^4 \quad (6-29)$$

where q is the heat transfer rate; σ is the Stephan-Boltzmann constant, which in the English system of units is 0.48×10^{-12} BTU/(sec) (ft²) (°R)⁴; A is the surface area of the body; and T is the absolute temperature of the body surface. Actual bodies radiate and absorb less heat than the black body. The ratio of heat emitted by a black body at the same temperature is called the emissivity ϵ and is a function of the body material, temperature, and surface conditions. The heat radiated by an actual body is equal to

$$q = \epsilon \sigma A T^4 \quad (6-30)$$

The ratio of heat absorbed by an actual body to the total amount of heat incident on the body (that which would be absorbed by a black body) is called the absorptivity α and is a function of body material, temperature, surface condition, and heat source temperature. Emissivity and absorptivity values may be obtained from standard material handbooks.

The net radiation heat transfer between two bodies is a function of the bodies' emissivities, absorptivities, geometries, temperatures and orientations. This transfer is equal to

$$q_1 = F_{12} A_1 \sigma (T_1^4 - T_2^4) \quad (6-31)$$

where q_1 is the radiation heat transfer rate of body 1; F_{12} is the combined emissivity, absorptivity, and orientation factor, which may be obtained from such sources as Reference 12; A_1 is the surface area of body 1; and T_1 and T_2 are the surface temperatures of bodies 1 and 2, respectively. Methods of obtaining the heat transfer between three or more bodies are described in Reference 13.

Following Reference 13, we may define a radiation heat transfer coefficient as

$$h_{Rad} = \frac{\sigma F_{12} (T_1^4 - T_2^4)}{(T_1 - T_2)} \quad (6-32)$$

By transposition and substitution in Eq. 6-31,

$$q_1 = h_{Rad} A_1 (T_1 - T_2) \quad (6-33)$$

6-6.1.3 Convection Heat Transfer

The convection heat transfer between a fluid in motion and a solid is equal to

$$q = hA(T_f - T_s) \quad (6-34)$$

where q is the convection heat transfer rate, h is the convection heat transfer coefficient, A is the area across which the heat is transferred, and T_f and T_s are the temperatures of the fluid and solid, respectively. The convection coefficient is a function of the temperatures, fluid properties, solid geometry, and solid surface conditions.

The methods of evaluating convection coefficients for a variety of conditions are presented in Reference 14.

6-6.1.4 Combined Heat Transfer

Often the heat transfer under consideration takes place by the modes of conduction, radiation, and convection acting simultaneously. Therefore, it is convenient to define an overall heat transfer coefficient U which will include all modes of heat transfer present. For illustration, consider the cylinder in Fig. 6-14 with a hot fluid at temperature T_H flowing on the inside and a cold fluid at temperature T_C flowing on the outside. Then the steady-state heat transfer from the inside fluid to the outside fluid is

$$q = UA(T_H - T_C) \quad (6-35)$$

where

$$U = \frac{1}{A} \left(\frac{1}{2\pi r_1 h_{is}} + \frac{\ln(r_2/r_1)}{2\pi k_1} + \frac{\ln(r_3/r_2)}{2\pi k_2} + \dots + \frac{\ln(r_n/r_{n-1})}{2\pi k_n} + \frac{1}{2\pi r_n h_{os}} \right)^{-1} \quad (6-36)$$

h_{is} and h_{os} are the inside and outside heat transfer coefficients, respectively, for convection plus radiation.

6-6.1.5 Transient Heat Transfer

When the heat transfer is transient, the rate at which heat is stored in a medium with a constant specific heat is equal to

$$q = mC_p \frac{dT}{d\theta} \quad (6-37)$$

where q is the rate at which heat is stored, m is the mass of the medium in which the heat is stored, C_p is the constant pressure specific heat of the medium, $dT/d\theta$ is the time rate of temperature change in the medium.

The solutions of three-dimensional transient heat transfer problems are more difficult than

AMCP 705-200

the above solutions and generally must be solved on high-speed digital computers.

6-3.2 COMBUSTION CHAMBER HEATING

The combustion process produces gas temperatures of 4000° to 7000°R depending on the propellant employed. Heat is transferred from the combustion chamber gases through the structure to the environment by conduction, convection, and radiation. The structure may be protected from overheating by employing insulating materials, a high heat capacity mass, or by transferring heat away to the environment.

The convection heat transfer coefficient on the inside of a cylindrical combustion chamber may be evaluated by the following relationship obtained from Reference 14:

$$N_{Nu} = \frac{hD}{k} = 0.023 (N_{Re})^{0.8} (N_{Pr})^{0.3} \quad (6-38)$$

$$N_{Re} = \frac{\rho VD}{\mu} \quad (6-39)$$

$$N_{Pr} = \frac{C_p \rho t}{k} \quad (6-40)$$

where N_{Nu} , N_{Re} , and N_{Pr} are the dimensionless Nusselt, Reynolds, and Prandtl numbers, respectively; h is the convection coefficient; D is the inside diameter of the chamber; k is the thermal conductivity; ρ is the density; V is the velocity; μ is the viscosity; and C_p the constant pressure specific heat of the chamber gas.

The convection heat transfer coefficient on the outside surface of the combustion chamber is a function of the airflow properties at the particular location under consideration. If the outside surface is exposed to the airstream, the heat transfer may be evaluated as indicated in par. 6-3.3. For other locations, the convection heat transfer coefficients may be evaluated from references cited previously.

If the combustion is over a short period of time, steady-state conditions may not be reached. In this case, for preliminary design, it is recommended that the net heat transfer to the structure at the initial temperature be evaluated over

an increment of time. The temperature rise in the structure due to heat storage can then be evaluated. Then the net heat transfer to the structure at the new temperature for the next increment of time is evaluated, and so on. The accuracy of this method can be increased by taking smaller time increments.

The methods outlined above can also be used on the rocket nozzle with sufficient accuracy for preliminary design.

6-3.3 EXHAUST PLUME HEATING

The rocket exhaust plume transfers heat by radiation to the rocket structure, and by convection to the launcher and surrounding equipment. The heat transferred is a function of the geometry, temperature, flow properties, and radiation properties of the plume; it is also a function of the orientation, temperature, radiation properties, and configuration of the rocket structure, launcher, and surrounding equipment.

The plume geometry is dependent on the exhaust gas pressure and atmospheric pressure as shown generally in Fig. 6-15. The plume geometry, temperature, and flow properties can be defined specifically, as outlined in Chapter 5, par. 5-2.1. The convection heat transfer coefficients on the launcher and surrounding equipment may be determined from references cited previously. The radiation properties of the plume depend on the operating characteristics of the rocket engine. Since this information is generally not available for preliminary design, the conservative approach should be taken and the emissivity and absorptivity assumed to be equal to 0.9.

6-3.4 AERODYNAMIC FRICTION HEATING

The heating due to aerodynamic friction on rockets of the class discussed in this handbook generally will not be significant enough for consideration in preliminary design. Therefore, only a cursory discussion of aerodynamic heating will be presented. For a more detailed presentation, consult such sources as Reference 15.

Kinetic energy is imparted by friction to the air surrounding a rocket in flight. Therefore, in the rocket boundary layer there is a kinetic tem-

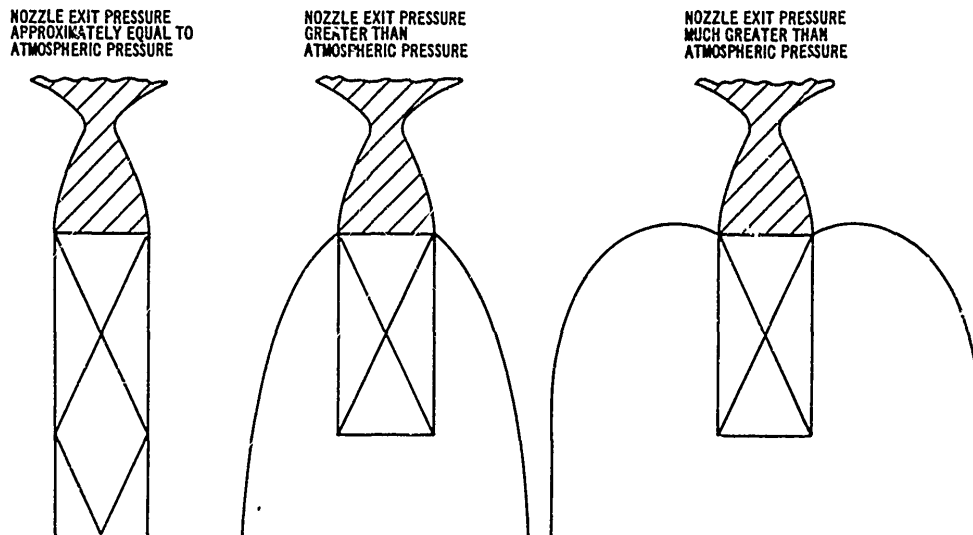


Figure 6-15. General Geometry of Rocket Exhaust Plumes

perature rise above the temperature of the atmospheric air. At stagnation points, such as the rocket nose and leading edge of the fins, the air temperature is equal to the atmospheric air temperature plus the complete kinetic temperature rise or

$$T_s = T_o + \left(\frac{\gamma - 1}{2}\right) M_\infty^2 T_o \quad (6-41)$$

where T_s is the stagnation air temperature in absolute units, T_o is the atmospheric air temperature in absolute units, γ is the ratio of the specific heat of air at constant pressure to the specific heat at constant volume, and M_∞ is the free stream Mach number. In regions other than stagnation points, the temperature in the boundary layer will be less than the stagnation temperature calculated above, due to the heat transfer within the boundary layer. This temperature, called the recovery temperature, is evaluated as follows:

$$T_R = T_o + r \left(\frac{\gamma - 1}{2}\right) M_\infty^2 T_o \quad (6-42)$$

where T_R is the recovery temperature in absolute units, and r is the recovery factor. The recovery factor for laminar and turbulent boundary layers

is equal to the Prandtl number (Eq. 6-39) raised to the one-half and one-third powers, respectively. For a smooth flat plate, the boundary layer may be considered as laminar at Reynolds numbers less than 10^5 and turbulent at Reynolds numbers greater than 10^5 .

The heat transfer to the rocket surface is evaluated as follows:

$$\frac{q}{A} = h(T_R - T_w) \quad (6-43)$$

where $\frac{q}{A}$ is the heat transfer rate to the surface per unit area, h is the heat transfer coefficient, and T_w is the rocket surface temperature in degrees Rankine. The heat transfer coefficient for laminar and turbulent flow on a flat plate may be evaluated as follows:

$$(C_{H_\infty})_{\text{laminar}} = \frac{h}{C_p \rho_\infty V_\infty} = \frac{1}{(N_{Pr})^{2/3}} \left(\frac{C_{f_{oc}}}{2}\right) \quad (6-44)$$

and

$$(C_{H_\infty})_{\text{turbulent}} = \frac{h}{C_p \rho_\infty V_\infty} = \frac{C_{f_{oc}}}{2} \quad (6-45)$$

where C_{H_∞} is the dimensionless Stanton number, h is the heat transfer coefficient, ρ_∞ is the

AMCP 706-200

density of the free stream air, V_∞ is the free stream velocity, C_{f_∞} is the free stream skin friction coefficient, which is obtained as outlined in Chapter 8, par. 8-3.2. The heat transfer coefficient on cones is approximately 73 percent and 15 percent higher than flat plate values for laminar and turbulent boundary layers, respectively. Fins and cylindrical bodies may be considered as flat plates for purposes of preliminary design.

6-7 TESTING

A test program is often required to supplement the structural analyses outlined above since these analyses do not consider such factors as stress concentrations, statistical variations, fabrication variations, and imperfections in structural materials and members. Although structural testing generally will not be performed during the preliminary phases of rocket design, a cursory discussion is presented here to indicate the types of tests usually conducted and the testing methods usually employed. Tests are classified as destructive if the test item is permanently deformed or fractured, and as nondestructive if the test item is structurally useful after the test.

The actual mechanical properties of materials may vary statistically from the generally published values. These variations may significantly affect the structural strength since factors of safety must be low to minimize weight. There-

fore, samples of materials are prepared and tested, conforming to standards set by organizations such as ASME and ASTM. A detailed discussion of the testing of materials is presented in Reference 16.

When evaluating structural members, it is generally desirable to employ nondestructive tests so as not to impair the usefulness of the tested item. Deep-seated irregularities such as cracks and voids in the structure can be identified by X-ray. Surface or near-surface irregularities can be identified by Magnaflux or Zyglo inspections. In the Magnaflux inspection the test item is covered by small magnetic particles which are attracted to local magnetic leakage fields around imperfections in the magnetized test item. In the Zyglo inspection, used on nonmagnetic materials, the test item is immersed in a fluorescent fluid that penetrates and thus reveals cracks, voids, and other imperfections. Observation of the properties of sound waves passed through the structure will also reveal imperfections.

When using small factors of safety and when uncertainties exist concerning the structural strength, it is usually desirable to verify the structure by subjecting it to a proof test. This is especially true for pressure vessels. In general, proof tests are designed to subject the structure to a load that will permanently deform it 0.01 percent or less.

For a more thorough discussion of structural testing—including vibration, creep, and impact—see Reference 16.

REFERENCES

1. M. Rhoden and D. Itsbin, *Simplified Method for Calculating the Area, Skin Weight, and Free Volume of Ogives*, Special Report, U. S. Army Missile Command, Redstone Arsenal, Alabama, 1 January 1965.
2. G. A. Greathouse and C. J. Wesel, Eds., *Deterioration of Materials, Causes and Preventative Techniques*, Division of Chemistry and Chemical Technology, National Academy of Sciences, National Research Council, Washington, D. C.
3. G. K. Guttwein, F. K. Priebe, and S. M. Jee, *Behavior of Electronic Equipment in Vehicular Transportation*, Tele-Tech and Electronic Industries, December 1964.
4. *Ride and Vibration Data*, Special Publication of the Society of Automotive Engineers, New York, N. Y.
5. *The Applicability of Existing Truck and Rail Shock, and Vibration Data to Freight Shipment Criteria*, Technical Report No. 58, Vitro Corporation of America, Silver Springs Laboratory, Silver Springs, Md., March 1954.
6. D. A. Firmage, *Transportation Shock and Vibration Studies*, Project No. 8-91-06-002, Engineering and Industrial Exp. Station, University of

REFERENCES (Cont)

- Florida, Engineering Research and Development Laboratories, Fort Belvoir, Va., February 1952.
7. L. E. Lamkin, *Packaging Criteria*, Shock and Vibration Bulletin No. 21, RDB.
 8. K. W. Johnson, *Design Criteria for Military Equipment Transported by Common Carrier*, Shock and Vibration Bulletin No. 16, October 1950.
 9. S. Kanemitsu and H. Nojima, *Axial Compression Tests of Thin Circular Cylinders*, M. S. Thesis, Guggenheim Aeronautical Laboratory, California Institute of Technology, 1939. Reviewed in H. S. Siefert, K. Brown, *Ballistic Missile and Space Vehicle Systems*, John Wiley and Sons, Inc., New York, N. Y. 1961.
 10. F. B. Seely and J. O. Smith, *Advanced Mechanics of Materials*, John Wiley and Sons, Inc., New York, N. Y. 1952.
 11. D. J. Peery, *Aircraft Structures*, McGraw-Hill Book Co. Inc., New York, N. Y. 1950.
 12. *Aero-Space Applied Thermodynamics Manual*, Society of Automotive Engineers Inc., Committee A-9, Aero-Space Environmental Control Systems, New York, February 1960.
 13. F. Kreith, *Principles of Heat Transfer*, International Textbook Co., Scranton, Pa., 1958.
 14. W. H. McAdams, *Heat Transmission*, McGraw-Hill Book Co. Inc., New York, 1954.
 15. Robert W. Truitt, *Fundamentals of Aerodynamic Heating*, The Ronald Press Co., New York 1960.
 16. Proceedings of the Society for Experimental Stress Analyses. All volumes, B. E. Rossi, Society for Experimental Stress Analyses, 21 Bridge Square, Westport, Conn.
 17. AMCP 706-134, *Engineering Design Handbook, Maintainability Guide for Design*.

CHAPTER 7 ACCURACY

LIST OF SYMBOLS

Symbol	Meaning	Symbol	Meaning
C_D	Aerodynamic drag coefficient, nondimensional	V	Estimate of population variance
C_{sq}	Aerodynamic damping moment coefficient, nondimensional	V	Projectile velocity, ft/sec
$C_{N\alpha}$	Aerodynamic normal force coefficient, per rad	V_w	Wind velocity, ft/sec
CPE	Circular probable error	w	Wind velocity in flight-path plane, ft/sec
d	Reference diameter of projectile or rocket, ft	w_Z	Wind velocity normal to flight path, ft/sec
G	Rocket acceleration due to thrust, ft/sec ²	X, Y, Z	Earth-fixed launch coordinate system
g	Gravitational acceleration, ft/sec ²	x, y	Specific sample value taken from a universe of statistical values
I	Moment of inertia, slug-ft ²	\bar{x}, \bar{y}	Estimate of μ based on available sample values
I_{sp}	Specific impulse, sec	α	Angle of attack, degrees or rad
k	Radius of gyration, ft	β	Dispersion reduction parameter (β = dispersion with reduction technique/dispersion with no reduction technique)
L	Thrust moment arm due to malalignment, ft	γ_{TS}	Steady state flight path angle with no disturbances, mils
l_x, l_y	Aerodynamic static margin, cal	Δ	Incremental change in the variable following the symbol
l_x, l_y	Distance from center of gravity to point of thrust application, ft	δ	Thrust malalignment angle, mils
\ln	Natural logarithm	δ_F	Aerodynamic malalignment angle, mils
m	Projectile mass, slug	ϵ	Angle between rocket longitudinal axis and principal axis, mils
N	Number of sample values taken from a universe of statistical values	θ	Projectile pitch attitude angle, measured from horizontal, rad
n_σ	Number of revolutions made by rocket during first wavelength of yaw	μ	Mean of a universe of statistical values
P	Nondimensional launcher length (actual launcher length / σ)	ρ	Atmospheric density, slug/ft ³
PE	Probable error	σ	Yaw oscillation distance or wavelength, ft; standard deviation of a sample of size N
p	Rocket spin rate, rad/sec	σ_0	Initial oscillation distance, ft
q	Component of projectile angular velocity in the direction of projectile y axis, rad/sec	σ_{sys}	Standard deviation of a system containing n statistical variables
R	Standard range, km	σ_x, σ_y	Standard deviation of the $x(y)$ values
s	Computed standard deviation	ϕ	Projectile roll angle, rad
S	Aerodynamic reference area, ft ²	ψ	Projectile yaw attitude angle, measured from vertical launch plane, rad
S	Nondimensional burning distance (actual burning distance / σ)	∂	Partial derivative
t	Time of flight, sec; Student's t value		
u, w	Components of projectile velocity in the direction of x and z axes, ft/sec		

AMCP 706-280

7-1 INTRODUCTION

Accuracy is the measure of the ability of the rocket system to position the payload at a given point at warhead event. Various error sources inherent in the rocket system, together with external conditions such as winds, cause a dispersion of the payload from its intended path. To determine the accuracy of a rocket system, a series of rockets are launched under carefully controlled conditions. The actual flight paths of the rockets are compared to an idealized trajectory in order to calculate the dispersion. As in the study of the accuracy of any mechanical instrument or system, the error sources are first identified and then categorized as to whether they are predictable (allowing a compensation to be made) or random. The most significant factors influencing the accuracy of free rockets have been identified by extensive comparisons between experimental tests and theory. This chapter is a detailed discussion of the error sources. The main objective is to describe how the designer must compensate for the errors in order to achieve the level of accuracy required by the mission specifications.

7-2 DEFINITIONS OF ERROR SOURCES

The flight of a rocket is divided into three phases: (1) the launch phase, (2) the propulsive or burning phase, and (3) the ballistic phase. Error sources are labeled according to the phase of flight during which the error causes the rocket to deviate from the idealized trajectory. For example, a burning phase error will cause a deviation to occur between launch and burnout. If no additional errors are encountered during the ballistic phase, the burning phase error will still result in a dispersion of the warhead event. The total error, including prelaunch errors not associated with flight, is the net dispersion due to all errors.

a. **Prelaunch Errors.** All errors, including aiming errors and prelaunch corrections, that are accrued before rocket ignition.

b. **Launch Phase Errors.** Those errors that are associated with and result from the launch phase, including the initial conditions transmitted to the rocket by the launcher and dynamic unbalance effects of the rocket.

c. **Propulsive Phase Errors.** The dispersions that result from such errors as thrust malalignment, nonstandard meteorological conditions, aerodynamic asymmetries, and propulsion variations.

d. **Ballistic Phase Errors.** Those dispersions that occur during the period from propulsion cut-off to the end of flight.

The following paragraphs will be concerned with the individual error sources and methods for computing approximate dispersions.

7-3 DESIGN CONSIDERATIONS INFLUENCING ACCURACY

The effect of design variables on accuracy and the delicate trade-off process involved in dispersion reduction can be more easily understood by dividing all errors into two groups: (1) speed change errors, and (2) angular errors.

7-3.1 DESIGN CONSIDERATIONS ASSOCIATED WITH SPEED CHANGE ERRORS

The speed change errors are characterized by a change from the nominal velocity attained at propellant burnout. These errors, which result in an error in the plane of the trajectory, are due primarily to the variability present in the propulsion system. Any variation in a parameter that influences the delivered total impulse will obviously result in a different burnout velocity of the rocket. These include variations in:

- a. Total loaded propellant
- b. Propellant specific impulse due to chemical composition
- c. Specific impulse due to physical quantities (e.g., nozzle throat diameter)
- d. Inert parts weight

In addition to propulsion system variability effects, the burning time and thrust of solid propellant rockets are effected by propellant temperature. Even though the temperature has a negligible effect on total impulse, it does affect the burnout velocity because the rocket is subjected to a different drag history.

Speed change errors are a function of mechanical design, manufacturing control, and propellant selection. These items are discussed in more de-

tail in Chapters 5 and 6. The remainder of this chapter will deal exclusively with the angular errors.

7-3.2 DESIGN CONSIDERATIONS ASSOCIATED WITH ANGULAR ERRORS

The angular errors are characterized by a change from the desired direction of the velocity vector at propellant burnout. The errors have components both in the plane of the nominal trajectory and normal to that plane, and are caused by:

- a. Wind normal to the velocity vector
- b. Thrust malalignment or the failure of the thrust vector to pass through the center of gravity
- c. Dynamic unbalance
- d. Aerodynamic asymmetries

Since the effect of the last two errors can be shown to be equivalent to thrust malalignment, in the paragraphs which follow we shall discuss only wind and thrust malalignment effects.

7-3.2.1 The Effect of Aerodynamic Stability

The aerodynamic stability of a rocket is the measure of the tendency of the rocket to align itself with the relative wind. If an aerodynamically stable rocket in steady flight with no aerodynamic moments should be given a disturbance such as a sudden increase in angle of attack, the aerodynamic forces caused by the disturbance direct the rocket back to its original state. The motion of the rocket immediately following the disturbance is generally a rotational oscillation about a lateral axis. One of the most important parameters in the study of the behavior of free rockets is the distance the rocket travels during one oscillation. The yaw oscillation distance σ is related to the aerodynamic stability of the rocket by the static margin (the moment arm of the corrective aerodynamic force):

$$\sigma = 2\pi \sqrt{\frac{2I}{\rho S l_s d C_{N\alpha}}} \quad (7-1)$$

where

σ = yaw oscillation distance or wavelength of yaw, ft

I = moment of inertia of the rocket about a lateral axis, slug/ft²
 ρ = atmospheric density, slug/ft³
 S = aerodynamic reference area, ft²
 l_s = rocket static margin, cal
 d = rocket reference diameter, ft
 $C_{N\alpha}$ = rocket normal force coefficient gradient, rad⁻¹

Since σ depends on the aerodynamic coefficients of the rocket, it is subject to a large change during flight as the velocity and/or altitude of the rocket change. Fig. 7-1 shows the variation of σ and the building of angular dispersion for a typical flight.

From the figure, it is seen that most of the dispersion takes place during the first yaw oscillation. During this time σ does not change appreciably (this has been found to be generally true). Therefore, the dependence of dispersion on σ is mainly determined by the initial wavelength of yaw. This initial value will be used to describe the wavelength of a flight.

7-3.2.2 The Effect of Wind

Fig. 7-2 illustrates the effect of a wind on a stable rocket.

It can be seen that the rotation of the rocket into the relative wind causes the thrust to drive the rocket from the intended path. Fig. 7-3 shows the effect of σ on the dispersion due to wind. As the rocket becomes less statically stable (thereby increasing σ), the sensitivity to wind reduces. This suggests that the designer should adjust parameters so as to maximize σ . However, as will be shown in the next paragraph, consideration of the dispersion due to thrust malalignment imposes a conflicting requirement on σ .

7-3.2.3 The Effect of Thrust Malalignment

Fig. 7-4 shows the effect of a malalignment of the rocket thrust with the vehicle axis. An angular malalignment is indicated. However, the same moment can also be caused by the vehicle center of gravity lying off the centerline of the vehicle. In fact, a displaced center of gravity has been shown to produce larger angular error than does an angular malalignment.

AMCP 706-280

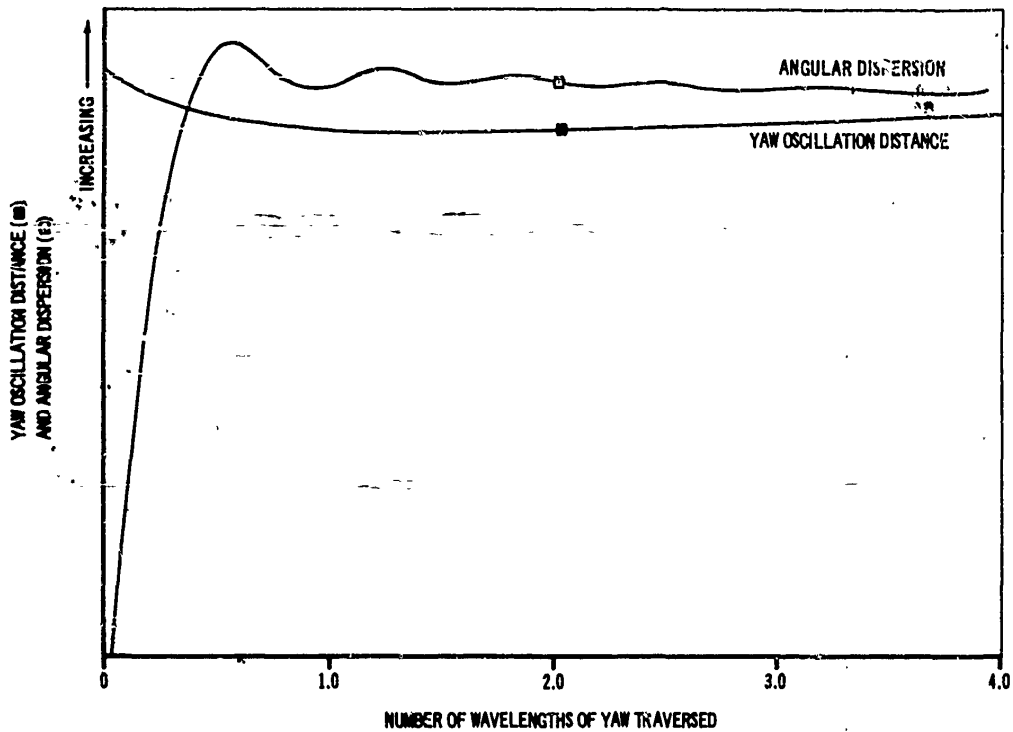


Figure 7-1. Variation of Angular Dispersion and Wavelength of Yaw During Flight

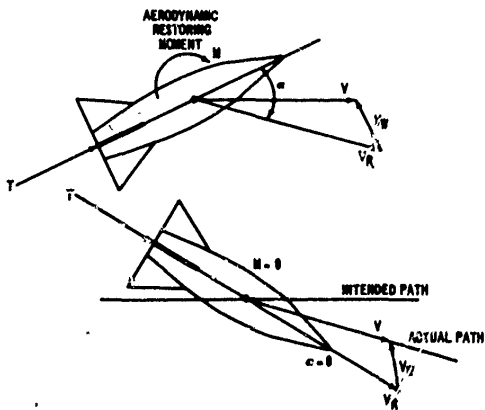


Figure 7-2. Effect of Wind on an Aerodynamically Stable Rocket

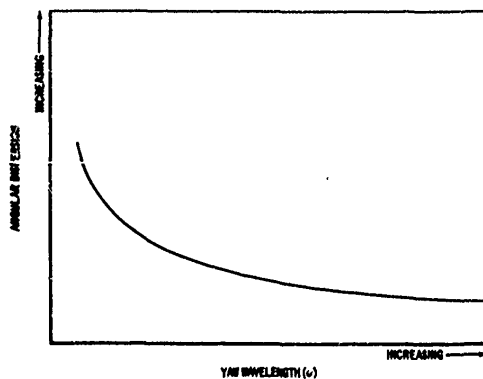


Figure 7-3. Effect of Wavelength of Yaw on Angular Dispersion Due to Wind

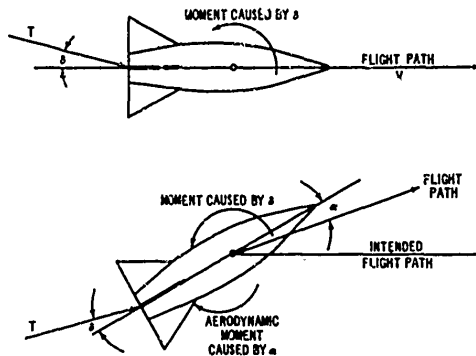


Figure 7-4. Effect of a Thrust Malalignment on an Aerodynamically Stable Rocket

The figure indicates that a thrust malalignment causes an aerodynamically stable rocket to rotate until the aerodynamic corrective moments are equal to the moment caused by the malaligned thrust.

Fig. 7-5 shows the effect of σ on the angular dispersion due to thrust malalignment.

For minimum thrust malalignment effects, the designer should select the smallest possible value of σ (maximum aerodynamic stability).

Combining the two error sources produces Fig. 7-6 which suggests an optimum value of σ for minimum total dispersion during burning. The designer may adjust the rocket parameters to obtain this value of σ .

The conflicting requirements on the wavelength of yaw result because an attempt was made to decrease two different types of errors by the same method, changing aerodynamic stability. We shall now consider a different method by which the dispersion caused by a body-fixed error, such as thrust or fin malalignment, can be reduced.

7-3.2.4 The Effect of a Slow Spin

Fig. 7-7 describes the build-up of the dispersion of a nonrotating rocket with a thrust malalignment. Because the thrust is applied in an unchanging direction, the dispersion grows steadily with time. Fig. 7-8 shows the effect of giving the rocket a slow spin about its longitudinal axis. In this case the direction of the thrust changes as the body rotates. The result is a reduction in the total angular dispersion.

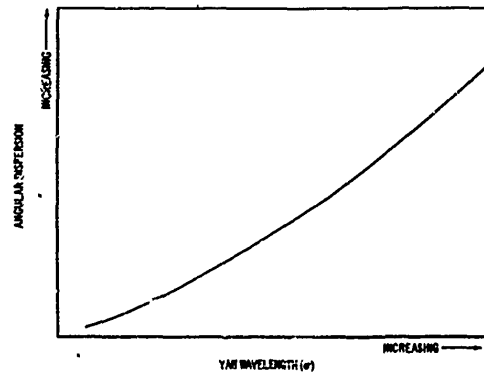


Figure 7-5. Effect of Wavelength of Yaw on Angular Dispersion Due to Thrust Malalignment

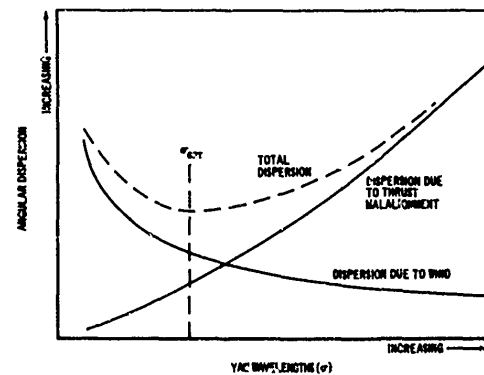


Figure 7-6. Optimum Wavelength of Yaw for Minimum Total Dispersion

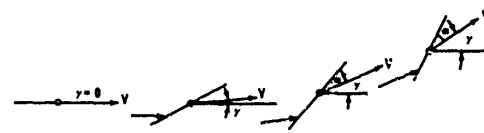


Figure 7-7. Growth of Angular Dispersion for a Rocket With a Thrust Malalignment and No Spin

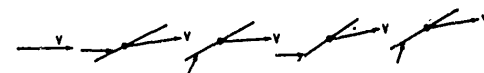


Figure 7-8. Growth of Angular Dispersion for a Rocket With a Thrust Malalignment and a Slow Spin

AMCP 706-280

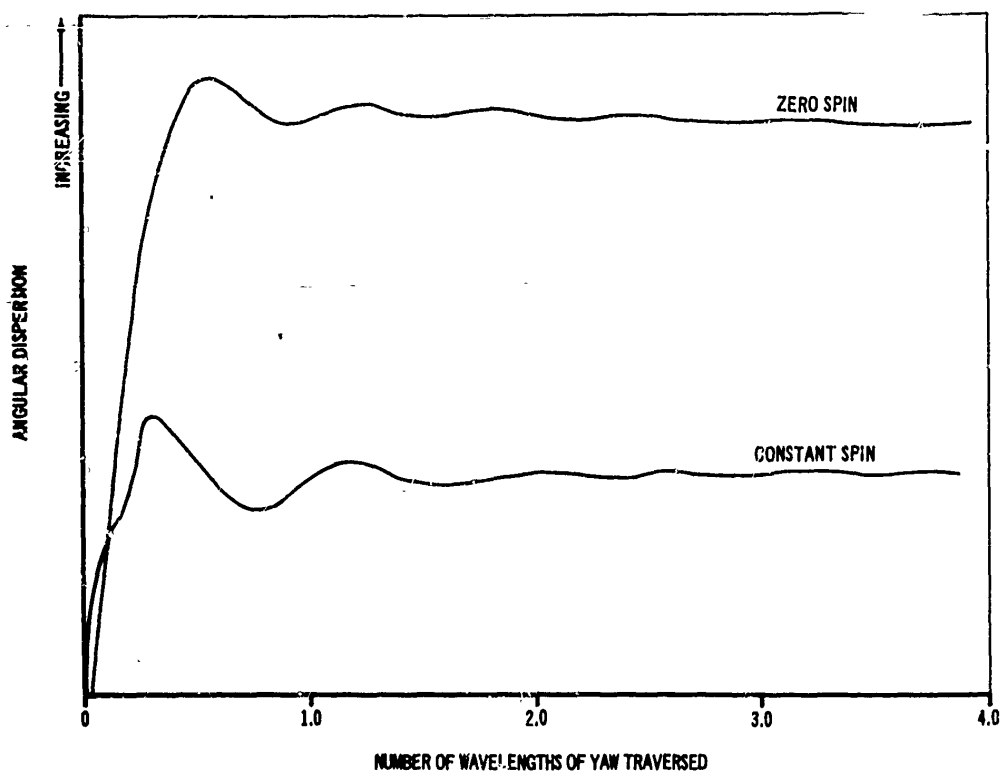


Figure 7-9. Effect of Spin on the Build-Up of Angular Dispersion Due to Thrust Misalignment

Fig. 7-9 describes the variation of the angular dispersion with distance for a typical rocket with and without a slow spin.

From the above discussion, it follows that spin of any kind will have some effect on the angular dispersion of a rocket. The significant factor that determines the effect of a spin technique is the relation between the rotational motion of the body-fixed error and the rotational motion of the rocket about a lateral axis. The rotational motion of the rocket has been shown to be characterized by the wavelength of yaw; therefore, it is expected that this parameter will have a strong influence on the effectiveness of any spin program.

As was shown in Fig. 7-1, most of the angular dispersion takes place during the first yaw oscillation. The spin motion during this period will have the most influence on the angular dispersion.

If the spin is constant or increasing in the same direction, the error will tend to accumulate because the acceleration of the rocket causes the influence of the misalignment to decrease as the rocket momentum increases. Therefore, the dispersion caused by the first half of the spin cycle is not completely compensated for by the second half. A uniform spin program will always result in some finite error.

The above considerations have led investigators to study nonuniform spin programs with the intention of developing techniques that would result in zero angular dispersion. The simplest program to visualize is the instantaneous, 180 deg rotation of the vehicle at some point in the trajectory. The point is chosen so that the accumulation of angular dispersion to that point is completely eliminated by reversing the direction of the error. This concept has been incor-

porated into the Spin-Buck Program which is discussed in par. 7-7.2.4.

Par. 7-7.2 discusses several spin programs which have been of interest to designers of free rockets.

7-3.2.5 The Effect of Dispersion Reduction on the Optimum σ

The amount of dispersion reduction obtained from any given spin program is measured by the parameter β which is the ratio of the dispersion with no spin to the dispersion with the spin program. Other paragraphs in this chapter indicate values of β for several spin programs. Once estimates of β are known, one can find the optimum value of σ which accounts for the combined effects of the spin program on thrust malalignment and of the effect of winds. For short launcher lengths:

$$\sigma_{opt} = \left[\frac{4 \pi k^2 V_w}{\sqrt{G} L \beta} \right]^{2/3} \quad (7-2)$$

where

- k = rocket radius of gyration, ft
- V_w = wind velocity, ft/sec
- G = rocket acceleration, ft/sec²
- L = thrust malalignment distance, ft
- β = dispersion reduction factor, dimensionless

The dispersion for this value of g is given by

$$\gamma_{TS} = \sqrt{\frac{3}{8}} \left[\frac{(4 \pi)^2 L \beta V_w^2}{G k^2} \right]^{1/3} \quad (7-3)$$

It is shown in the following paragraphs that the optimum design depends on yaw oscillation wavelength, launching technique, and error source magnitude. In order that these items may be evaluated, these paragraphs present more detailed discussion of the errors and the means of computing dispersion under varying conditions.

7-4 PRELAUNCH ERRORS

When preparing to launch a rocket at a specified target, we must first establish the launch

angle in the vertical plane (QE) and the azimuth angle under standard conditions. The term *standard* here applies to the flight that exists under arbitrarily chosen meteorological, positional, and material conditions. Corrections must then be made to this standard aiming for variations of the conditions existing for a given flight from the standard. Both the standard aiming and the corrections are generally obtained from a firing table which is a catalog of standard trajectories and corrections for nonstandard conditions. For example, the usual rocket firing table includes the following:

- a. Pertinent data for the standard trajectories of the rocket.
- b. Corrections to the standard aiming to compensate for rotation of the earth.
- c. Corrections to the standard launch elevation (QE) to compensate for variation in propellant temperature, uninhibited propellant weight, atmospheric pressure, density and temperature, inert weight, and wind.
- d. Corrections to the standard azimuth aiming for wind.

7-4.1 AIMING ERRORS

Aiming errors may exist due to any combination of the following:

- a. Incorrect determination of the standard aiming from the firing table.
- b. Error in positioning of the launcher.
- c. Incorrect determination of the corrections to be applied for the nonstandard flight.

These errors, while due to different causes, all result in a physical displacement of the launcher from that position required for the rocket to acquire the target. The errors at payload disposition resulting from aiming errors of the launcher are:

$$\Delta Y = \Delta \psi_o R \quad (7-4)$$

$$\Delta X = \Delta \theta_o \left. \frac{\partial R}{\partial \theta} \right|_{\gamma = \text{const}} \quad (7-5)$$

$$\Delta t = \Delta \theta_o \left. \frac{\partial t}{\partial \theta} \right|_{R = \text{const}} \quad (7-6)$$

AMCP 706-280

$$\Delta Z = \Delta \theta_0 \left. \frac{\partial Z}{\partial \theta} \right|_{t = \text{const}} \quad (7-7)$$

$$\Delta \psi_0 = \psi_{0STD} - \psi_0 \quad (7-8)$$

$$\Delta \theta_0 = \theta_{0STD} - \theta_0 \quad (7-9)$$

where

 ΔY = deflection error, m ΔX = range error, m Δt = time of flight error, sec ΔZ = altitude error, m R = standard range, km $\Delta \psi_0$ = azimuth aiming error, mils $\Delta \theta_0$ = elevation aiming error, mils

The errors are determined by calculating the difference between a flight with an error and a standard trajectory. Fig. 7-10 illustrates these quantities.

The derivatives— $\partial R/\partial \theta$, $\partial t/\partial \theta$, and $\partial Z/\partial \theta$ —will be discussed in more detail in par. 7-8.

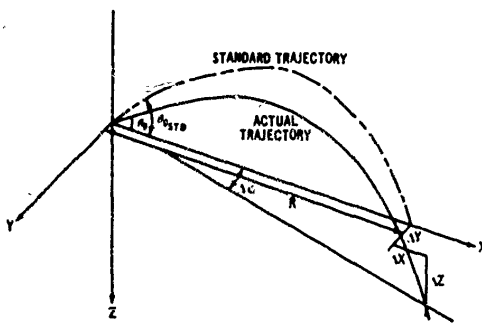


Figure 7-10. Aiming Errors

7-4.2 ERRORS DUE TO VARIATIONS IN METEOROLOGICAL CONDITIONS

In making corrections for nonstandard conditions, one assumes a knowledge of the existing nonstandard conditions. Any variation in conditions from the assumed values introduces an error at the point of warhead disposition. These errors may be treated in the same manner as those described below for the launch, propulsive, and ballistic phases.

7-5 CALCULATIONS OF ANGULAR ERRORS

The angular error of a rocket is obtained by solving the differential equations of motion throughout the flight. The equations can be solved with as much generality as desired on an automatic computer. Values are chosen for the error sources and a number of parametric runs are made. The results can then be combined statistically as outlined in par. 7-10.

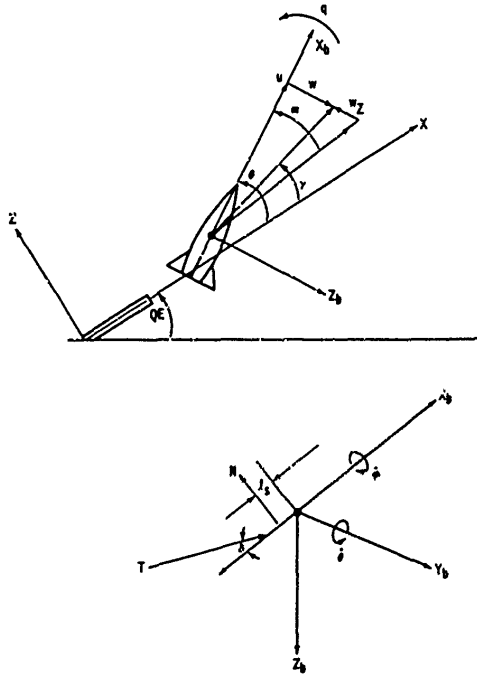


Figure 7-11. Definitions of Sign Conventions for the Rocket Equations of Motion

If we assume missile symmetry about the longitudinal axis (Fig. 7-11)—so that normal small angle approximations are valid—and if we omit gyro effects due to missile roll, then the six-degree-of-freedom equations of motion become decoupled in the vertical and horizontal planes. Furthermore, the motion in the two planes is identical except for the gravity terms in the vertical plane. (The effect of gravity is equivalent to a bias error and will not be considered in these equations.) We can then determine the solution

in only one plane, thus simplifying the problem considerably. The equations to be solved then become

$$\dot{u} = [G] - \frac{\rho u^2}{2} \left[\frac{C_D S}{m} \right] \quad (7-10)$$

$$\dot{w} = qu - \frac{\rho u}{2} \left[\frac{C_{N\alpha} S}{m} \right] (w + w_Z) + [G] \delta \cos \phi \quad (7-11)$$

$$\dot{q} = -u \left[\frac{4\pi^2}{\sigma^2} \right] \left\{ w + w_Z \right.$$

$$\left. - \left[\frac{C_{nq} d}{2C_{N\alpha} l_s} \right] q + \delta_F \cos \phi \right\} + \left[\frac{G l_t}{k^2} \right] \delta \cos \phi \quad (7-12)$$

$$\dot{X} = u \quad (7-13)$$

$$\dot{Z} = w - u \theta \quad (7-14)$$

$$\dot{\theta} = q \quad (7-15)$$

$$\dot{\phi} = f(t) \quad (\text{This is specified by the spin program.}) \quad (7-16)$$

where

- u, w = components of the rocket velocity in the directions of the X_b and Z_b body axes, ft/sec
- $q, \dot{\phi}$ = components of the rocket angular velocity in the directions about the Y_b and X_b body axes, rad/sec
- θ = rocket pitch angle, rad
- ϕ = rocket roll angle, rad
- \dot{X} = component of the rocket velocity in the slant range direction, ft/sec
- \dot{Z} = component of the rocket velocity normal to the slant range direction, ft/sec
- G = rocket acceleration due to the thrust, ft/sec²
- C_D = aerodynamic drag coefficient, nondimensional
- m = rocket mass, slug
- S = aerodynamic reference area, ft²

$C_{N\alpha}$ = aerodynamic normal force gradient, rad⁻¹

C_{nq} = aerodynamic damping moment coefficient, dimensionless

l_s = aerodynamic static margin, cal

l_t = distance from center of gravity to point of thrust application, ft

d = reference body diameter, ft

k = rocket radius of gyration, ft

δ = thrust malalignment angle, rad

δ_F = aerodynamic malalignment angle, rad

w_Z = component of wind in direction of the Z_b body axis, ft/sec

σ = wavelength of yaw, ft

ρ = atmospheric density, slug/ft³

X_b, Y_b, Z_b = body-fixed axes with origin at the center of gravity and X_b along the missile axis

The six expressions in brackets completely specify all the rocket characteristics needed to calculate its motion. Therefore, if the rocket motion is tabulated for variations in each of the six expressions, the results will be applicable to any configuration for which these parameters are known.

Examination of the solutions of the above equations for typical rocket systems indicates that only a relatively few parameters have first-order effects on the angular dispersion. These are the rocket acceleration G , the wavelength of yaw σ , the nondimensional launcher length P , and the burning distance S .

For the equations above, the launcher affects the motion of the rocket through the initial conditions. For convenience, we shall use a nondimensional expression for the launcher length:

$$P = \frac{\text{launcher length}}{\sigma}$$

The effect of launcher length, then, is represented by an initial value of velocity;

$$u_p = \sqrt{2PG\sigma} \quad (7-17)$$

where u_p = velocity in ft/sec at the end of the launcher.

These equations can now be solved on an analog or digital computer and the dispersion at the end of flight determined for any given error source.

AMCP 706-280

A more informative approach for the designer is to consider each phase separately and identify the major contributors to the latent error.* In each flight phase different forces predominate; therefore, the important parameters change. In the following subparagraphs the important parameters for each phase will be discussed.

Considering the errors in each flight phase separately has two advantages: (1) the equations can be simplified by including only the forces that predominate during the phase, and (2) the simplified equations can be manipulated to provide analytical solutions. The availability of analytical solutions is of great benefit to the designer because the important variables or combinations of variables that determine the angular error can be easily identified. These results can then be combined with computer calculations that provide the required accuracy.

Analytical results have been prepared wherever possible and have been plotted with computer results to illustrate their accuracy.

The criterion chosen for determining the accuracy of a rocket system during the launch and propulsive phases is the dispersion at warhead event. The effects of various errors and the effectiveness of several dispersion reduction techniques will be considered in terms of the steady-state flight path angular error. This representation allows rapid evaluation of the accuracy of the rocket without resorting to the complex methods of accounting for ballistic phase errors presented in par. 7-9.

The rocket equations were solved, using an automatic computer, for the burning phase of flight. The angular dispersion at the end of the boost phase is approximated by the following expression:

$$\gamma_{TS} = \theta - \frac{r}{u} + \frac{qk^2}{ul_s} - \frac{\rho S d C_{nq}}{4m u l_s} (w + w_z) \quad (7-18)$$

where the values of θ , w , u , q and the aerodynamic parameters are those at burnout. γ_{TS} is determined by computing $\lim_{t \rightarrow \infty} \frac{z}{u}$ which is the

*The latent angular error is the error at the end of a given phase. The idealized trajectory must then be used to determine the error at the end of flight.

steady state, post-boost angular dispersion of the direction of the velocity. Thus, for calculating the effect of the boost phase on dispersion at warhead event, γ_{TS} may be treated as an aiming error. The missile is assumed to be launched with the initial conditions taken from booster burnout.

7-6 LAUNCH PHASE ERRORS

During the launching process the rocket is deflected from its intended path by motion of the launcher and motion caused by the release of the launcher constraints. The results are conditions undesirable at the beginning of the propulsion phase. These conditions are separated into three modes of motion: (1) initial angular velocity about a lateral axis, (2) initial translational velocity normal to the launcher axis, and (3) angular velocity resulting from rocket dynamic unbalance when some form of spin on the launcher is used. Subparagraphs 7-6.1 through 7-6.3 present the angular dispersion at flight termination caused by these initial conditions.

7-6.1 ANGULAR VELOCITY

Figs. 7-12 (A), (B), (C) show the angular dispersion caused by an initial angular velocity of 100 mils per sec. The launcher length, the wavelength of yaw, and acceleration have substantial effects on the dispersion. The dispersion is minimized by increasing the launcher length and the rocket acceleration while keeping the aerodynamic stability as high as possible, i.e., a small value of σ .

7-6.2 TRANSLATIONAL VELOCITY

Figs. 7-13 (A), (B), (C) show the effect of an initial translational velocity of 1 ft per sec, normal to the launcher line, on the angular dispersion. The launcher length does not significantly affect the dispersion. An increase in the wavelength of yaw has a beneficial effect that is significant for rockets with high aerodynamic stability. Increasing the rocket acceleration causes a decrease in the dispersion for all cases considered.

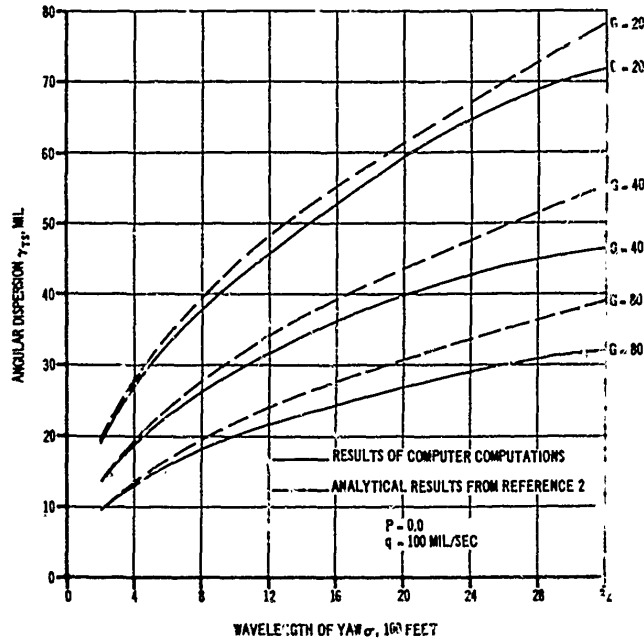


Figure 7-12(A). Angular Dispersion Due to Malfunction - Initial Angular Rate

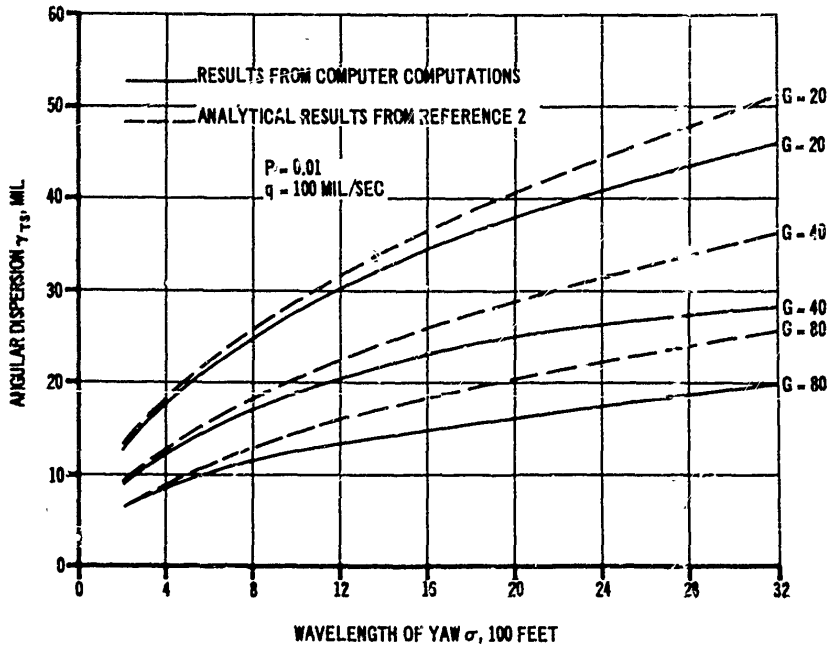


Figure 7-12(B). Angular Dispersion Due to Malfunction - Initial Angular Rate

AMCP 706-280

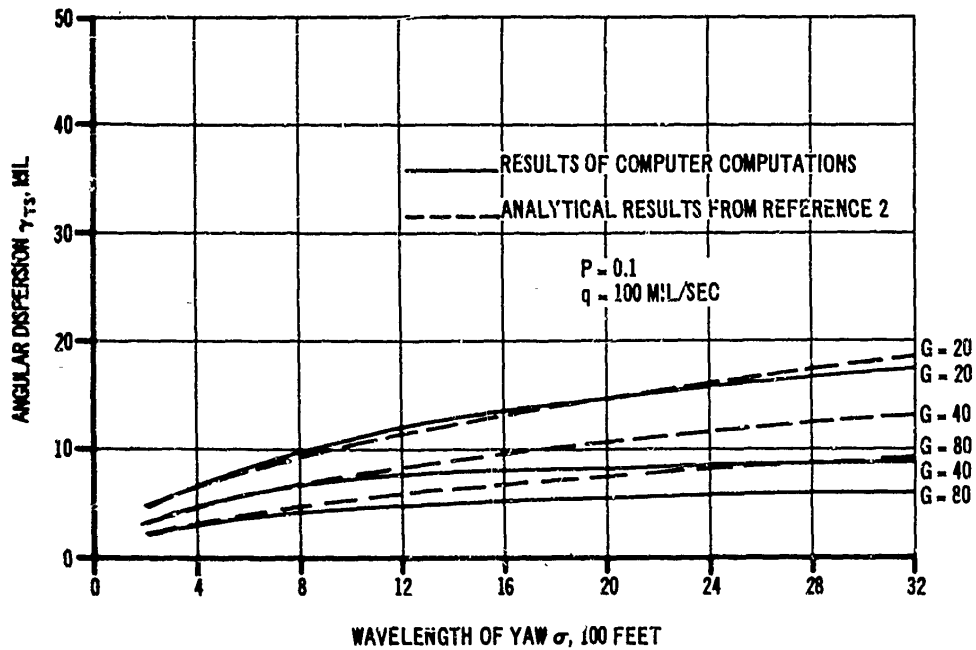


Figure 7-12(C). Angular Dispersion Due to Mallaunch - Initial Angular Rate

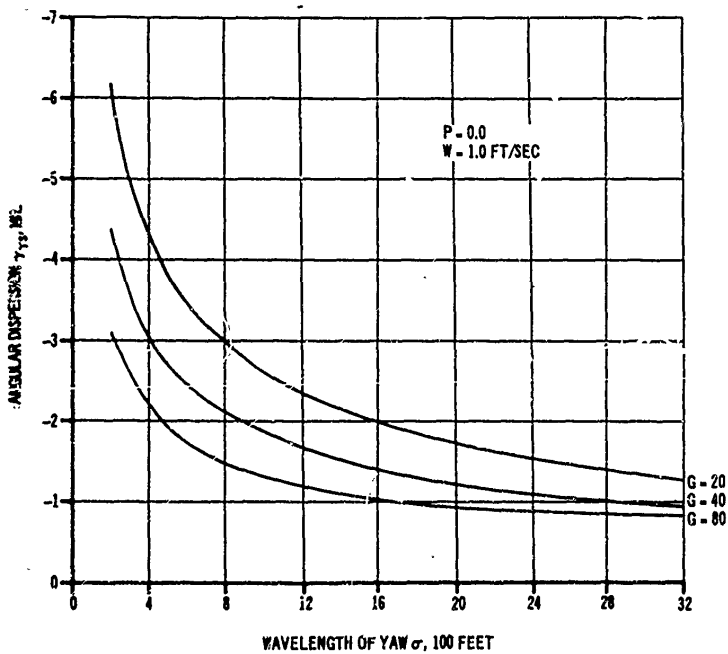


Figure 7-13(A). Angular Dispersion Due to Mallaunch - Initial Translational Velocity

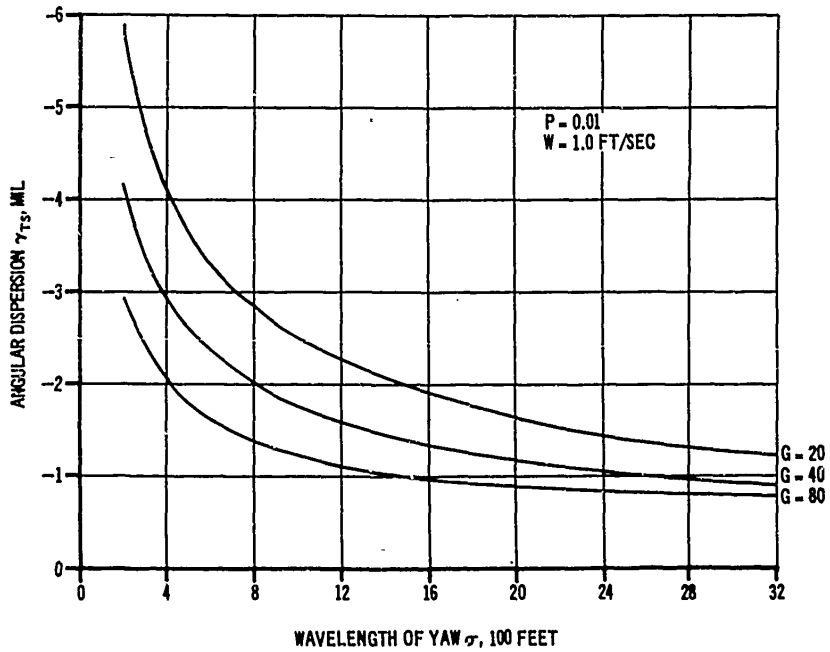


Figure 7-13(B). Angular Dispersion Due to Mallaunch - Initial Translational Velocity

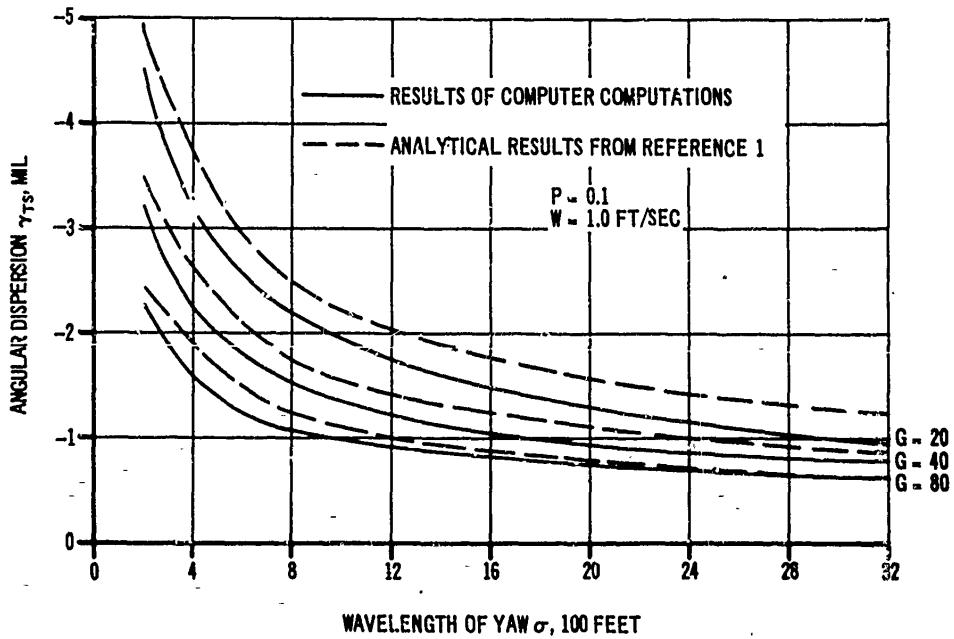


Figure 7-13(C). Angular Dispersion Due to Mallaunch - Initial Translational Velocity

AMCP 706-280

The angular dispersion due to initial translational velocity is minimized by making the rocket acceleration as high as possible and the aerodynamic stability low.

7-6.3 DYNAMIC UNBALANCE

Dynamic unbalance is caused by spinning the rocket about its geometric longitudinal axis rather than its principal axis of inertia. When the rocket is spun on the launcher, release of the launcher constraints will result in a motion characteristic of the force-free precession of a rigid body unless the rocket is spinning about its principal axis of inertia (i.e., its dynamic axis). The dynamic unbalance effect limits the spin rate that can be used to reduce thrust malalignment effects.

The precession motion is, for all practical purposes, an angular velocity at launch. The magnitude of this initial angular velocity is:

$$q_{equiv} = p\epsilon$$

where:

- p = rocket spin rate, rad/sec
- q_{equiv} = equivalent initial angular rate due to dynamic unbalance, rad/sec
- ϵ = angle between the rocket longitudinal and principal axes, rad

After determining the equivalent angular velocity, Figs. 7-12, 7-13, and 7-14 can be used to determine the angular dispersion.

The dispersion due to dynamic unbalance is minimized by increasing the launcher length and the rocket acceleration while maintaining a high level of aerodynamic stability. In addition, the dynamic unbalance angle ϵ should be kept as small as possible by careful design and care in manufacturing. The spin rate should be kept as low as possible after considering the requirement for reducing the dispersion due to thrust malalignment.

Par. 7-7.2.6 describes how the effect of dynamic unbalance at launch can be reduced by a unique launcher design.

7-7 PROPULSION PHASE ERRORS

Angular errors which originate during the propulsion phase of flight are primarily caused by

wind normal to the direction of flight, and thrust malalignment. A qualitative description of the effect of wind and thrust malalignment was given in par. 7-3. This paragraph presents some quantitative results which describe the effects of the important rocket parameters on the angular dispersion caused by the same two error sources, wind and thrust malalignment. These results can be used for preliminary accuracy estimates.

Par. 7-3 showed how spinning the rocket about its longitudinal axis will reduce dispersion caused by body-fixed error sources such as thrust malalignment. The major portion of this paragraph is devoted to describing the effectiveness of several spin programs developed to minimize the angular error due to body-fixed error sources. In most applications, the choice of a spin technique is heavily influenced by the difficulty of mechanically implementing it. Therefore, while several of the methods presented here result in near-zero dispersion, complexity of the devices needed to carry out the spin program limit its use to systems where high accuracy requirements justify extreme measures.

7-7.1 NONROTATING ROCKET

Figs. 7-14 (A), (B), (C) and 7-15 (A), (B), (C) show the angular error caused by a 10 ft per sec wind normal to the flight path of the rocket and by a 0.5-mil thrust malalignment on a non-rotating rocket.

Since the wind force on a symmetric rocket does not depend on the roll orientation, spin does not affect the dispersion due to wind. Therefore, Figs. 7-14 (A), (B), (C) are applicable to any rocket system.

As was pointed out in par. 7-3, the angular dispersion due to wind is minimized by keeping the aerodynamic stability as low as possible. The figures indicate that launcher length has very little effect on the wind dispersion. The rocket acceleration should be large.

The dispersion due to thrust malalignment is minimized by keeping the aerodynamic stability as high as possible. The effect of acceleration is most significant for rockets with low stability. The angular dispersion increases with increasing acceleration. The effect of launcher length is significant under all conditions—a long launcher is desirable.

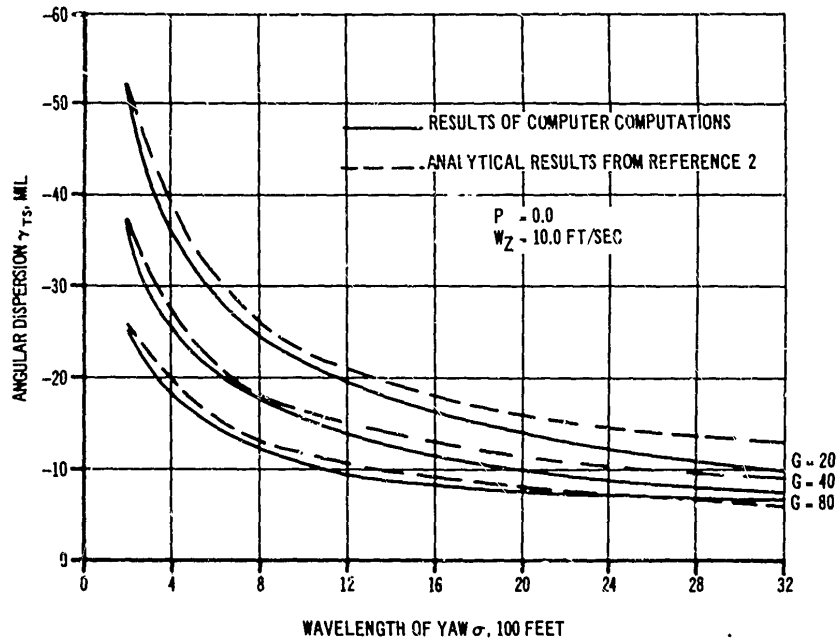


Figure 7-14(A). Angular Dispersion Due to Wind

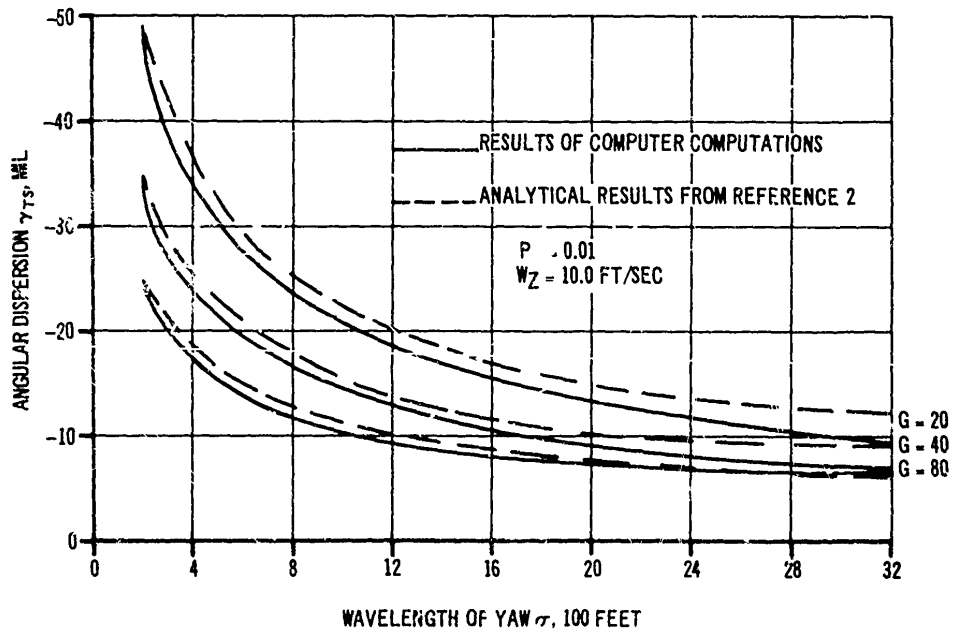


Figure 7-14(B). Angular Dispersion Due to Wind

AMCP 703-280

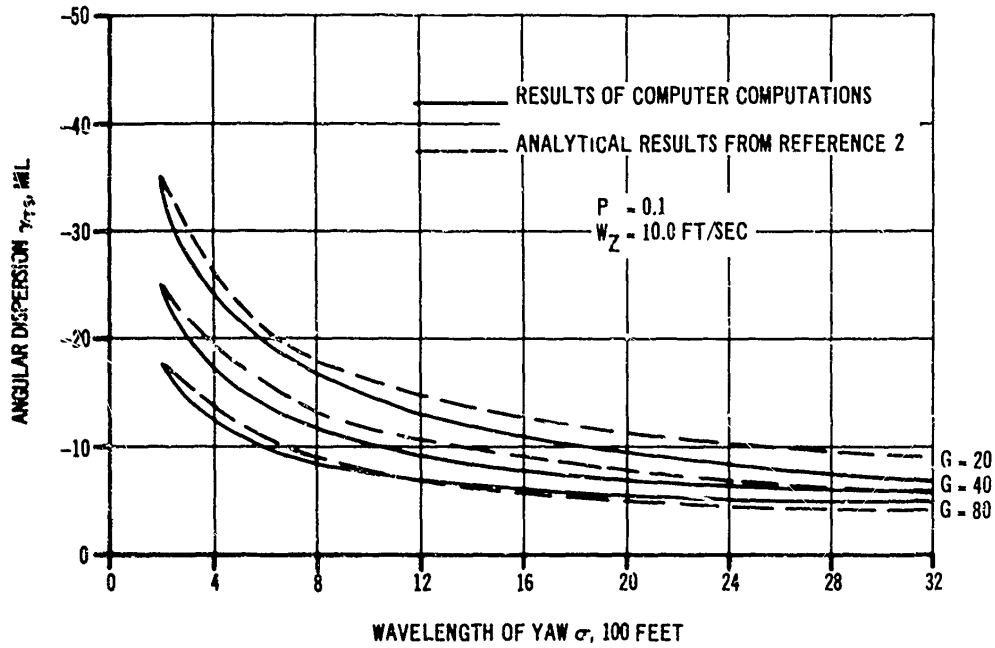


Figure 7-14(C). Angular Dispersion Due to Wind - Initial Translational Velocity

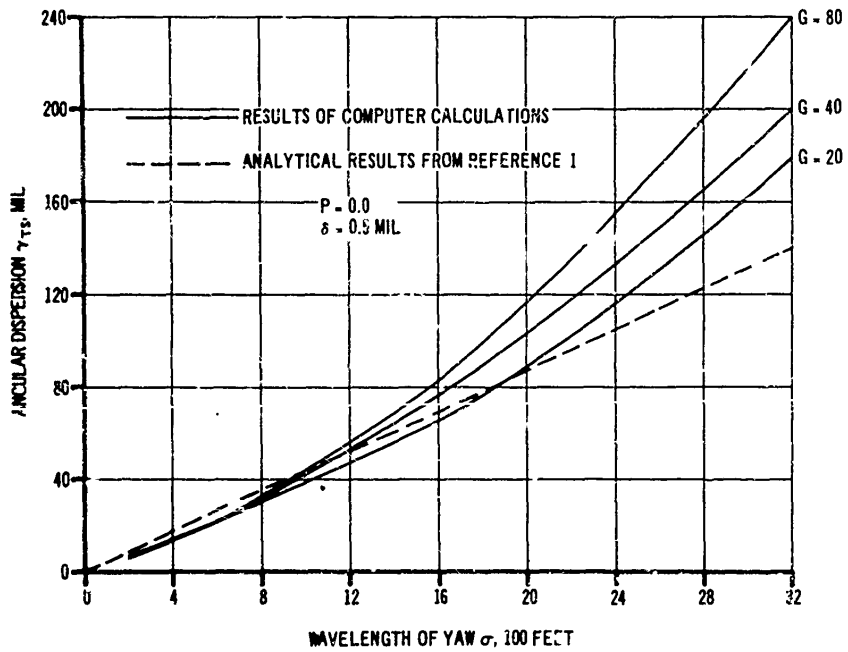


Figure 7-15(A). Angular Dispersion Due to Thrust Malalignment - Zero Spin

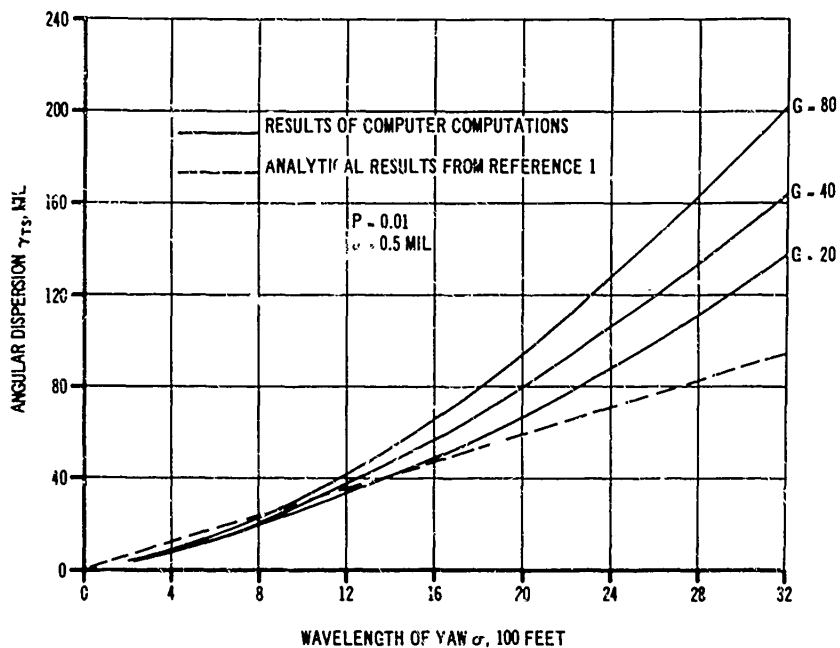


Figure 7-15(B). Angular Dispersion Due to Thrust Malalignment - Zero Spin

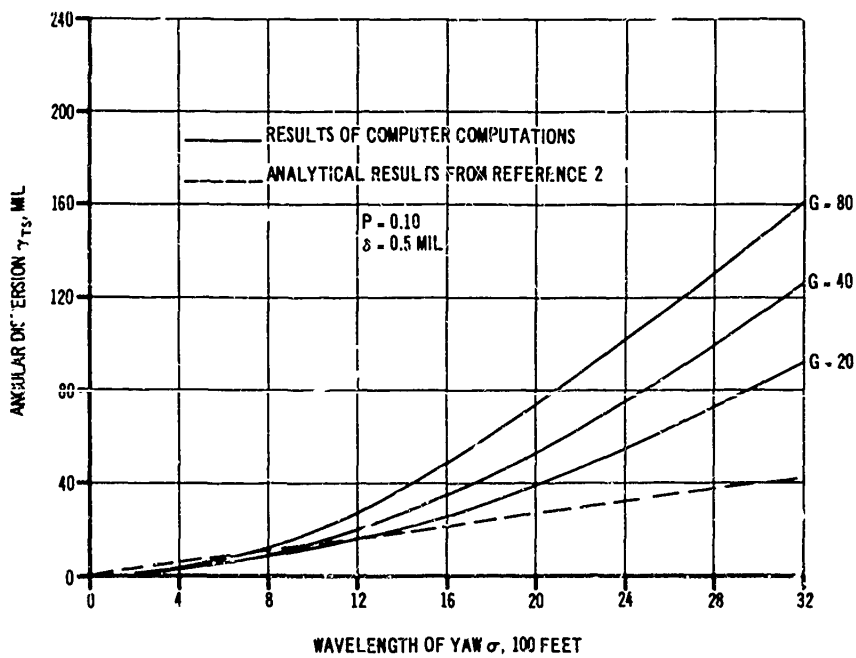


Figure 7-15(C). Angular Dispersion Due to Thrust Malalignment - Zero Spin

AMCP 706-280

7-7.2 DISPERSION REDUCTION TECHNIQUES

Par. 7-3 pointed out that the conflicting requirements on aerodynamic stability caused by wind and thrust malalignment could be overcome by reducing the effects of the malalignment with a separate technique. The most common methods used to reduce the malalignment error employ spin; however, there are other possibilities, such as the variable acceleration program described in par. 7-7.2.6.

The effectiveness of a given method in reducing angular dispersion is represented by the dispersion reduction factor β . β is the ratio of the value of angular dispersion associated with the dispersion reduction scheme being considered to the value of dispersion for a nonrotated rocket.

7-7.2.1 Constant Spin Rate

Fig. 7-9 indicates that, with constant spin, thrust malalignment has its greatest effect during the first wavelength of yaw, but is almost negligible during the remainder of the flight. This observation leads to the use of the number of revolutions made by the rocket during this initial period as one of the most important spin parameters. n_{σ} is the number of revolutions the rocket makes during the first wavelength. Fig. 7-16 shows the dependence of the dispersion reduction factor β on n_{σ} .

Various techniques can be used to achieve spin. Any method used must be capable of spinning the rocket without imparting unwanted motion to the rocket. The importance of spin during the early portion of flight eliminates aerodynamic fins as a means of obtaining it since fins are least effective during this time. The most common method of providing spin is through auxiliary rockets fired in a circumferential direction.

The importance of early spin has led to the development of systems where the spin is accomplished while the rocket is still on the launcher. These systems involve many mechanical problems because of the difficulties involved in clearing the rocket fins and in releasing the launcher constraints without introducing translational or angular motion to the rocket.

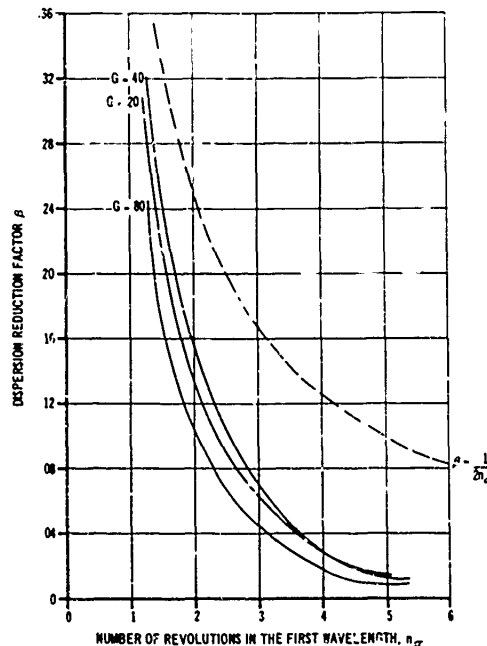


Figure 7-16. Effect of Constant Spin on Angular Dispersion

Fig. 7-16 shows that the angular dispersion decreases as the number of revolutions in the first wavelength increases. On the other hand, the dispersion due to dynamic unbalance increases with spin. These two effects result in an optimum spin rate, beyond which the dispersion reduction associated with thrust malalignment is lost to the dynamic unbalance effect. The spin rates used for the constant-spin results are the optimum values for a dynamic axis malalignment ϵ of 0.5 mil.

Figs. 7-17(A), (B), (C)—for the case of constant spin—present the effects of rocket acceleration G , nondimensional launcher length P , and wavelength of yaw σ , on the dispersion reduction factor β . The wavelength of yaw can be seen to have the greatest influence on the dispersion reduction.

In practice, constant spin is not achieved. The programs that are called constant spin are actually composed of a period of high angular acceleration when the spin rockets are fired, followed by a slow deceleration caused by aerodynamic forces on the fins.

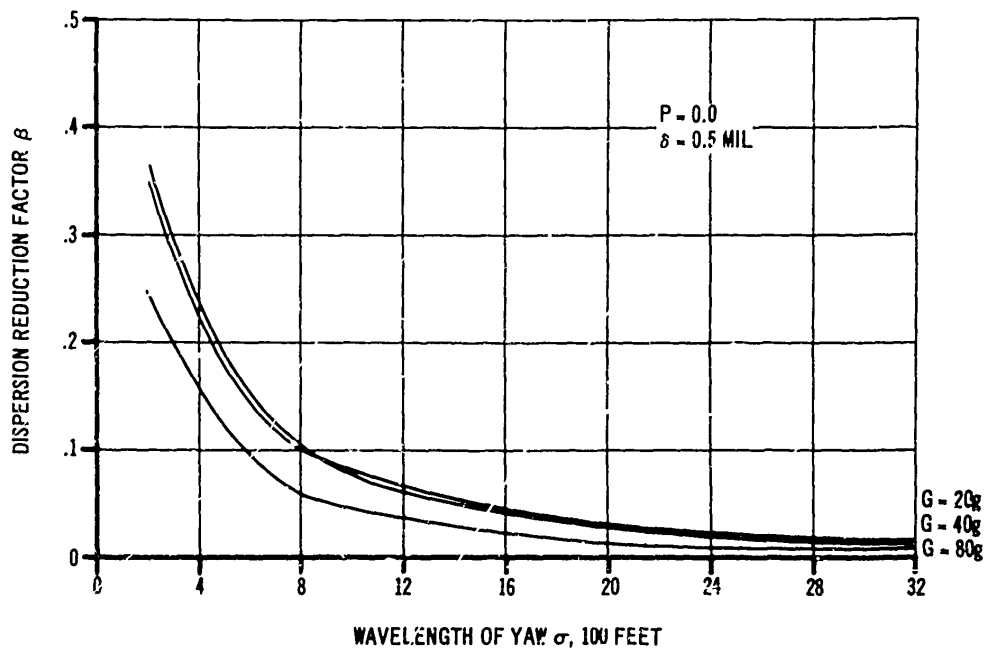


Figure 7-17(A). Constant Spin

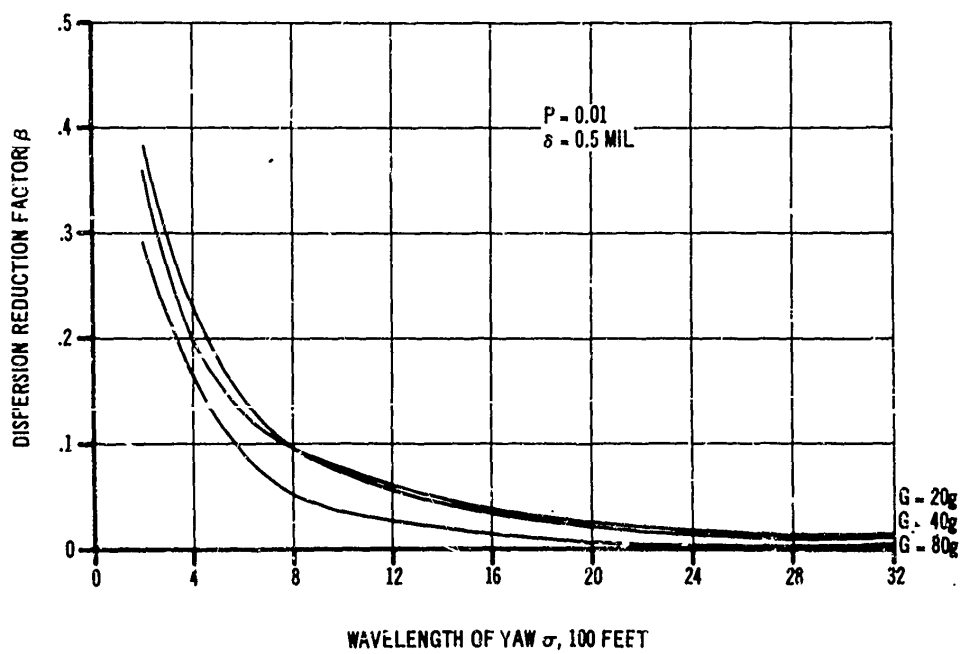


Figure 7-17(B). Constant Spin

AMCP 706-280

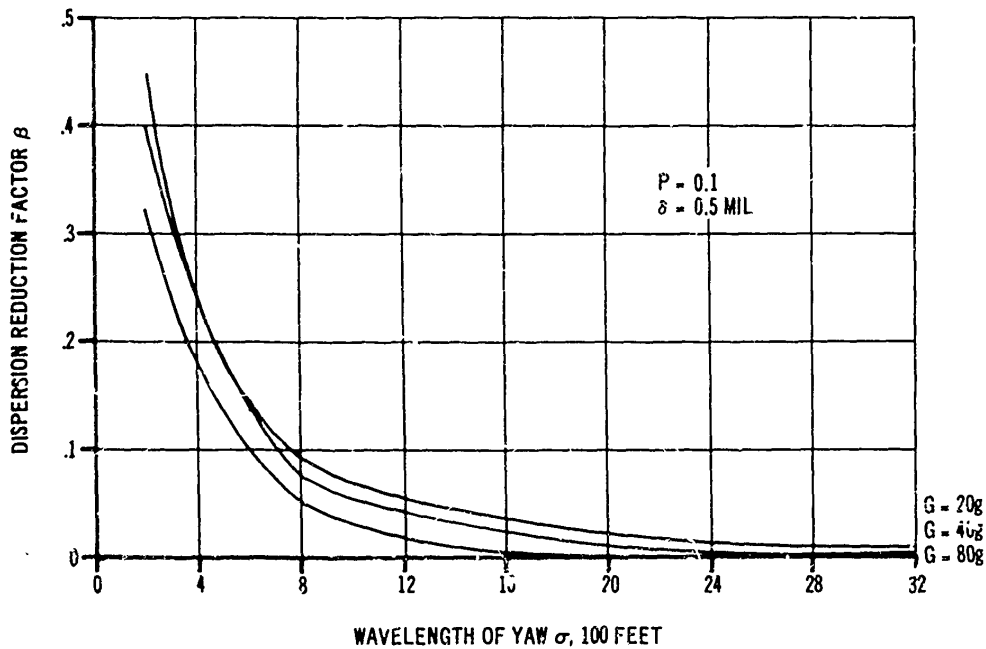


Figure 7-17(C). Constant Spin

7-7.2.2 Constant Spin Acceleration

The dispersion reduction technique which is probably the easiest to implement is the constant spin acceleration. This can be achieved by canting the nozzles of the rocket motors (if more than one motor is used) or by placing fins in the rocket exhaust. Unfortunately, due to the slow initial spin, the technique is not as effective as the constant spin.

Figs. 7-18 (A), (B), (C) present the effects of the rocket variables on the dispersion reduction factor for constant spin acceleration. The most significant variable is the wavelength of yaw. The wavelength should be long to minimize the dispersion.

7-7.2.3 Slowly Uniformly Decreasing Spin (SUDS)

The preceding spin programs always result in some finite dispersion. According to the mathematical theory of rocket flight (see Reference 6), it is possible to devise spin programs which re-

sult in zero angular dispersion. One such program is that of a Slowly Uniformly Decreasing Spin (SUDS); another is the Spin-Buck program.

The SUDS program begins with a constant spin which is followed by a constant deceleration. The initial spin rate and the value of the deceleration are functions of the rocket parameters. The angular error is very sensitive to changes in the spin rate or the deceleration. For this reason it is not possible to achieve zero dispersion in practice. Also, the limitations of the rocket theory make the zero dispersion result invalid. Figs. 7-19 (A), (B), (C) present the dispersion reduction for SUDS when the assumptions of the rocket theory are removed.

7-7.2.4 Spin-Buck

The Spin-Buck program is an attempt to eliminate the angular dispersion caused by thrust misalignment by reversing the spin direction of the rocket. By this reversal, the error accumulated prior to the reversal should be cancelled by the

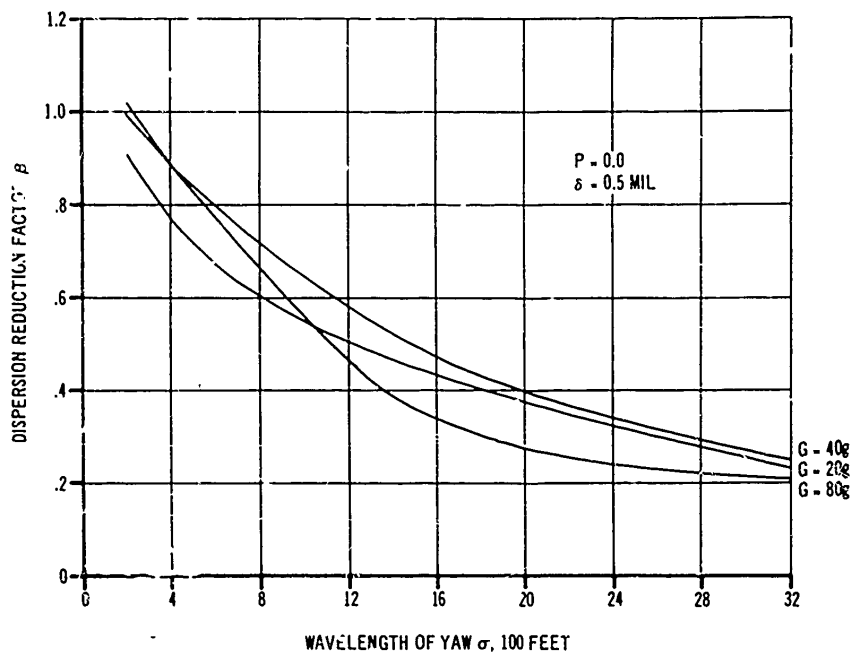


Figure 7-18(A). Constant Spin Acceleration

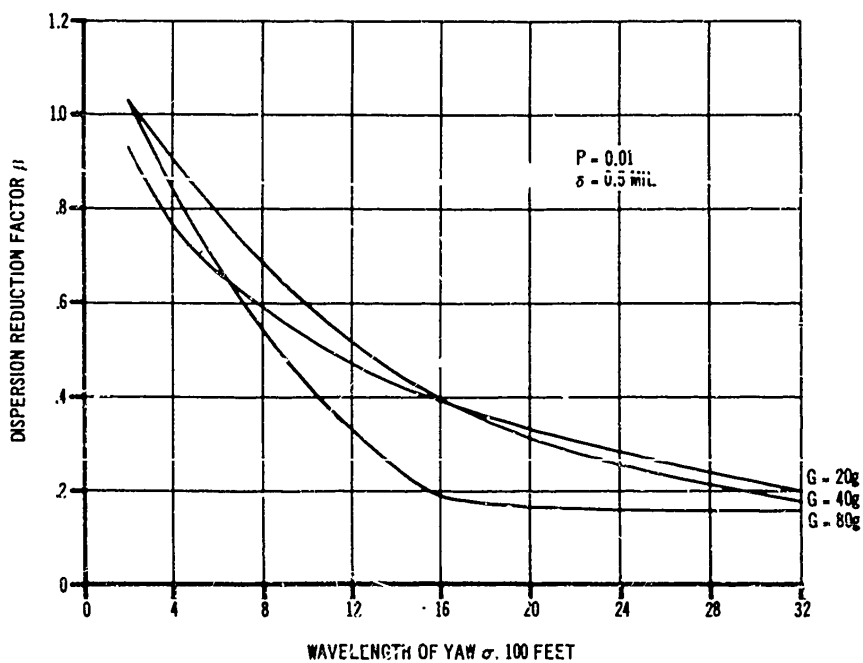


Figure 7-18(B). Constant Spin Acceleration

AMCP 706-280

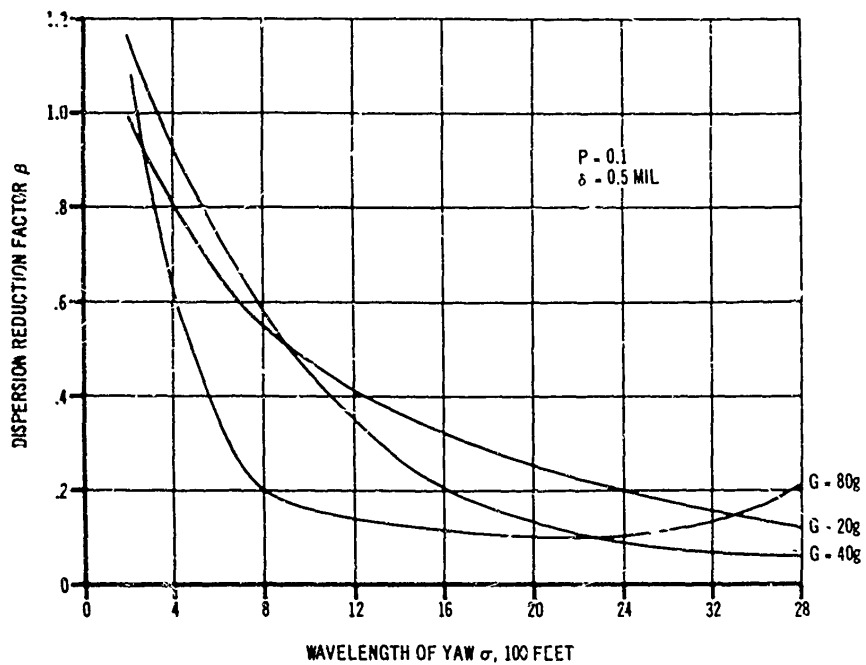


Figure 7-18(C). Constant Spin Acceleration

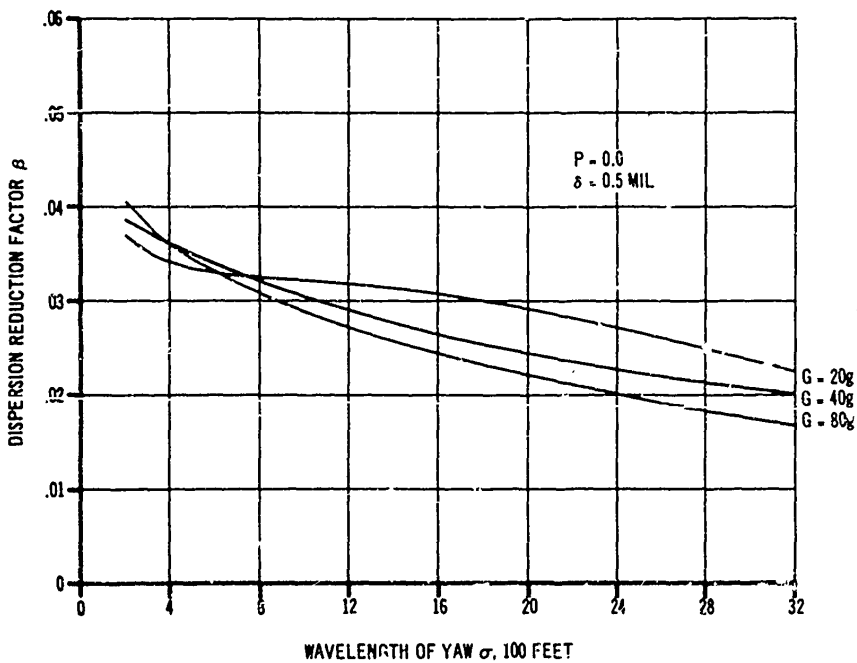


Figure 7-19(A). Slowly Uniformly Decreasing Spin (SUDS)

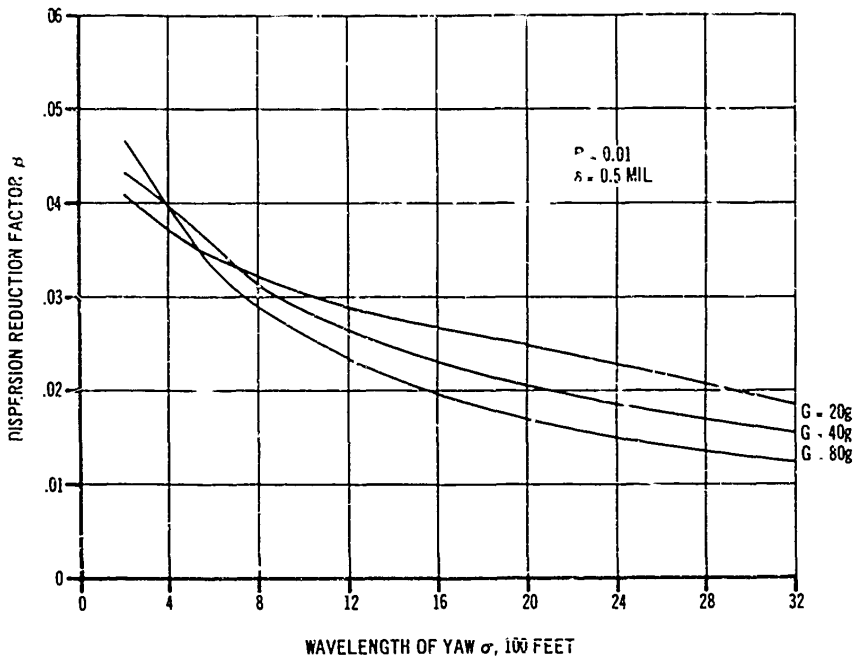


Figure 7-19(B). Slowly Uniformly Decreasing Spin (SUDS)

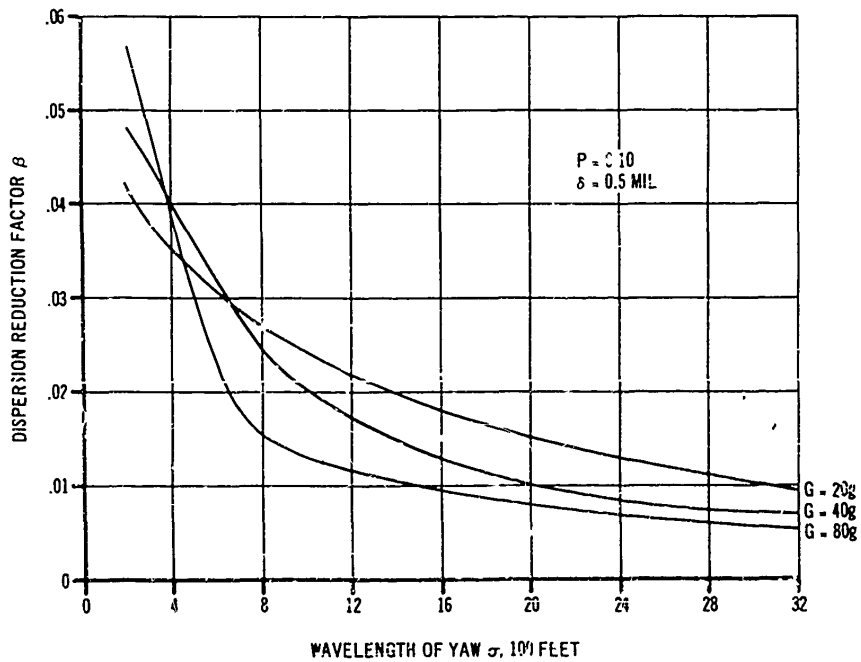


Figure 7-19(C). Slowly Uniformly Decreasing Spin (SUDS)

AMCP 706-280

subsequent error. The motivation behind this concept can be better understood if we consider the case of a nonrotating rocket with a thrust malalignment. We know from Fig. 7-1 that the dispersion builds up rapidly during the first wavelength. If at some instant during this build-up the rocket were rotated 180 degrees, the thrust malalignment would cause the dispersion to go to the negative direction. With the proper choice of the rotation point, the resultant dispersion will be zero.

Since most of the angular dispersion occurs in a very small portion of the flight, it might be expected that the point at which the rotation occurs is very near the launch point. Fig. 7-20 shows how the distance for the instantaneous rotation varies with rocket acceleration and wavelength of yaw.

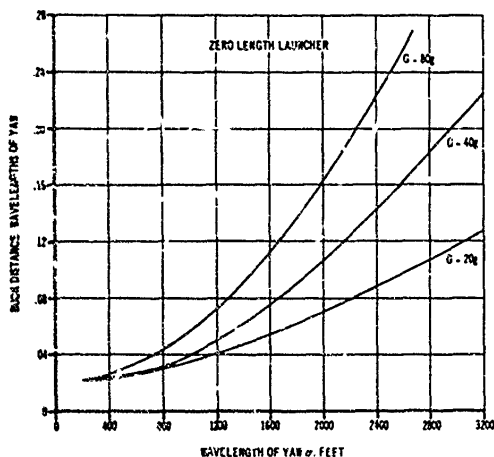


Figure 7-20. Effect of Wavelength of Yaw on Buck Distance for Zero Angular Dispersion

From a practical standpoint, one shortcoming of this concept is the high sensitivity of the dispersion reduction factor to errors in the rotation distance. Fig. 7-21 indicates that, for a rocket acceleration of 40 g's, an error in rotation or buck distance of 7 percent produces a 40-percent change in the dispersion reduction factor.

The Spin-Buck program is accomplished by firing two banks of spin rockets, one following the other and in opposing directions. The net result is similar to the idealized case discussed above. A small residual spin is allowed, to re-

duce the effect of any error related to inaccuracies in the system.

Field tests of the Spin-Buck program indicate that a dispersion reduction factor of 0.1 is possible.

7-7.2.5 Prespin Automatic Dynamic Alignment (PADA)

The PADA concept for dispersion reduction differs from those discussed above in that it is not simply a method of spinning the rocket to reduce the effect of thrust malalignment, but incorporates a novel launcher design to reduce errors due to mallaunch, thrust malalignment, and dynamic unbalance. Par. 7-3.2.2 pointed out that control of these errors allows the aerodynamic stability requirement to be reduced. This control also results in a decrease in the rocket's wind sensitivity.

Development of the PADA launcher evolved from the desire to launch a rocket with an initial spin rate. The problem of bulky launchers, which developed in past attempts at launching spinning rockets, was eliminated by mounting the launching shoes on rings attached to the rocket by bearings. The dynamic unbalance effect—which normally limits the maximum spin rate (par. 7-7.2.1)—has been overcome by a spring suspension system, designed so that natural frequency of transverse angular motion of the rocket on the launcher is considerably less than the rocket spin frequency. The result is that the rocket dynamic axis aligns itself with the spin axis. Theoretically (Reference 8), PADA launchers can be constructed that will reduce the effect of dynamic unbalance by more than 90 percent, and possibly even by as much as 99 percent.

7-7.2.6 Variable Acceleration

The final dispersion reduction technique is unusual in that it does not utilize spin of any kind. Instead, the dispersion reduction is accomplished by changing the acceleration history of the rocket. This can be done with a throttleable rocket motor or with a combination of rocket motors. The example we shall consider here is a rocket with two levels of acceleration. The thrust level is assumed to vary instantaneously at the same point in the flight (Reference 9).

AMCP 706-280

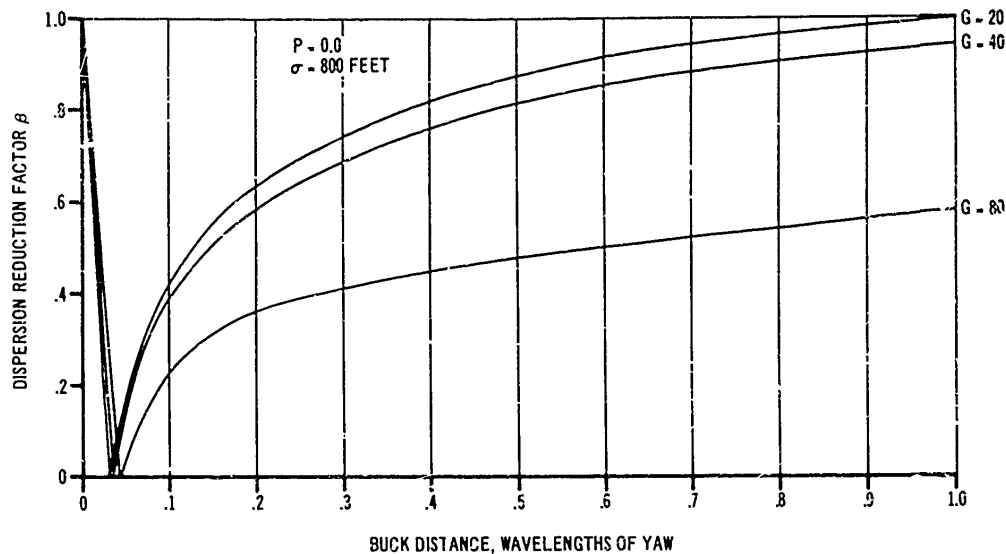


Figure 7-21. Effect of Buck Distance on Dispersion Reduction

How the rocket translational acceleration affects the angular dispersion is not immediately obvious. Reference 9 indicates that the dispersion due to various error sources, such as malalignment and thrust malalignment, is affected differently by the change of acceleration. However, the descriptor below, taken from Reference 9, describes the phenomenon.

The dispersion γ is found by integrating $\dot{\gamma}$ with flight time. It can be shown that $\dot{\gamma}$ is an oscillating function whose magnitude varies as $1/V^2$. Therefore, the first half-cycle (when $\dot{\gamma}$ has one sign) has greater amplitude than the second half-cycle (when $\dot{\gamma}$ has the opposite sign). The result obtained when $\dot{\gamma}$ is integrated over the entire cycle is that the first half-cycle dominates the second. If the acceleration is decreased at some time before the second cycle begins, the contribution of the second half-cycle can be increased and made to offset the first half.

The variable acceleration technique is presented here to show that there is a possibility for dispersion reduction without spin. However, the technique requires more research before its usefulness can be evaluated.

7-8 BALLISTIC PHASE ERRORS

7-8.1 FORCES ACTING ON THE PROJECTILE

The only forces acting during the ballistic phase are aerodynamic and gravitational. The aerodynamic forces can be separated into drag and those forces acting normal to the flight path.

The aerodynamic forces acting normal to the flight path are due to lift and cross spin. The aerodynamic lift force is well known; the cross spin force is a result of the air flow being disturbed by rotation of the projectile about a lateral axis. The rotation causes a variation of the angle of attack along the body, resulting in an unsymmetric force.

7-8.2 SOURCES OF ERROR

From the definition of dispersion, any force which causes the projectile to deviate from the idealized trajectory will be included as a source of error. Since only drag is considered in calculating the idealized trajectory, normal forces as well as changes in drag will introduce dispersion

AMCP 706-280

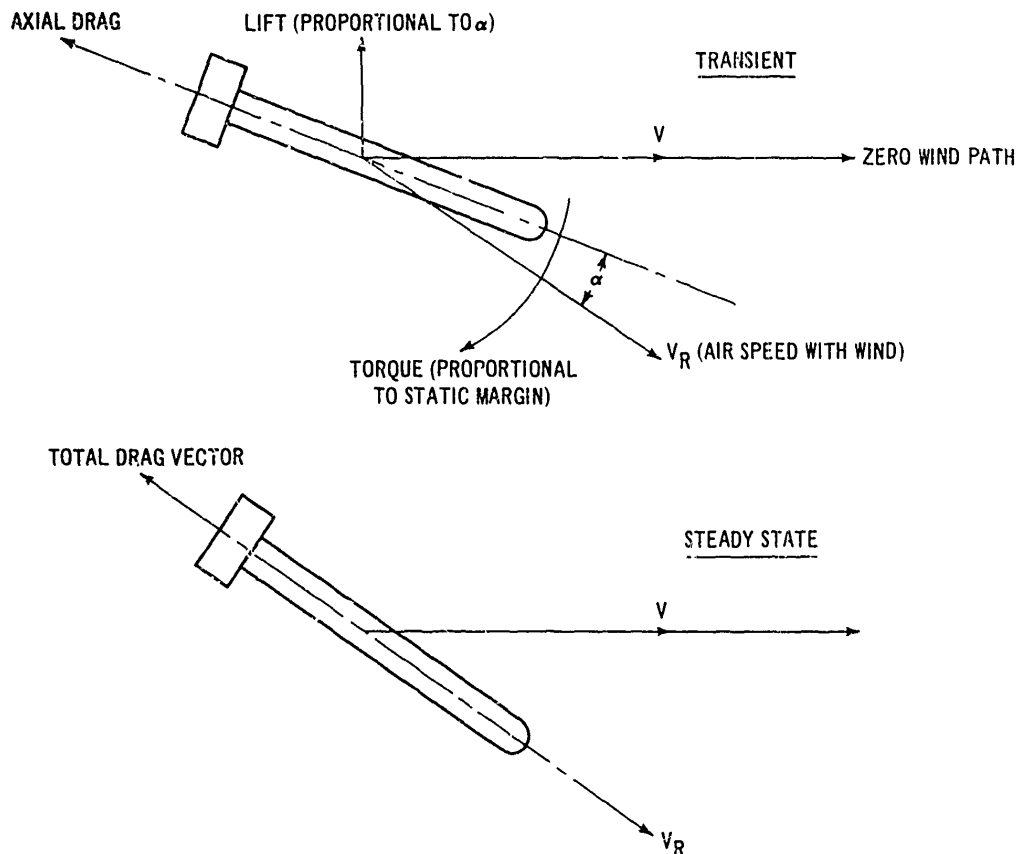


Figure 7-22. Action of Winds on a Free Rocket

In addition to dispersion of the flight path, errors associated with fuzing the warhead must also be considered.

7-8.2.1 Errors Due to Winds

The action of winds on a free rocket in its ballistic phase (Figure 7-22) generates three perturbing forces that affect the missile trajectory:

a. **Change in Drag Magnitude.** Ballistic wind will cause a change in air speed and, consequently, in dynamic pressure and drag force magnitude. This effect will usually be negligible.

b. **Lift Forces.** A change in wind velocity normal to the ballistic flight path will cause an angle of attack, and consequently, the develop-

ment of a lift force. Since this is a transient effect, it is usually very small.

c. **Change in Drag Direction.** In its steady state response to a normal wind, a stable missile will be oriented at some angle with respect to its zero-wind flight path. Since the total drag force vector still lies along the missile axis, it will cause an acceleration in the downwind direction until the missile dispersion velocity reaches the wind velocity. This is the predominant force causing ballistic wind error. Since high-altitude winds can reach high velocity—e.g., the jet stream—an attempt is frequently made to compensate for the winds in the aiming process. This can be accomplished by use of data from firing tables, weather balloons, etc.

7-8.2.2 Change in Drag

A projectile will seldom have an actual drag history exactly the same as the one used in the calculation of the idealized trajectory. Inaccuracies inherent in the methods of determining drag—as well as inaccuracies resulting from manufacturing errors and damage in handling—are typical causes of these drag deviations. Therefore, the effect of changes in the ballistic coefficient C must be considered as a source of dispersion.

7-8.2.3 Nonstandard Conditions

A departure from nonstandard atmospheric conditions will also be considered. This effect is equivalent to a change in drag.

7-8.2.4 Malalignment of Fins

Projectiles with fins that have become malaligned or bent due to careless handling or manufacturing error will cause aerodynamic forces resulting in dispersion. However, fin malalignment will also cause a slow spin which tends to reduce the effect of the error (Reference 1, p. 60).

7-8.2.5 Static Unbalance

Manufacturing tolerances usually result in the projectile center of gravity being located off the longitudinal axis. The aerodynamic forces will then produce a moment resulting in an angle of attack. The dispersion due to static unbalance can be reduced by a slow spin.

7-8.2.6 Dynamic Unbalance

Manufacturing tolerances plus the unavoidable unsymmetric placement of small components or uneven propellant-burning will result in the inertial spin axis being displaced from the projectile centerline. Therefore, if spin is used to reduce other sources of dispersion, error will be introduced due to dynamic unbalance. Fortunately this effect can usually be kept small by careful design and manufacturing control so that the conflicting requirements can be satisfied without introducing a significant amount of dispersion.

7-8.2.7 Curvature of the Trajectory

The trajectory of the projectile during the ballistic phase will approximate a parabolic arc. An aerodynamically stable vehicle will attempt to keep its axis aligned with the flight path. However, the inherent resistance of the body to rotation (aerodynamic damping) will cause the projectile axis to lag behind the changing flight path direction. This phenomenon is called the yaw of repose (Reference 1, p. 58), which causes a small dispersion unaffected by spin.

7-8.2.8 Fuzing Errors

a. Impact Fuzing: With impact fuzing (a special case of altitude fuzing), the errors are those associated with the dispersion of the trajectory. There are no errors introduced by the fuzing technique itself.

b. Time Fuzing: With time fuzing, variation in fuze action time introduces errors in addition to those associated with the dispersion of the trajectory. The result will be additional range and altitude dispersions of the warhead at the time of detonation.

7-8.3 CALCULATION OF DISPERSION

The preceding paragraphs have presented methods that can be used to determine the condition of the rocket at motor burnout. The dispersion at burnout associated with the launch and propulsion phases has been given. With the burnout conditions as inputs, the graphs in this paragraph determine the dispersion of the rocket at warhead event. In addition to the launch and propulsion errors, the errors associated with the ballistic phase are introduced. The final results are the dispersions of the rocket at warhead event, caused by the error sources throughout the flight. For the purpose of this handbook only those ballistic phase errors which have the greatest influence on the accuracy have been included. These errors have been taken to be (1) change in atmospheric density, (2) change in the ballistic coefficient, and (3) ballistic wind.

The graphs in this paragraph give the changes in range and deflection for unit changes in the several rocket variables. The plotted data are

AMCP 706-280

TABLE 7-1. ERROR BUDGET FOR INDIRECT FIRE ROCKET WITH IMPACT FUZE

LAUNCH QUADRANT ELEVATION 45 DEGREES

Source	One Sigma Magnitude	ΔY , meters	ΔR , meters	ΔY , mils	ΔR , mils
I. Launch Errors					
A. Malaim	0.5 mil	14.2	0	0.5	0
B. Mallaunch					
a. Translation	1.0 ft sec	-71.0	0	-2.50	0
b. Rotation	$q = 10.0$ ft sec	55.6	0	1.95	0
c. Dynamic Unbalance	1.0 mil	55.6	0	1.95	0
II. Propulsive Errors					
A. Wind	3.9 ft/sec	222.0	0	7.80	0
B. Thrust Malalignment	1.0 mil	182.0	0	6.40	0
C. Impulse	2.0%	0	76.0	0	2.67
III. Ballistic Errors					
A. Density	1.0%	0	222.0	0	7.80
B. Ballistic Wind	8.1 ft. sec	117.0	148.0	4.11	5.20
C. Ballistic Coefficient	1.0%	0	222.0	0	7.80

the results of numerous digital computer calculations. The graphs are used by determining the nominal quadrant elevation and range, which in turn are used to establish the unit effects. The example calculations in pars. 7-8.3.1 through 7-8.3.4 illustrate how the dispersion at warhead event is calculated and tabulated into an error budget, used in the further calculation of probable error components (see par. 7-19).

Given: Indirect fire rocket with impact fuze and constant spin; ballistic coefficient $C = \frac{W_{BO}}{id^2} = 4.0$; range at quadrant elevation for maximum range = 28.5 km; wavelength of yaw $\sigma = 510$ ft; specific

impulse $I_{sp} = 250$ sec; mass ratio $r_B = 1.4$; $G = 48.0$ g; quadrant elevation $QE = 45$ deg; nondimensional launcher length $P = 0.0$. Typical one-sigma values assumed for the errors are as listed in Table 7-1.

Find: The dispersions at warhead event.

Solution: See calculations which follow.

7-8.3.1 Launch Errors

7-8.3.1.1 Malaim

Malaim errors will result in the impact point being deflected off to the side of the desired im-

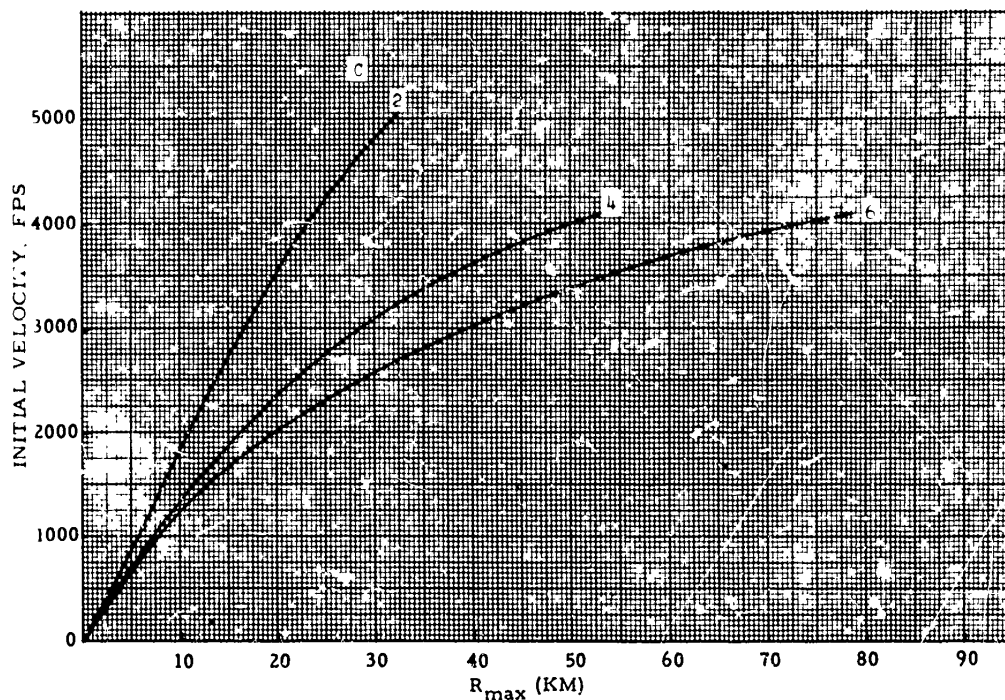


Figure 7-23. Initial Velocity Versus Maximum Range

pact. If the malaim error $\Delta\psi$ is 0.5 mil, the error will be

$$\Delta Y = (\Delta\psi)R$$

$$\Delta Y = 0.5 \text{ mil} \left(\frac{\text{rad}}{1000 \text{ mils}} \right) 28,500 \text{ m}$$

$$\Delta Y = 14.23 \text{ m}$$

With a ballistic coefficient C of 4.0, a maximum range R of 28,500 m and with the use of Fig. 7-23, the initial velocity is determined to be 3000 fps. By use of Fig. 7-24(B) in conjunction with the above information, the ratio of a percent change in range per change in departure angle is determined. In this example, the range we are interested in is the maximum value. Thus, the ratio of range desired to maximum range is unity. As seen in Fig. 7-24(B), the partial derivative $\frac{\partial R}{\partial \theta}$ is zero; thus, an error in malaim results in a negligible error in range for maximum range.

7-8.3.1.2 Mallaunch

A translational error of 1.0 fps will result in an angular dispersion, γ_{TS} , of -2.5 mils as obtained from Fig. 7-13(A). If the same formula is used as in par. 7-8.3.1.1 above, the error in deflection becomes

$$\Delta Y = \left(\frac{-2.5}{1000} \right) 28,500$$

$$\Delta Y = -71. \text{ m}$$

The change in range as the result of a mallaunch is zero for the same reason as presented above. A rotation error q of 10 mil/sec will result in an angular dispersion, as found in Fig. 7-12(A), of

$$\gamma_{TS} = 19.5 \text{ mils} \left(\frac{10 \text{ mil/sec}}{100 \text{ mil/sec}} \right)$$

$$\gamma_{TS} = 1.95 \text{ mils}$$

AMCP 706-280

This assumes that the angular dispersion, as a function of G and σ , is affected linearly by rotation rate q .

$$\Delta Y = \left(\frac{1.95}{1000} \right) 28,500$$

$$\Delta Y = 55.6 \text{ m}$$

$$\Delta R = 0$$

For a dynamic unbalance error of 1.0 mil with a spin rate of 10 rad./sec

$$q = P\epsilon = 10(1) = 10 \text{ mil/sec}$$

From Fig. 7-12

$$\gamma_{TS} = 1.95 \text{ mils}$$

$$\Delta Y = \left(\frac{1.95}{1000} \right) 28,500$$

$$\Delta Y = 55.6 \text{ m}$$

$$\Delta R = 0$$

7-8.3.2 Propulsion Errors

7-8.3.2.1 Wind

With a wind error of 3.9 fps, and the use of Fig. 7-14(A), the angular dispersion is

$$\gamma_{TS} = 20 \left(\frac{3.9}{10} \right) = 7.8 \text{ mil}$$

$$\Delta Y = \left(\frac{7.8}{1000} \right) 28,500$$

$$\Delta Y = 222 \text{ m}$$

$$\Delta R = 0$$

7-8.3.2.2 Thrust Malalignment

The spinning of the vehicle is an attempt to minimize the thrust malalignment error. Fig. 7-17(A) gives a dispersion reduction factor β :

$$\beta = 0.16 \left(\frac{1}{0.5} \right) = 0.32$$

Fig. 7-15(A) gives the angular dispersion

$$\gamma_{TS} = 20 \text{ mils}$$

$$\Delta Y = \beta \gamma_{TS} R$$

$$\Delta Y = 0.32 \left(\frac{20}{1000} \right) 28,500$$

$$\Delta Y = 182 \text{ m}$$

$$\Delta R = 0$$

7-8.3.2.3 Impulse Variation

From Fig. 4-8, if we generate a plot of I_{sp} versus burnout velocity for a constant booster-mass-ratio and calculate

$$\frac{\Delta V_B}{\Delta I_{sp}} = 9.1$$

For an impulse error of 2 percent

$$\Delta V_B = 9.1 \Delta I_{sp}$$

$$\Delta I_{sp} = 0.02 I_{sp}$$

$$\Delta V_B = 9.1 (0.02 I_{sp})$$

$$= 0.182 (250) \text{ ft/sec}$$

$$\Delta V_B = 45.5 \text{ ft/sec}$$

From Fig. 7-25(B)

$$\frac{\partial R}{\partial V} = 1.67$$

$$\Delta R = (1.67)(45.5)$$

$$\Delta R = 76 \text{ m}$$

$$\Delta Y = 0$$

7-8.3.3 Ballistic Errors

7-8.3.3.1 Density

The density error is 1.0 percent.

From Fig. 7-20(B)

$$\frac{\partial R}{\partial \rho} = 0.78$$

$$\% \Delta R = 1\%(0.78) = 0.0078$$

$$\Delta R = 0.0078 (28,500)$$

$$\Delta R = 222 \text{ m}$$

$$\Delta Y = 0$$

7-8.3.3.2 Ballistic Wind

The ballistic wind error is 8.1 fps.
From Fig. 7-27(B)

$$\frac{\partial R}{\partial V_w} = 0.064 \frac{\%}{\text{fps}}$$

$$\% \Delta R = 0.064 (9.1)$$

$$= 0.519\% \approx 0.0052$$

$$\Delta R = 0.0052 (28,500)$$

$$\Delta R = 148 \text{ m}$$

From Fig. 7-28(B)

$$\frac{\partial Y}{\partial V_w} = 0.05 \frac{\%}{\text{fps}}$$

$$\% \Delta Y = 0.05 (8.1)$$

$$= 0.405\% \approx 0.0041$$

$$\Delta Y = 0.0041 (28,500)$$

$$\Delta Y = 117 \text{ m}$$

7-8.3.3.3 Ballistic Coefficient

The ballistic coefficient error is 1.0 percent.

This error is estimated as if it were an error in density. Thus, from Fig. 7-26(B)

$$\frac{\partial R}{\partial C} = 0.78$$

$$\% \Delta R = 1\%(0.78) = 0.78\% = 0.0078$$

$$\Delta R = 0.0078 (28,500)$$

$$\Delta R = 222 \text{ m}$$

$$\Delta Y = 0$$

7-8.3.4 Tabulation of Results

The results of the above calculations are tabulated in Table 7-1.

7-8.3.5 Additional Reference Graphs

The sample calculations above have all dealt with a rocket armed with an impact fuze. Figs. 7-29 and 7-30 give additional reference data for this type of rocket, and Figs. 7-31 through 7-41 give similar reference data for a rocket with a time fuze.

7-9 STATISTICAL METHODS

Up to this point, this chapter has been concerned with identifying the sources of error in a rocket system and determining the effect of each error source on the dispersion of the rocket at warhead event. We shall now consider how to use this information to determine the probability of hitting a given target with a rocket system subject to known error sources. More precisely, the problem is find the radius of the circle within which one-half of all the rockets will impact.

Since the error sources are statistical in nature, we can only speak in terms of expected values and probabilities, and it will be necessary to separate the error sources according to their statistical nature. Let us first summarize the basic concepts of statistical analysis used to determine the accuracy of rocket systems. We shall then apply these concepts to determine the circular probable error *CPE* for the example problem of par. 7-8.3. The following definitions are useful:

a. **Fixed Bias Errors.** Let us assume that, because of a manufacturing error, the sight for a particular rocket launcher is malaligned with the launcher rail. This will result in a center of impact that is not in line with the intended direction as established by the sight. This type of error is called a fixed bias error. We shall not consider fixed bias errors further because we may assume that they can always be discovered, and compensated for, by systematic tests.

b. **Random Bias Errors.** Errors which exist for a specific set of shots fixed at the same ele-

AMCP 706-280

vation and deflection setting—such as the misreading of an unchanging wind or the missetting of the quadrant elevation angle—are called random bias errors. Methods will be described for computation of these errors; however, in the description of dispersion, the errors will not be considered since, when prior knowledge of these disturbances exists, correction can be made through such methods as prelaunch computation and aiming.

c. **Random Errors.** The computation of these errors is the main topic of pars. 7-4 through 7-8. These errors are due to thrust malalignment, weight variations, malaim, incomplete compensation for random bias errors, and many other causes.

The remainder of this chapter is concerned with determining the CPE from a knowledge of the random errors.

7-9.1 MEASURES OF DISPERSION FOR ONE ERROR SOURCE

In reducing sample dispersion data to determine the accuracy of a missile system, we must show how the values are distributed about their center of impact. This discussion will include procedures used to compute these measures of dispersion in one- and two-dimensional distributions.

The most common measures of dispersion for one-dimensional distribution are the variance, standard deviation, and probable error.

7-9.1.1 Variance

The variance σ^2 of a population (the whole class about which conclusions are to be made) is defined as the average of the squares of the distances from the universe mean. If a sample of N values is drawn from a population, with mean μ , the variance of the population is estimated by the equation

$$V = \sum_{i=1}^N \frac{(x_i - \mu)^2}{N} \quad (7-19)$$

where x_i are the sample values.

Generally, μ is not known, and an estimated mean \bar{x} of the sample values must be used. If \bar{x} is substituted for μ , V becomes a biased estimator of the variance. (Reference 17, pp. 31-32) This bias can be corrected by using $(N-1)$ instead of N . The unbiased estimator s^2 of the population variance then becomes

$$s^2 = \frac{\sum_{i=1}^N (x_i - \bar{x})^2}{N - 1} \quad (7-20)$$

7-9.1.2 Standard Deviation

The standard deviation σ is the most important measure of dispersion. The standard deviation is the deviation from the mean value μ of a set of random values such that approximately 68 percent of the values are between μ minus σ and μ plus σ . It is a more understandable measure of dispersion than the variance, because the standard deviation is the square root of the variance and, therefore, has the same dimensions as the variable. The standard deviation is estimated from a sample of size N by the equation

$$s = \left[\frac{1}{N-1} \sum_{i=1}^N (x_i - \bar{x})^2 \right]^{1/2} \quad (7-21)$$

where s is the estimator of σ . Computation can be simplified by the algebraically equivalent form

$$s = \frac{1}{N(N-1)} \left[N \sum_{i=1}^N x_i^2 - \left(\sum_{i=1}^N x_i \right)^2 \right]^{1/2} \quad (7-22)$$

7-9.1.3 Probable Error

The probable error PE is the deviation from the mean μ such that 50 percent of the observations are expected to lie between μ minus the probable error and μ plus the probable error. It can be found from a percentage of the normal distribution table (Reference 20, p. 230), that the

probable error for a normal distribution is equal to 0.674 times the standard deviation.

$$PE = 0.674\sigma \quad (7-23)$$

To convert probable error to the standard deviation, multiply by 1.48:

$$\sigma = 1.48 PE \quad (7-24)$$

The standard deviation is also a very important measure of dispersion for two-dimensional distributions. Considering a sample size of less than 30 items, for a two-dimensional distribution (x and y), the standard deviation can be estimated by using the formula

$$s = \left[\sum_{i=1}^N \frac{(x_i - \bar{x})^2 + (y_i - \bar{y})^2}{2(N-1)} \right]^{1/2} \quad (7-25)$$

It is often desirable to establish an interval about the sample standard deviation or mean in which we can state, with a specified confidence, that the true standard deviation or true mean lies. This is the confidence interval. The confidence interval for the standard deviation can be computed from the formula

$$\left[\frac{(N-1) s^2}{X_{\frac{\alpha}{2}}^2} \right]^{1/2} \leq \sigma \leq \left[\frac{(N-1) s^2}{X_{\frac{\alpha}{2}}^2} \right]^{1/2} \quad (7-26)$$

where

$$X_{\frac{\alpha}{2}}^2 = X_{\frac{\alpha}{2}}^2$$

and

$$X_{\frac{\alpha}{2}}^2 = X_{\frac{\alpha}{2}}^2, \text{ with } N-1 \text{ degrees of freedom}$$

and s is the computed standard deviation. The value of α is found by subtracting the desired confidence interval from 1:

$$\alpha = 1 - (\text{confidence interval}) \quad (7-27)$$

The values for $X_{\frac{\alpha}{2}}^2$ and $X_{1-\frac{\alpha}{2}}^2$ are obtained from

a chi-squared distribution table.

The confidence interval about the mean is computed by the formula

$$\left[\bar{x} - \frac{t_1 s}{N}, \bar{x} + \frac{t_2 s}{N} \right]$$

where

t_1 = Student's t value for $(N-1)$ degrees of freedom at the $\frac{\alpha}{2}$ point and t_2 is the same for the $(1-\frac{\alpha}{2})$ -point.

The most widely used measure of dispersion for determining missile accuracy for a two-dimensional distribution is the Circular Probable Error CPE . The CPE is defined as the radius of a circle within which one-half of the values are expected to fall. The center of the circle is the mean of the values. The most popular formula used to compute the CPE is

$$CPE = 1.1774 \sigma \quad (7-28)$$

which can be estimated by

$$CPE = K \left[\sum \frac{(x_i - \bar{x})^2 + (y_i - \bar{y})^2}{2(N-1)} \right]^{1/2} \quad (7-29)$$

where

$$K = 1.1774$$

This formula is true only when the horizontal positions x and vertical positions y are independent, normally distributed, and have a common standard deviation σ , where $\sigma_y = \sigma_x = \sigma$.

For distributions where there is no common standard deviation, the distribution becomes elliptical instead of circular. An approximation of the CPE for an elliptical distribution can be determined by the equation

$$CPE = 1.1774 \left(\frac{\sigma_y + \sigma_x}{2} \right) \quad (7-30)$$

where σ_x and σ_y are the standard deviations in the x and y positions. This approximation is correct to within 2.5 percent if the ratios of the standard deviations are less than 7:1. (Reference 22.)

If a more accurate estimation of the CPE for an elliptical distribution ($\sigma_y + \sigma_x$) is desired,

AMCP 706-280

Figs. 7-42 and 7-43 can be used. Their use will be described in par. 7-9.3.

7-9.2 MEASURES OF DISPERSION FOR SEVERAL ERROR SOURCES

The measures of dispersion previously discussed are used when the errors are from one source. For the total error resulting from several independent error sources, the root-sum-square (vector sum) method is used. The total error is determined by squaring the errors from each source and then summing them. The square root of this summation is the total error. (Reference 15, p. 201.) In equation form

$$\sigma_{tot} = \sqrt{\sigma_1^2 + \sigma_2^2 + \dots + \sigma_N^2} \quad (7-31)$$

For a two-dimensional distribution, the total error in each dimension must be found and the average of the two taken to obtain the total error for the system

$$(\sigma_x)_{tot} = \sqrt{\sigma_{x1}^2 + \sigma_{x2}^2 + \dots + \sigma_{xN}^2} \quad (7-32)$$

$$(\sigma_y)_{tot} = \sqrt{\sigma_{y1}^2 + \sigma_{y2}^2 + \dots + \sigma_{yN}^2} \quad (7-33)$$

$$\sigma_{sys} = \frac{(\sigma_x)_{tot} + (\sigma_y)_{tot}}{2} \quad (7-34)$$

The CPE is then found by the equation

$$CPE = 1.1774\sigma_{sys} \quad (7-35)$$

This method is used extensively in the research and development phase of a missile system. The CPE required in order for the missile system to meet its overall accuracy requirement is found. The average (one-sigma) errors of each of the independent error sources are found by testing each of these components. By simulation, the effects of these one-sigma values on the range and deflection of the missile at the impact point are found. These errors in range and deflection are then combined by the root-sum-square method to get the total error for the system. The CPE is computed and compared with the required CPE. If this computed CPE does not meet the

7-34

requirements, some or all of the components that contribute to the total error must be improved. In this manner, the best design of the missile components can be determined.

Figs. 7-42 and 7-43 can be used to estimate the CPE of an elliptical distribution.

7-9.3 USE OF FIGS. 7-42 AND 7-43

Figs. 7-42 and 7-43 provide a more accurate estimate of the circular probable error for an elliptical distribution. The value of K in the equation

$$CPE = K \times (\text{Standard Deviation}) \quad (7-36)$$

can be more accurately determined. The value 1.1774 is the standard value used for K , but this value is correct only when the horizontal and vertical standard deviations are equal:

$$\sigma_x = \sigma_y.$$

The major difference between Figs. 7-42 and 7-43 is that Fig. 7-42 uses the average of the standard deviation in the horizontal and vertical position for the computation of the CPE while Fig. 7-43 uses the larger of the two standard deviations, i.e.:

$$CPE = K \left(\frac{\sigma_x + \sigma_y}{2} \right) \quad (\text{Fig. 7-42}) \quad (7-37)$$

$$CPE = K \sigma_{max} \quad (\text{Fig. 7-43}) \quad (7-38)$$

For Fig. 7-42, the smaller of the two standard deviations is divided by the larger. The ratio is then read on the horizontal axis and extended to the curve. The vertical value of this point on the curve is the value of K in Eq. 7-37.

For Fig. 7-43, the minimum value of the two standard deviations is divided by the maximum and the ratio is the vertical value on the curve. This point on the curve is the value of k in Eq. 7-38.

7-10 COMPUTATION OF ACCURACY

Using the results of the example dispersion calculation which are presented in Table 7-1, one can determine the probable errors in range and

deflection as well as the *CPE*. The example calculation considers only one quadrant elevation. The change in the accuracy of a rocket system with range is very important since a variation in target range is to be expected.

7-10.1 RANGE PROBABLE ERROR (RPE)

The values given in Table 7-1 are one-sigma dispersions. Therefore, using the formula from par. 7-9.2

$$\begin{aligned}\sigma_{\text{RANGE}} &= \sigma_{\text{R TOTAL}} \\ &= \sqrt{(2.67)^2 + (7.80)^2 + (5.20)^2 + (7.80)^2} \\ &= 12.5 \text{ mils}\end{aligned}$$

From par. 7-9.1.3, range probable error

$$\begin{aligned}\text{RPE} &= 0.674 (\sigma_{\text{RANGE}}) \\ &= 0.674 (12.5) = 8.42 \text{ mils}\end{aligned}$$

Fig. 7-44 indicates the variation of *RPE* with range for a typical free rocket with an impact fuze.

7-10.2 DEFLECTION PROBABLE ERROR (DPE)

Again from Table 7-1

$$\sigma_{\text{DEFLECTION}} = \sigma_{\text{D TOTAL}}$$

$$\begin{aligned}&= \left[(0.5)^2 + (2.50)^2 + (1.95)^2 \right. \\ &\quad \left. + (1.95)^2 + (7.80)^2 + (6.40)^2 + (4.11)^2 \right]^{1/2} \\ &= 11.5 \text{ mils}\end{aligned}$$

Deflection probable error

$$\text{DPE} = (0.674) (11.5) = 7.75 \text{ mils}$$

Fig. 7-45 indicates the variation of *DPE* with range for a typical free rocket with impact fuze.

7-10.3 CIRCULAR PROBABLE ERROR (CPE)

From the results presented in par. 7-9.2

$$\begin{aligned}\sigma_{\text{sys}} &= \frac{\sigma_{\text{R TOTAL}} + \sigma_{\text{D TOTAL}}}{2} \\ &= \frac{12.5 + 11.5}{2} \\ &= 12.0 \\ \text{CPE} &= 1.1774 \sigma_{\text{sys}} \\ &= 1.1774(12.0) \\ &= 14.1 \text{ mils}\end{aligned}$$

Fig. 7-46 indicates the variation of *CPE* with range for a typical free rocket with impact fuze.

AMCP 706-280

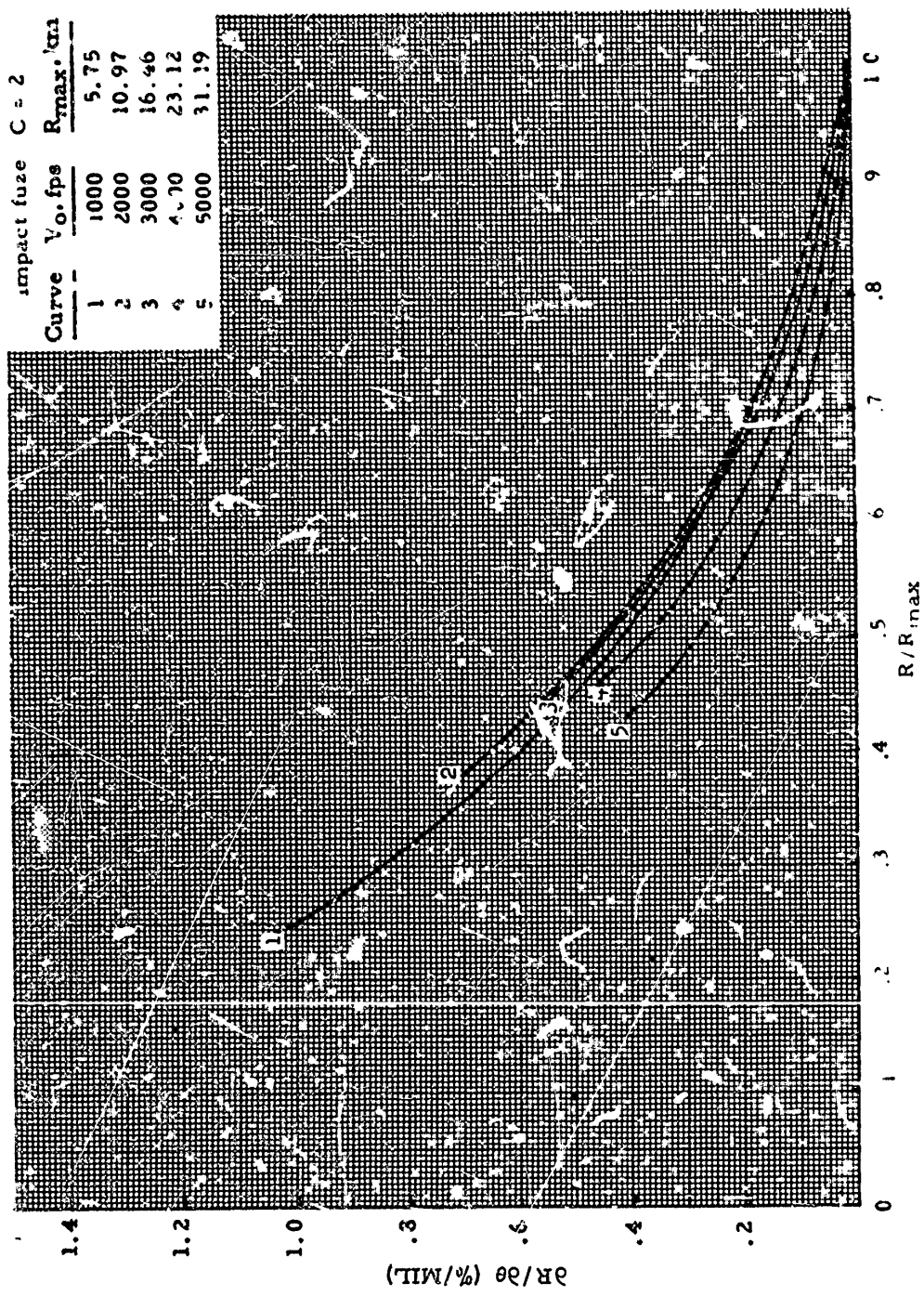


Figure 7-24(A) Unit Effect, Range/Departure Angle Versus R_{max} - Impact Fuze

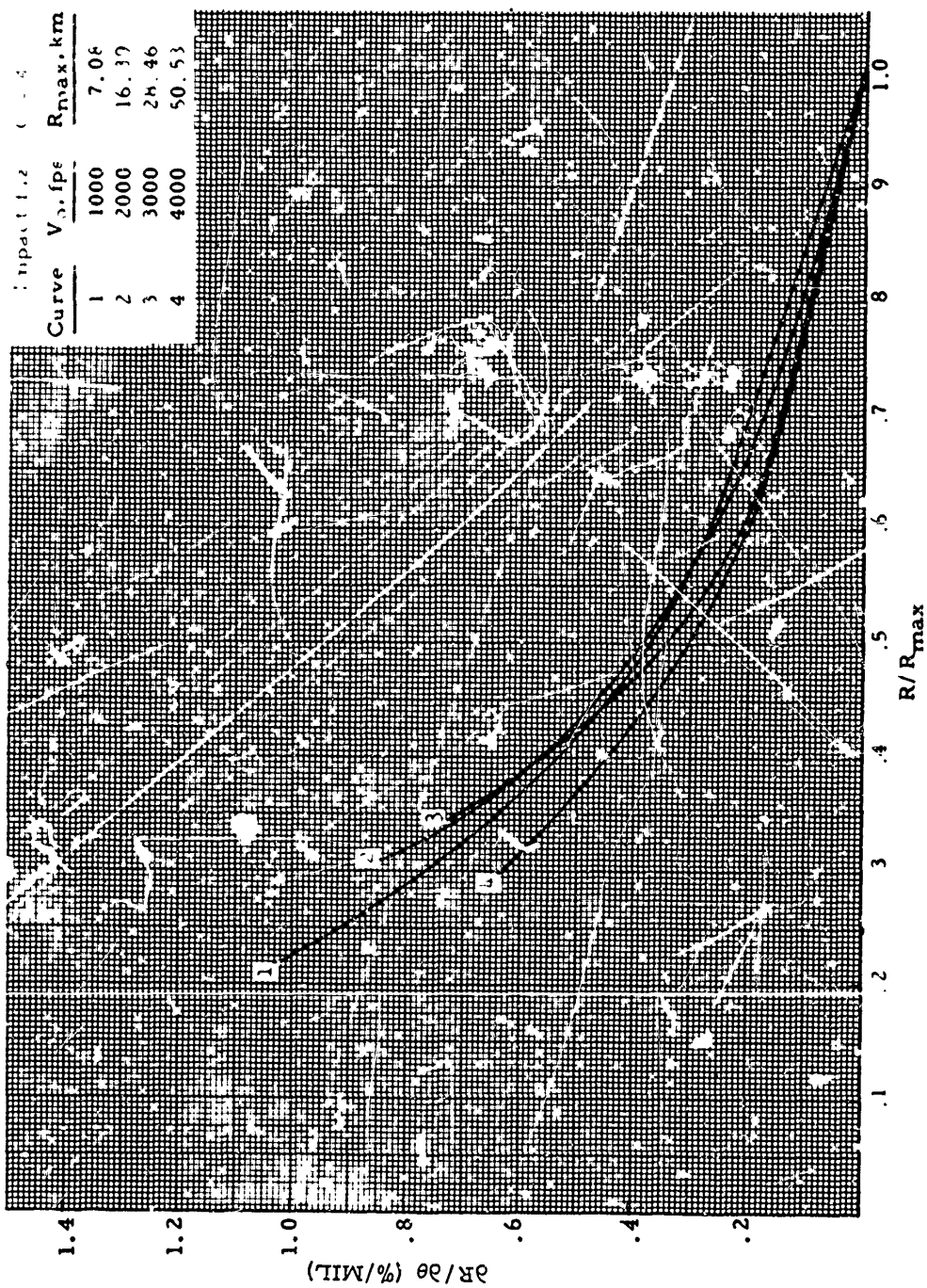


Figure 7-24(B). Unit Effect, Range Departure Angle Versus R/R_{max} - Impact Fuse

AMCP 763-280

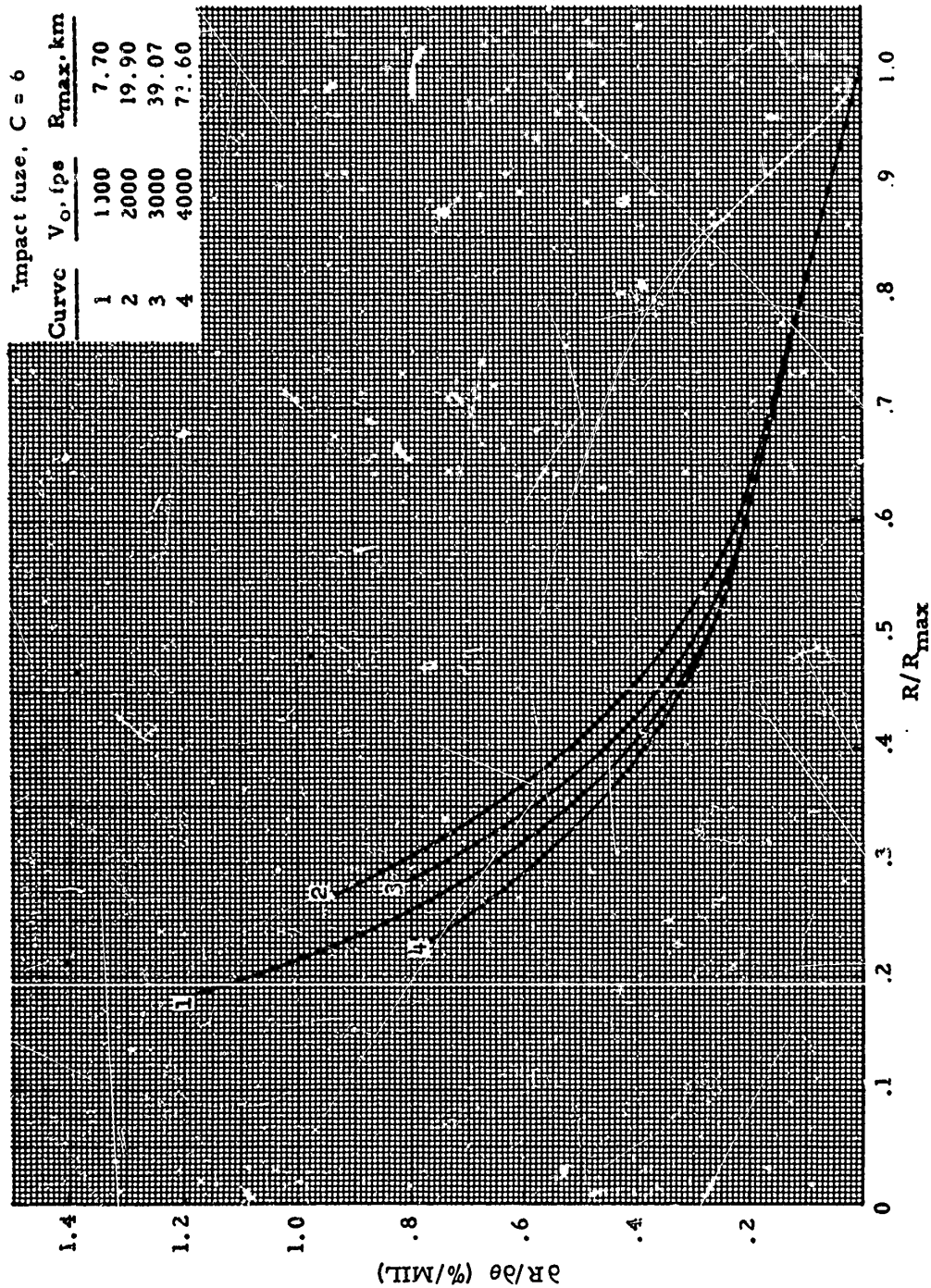


Figure 7-24(C). Unit Effect, Range/Departure Angle Versus R/R_{max} - Impact Fuze

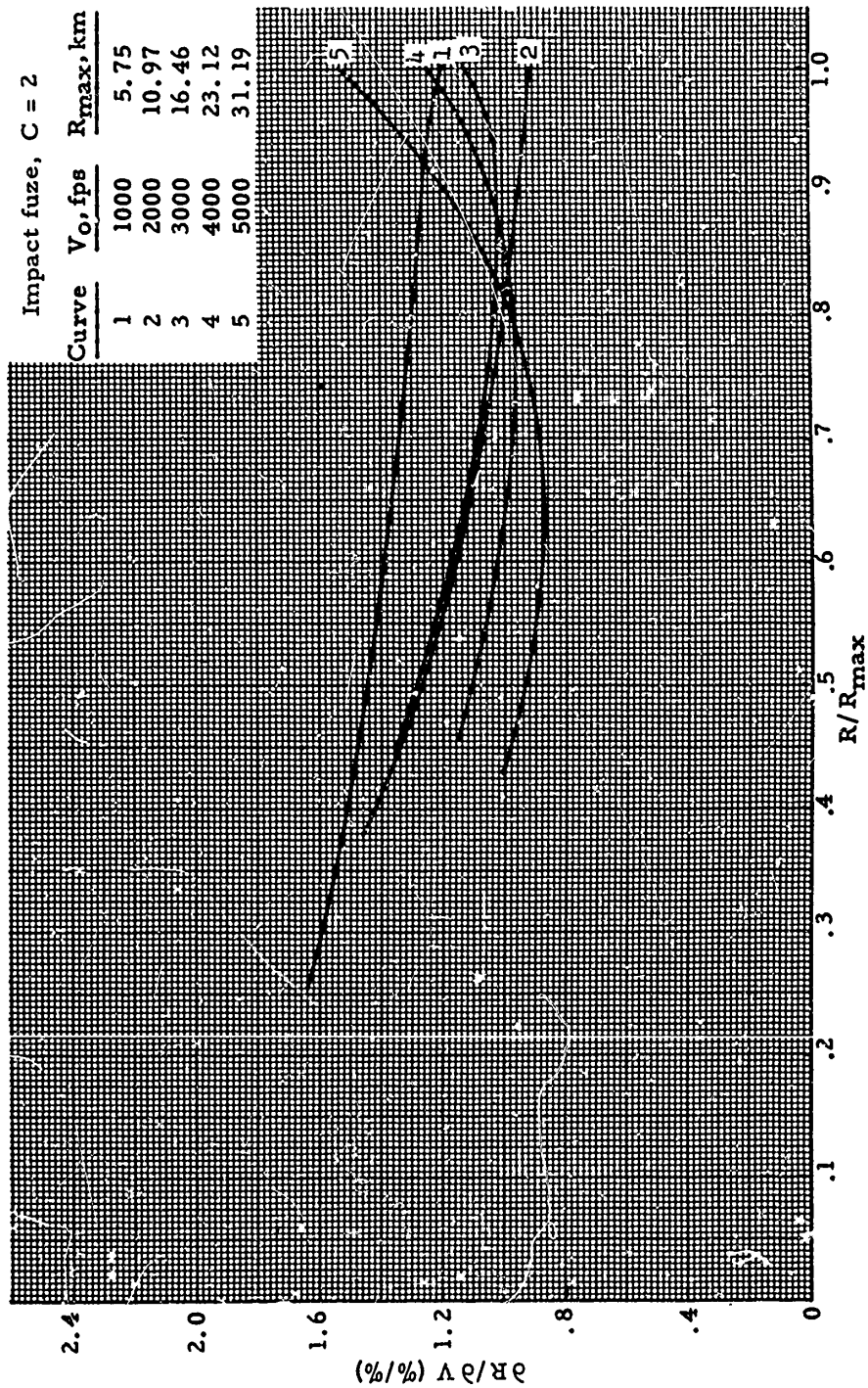


Figure 7-25(A). Unit Effect, Range/Velocity Versus R/R_{max} - Impact F_{0x}

AMCP 706-280

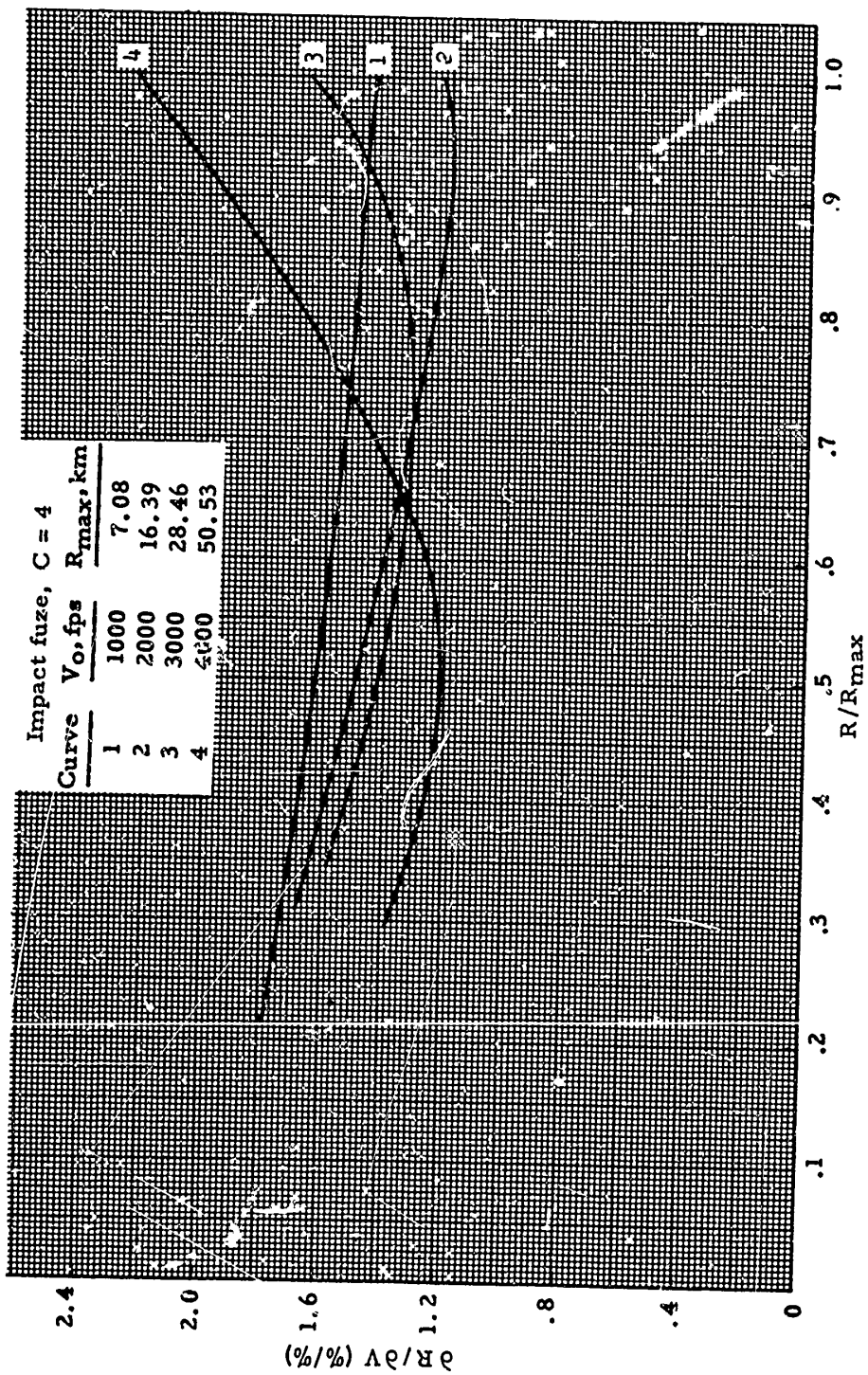


Figure 7-25(B). Unit Effect, Range/Velocity Versus R/R_{max} - Impact Fuze

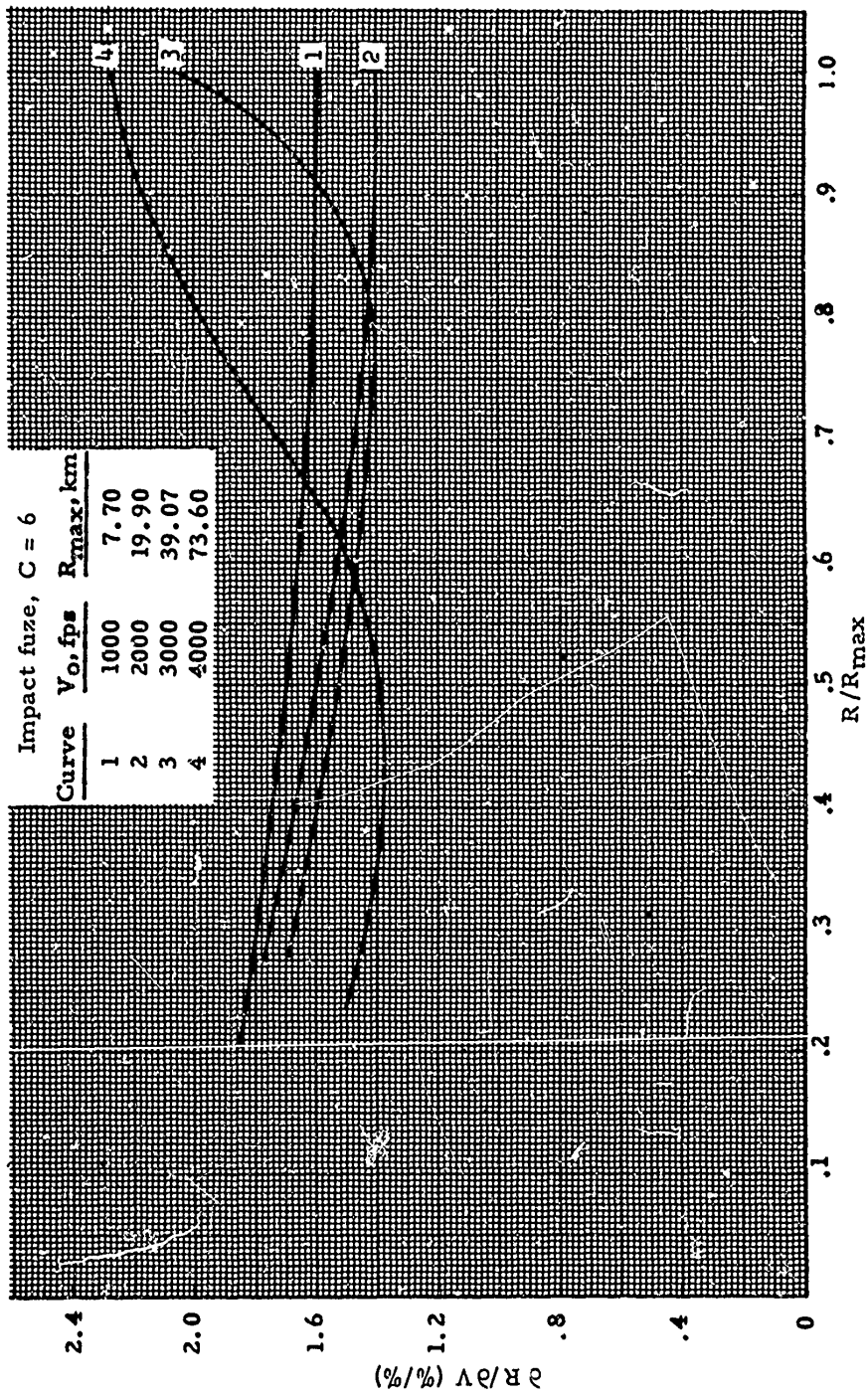


Figure 7-25(C). Unit Effect, Range/Velocity Versus R/R_{max} - Impact Fuze

AMCP 706-280

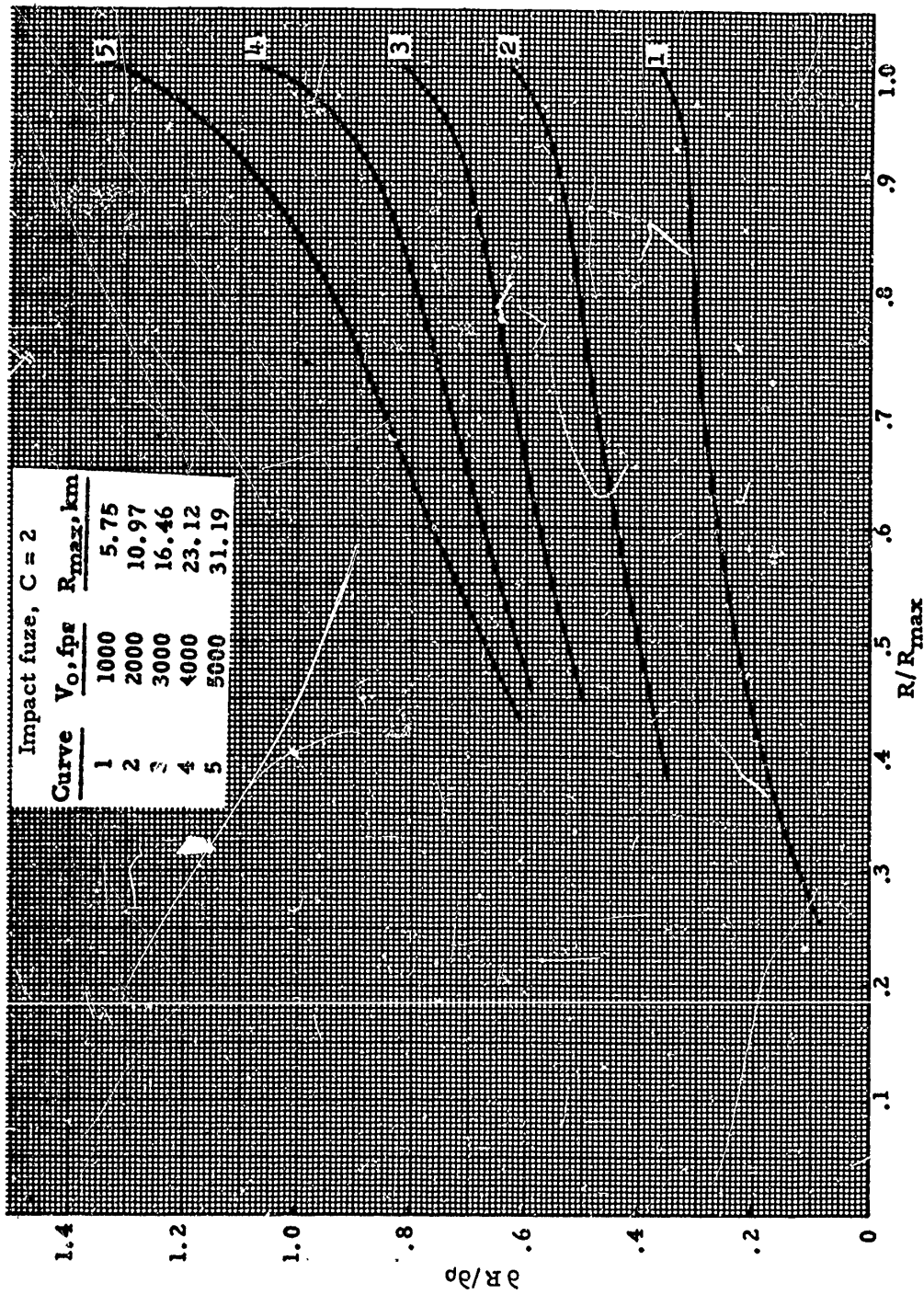


Figure 7-26(A). Unit Effect, Range/Density Versus R/R_{max} - Impact Fuze

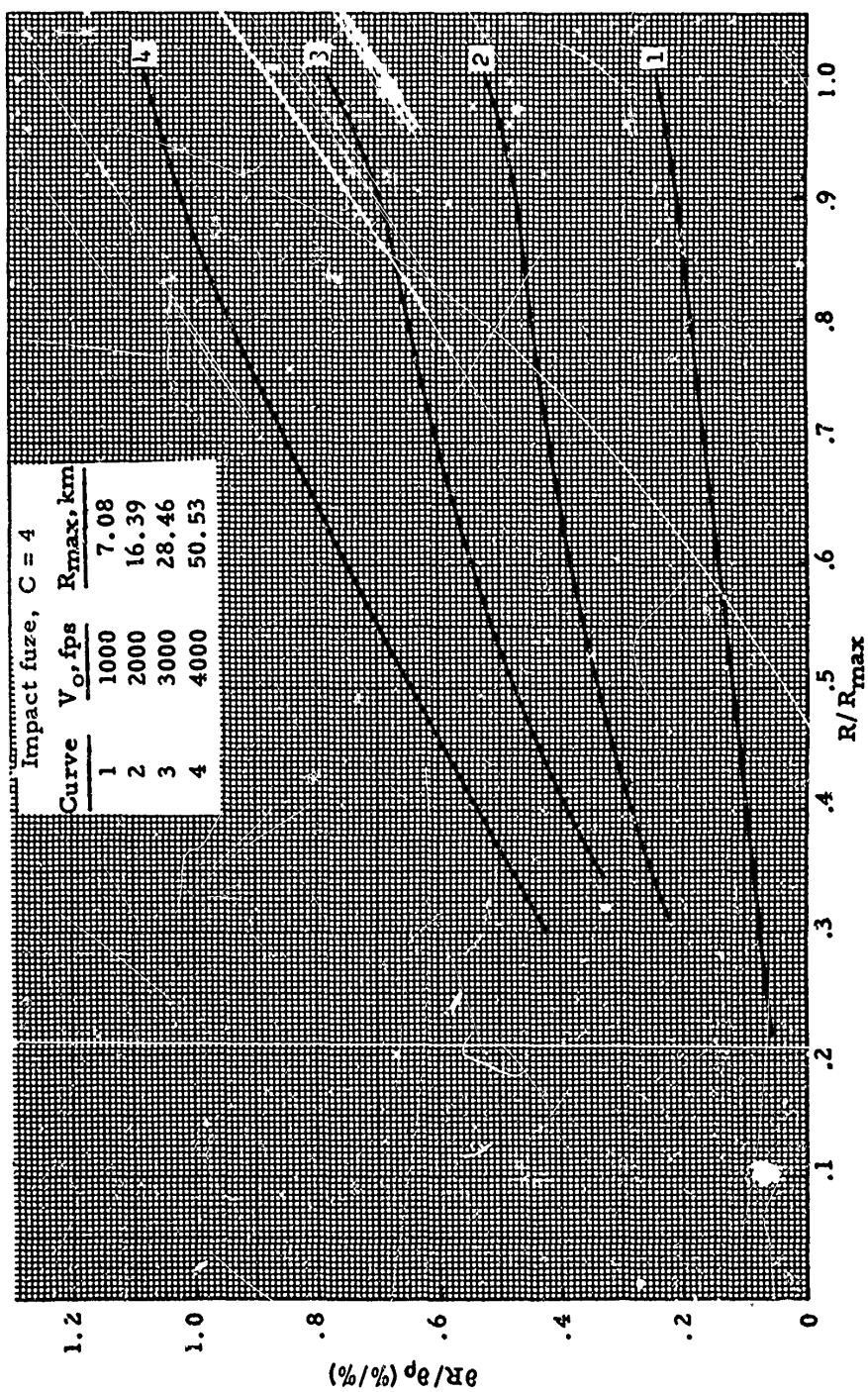


Figure 7-26(B). Unit Effect, Range/Density Versus R/R_{max} - Impact Fuze

AMCP 706-280

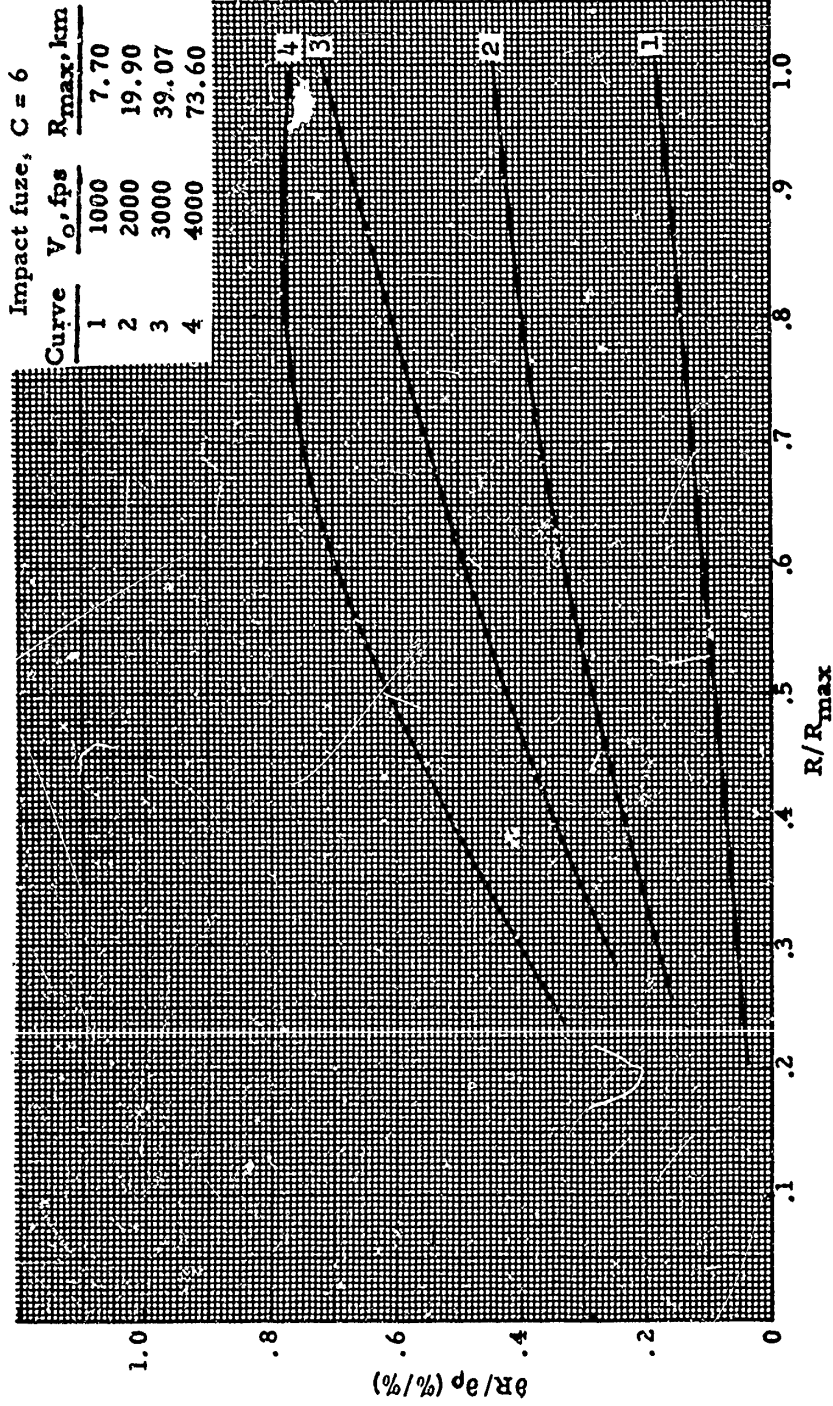


Figure 7-26(C). Unit Effect, Range/Density Versus R/R_{max} - Impact Fuze

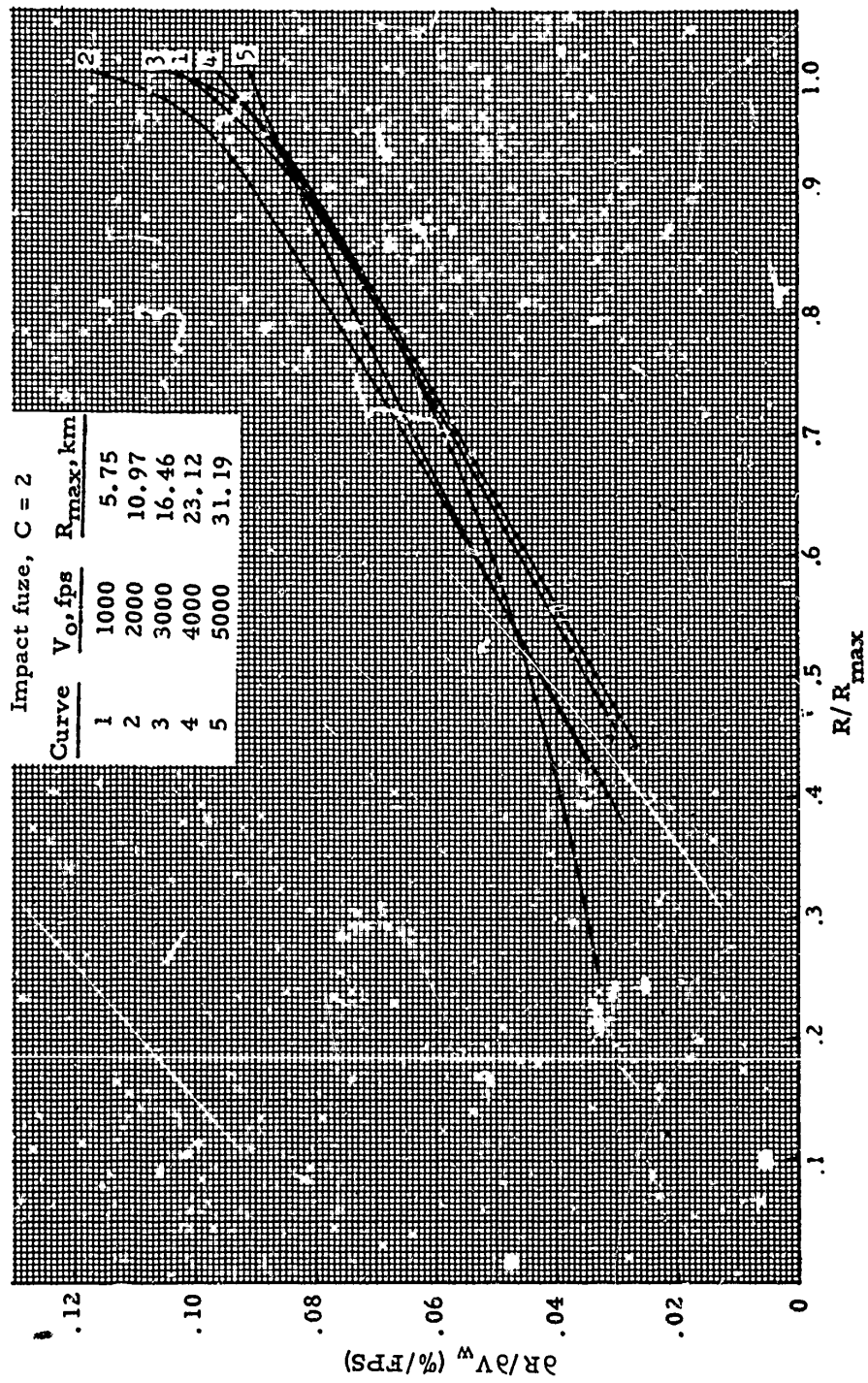


Figure 7-27(A). Unit Effect, Range/Wind Versus R/R_{max} - Impact Fuze

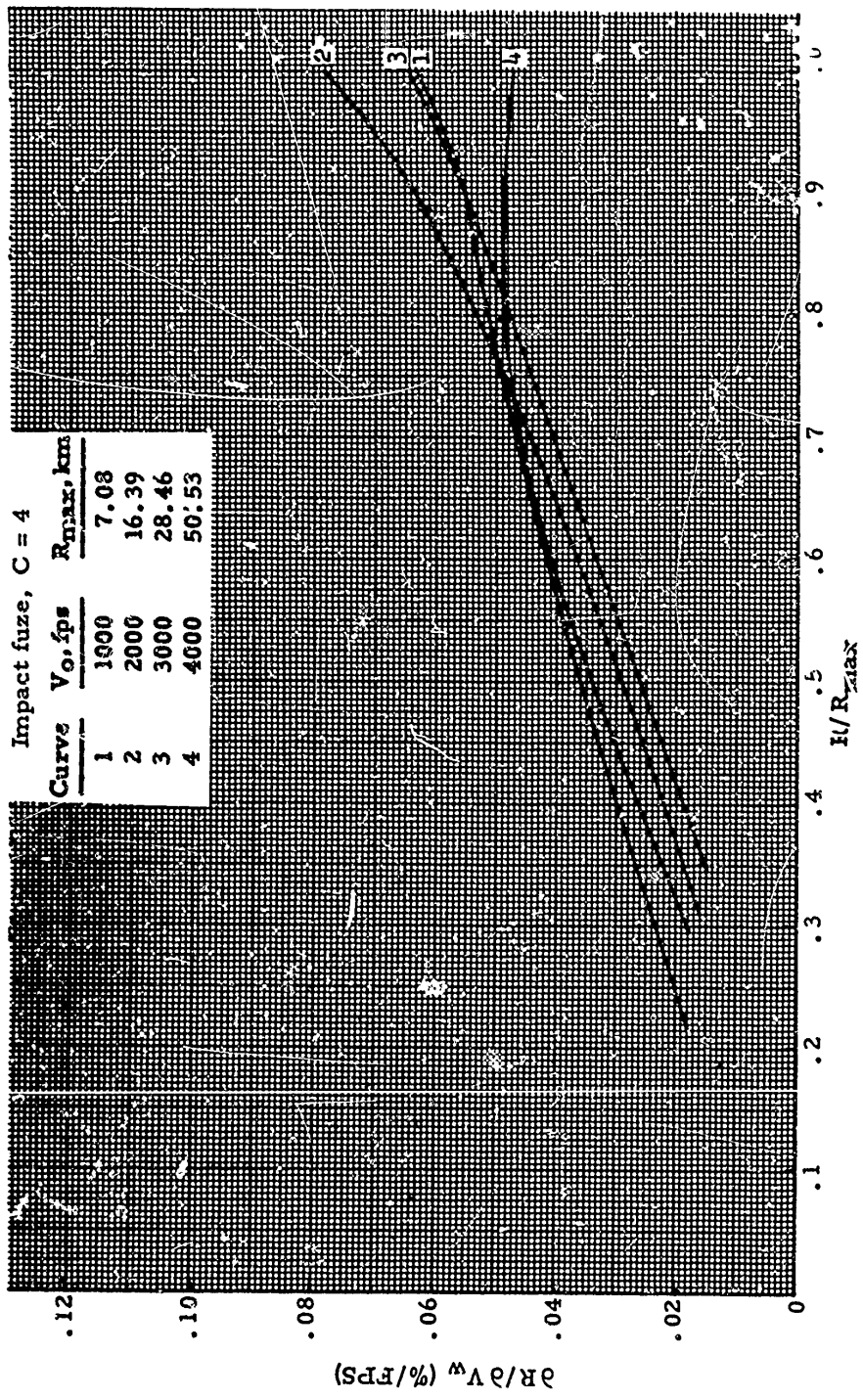


Figure 7-27(B). Unit Effect, Range/Wind Versus R/R_{max} - Impact Fuze

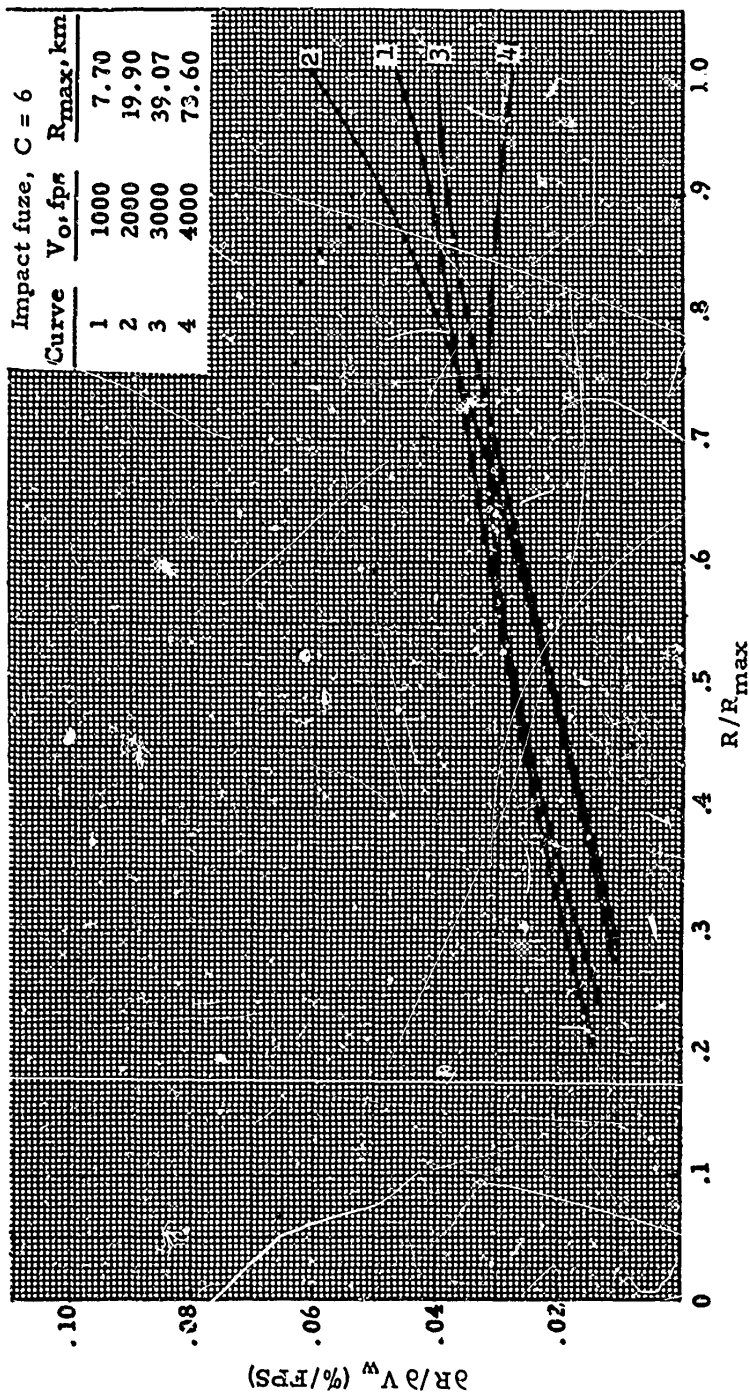


Figure 7-27(C). Unit Effect, Range/Wind Versus R/R_{max} - Impact Fuze

AMCP 706-280

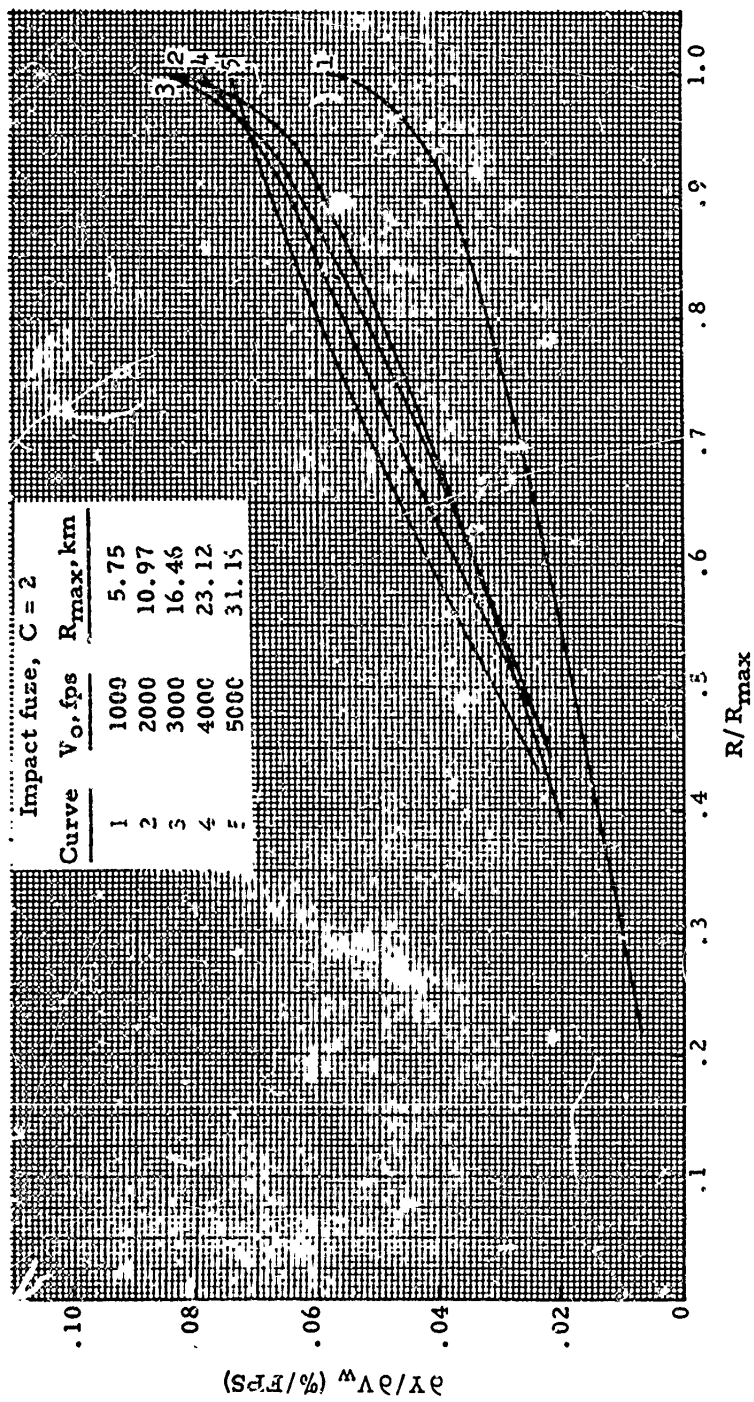


Figure 7-28(A). Unit Effect, Deflection/Wind Versus R/R_{mo} - Impact Fuze

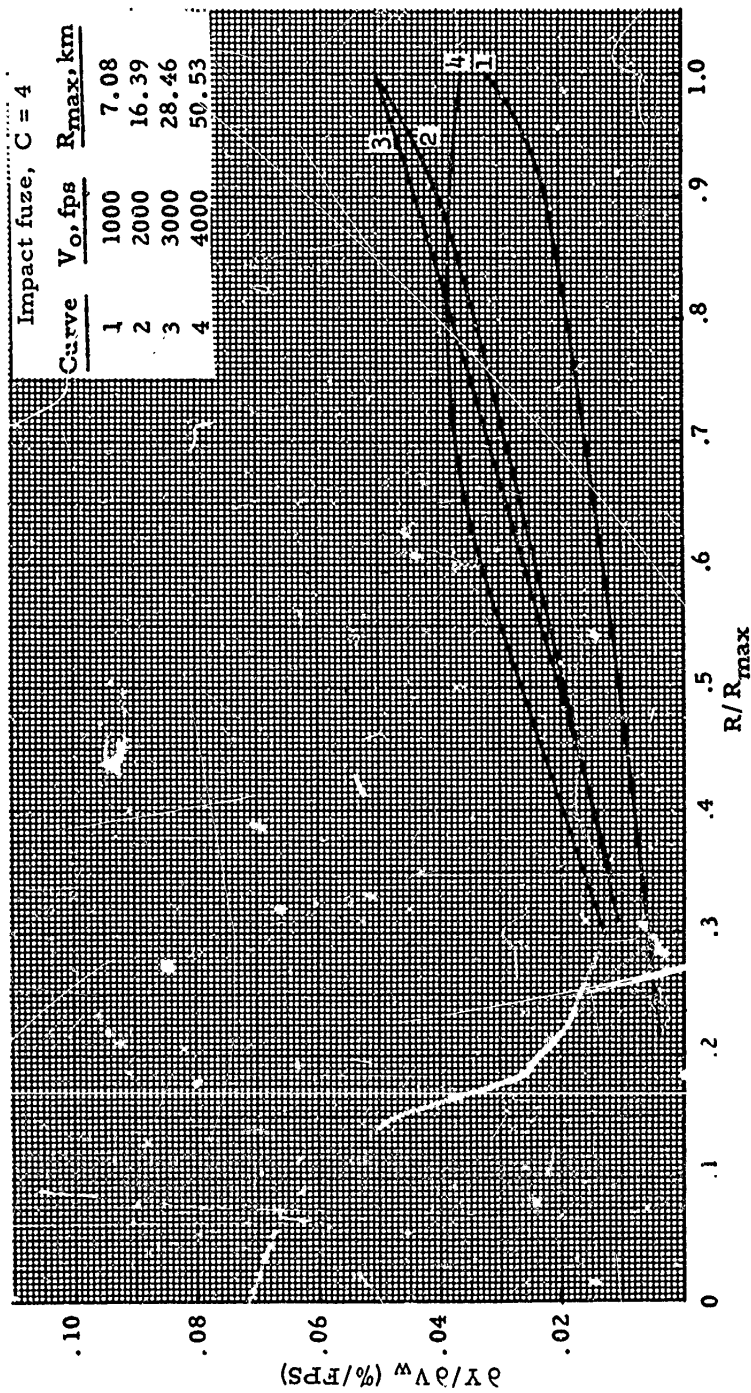


Figure 7-28(B). Unit Effect, Deflection/Wind Versus R/R_{max} - Impact Fuze

AMCP 706-280

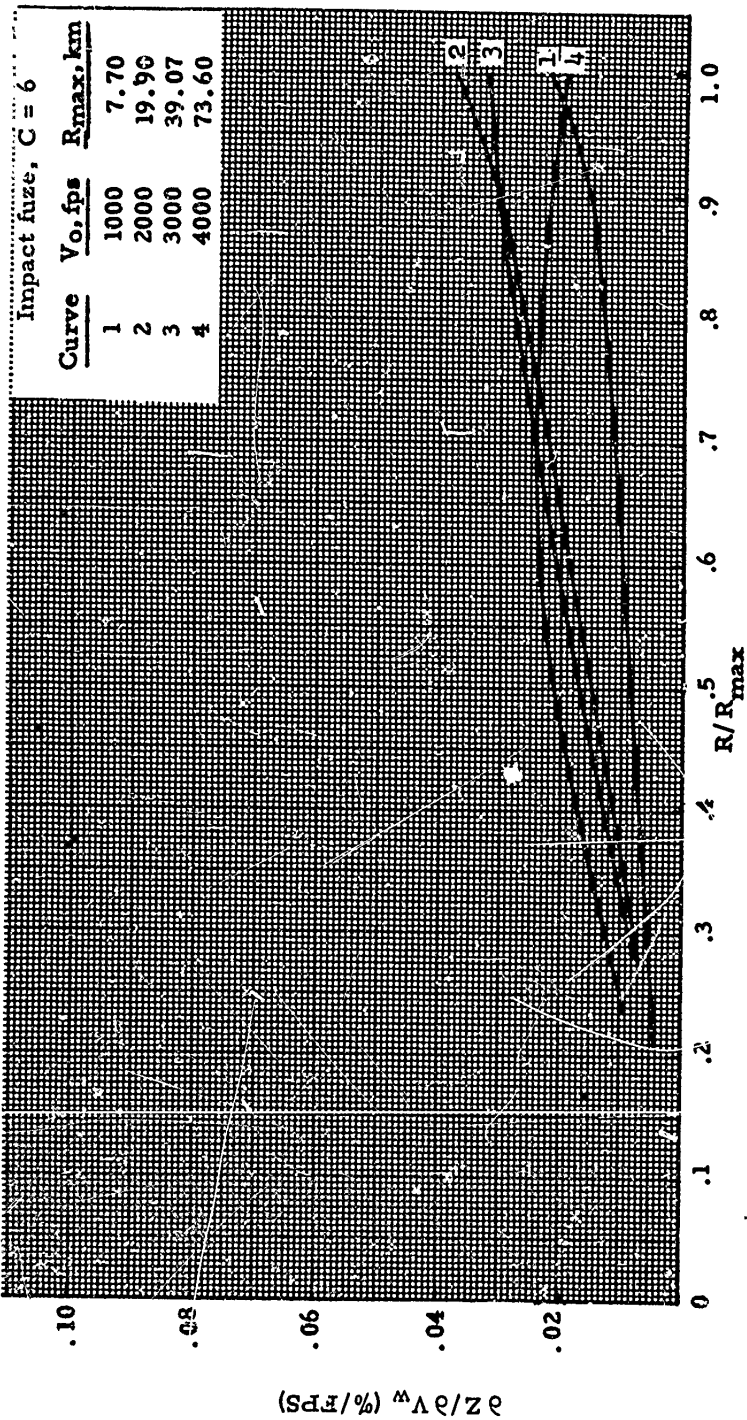


Figure 7-28(C). Unit Effect, Deflection/Wind Versus R/R_{max} - Impact Fuze

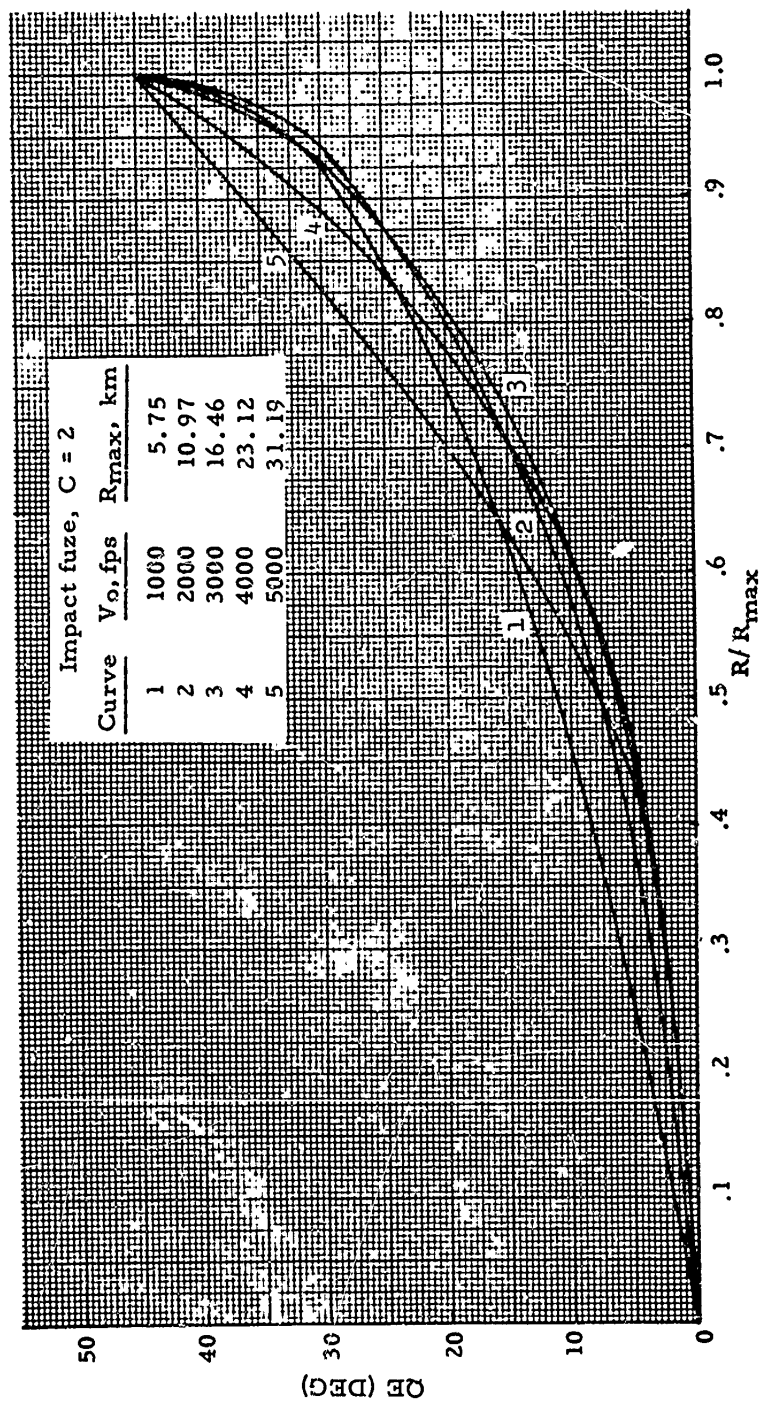


Figure 7-22(A). QE Versus R/R_{max} - Impact Fuze

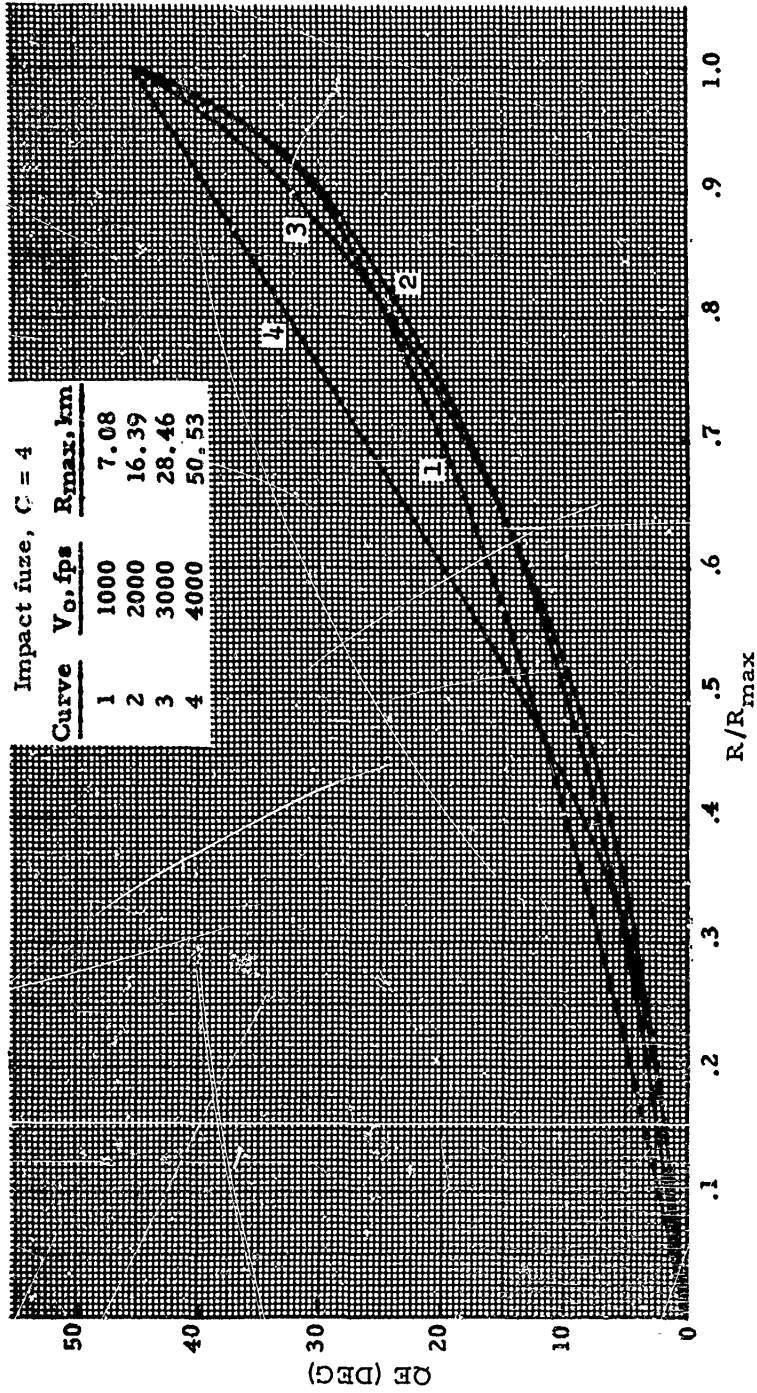


Figure 7-29(B). QE Versus R/R_{max} - Impact Fuze

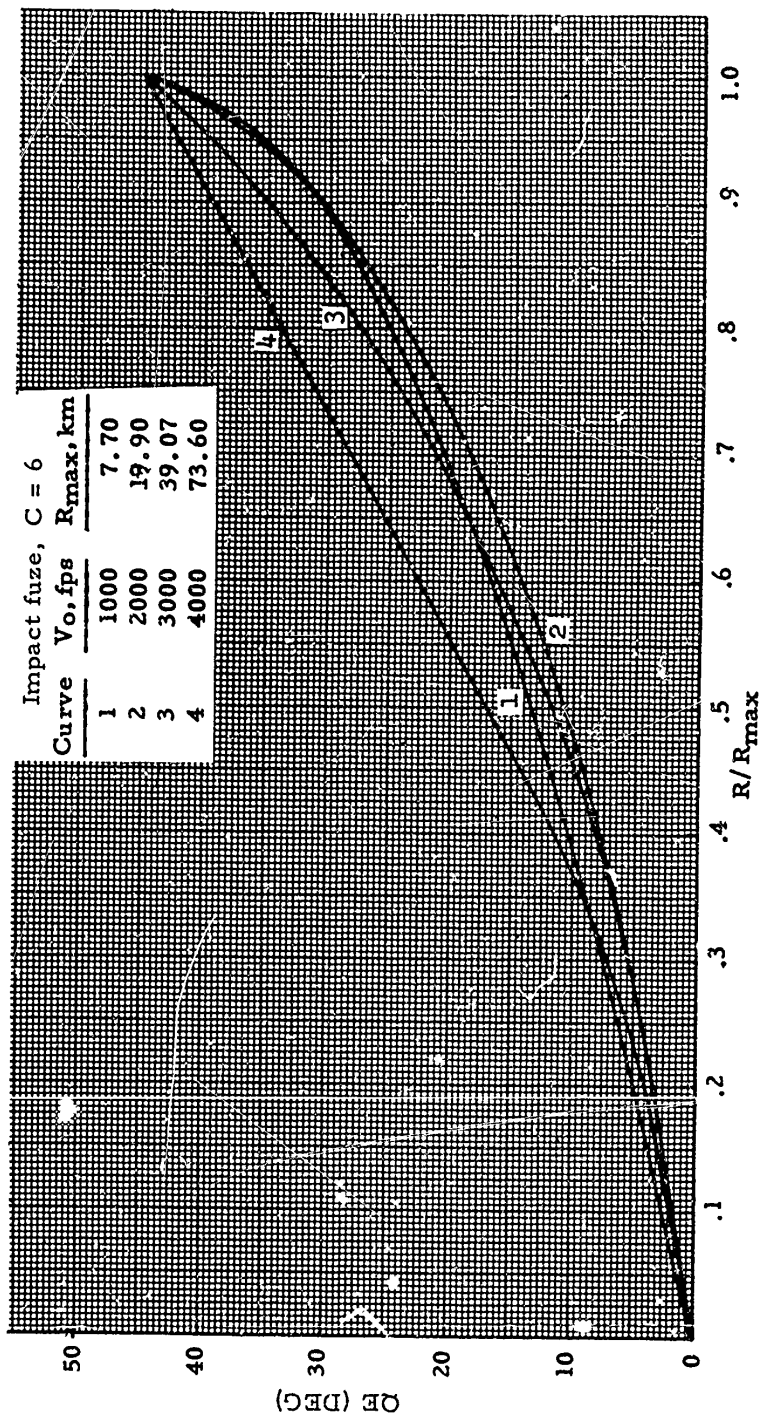


Figure 7-29(C). OE Versus R/Rmax - Impact Fuze

AMCP 706-280

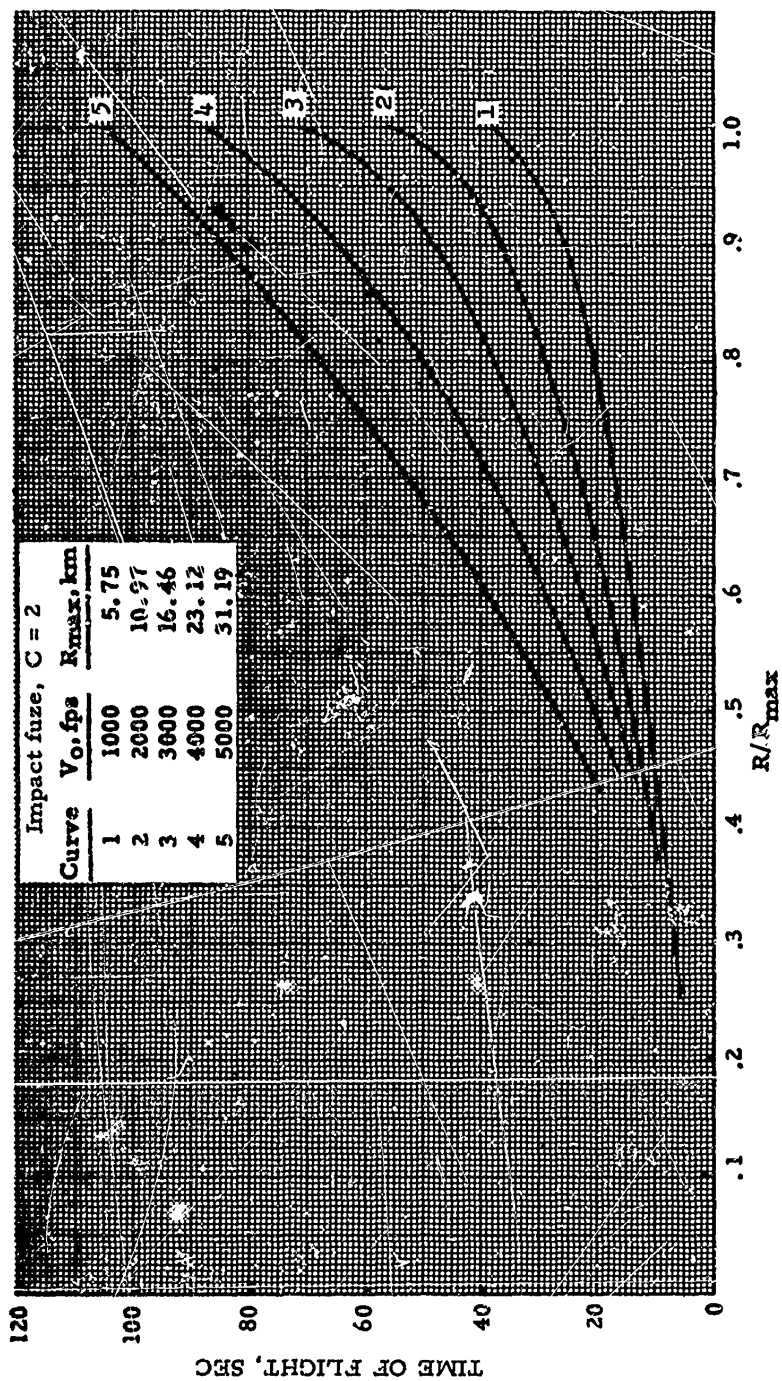


Figure 7-30(A). Time of Flight Versus R/R_{max} - Impact Fuze

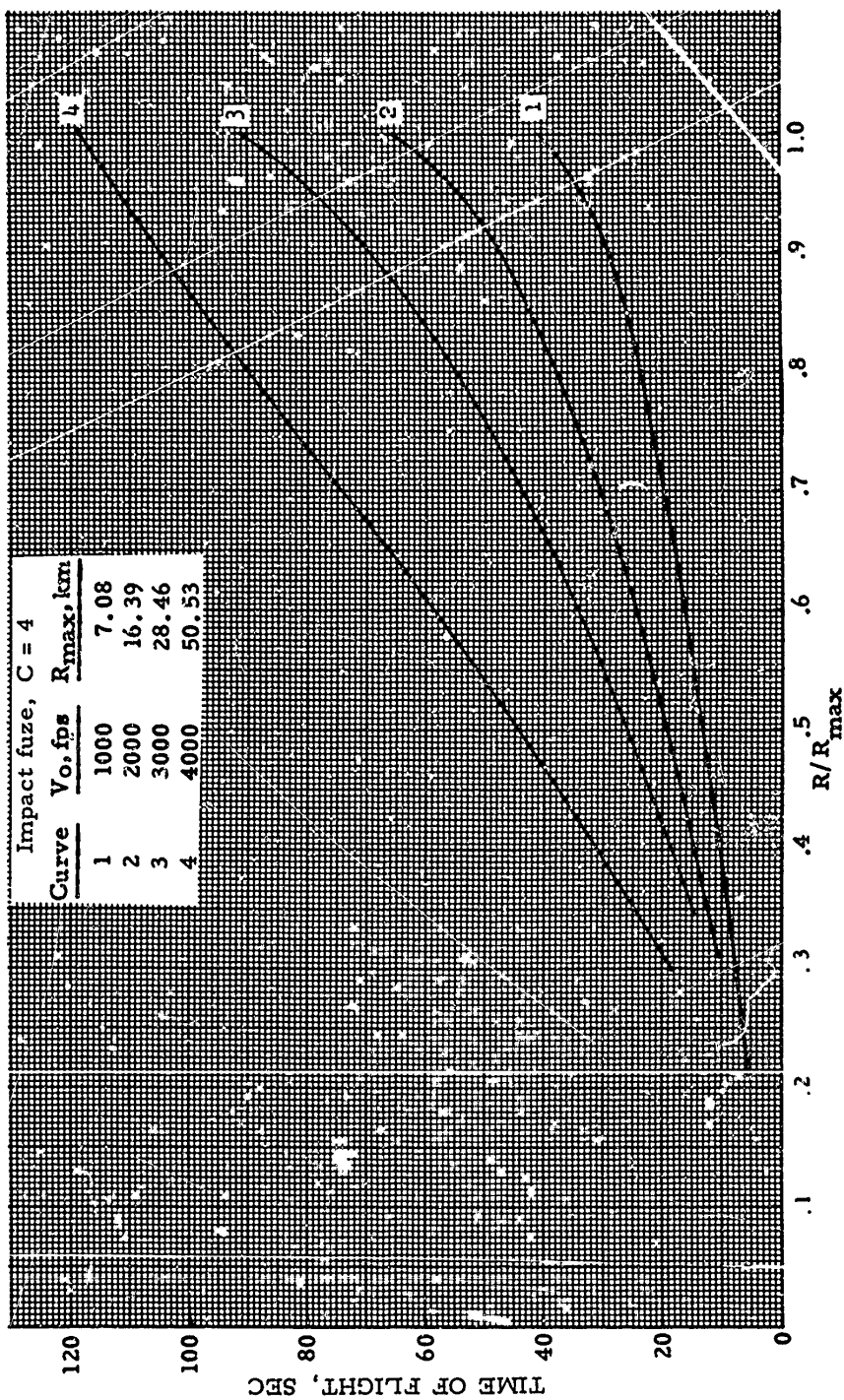


Figure 7-30(B). Time of Flight Versus R/R_{max} - Impact Fuze

AMCP 703-280

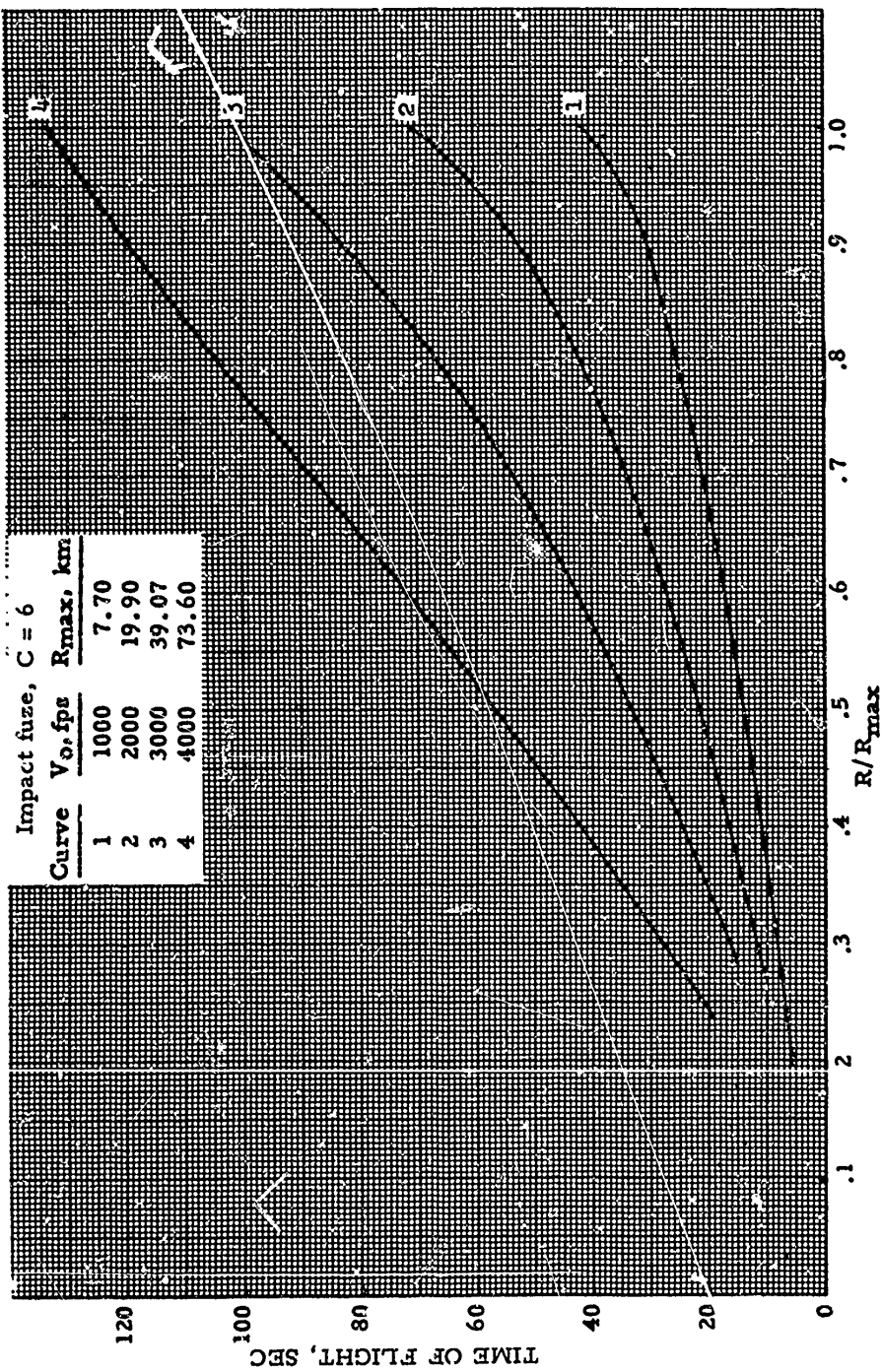


Figure 7-30(C). Time of Flight Versus R/R_{max} - Impact Fuze

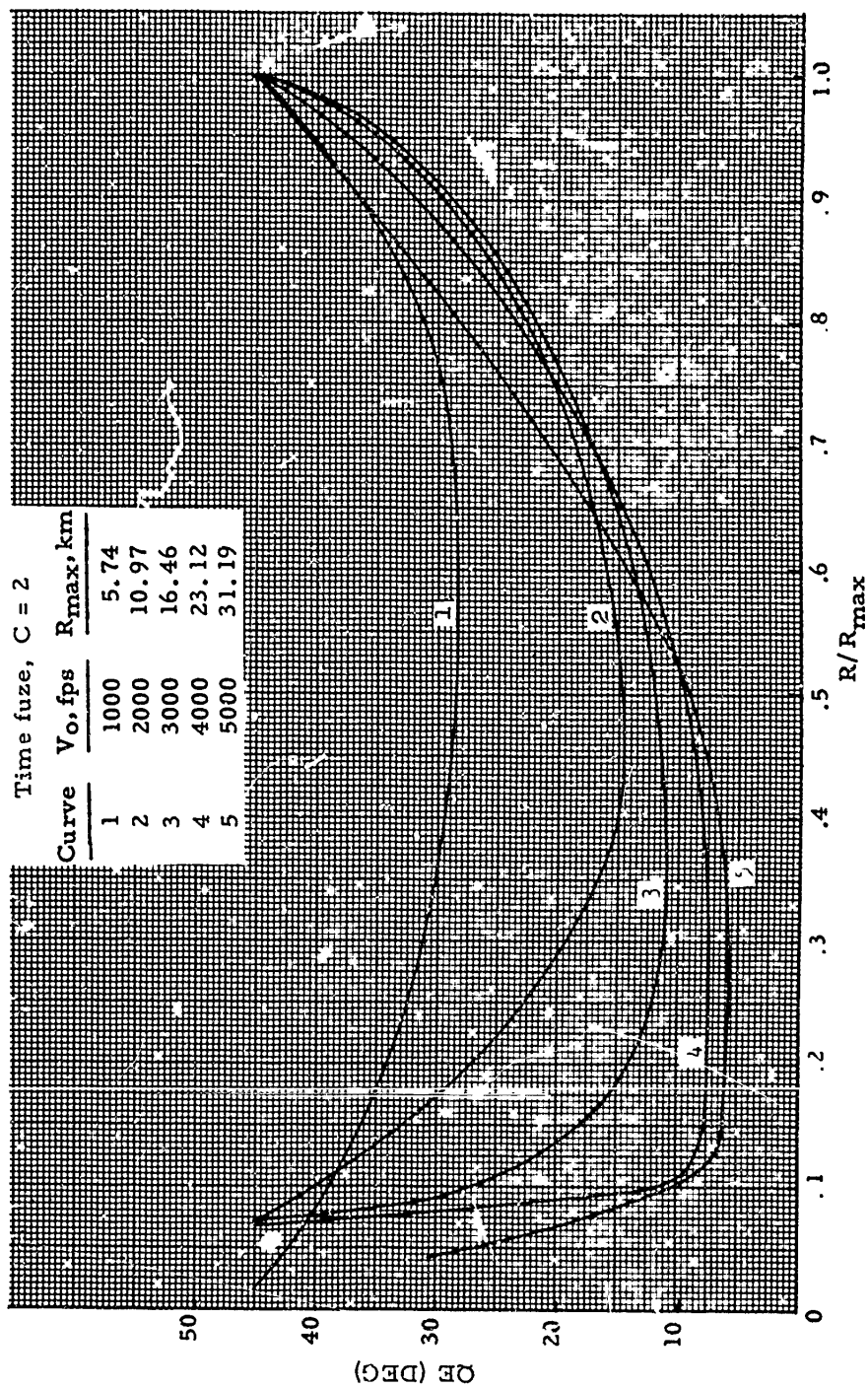


Figure 7-31(A). QE Versus R/R_{max} - Time Fuze

AMCP 706-280

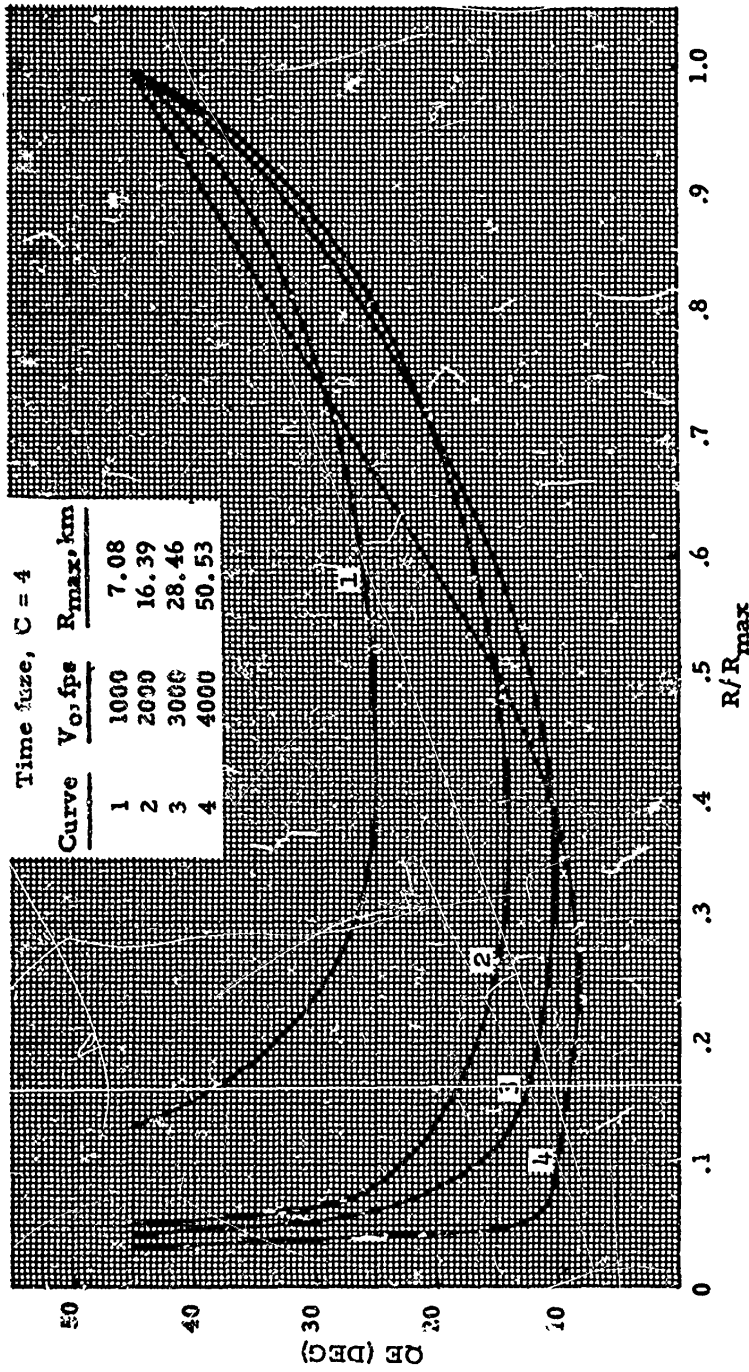


Figure 7-31(B). QE Versus R/R_{max} - Time Fuze

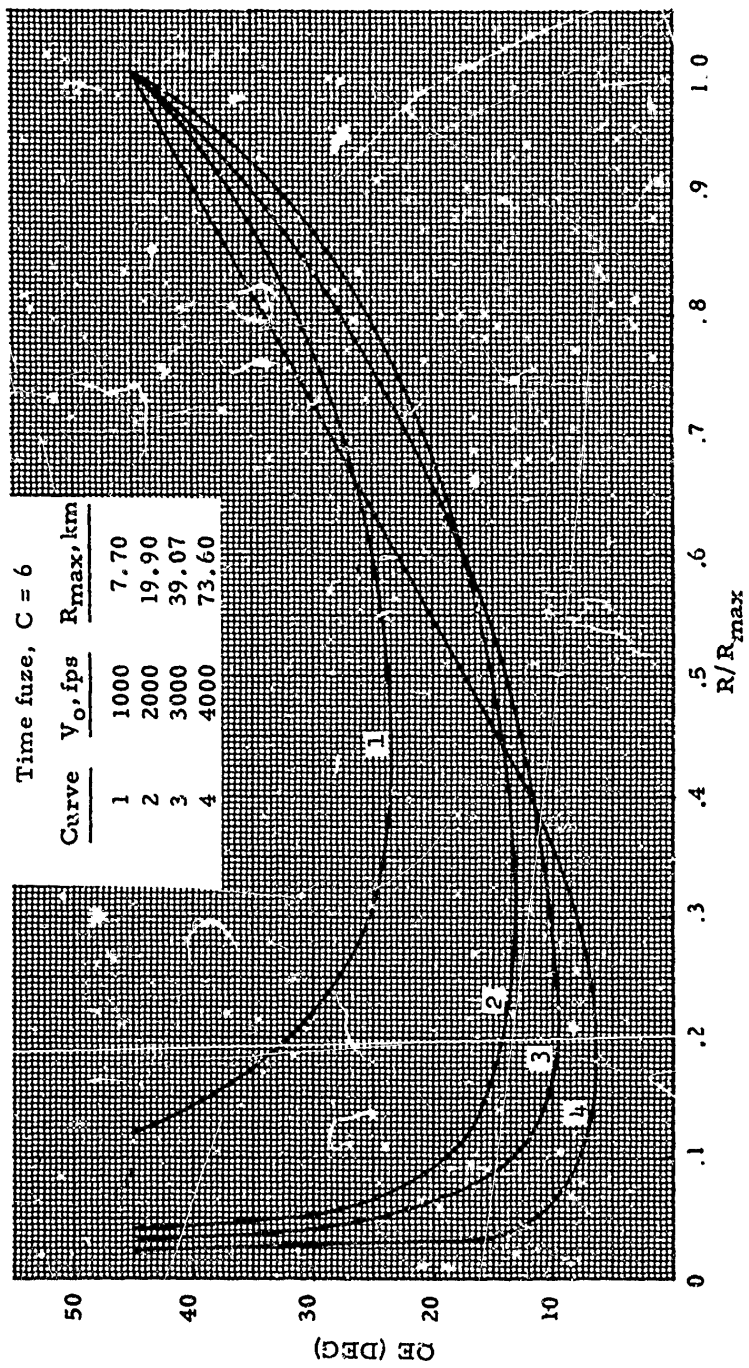


Figure 7-31(C). QE Versus R/R_{max} - Time Fuze

AMCP 706-280

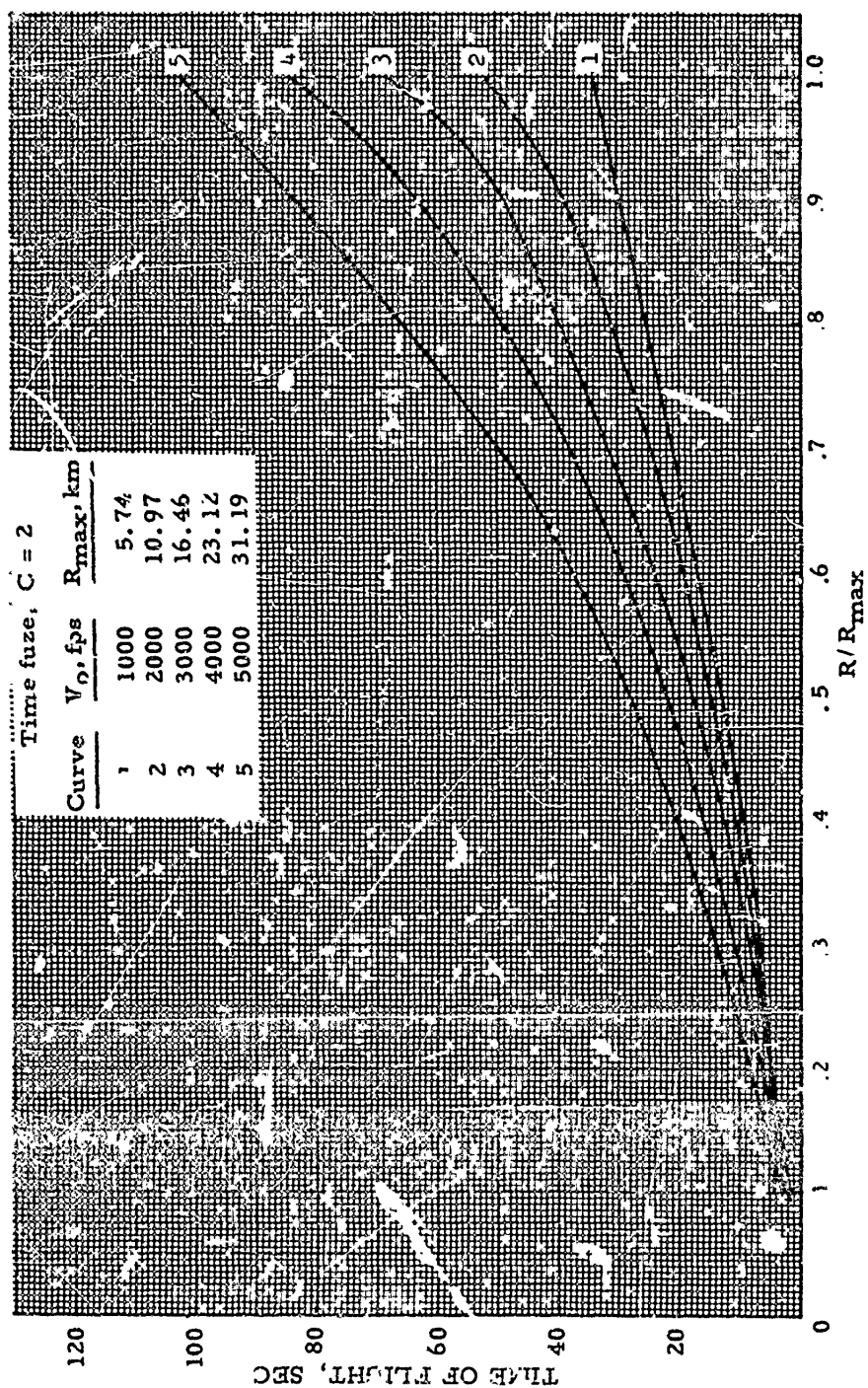


Figure 32.4). Time of Flight Versus R/R_{max} - Time Fuze

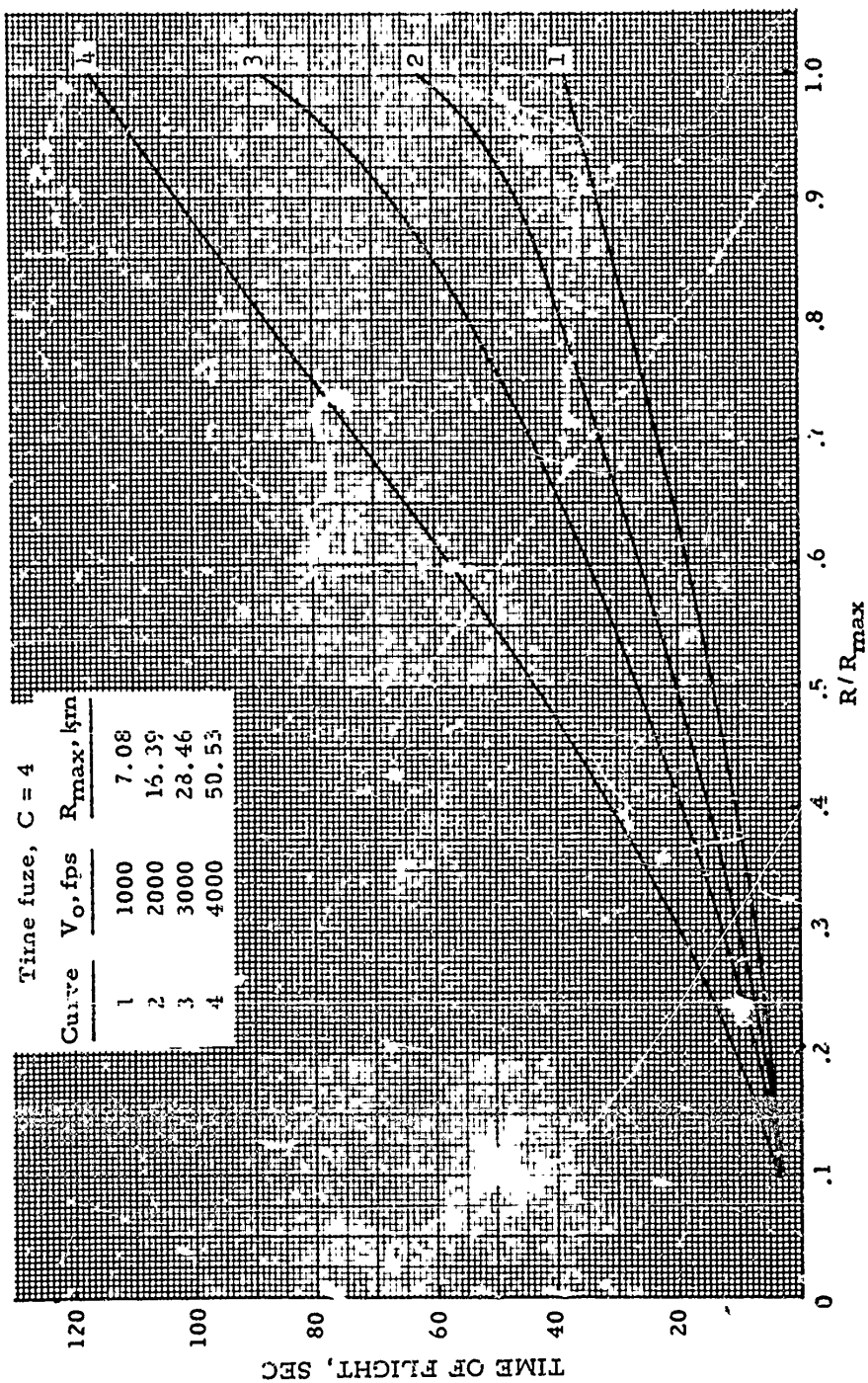


Figure 7-32(B). Time of Flight Versus $P'_{r,v}$ - Time Fuze

AMCP 706-200

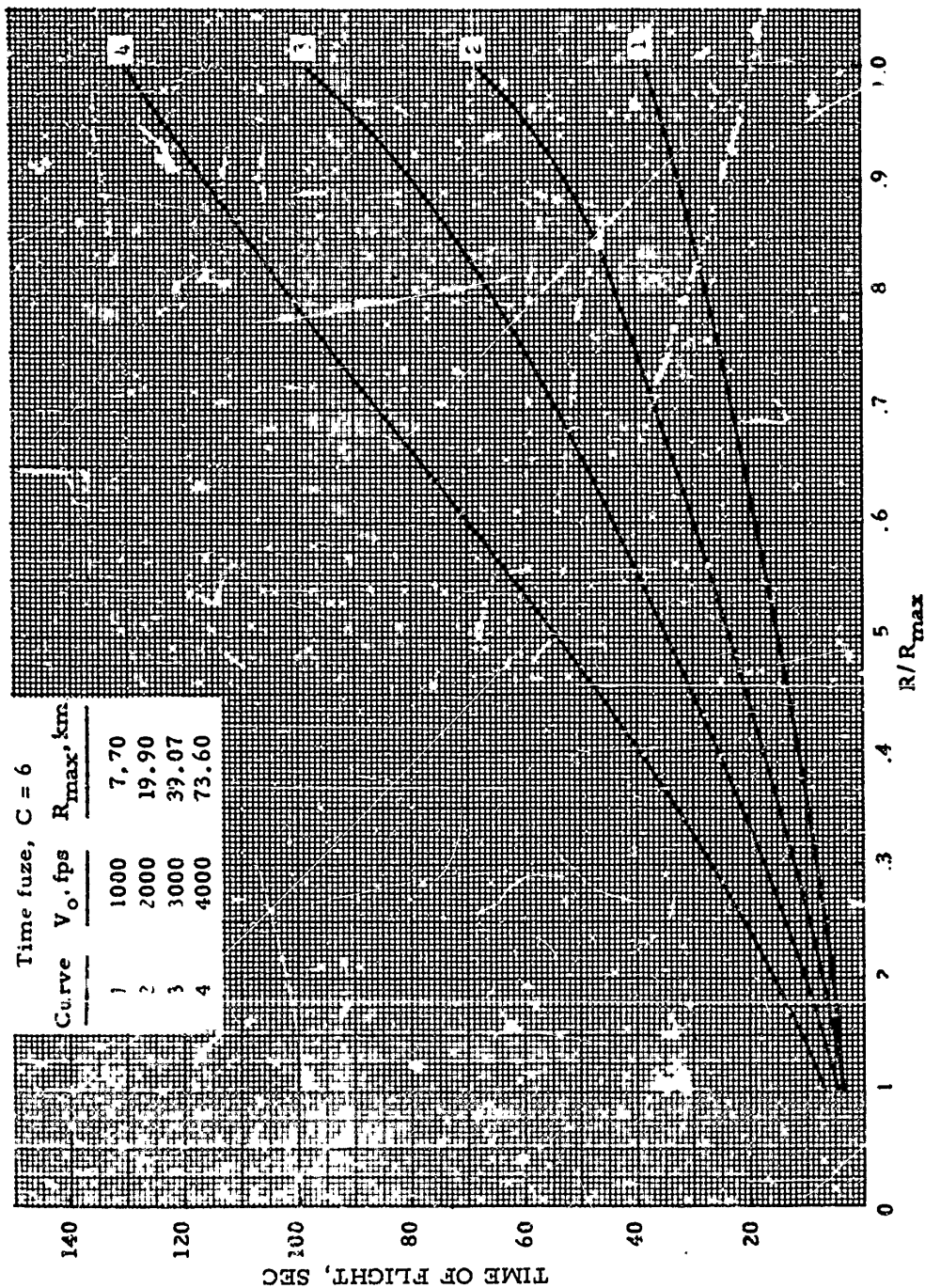


Figure 7-32(C). Time of Flight Versus R/R_{max} - Time Fuze

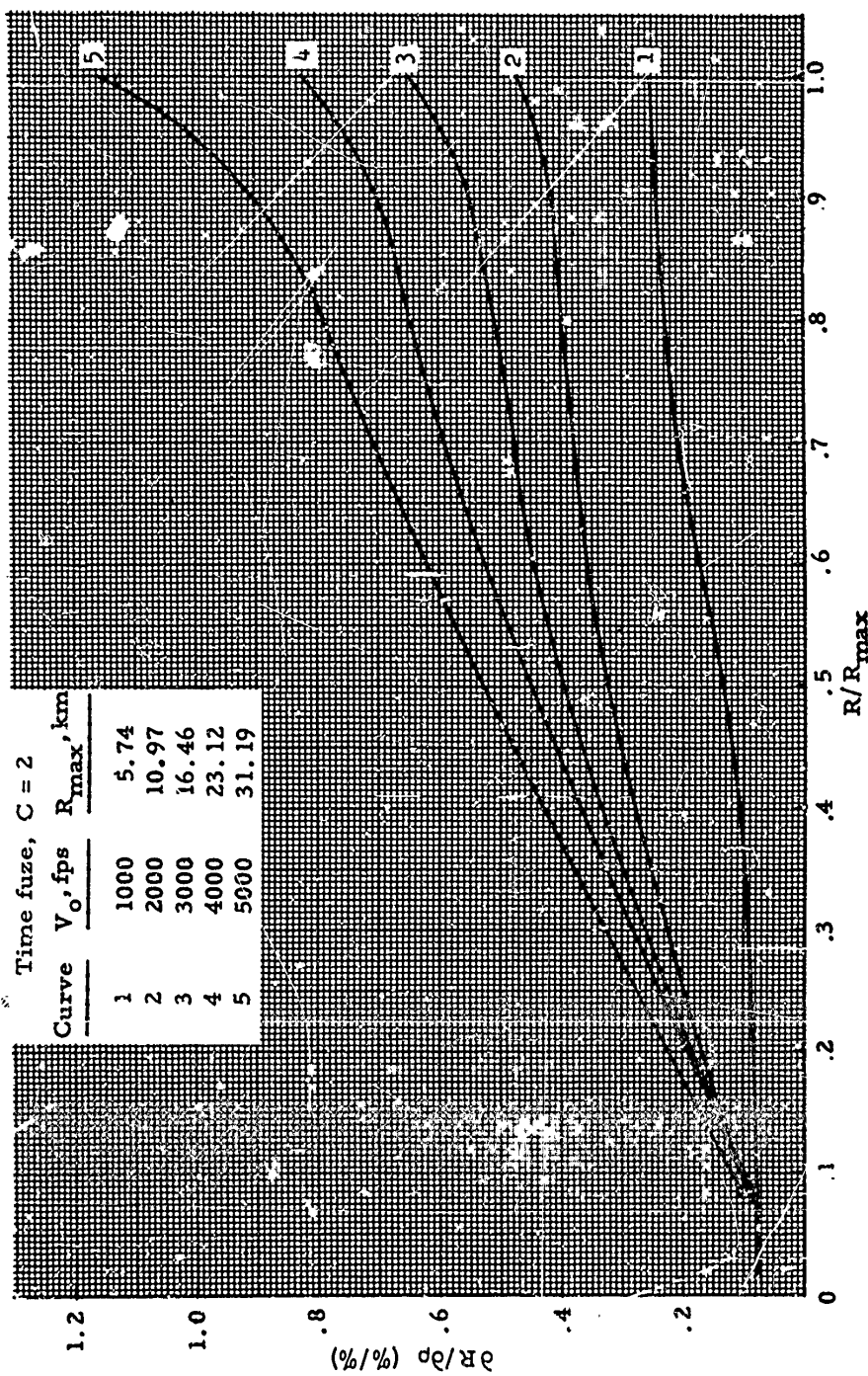


Figure 7-33(A). *Unir Effect, Range/Density Versus R/R_{max} - Time Fuze*

AMCP 706-280

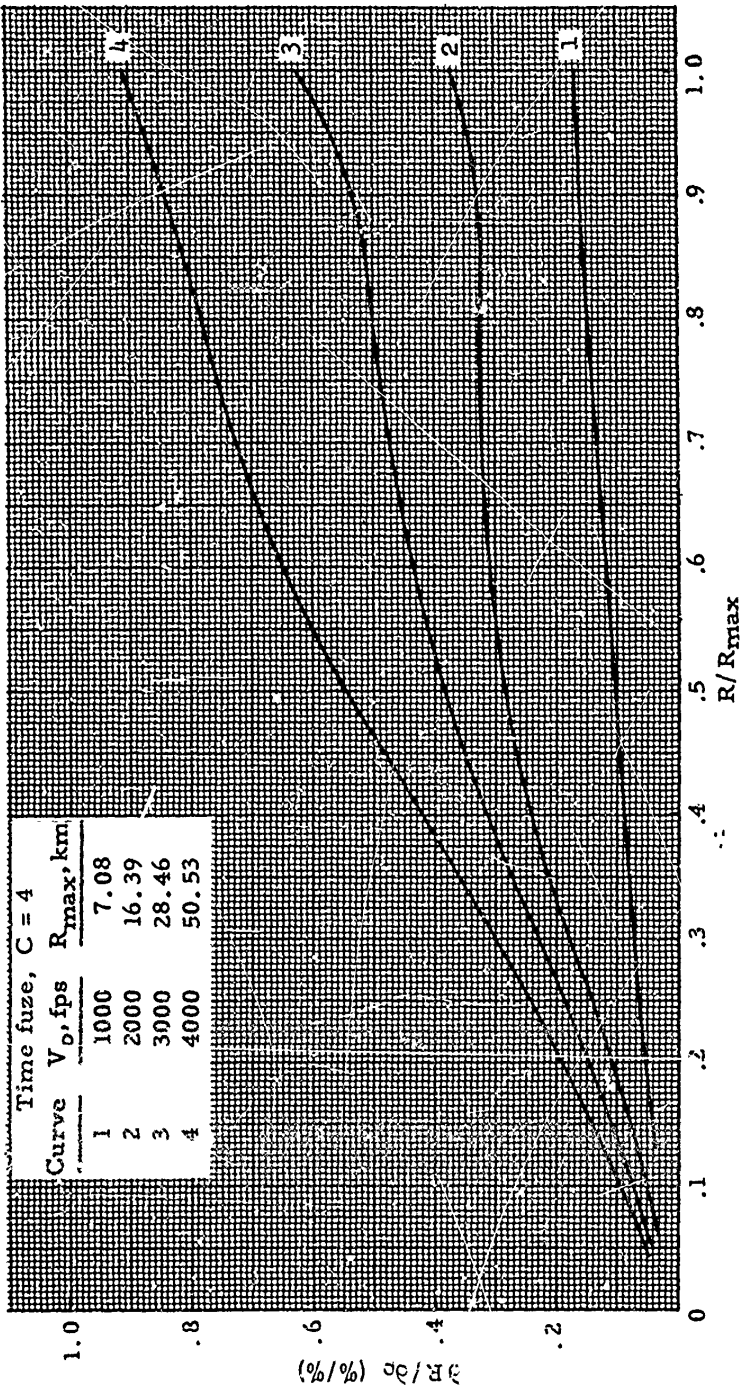


Figure 7-33(B). Unit Effect, Range/Density Versus R/R_{max} - Time Fuze

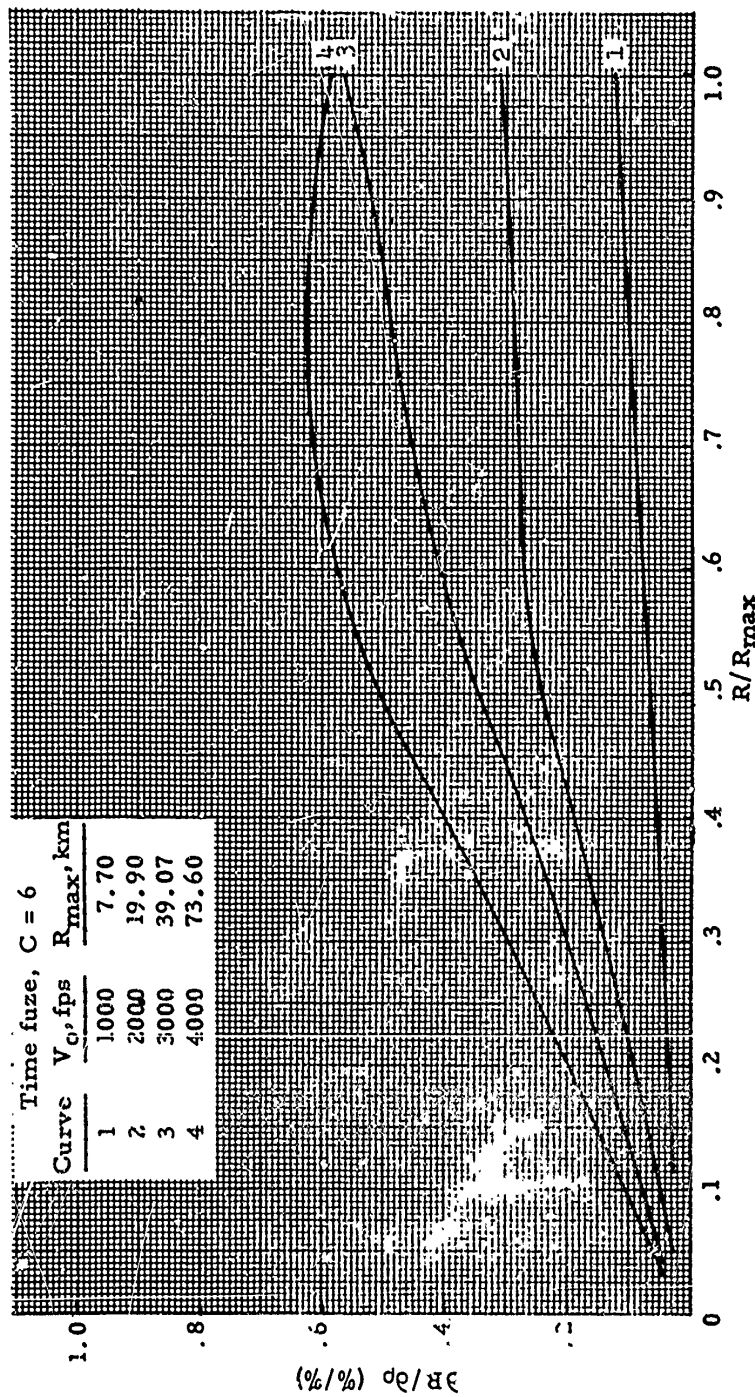
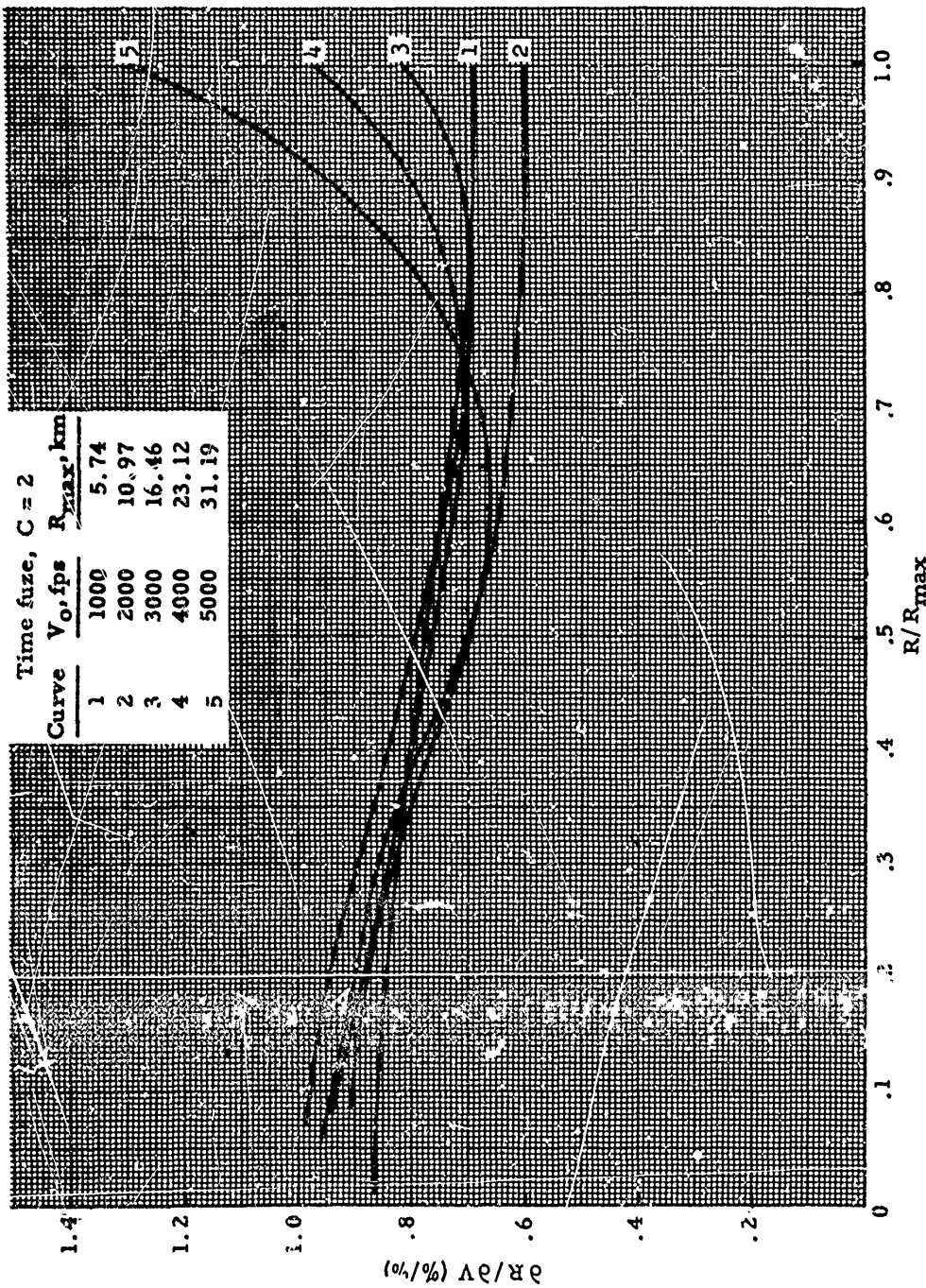


Figure 7-33(C). Unit Effect, Range/Density Versus R/R_{max} - Time Fuze

AMCP 706-280



Time fuze, C = 2

Curve	V_0 , fps	R_{max} , km
1	1000	5.74
2	2000	10.97
3	3000	16.46
4	4000	23.12
5	5000	31.19

Figure 7-34(A). Unit Effect, Range/Velocity Versus R/R_{max} - Time Fuze

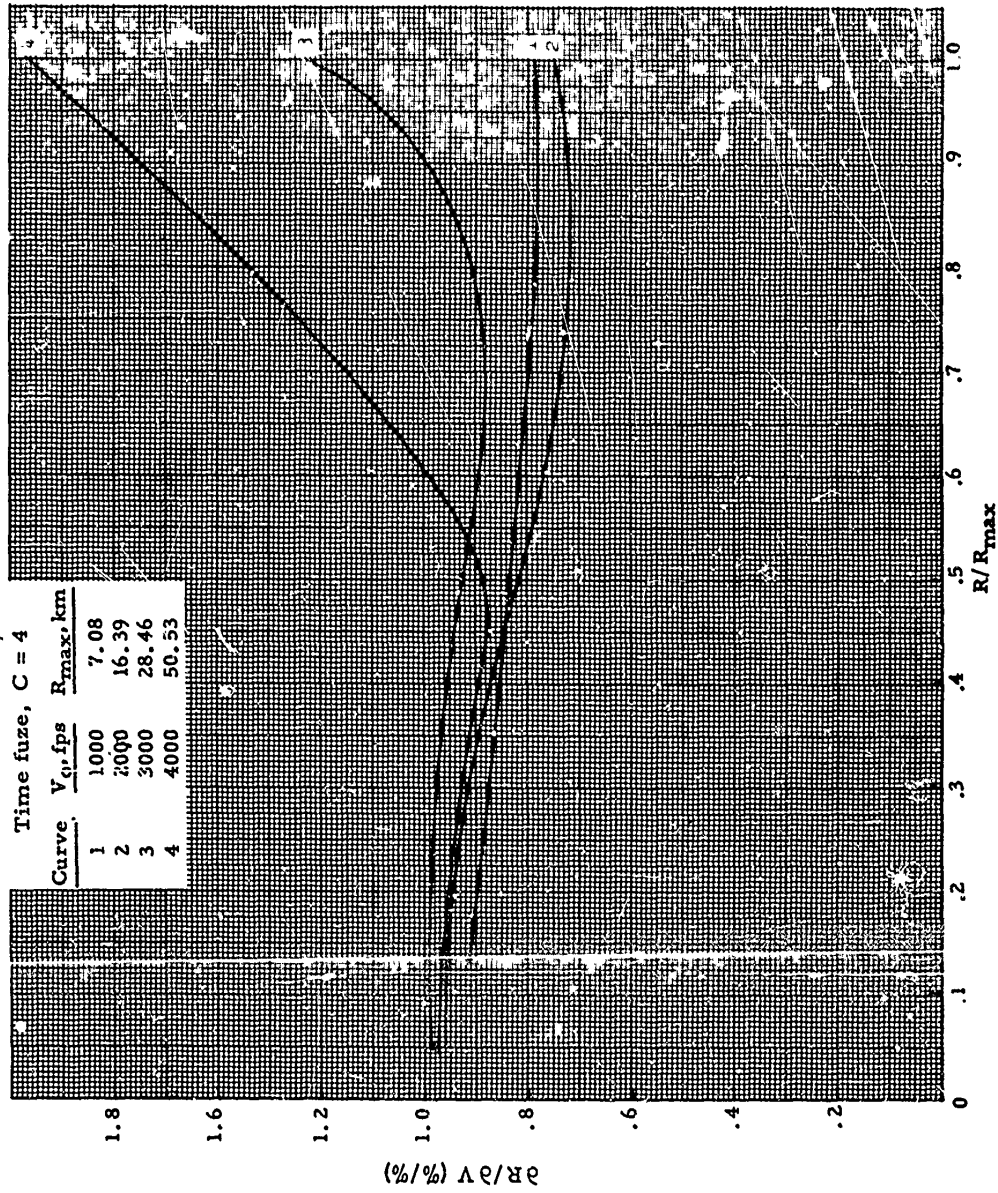


Figure 7-34(B). Unit Effect, Range/Velocity Versus R/R_{max} - Time Fuze

AMCP 706-200

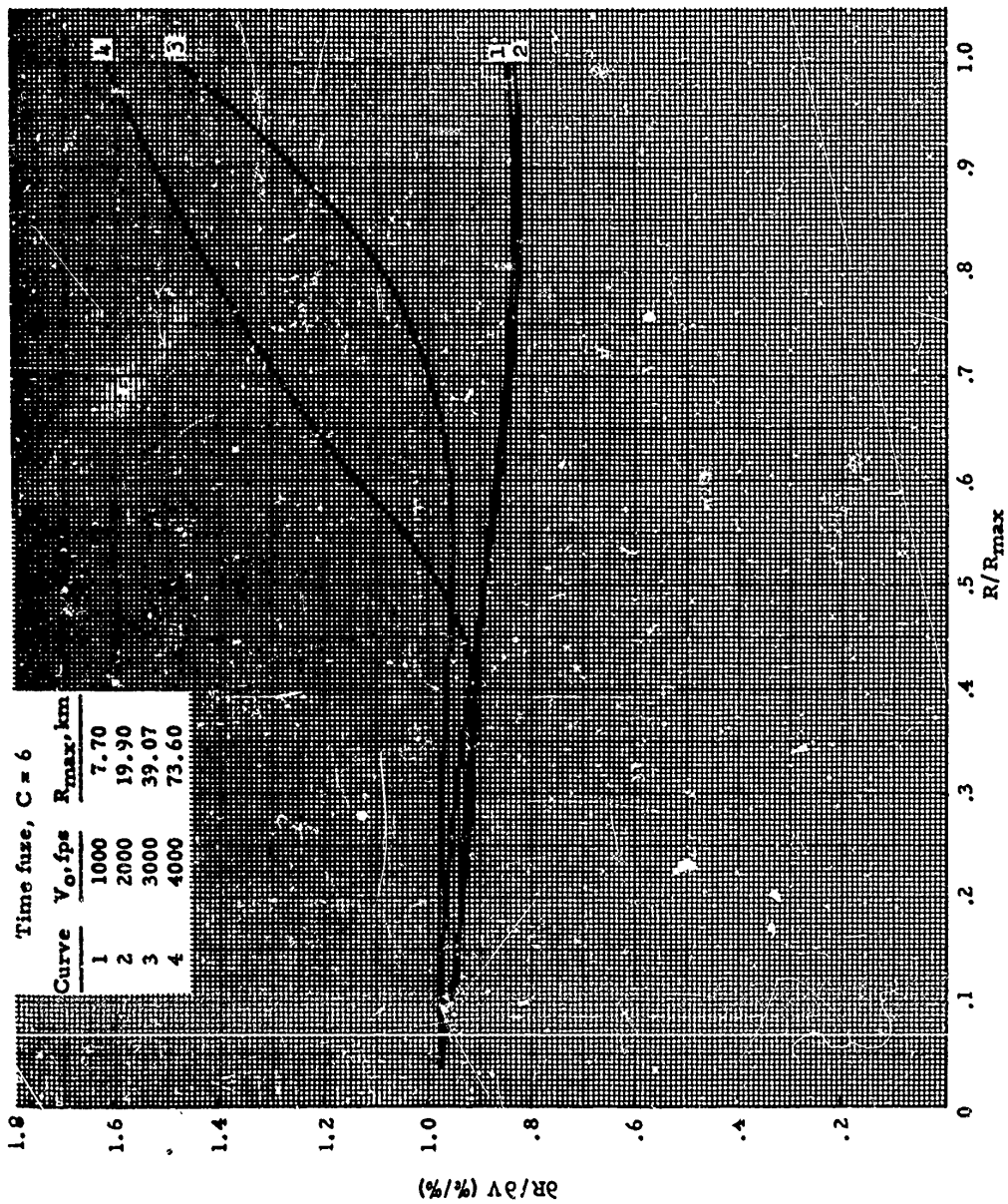


Figure 7-34(C). Unit Effect, Range/Velocity Versus R/R_{max} - Time Fuse

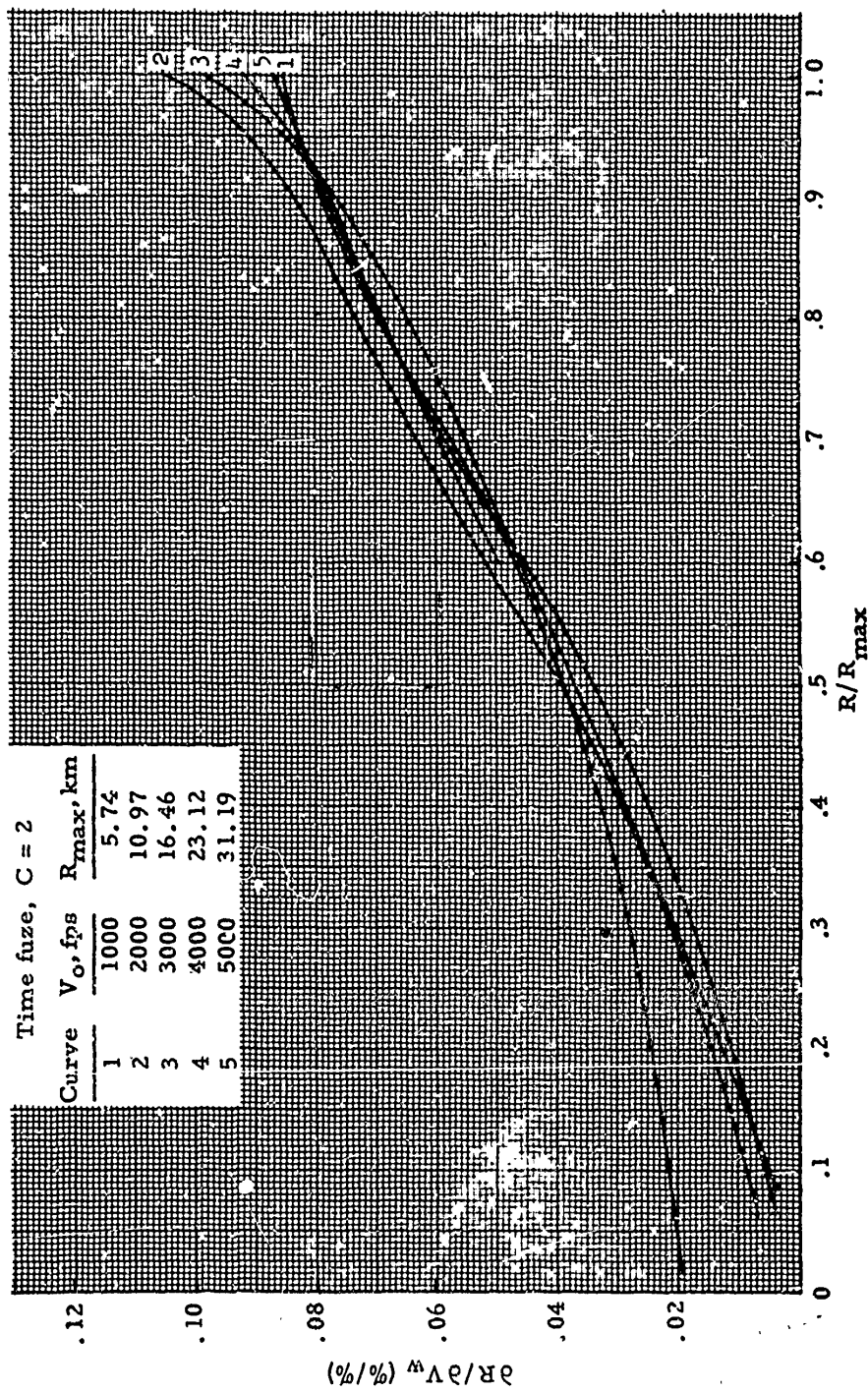


Figure 7-35(A). Unit Effect, Range/Wind Versus R/R_{max} - Time Fuze

AMCP 708-280

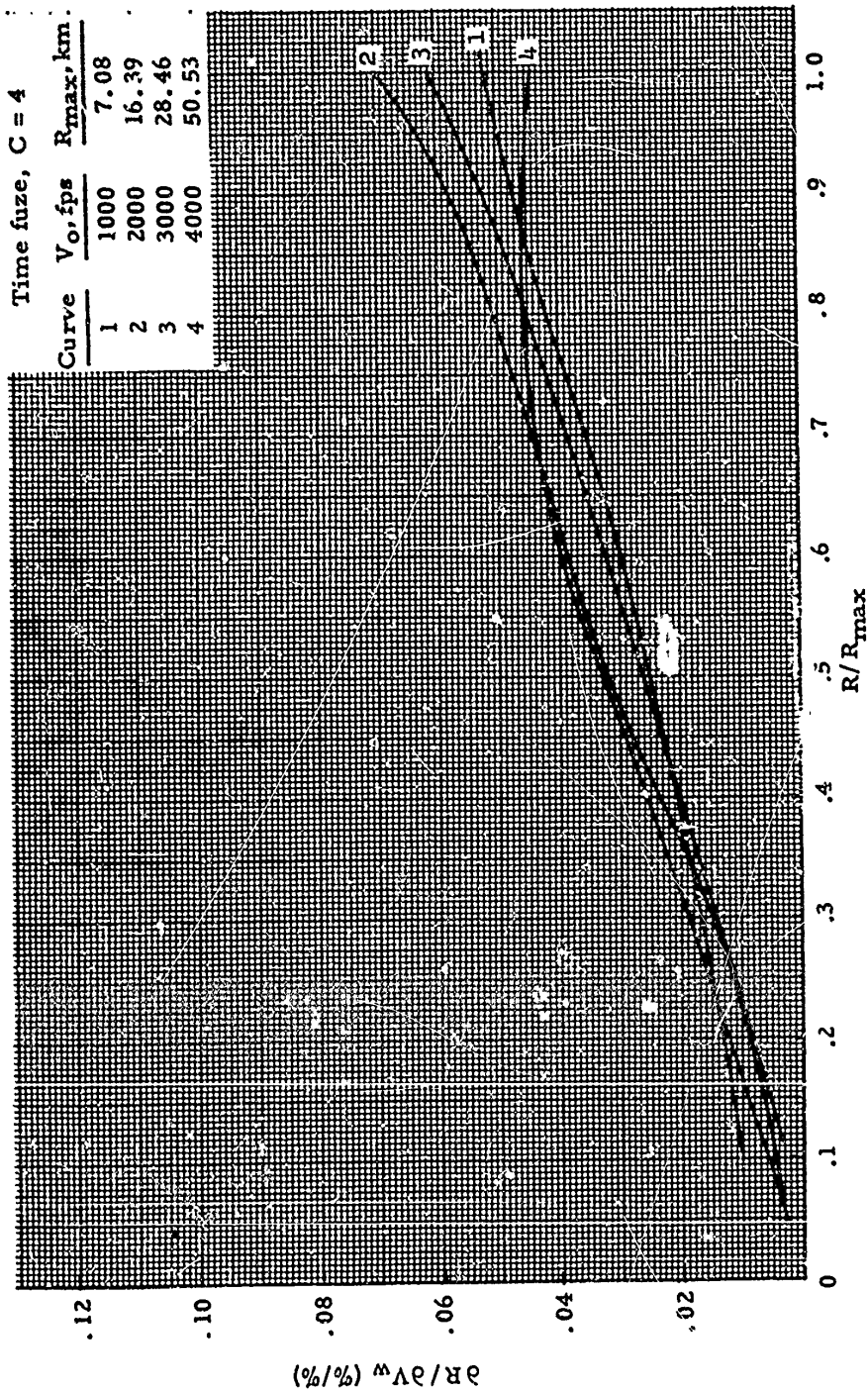


Figure 7-35(B). Unit Effect, Range/Wind Versus R/R_{max} - Time Fuze

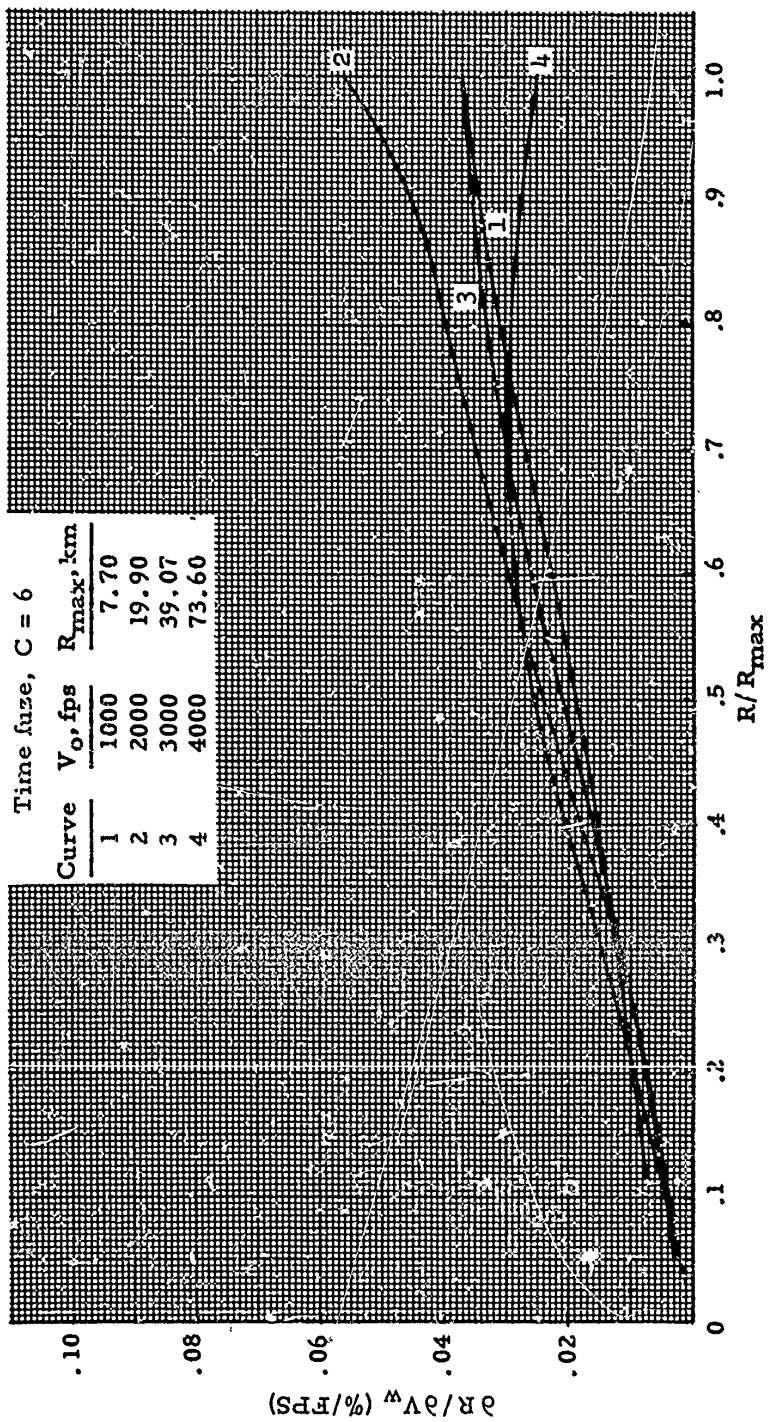


Figure 7-35(C). Unit Effect, Range/Wind Versus R/R_{max} - Time Fuze

AMCP 706-280

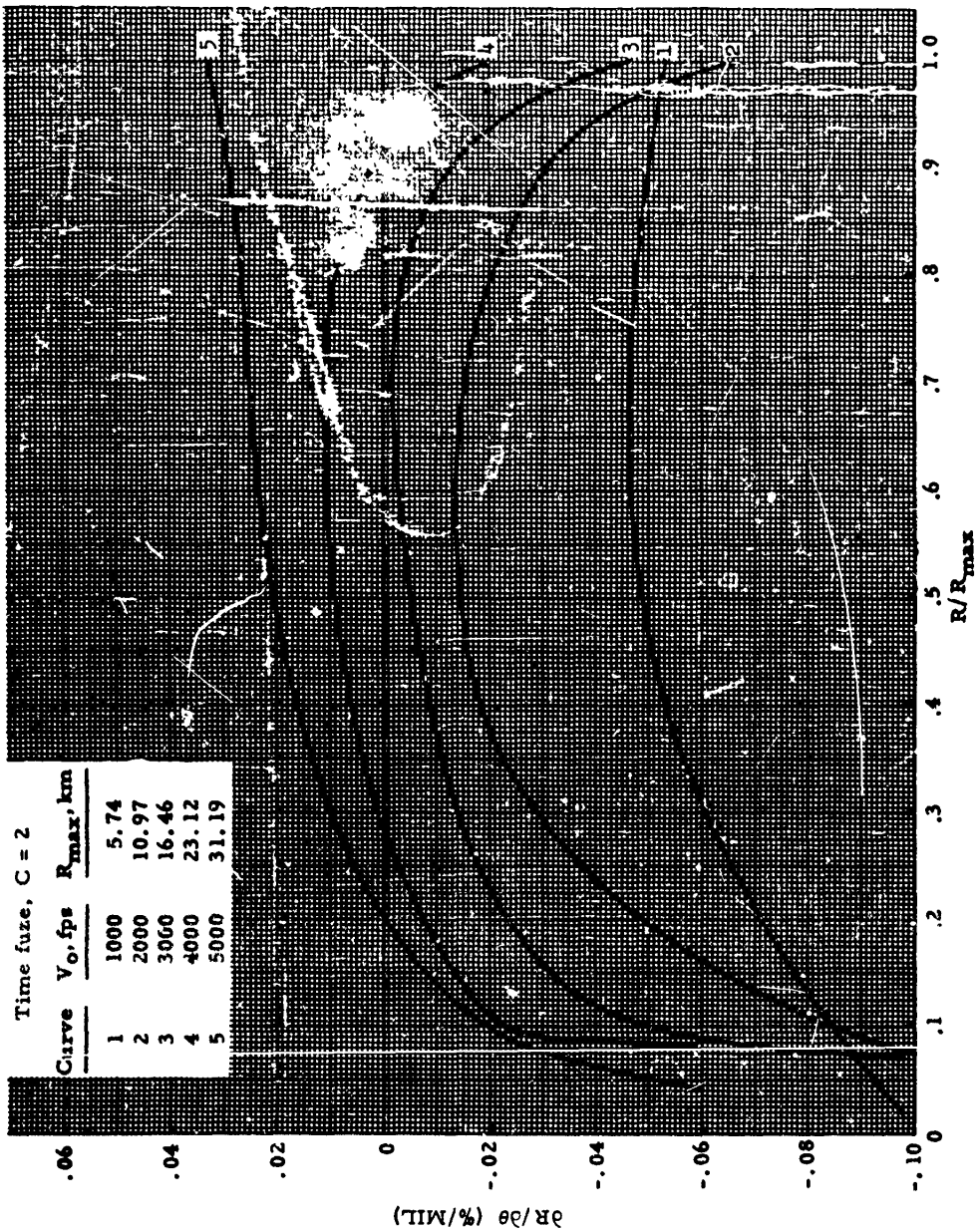


Figure 7-36(A). Unit Effect, Range/Departure Angle Versus R/R_{max} - Time Fuze

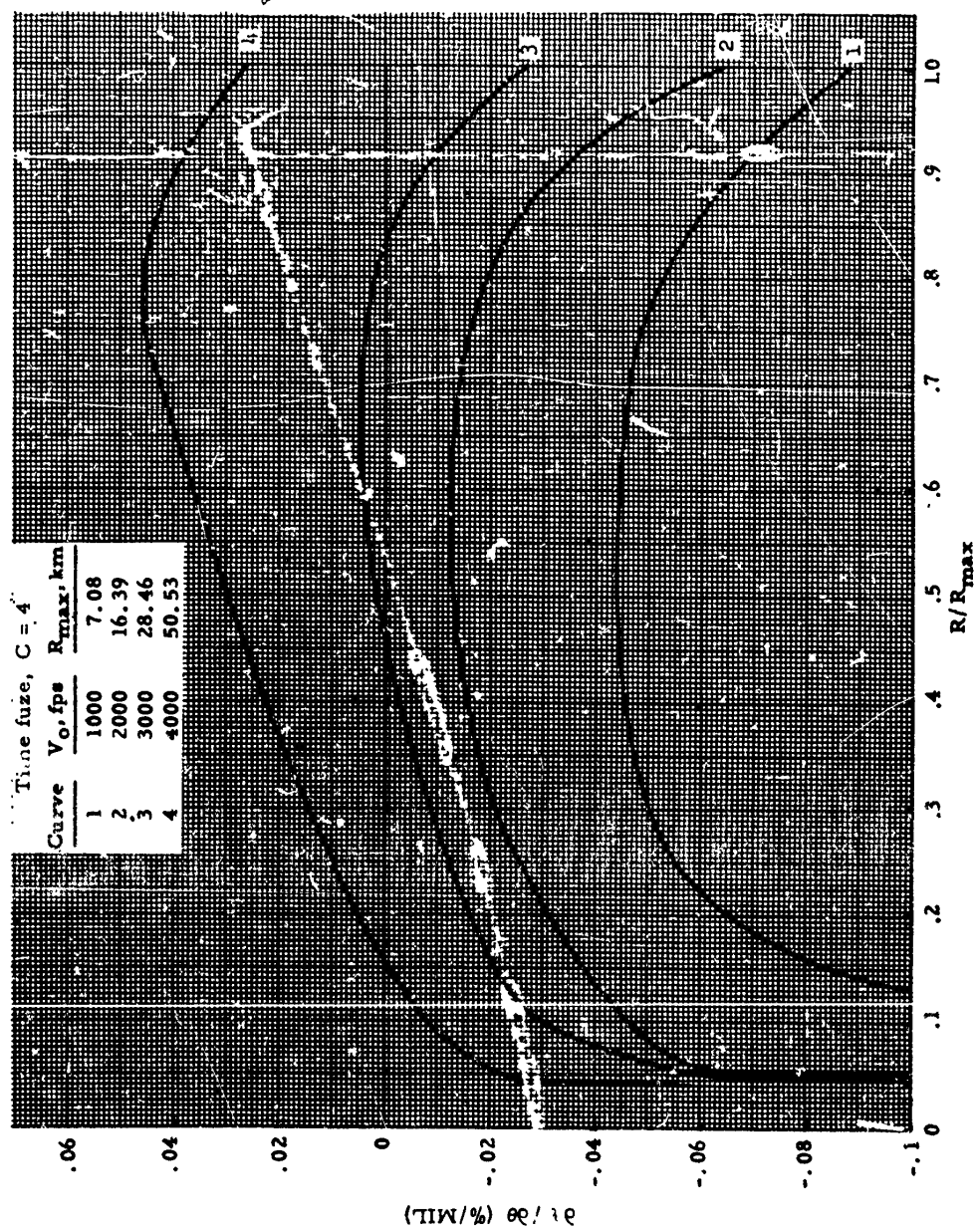


Figure 7-36(B). Unit Effect, Range/Departure Angle Versus R/R_{max} - Time Fuze

AMCP 706-280

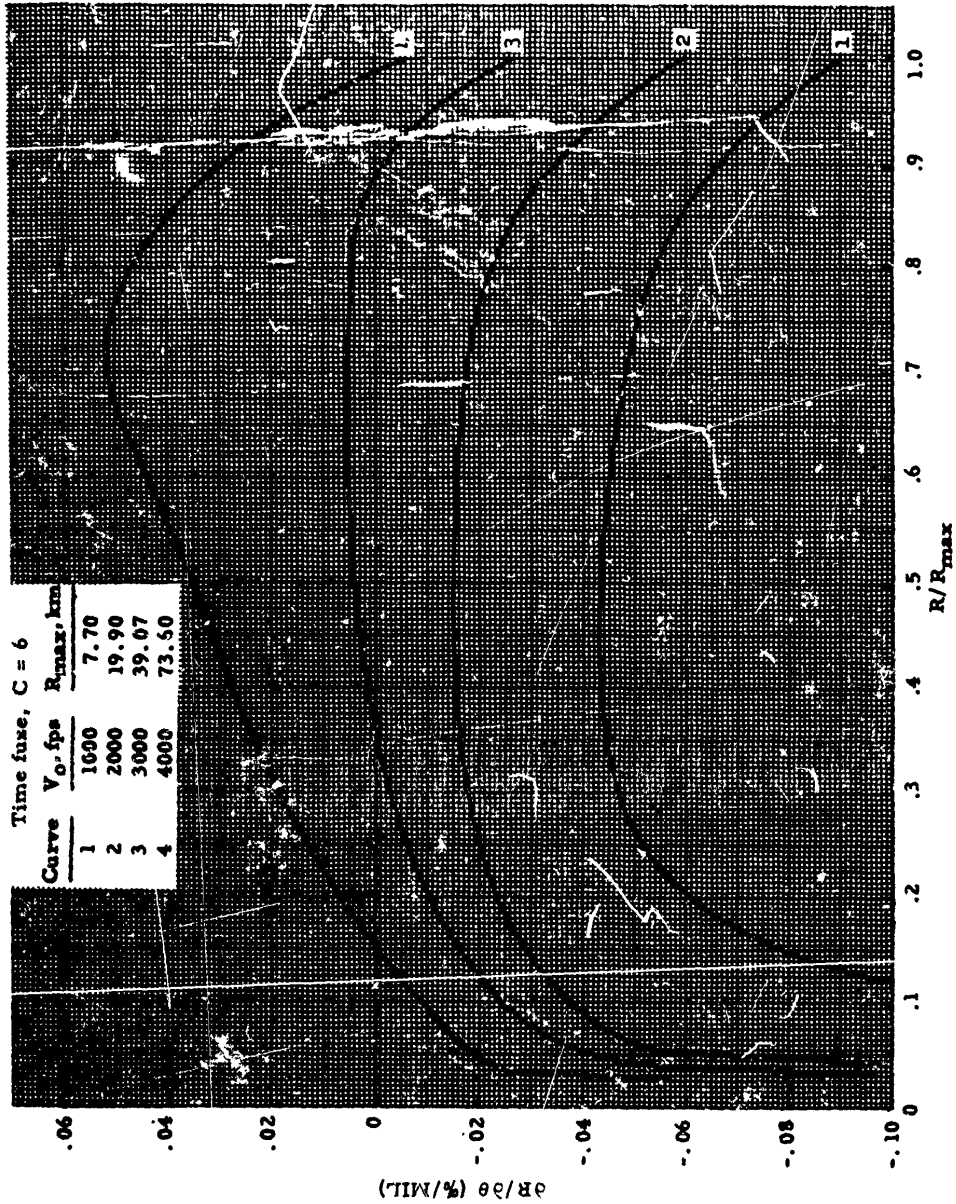


Figure 7-36(C). Unit Effect, Range/Departure Angle Versus R/R_{max} - Time Fuse

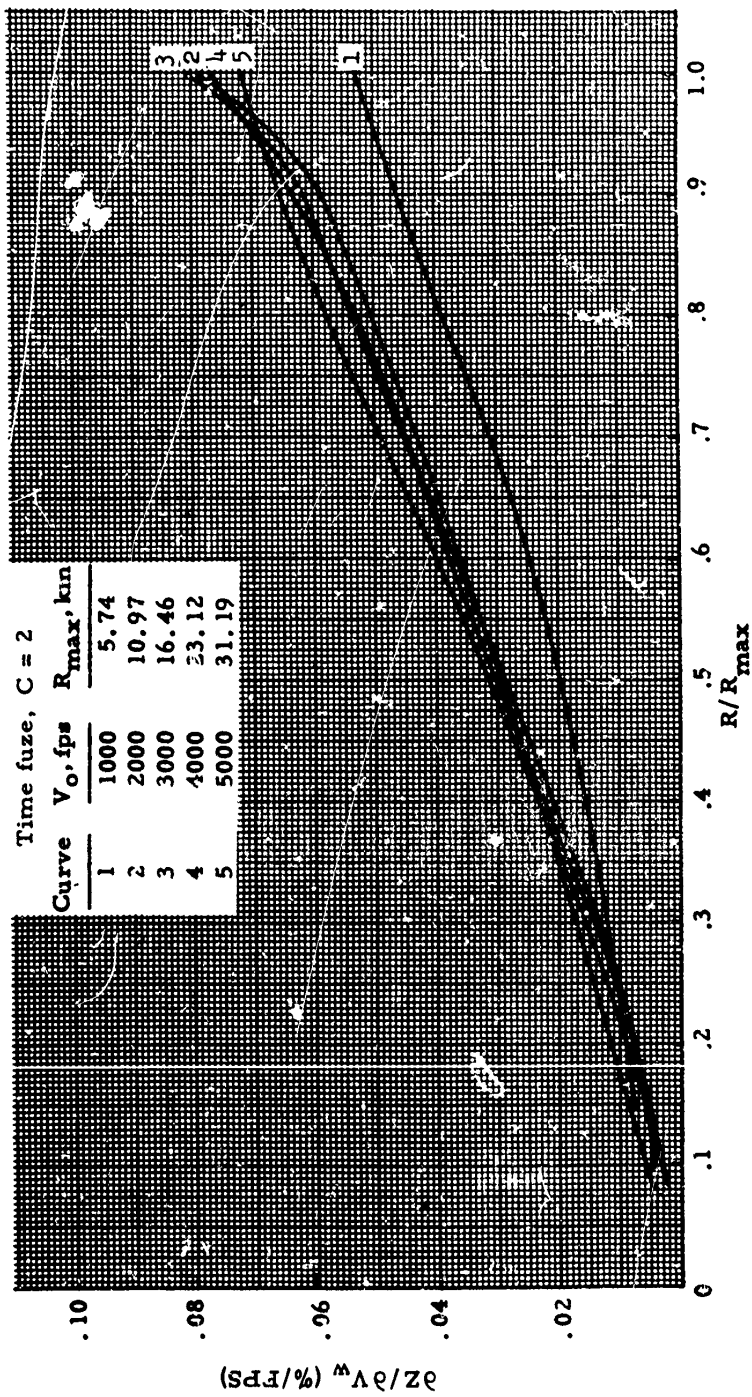


Figure 7-37(A). Unit Effect, Deflection/Wind Versus R/R_{max} - Time Fuze

AMCP 706-280

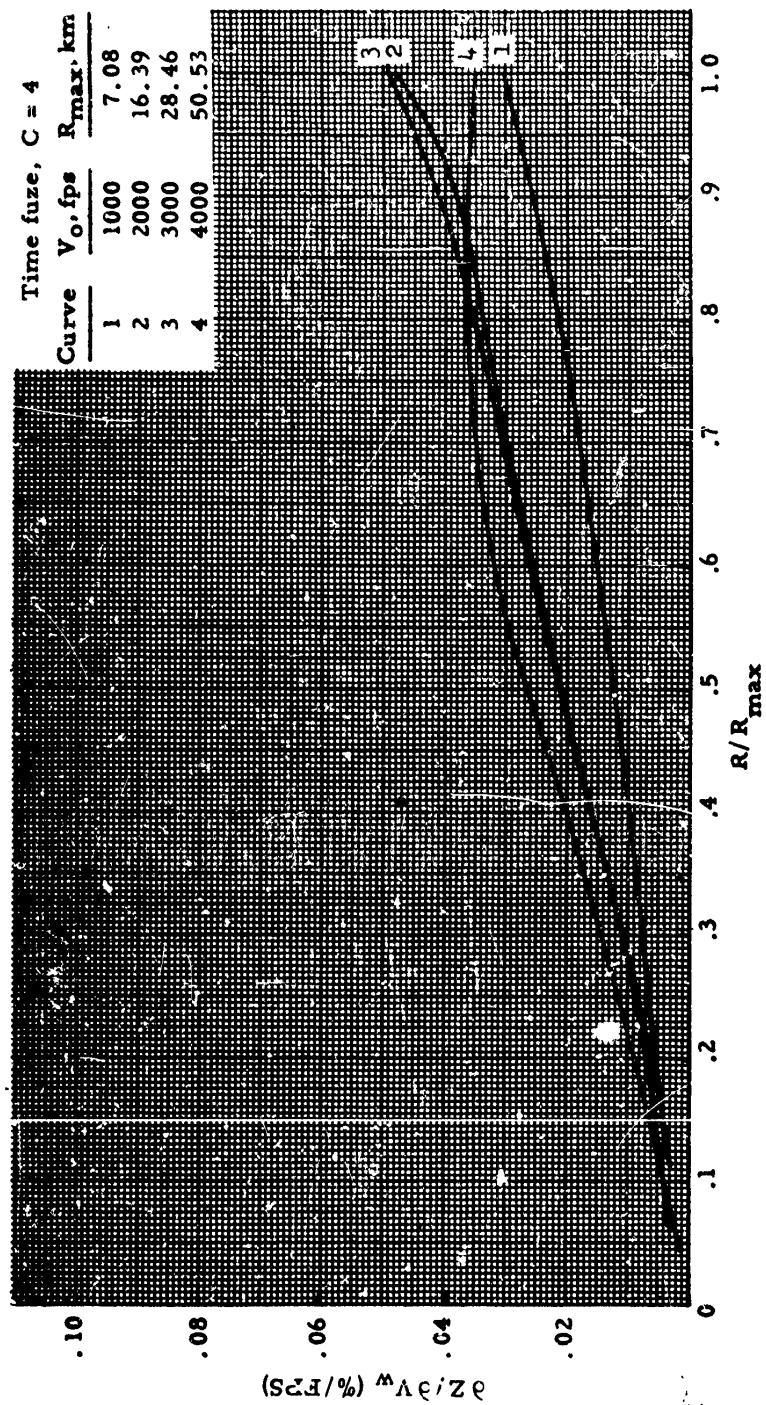


Figure 7-37(B). Unit Effect, Deflection/Wind Versus R/R_{max} - Time Fuze

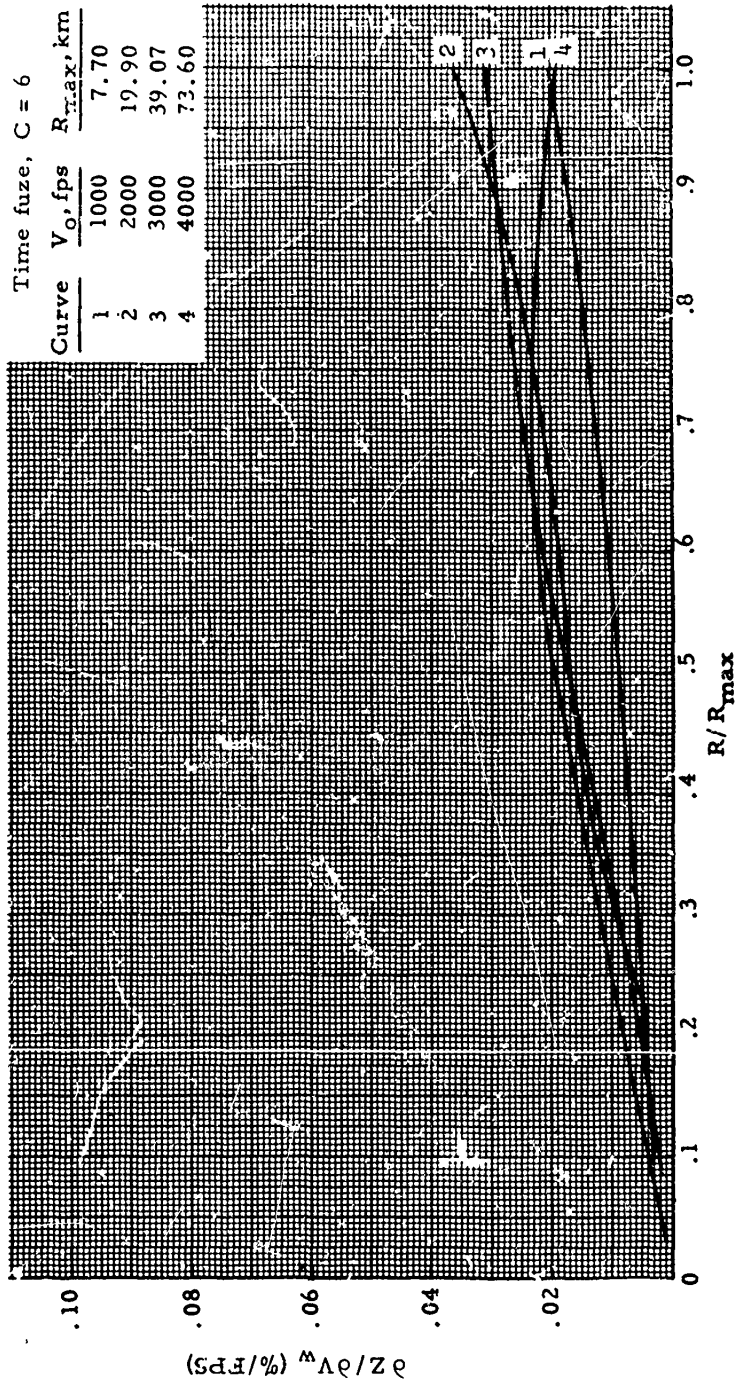


Figure 7-37(C). Unit Effect, Deflection/Wind Versus R/R_{max} - Time Fuze

AMCP 700-280

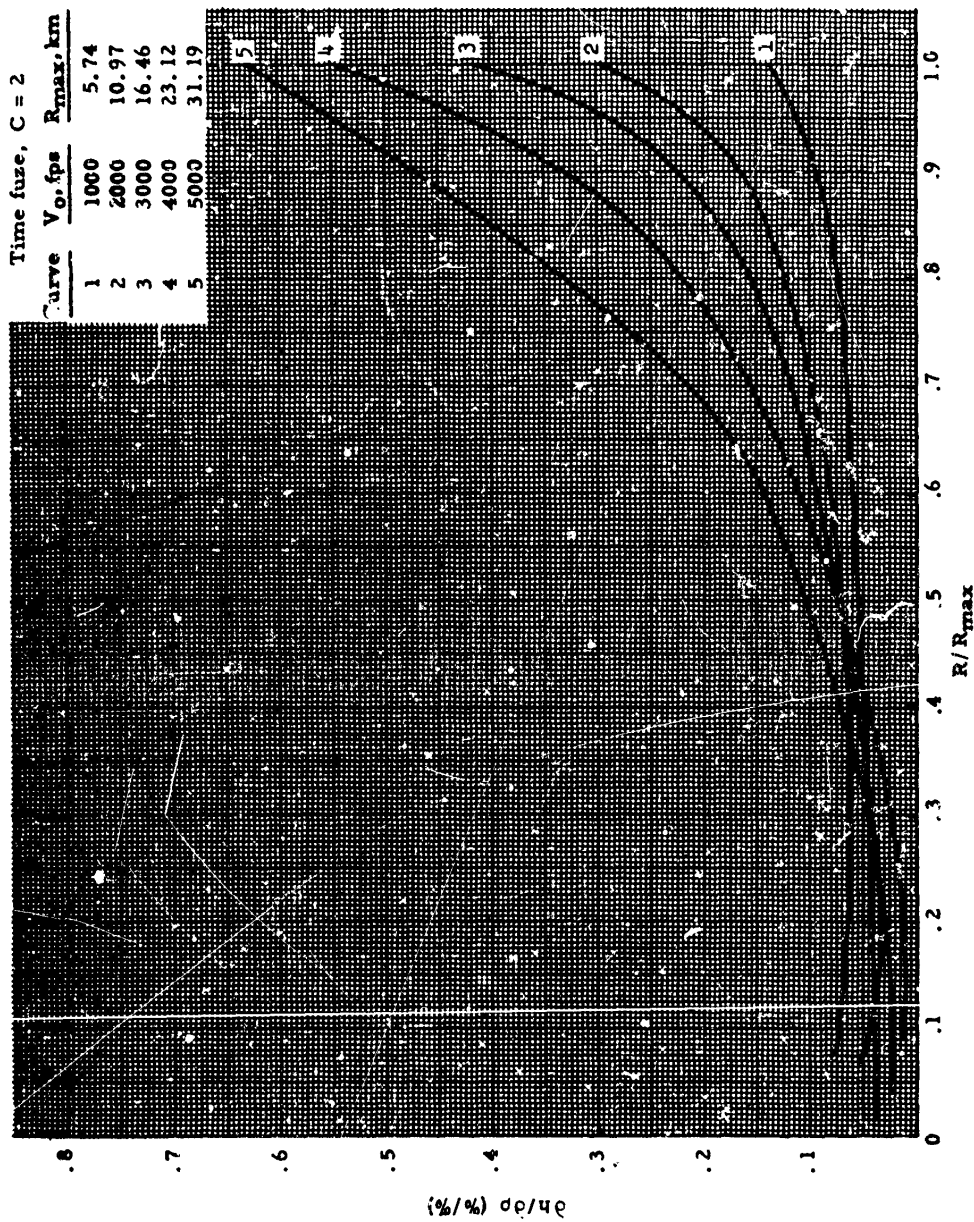


Figure 7-38(A). Unit Effect, Altitude/Density Versus R/R_{max} - Time Fuze

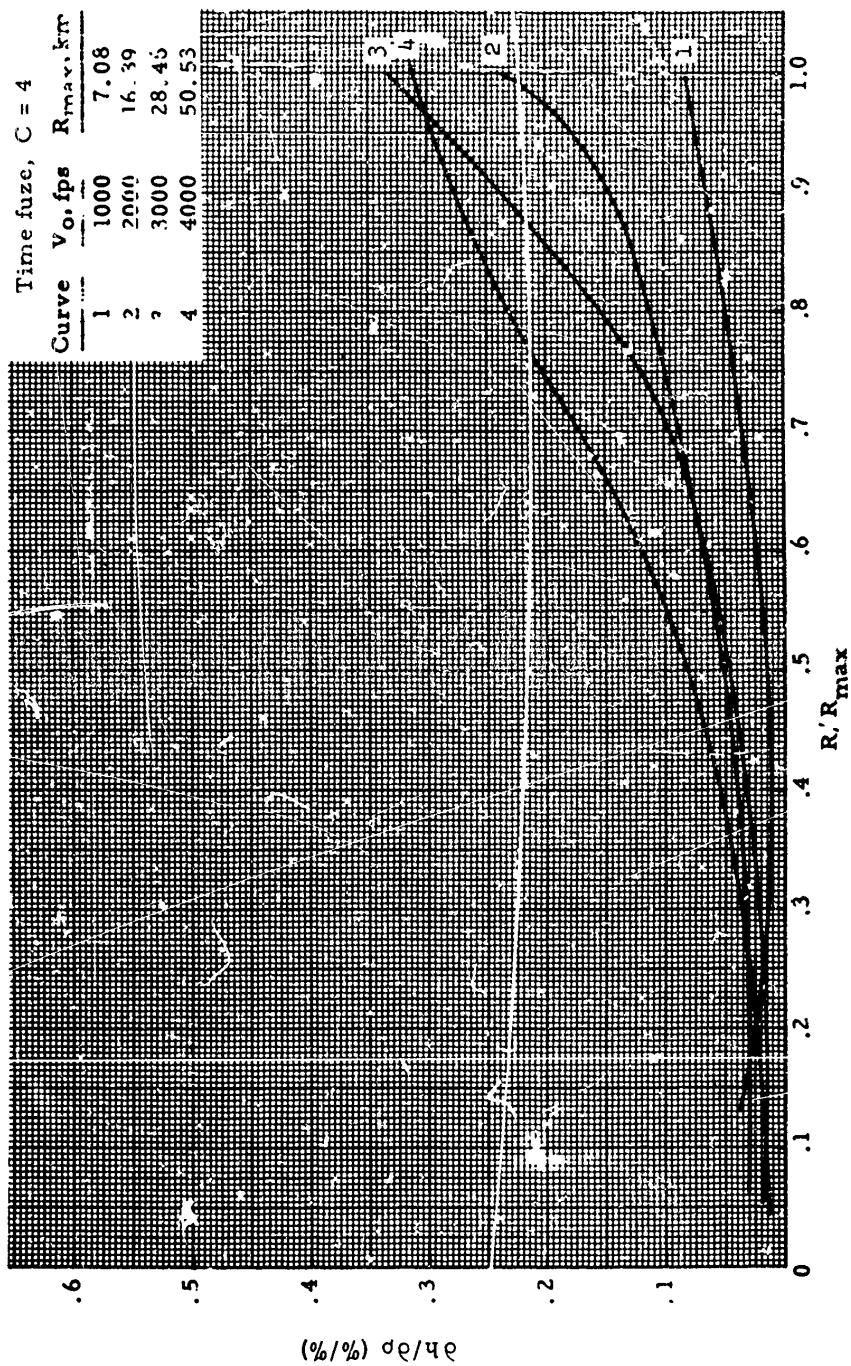


Figure 7-38(B). Unit Effect, Altitude/Density Versus R/R_{max} - Time Fuze

AMCP 706-280

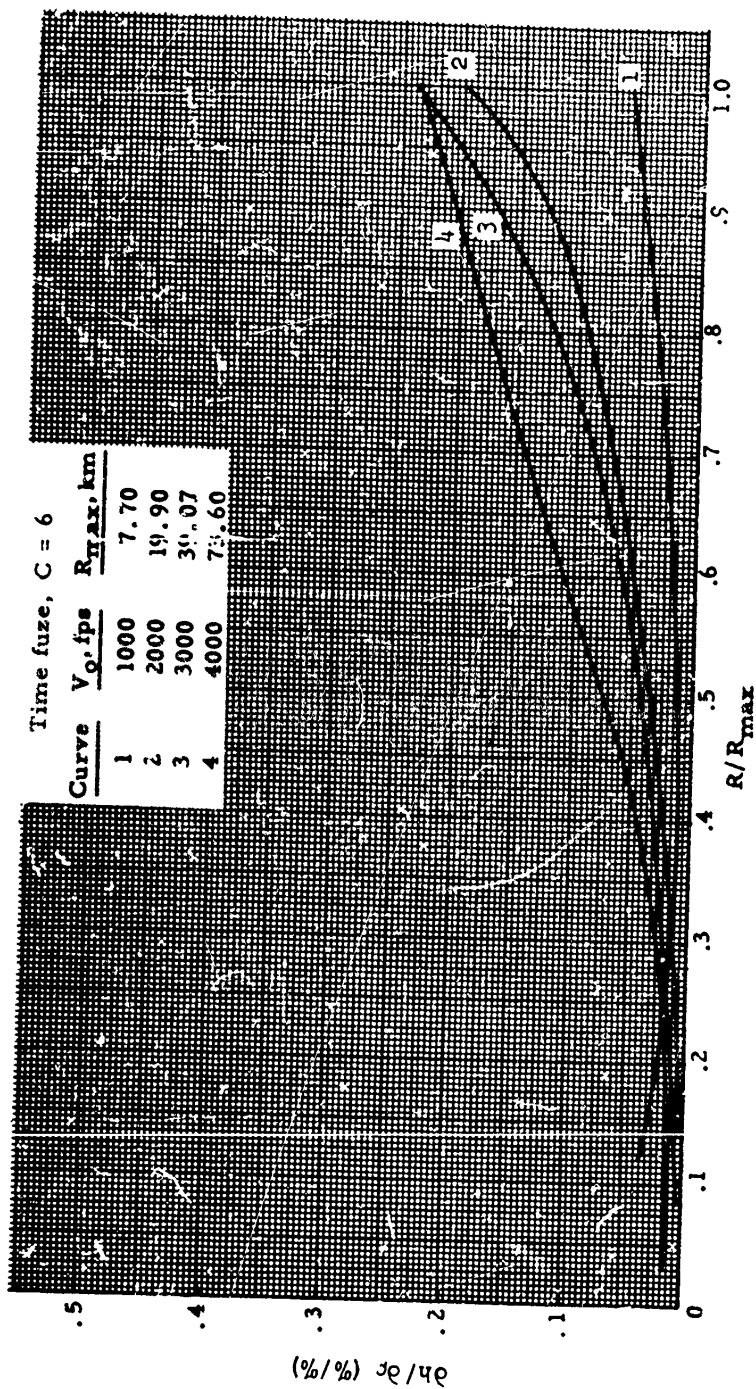


Figure 7-38(C). Unit Effect, Altitude/Density Versus R/R_{max} - Time Fuze

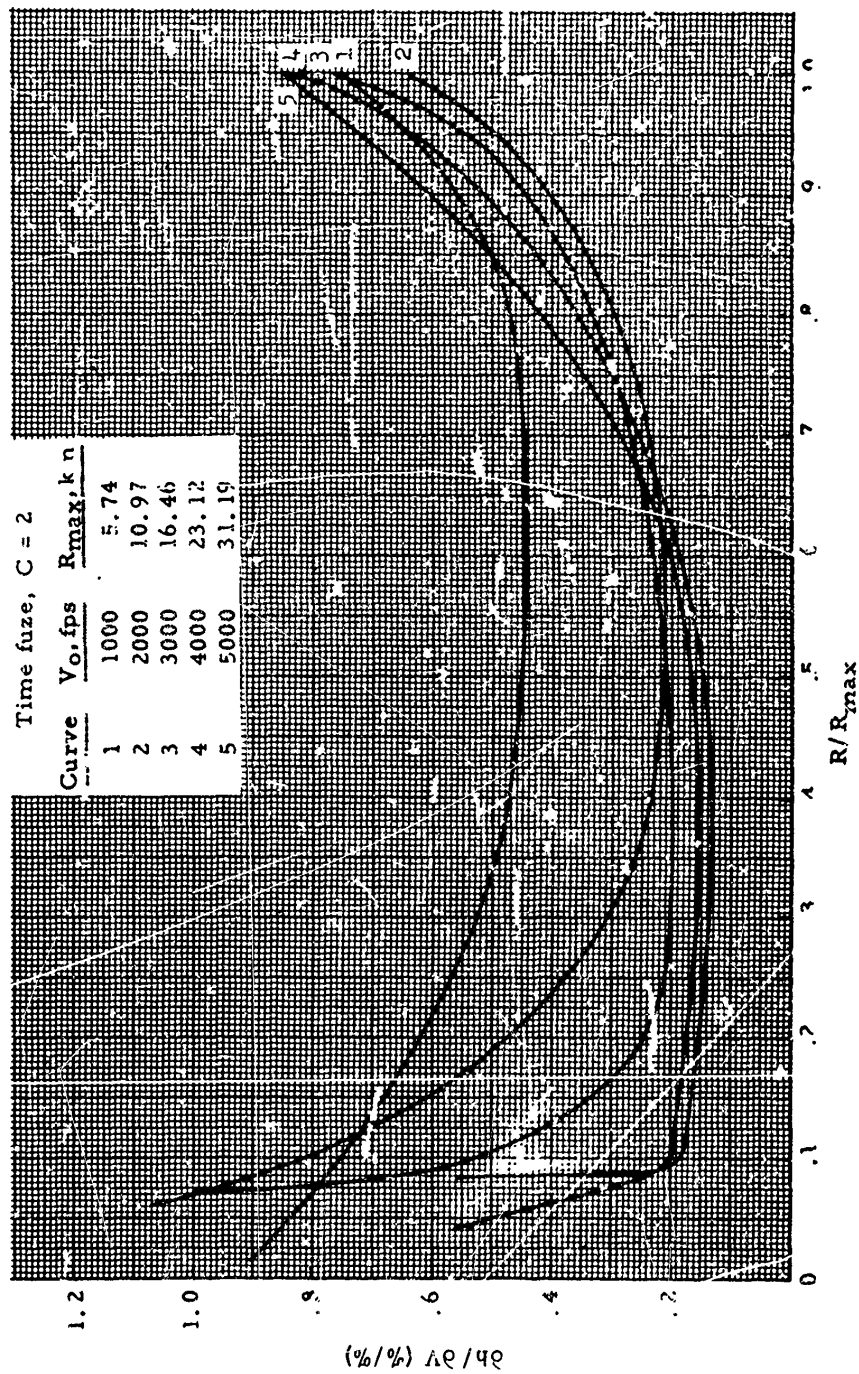


Figure 7-39(A). Unit Effect, Altitude/Velocity Versus R/R_{max} ~ Time Fuze

AMCP 706-280

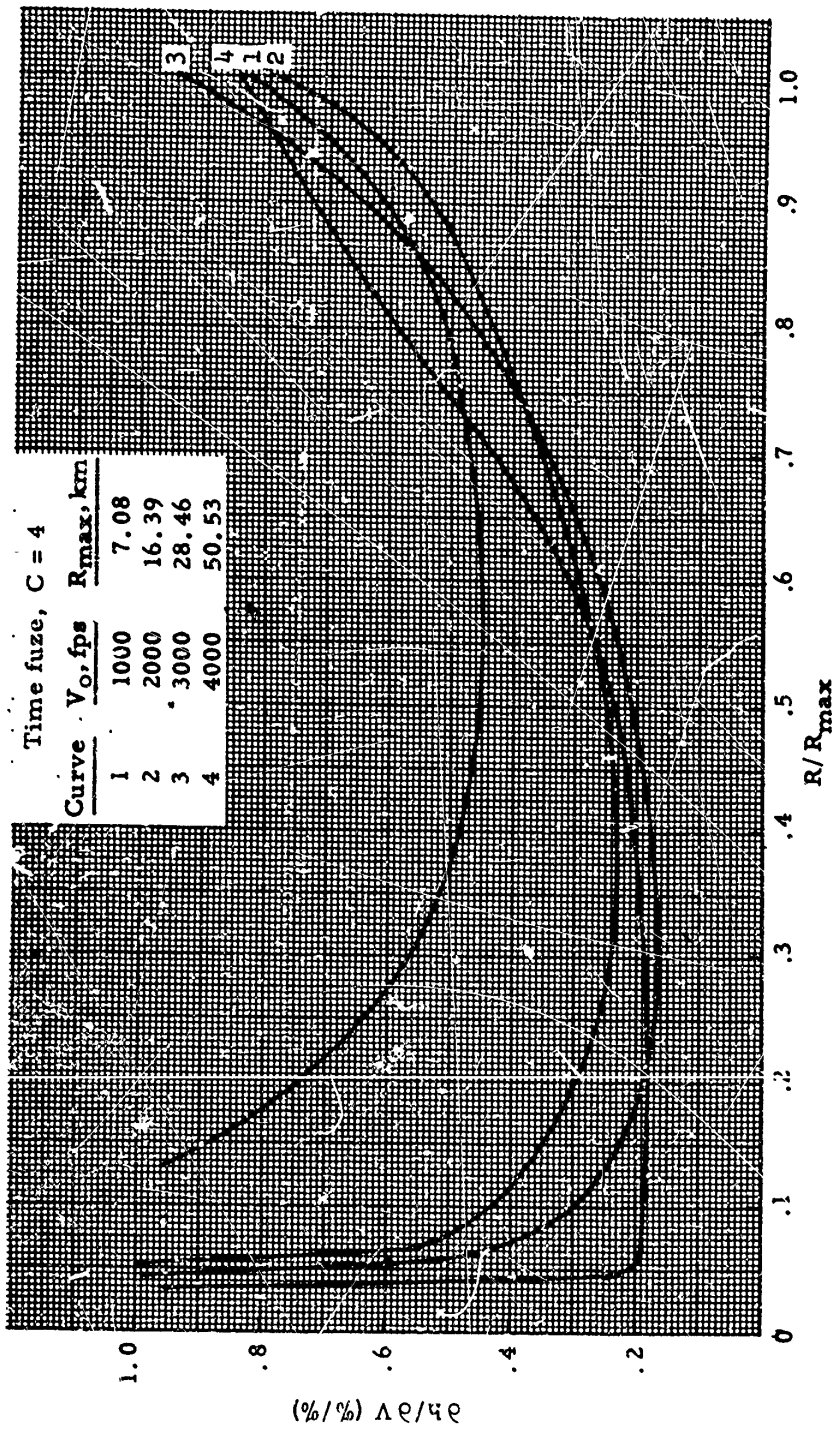


Figure 7-39(B). Unit Effect, Altitude/Velocity Versus R/R_{max} - Time Fuze

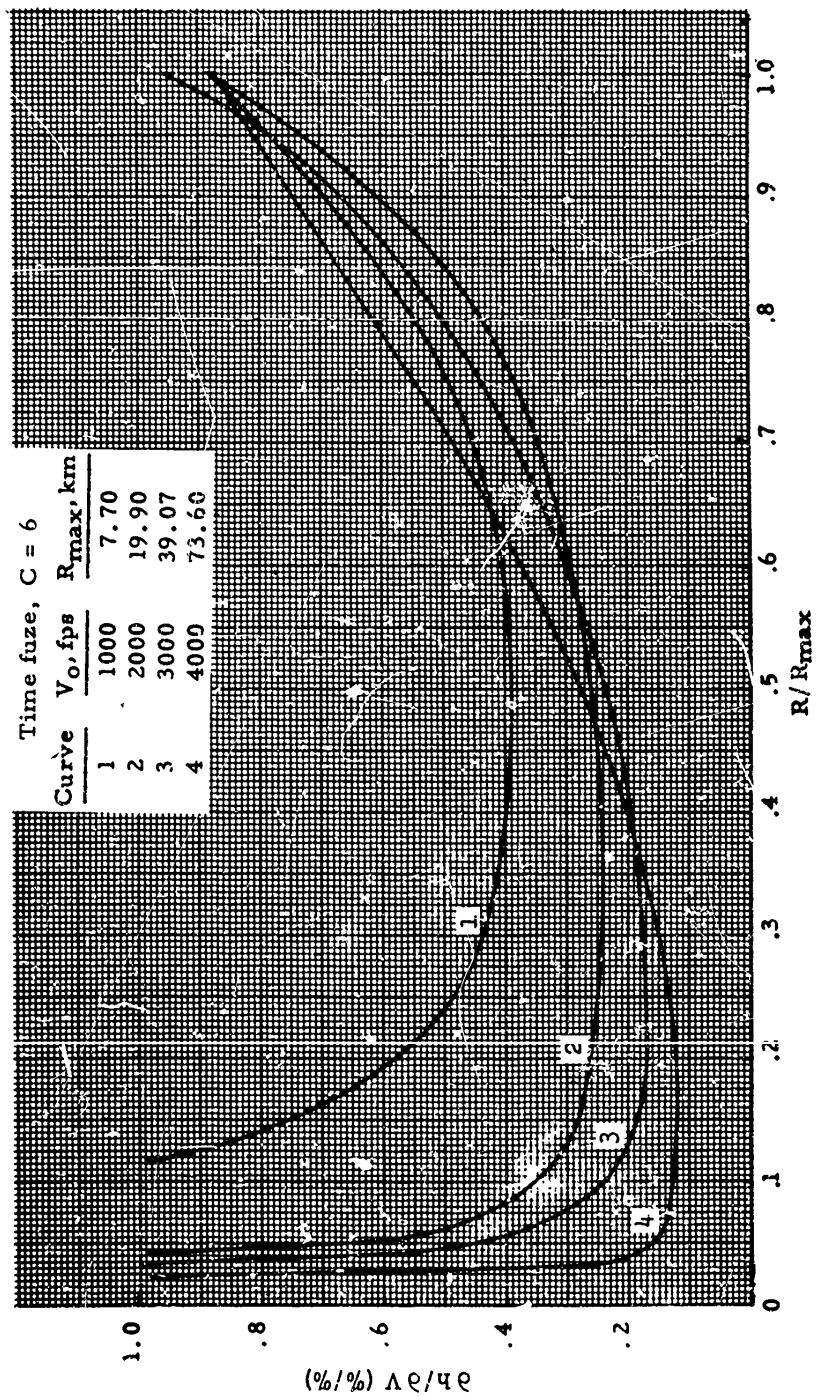


Figure 7-39(C). Unit Effect, Altitude/Velocity Versus R/R_{max} - Time Fuze

AMCP 706-260

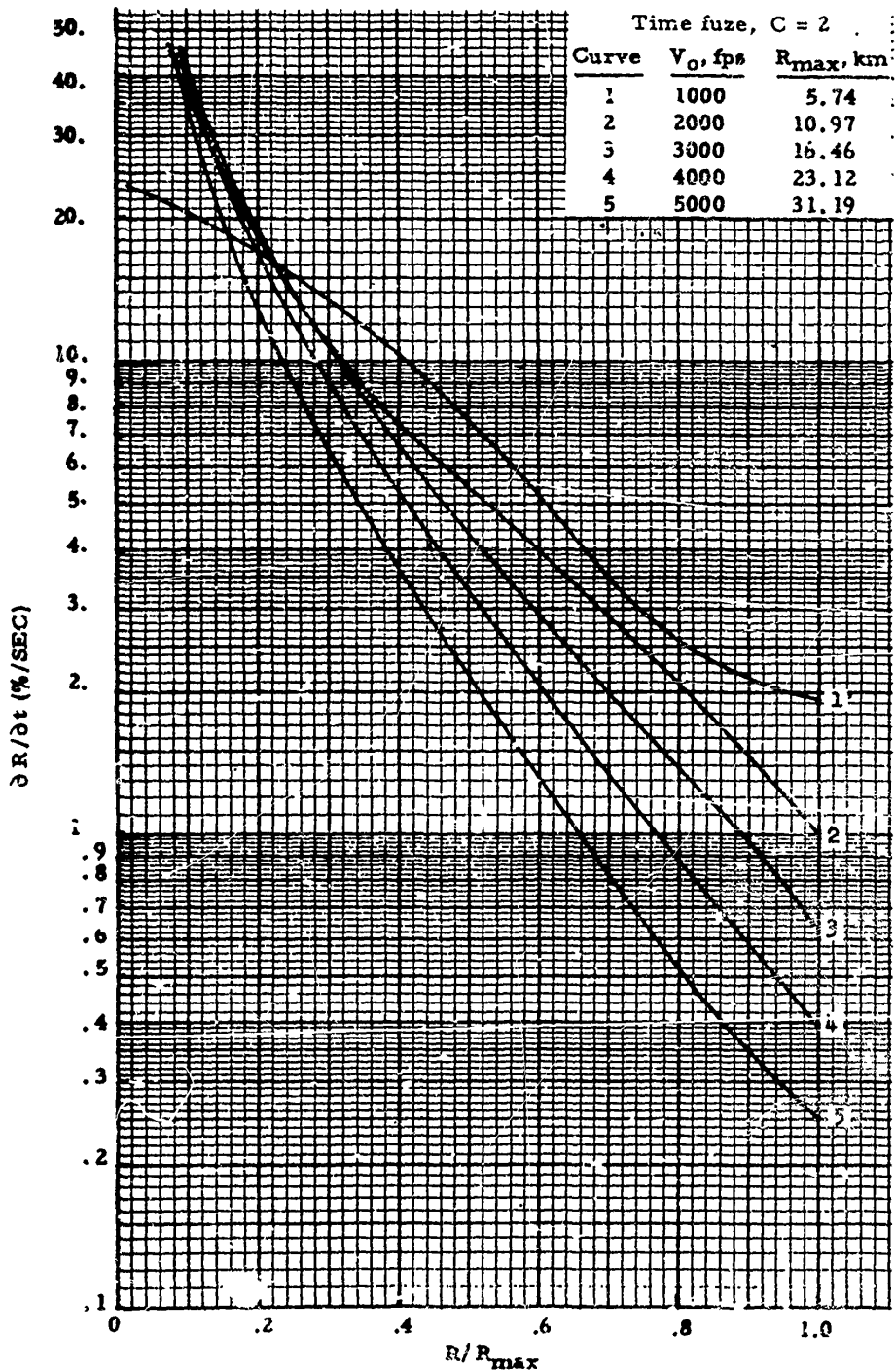


Figure 7-40(A). Unit Effect, Range/Time Versus R/R_{max} - Time Fuze

AMCP 706-280

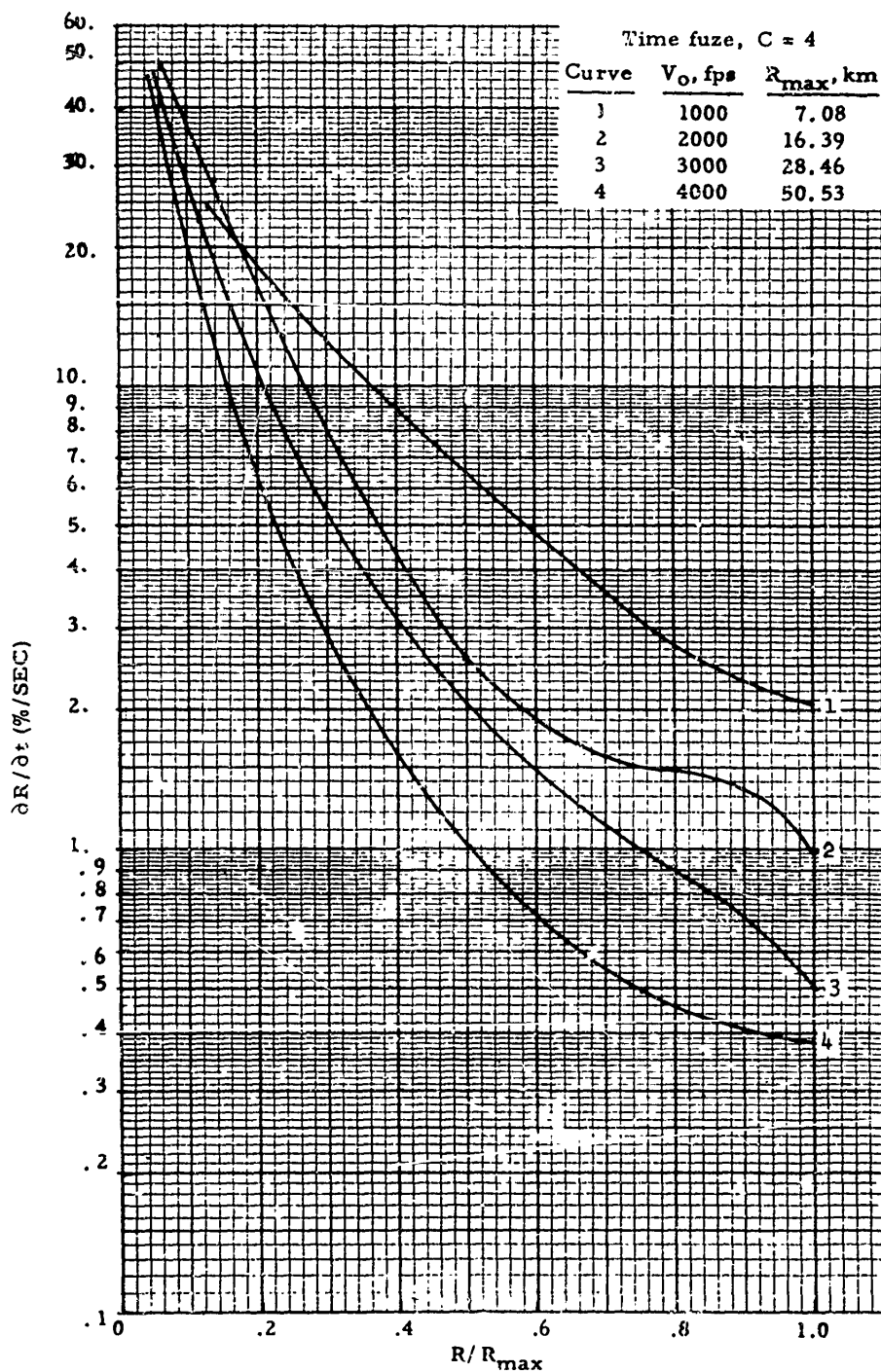


Figure 7-40(B). Unit Effect, Range/Time Versus R/R_{max} - Time Fuze

AMCP 708-280

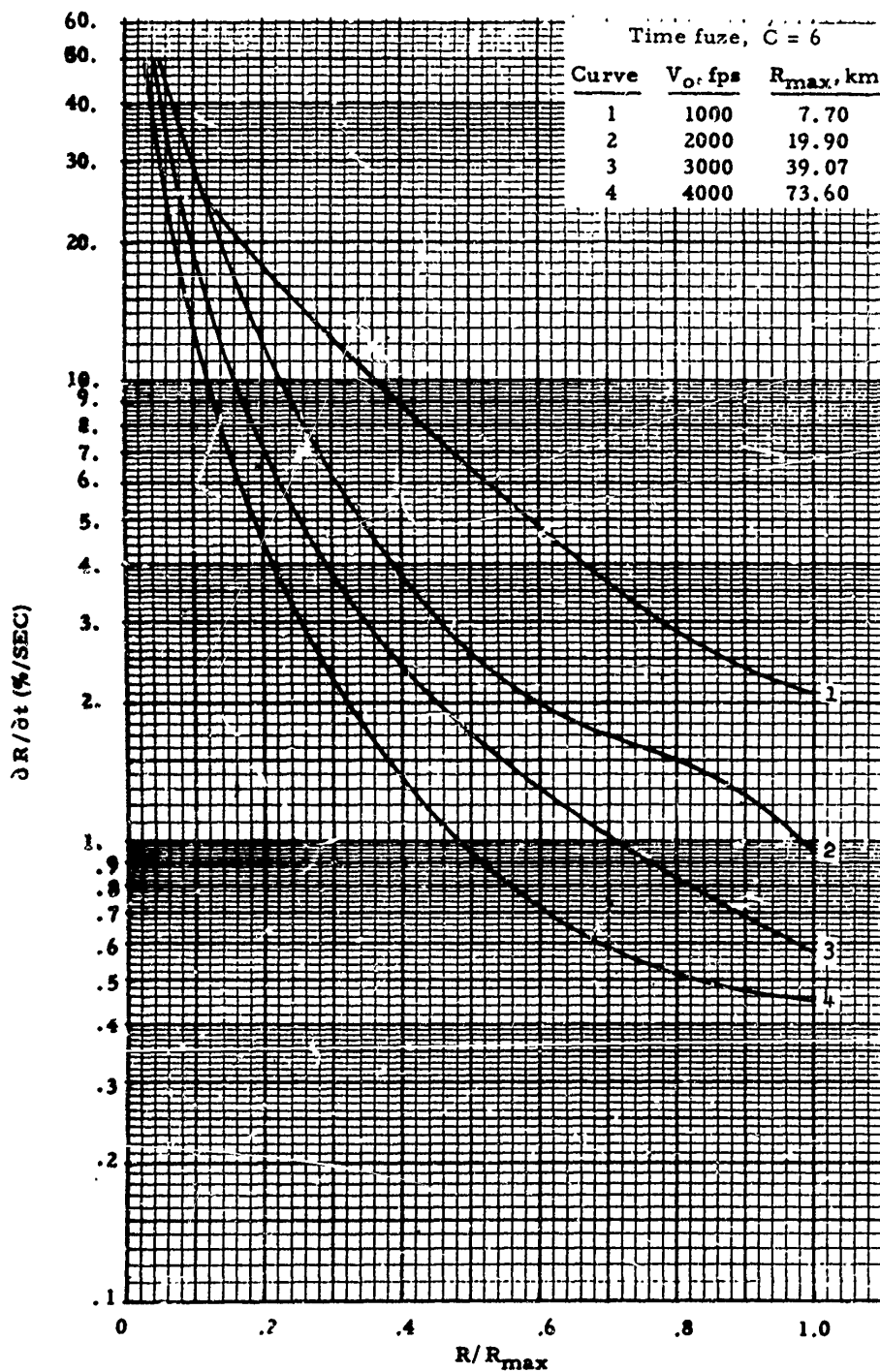
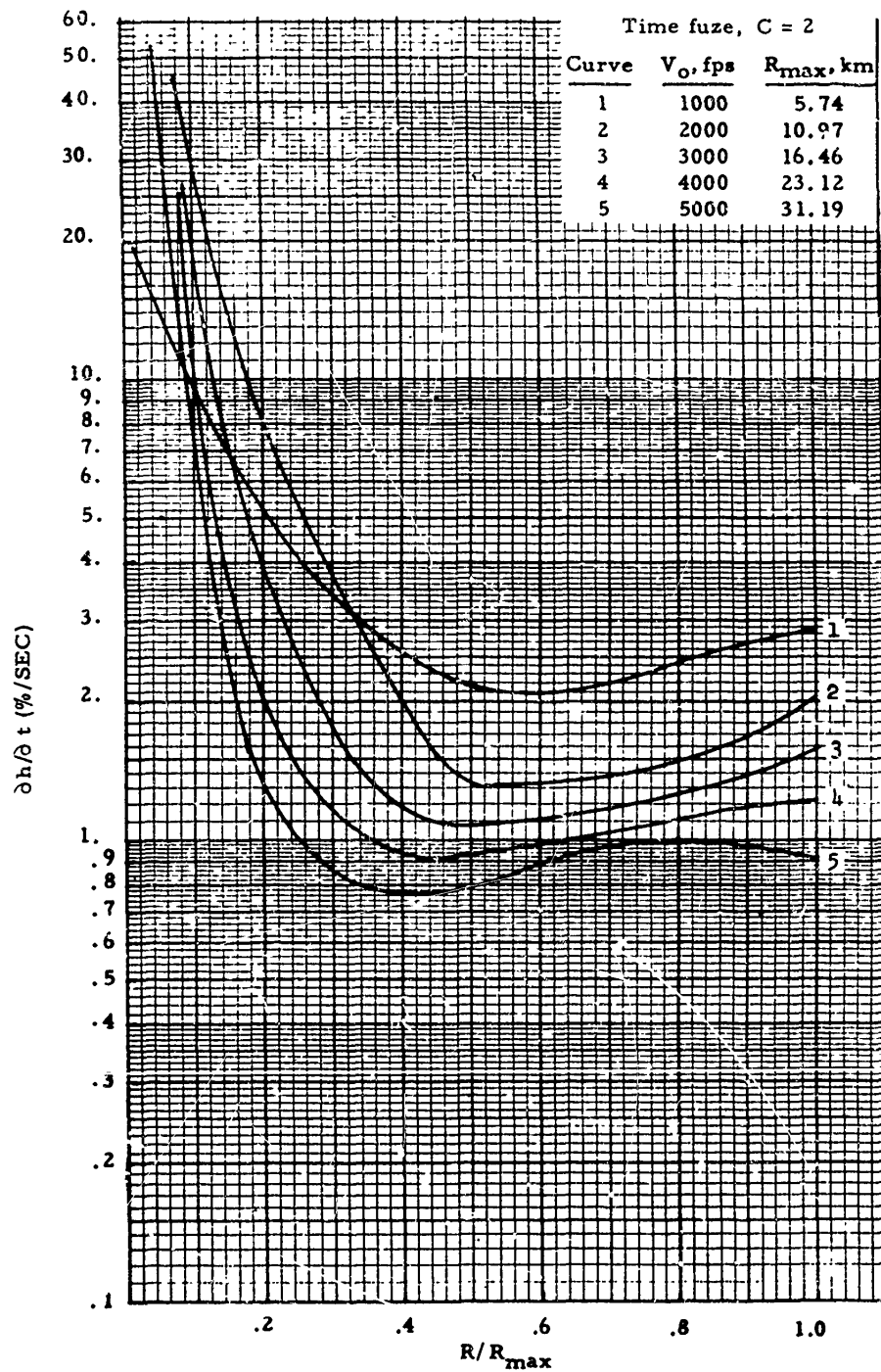


Figure 7-40(C). Unit Effect, Range/Time Versus R/R_{max} - Time Fuze

AMCP 706-280

Figure 7-41(A). Unit Effect, Altitude/Time Versus R/R_{max} - Time Fuze

AMCP 706-280

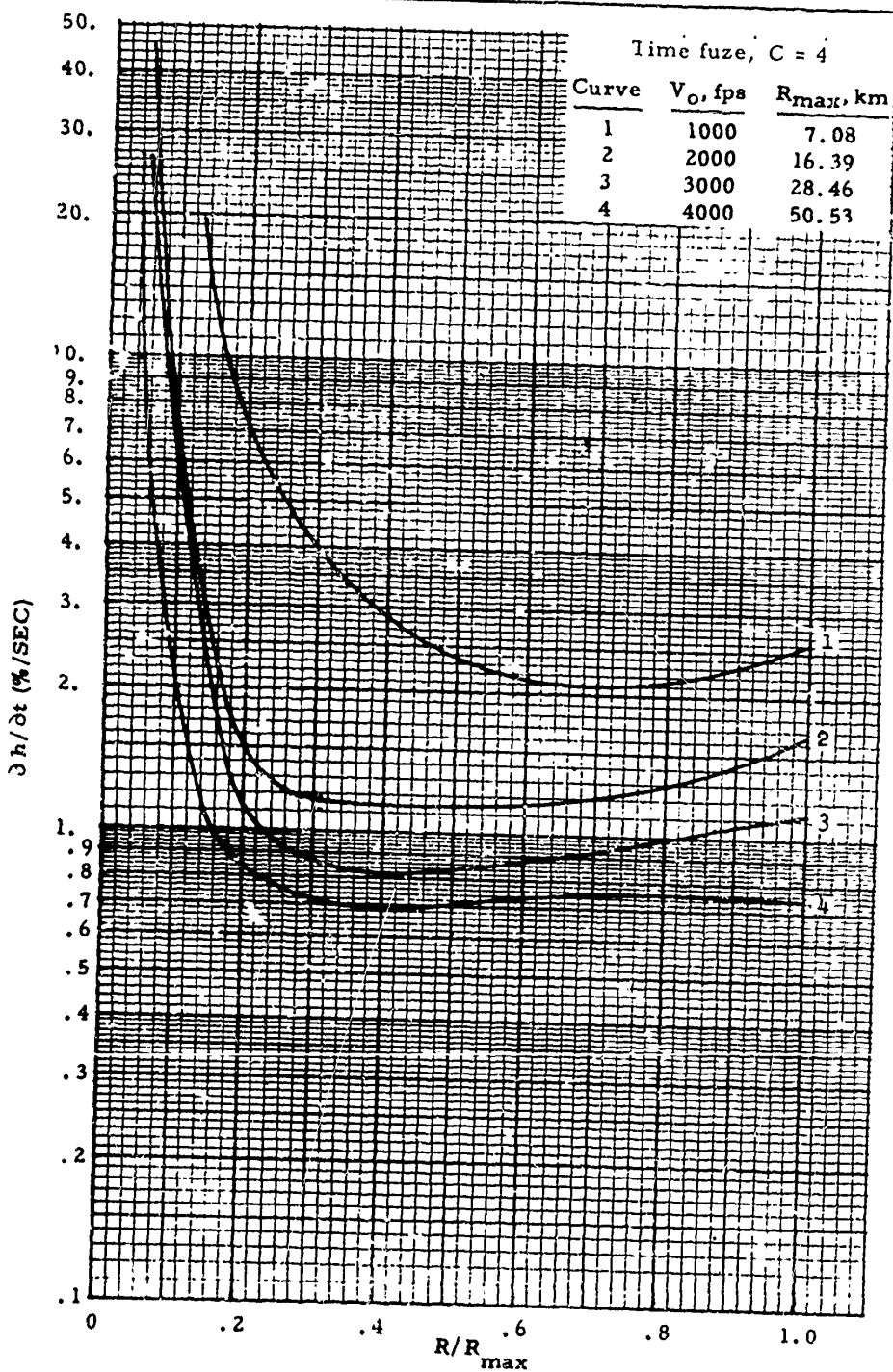
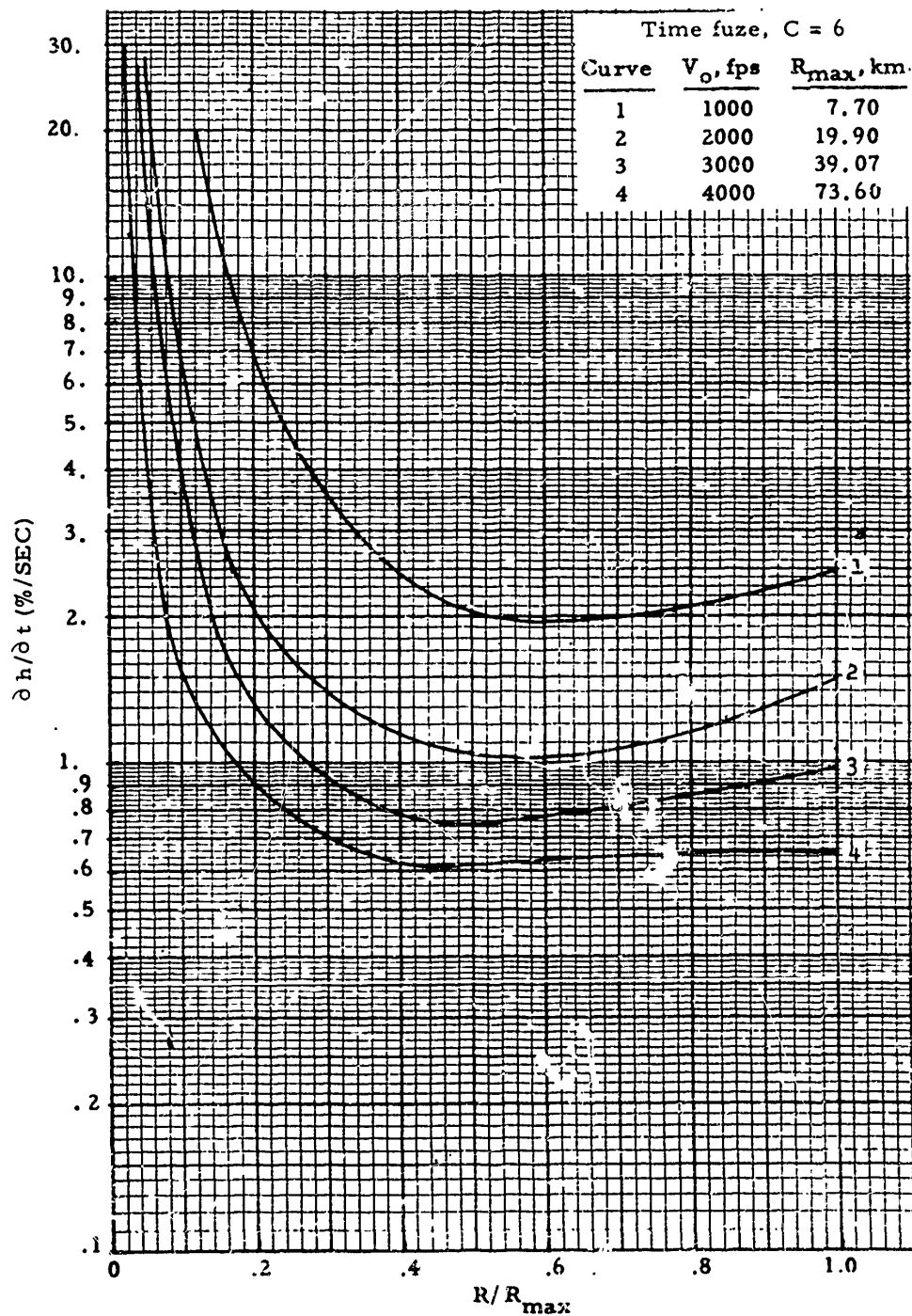


Figure 7-41(B). Unit Effect, Altitude/Time Versus R/R_{max} - Time Fuze



Figurs 7-41(C). Unit Effect, Altitude/Time Versus R/R_{max} - Time Fuze

AMCP 706-280

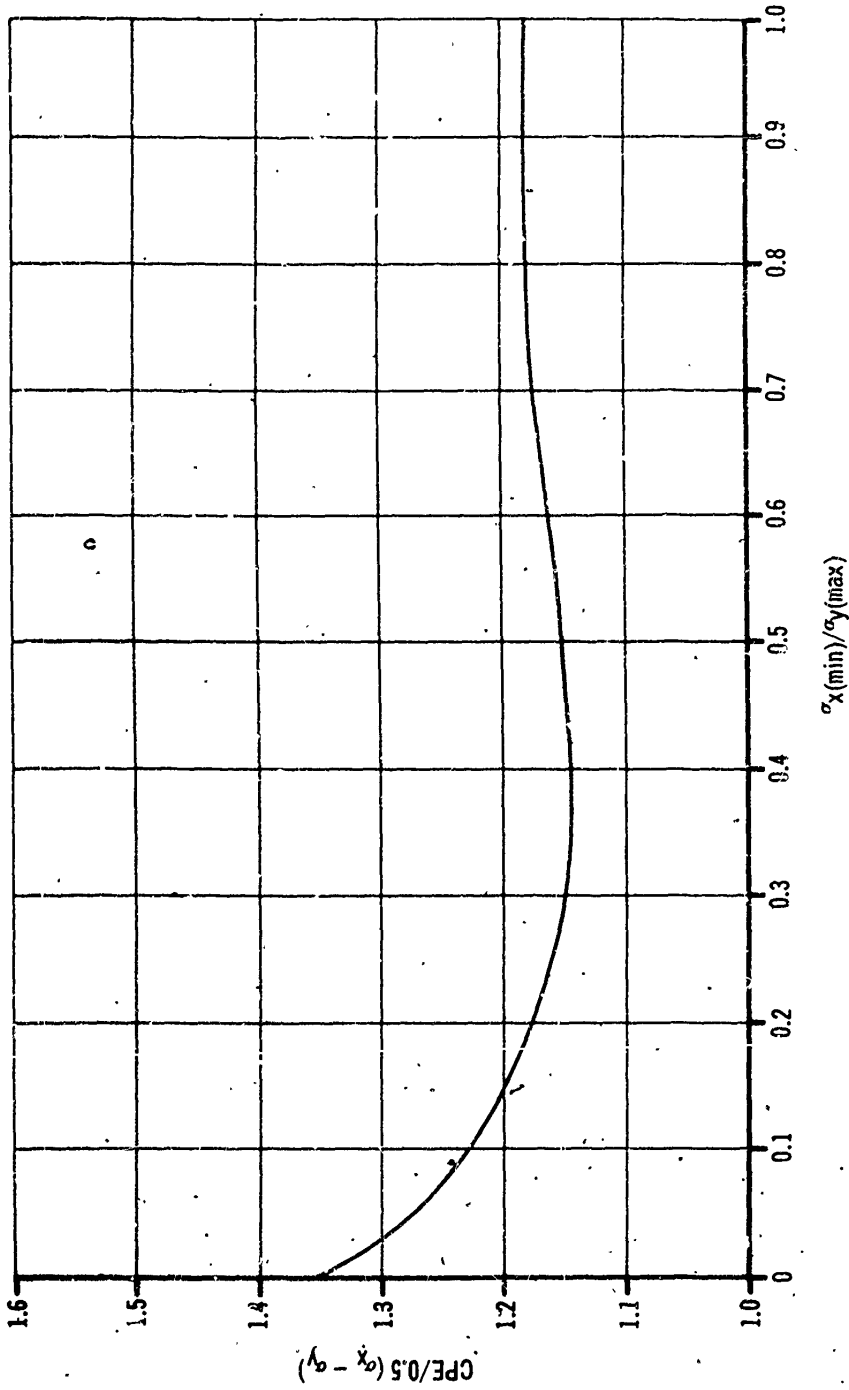


Figure 7-42. Ratio of CPE to σ_x/σ_y for Elliptical Distribution

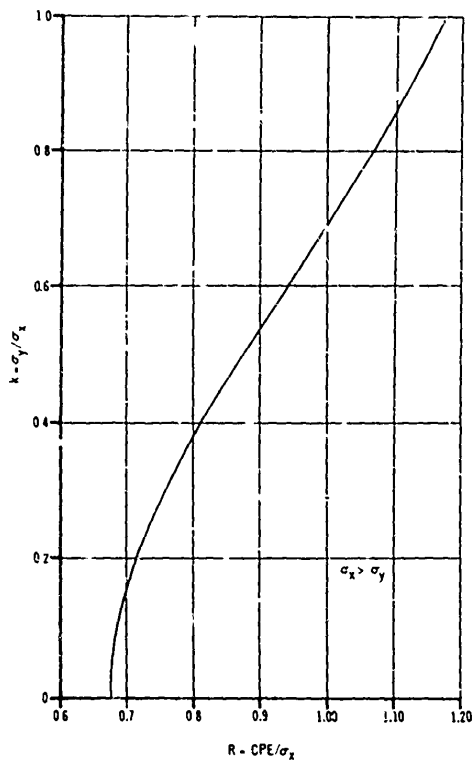


Figure 7-43. Chart for Determination of Circular Probable Error

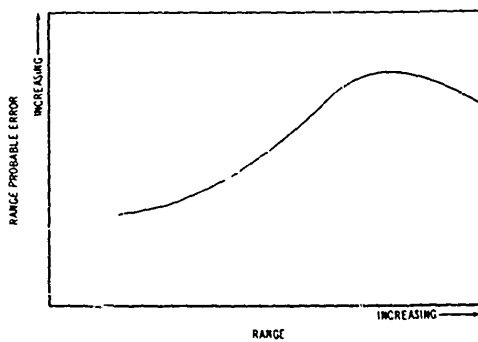


Figure 7-44. Variation of Range Probable Error With Range - Impact Fuze

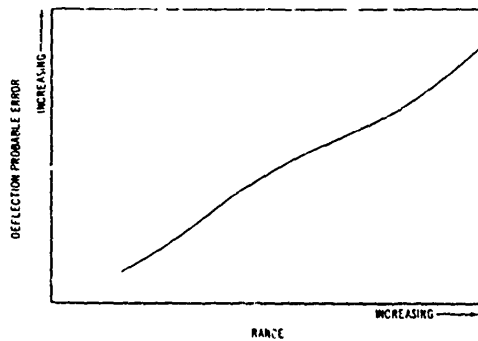


Figure 7-45. Variation of Deflection Accuracy With Range - Impact Fuze

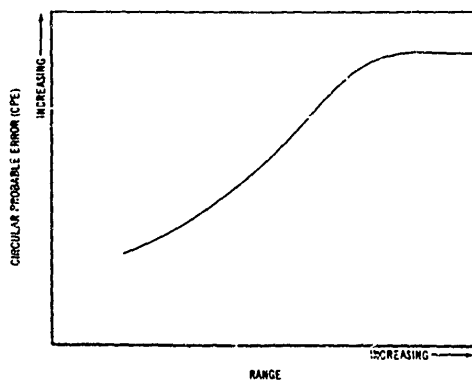


Figure 7-46. Variation of CPE With Range - Impact Fuze

REFERENCES

1. J. B. Rosser, et al, *Mathematical Theory of Rocket Flight*, McGraw-Hill, Inc., New York, 1947.
2. L. Davis Jr., et al, *Exterior Ballistics of Rockets*, D. Van Nostrand Co., 1958.
3. R. A. Rankin, "The Mathematical Theory of the Motion of Rotated and Unrotated Rockets", *Philosophical Transactions of the Royal Society of London, Series A, No. 837*, **241**, 457-585, Cambridge University Press, London, 1949.
4. R. R. Newton, *Spin Programs Which Cause the Dispersion Produced by Thrust Malalignment to Vanish*, The University of Tennessee, Knoxville, Tenn., 1955.
5. R. E. Maerker and R. R. Newton, *Spin Programs Which Cause Dispersion Produced by Thrust Malalignment to Vanish, Part II*, The University of Tennessee, Knoxville, Tenn., 1955.
6. R. R. Newton, *Spin Programs Which Cause Dispersion Produced by Thrust Malalignment to Vanish, Part III*, Department of Physics, Tulane University, New Orleans, La., 1956.
7. M. W. Hunter, et al, "Some Recent Aerodynamic Techniques in Design of Fin-Stabilized Free-Flight Missiles for Minimum Dispersion," *Journal of the Aeronautical Sciences*, 571-7 (June 1956).
8. W. C. McCorkle, *Recent Developments in High Accuracy Free Rocket Weapons Systems (U)*, Carde Report # AXP 8, Redstone Scientific Information Center, Redstone Arsenal, Ala., April, 1959.
9. R. R. Newton, *Effect of Variable Acceleration Upon the Dispersion of Fin-Stabilized Rockets*, Report PH-RR-10, University of Tennessee Department of Physics, Knoxville, Tenn., April 1, 1953.
10. R. S. Burrington and D. C. May, Jr., *Handbook of Probability and Statistics With Tables*, Handbook Publishers, Inc., Sandusky, Ohio, 1953.
11. S. S. Chun, *Missile Configuration Design*, McGraw-Hill, Inc., 1961.
12. L. Davis, *Statistical Methods in Research and Production*, Third Edition, Fisher, New York, 1961.
13. E. Freud, *Modern Elementary Statistics*, Prentice-Hall, New York, 1952.
14. E. S. Keeping and J. F. Keeney, *Mathematics of Statistics, Part One*, Third Edition, D. Van Nostrand, New York, 1954.
15. G. A. Korn and E. M. Korn, *Mathematical Handbook for Scientists and Engineers*, McGraw-Hill, Inc., New York, 1931.
16. F. Mosteller, R. E. F. Rourke, and G. B. Thomas, Jr., *Probability and Statistics*, Addison-Wesley, Reading, Massachusetts, 1961.
17. E. L. Crow, F. A. Davis, and M. W. Maxfield, *Statistics Manual*, U. S. Naval Ordnance Test Station, China Lake, California, 1955.
18. W. Volk, *Applied Statistics for Engineers*, McGraw-Hill, Inc., New York, 1955.
19. H. S. Seigjent, *Required Accuracy of Corporal Fire*, JPL Publication 25, 15 April 1954.
20. J. W. Haughy, *Calculation of Missile Accuracy From Actual Test Flight Data*, Army Ballistic Missile Agency Report No. RG-TN-2-61, 13 Jan 1961.
21. *C.E.P. for Correlated Unequal Standard Deviations*, G.M. 41.2-108, Ramo-Woolridge, 28 Oct 1957.
22. *Approximating to the Circular Probable Error of an Elliptical Gaussian Distribution (C)*, Royal Aircraft Establishment, T. M. No. G. W. 300, March 1957.
23. Pat Maxwell, Jr., *Estimation of the C.E.P. of a Missile System from the Results of Firings*, G. M. TR-139, Ramo-Woolridge, 3 April 1957.
24. M. L. Eaton, *Accuracy C.E.P. Estimates*, NAMTC TMR 105, Bureau of Aeronautics, 1 Jan 1957.

AMCP 706-260

LIST OF SYMBOLS (Cont)

Subscript:	Meaning	Subscript:	Meaning
<i>e</i>	Exposed value	<i>r</i>	Root chord
<i>f</i>	Flare; fin; friction	<i>re</i>	Exposed root chord
<i>fb</i>	Forebody	<i>ref</i>	Reference condition
<i>fe</i>	Exposed fin	<i>rt</i>	Ring tail
<i>fl</i>	Flare	<i>T</i>	Total
<i>g</i>	Rocket launch condition	<i>t</i>	Tip chord
<i>IF</i>	Interference free	<i>te</i>	Trailing edge
<i>J</i>	Jet (or nozzle exit plane) conditions	<i>theory</i>	Theoretical prediction
<i>le</i>	Leading edge	<i>w</i>	Wave drag; "wetted" condition
<i>n</i>	Nose	<i>2D</i>	Two dimensional consideration
<i>o, ∞</i>	Free stream or stagnation conditions	<i>⊥</i>	Perpendicular measure
<i>p</i>	Planform		

8-1 GENERAL DESIGN CONSIDERATIONS

This chapter will discuss the aerodynamic aspects of free rocket design and will indicate means of predicting the significant aerodynamic coefficients. *Simply stated, the usual aerodynamic design goal is to select an external configuration which provides stable flight with minimum drag through the desired altitude-velocity range.*

For a rocket to possess flight stability, a restoring moment must be produced when its longitudinal axis is rotated from the flight direction, i.e., when an angle of attack exists. This flight stability is achieved in the case of aerodynamically stabilized rockets by selecting the external configuration such that the center of pressure of aerodynamic forces normal to the longitudinal axis is located farther aft of the rocket's nose tip than the center of gravity. Since the aerodynamic forces are proportional to angle-of-attack (the angle between the flight direction or velocity vector and the longitudinal axis of the rocket), any deviation will produce a moment to restore the axis to its aligned condition. When the center of pressure is aft of the center of gravity, the rocket is said to be statically stable.

The degree of aerodynamic stability, or the static margin requirement, varies with the desired accuracy of each rocket and its design approach. For example, a rocket designed for minimum dispersion during powered free flight requires a specific tailoring of the static margin over its Mach number regime, while a high-acceleration rocket which achieves most of its velocity prior to release from the launcher requires only that the stability margin remain within certain upper and lower bounds. The width of this stability band is governed primarily by the requirement to maintain a significant spread between the roll and pitch-yaw frequencies.

Although the static margin is of paramount interest to the accuracy of a free rocket during the powered, high-acceleration phase, the aerodynamic drag or axial force is a prime factor affecting the accuracy and performance during the sustain and ballistic flight phases. For an unguided rocket, the angle of attack is nominally zero; therefore, the axial and drag forces are equal. The general goal is to keep the axial force coefficient as low as possible, consistent with other design considerations such as body

length, weight, and structural rigidity. Reduction of the axial force coefficient is more important generally for indirect-fire, artillery-type rockets where the sustain and ballistic flight times are much greater than that of the boost phase. Axial force reduction in this case can result in either a lighter and smaller rocket for a specified maximum range, or increased range for a fixed rocket size and weight. In addition, improved accuracy is achieved by reduced sensitivity to atmospheric variations during the ballistic flight because it is primarily through the aerodynamic axial force that non-gravitational accelerations are transmitted to the rocket.

The external configuration of a free rocket can vary significantly depending on the trade-off between aerodynamic requirements imposed by performance and accuracy considerations, and other system requirements. Some generalization can be made, however, based on past designs. Typically, the rocket's external configuration consists of a pointed body-of-revolution housing payload and propulsion unit, with a stabilizing device attached to the aft section. A circular cross-section is preferred because its symmetry about the longitudinal axis makes for simplicity, both in manufacturing and in determining aerodynamic coefficients and mass-inertia properties. To the rocket body, which normally is aerodynamically unstable, various normal-force-producing devices are attached at its aft end to provide the necessary restoring moment for stability. Thin-profile planar fins, spaced evenly around the circumference of the body, are used in many rocket designs as stabilizing devices. This type of fin usually will produce the maximum stabilizing moment with minimum weight and axial force penalties. When minimum overall diameter is a dominant design consideration, the ring-tail and conical flare become of greater interest. A ring-tail will produce, at both subsonic and supersonic velocities, approximately twice the restoring moment of a cruciform planar fin with equal total span and chord. The conical flare is of interest for restricted-diameter rockets with maximum velocities above approximately 5000 ft/sec. On the basis of projected planform area, a conical flare will produce better than twice the normal force of cruciform fins at hypervelocity speeds. However, the axial force of a flare greatly exceeds that of fins providing equal restoring moment.

AMCP 706-280

It should be clear from the preceding discussion that a "best" aerodynamic configuration does not exist. The great multitude of parameters affecting the configuration selection usually results in its choice being based on past design experience and aesthetic values rather than an optimization study.

In order to estimate the aerodynamic stability characteristics for complete rocket configurations and to provide design guidance, it is necessary to know the aerodynamic coefficients of each major rocket component and interference between components. The paragraphs which follow will discuss first the stability parameters for various rocket forebody shapes, fins, ring-tails, conical flares, and boattails; and then will discuss how these component aerodynamic coefficients are combined to arrive at values for the complete configuration. Wherever possible, simple analytical or semi-empirical equations will be presented along with charts to make aerodynamic estimates. No effort will be made to provide the theoretical basis or experimental substantiation for the data presented since numerous textbooks and reports exist which discuss these topics in great detail. Finally, a detailed computational chart will summarize sources and methods of obtaining design data, and will provide a format and check list for design computation.

8-2 STABILITY CHARACTERISTICS OF ROCKETS

8-2.1 BODIES OF REVOLUTION

8-2.1.1 Nose Cylinder

The forebody of a rocket normally consists of a pointed cone, an ogive, or a power series curve, followed by a cylindrical section. The slender-body theory provides a simple means of expressing the stability characteristics of these bodies in terms of the geometric parameters only, as follows:

$$\left(\frac{dC_N}{dx}\right)_b = \frac{(k_2 - k_1)}{S_{ref}} \left(\frac{dS}{dx}\right) \sin 2\alpha \quad (8-1)$$

which, when integrated from $x = 0$ to $x = l$, gives

$$\left(C_{N\alpha}\right)_b = 2(k_2 - k_1) \frac{S_B}{S_{ref}} \quad (8-2)$$

In the above expressions

- C_N = normal force coefficient
- $C_{N\alpha}$ = normal force coefficient gradient, per rad or per deg (see par. 8-2.4.1)
- b = body
- α = angle of attack, the angle between the longitudinal axis of the rocket and the velocity vector, in rad or deg
- $k_2 - k_1$ = apparent mass factor
- l = body length, ft
- dS = incremental cross-sectional area, ft²
- dx = incremental axial distance, ft
- S_B = body base area, ft²
- S_{ref} = reference area, ft²

The factor $(k_2 - k_1)$ is the apparent mass factor as derived by Munk (Reference 1). The values for ellipsoids of revolution presented in Fig. 8-1 represent a reasonable approximation for any axisymmetrical body of comparable fineness ratio. The center of pressure may be assumed to act at the centroid of the nose projected area for $M_\infty < 1$.

The fundamental assumptions of the theory are that all second order partial derivatives of velocity can be neglected, and that velocity perturbations along the body axis are small compared to the transverse values. The solution implies that adding cylinder length to the nose has no effect, and that there is no compressibility effect due to varying Mach number. However, experimental data and more refined theoretical solutions, too complex to discuss here, show these effects to be significant. The reader is referred to References 2, 3, and 4 for further details of

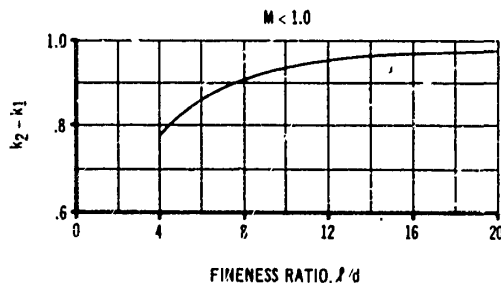


Figure 8-1. Apparent Mass Factor

these solutions. In the absence of more precise solutions, the slender-body theory should be used in the subsonic-through-sonic Mach number range.

At supersonic Mach numbers, the normal-force coefficient gradient and center-of-pressure estimates should be obtained, respectively, from Figs. 8-2 and 3-3 for tangent-ogive-cylinder bodies, and from Figs. 8-4 and 8-5 for cone-cylinder bodies. These curves were extracted from Reference 5 and were constructed from empirical data covering a Mach-number range from 1.4 to 7.0 and a nose-fineness ratio range from 3.0 to 7.0. Stated accuracies are ± 10 percent for normal-force coefficient and 0.5 calibers for center of pressure.

A fairly extensive experimental study of the effects of particular nose shapes and cylindrical lengths is presented in Reference 6. Aerodynamic-stability parameters were determined at Mach numbers from 0.8 to 4.5 for tangent-ogive, conical, and power-series noses, all with a fineness ratio of four, combined with cylinder lengths of from 4 to 11 calibers. The effect of changing the nose-fineness ratio from 3 to 5 for conical and tangent-ogive shapes was determined for a cylindrical afterbody length of 6 calibers. Since the overall study covers body configurations of general interest to free rocket design, the pertinent results are presented in Figs. 8-6(A), (B), (C) and 8-7(A), (B), (C). These results should give normal-force coefficient gradients within ± 5 percent and center of pressure within $\pm .1$ caliber for the range of test variables. Whenever the body of interest falls within the range of test variables, it is recommended that the stability parameters be established from these data.

8-2.1.2 Boattail

Where the rocket propulsive nozzle is smaller in diameter than the body cylinder, the rocket afterbody may be tapered to form a boattail, which reduces base drag. The normal loading over this boattail is negative, thus reducing the total normal-force coefficient and shifting the center of pressure forward. The slender-body theory predicts the normal-force coefficient gradient to be:

$$\left(\Delta C_{N_{\alpha}}\right) = -2 \frac{S_{bt}}{S_{ref}} \left[1 - \left(\frac{d_{bt}}{d_c}\right)^2 \right] \quad (8-3)$$

where

S_{bt}	=	cross-sectional area of boattail at its smallest diameter, ft^2
d	=	diameter, ft
bt	=	boattail
c	=	cylinder
Δ	=	increment

It is recommended that slender-body theory predictions be used for the subsonic-to-sonic Mach-number range since systematic empirical investigations are not available.

At supersonic Mach numbers, Fig. 8-8 (Reference 5) will provide normal-force coefficient gradients for conical boattails located behind a semi-infinite cylinder; i.e., the local flow conditions upstream of the boattail are equal to the free stream conditions. These data, derived from linearized theory calculations and slender-body theory predictions, have not been verified by a detailed comparison with experimental data. Therefore, no statement can be made concerning the expected accuracy.

The center-of-pressure for the boattail normal force is located approximately $0.6 l_{bt}$ from the cylinder-boattail juncture at subsonic Mach numbers. The center of pressure at supersonic Mach numbers may be evaluated from Fig. 8-9, taken from Reference 5.

It is recommended that the data in this section be used for boattail angles of less than 10 deg and ratios of $\frac{d_{bt}}{d_c}$ greater than 0.8 to avoid flow separation from the boattail.

8-2.1.3 Conical-Flare Afterbody

A conical-flare afterbody can be added to nose cylinder configurations to provide aerodynamic stability. The slender-body prediction for the incremental normal force coefficient gradient of a flared afterbody is

$$\left(\Delta C_{N_{\alpha}}\right)_{flare} = 2 \frac{S_f}{S_{ref}} \left[1 - \left(\frac{d_c}{d_f}\right)^2 \right] \quad (8-4)$$

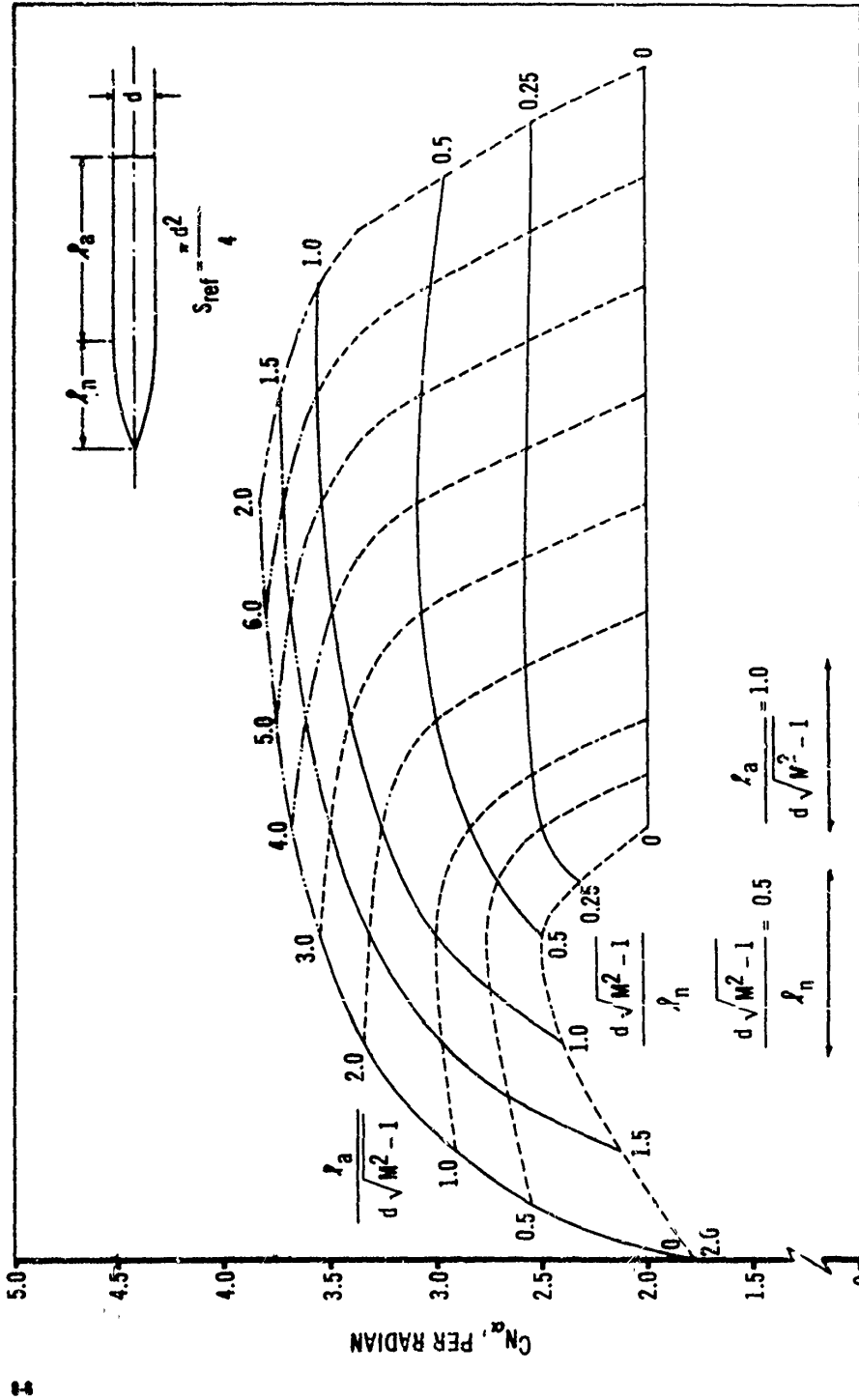


Figure 8-2. Normal Force Coefficient Gradient for Tangent Ogive-Cylinder Configurations

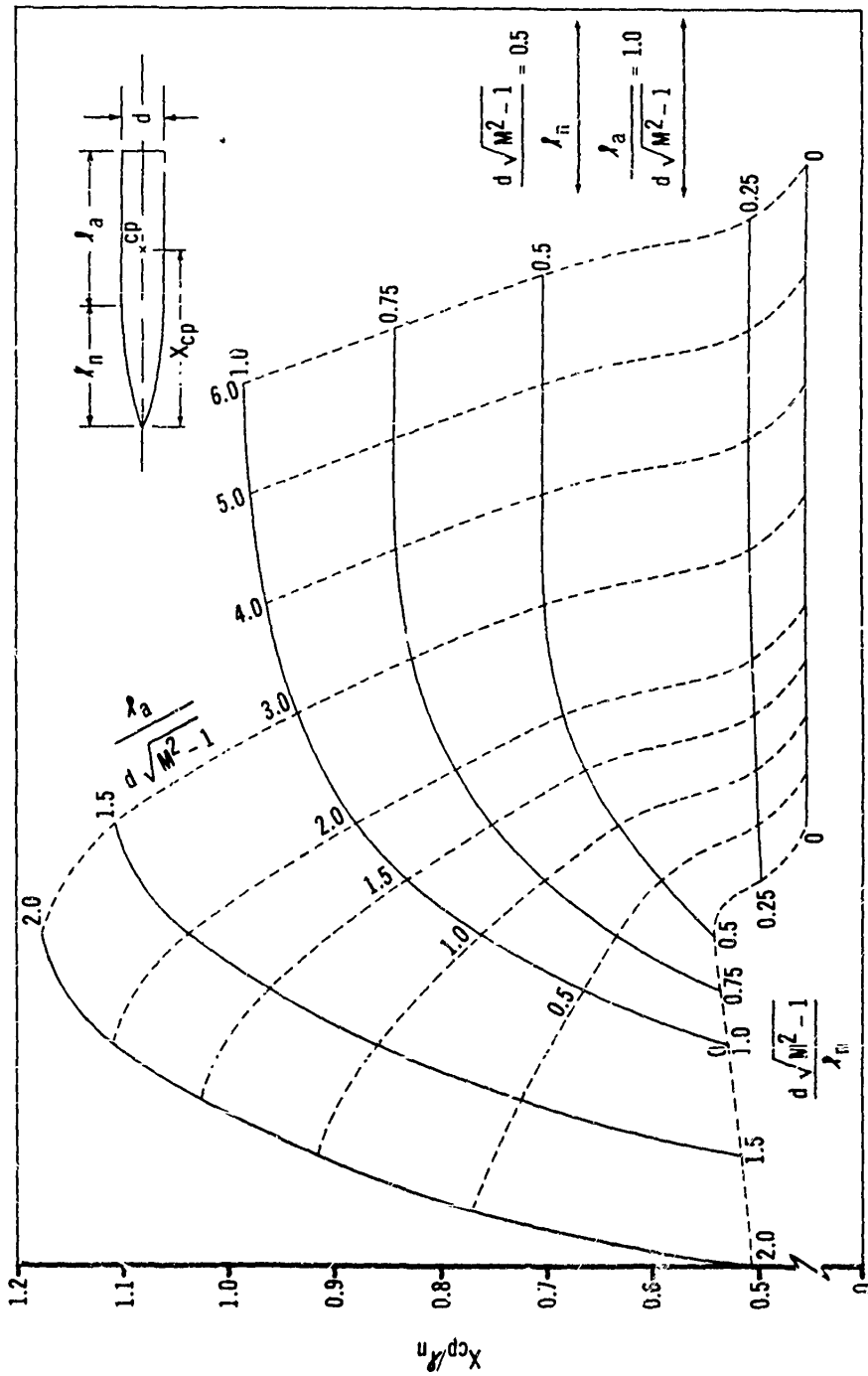


Figure 8-3. Center of Pressure for Tangent Ogive-Cylinder Configurations

AMCP 716-380

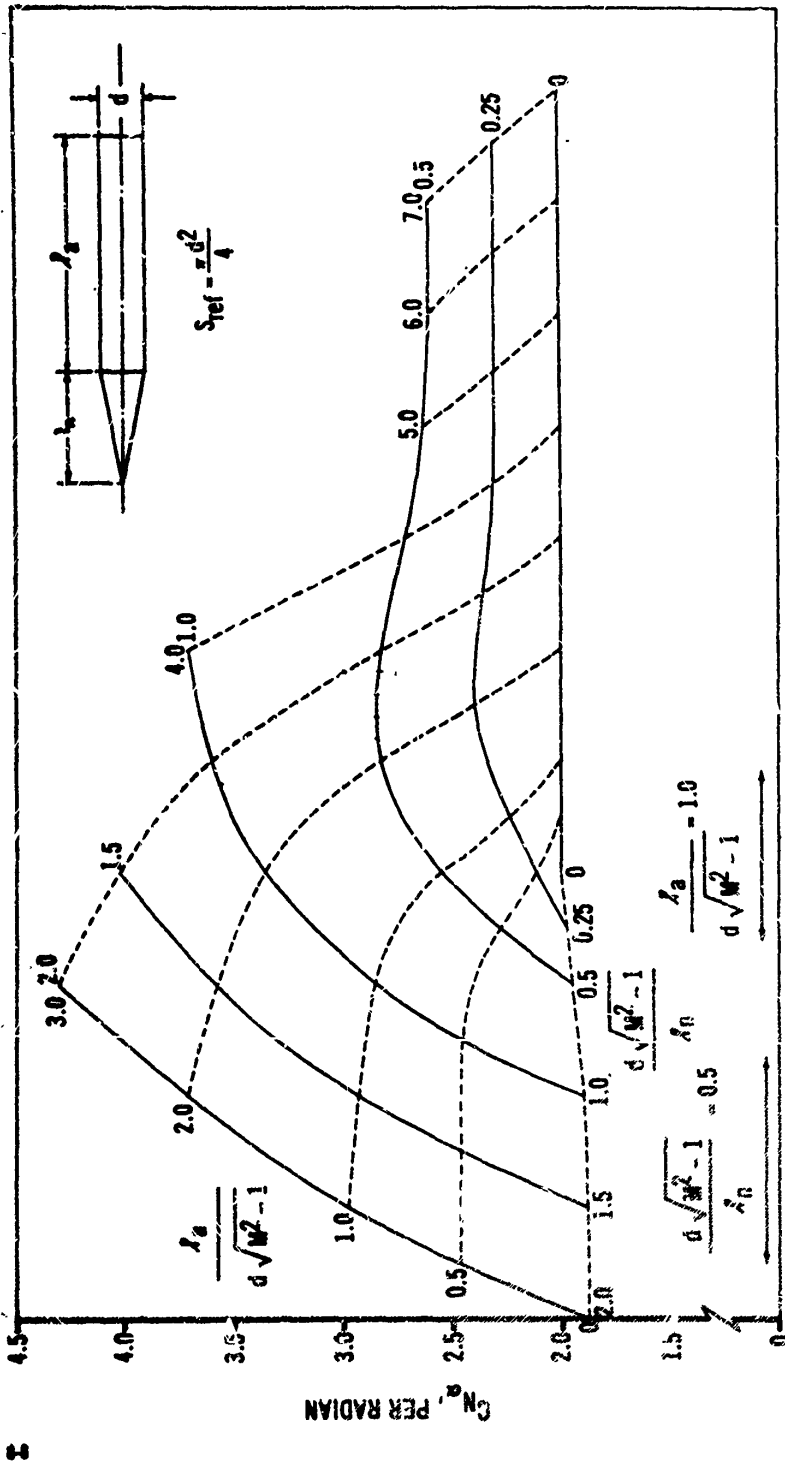


Figure 2-4. Normal Force Coefficient Gradient for Cone-Cylinder Configurations

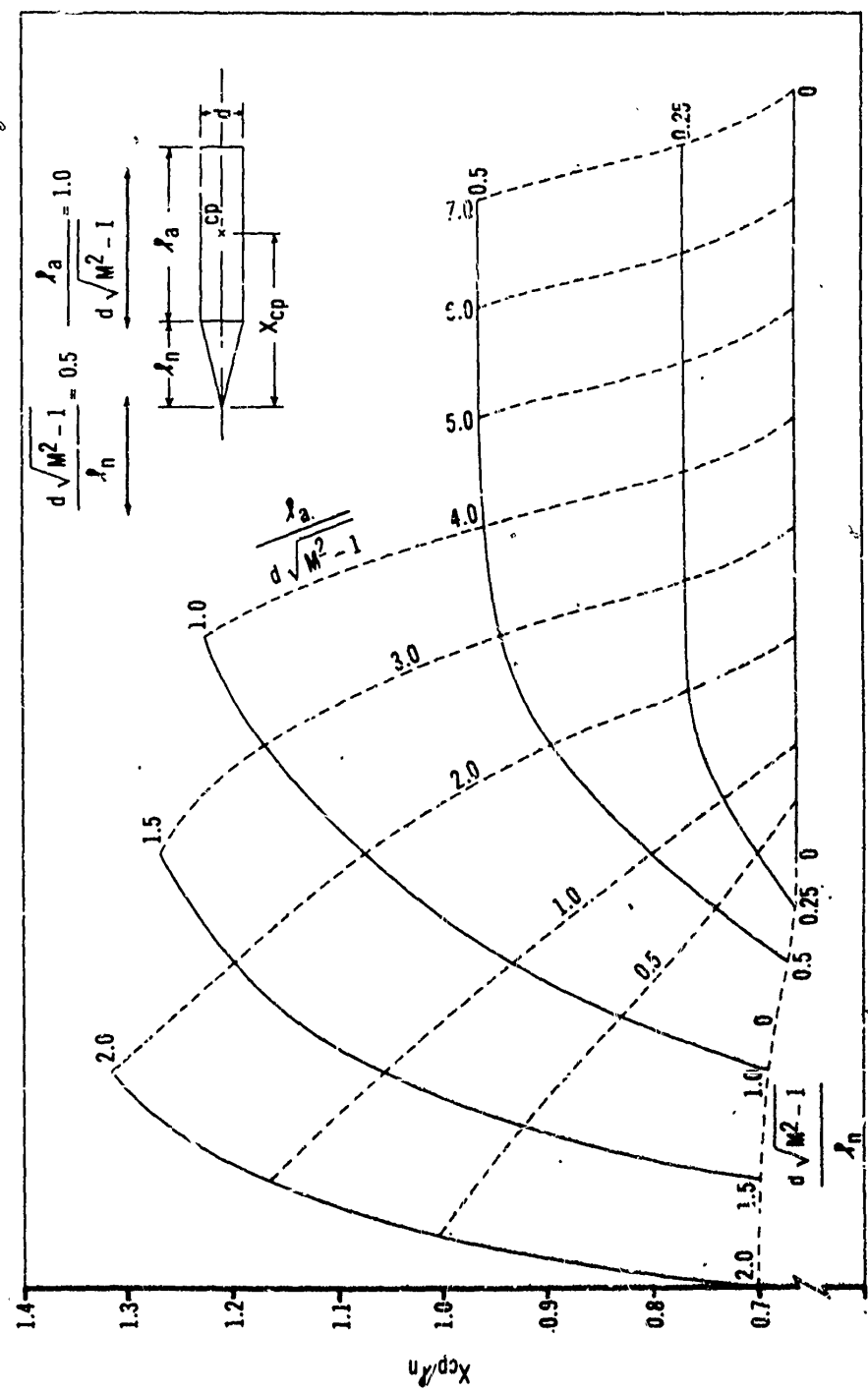


Figure 8-5. Center of Pressure for Cone-Cylinder Configuration

AMCP 706-200

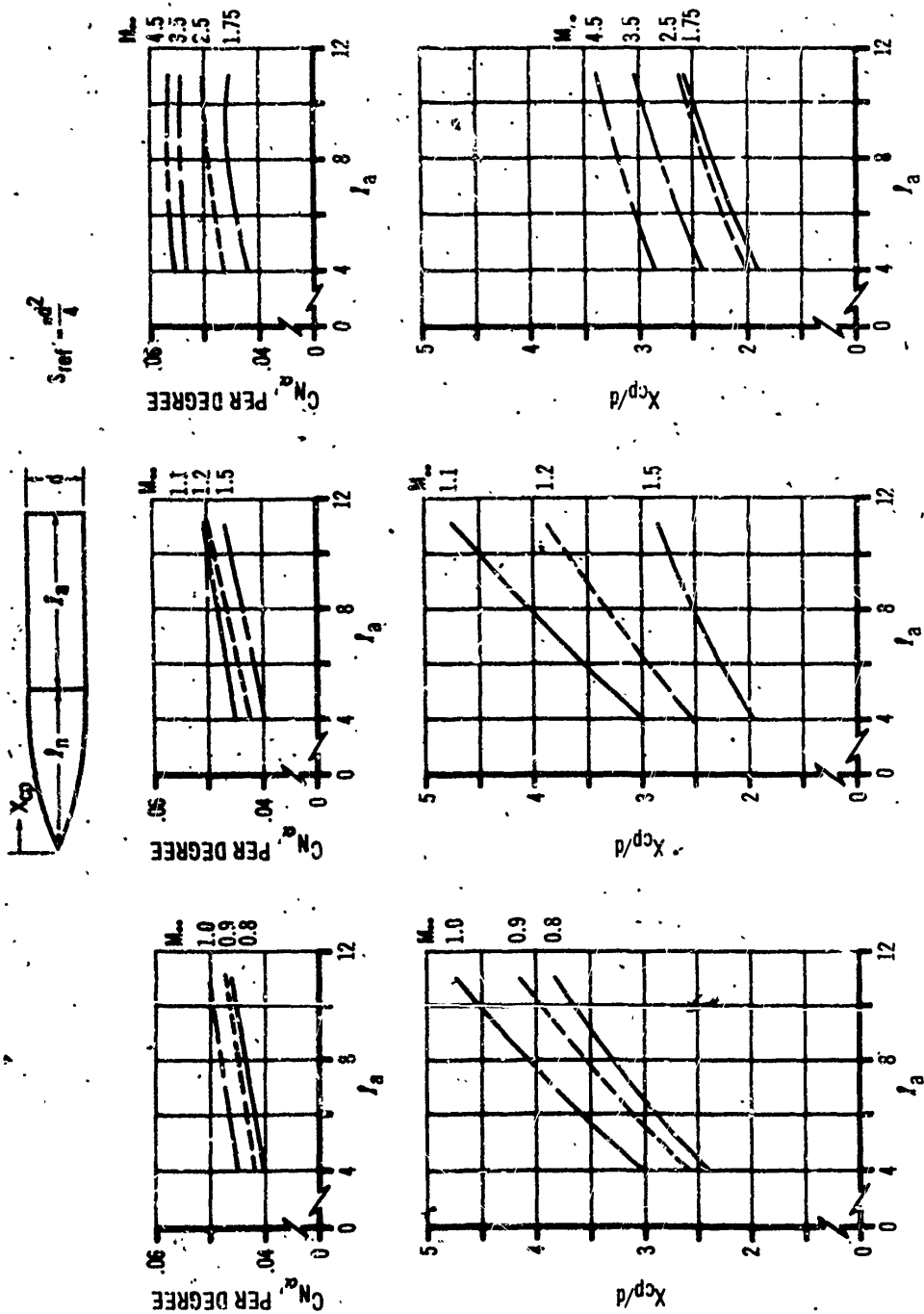


Figure 8-6(A). Normal Force Coefficient Gradient and Center of Pressure - 4-Caliber Tangent Ogive With Varying Afterbody Length

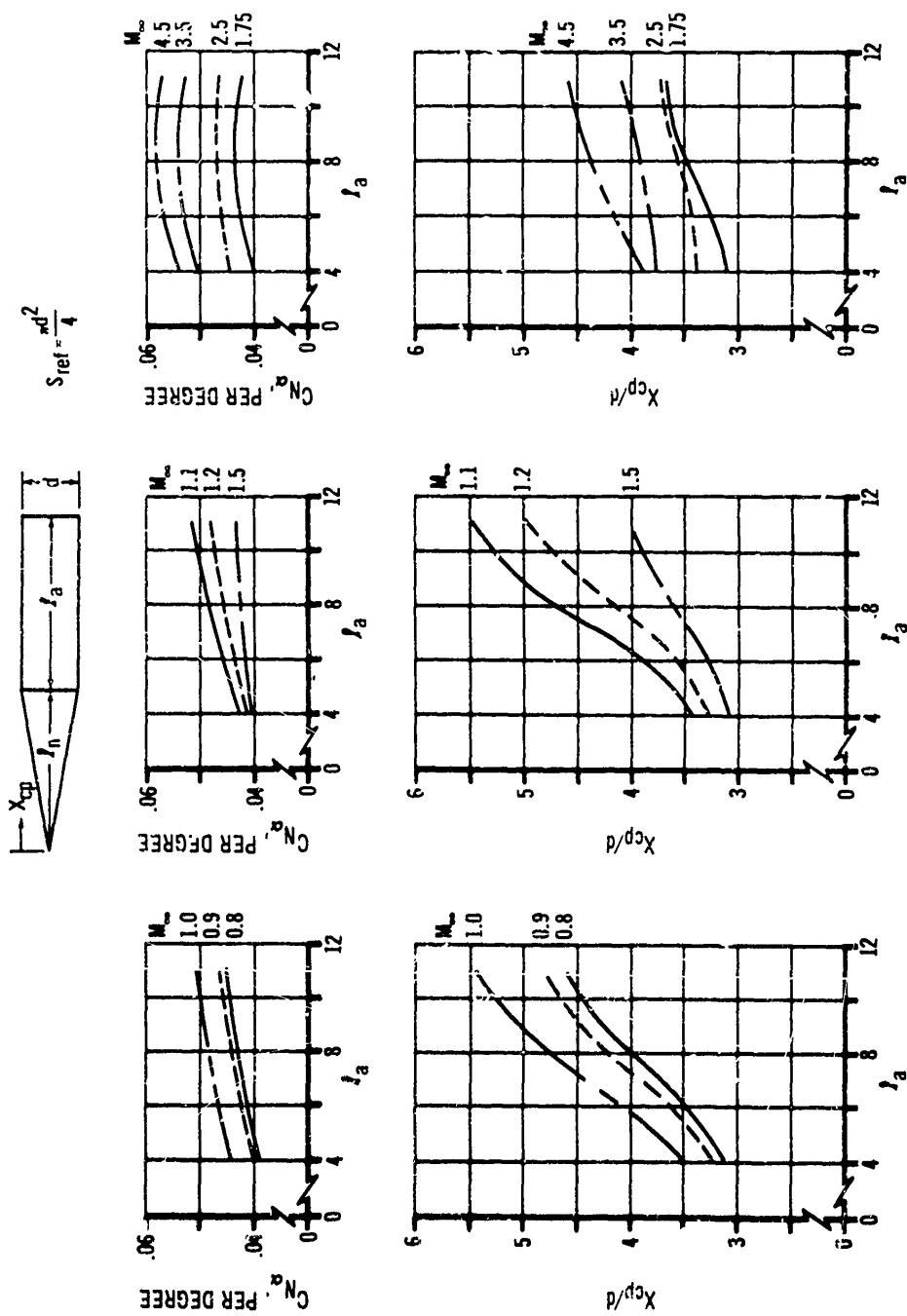
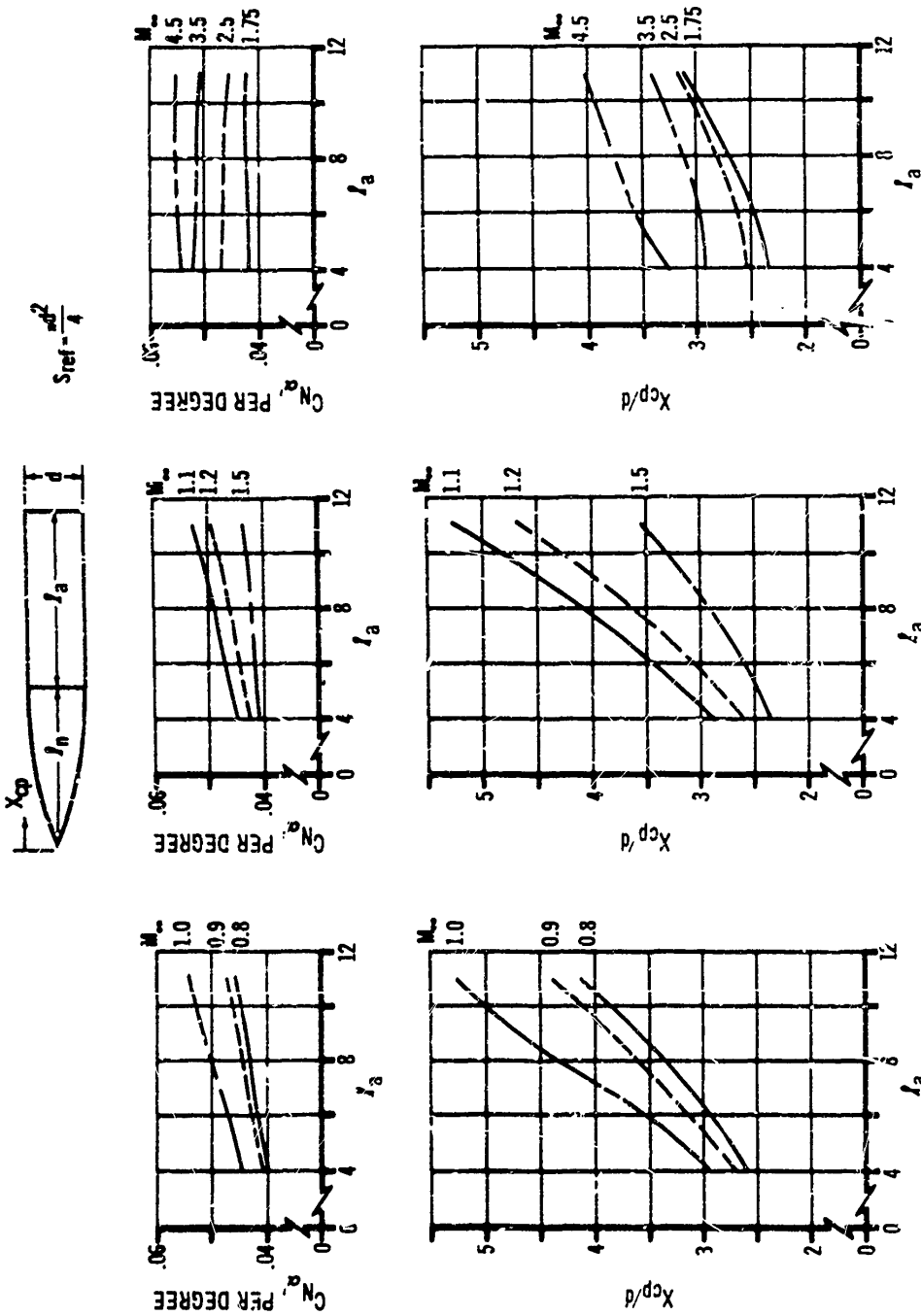


Figure 8-6(B). Normal Force Coefficient Gradient and Center of Pressure - 7.125° Cone With Varying Afterbody Length

AMCP 706-280



Figures 3-6(f). Normal Force Coefficient Gradient and Center of Pressure - 1/2-Power Nose With Varying Afterbody Length

AMCP 706-280

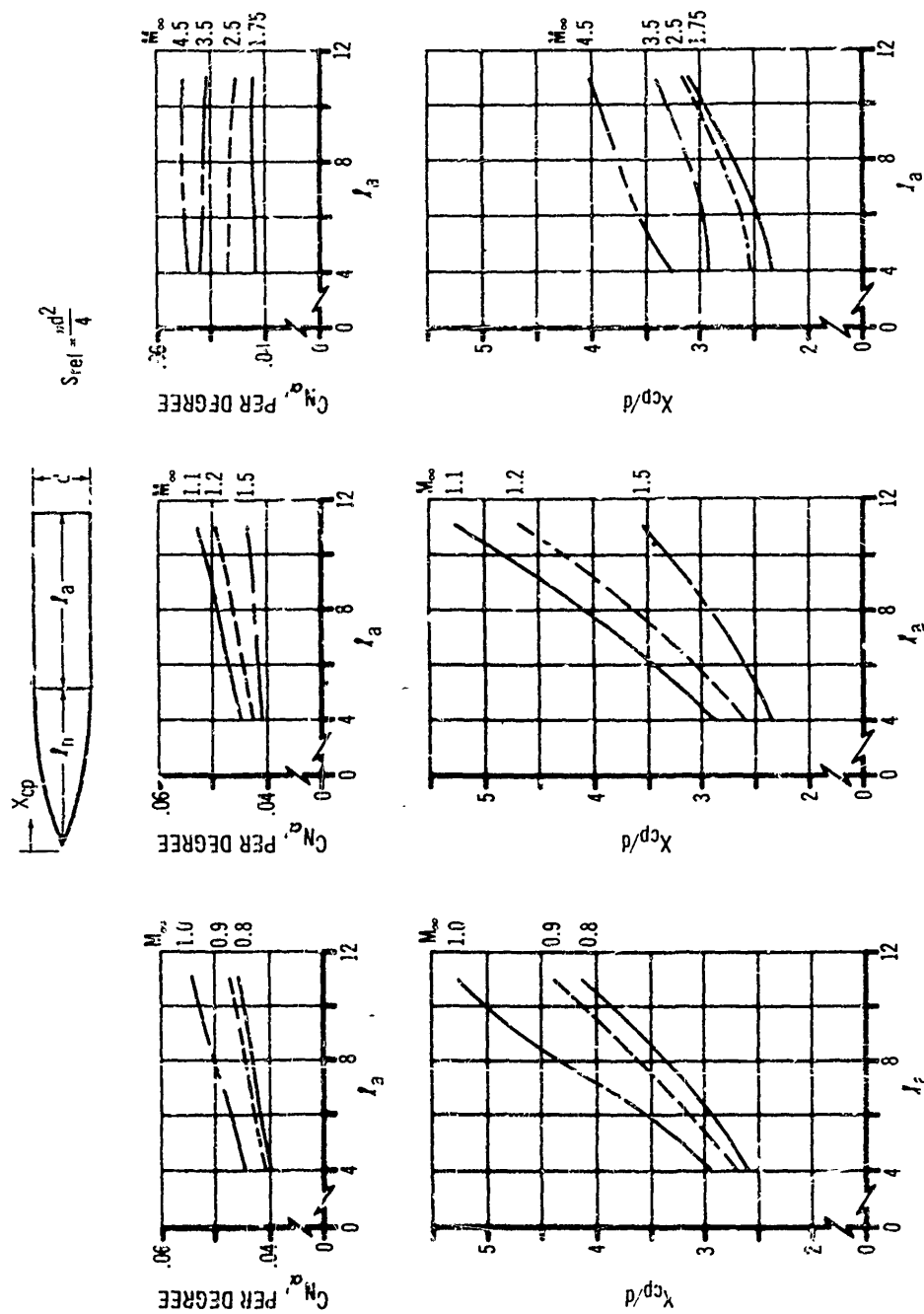


Figure 8-5(C). Normal Force Coefficient Gradient and Center of Pressure -- 1/2-Power Nose With Varying Afterbody Length

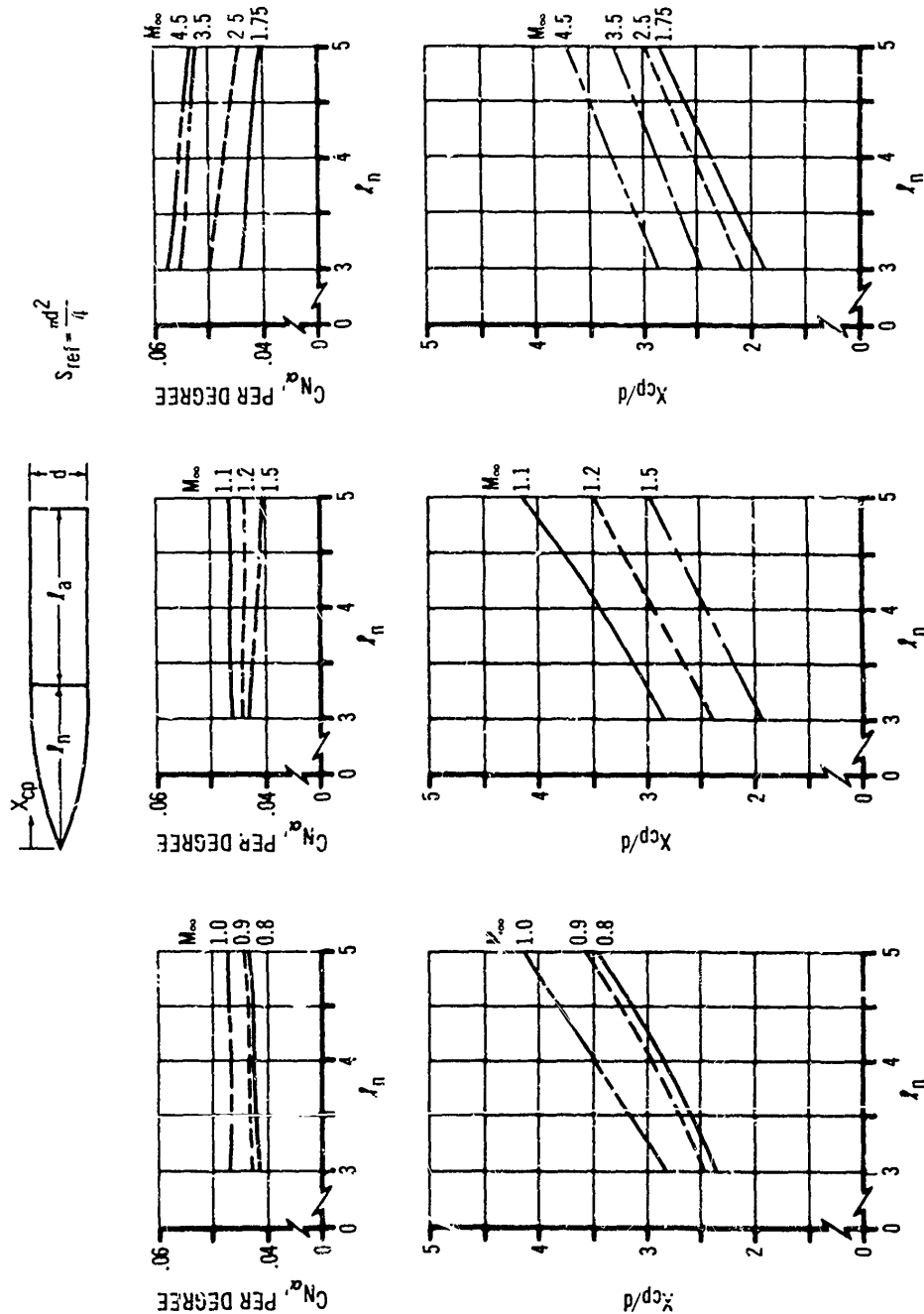


Figure 8-7(A). Normal Force Coefficient Gradient and Center of Pressure - Varying Tangent Ogive Nose Length With Constant Afterbody Length of 6 Calibers

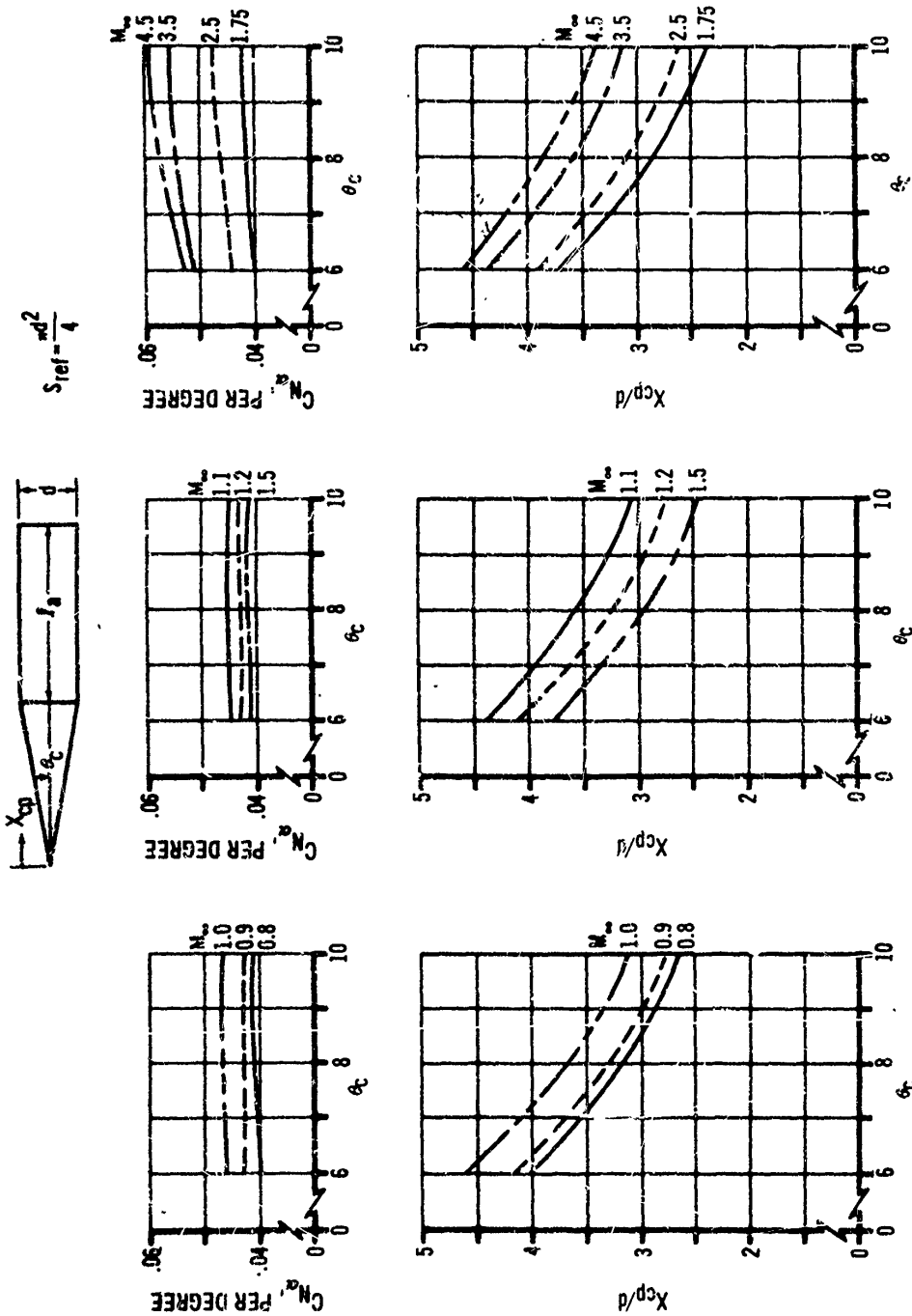


Figure 8-7(B). Normal Force Coefficient Gradient and Center of Pressure - Varying Conical Nose Angle With Constant Afterbody Length of 6 Calibers

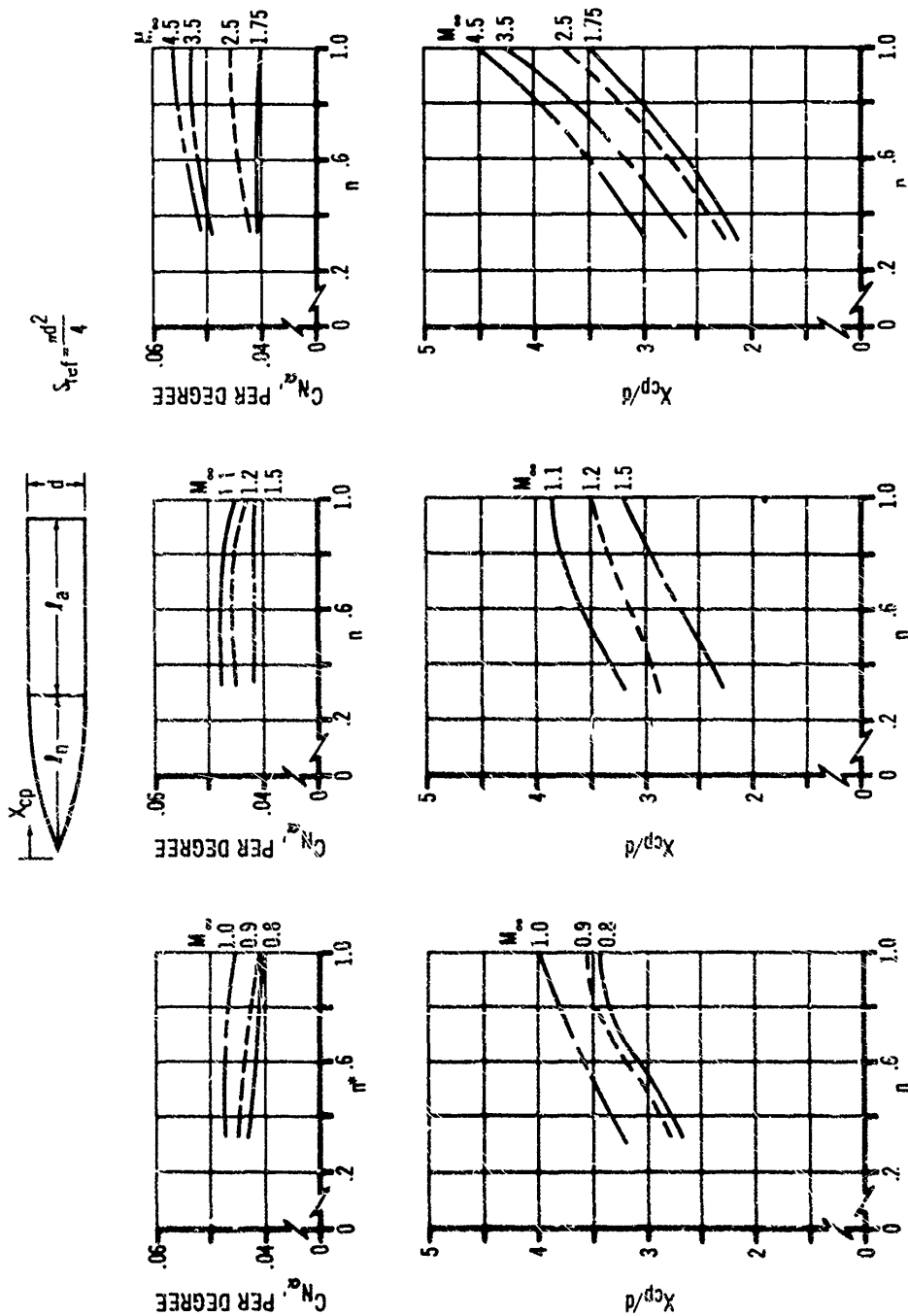


Figure 8-7(C). Normal Force Coefficient Gradient and Center of Pressure - Varying n -Power Nose Shape With Constant Afterbody Length of 6 Calibers
 n (n is exponent for power law nose)

AMCP 70S-200

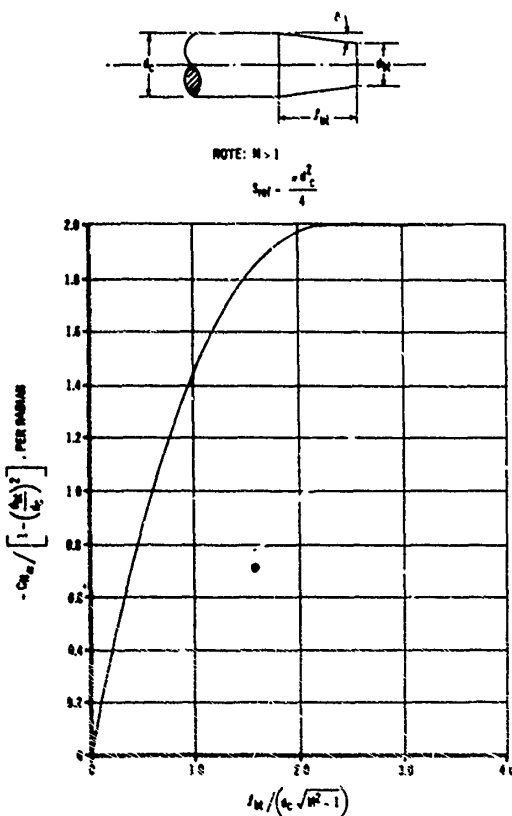


Figure 8-8. Normal Force Coefficient Gradient for a Boattail

and center of pressure of the normal-force increment is

$$\left(\frac{X_{cp}}{l_f}\right)_f = \frac{\frac{d_c}{d_f} \left(\frac{d_c}{d_f} + 1\right) - 2}{3 \left[1 - \left(\frac{d_c}{d_f}\right)^2\right]} \quad (8-5)$$

where

- X_{cp} = axial distance from cylinder-flare juncture to the flare center of pressure, ft
 l_f = total flare length, ft
 f = flare
 d_c = cone diameter, ft
 d_f = flare diameter ft

8-18

NOTE: Values of $\frac{X_{cp}}{l_f}$ measured rearward from the cylinder-flare juncture are negative.

The important geometric parameter is seen to be the ratio of forebody cylinder diameter to base diameter. Flare angle and Mach number do not influence the flare normal-force within the limitations of the slender-body assumptions. To a limited degree, the experimental data of Reference 7 verify this trend at transonic Mach numbers and for flare angles of less than 8 degrees.

The actual normal-force contribution of flared afterbodies is shown by other theories (References 8 and 9) and by experimental results to be influenced by flow conditions forward of the flare, as well as by flare angle and length. Also, large flare angles (greater than about 10 deg) are known to cause flow separation at the cylinder-frustum juncture, which alters considerably the local normal-force loading in this region. Precise estimates of the flared-afterbody stability contribution must consider the complete upstream flow field, including boundary-layer characteristics.

For preliminary design estimates, however, the incremental normal-force coefficient gradients presented in Figs. 8-10(A) through (E) are considered adequate. These data were computed from slender-body theory and correlate fairly well with the experimental data presented in Reference 10.

For values of d_f/d_c greater than 1.5, location of the center of pressure of the incremental normal force — as predicted by slender-body theory — varies from approximately 50 percent to 68 percent of the flare length aft of the flare leading edge. The use of 60 percent, for flare geometric variations within the parameters of the investigations described in References 7 and 10, is therefore consistent with the overall experimental accuracy. The combination of data in Figs. 8-10 with cone-cylinder or ogive-cylinder forebody data derived from par. 8-2.1.1 should provide overall normal-force coefficient gradients within ± 10 percent and center-of-pressure locations within ± 0.5 caliber.

8-2.1.4 Oversize Head Configurations

Occasionally the nose section is required to have a larger diameter than that of the cylindrical

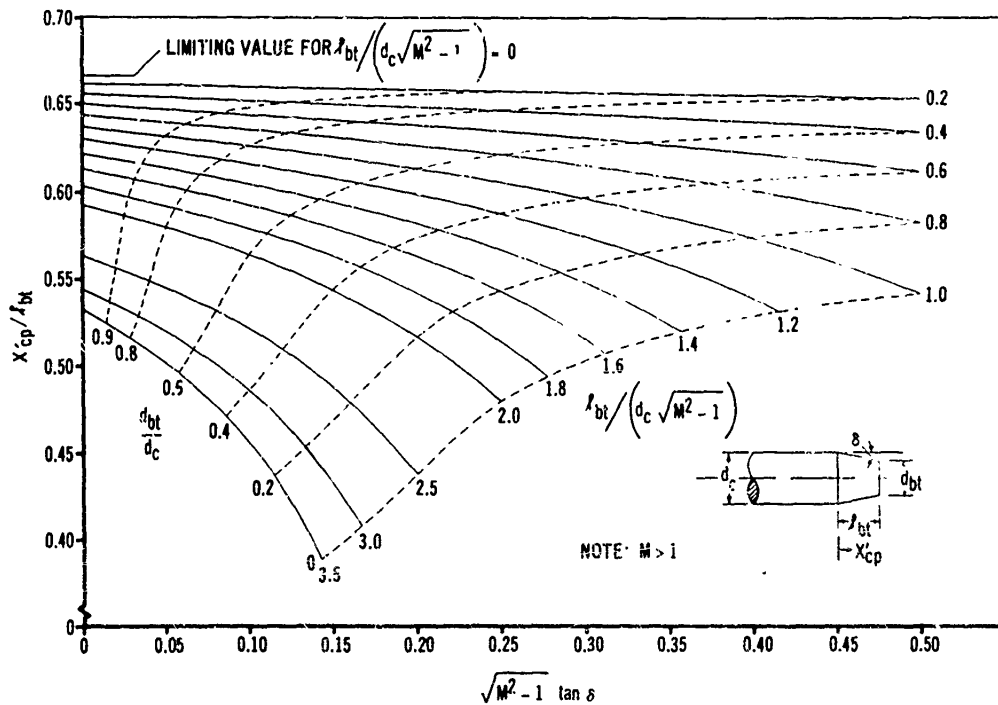


Figure 8-9. Center of Pressure for a Boattail

afterbody because of warhead considerations. Slender-body theory can be used to estimate normal force and center of pressure through the subsonic-transonic Mach number region. At supersonic Mach numbers, methods provided in the previous paragraphs can be used to calculate the nose-cylinder and boattail characteristics, neglecting the aft-cylinder normal-force contribution. If a tapered boattail is not used to provide a transition section between the nose and cylinder, or if the boattail angle exceeds 12 deg, then the normal-force and center of pressure characteristics should be calculated assuming an effective 12-deg boattail angle.

8-2.2 FINS

The geometric and flow parameters affecting the normal force and center of pressure of two isolated coplanar fins (2 fins in the same plane) will be discussed initially, followed by a discussion of fin-body and fin-fin interference effects

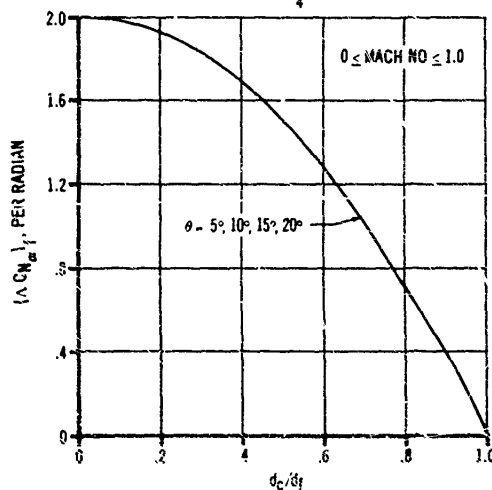
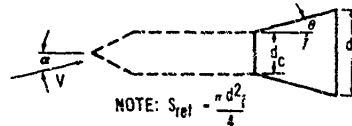


Figure 8-10(A). Incremental Normal-Force Coefficient Gradient for a Flare

AMCP 706-260

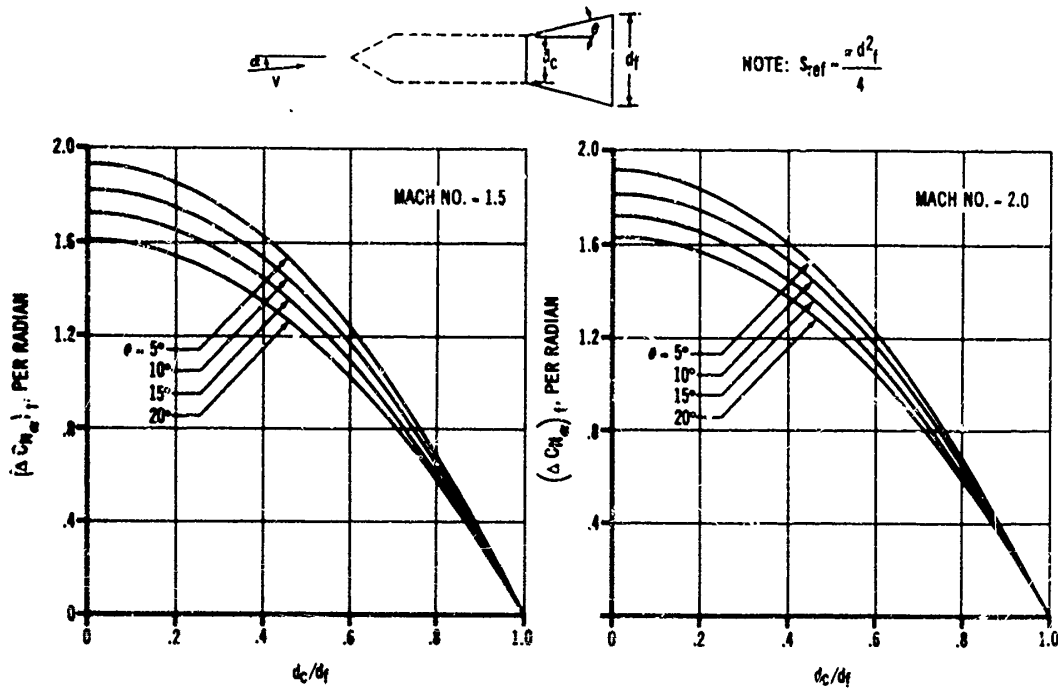


Figure 8-10(B). Incremental Normal-Force Coefficient Gradient for a Flare

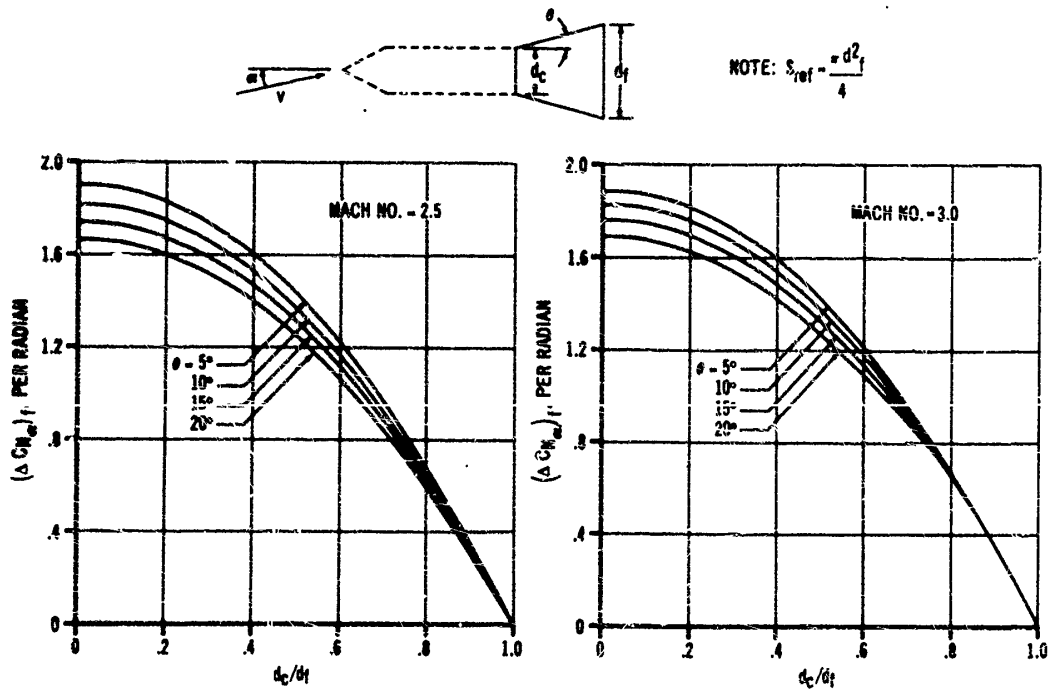


Figure 8-10(C). Incremental Normal-Force Coefficient Gradient for a Flare

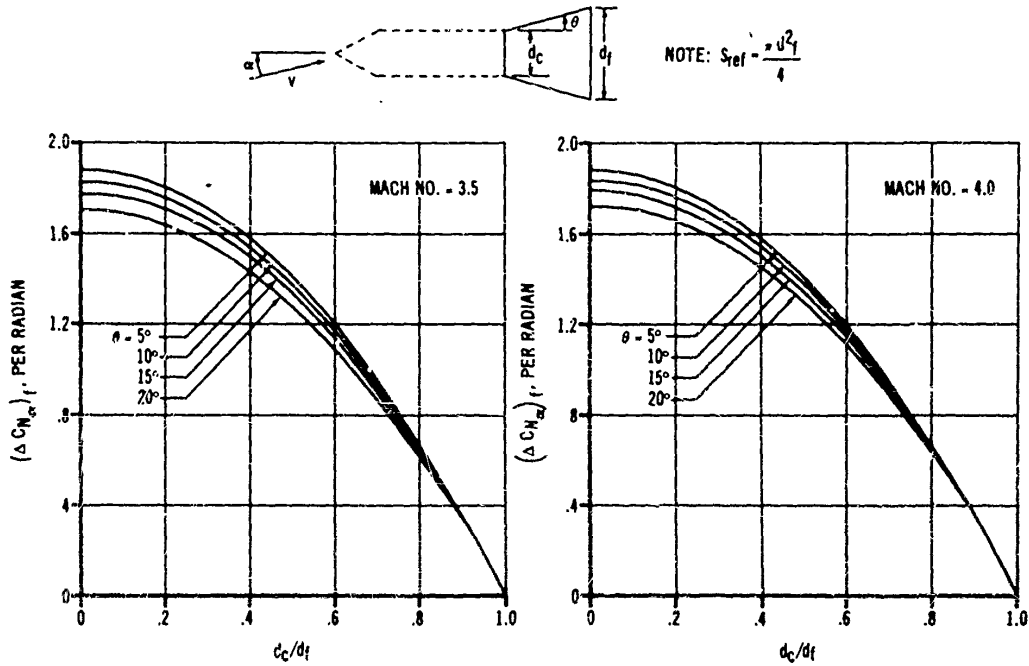


Figure 8-10(D). Incremental Normal-Force Coefficient Gradient for a Flare

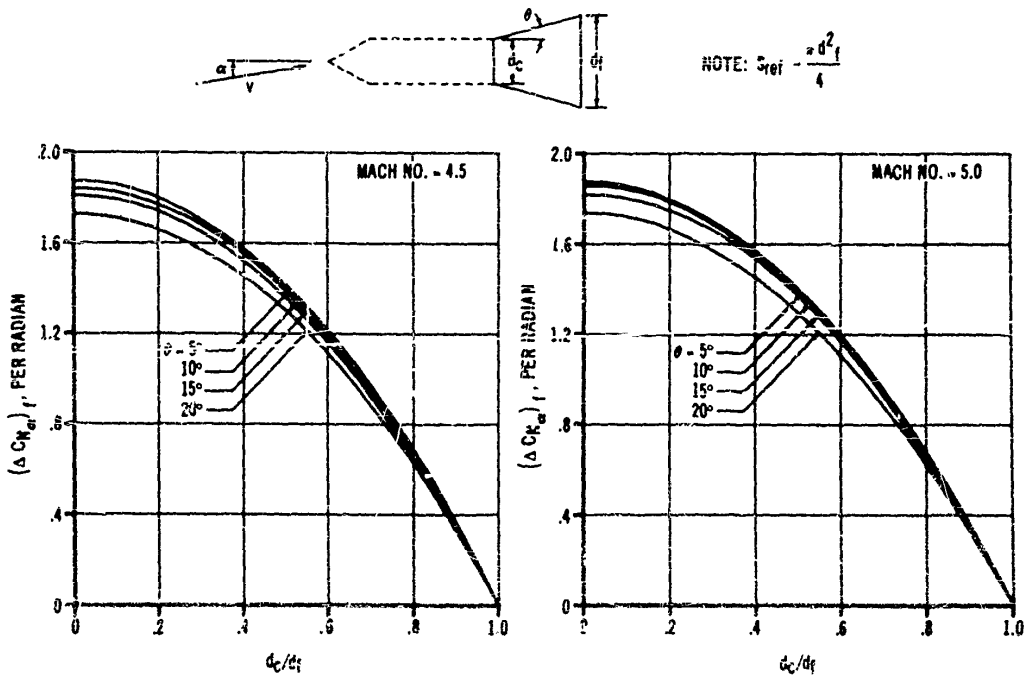


Figure 8-10(E). Incremental Normal-Force Coefficient Gradient for a Flare

AMCP 706-289

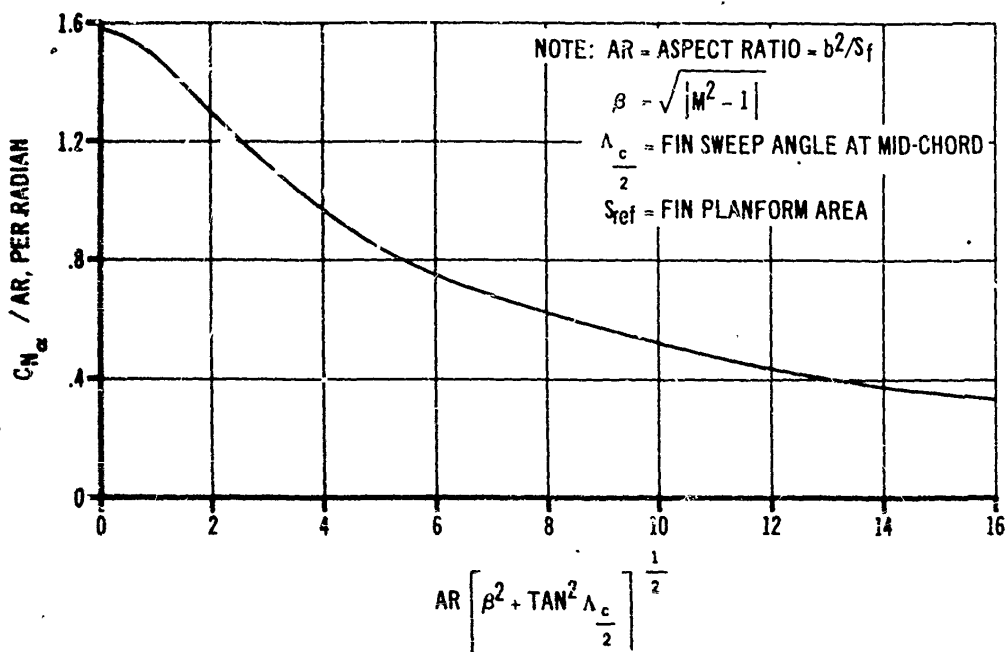


Figure 8-11. Subsonic Fin Normal-Force Coefficient Gradient

(par. 8-2.4). Throughout this discussion, thickness will be considered small relative to fin chord since the general practice is to minimize profile thickness for reduction of drag and weight.

Theoretical studies have shown the aspect ratio to be the dominant geometric factor governing the lifting characteristics of unswept wings or fins. The normal-force coefficient slope varies from $\frac{\pi(AR)}{2}$ for a very low aspect ratio (approaching zero), to 2π for an aspect ratio approaching infinity. A simple correlation based on lifting-line theory (Reference 11) gives

$$\frac{C_{N_{\alpha}}}{AR} = \frac{2\pi}{2 + \left[(AR)^2 \left(\beta^2 + \tan^2 \Lambda_c \frac{c}{2} \right) + 4 \right]^{1/2}} \quad (8-6)$$

assuming that the section lift coefficient equals 2π and where

$$AR = \frac{\text{fin span squared}}{\text{fin area}}$$

$$\beta = \sqrt{M_{\infty}^2 - 1}$$

8-18

$M_{\infty} =$ free stream Mach number
 $\Lambda_c =$ fin sweep angle, degrees
 $\frac{c}{2} =$ fin mid-chord position

This equation, plotted in Fig. 8-11, is valid for thin unswept or swept fins of any aspect ratio and for Mach numbers to 0.6. However, for low-aspect-ratio fins which are of primary interest to rocket designers, valid results can be expected up to Mach numbers approaching one. Subsonically, the fin center of pressure may be assumed at 25 percent of the mean aerodynamic chord \bar{c} measured rearward from the leading edge.

The complex nature of transonic flow has precluded reasonably simple mathematical solutions for the flow field about fins, except in the case of thin fins with very low aspect ratios. The linearized slender-wing theory predicts that

$$C_{N_{\alpha}} = \frac{\pi}{2} (AR) \quad (8-7)$$

Utilizing transonic-similarity laws, McDevitt (Reference 12) obtained from experimental data the correlation shown in Figs. 8-12(A) and (B) for rectangular planform fins. At Mach number

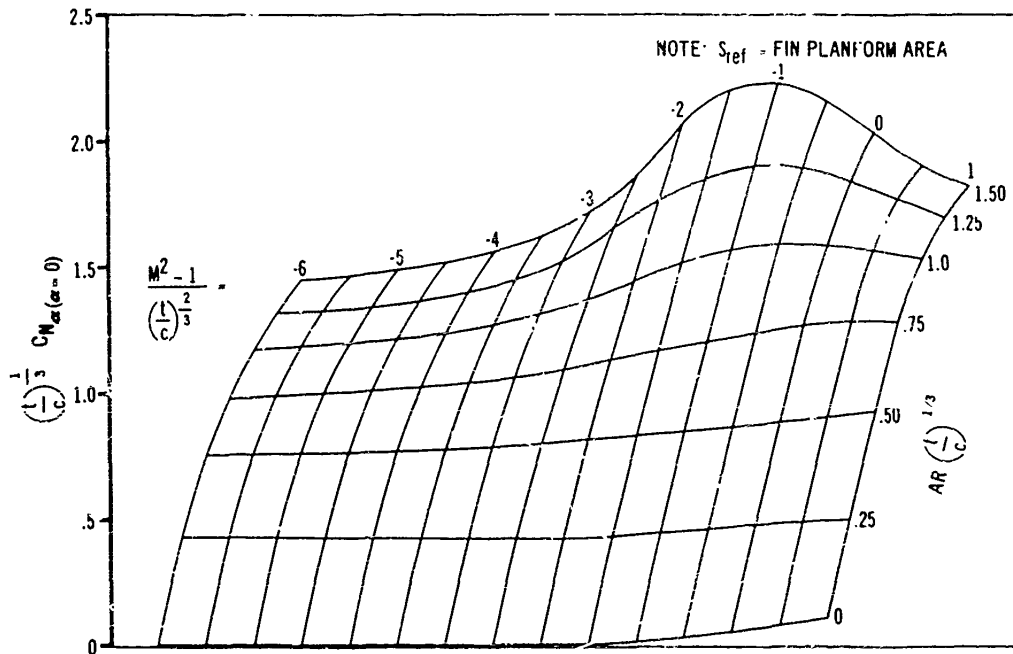


Figure 8-12(A). Normal-Force Coefficient Gradient for Rectangular Fins

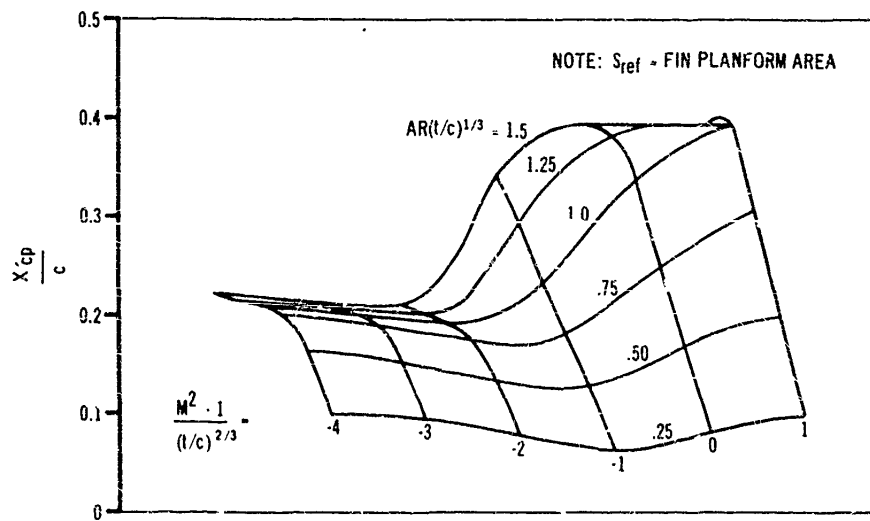
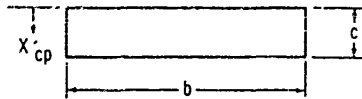


Figure 8-12(B). Center of Pressure for Rectangular Fins

AMCP 706-280

1, linearized-wing-theory prediction matches the experimental data where $(AR)(t/c)^{1/3}$ is less than one. Therefore, it is suggested that linearized-wing theory be used as a guide for planforms other than rectangular in the sonic region.

Linearized flow theory has been found to be an accurate means of predicting supersonic stability characteristics of thin-profile fins. Thickness effects are important, primarily when the Mach line emanating from the leading edge root-section lies close to the leading edge. Reference 13 presents charts, based on linearized theory, to estimate normal-force coefficient gradient and center of pressure for swept leading-edge fins of nearly arbitrary planform.

Figs. 8-13(A), (B), (C) and 8-14(A), (B), (C), respectively, are duplications of the generalized charts for normal-force coefficient gradient and center of pressure. Fig. 8-14 provides reasonable estimates of center of pressure for the subsonic, transonic, and supersonic regions for all fin planforms other than rectangular. A correction to the theoretical $C_{N\alpha}$ for thickness effects is given in Fig. 8-15 for swept fins with wedge leading edges. Use of this figure is explained in the computational sheets, par. 8-2.4.4. Thickness has only a minor effect on center-of-pressure, and no correction to the theoretical estimates is considered necessary.

The supersonic normal-force coefficient slope and center-of-pressure of rectangular-planform fins as derived by linearized theory (Reference 14) are presented in Fig. 8-16. These data are valid for $\beta(AR) \geq 0.5$.

A general presentation of linearized-supersonic-wing theory and aerodynamic estimation charts can be found in Reference 15; the reader is referred to this work for fin planform not covered by the charts herein.

8-2.3 RING TAIL

The normal-force coefficient gradients for ring fins installed in a cylindrical afterbody are presented in Figs. 8-17(A) through (F), taken from Reference 16, for Mach numbers from 0.8 to 3.0. The figure shows the normal-force coefficient gradient for various chord lengths and ring diameters plotted in a "carpet plot". Three different positions of the ring trailing-edge relative to the body base are indicated by the solid, chain-

dashed, and dashed lines.

As ring tails are often used in conjunction with oversized heads, it should be noted that the reference area of the lift curve is the cross-sectional area of the cylindrical afterbody on which the ring is installed. The data used in Fig. 8-17 were obtained from wind tunnel tests on rings having a 4° double-wedge section, with the inside surface of the ring diverging at 4° from the body centerline. (See sketch on Fig. 8-17.) Included are the effects of interference between the body, support strut, and ring on the normal-force coefficient gradient.

It should be noted that the test data are for rings whose trailing-edge diameter is larger than the leading-edge diameter. However, the charts should provide reasonably accurate lift estimates for other ring configurations, provided that the minimum and maximum diameters of the ring are within the limits of minimum and maximum diameters of the 4° ring case.

The center-of-pressure is assumed to be at the ring mid-chord point.

8-2.4 STABILITY OF COMPLETE CONFIGURATION

8-2.4.1 General

In the previous paragraphs, consideration has been given to the prediction of force and moment characteristics of individual free flight rocket components. When the force and moment characteristics of the complete configuration are computed, two major factors must be considered:

- a. The data for the individual components may be summed for the total *only* if a consistent set of data is used.
- b. Certain interference effects must be accounted for when the components are joined to form the complete configuration.

The first factor concerns equatibility between the force and moment coefficients; i.e., the force coefficients must be reduced on a common reference area and the moment coefficients must be reduced on a common reference area and length as well as a common reference point.

To explain further, the normal force coefficient gradient is defined as

$$C_{N\alpha} = \frac{N}{q\alpha A_{ref}} \quad \text{for small values of } \alpha \quad (8-8)$$

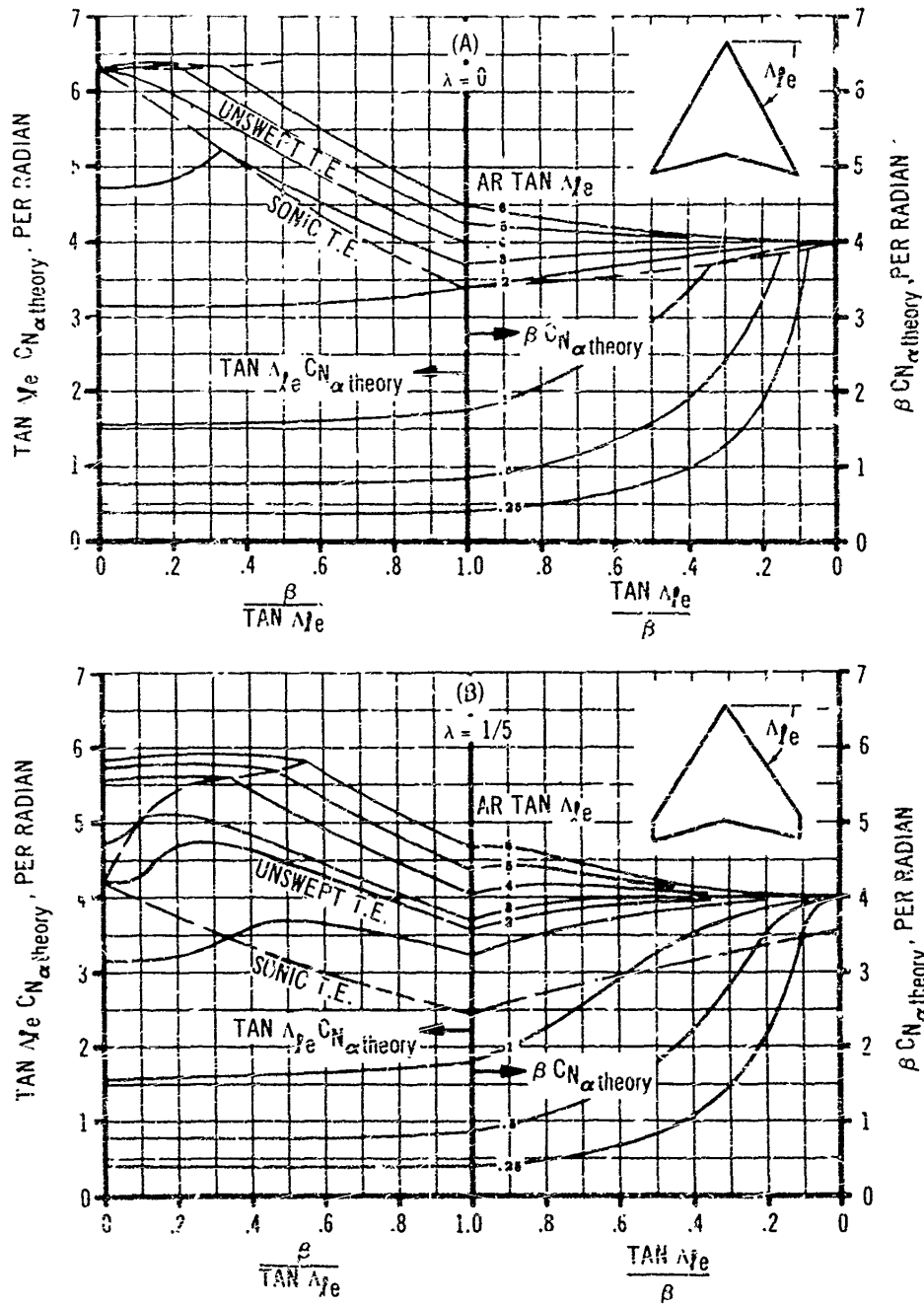


Figure 8-13(A). F: Normal Force Coefficient Gradient at Supersonic Mach Numbers

AMCP 706-280

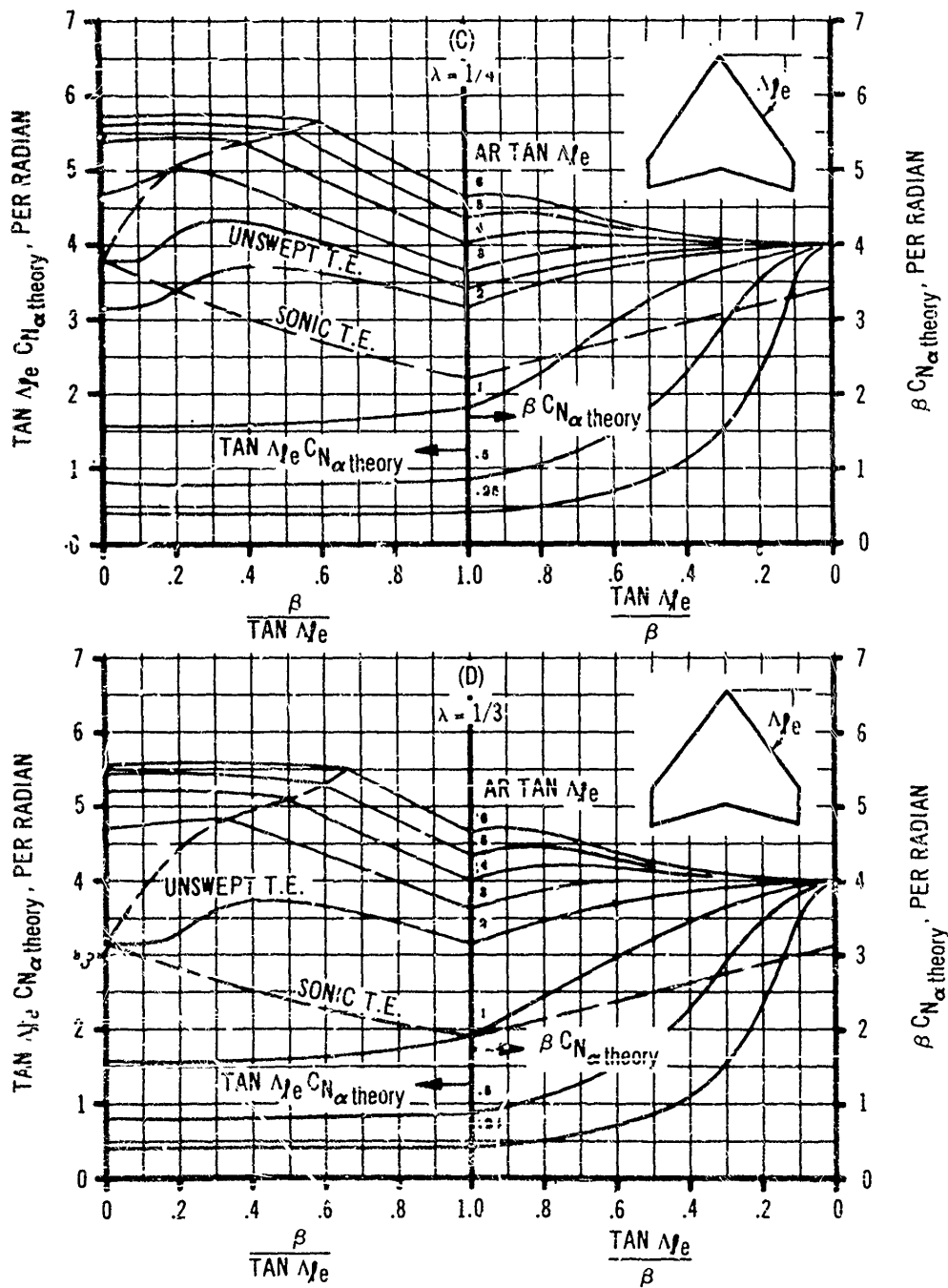


Figure 8-13(B). Fin Normal Force Coefficient Gradient at Supersonic Mach Numbers

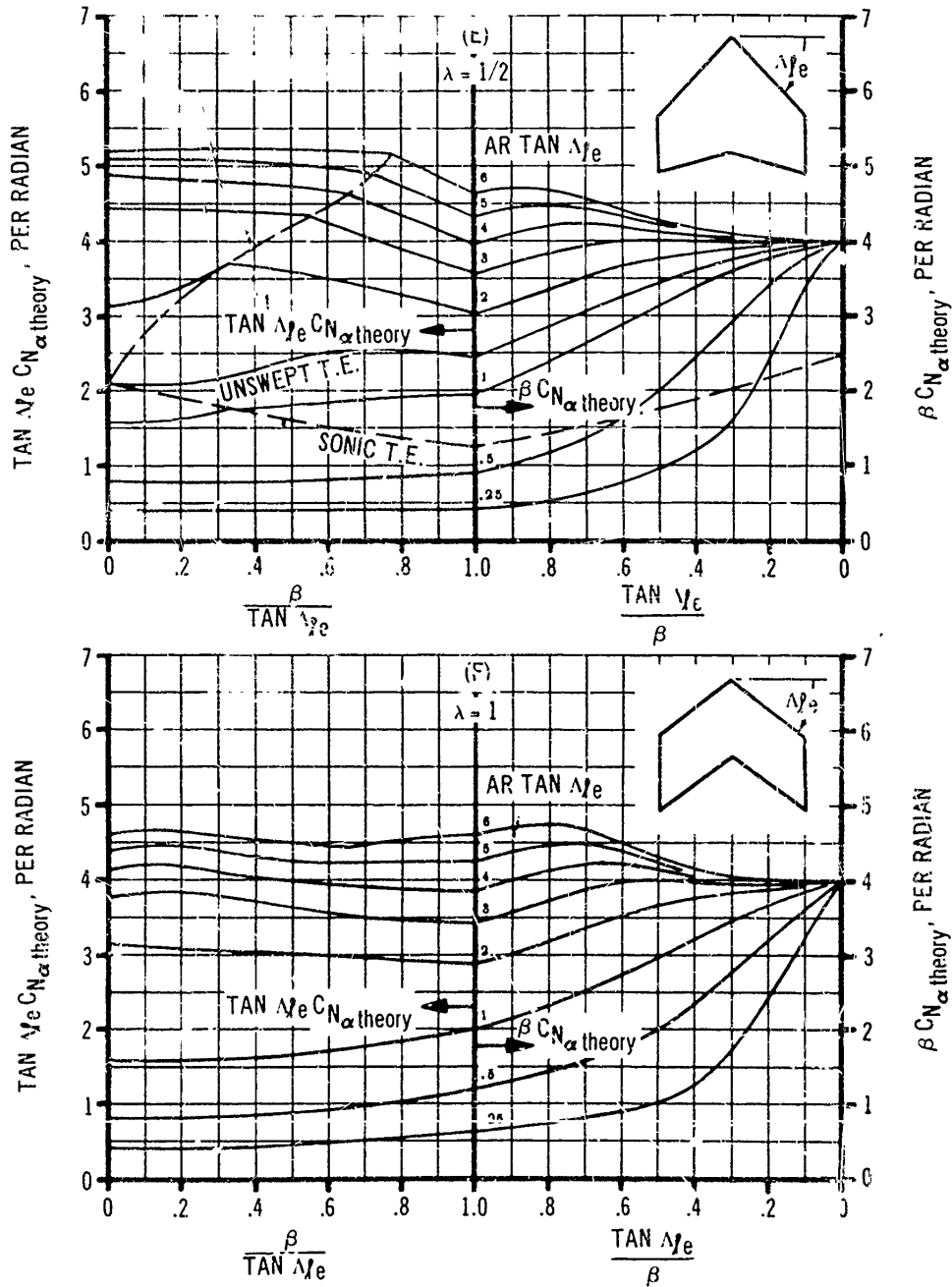


Figure 8-13(C). Fin Normal Force Coefficient Gradient at Supersonic Mach Numbers

AMCP 706-280

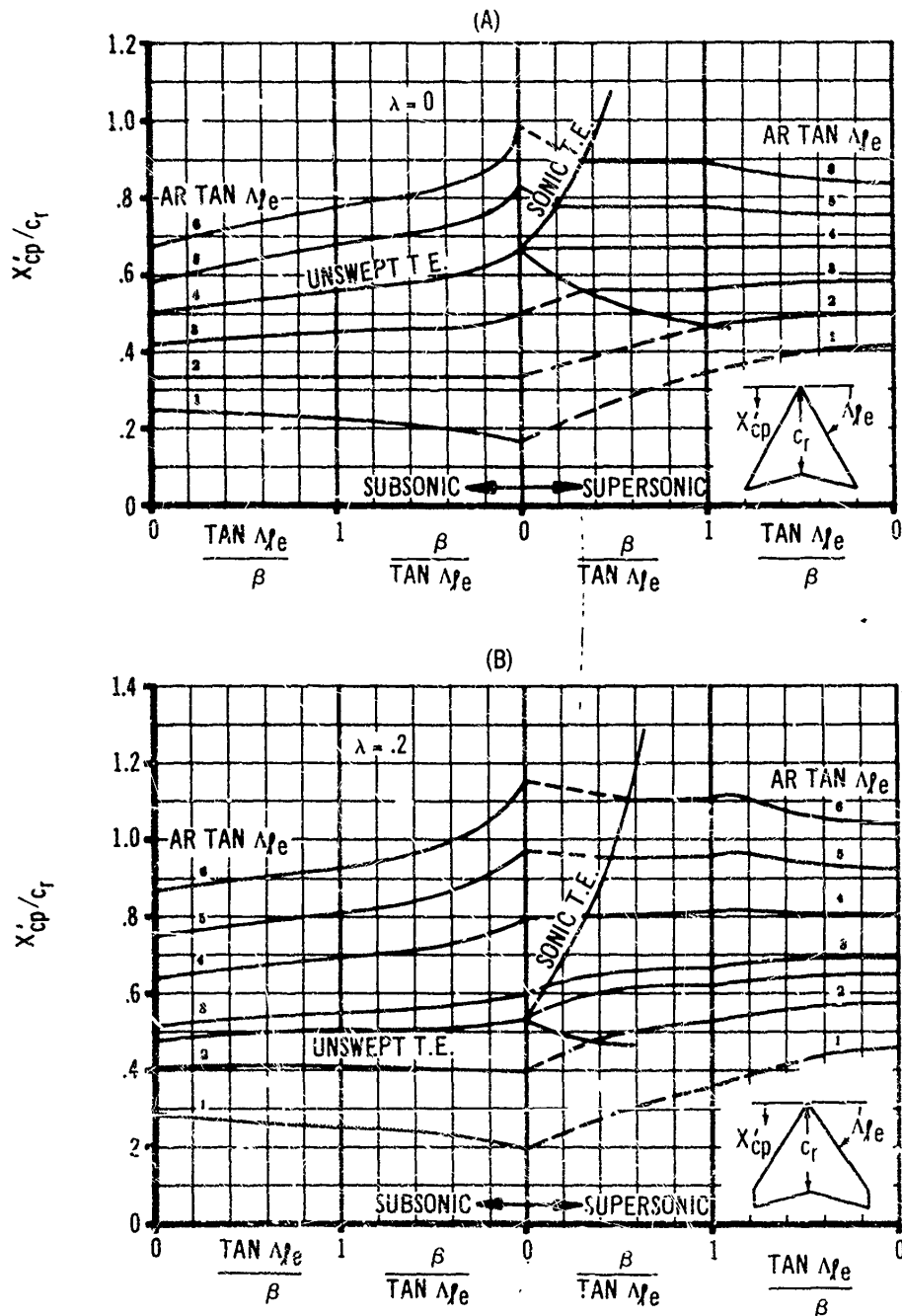


Figure 8-14(A). Fin Center of Pressure

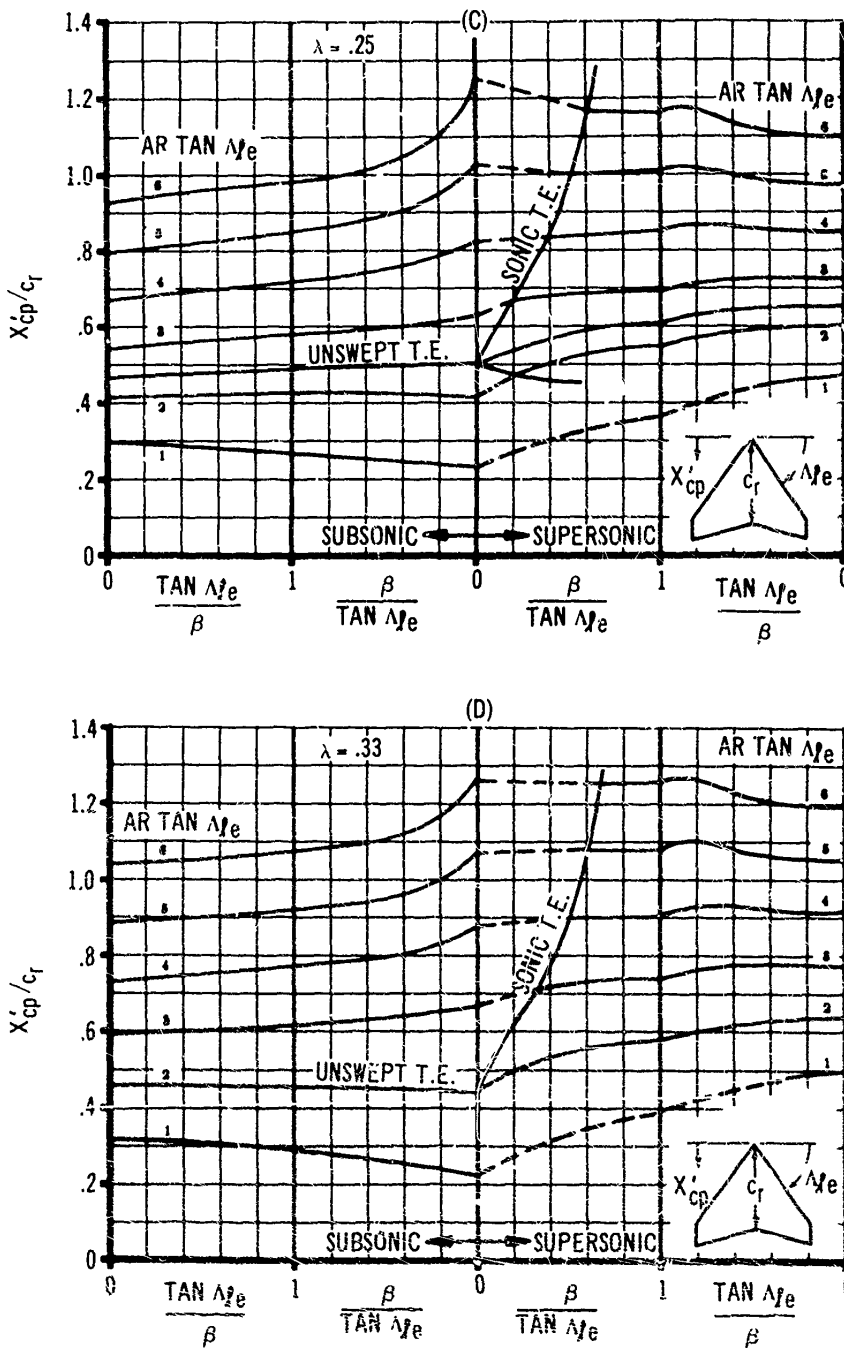


Figure 8-14(B). Fin Center of Pressure

AMCP 706-250

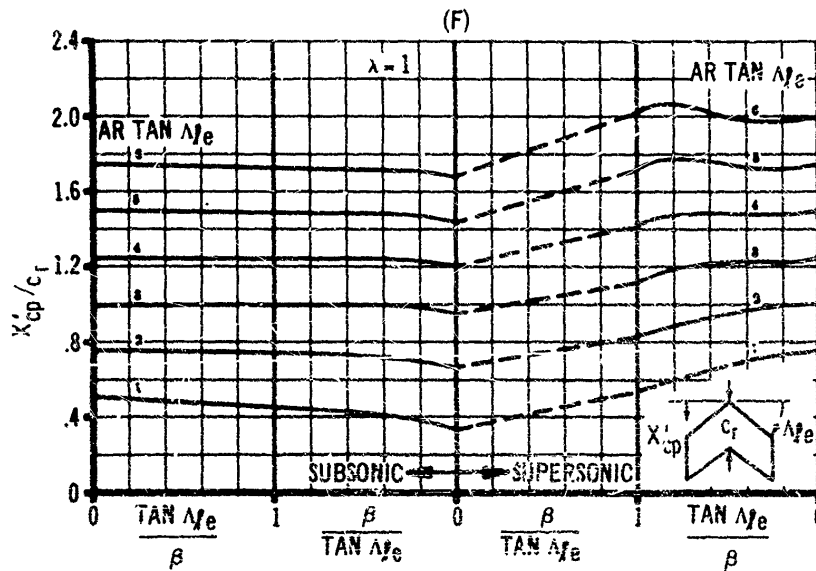
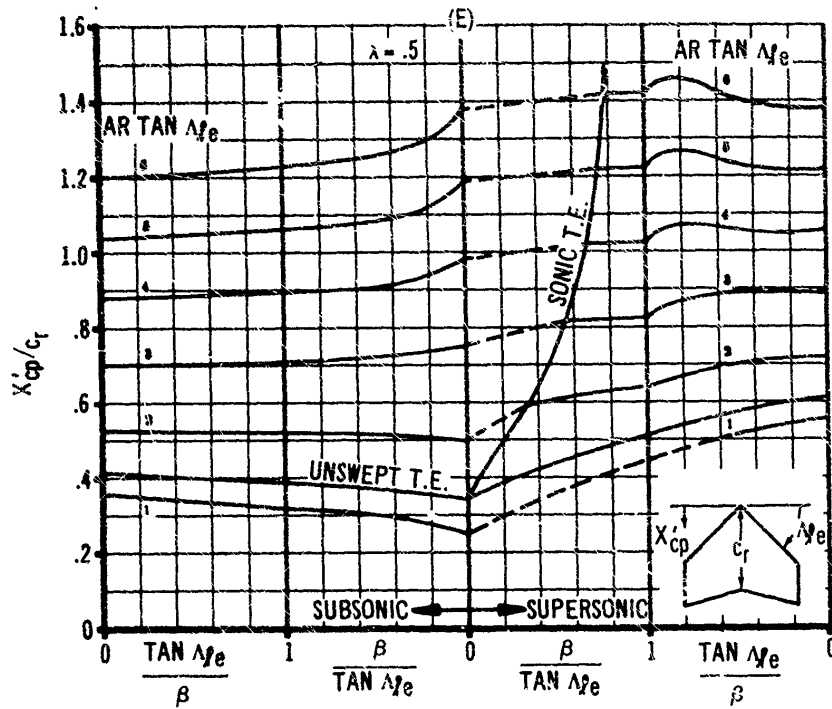


Figure 8-14(C). Fin Center of Pressure

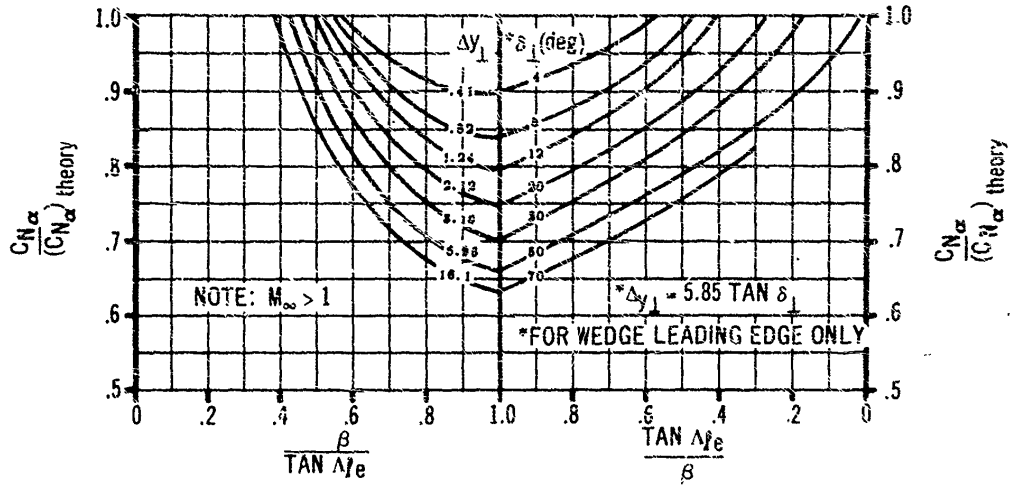


Figure 8-15. Fin Normal Force Coefficient Gradient Correction Factor for Sonic Leading Edge Region

where

- N = normal force, lb
- q = dynamic pressure (1/2 rho V^2), lb/ft^2
- alpha = angle of attack, rad or deg, and
- A_ref = reference area, ft^2

Thus the unit of measure for C_N_alpha simplifies to units per radian for a measured in radians (representing a slope). C_N_alpha is also sometimes presented as units per degree, which can be converted to radian-measure by the formula:

$$C_{N_{\alpha}} \text{ (per degree)} \times 57.3 = C_{N_{\alpha}} \text{ (per radian)} \quad (8-9)$$

Either radian- or degree-measure may be used; however, all coefficients must be consistent.

To illustrate, assume we have obtained the following data:

$$C_{N_{\alpha \text{ body}}} = 2.0/\text{rad with } S_{ref}$$

$$= \text{body cross-sectional area} = A_{cyl}$$

and

$$C_{N_{\alpha \text{ fin}}} = .060/\text{deg with } S_{ref}$$

$$= \text{fin planform area} = A_p$$

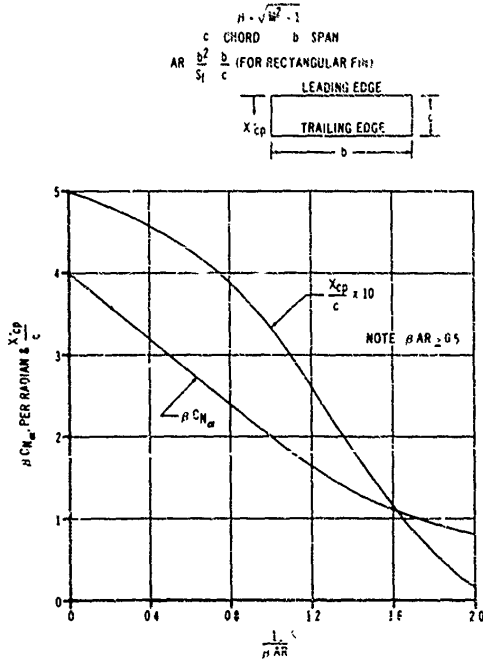


Figure 8-16. Normal Force Coefficient Gradient and Center of Pressure for Rectangular Fins

AMCP 706-250

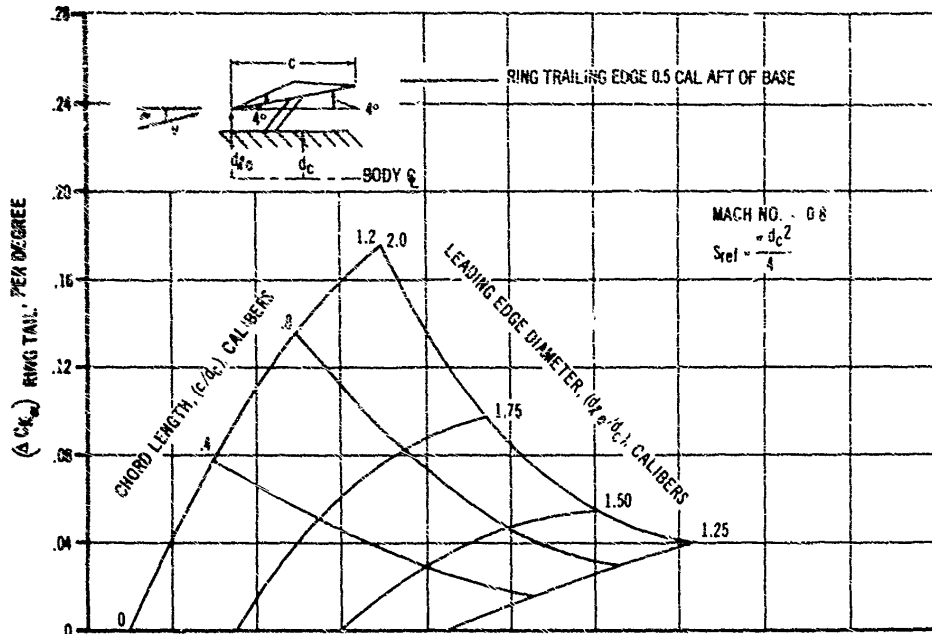


Figure 8-17(A). Incremental Normal Force Coefficient Gradient for a Ring Tail Mounted on a Cylindrical Afterbody

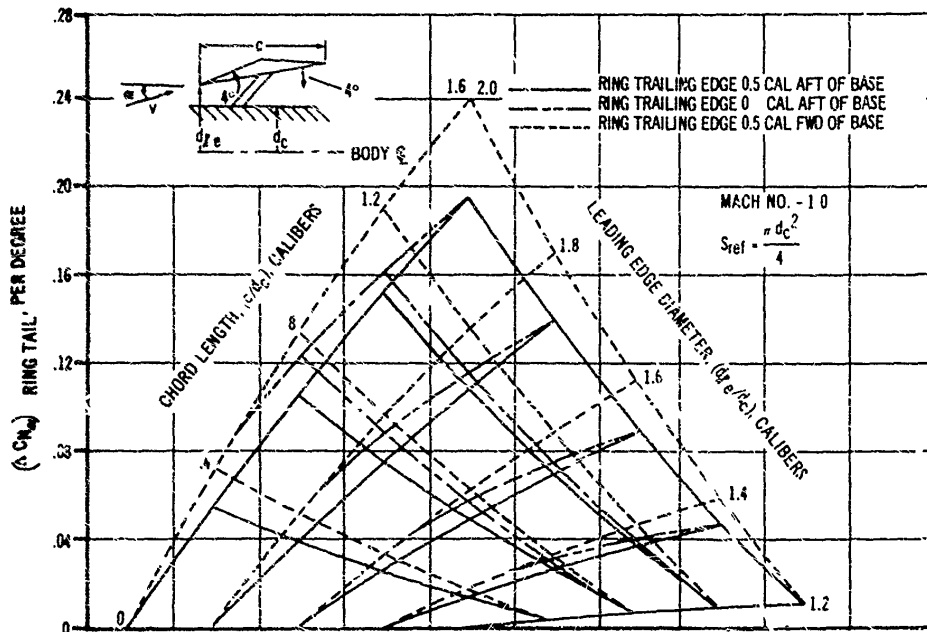


Figure 8-17(B). Incremental Normal Force Coefficient Gradient for a Ring Tail Mounted on a Cylindrical Afterbody

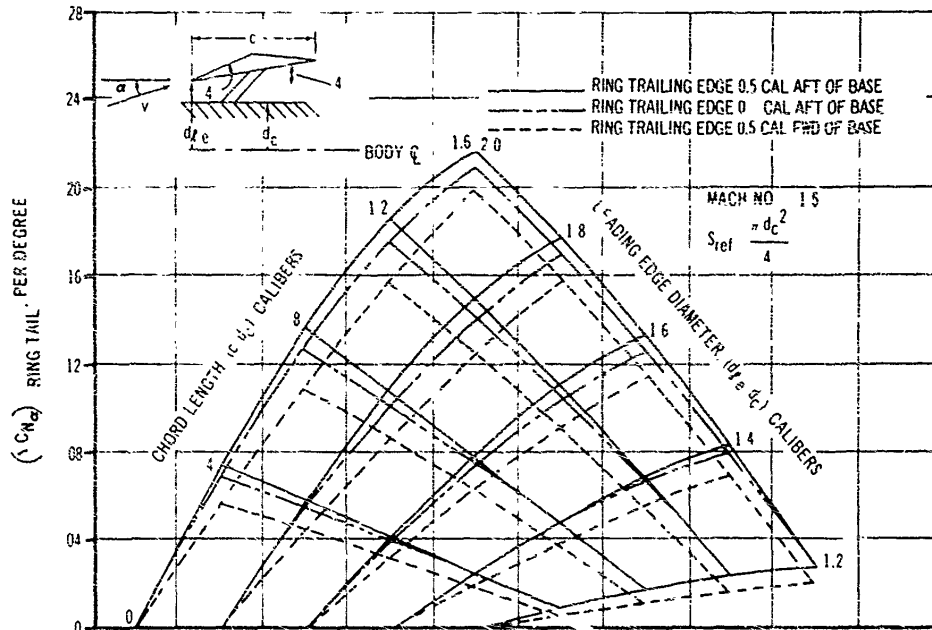


Figure 8-17(C). Incremental Normal Force Coefficient Gradient for a Ring Tail Mounted on a Cylindrical Afterbody

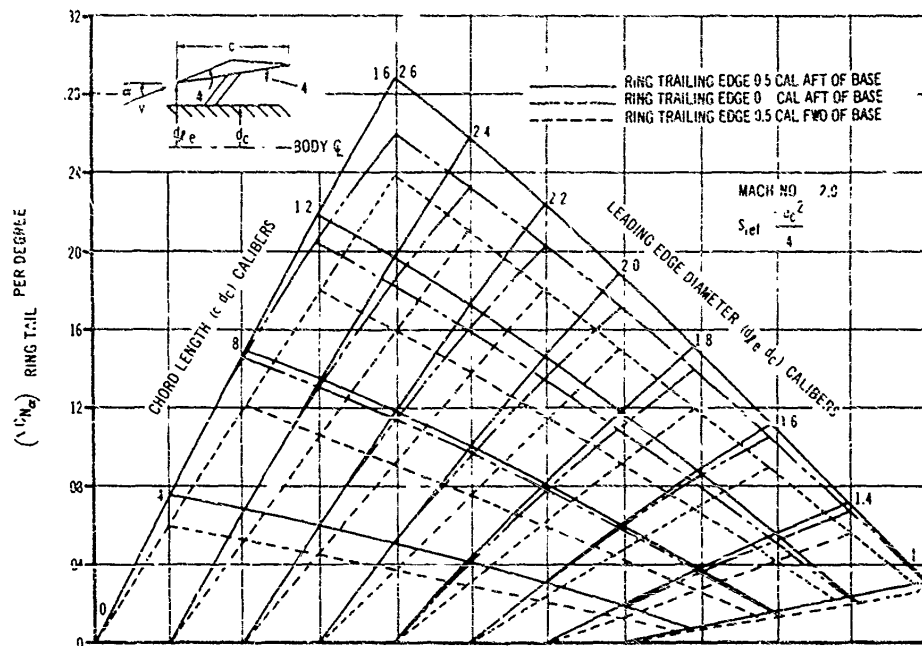


Figure 8-17(D). Incremental Normal Force Coefficient Gradient for a Ring Tail Mounted on a Cylindrical Afterbody

AMCP 700-280

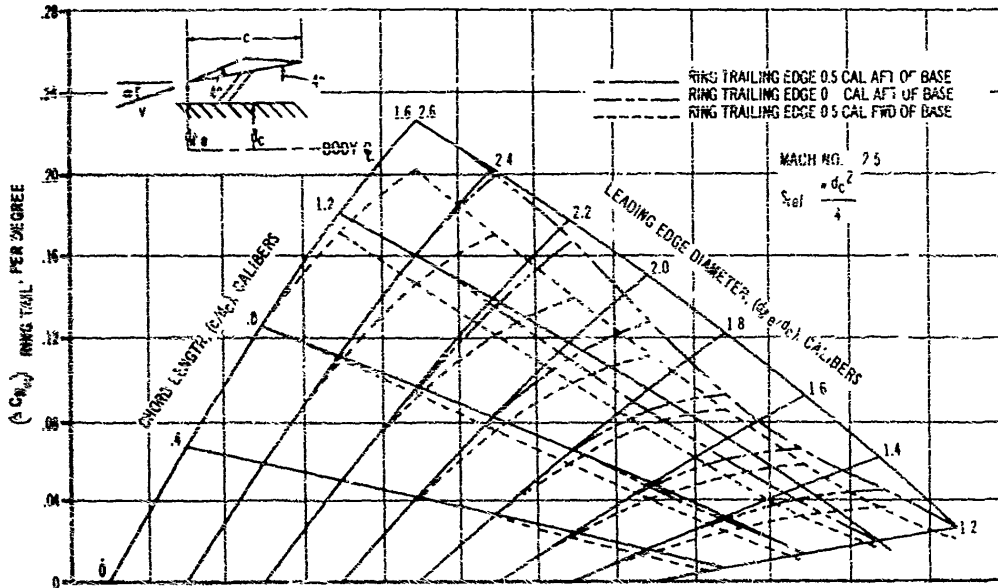


Figure 8-17(E). Incremental Normal Force Coefficient Gradient for a Ring Tail Mounted on a Cylindrical Afterbody

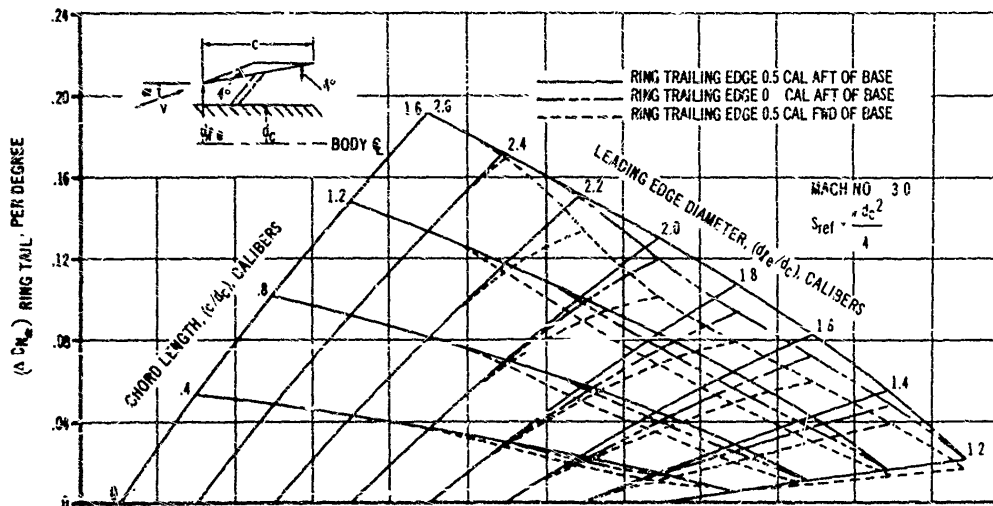


Figure 8-17(F). Incremental Normal Force Coefficient Gradient for a Ring Tail Mounted on a Cylindrical Afterbody

First, convert $C_{N_{\alpha}}^{\text{fin}}$ to radian measure

$$\begin{aligned} C_{N_{\alpha}}^{\text{fin}} &= .960/\text{deg} \\ &= (.960)(57.3)/\text{rad} = 3.43/\text{rad} \end{aligned}$$

Next select a common reference area (usually the body cylindrical cross-sectional area is selected) as $A_{\text{ref}} = A_{\text{cyl}}$.

Then,

$$\begin{aligned} C_{N_{\alpha}}^{\text{body}} &= 2.0/\text{rad} \\ &\text{(based on body cross-sectional area)} \end{aligned}$$

$$\begin{aligned} C_{N_{\alpha}}^{\text{body}} &= 2.0/\text{rad} \left(\frac{A_{\text{cyl}}}{A_{\text{ref}}} \right) \\ &\text{(based on common area } A_{\text{ref}}) \end{aligned}$$

$$\begin{aligned} C_{N_{\alpha}}^{\text{fin}} &= 3.43/\text{rad} \\ &\text{(based on fin planform area } A_p) \end{aligned}$$

$$\begin{aligned} C_{N_{\alpha}}^{\text{fin}} &= 3.43 \left(\frac{A_p}{A_{\text{ref}}} \right) \\ &\text{(based on common area } A_{\text{ref}}) \end{aligned}$$

The total (sum of body and fin) normal-force coefficient gradient is, then, expressed as

$$\begin{aligned} C_{N_{\alpha T}} &= C_{N_{\alpha}}^{\text{body}} + C_{N_{\alpha}}^{\text{fin}} \\ &= 2.0/\text{rad} + 3.43 \left(\frac{A_p}{A_{\text{ref}}} \right) / \text{rad} \end{aligned} \quad (8-10)$$

and the reference area for the total coefficient $C_{N_{\alpha T}}$ is A_{ref} .

The moment coefficient gradient is defined as follows for small values of α :

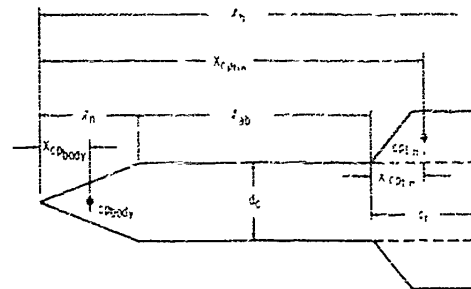
$$C_{M_{\alpha}} = C_{N_{\alpha}} \left(\frac{\lambda_{cp}}{l_{\text{ref}}} \right) = \frac{M}{q A_{\text{ref}} l_{\text{ref}} \alpha} \quad (8-11)$$

where

M = pitching moment, ft-lb
 λ_{cp} = axial distance from reference point to center of pressure, ft

As previously explained, radian or degree measures may be used. A comparison of the expressions for $C_{N_{\alpha}}$ and $C_{M_{\alpha}}$ indicates that, in addition to a common area reference, the moment coefficient must be reduced on a common reference length and a common reference point.

To illustrate, assume we have obtained the following data concerning the configurations shown in the sketch below:



$$C_{N_{\alpha}}^{\text{body}} = 2.0/\text{rad} \text{ (based on } \frac{\pi d_c^2}{4} \text{)}$$

$$l_{cp, \text{body}} = \frac{2}{3} l_n \text{ (in ft)}$$

$$C_{M_{\alpha}}^{\text{fin}} = 3.0/\text{rad} \text{ (based on } \frac{\pi d_c^2}{4} \text{)}$$

$$\left(\frac{\lambda_{cp}}{c_r} \right)_{\text{fin}} = 0.5 \text{ (in root-chord lengths)}$$

First, a reference length and point must be selected (usually the body diameter and nose of the body, respectively, are selected).

Then, when

$$A_{\text{ref}} = \frac{\pi d_c^2}{4}, \quad l_{\text{ref}} = d_c \quad \text{and}$$

Reference point = nose tip

$$C_{M_{\alpha}}^{\text{body}} = \left(C_{N_{\alpha}}^{\text{body}} \right) \left(\frac{2}{3} \cdot \frac{l_n}{d_c} \right) \quad (8-12)$$

$$C_{M_{\alpha}}^{\text{body}} = 2.0 \left(\frac{2}{3} \cdot \frac{l_n}{d_c} \right) \quad (8-13)$$

AMCP 706-280

When

$$A_{ref} = \frac{\pi d_c^2}{4}, \quad l_{ref} = c_r \quad \text{and}$$

Reference point = junction of fin root chord and body surface

$$C_{N\alpha \text{ fin}} = C_{N\alpha \text{ fin}} \left(\frac{X'_{cp}}{c_r} \right)_{\text{fin}} \quad (8-14)$$

Changing reference, when

$$A_{ref} = \frac{\pi d_c^2}{4}, \quad l_{ref} = d_c \quad \text{and}$$

Reference point = nose tip

$$C_{N\alpha \text{ fin}} = (3.0) \left[\frac{l_n + l_{ab} + \left(\frac{X'_{cp \text{ fin}}}{c_r} \right)}{d_c} \right] c_r \quad (8-15)$$

Now, since both moment coefficients have a common reference area, reference length, and reference point, we can write

$$C_{N\alpha \tau} = C_{N\alpha \text{ body}} + C_{N\alpha \text{ fin}} \quad (8-16)$$

or

$$C_{N\alpha \tau} = 2.0 \left(\frac{2}{3} \cdot \frac{l_n}{d_c} \right) + 3.0 \left[\frac{l_n + l_{ab} + \left(\frac{X'_{cp \text{ fin}}}{c_r} \right)}{d_c} \right] c_r \quad (8-17)$$

where

$$A_{ref} = \frac{\pi d_c^2}{4}, \quad l_{ref} = d_c \quad \text{and}$$

Reference point = nose tip

The total center-of-pressure may be found as

$$\left(X_{cp} \right)_{\text{Total}} = \left(\frac{C_{M\alpha}}{C_{N\alpha}} \right)_{\text{Total}} (d_c) \quad (8-18)$$

measured rearward from the nose tip, or the total center-of-pressure expressed in body diameters (or calibers) is

$$\left(\frac{X_{cp}}{d_c} \right)_{\text{Total}} = \left(\frac{C_{M\alpha}}{C_{N\alpha}} \right)_{\text{Total}} \quad (8-19)$$

measured rearward from the nose tip.

The second major factor to be considered concerns the fin-body and fin-fin interference effects. These are covered in greater detail in the paragraphs which follow.

8-2.4.2 Fin-Body Interference

When fins are attached to a body-of-revolution, interference effects increase the normal force over that for the isolated fins. This interference effect is particularly important for low-aspect-ratio fins where the fin span is approximately equal to the body diameter.

The presence of a cylindrical afterbody induces an increased local angle-of-attack along the fin span. If we neglect the nose effects a reasonably accurate prediction of the upwash distribution in the horizontal plane is given by Eskin (Reference 17) to be

$$\alpha = \left[i + \left(\frac{r}{y} \right)^2 \right] \quad (8-20)$$

where α_0 is the body angle of attack, r is the body radius in feet, and y is the lateral distance from the body centerline in feet. If we utilize the approach of Reference 18 slender-body theory, the ratio of fin normal force in the presence of a body to fin normal force of the isolated fin (interference factor) is

$$k_{f(b)} = \frac{C_{N\alpha \text{ f(b)}}}{C_{N\alpha \text{ f}}} = \frac{2}{(1 - \frac{r}{b})^2} \left\{ \left(1 + \frac{r^4}{b^4} \right) \left[\frac{1}{2} \tan^{-1} \frac{1}{2} \left(\frac{b}{r} - \frac{r}{b} \right) + \frac{\pi}{4} \right] - \frac{r^2}{b^2} \left[\left(\frac{b}{r} - \frac{r}{b} \right) + 2 \tan^{-1} \frac{r}{b} \right] \right\} \quad (8-21)$$

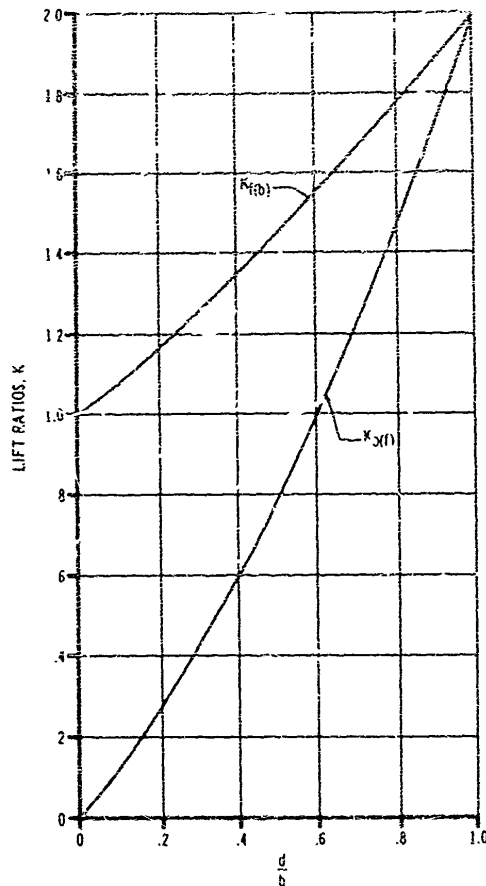


Figure 8-18. Values of Lift Ratios Based on Slender-Body Theory

The primary parameter is seen to be the ratio of fin span b to body radius r . Although a more precise analysis would show dependence on Mach number, fin planform, and location of the fin on the body, the slender-body result will give adequate preliminary design estimates of the ratio $K_{f(b)}$. Fig. 8-18 presents $K_{f(b)}$ as a function of d/b .

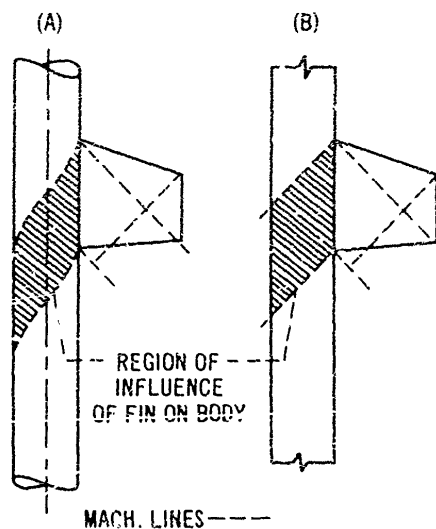
Additional normal force is produced on the cylindrical body adjacent to the fins by carryover to the body of lifting pressure distribution on the fins. Subsonically, the method for determining this carryover by slender-body theory is

$$K_{b(f)} = \frac{C_{v \text{ eff}}}{C_{v \text{ eff}}} \left(1 + \frac{r}{b}\right)^2 = K_{f(b)} \quad (8-22)$$

for values of $M \leq 1$. Fig. 8-18 presents $K_{b(f)}$ as a function of d/b .

Contrary to the case for subsonic Mach numbers, fin planform and Mach number are important parameters in determining the supersonic fin carryover normal force to the body. The ratio of carryover normal force to the isolated-fin normal force $K_{b(f)}$ is determined adequately by the method of Reference 18. This method, based on slender-body theory, integrates the carryover pressure distribution over the region defined by the Mach cones emanating from the root-chord leading edge and trailing edge as shown in Fig. 8-19 taken from Reference 18.

If the fin trailing edge is located flush with the body base, as is the case in many rocket designs, the body area influenced by fin carryover pressures is restricted to that defined by the Mach cone from the root-chord leading edge and the body base. Values of the ratio $K_{b(f)}$ are presented in Fig. 8-20 for configurations with no



(A) NONPLANAR MODEL (B) PLANAR MODEL

Figure 8-19. Interference Effects of Fin on Body

AMCP 706-240

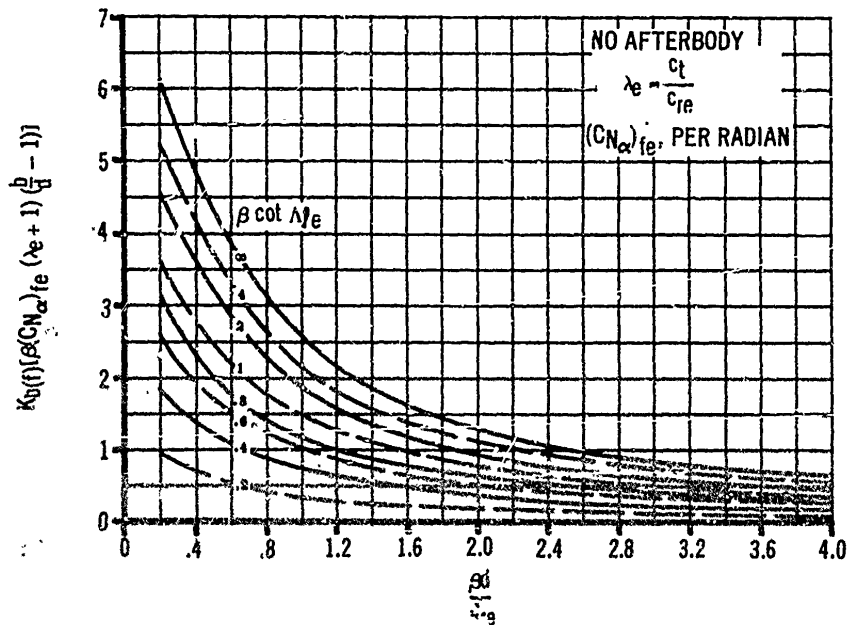
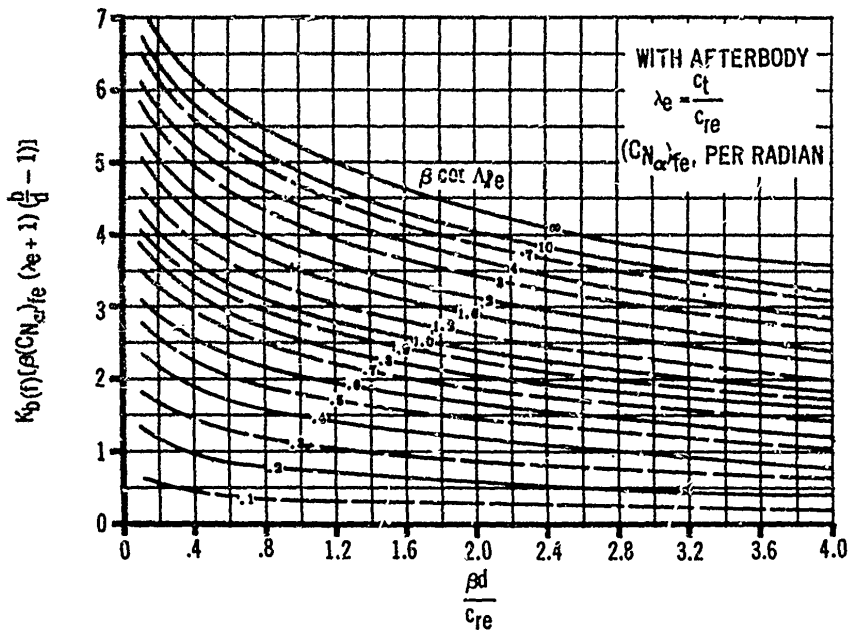


Figure 8-20. Lift Factors - Influence of Fin on Body

afterbody and with an afterbody. These represent more refined estimates than those presented in Fig. 8-18.

A second method of estimating total fin-body interference for all Mach numbers and unswept planforms ($0 < \beta(AR) < \infty$) was developed by Morikawa (References 19 and 20). This method gives the total interference, $K = K_{f(b)} + K_{b(f)}$, only when the trailing edge of the fin is unswept and flush with the base. Figs. 8-21(A)-(F) pre-

sent the total interference, $K = \frac{C_{N\alpha}}{C_{N\alpha f}}$ (ratio of

fin $C_{N\alpha}$ with interference to basic "isolated" fin), as a function of fin to body geometry, Mach number, and taper ratios from 0.0 to 1.0. This method is generally easier to use when compared to that previously presented and gives preferred data if the configuration being analyzed meets the stated restrictions.

8-2.4.3 Fin-Fin Interference

Cruciform fins—4 fins equally spaced around the body circumference—are the most common means of stabilizing free-flight rockets. In most cases, this type of fin provides the highest ratio of restoring moment to axial force. The data previously presented will permit the prediction of force and moment characteristics of this type of configuration. However, some designs might require more than four fins to obtain the necessary restoring moment. This could be particularly true for a configuration that was span-limited, with a center of gravity located farther aft than normal. The information below will permit reasonably accurate estimates for certain multi-finned configurations or planforms, and also serve as a guide in estimating the force and moment characteristics of other planforms.

The slender-body theory predicts that, at subsonic speeds, the ratios of the normal-force coefficient gradients for eight and six fin—equally spaced around the body circumference—to the gradient for twin fins—4 fins, 2 equally loaded—are 1.62 and 1.37, respectively. Thus for speeds from subsonic up to sonic, the following relations are expected to apply:

$$\frac{C_{N\alpha \ 6 \ fins}}{C_{N\alpha \ 4 \ fins}} = 1.37$$

and

$$\frac{C_{N\alpha \ 8 \ fins}}{C_{N\alpha \ 4 \ fins}} = 1.62$$

where $C_{N\alpha \ 4 \ fins}$ can be determined from methods previously presented, and the center of pressure may be assumed at 25 percent of the mean aerodynamic chord \bar{c} , measured from the fin leading edge.

At supersonic speeds, shock waves from the leading edge can be expected to impinge on adjacent surfaces, causing considerable interference. Wind tunnel tests (Reference 21) on a series of clipped-delta planforms were conducted, and a correlation parameter determined. This correlation parameter is defined as follows:

$$I = \frac{c_{rc}}{\beta d_c \sin \frac{\pi}{n}} \quad (8-23)$$

where

$$\begin{aligned} c_{rc} &= \text{exposed root chord} \\ \beta &= \sqrt{M^2 - 1} \\ d_c &= \text{body diameter} \\ n &= \text{number of fins} \end{aligned}$$

This parameter is shown as the abscissa in Fig. 8-22. The ordinate represents the value of $C_{N\alpha}$, based on an effective area S_{eff} , which is a function of the number of fins n , in accordance with the table below:

No. of fins n	$\frac{I}{S_j}$
4	1.63
6	2.43
8	3.24

S_j is the exposed area of a single fin.

Thus, data for a multi-finned configuration may be obtained by computing the parameter I , entering Fig. 8-22 at this value of I and reading

AMCP 706-219

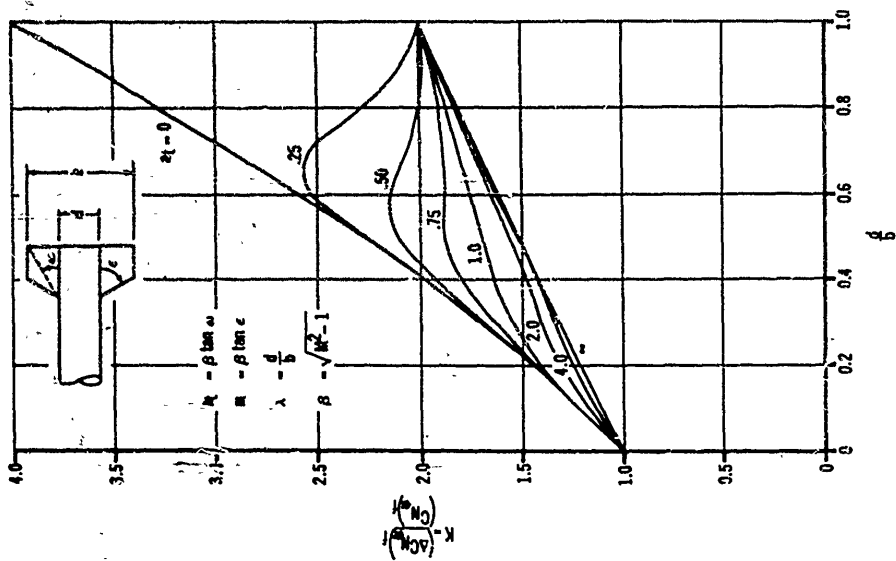


Figure 8-21(B). Lift of Fin (Body) for $a_f/m = 0.2$
(Clipped Delta Fin)

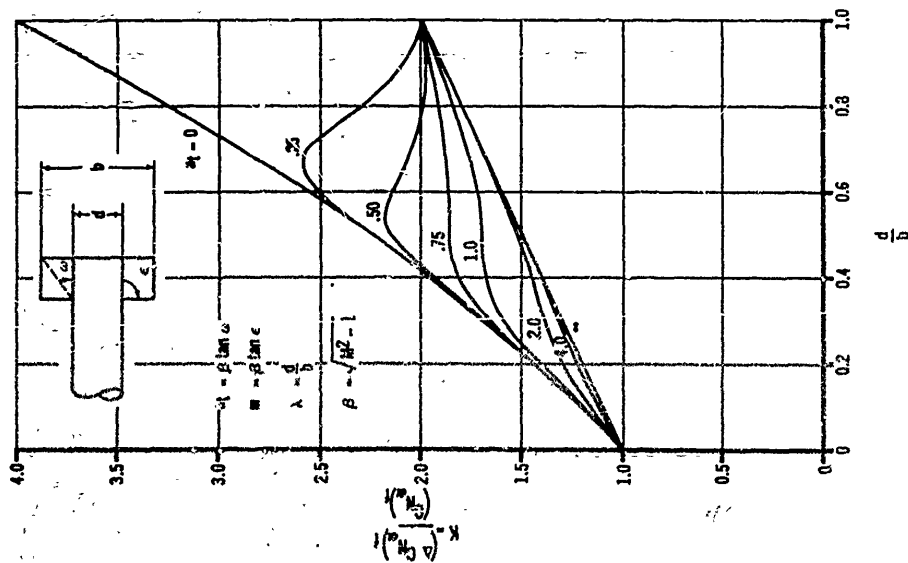


Figure 8-21(A). Lift of Fin (Body) for $a_f/m = 0$
(Rectangular Fin)

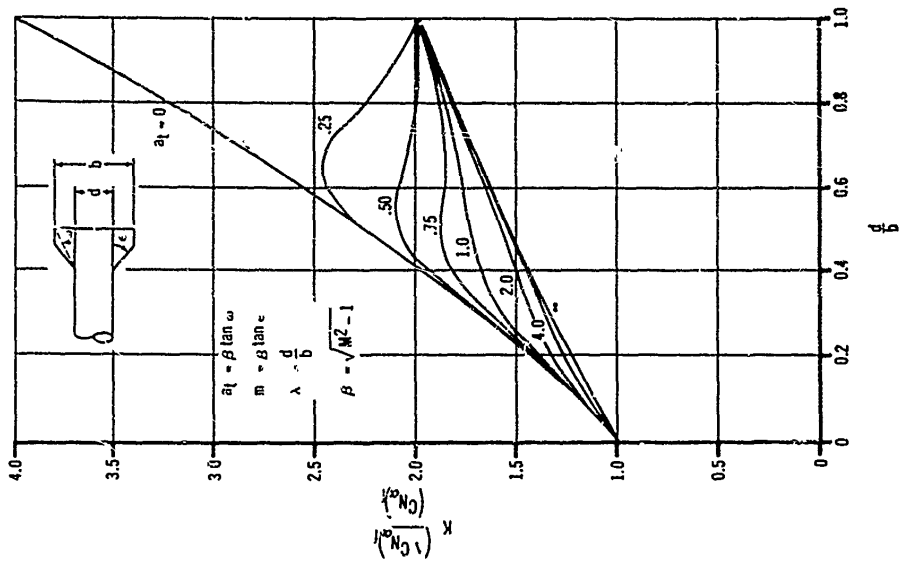


Figure 8-21(D). Lift of Fin (Body) for $\alpha_r/m = 0.6$ (Clipped Delta Fin)

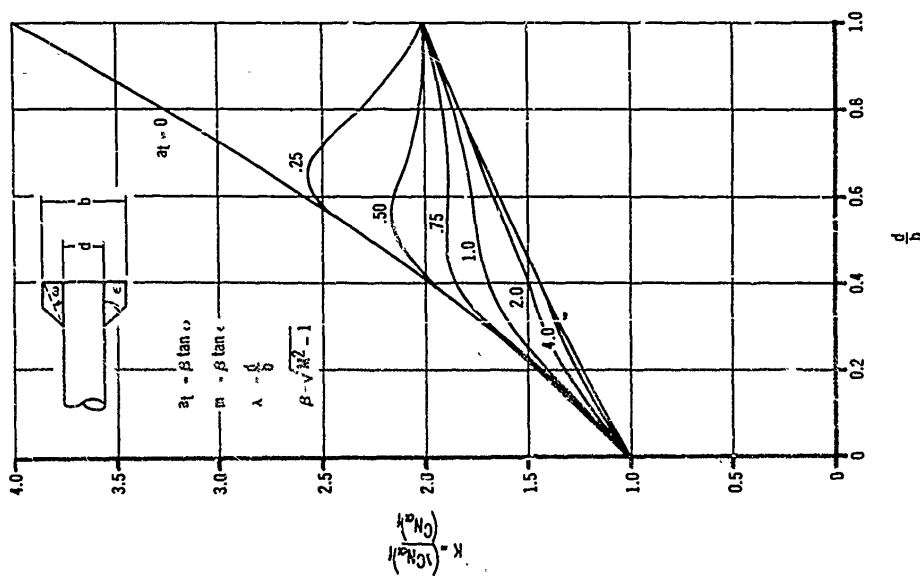


Figure 8-21(C). Lift of Fin (Body) for $\alpha_r/m = 0.4$ (Clipped Delta Fin)

AMCP 705-200

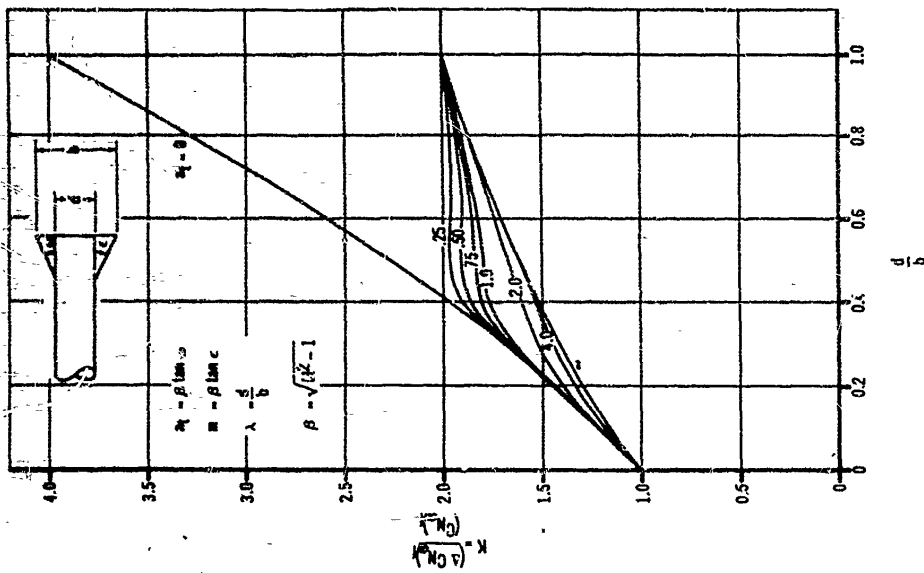


Figure 8-21(F). Lift of Fin (Body) for $a_f/m = 1.0$ (Delta Fin)

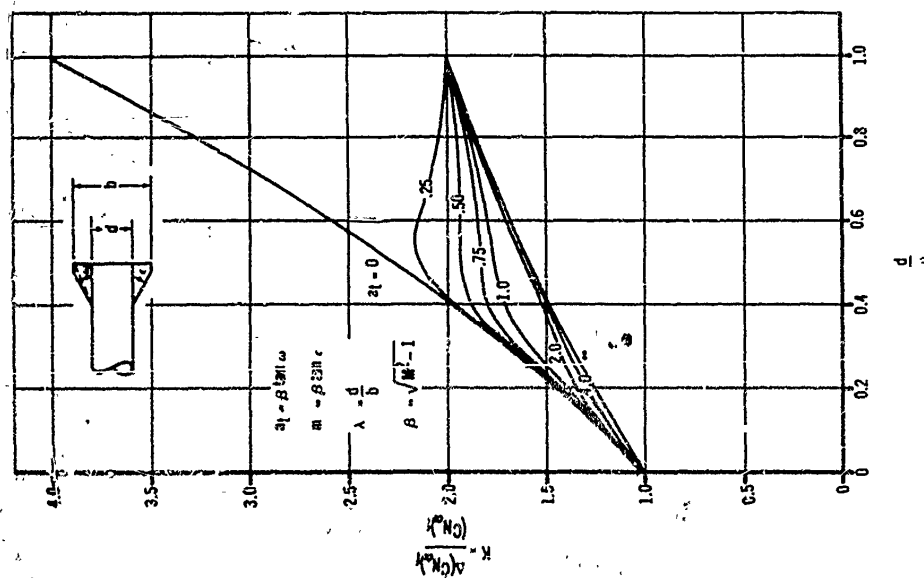


Figure 8-21(E). Lift of Fin (Body) for $a_f/m = 0.8$ (Clipped Delta Fin)

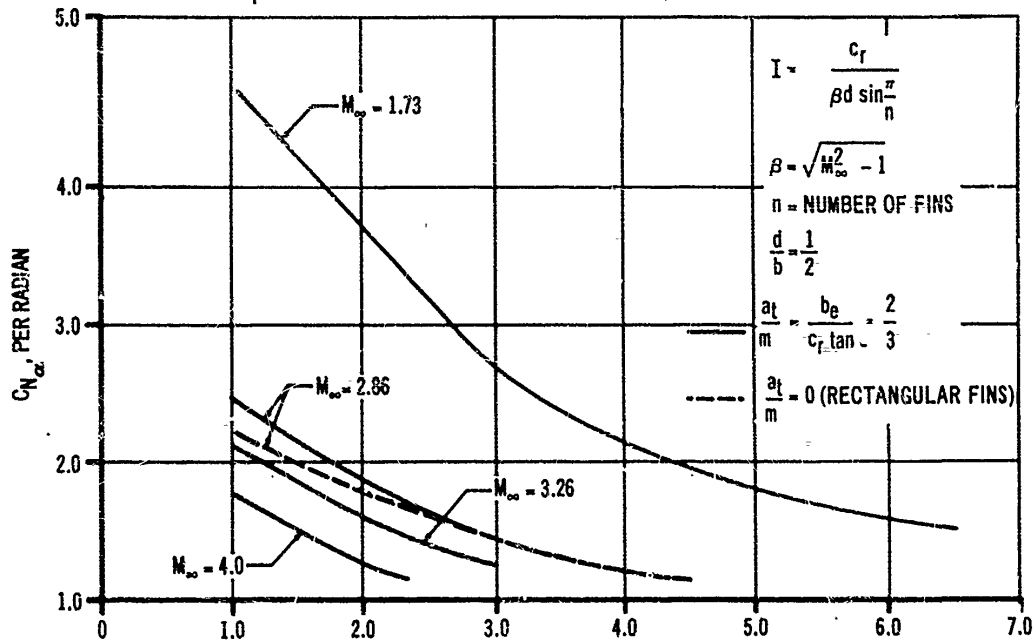
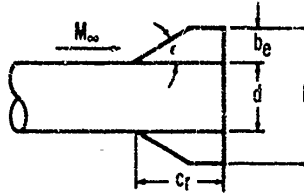
REFERENCE AREA = S_{eff} (EFFECTIVE AREA)

$$\frac{S_{eff}}{S_f} = 1.63 \text{ (4 FINS)}$$

$$\frac{S_{eff}}{S_f} = 2.43 \text{ (6 FINS)}$$

$$\frac{S_{eff}}{S_f} = 3.24 \text{ (8 FINS)}$$

S_f = PLANFORM AREA OF SINGLE FIN



CORRELATION PARAMETER FOR FIN-FIN INTERFERENCE, I

Figure 8-22. Normal Force Coefficient Gradient of Multiple Fins at Supersonic Speeds

$C_{N_{\alpha \text{ fin}}}$ for the appropriate Mach number. Then, multiplying the value of $C_{N_{\alpha \text{ fin}}}$ by the appropriate value of S_{eff}/S_f (dependent on number of fins) yields the total fin contribution, based on a reference area equal to the exposed planform area of one fin. It should be emphasized that the data in Fig. 8-22 were developed for, and are directly applicable only to, the particular planforms indicated. However, the data may be used as a guide for predicting the characteristics of other planforms.

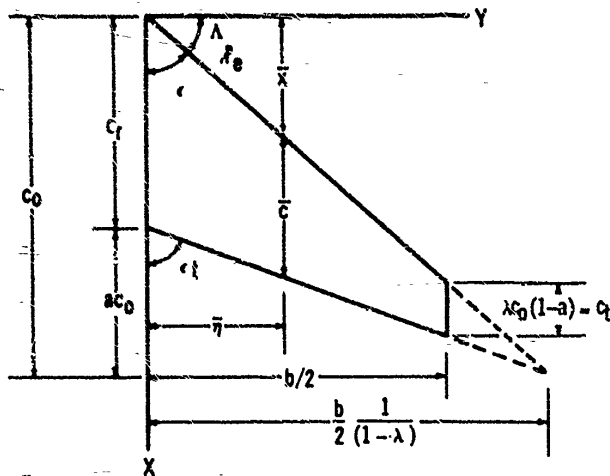
When the value of I is less than one, the Mach cone emanating from the leading edge of one fin does not impinge on adjacent fins. Therefore, the ratio of the multi-fin normal-force coefficient

gradient to the twin-fin gradient (4 fins, 2 equally loaded) is a function of the number of fins only, and can be written as

$$\left. \begin{aligned} \frac{C_{N_{\alpha \text{ 6 fins}}}}{C_{N_{\alpha \text{ 4 fins}}}} &= 1.50 \\ \frac{C_{N_{\alpha \text{ 8 fins}}}}{C_{N_{\alpha \text{ 4 fins}}}} &= 2.00 \end{aligned} \right\} \text{ for } I < 1$$

and the four-fin data may be computed by methods previously presented.

AMCP 705-280



$$\lambda = \text{TAPER RATIO} = c_t/c_r$$

$$a = \text{CUTOUT FACTOR} = \text{TAN } \epsilon_c / \text{TAN } \epsilon_t$$

FIN AREA (S_f)

$$S_f = \frac{bc_0}{2} (1-a)(1+\lambda) \\ = c_0^2 \text{TAN } \epsilon (1-a)(1+\lambda^2)$$

ASPECT RATIO (AR)

$$AR = \frac{b^2}{S_f} = \frac{4 \text{TAN } \epsilon (1-\lambda)}{(1-a)(1+\lambda)}$$

CUTOUT FACTOR

$$a = \text{TAN } \epsilon_c / \text{TAN } \epsilon_t$$

$$= 1 - \frac{4(1-\lambda) \text{TAN } \epsilon}{AR(1+\lambda)}$$

SWEEP ANGLES

$$\text{TAN } \epsilon_c = a \text{TAN } \epsilon_t = \frac{b}{2c_0(1-\lambda)} = \frac{3+a}{4 \text{TAN } \Lambda_c/4}$$

$$\text{TAN } \Lambda_{kc} = \text{TAN } \Lambda_c/4 + \frac{(1-4k)(1-\lambda)}{AR(1+\lambda)}; k = \text{PERCENT CHORD FOR DESIRED SWEEP}$$

MEAN AERODYNAMIC CHORD

$$c = (2/3)c_0 (1-a) \left(1 + \frac{\lambda^2}{1+\lambda}\right) = 4/3 \sqrt{\frac{S_f}{AR}} \left(\frac{1}{1+\lambda}\right) \left(1 + \frac{\lambda^2}{1+\lambda}\right)$$

$$\bar{x} = 1/3 \left(\frac{1+2\lambda}{1+\lambda}\right); \bar{x} = \bar{x} \left(\frac{b}{2}\right) \text{TAN } \Lambda_c/4$$

Figure 8-23. Fin Geometry

Supersonically, the center of pressure may be assumed⁸ at the mid-point of the mean aerodynamic chord \bar{x} , measured rearward from the leading edge of the fin.

8-2.4.4 Sample Calculation Sheet

Table 8-1 was constructed to summarize the principles and formulas presented in par. 8-2 Stability Characteristics of Rockets. The table also illustrates in numerical examples the use of the formulas and data curves presented in par.

8-2. Fig. 8-23 gives the geometric relationships for computation of fin geometry. Fig. 8-24 defines lengths and diameters associated with boat-tail, flare, and finned configurations. Finally, Fig. 8-25 presents an example configuration, with pertinent design data, as a basis for computation of force and moment characteristics. Entries shown in Table 8-1 were developed for this configuration. The superscript circled numbers appearing in Table 8-1 indicate that values for the expressions so annotated come from the column number corresponding to the superscript.

AMCP 706-280

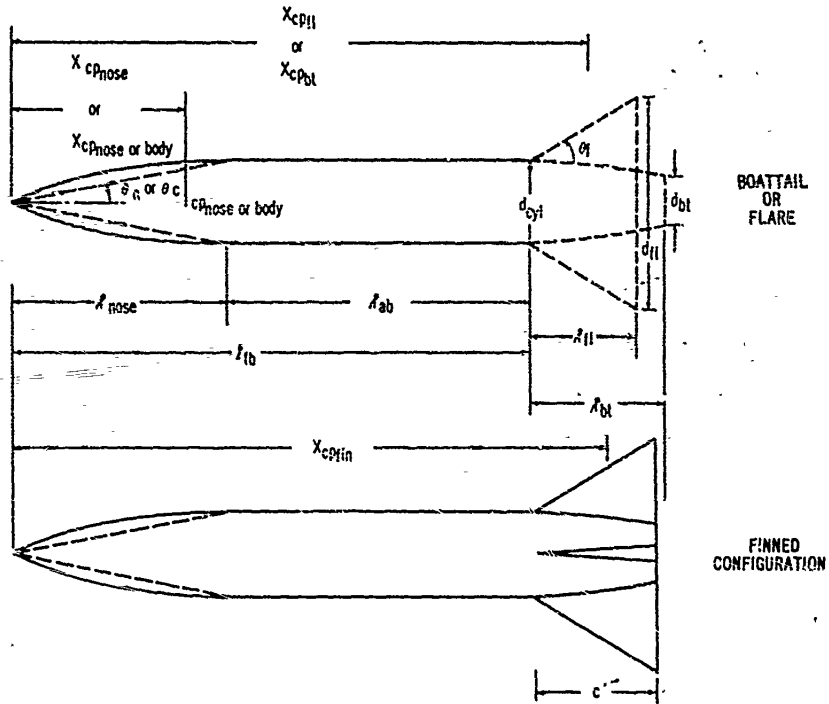
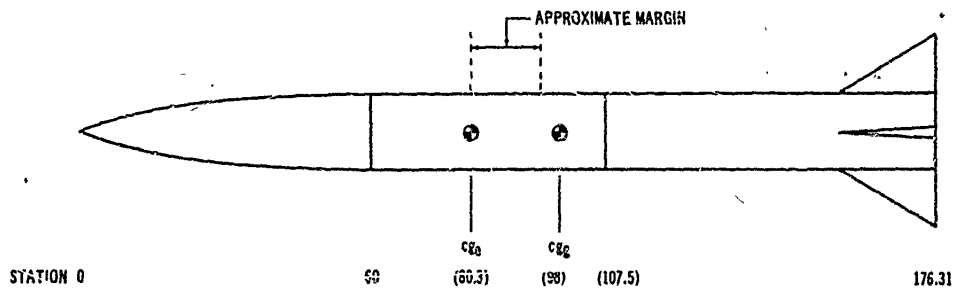


Figure 8-24. Body Geometry



DESIGN DATA	
BODY	FIN
1. $0 < \text{Mach NO.} < 4.5$	5. DESIGNED TO PROVIDE ONE CALIBER OF STATIC MARGIN AT $M = 4.5$ (PLANFORM NOT OPTIMIZED).
2. $l_n = 4.0$ (TANGENT OGIVE)	6. $c_{Te} = 21.6''$
3. $l_{ab} = 7.76$	7. $\Delta \lambda_2 = 60^\circ$
4. $c_D = 15''$	8. $\Delta c/2 = 40.9^\circ$
5. $c_{B_{gross}} = 98''$	9. $\lambda_{Te} = 0$
6. $c_{B_{b.o.}} = 80.3''$	4. $S_f = 1.882 \text{ ft}^2$

Figure 8-25. Configuration and Design Data for Numerical Example

AMCP 704-200

8-3 DRAG

Estimation of drag for free rockets can be restricted to zero-lift since the rocket follows a ballistic path. The total drag on the rocket is the sum of the wave drag produced by pressure forces normal to all surfaces except the base, plus the skin friction drag produced by forces tangential to the surfaces, plus the base drag produced by pressure forces acting normal to the base. The drag coefficient C_D is equal to the drag force D in pounds divided by $1/2\rho V^2 S_{ref}$, where ρ is the atmospheric density in slugs per ft³, V is the rocket velocity in ft per sec, and S_{ref} is the reference area, in square feet, on which C_D is based.

8-3.1 WAVE DRAG

Wave drag is present on the rocket nose, the afterbody (boattail or flare), and the fins or other stabilizing surfaces. Since wave drag is produced by pressures normal to the surface, no wave-drag component is present on the cylindrical section.

8-3.1.1 Nose Wave Drag

The nose shapes of free rockets are usually slender since there are no large volume requirements to enclose guidance systems or related components. Blunting the nose with a radius equal 0.1 times the maximum body diameter avoids a sharp point for manufacturing and safety reasons, yet causes only a negligible increase in drag and has no appreciable effect on aerodynamic estimates.

Nose wave drag is influenced primarily by fineness ratio, nose shape, and Mach number. The general trend of nose wave-drag characteristics is shown in Figs. 8-26(A) and (B). For most slender nose shapes, the coefficient is zero below a Mach number of about 0.8 to 0.9; rises sharply through the transonic region; and decreases with increasing supersonic Mach number. The coefficient decreases with increasing nose fineness ratio. However, in practical design, nose fineness ratios are limited by rocket total-length requirements, weight requirements, and increasing friction drag.

For preliminary design estimates, the family of nose shapes-of-interest for free rockets is bounded

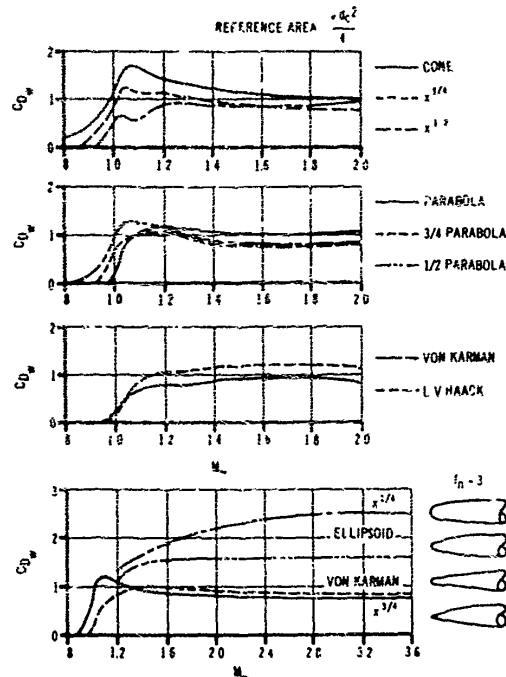


Figure 8-26(A). Effects of Mach Number and Nose Fineness Ratio on Wave Drag

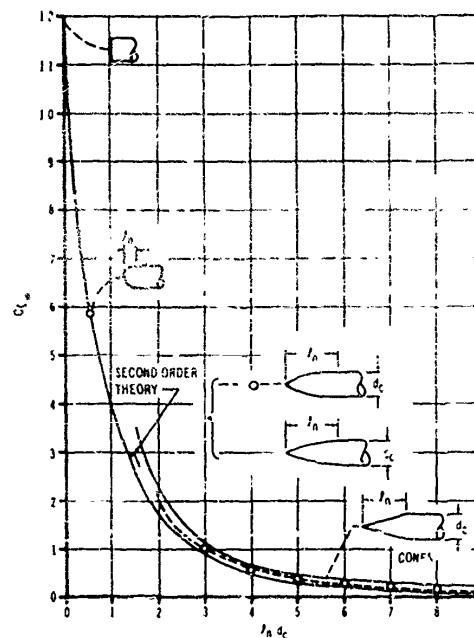


Figure 8-26(B). Effects of Mach Number and Nose Fineness Ratio on Wave Drag

AMCP 706-280

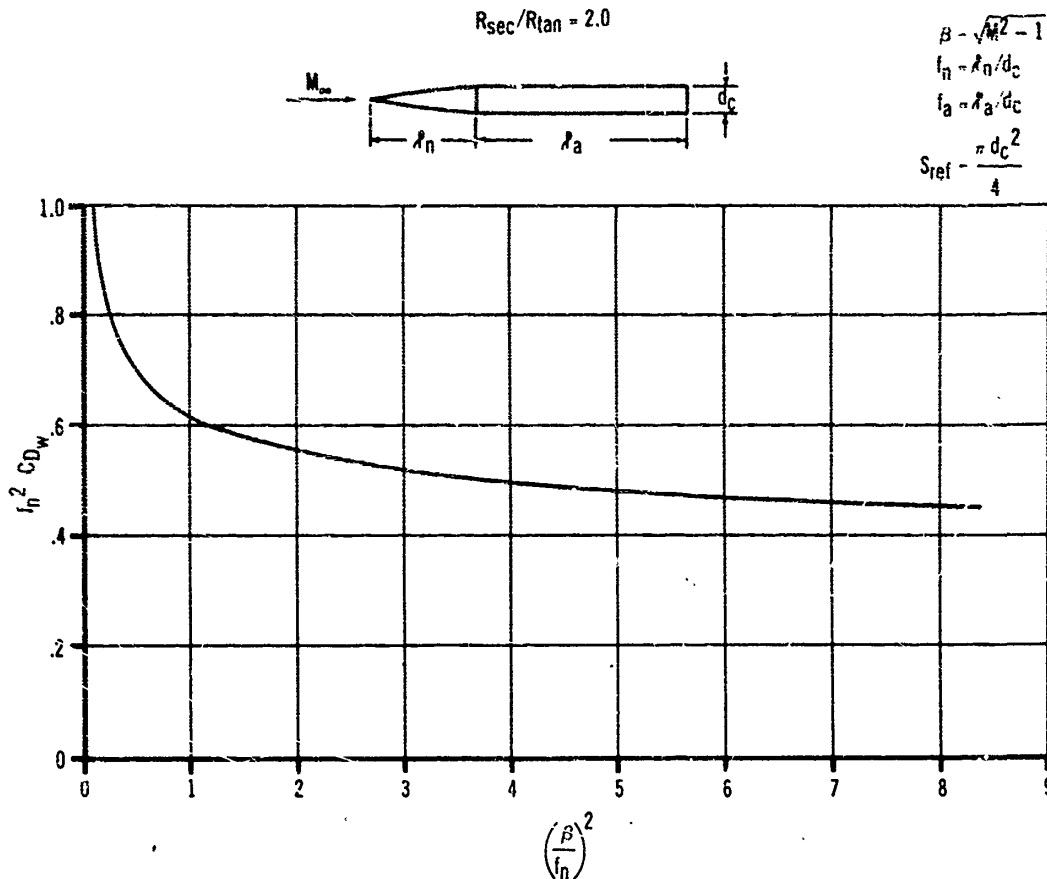


Figure 8-27. Wave Drag Coefficient of Optimum Secant Ogive Cylinder at Transonic Speed

by cones and ogives. A secant ogive, formed by a circular arc with twice the radius of a tangent ogive, yields minimum wave drag for low supersonic Mach numbers (Reference 22); drag characteristics of this nose shape are presented in Fig. 8-27. For higher Mach numbers, a secant ogive with 2.5 to 3 times the radius of a tangent ogive is optimum. However, when optimizing overall-configuration nose shape, factors other than drag must be considered.

The transonic wave-drag coefficient of general ogives is presented in Fig. 8-28. Unfortunately, there is no apparent, reliable correlation of transonic wave-drag for cones. It is suggested that estimates be guided by Fig. 8-26 and other experimental data, such as References 23 and 24.

Values of supersonic wave drag for cones and general ogives are presented in Fig. 8-29 as a more detailed extension of values presented in Fig. 8-26.

8-3.1.2 Boattail Wave Drag

When the exit diameter of the rocket nozzle is smaller than the body-cylinder diameter, the afterbody of the rocket may be tapered to form a boattail and reduce the base drag. This technique, however, increases the wave drag on the configuration. An optimum boattail configuration, therefore, results from balancing the increase in wave drag with the reduction of base drag.

AMCP 700-200

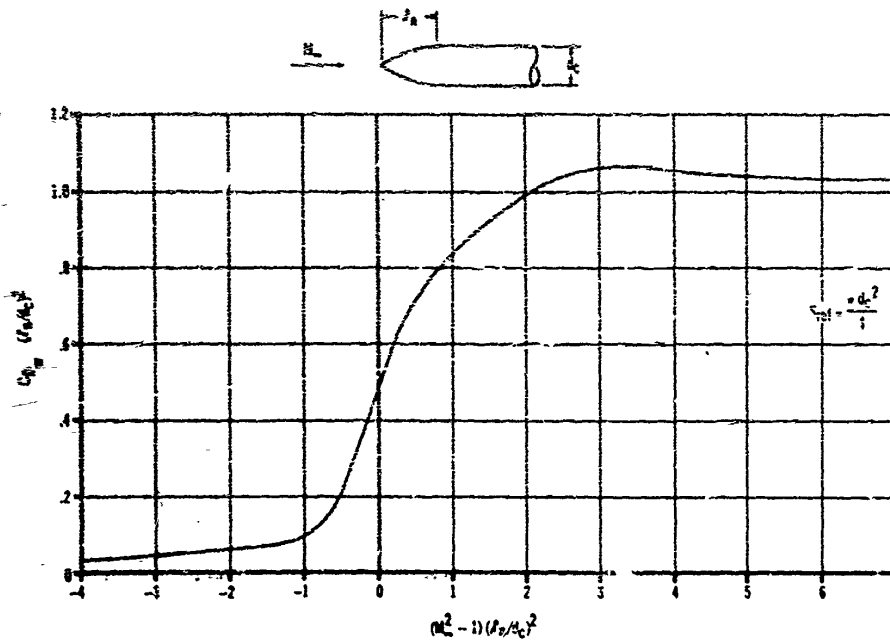


Figure 8-28. Wave Drag Coefficient of Slender Ogives at Transonic Speeds

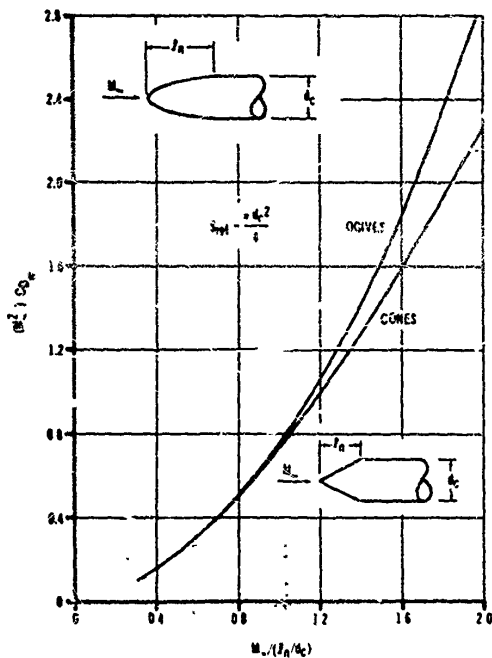


Figure 8-29. Wave Drag Coefficient of Cones and Ogives at Supersonic Speeds

The supersonic wave drag of conical and parabolic boattails is presented in Figs. 8-30 and 8-31. No analytical method or suitable parametric experimental data exist for accurate prediction of boattail wave drag at subsonic and transonic speeds. If experimental data for a particular configuration cannot be found, it is suggested that supersonic data be extrapolated to peak value at a Mach number of 1.0 to 1.2, with a sharp reduction to a lower value at subsonic speeds. A curve of boattail wave drag, to act as a guide, is shown in Fig. 8-32.

8-3.1.3 Flare Wave Drag

Flared afterbodies are useful for rocket stabilization where precise stability margin control is required. The drag on flares, however, is higher than the drag on fins giving equivalent stabilization. Parametric experimental data and several theoretical methods, which agree well with experimental results, are available for estimating flare wave drag. Care should be exercised in the use of experimental data for large flare angles since flow separation at the cylinder-flare juncture may be more pronounced in some

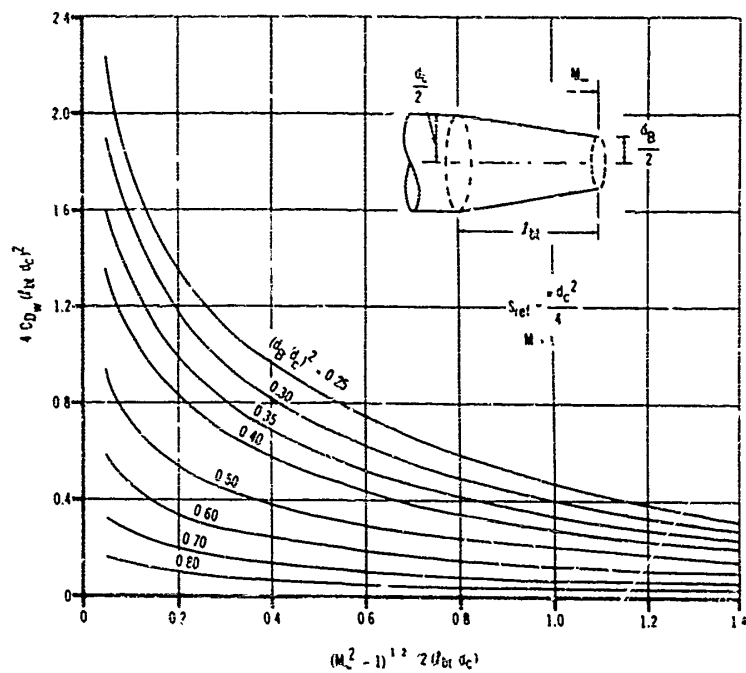


Figure 8-30. Wave Drag Coefficient of Conical Boattails at Supersonic Speeds

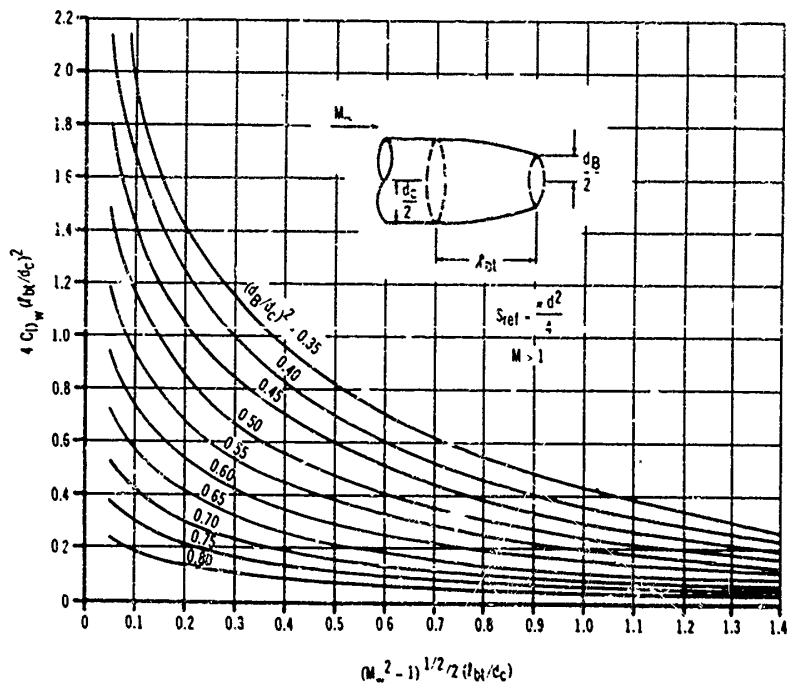


Figure 8-31. Wave Drag Coefficient of Parabolic Boattails at Supersonic Speeds

AMCP 706-280

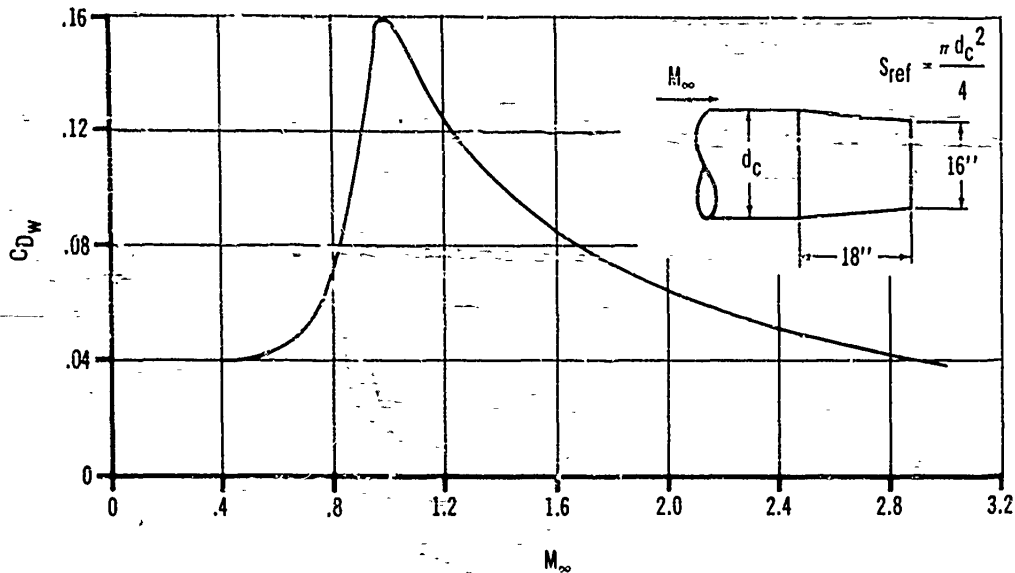


Figure 8-32. Wave Drag Coefficient of a Boattail at Transonic Speeds

tests where the Reynolds numbers are lower than would be expected in actual flight. The wave-drag coefficient determined experimentally (Reference 27) for a series of flares is presented in Figs. 8-33(A)-(I).

8-3.1.4 Fin Wave Drag

The wave drag on fins is small (on the order of 10 percent) compared to the total rocket drag. The drag is influenced strongly by thickness-to-chord ratio and sectional shape. Figs. 8-34(A)-(H) present the theoretical wave drag coefficient, based on planform area, at zero-lift for various sectional shapes and planforms. The discontinuities in the curves will not exist in practice, and values at transonic speeds are not precise. The wave drag for sectional shapes not shown in Fig. 8-34 may be evaluated as follows: in Fig. 8-34, find the wave drag coefficient for a double-wedge section having the same thickness and planform geometry as the sectional shape-of-interest; multiply the value so obtained by the factor for the particular shape from Fig. 8-35. The product will be the desired wave drag coefficient.

The transonic wave drag coefficient of rectangular and delta planform fins is shown in Figs.

8-36 and 8-37. The wave drag for other planforms will be between the values on these two curves for fins with the same sectional shape, thickness-to-chord ratio, and aspect ratio.

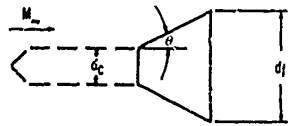
8-3.1.5 Ring Tail Wave Drag

The ring tail wave drag coefficient, based on an arbitrary reference area S_{ref} , may be evaluated by multiplying the two-dimensional drag coefficient by the product of ring-tail circumference times chord length (or "rolled out" planform area):

$$C_{D_v} = \frac{\pi d_r(c) (C_{D_v})_{(2 \text{ dimensional})}}{S_{ref}} \quad (8-24)$$

At supersonic speeds, the two-dimensional drag coefficients for particular sectional shapes may be obtained from Fig. 8-35. At transonic speeds, the two dimensional drag coefficient for a symmetrical double-wedge may be obtained from Fig. 8-38. For other sections, the double-wedge value should be multiplied by the appropriate modifying factor in Fig. 8-35.

The drag evaluated above will be slightly higher than the actual flight data due to the interfer-



$$S_{rel} = \frac{\pi d_c^2}{4}$$

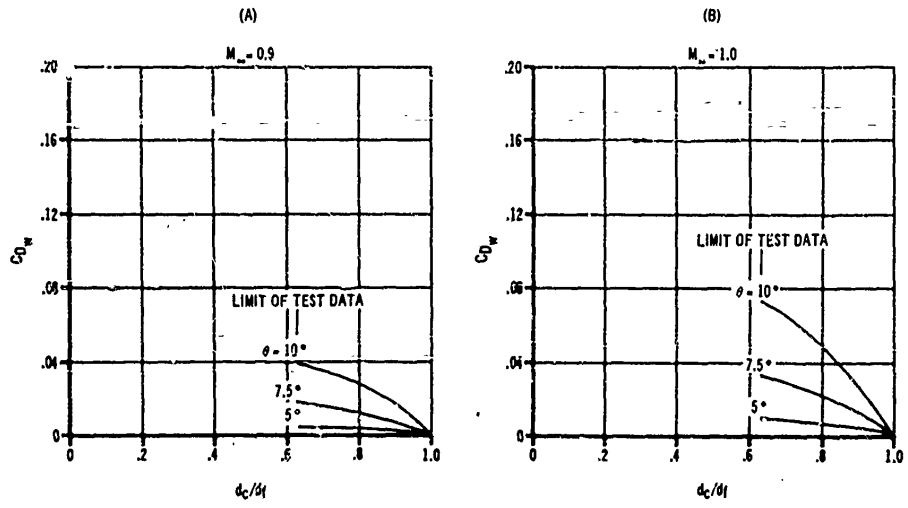
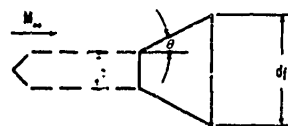


Figure 8-33(A) & (B). Wave Drag Coefficient of Conical Flare



$$S_{rel} = \frac{\pi d_c^2}{4}$$

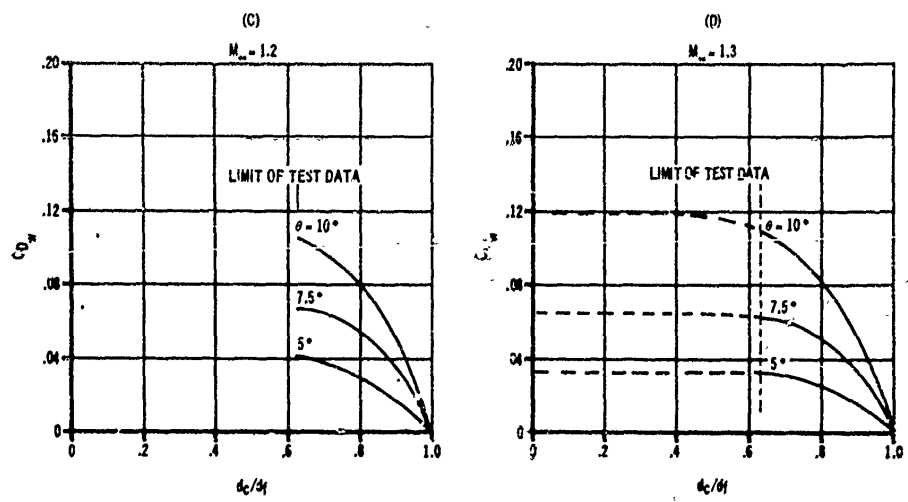


Figure 8-33(C) & (D). Wave Drag Coefficient of Conical Flare

AMCP 706-280

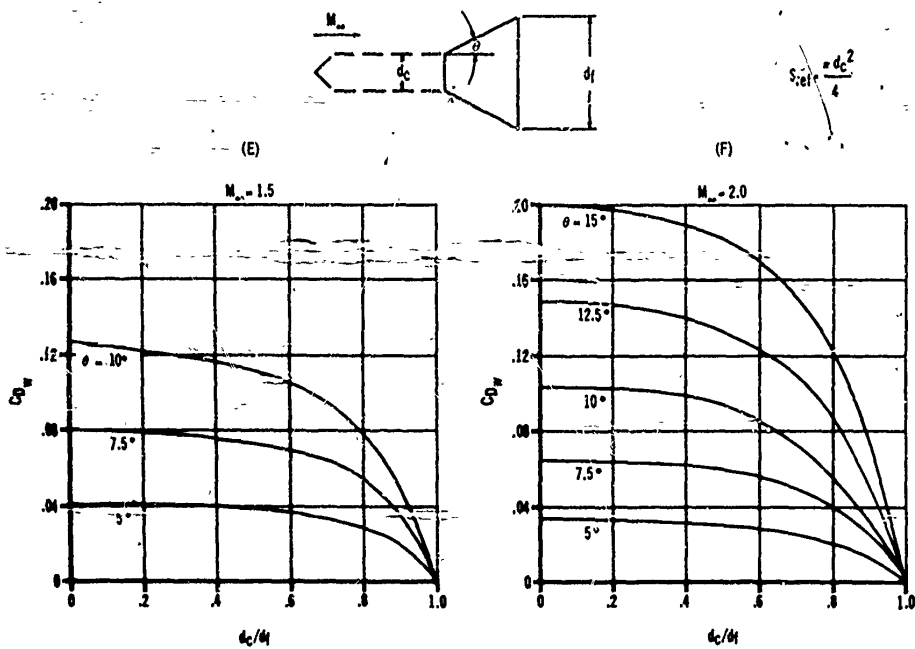


Figure 8-33(E) & (F). Wave Drag Coefficient of Conical Flare

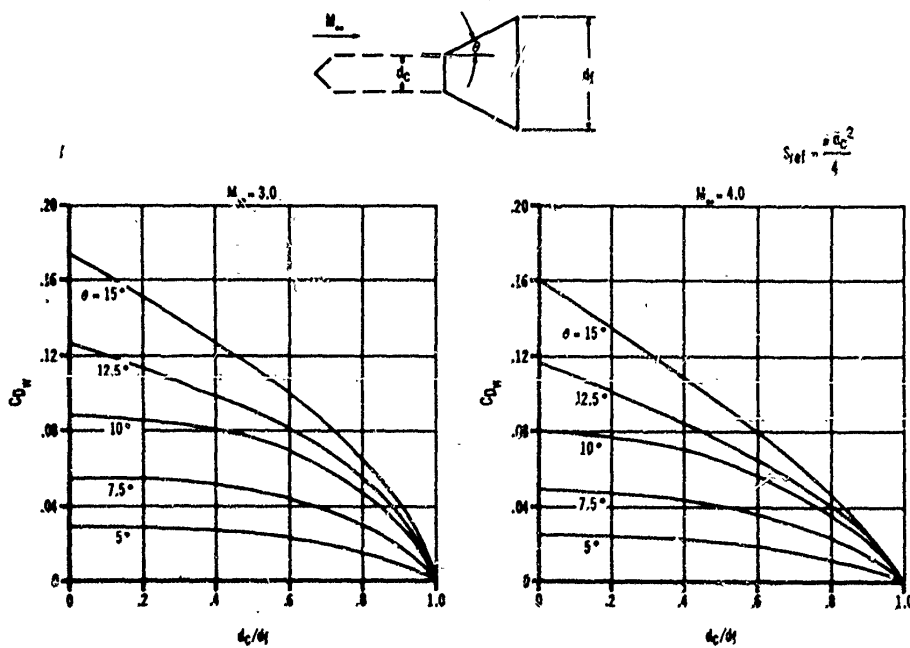


Figure 8-33(G) & (H). Wave Drag Coefficient of Conical Flare

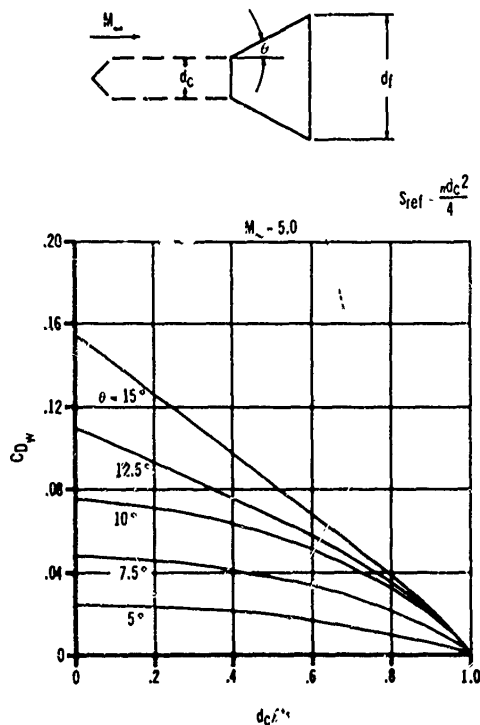


Figure 8-33(I). Wave Drag Coefficient of Conical Flare

ence effects of the struts attaching the ring tail to the rocket body. However, since these effects are small compared to the total rocket drag and the computation of the effects is complex, interference may be neglected for preliminary design.

For further discussion of interference, see Reference 25.

8-3.2 FRICTION DRAG

The friction drag depends primarily on conditions of heat transfer, position of transition from laminar to turbulent boundary layer, Reynolds number, and Mach number. The method presented in this paragraph for evaluating the friction-drag coefficient is a rapid approximate method. More precise solutions are presented in References 26 and 27.

The average skin-friction coefficient (friction-drag coefficient) for flat plates, based on the

wetted area, is presented in Fig. 8-39 as a function of Mach number and Reynolds number. Reynolds number per foot of length, as a function of Mach number and altitude, may be obtained from Fig. 8-40. The flat-plate coefficient should be used for fin and ring tail surfaces. Correlation of experimental data has shown that the skin-friction coefficient for bodies of revolution is approximately 15 percent higher than the flat-plate values (Reference 28). Therefore, for preliminary design purposes, the values obtained from Fig. 8-39 should be multiplied by 1.15 when the surface is a body of revolution.

8-3.3 BASE DRAG

Base drag is the result of pressure forces due to airflow separation from rearward-facing steps such as body bases and fin trailing edges. The drag is affected by the geometry of the rearward-facing step and by the properties of the airstream approaching the step, including boundary-layer conditions. A rocket exhaust complicates the base flow phenomenon by adding a second stream with different properties, boundary layer conditions, and approach geometry. The mixing of and interaction between the air and rocket exhaust streams produce a complex fluid mechanics problem.

General curves and empirical relations will be presented to allow a rapid estimation of base drag of a quality suitable for preliminary estimates. No attempt will be made to discuss in detail the effects of various parameters on base drag. Insufficient experimental data exist, throughout the range of parameters, to allow use of design charts.

8-3.3.1 Body-of-Revolution Base Drag, Rocket Jet Off

The boundary layer approaching the body base of free rockets is generally turbulent. For cylindrical afterbodies, the variation of base-pressure coefficient (negative of base-drag coefficient, based on the area seen by base pressure) with Mach number is well defined. For boat-tailed and flared afterbodies, several methods of estimating base pressures are presented in References 22 and 29. These methods, however, have

AMCP 706-280

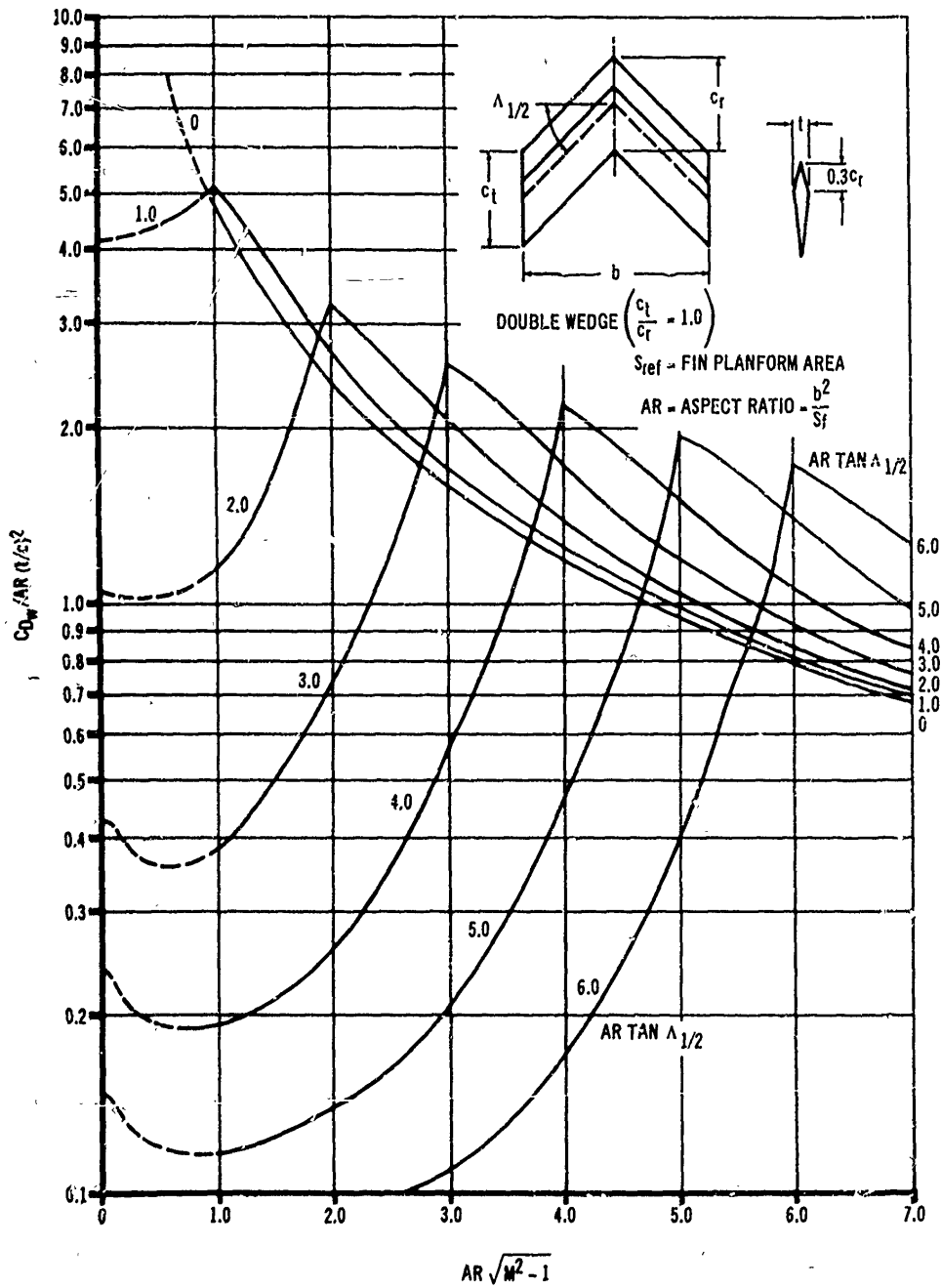


Figure 8-34(A). Wave Drag Coefficient of Fins at Supersonic Speeds

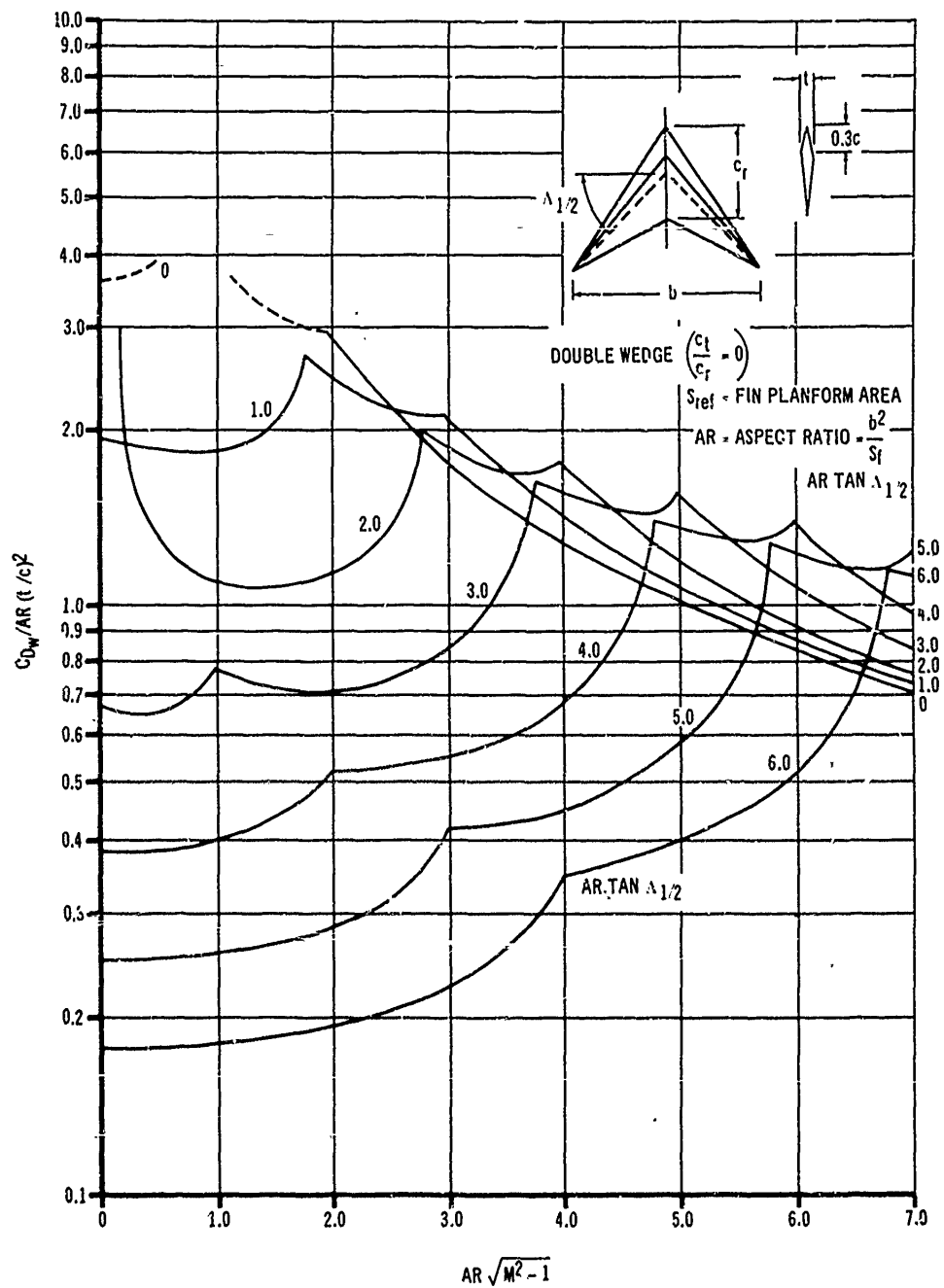


Figure 8-34(B). Wave Drag Coefficient of Fins at Supersonic Speeds

AMCP 706-280

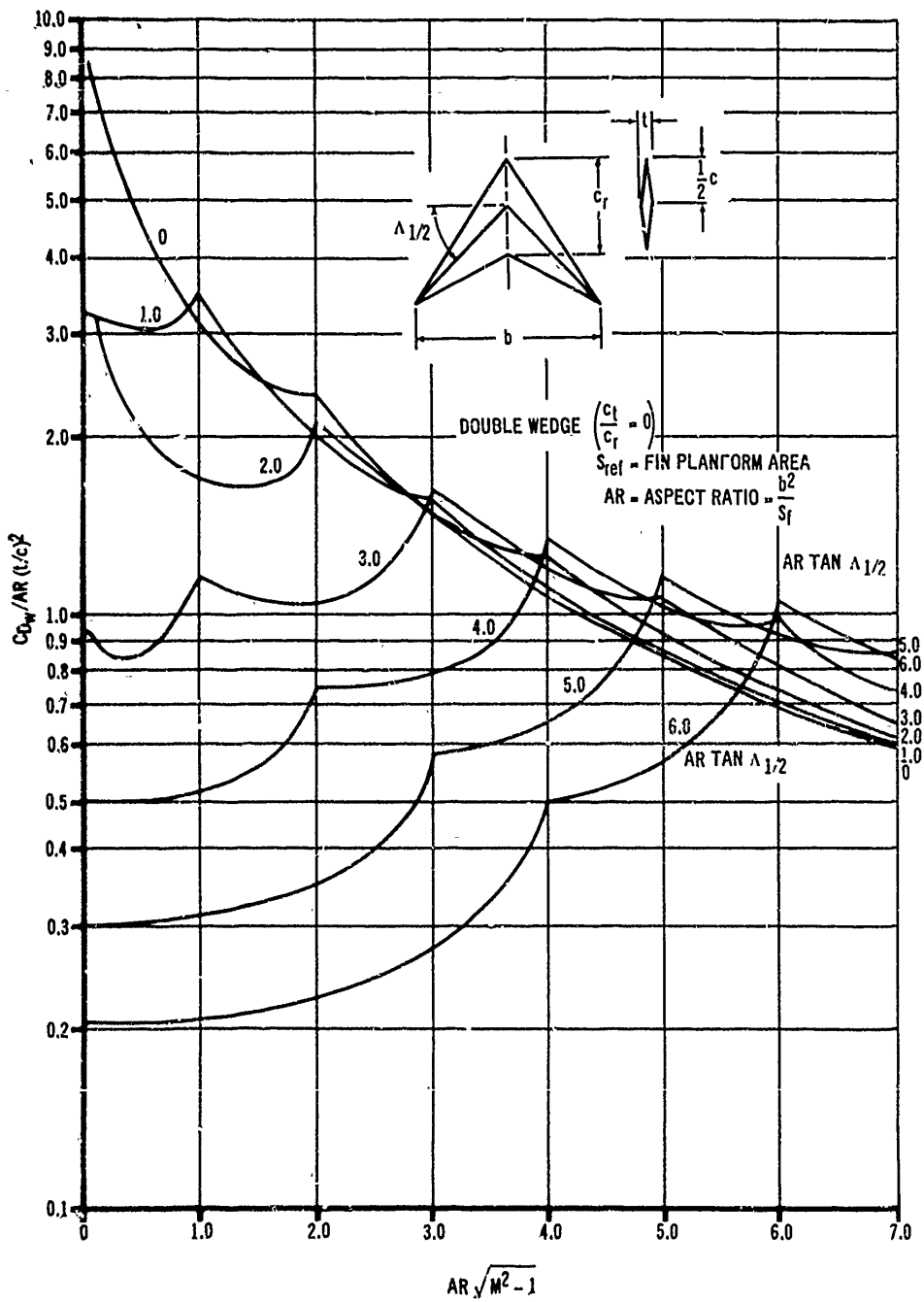


Figure 8-34(C). Wave Drag Coefficient of Fins at Supersonic Speeds

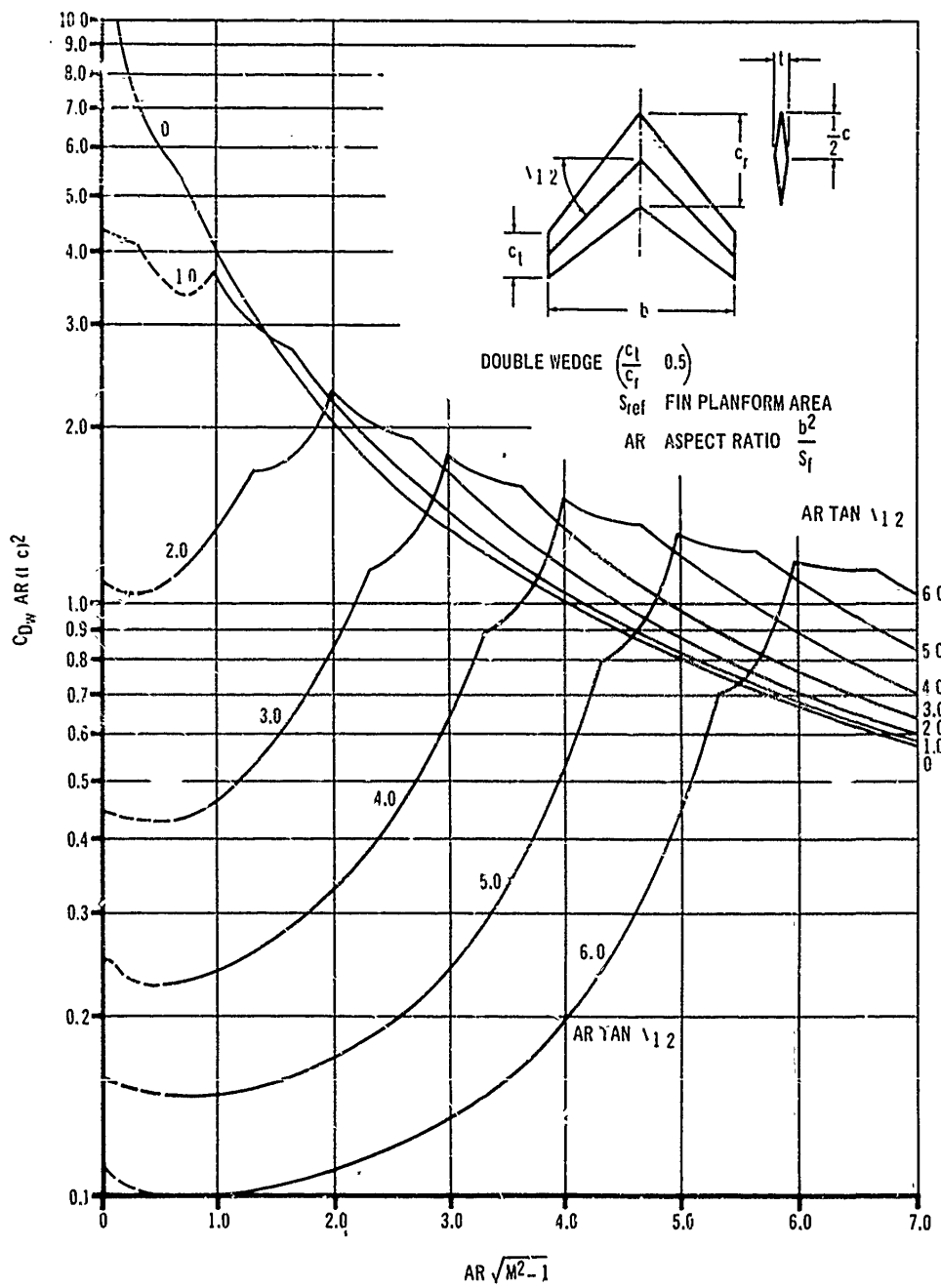


Figure 8-34(D). Wave Drag Coefficient of Fins at Supersonic Speeds

AMCP 706-280

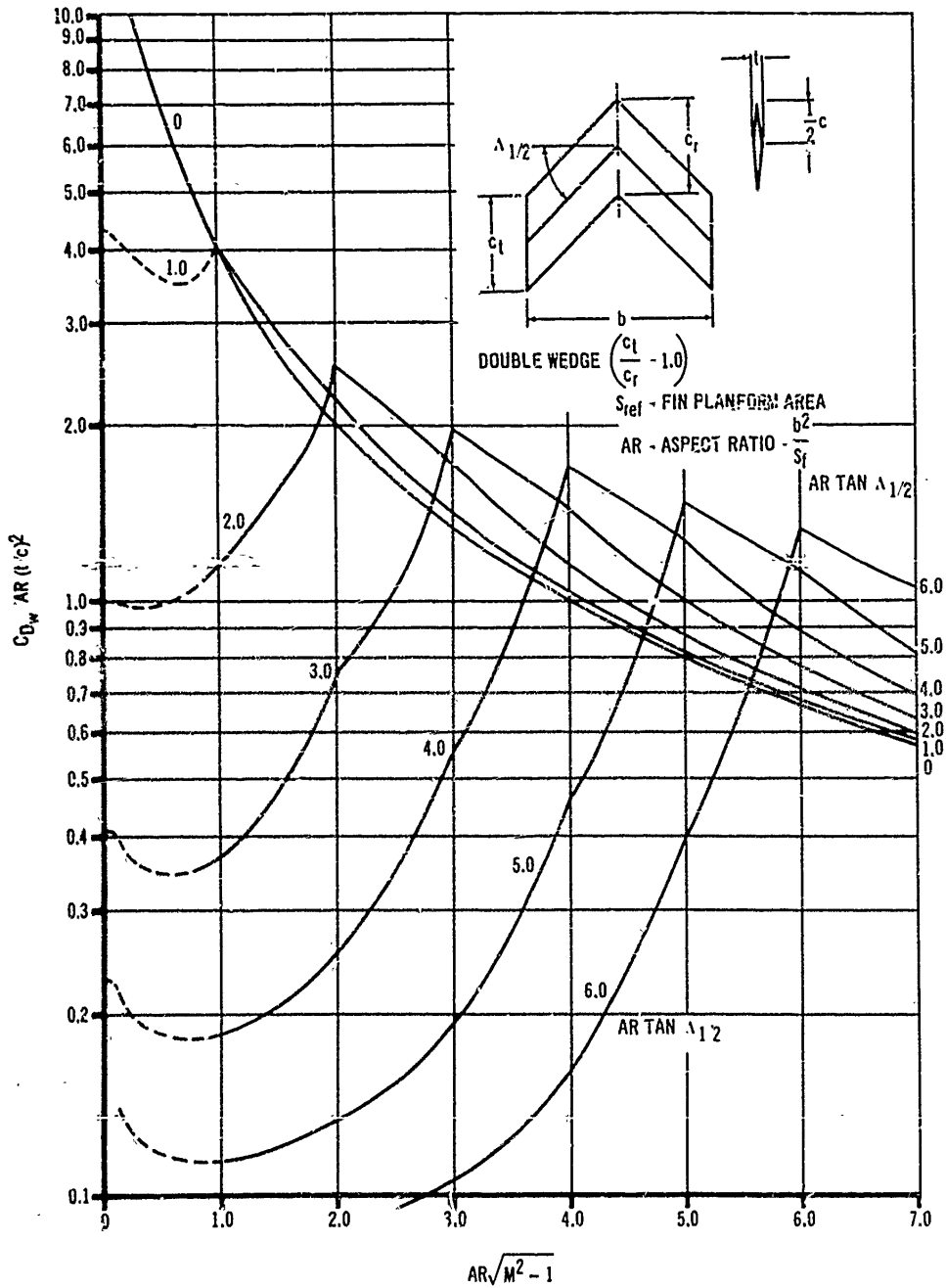


Figure 8-34(E). Wave Drag Coefficient of Fins at Supersonic Speeds

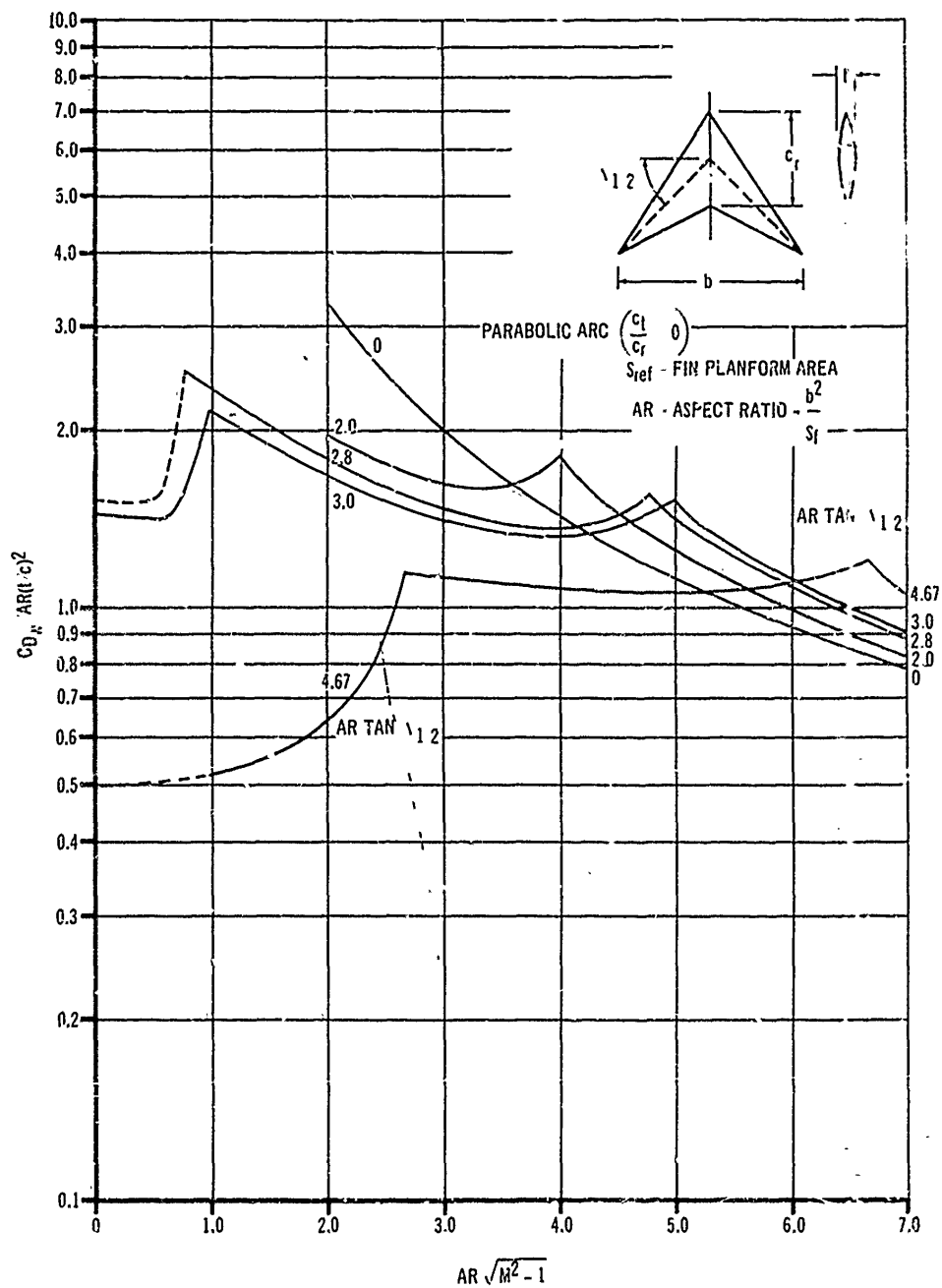


Figure 8-34(F). Wave Drag Coefficient of Fins at Supersonic Speeds

AMCP 706-280

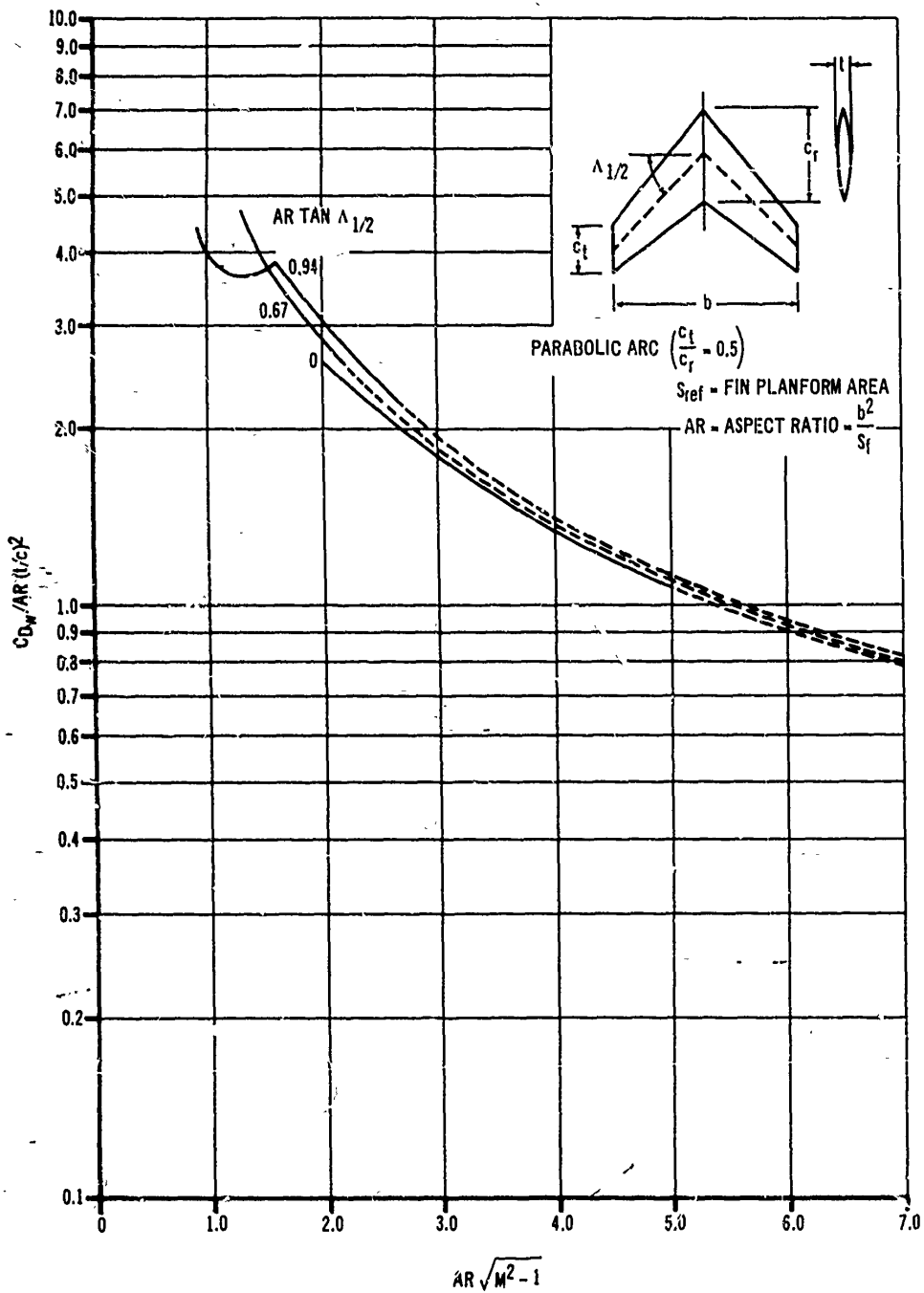


Figure 8-34(G). Wave Drag Coefficient of Fins at Supersonic Speeds

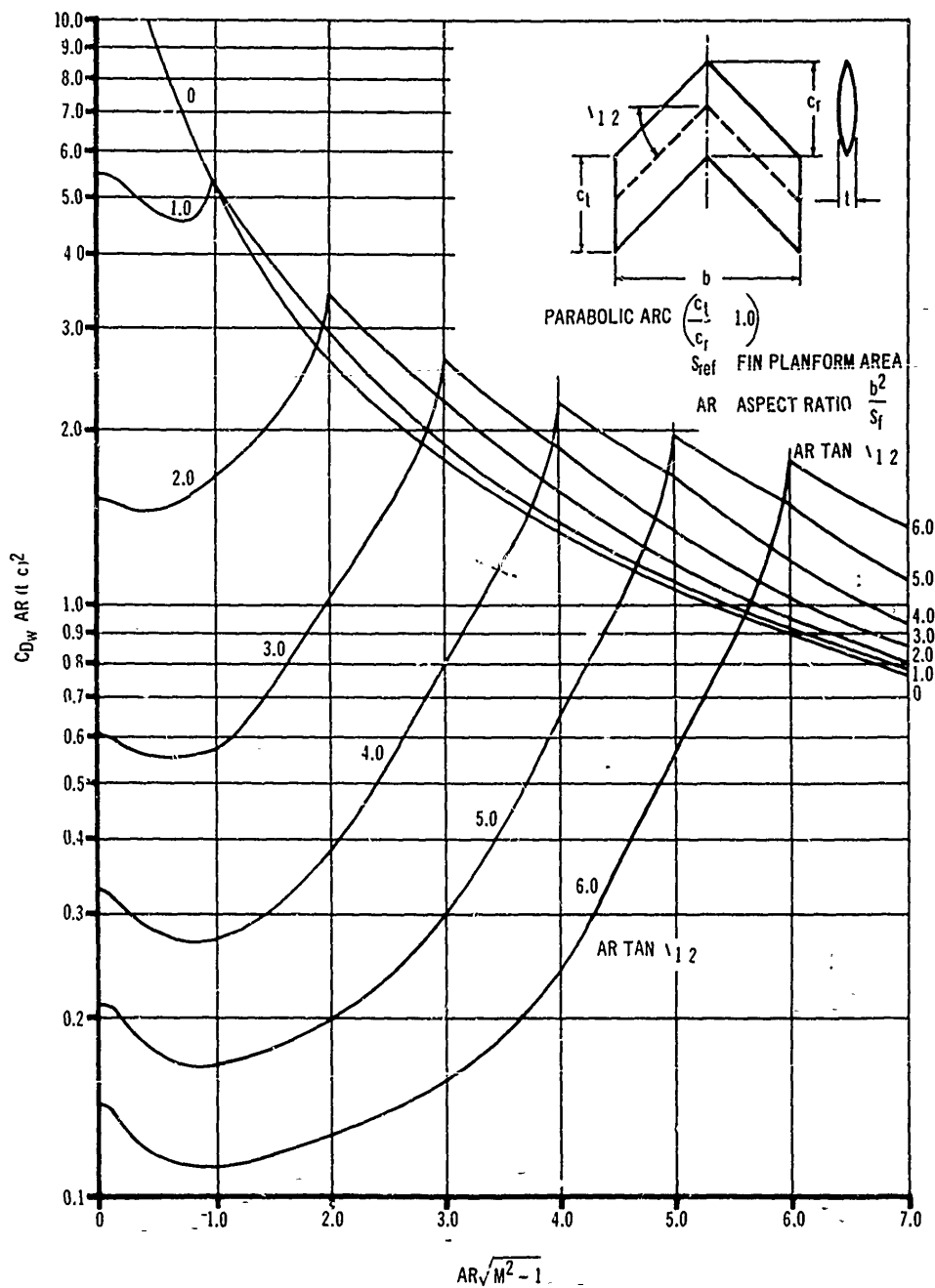


Figure 8-34(H). Wave Drag Coefficient of Fins at Supersonic Speeds

AMCP 708-280

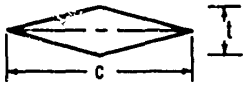
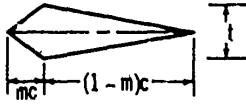
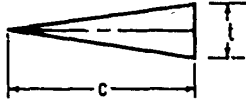
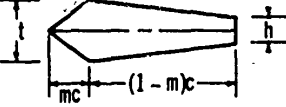
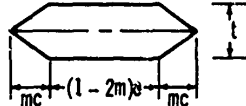

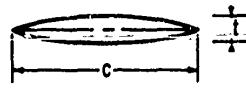
TYPE	PROFILE	TWO DIMENSIONAL DRAG COEFFICIENT BASED ON PLANFORM AREA	FACTOR
SYMMETRICAL DOUBLE WEDGE		$\frac{4}{M} \left(\frac{t}{c}\right)^2$	1
DOUBLE WEDGE		$\frac{1}{M} \left(\frac{t}{c}\right)^2 \cdot \frac{1}{m(1-m)}$	$\frac{1}{4m(1-m)}$
SINGLE WEDGE		$\frac{1}{M} \left(\frac{t}{c}\right)^2$	$\frac{1}{4}$
CROPPED DOUBLE WEDGE		$\frac{1}{M} \left[\left(\frac{t}{c}\right)^2 \cdot \frac{1}{m} + \frac{(t-h)^2}{c^2(1-m)} \right]$	$\frac{1}{4} \left[\frac{1}{m} + \frac{(1-h/t)^2}{1-m} \right]$
SYMMETRICAL PARALLEL DOUBLE WEDGE		$\frac{2}{M} \left(\frac{t}{c}\right)^2 \cdot \frac{1}{m}$	$\frac{1}{2m}$
PARALLEL DOUBLE WEDGE		$\frac{1}{M} \left(\frac{t}{c}\right)^2 \left[\frac{1}{m_1} + \frac{1}{m_2} \right]$	$\frac{1}{4} \left[\frac{1}{m_1} + \frac{1}{m_2} \right]$
SYMMETRICAL BICONVEX (CIRCULAR OR PARABOLIC ARCS)		$\frac{4}{M} \cdot \frac{4}{3} \left(\frac{t}{c}\right)^2$	$\frac{4}{3}$

Figure 8-35. Wave Drag Coefficient of Fins of Various Sectional Shapes

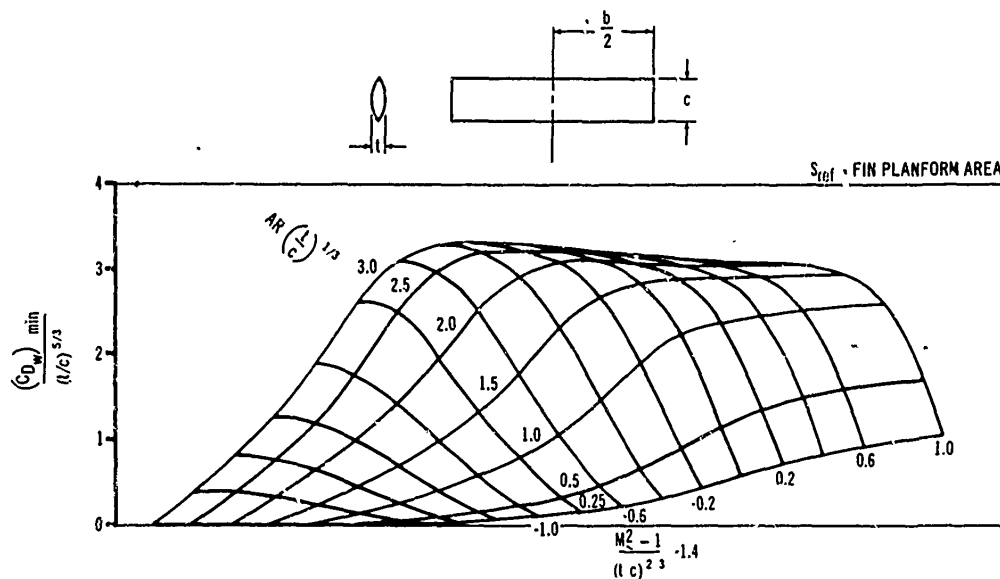


Figure 8-36. Wave Drag Coefficient of Rectangular Fins at Subsonic and Transonic Speeds

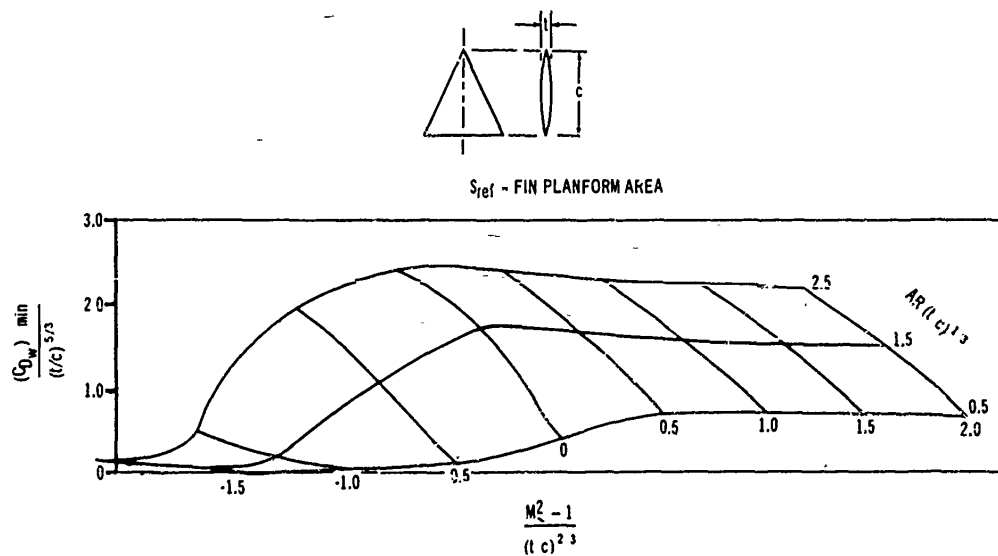


Figure 8-37. Wave Drag Coefficient of Delta Fins at Subsonic and Transonic Speeds

AMCP 706-280

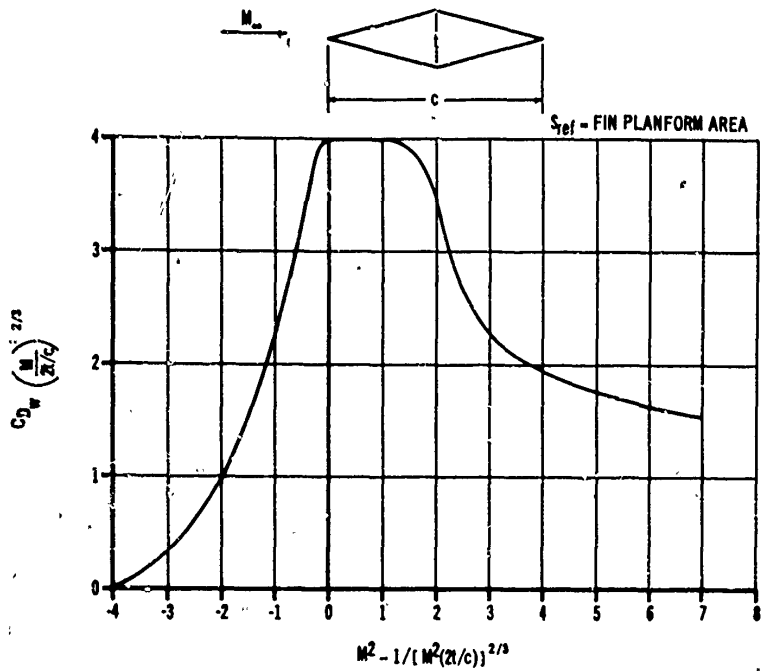


Figure 8-38. Wave Drag Coefficient of a Double Wedge Fin at Transonic Speeds

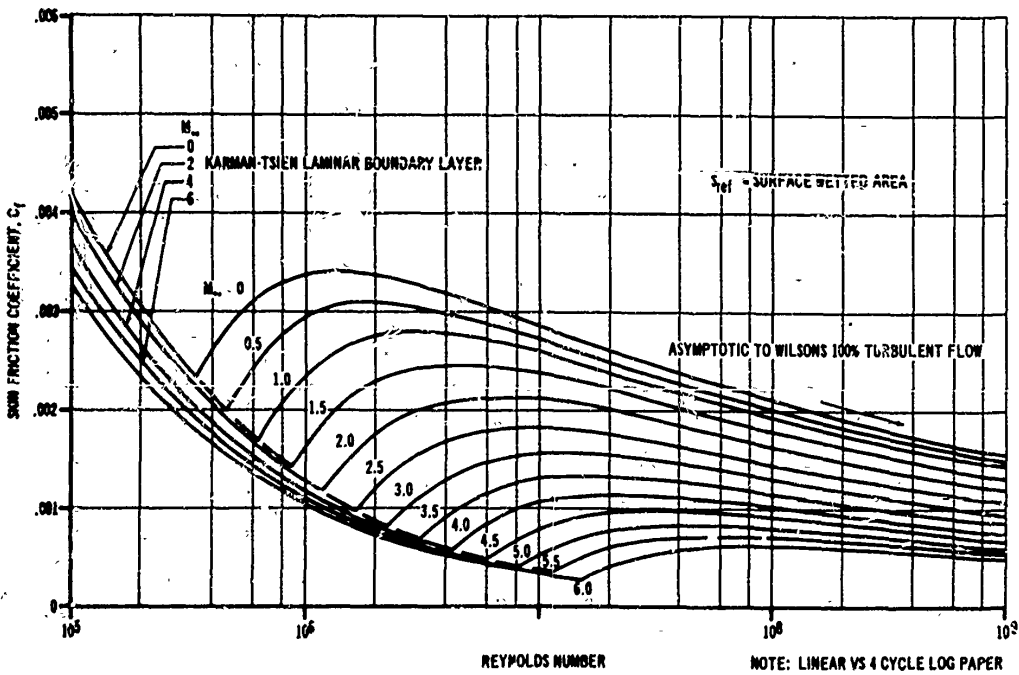


Figure 8-39. Flat Plate Average Skin Friction Coefficient

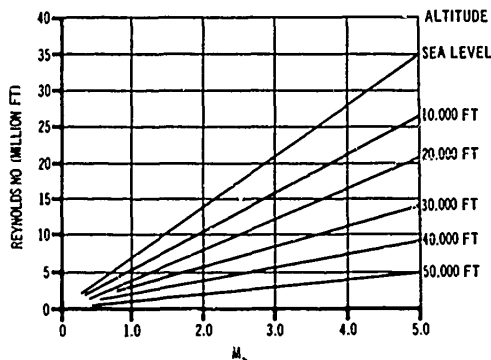


Figure 8-40. Reynolds Number as a Function of Flight Mach Number and Altitude

not been confirmed by experiment throughout the Mach-number range or through a sufficient range of afterbody geometric parameters.

The variation of base pressure with Mach number for a cylindrical body (based on experimental correlations) and boattailed or flared afterbodies is presented in Fig. 8-41. Although it is uncertain that afterbody angle is the major parameter affecting base pressure, it is presented in this manner for convenience. If nominal-length boattails and flares are considered, the data presented will be adequate for preliminary design purposes.

8-3.3.2 Body-of-Revolution Base Drag, Rocket Jet On

A typical example of the base pressure, with the effects of the rocket jet considered, is shown in Fig. 8-42. Examination of the figure reveals several important facts concerning free rocket design. During boost, when the jet exit diameter usually approaches the base diameter, base drag is relatively unimportant. The combination of high chamber pressure, high base pressure, and small base-annulus area results in a low base drag or even a base thrust. For sustainer operation, the jet-exit-to-base-diameter ratio and jet-to-free-stream pressure ratio are usually low, resulting in high values of base drag, amounting to as much as 50 to 70 percent of the total drag. After burnout, the effect of residual burning must be considered. Mass added to the base region as a result of residual burning serves to increase the pressure ratio in the base region, re-

sulting in base pressures considerably higher than would be predicted for the jet-off case. This phenomenon is shown by the peak in base pressure at low jet-to-free-stream pressure ratios. This decrease in base drag due to residual burning effects may lead to errors in range prediction if not considered.

Previous design charts for engineering estimates of jet-on base pressure have been based on a limited amount of unrelated experimental data from various sources, which give reasonable estimates only if the configuration closely matches that on which the data were obtained. A theoretical method for predicting base pressure is presented in Reference 30. This method predicts trends of various parameters independently and can handle several parameters not easily simulated in wind tunnel tests. The method, however, is very complex and requires the use of high-storage-capacity computers.

A method, based on the thrust coefficient, has been developed (Reference 31) which allows rapid prediction of base pressures suitable for engineering estimates. For a cylindrical afterbody, the base pressure is given by

$$\frac{p_B}{p_\infty} = \frac{\frac{3}{5} (C_F)^{\frac{1}{2}}}{\frac{\gamma}{a^*}} \quad (8-25)$$

where

$$C_F = \frac{\text{Thrust}}{P_c A_T} \quad (8-26)$$

and

$$\frac{1}{a^*} = \sqrt{\left(\frac{\gamma + 1}{2}\right) M^2 \left(1 - \frac{\gamma - 1}{2} M^2\right)^{-1}} \quad (8-27)$$

and the base pressure coefficient is defined as

$$C_{p_B} = \frac{P_\infty - p_B}{\frac{1}{2} \rho_\infty V_\infty^2} = \frac{1 - \frac{p_B}{P_\infty}}{\frac{\gamma}{2} M_\infty^2} \quad (8-28)$$

In the above equations,

$$\begin{aligned} p_B &= \text{base pressure, lb/ft}^2 \\ P_c &= \text{motor chamber pressure, lb/ft}^2 \end{aligned}$$

AMCP 708-200

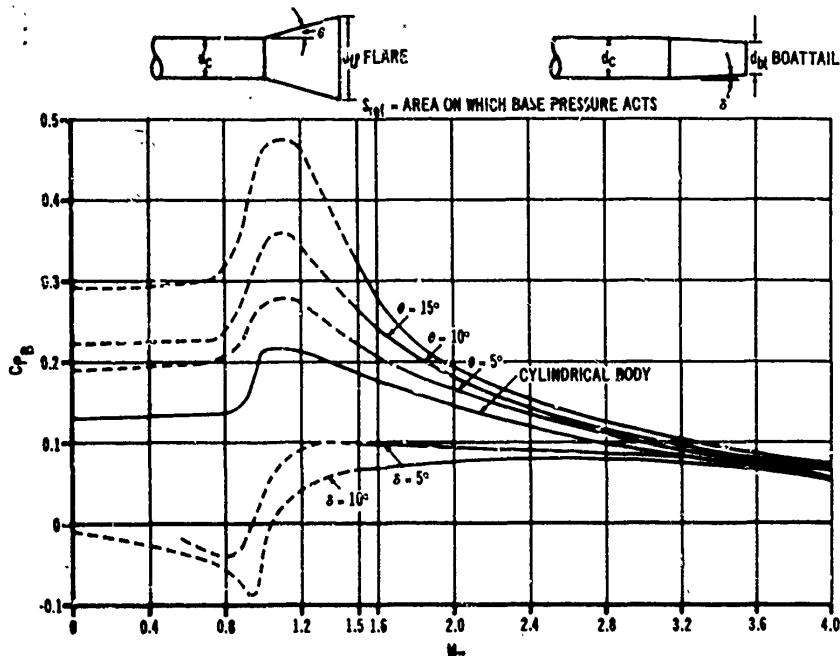


Figure 8-41. Base Pressure Coefficient of Cylinders, Boattails, and Flares With Rocket Jet Off

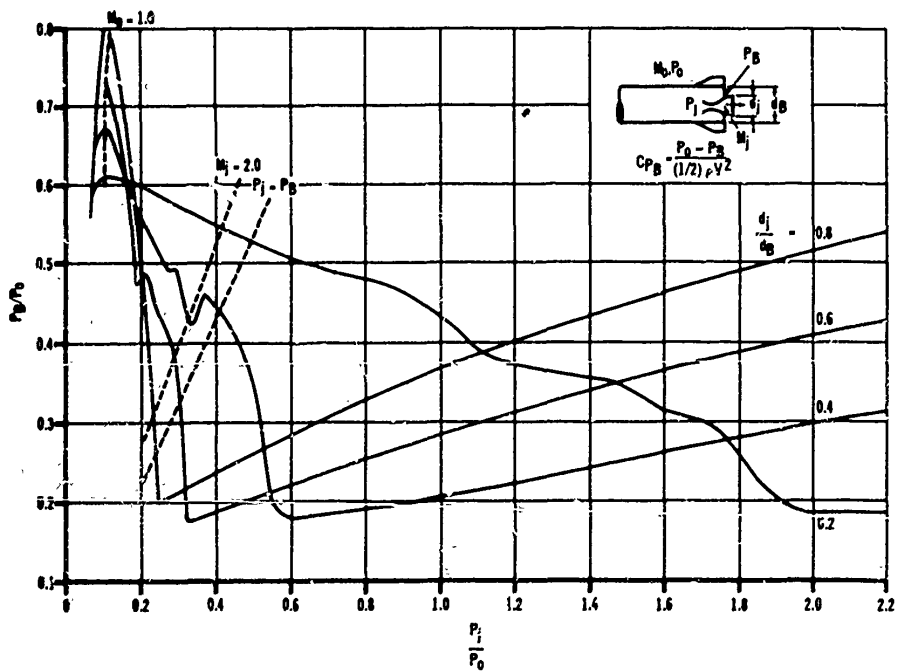


Figure 8-42. Effect of Rocket Set on Base Pressure

P_∞	=	free stream pressure, lb/ft ²
V	=	velocity, fps
V_∞	=	free stream velocity, fps
a^*	=	sonic velocity, fps
C_F	=	thrust coefficient
A_T	=	jet throat area, ft ²
C_{PB}	=	base pressure coefficient
ρ_∞	=	atmospheric density, slug ft ³
γ	=	ratio of specific heats
M	=	Mach number

For bodies with flared or boattailed afterbodies, $P_{B_i} P_\infty$ is corrected by use of Fig. 8-43. The stated correlation agrees well with most of the available experimental data. It is applicable at jet-to-free-stream pressure ratios above the value where base pressure is minimum (represented by the nearly linear portion of the curves in Fig. 8-42).

To give an indication of the characteristics of base pressure through a more complete Mach number and jet-pressure range, Fig. 8-44 has been prepared. This figure represents a cylindrical body and a nozzle having a jet Mach number of about 3.0. The solid curves represent either experimental data or the correlation curve. The dashed curves are extrapolated values.

8-3.3.3 Fin Base Drag

The boundary layer approaching the base of fins and other stabilizing surfaces is generally turbulent. The effects of profile shape on the base-pressure coefficient at supersonic speeds with a turbulent boundary layer is small. Fig. 8-45 provides a good estimate of fin base-pressure coefficient at supersonic speeds. At transonic and subsonic speeds, the ratio of trailing edge thickness to chord length is significant, and Fig. 8-46 should be used as a guide for estimating the base pressures.

8-3.4 DRAG CHARACTERISTICS OF COMPLETE CONFIGURATIONS

8-3.4.1 Interference Effects—Fin on Base

The presence of fins on rockets affects the external flow characteristics and usually results in increased base drag. The most important parameters appear to be fin thickness, fin longitudinal position, number of fins, and free-stream Mach number. Experimental data on the effects of fins are sparse if all important parameters

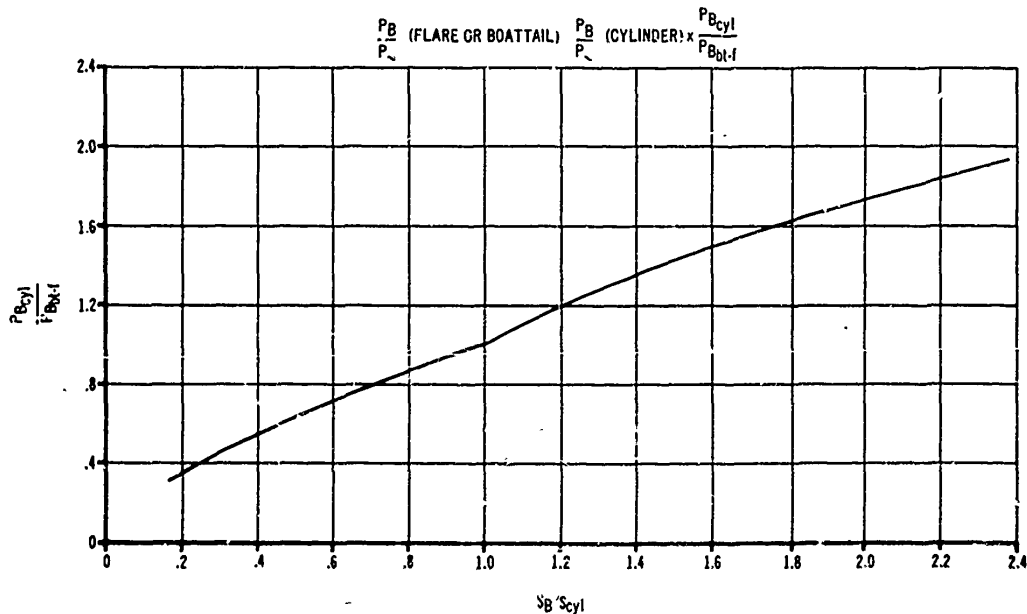


Figure 8-43. Base Pressure Correction for Boattailed and Flared Afterbodies

AMCP 706-200

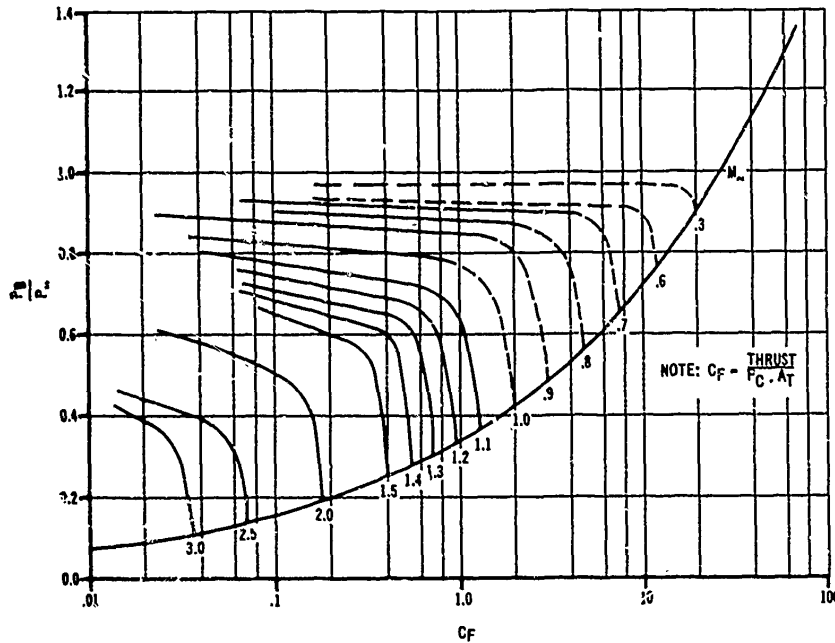


Figure 8-44. Base Pressure on Cylindrical Bodies

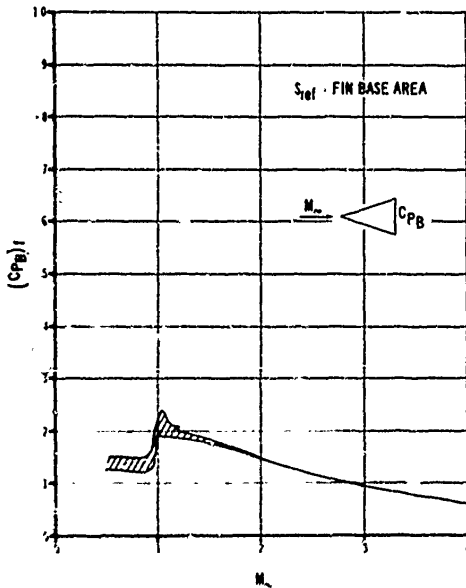


Figure 8-45. Base Pressure Coefficient of Fins at Supersonic Speeds

are considered. It is suggested that the empirical relation developed in Reference 29 be used in estimating fin effects on base drag:

$$\Delta C_{D_b} = \frac{t}{c} \left(\frac{0.825}{M^2} - \frac{0.05}{M} \right) n \quad (8-29)$$

where

- $t, c =$ thickness-to-chord ratio of fins and
- $n =$ number of fins

This relation is limited to the case where the fin trailing edge is flush with the base. Predicted values using this relation appear to be high at Mach numbers below about 2; with reasonable agreement for Mach numbers greater than 2.

8-3.4.2 Computational Table

The drag characteristics of the complete configuration are computed by summing the individual component drag coefficients, based on a common reference area. Table 8-2, Drag Force Calculation Sheets, which follow, indicate the method of obtaining the drag coefficients of the

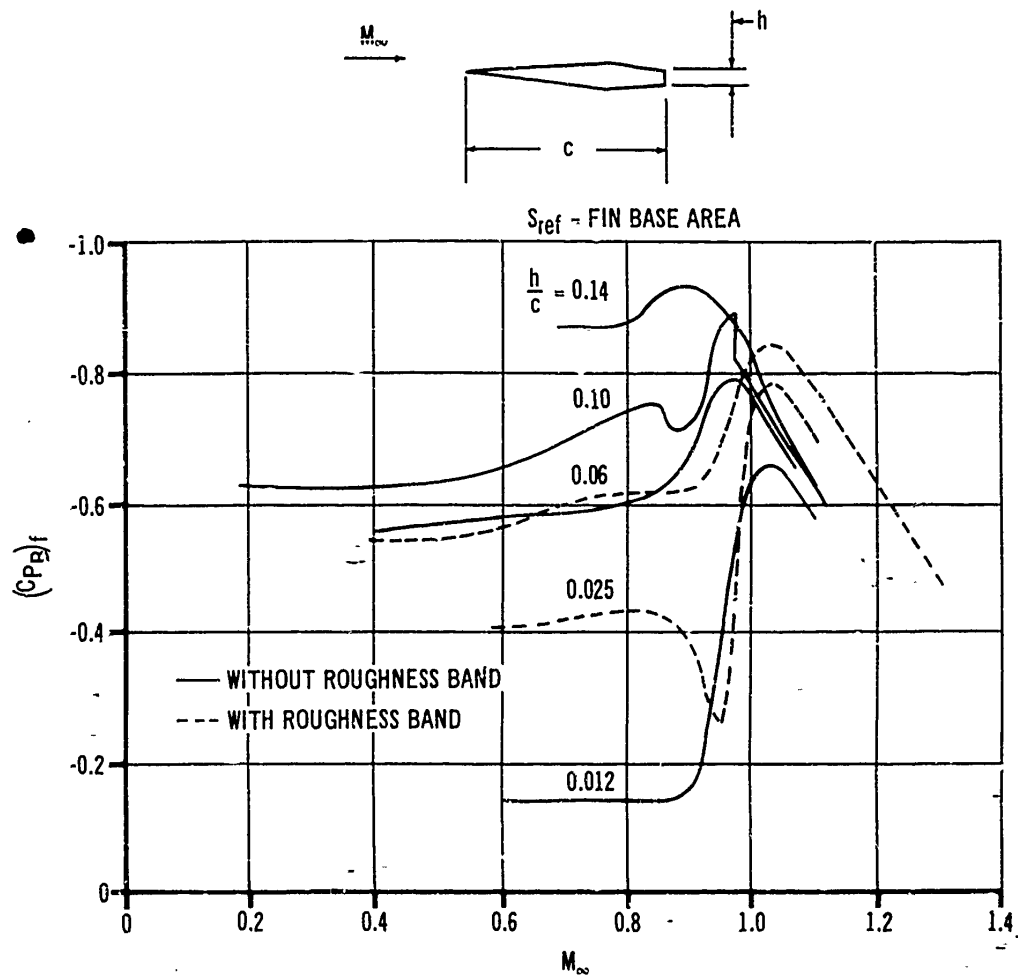


Figure 8-46. Base Pressure Coefficient of Fins at Transonic Speeds

individual components and of the complete configuration based on the configuration presented in Fig. 8-25.

8-4 AERODYNAMIC TESTING

The aerodynamic performance of rockets may be evaluated by theoretical estimates, flight testing, or wind tunnel testing. Theoretical estimates, due to lack of refinement, often fail to provide adequate quantitative aerodynamic data. Flight testing provides a slow rate of data collection; does not allow adequate control of the test ar-

ticle; and is expensive because the test article is usually expended. Wind tunnel testing, however, allows precise control of the parameters influencing flight characteristics. A wide scope of the problems associated with placing a rocket in a selected trajectory—such as stability, drag, and propulsion system influence—may be investigated in a complete wind tunnel program.

An indication of the wind tunnels available in the United States is given in References 32 and 36. While this list is not current and therefore incomplete, the uniqueness of the available tunnels dictates the necessity for matching particular

AMCP 706-280

tunnel characteristics to the particular test requirements. Tunnel operating capabilities and size are foremost among the considerations in selecting a test facility. However, consideration of availability, accessory equipment, and cost of test time cannot be ignored.

Wind tunnels are normally classified according to their operating speed range as follows:

<u>Tunnel Classification</u>	<u>Mach Number Range</u>
<i>Subsonic</i>	<i>Less than 0.7</i>
<i>Transonic</i>	<i>0.7 to 1.2</i>
<i>Supersonic</i>	<i>1.2 to 5.0</i>
<i>Hypersonic</i>	<i>Greater than 5.0</i>

Due to inherent problems associated with operating at different speed (or Mach number) ranges, wind tunnel facilities usually elect to operate only within the range of their classification Mach numbers. Since a large portion of the rockets considered in this handbook operate over a wide range of the Mach number spectrum, complete testing will require more than one facility. The upper limit for supersonic tunnels, $M = 5.0$, has been set from considerations of operating procedures and not abrupt changes in flight characteristics. When air is expanded to a Mach number of approximately five and above, the attendant large change in the temperature results in liquefaction of the air. To prevent this, heaters of large capacity, or a medium other than air, may be used to maintain temperatures above the liquefaction point.

The Reynolds-number capability of a wind tunnel is an important consideration. Matching the full-size-rocket Mach number and Reynolds number on the scale model insures that flow patterns are similar and that the measured forces and moments may be scaled up to the full-size rocket. Reynolds-number as a function of Mach number and altitude is presented in Fig. 8-40. The flow patterns become fully established at a Reynolds number of approximately two million, and therefore the requirement for matching Reynolds number above this value may be relaxed.

The capability for matching flight environment temperature in a wind tunnel is only important in the study of high velocities, such as may be

produced by reentry trajectories. Flight environment temperatures are not significant on the classes of rocket considered in this handbook.

The investigation of the influence of a propulsion system on the aerodynamic characteristics of a rocket requires a facility with the capability of propulsion testing or propulsion jet simulation. Operation of a propulsion system in a tunnel requires a means for removing the combustion products from the tunnel airstream, and creates fire and explosion hazards. Propulsion jet simulation is much simpler. Jets of compressed gases such as air or nitrogen will closely simulate exhaust flow patterns. The hazards connected with this technique are only those normal to high pressure storage and transmission. Jet exhaust conditions may be more closely simulated by the decomposition of hydrogen peroxide, but personnel hazards require special storage and handling procedures.

It is desirable to test the full-size rocket in order to have the maximum degree of confidence in the data. Generally, however, this is not practical, and a scaled-down test model must be fabricated. Model-size decisions must be based on (1) characteristics to be investigated, (2) instrumentation located in the model interior, (3) model support capabilities, and (4) size of available test facilities.

The model scale must be large enough so that the component parts which are normally exposed to free stream flow on the full-size article will not be submerged in the boundary layer of the test model. It is desirable that the selected scale provide a boundary layer of the same character that will exist on the full-size article. To maintain a desirable scale and duplicate boundary-layer conditions, the boundary layer often must be controlled by artificial means. There are practical limits to the duplication of small details of the full-size rocket. Duplicated details such as surface condition, small protuberances, screw heads, and small gaps in the scale model usually serve only to increase the fabrication cost, and affect the data to such a small extent that measuring accuracies do not reveal their presence. The tolerances used in manufacturing the full-size rocket should be considered in development of the test model. The data presented in Fig. 8-47 show a comparison of the test results obtained from a full-size model and an eight-percent scale

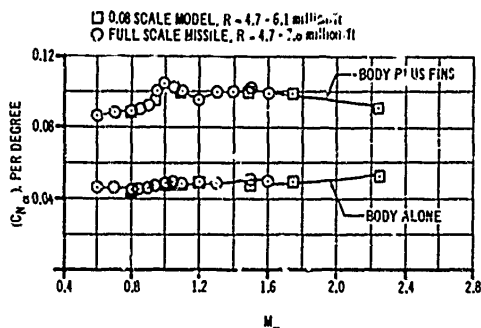


Figure 8-47. Comparison of Test Results on Full Size and Scale Model Artillery Missile

model of a typical artillery rocket, it can be seen that the agreement is excellent.

The amount of instrumentation that must be located inside the model often determines the minimum scale that can be used. Also, the scale of the model is often determined by the ability of the support to withstand the loads imposed on it.

The dimensions of the wind tunnel test section must be large enough so that the model does not significantly alter the velocity of the airstream and so that disturbances imparted to the airstream do not reflect from the tunnel boundaries to the model. It is not possible to quote maximum allowable model dimensions which will avoid these difficulties since they are dependent on overall configuration, position in tunnel, operating conditions, efforts made to attenuate these effects in each tunnel, and the precision of test measurements. Theoretical means of defining the relationship between model maximum size and test section size are not precise. Design decisions must be based on experimental investigations and an intimate knowledge of the testing facility. Fig. 8-48, from Reference 33, gives an indication of the relationship between the geometry of a typical body-of-revolution model and the allowable test-section size for a range of supersonic Mach numbers. However, this information was obtained experimentally, in part, and cannot be applied directly to other test facilities.

A survey of the descriptive literature on several transonic tunnels indicates that the model maximum cross-sectional area should be less than two percent of the test cross-sectional area. This ratio may be slightly increased if the model is not

to be tested at large angles of attack. The allowable model cross-sectional area in subsonic tunnels is less restrictive and may be as high as 10 percent of the test cross-sectional area. The maximum model length in subsonic tunnels is determined by the length of the test sector containing the desired flow properties.

The necessity of supporting the model in the airstream prevents exact duplication of flow patterns over the base of the model. The normal means of supporting the model is a horizontal sting which extends from the interior of the model through the base and is cantilevered from a vertical support member downstream. Unlike flight conditions, the sting promotes wake stabilization and creates disturbances that might propagate into the base region. To reduce these effects, the sting should be as small as structural considerations will allow, and abrupt increases in the lateral dimensions should be avoided to provide a relatively straight member over a considerable length. A rule of thumb often applied is that the flow disturbances created by abrupt changes in the support system may be propagated upstream through the support boundary layer and model wake for a distance five times greater than the lateral dimensions of the disrupting portion.

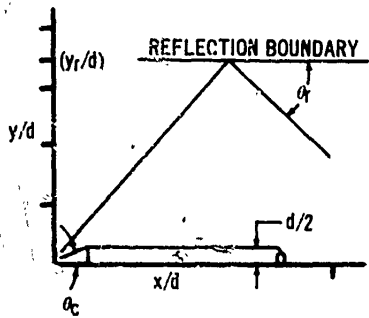
Design decisions on the materials and fabrication of a model must be based on the anticipated loads, severity of vibrations, and structural temperature gradients. The majority of test facilities require that model construction provide a factor of safety of at least four, based on maximum anticipated loads which, in supersonic tunnels, often occur during the establishment of flow in the test section. At Mach numbers of 5.0, the stagnation temperature at some points on the model is approximately six times greater than the static temperature at other points.

The high cost of tunnel test time requires that model changes, necessary during the test, be made in a minimum of time. The expense of designing and fabricating quick-change capability in a model can usually be justified by savings realized through increased utilization of tunnel time.

Balances, fitted in the interior of the test model, resolve the net aerodynamic forces acting on the model into the components shown in Fig. 8-49. The measuring elements of these balances are electrical strain gages, with an accuracy of approximately 1/2 to 1 percent of the maximum

AMCP 706-230

θ_c , deg	x/d	MACH NUMBER						
		1.5	2	2.5	3	4	5	6
10	2	y/d = 1.90	1.20	0.95	0.80	0.65	0.60	0.55
	4	3.80	2.40	1.90	1.70	1.30	1.15	1.00
	6	5.60	3.65	2.80	2.50	2.00	1.70	1.50
	8	7.50	4.90	3.80	3.30	2.60	2.30	2.13
	10	9.60	6.10	4.70	4.15	3.30	2.90	2.63
20	2	2.30	1.60	1.35	1.20	1.00	1.00	0.95
	4	4.45	3.20	2.60	2.30	1.90	1.70	1.55
	6	6.50	4.65	3.65	3.10	2.55	2.30	2.15
	8	8.60	5.95	4.65	4.00	3.25	2.85	2.65
	10	10.70	7.20	5.60	4.90	3.95	3.40	3.10
HEMI	2	3.75	2.65	2.20	2.00	1.70	1.65	1.60
	4	5.95	4.10	3.35	3.00	2.75	2.30	2.20
	6	8.00	5.37	4.45	3.90	3.20	2.95	2.80
	8	10.05	6.70	5.40	4.70	3.90	3.60	3.40
	10	7.95	6.35	5.60	4.65	4.20	3.90	3.90
θ_c deg = 44.5		32.5	23.5	21.5	16.0	13.0	11.0	



A_M = MODEL FRONTAL AREA
 A_T = AERODYNAMIC TEST SECTION AREA
 θ_c = MODEL NOSE HALF ANGLE

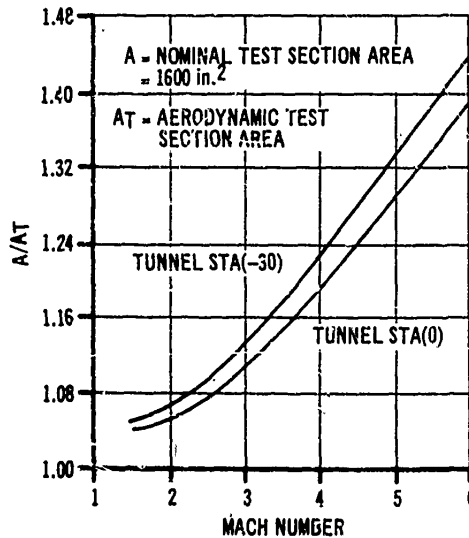
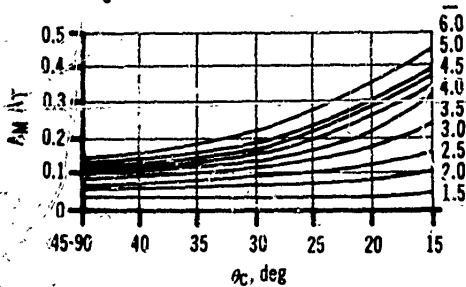


Figure C-48. Relationship Between Maximum Allowable Model Dimensions and Test Section Dimension in a Specific Wind Tunnel Facility

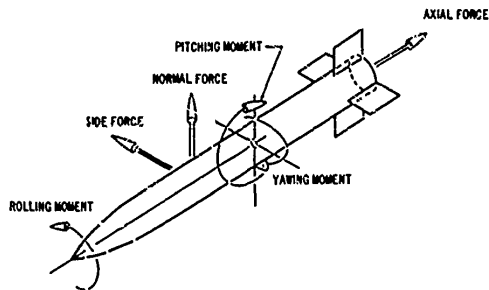


Figure 3-49. Aerodynamic Force Components

rated load. To obtain the greatest accuracy, a balance should be selected with a maximum load rating corresponding closely to the predicted test loads, especially if small changes in the total loads are to be measured.

Balances are compensated to operate in temperature environments as high as 180°F. At higher temperatures, a means of cooling must be provided.

Detailed knowledge of the effect of the flow over a model may be obtained by measuring surface pressure with manometers or transducers. Transducers are preferred for greater accuracy and faster response time. Measuring devices should be located near the test model, and the orifices and connecting lines should be large enough

to prevent unnecessary time delays in sensing pressure changes.

Temperature measurements are made by thermocouples which are selected for the expected temperature range and compatibility with tunnel read-out instrumentation. Reference 34 presents information on the performance of various types of thermocouples.

Flow visualization techniques are useful in making qualitative evaluations of the flow over a model. Subsonic flow patterns may be determined by observing tufts attached to the surface of the model. Areas where the flow exhibits unusual turbulence or separates from the model surface may be identified by coating the surface with a volatile substance and observing evaporation rates. At supersonic velocities, the compression and expansion waves emanating from the model surfaces are characterized by marked changes in density which may be identified by shadowgraphs, schlierens, or interferometers.

A recommended source of information in planning wind tunnel tests is the descriptive literature issued by each test facility. This literature provides detailed information for all problem areas covered in the foregoing discussion. The Ballistic Research Laboratories at Aberdeen Proving Ground, Maryland, described in Reference 35, provide the most readily available facilities for Army-sponsored wind tunnel tests.

REFERENCES

1. M. M. Munk, *The Aerodynamic Forces on Airship Hulls*, NAC-TR-187, 1924.
2. M. D. Van Dyke, "First and Second Order Theory of Supersonic Flow Past Bodies of Revolution," *Journal of Aeronautical Sciences* **18**, 161-78 (March 1951).
3. H. S. Tsien, "Supersonic Flow Over an Inclined Body of Revolution," *Journal of Aeronautical Sciences* **12**, 480-3 (October 1955).
4. M. D. Van Dyke, *Practical Calculation of Second-Order Supersonic Flow Past Nonlifting Bodies of Revolution*, NACA TN 2744, July 1952.
5. Royal Aeronautical Society Data Sheets, *Aerodynamics*, London, England, 1960.
6. D. J. Spring, *The Effect of Nose Shape and Afterbody Length on the Normal Force and Neutral Point Location of Axisymmetrical Bodies at Mach Numbers from 0.8 to 4.5*, Report No. RF-TR-64-13, Army Missile Command, Huntsville, Alabama, August 1964.
7. D. J. Spring, *The Static Stability Characteristics of Several Cone-Cylinder-Flare-Cylinder Configurations at Mach Numbers 0.4 to 4.5*, Report No. RF-TR-63-14, Army Missile Command, Huntsville, Alabama, 1963.
8. C. A. Syvertson and D. H. Dennis, *A Second Order Shock Expansion Method Applicable to Bodies of Revolution Near Zero Lift*, NACA TR 1828, 1957.
9. A. H. Shapiro, *The Dynamics and Thermodynamics of Compressible Fluid Flow*, The Ronald Press Company, New York, 1953.

REFERENCES (Cont)

10. J. H. Henderson, *Normal Force Pitching Moment and Center of Pressure of Eighty Cone-Cylinder-Frustum Bodies of Revolution at Mach Numbers 1.5 to 4.04*, Report No. 6R8F, Ordnance Missile Laboratories, Huntsville, Alabama, 1956.
11. J. G. Lowry and E. C. Polhamus, *A Method for Predicting Lift Increments Due to Flap Deflection at Low Angles of Attack in Incompressible Flow*, NACA TN 8911, January 1957.
12. J. B. McDevitt, *A Correlation by Means of Transonic Similarity Rules of Experimentally Determined Characteristics of a Series of Symmetrical and Cambered Wings of Rectangular Planform*, NACA TR 1258, 1955.
13. D. E. Hook and J. W. Carlson, *USAF Stability and Control Handbook*, Wright Patterson Air Force Base, Ohio.
14. P. A. Lagerstrom and M. E. Graham, *Low Aspect Ratio Rectangular Wings in Supersonic Flow*, Report No. SM 18110, Douglas Aircraft Company, Santa Monica, California, December 1947.
15. E. Lapin, *Charts for the Computation of Lift and Drag of Finite Wings at Supersonic Speeds*, Report No. SM 13480, Douglas Aircraft Company, Santa Monica, California, 1949.
16. *Longitudinal Stability Characteristics of a Series of Ring Tails on Bodies of Revolution at Mach Numbers from 0.8 to 4.5*, Report No. BF-TR-65-7, Army Missile Command, Huntsville, Alabama.
17. L. Reekin, *Determination of Upwash Around a Body of Revolution at Supersonic Velocities*, Report No. CM-251, Applied Physics Laboratory, The John Hopkins University, 1946.
18. W. C. Pitts, J. N. Nielsen, and G. E. Kaattari, *Lift and Center of Pressure of Wing-Body-Tail Combinations at Subsonic, Transonic, and Supersonic Speeds*, NACA TR 1807, 1959.
19. G. Morikawa, "Supersonic Wing Body Lift," *Journal of Aeronautical Sciences* 18, 217-28 (April 1951).
20. G. Morikawa, *The Wing-Body Problem for Linearized Supersonic Flow*, Progress Report No. 4-116, Jet Propulsion Laboratory, California Institute of Technology, 1949.
21. J. L. Potter, N. M. Shapiro, and W. D. Murphree, *An Interference Factor for Multifinned Tail Assemblies in Supersonic Flow*, Report No. 2R12F, Ordnance Missile Laboratories, Huntsville, Alabama, May 1956.
22. *Handbook of Supersonic Aerodynamics*, Section 8, "Bodies of Revolution," Report 1488 (Volume 3), Bureau of Naval Weapons, Department of the Navy, Washington, D. C., October 1961.
23. W. E. Stoney, Jr., *Collection of Zero-Lift Drag Data on Bodies of Revolution from Free-Flight Investigations*, NASA TR-R-100, 1961.
24. Aerodynamics Facilities Section Staff, *Aerodynamic Characteristics of Spherically Blunted Cones at Mach Numbers from 0.5 to 5.0*, Report MTP-AERO-61-38, Marshall Space Flight Center, Huntsville, Alabama, 1961.
25. P. R. Connolly, *The Zero-Lift Fore Drag and Body Base Drag Coefficient of a Series of Ring-Tail-Strut-Body Configurations at Mach Numbers from 0.8 to 4.5*, Report No. RD-TR-65-8, Army Missile Command, Huntsville, Alabama, 1963.
26. D. R. Chapman and M. W. Rubesin, "Temperature and Velocity Profiles in the Compressible Laminar Boundary Layer with Arbitrary Distribution of Surface Temperature," *Journal of Aeronautical Sciences* 16, 547-65 (September, 1949).
27. D. B. Lee and M. A. Faget, *Charts Adapted from Van Driest's Turbulent Flat Plate Theory for Determining Values of Turbulent Aerodynamic Friction and Heat Transfer Coefficient*, NACA TN 3811, October, 1956.
28. R. W. Truitt, *Fundamentals of Aerodynamic Heating*, The Ronald Press Company, New York, 1960.
29. E. E. Honeywell, *Completion of Power-Off Base Drag Data and Empirical Methods for Predicting Power-Off Base Drag*, Report No. TM 334-337, Convair, Pomona, California, 1959.
30. H. H. Korst, W. L. Chow, and G. W. Zumwalt, *Research on Transonic and Supersonic Flow of a Real Fluid at Abrupt Increases in Cross Section*, ME Tech Note 892-5, University of Illinois, Urbana, Illinois, December 1959.
31. C. E. Brazzell, *A Correlation of the Base Pressure on a Body of Revolution With a Cold Jet Exhausting Through the Base*, Army Missile Command, Huntsville, Alabama.
32. *National Wind Tunnel Summary*, Aeronautics Panel of the Aeronautics and Astronautics Coordination Board, Department of Defense and

REFERENCES (Cont)

- National Aeronautics and Space Administration, Washington, D. C., 1961.
33. *Test Facilities Handbook*, Arnold Engineering and Development Center, Arnold Air Force Station, Tennessee, July 1968.
34. R. L. Walker, *Heat and Temperature Measurement*, Prentice-Hall, Inc., New York, 1950.
35. J. C. McMullen, *Wind Tunnel Testing Facilities at the Ballistic Research Laboratories*, Aberdeen Proving Ground, Maryland, 1960.
36. AMCP 706-342, *Engineering Design Handbook, Design for Control of Projectile Flight Characteristics*.

AMCP 706-280

TABLE 8-1. COMPUTATIONAL TABLE

Reference Data				
1	2	3	4	5
Mach No.	β	ref area (A_{ref}) Ft^2	ref length (l_{ref}) Ft	ref point (body sta)
0	1	1.225	1.25	0
.5	.866	1.225	1.25	0
1.0	0	1.225	1.25	0
1.5	1.12	1.225	1.25	0
2.0	1.73	1.225	1.25	0
2.5	2.29	1.225	1.25	0
3.5	3.36	1.225	1.25	0
4.5	4.39	1.225	1.25	0
arbitrarily selected	$\beta = \sqrt{M^2 - 1}$	arbitrarily selected (usually cross sectional area of body cylindrical section or $\frac{\pi d_{cyl}^2}{4}$)	arbitrarily selected (usually diameter of body cylindrical section, d_{cyl})	arbitrarily selected (usually nose tip)

TABLE 8-1. COMPUTATIONAL TABLE (cont)

Ref Data	Subsonic and Sonic Computation								
	Body - Force and Moment Characteristics								
1	6	7	8	9	10	11	12	13	14
Mach No.	$k_2 - k_1$	$\frac{S_B}{A_{ref}}$	$C_{N_{\alpha \beta}}$	S_{bt}	$\Delta C_{N_{\alpha \beta t}}$	S_{fl}	$\Delta C_{N_{\alpha fl}}$	$C_{N_{\alpha \text{ body}}}$	$X_{cp \beta}$
0	.95	1.0	1.90		0		0	1.90	
.5	.95	1.0	1.90		0		0	1.90	
1.0	.95	1.0	1.90		0		0	1.90	
1.5									
2.0									
2.5									
3.5									
4.5									
	from Fig. 8-1		$C_{N_{\alpha \beta}} = 2(k_2 - k_1) \frac{S_B}{A_{ref}}$ see also Figs. 8-6 & 8-7 for specific configuration; per rad; ref area = A_{ref}	Boattail cross-sectional area at minimum diameter sections	$\Delta C_{N_{\alpha \beta t}} = 2 \frac{S_{bt}}{S_{ref}} \left[1 - \left(\frac{d_{bt}}{d_c} \right)^2 \right]$ per rad; ref area = A_{ref}	Flare cross-sectional area at maximum diameter section	$\Delta C_{N_{\alpha fl}} = -2 \frac{S_{fl}}{A_{ref}} \left[1 - \left(\frac{d_c}{d_{fl}} \right)^2 \right]$ from Fig. 8-10(A); per rad; ref area = A_{ref}	$C_{N_{\alpha \text{ body}}} = C_{N_{\alpha \beta}}$ per rad; ref area = A_{ref} ; add $\Delta C_{N_{\alpha \beta t}}$ or $\Delta C_{N_{\alpha fl}}$ if applicable	Centroid of projected nose area (measured rearward from nose tip)

TABLE 8-1. COMPUTATIONAL TABLE (cont)

Ref Data xxx	Subsonic and Sonic Computation					
	Body - Force and Moment Characteristics					
1	15	16	17	18	19	20
Mach No.	$C_{N_{\alpha \beta}}$	$X_{cp_{bt}}$	$\Delta C_{N_{\alpha \beta t}}$	$X_{cp_{fl}}$	$\Delta C_{N_{\alpha \beta l}}$	$C_{N_{\alpha \text{ body}}}$
0	5.06	--	--	--	--	5.06
0.5	5.06	--	--	--	--	5.06
1.0	5.06	--	--	--	--	5.06
1.5						
2.0						
2.5						
3.5						
4.5						
	$C_{N_{\alpha \beta}} = C_{N_{\alpha \beta}} \left(\frac{X_{cp_{bt}}}{l_{ref}} \right)$ per rad; ref area = A_{ref} ; ref length = l_{ref} ; with respect to nose tip	$X_{cp_{bt}} = 0.6 l_{bt} + l_{nose} + l_s$ (measured aft from nose tip)	$\Delta C_{N_{\alpha \beta t}} = \Delta C_{N_{\alpha \beta t}} \left(\frac{X_{cp_{bt}}}{l_{ref}} \right)$ per rad; ref area = A_{ref} ; ref length = l_{ref} ; with respect to nose tip	$X_{cp_{fl}} = l_n + l_{ob} + \left[\frac{\frac{d_c}{d_{fl}} \left[\frac{d_c}{d_{fl}} + 1 \right]^{-2}}{3 \left[1 - \left(\frac{d_c}{d_{fl}} \right)^2 \right]} \right]$ (measured aft from nose tip)	$\Delta C_{N_{\alpha \beta l}} = \Delta C_{N_{\alpha \beta l}} \left(\frac{X_{cp_{fl}}}{l_{ref}} \right)$ per rad; ref area = A_{ref} ; ref length = l_{ref} ; with respect to nose tip	$C_{N_{\alpha \text{ body}}} = C_{N_{\alpha \beta}}$ ref area = A_{ref} ; ref length = l_{ref} ; per rad; with respect to nose tip with incremental terms $\Delta C_{N_{\alpha \beta t}}$, $\Delta C_{N_{\alpha \beta l}}$ added if applicable

TABLE 8-1. COMPUTATIONAL TABLE (cont)

Ref Data	Subsonic and Sonic Computation							
	Fin - Force and Moment Characteristics							
1	21	22	23	24	25	26	27	28
Mach No.	b	S_f	AR	β^2	$\tan^2 \Lambda_{c/2}$	F_1	$\frac{C_{N_{\alpha f}}}{AR}$	$C_{N_{\alpha f}}$
0	2.08	1.882	2.31	1.0	0.75	3.06	1.11	2.56
.5	2.08	1.882	2.31	.75	0.75	2.83	1.15	2.66
1.0	2.08	1.882	2.31	0	0.75	2.00	1.30	3.00
1.5								
2.0								
2.5								
3.5								
4.5								
	span (see Fig. 8-23)	fin planform area (see Fig. 8-23)	$AR = \frac{b^2}{S_f}$	$\beta^2 = 1 - M^2$	(tangent of mid-chord sweep angle) ²	$F_1 = AR(\beta^2 + \tan^2 \Lambda_{c/2})^{1/2}$ abscissa entry for Fig. 8-11	from Fig. 8-11	$C_{N_{\alpha f}} = \left(\frac{C_{N_{\alpha f}}}{AR}\right) (AR)$ per rad; ref area = S_f

AMCP 706-200

TABLE 8-1. COMPUTATIONAL TABLE (cont)

Ref Data	Subsonic and Sonic Computation						
	Fin - Force and Moment Characteristics			Rectangular Fins - Force and Moment Characteristics			
1	29	30	31	32	33	34	35
Mach No.	$C_{N_{\alpha f}}$	λ_{ref}	$C_{M_{\alpha f}}$	$\frac{t}{c}$	$AR \left(\frac{t}{c}\right)^{1.5}$	$\frac{M^2 - 1}{\left(\frac{t}{c}\right)^{2.5}}$	$\left(\frac{t}{c}\right)^{1.5} C_{N_{\alpha f}}$
0	3.93	165.5	43.4				
.5	4.09	165.5	45.1				
1.0	4.61	165.5	50.9				
1.5							
2.0							
2.5							
3.5							
4.5							
	$C_{N_{\alpha f}} \left(\frac{S_f}{l_{ref}}\right)$ per rad; ref area A_{ref}	$\lambda_{ref} = 0.75 \bar{c}$ measured from nose tip (see Fig. 8-23 for \bar{c}); assumes fin trailing edge flush with base. [] indicates term could or could not be in the equation, depending upon configuration being analyzed.	$C_{M_{\alpha f}} \left(\frac{N_{ref}}{l_{ref}}\right)$ per rad; ref area A_{ref} ; ref length l_{ref} ; with respect to nose tip	ratio of fin maximum thickness to maximum chord length	entry for horizontal variable, Fig. 8-12(A)	entry for vertical variable, Fig. 8-12(A)	from Fig. 8-12(A)

TABLE 8-1. COMPUTATIONAL TABLE (cont)

Ref Data	Subsonic and Sonic Computation				
	Rectangular Fins - Force and Moment Characteristics				
1	36	37	38	39	40
Mach No.	$C_{N_{\alpha f}}$	$C_{M_{\alpha f}}$	$\left(\frac{\lambda_{cpf}}{c}\right)_f$	λ_{cpf}	$C_{V_{\alpha f}}$
0 .5 1.0 1.5 2.0 2.5 3.5 4.5	$\left[\left(\frac{l}{c}\right)^{1/3} C_{N_{\alpha f}} \sqrt{\left(\frac{l}{c}\right)}\right]^{1/3}$ per rad; ref area S_f	$C_{M_{\alpha f}} \left(\frac{S_f}{\lambda_{ref}}\right)$ per rad; ref area λ_{ref}	from Fig. 8-12(B), measured from fin leading edge	measured from nose tip; assumes fin trailing edge is flush with body base. [] indicates term could or could not be in the equation, depending upon configuration being analyzed.	per rad; ref area λ_{ref} ; ref length l_{ref} ; with respect to nose tip
				$\lambda_{cpf} = l_n + l_{ab} + [l_{bt}] - \left[1 - \left(\frac{\lambda_{cp}}{c}\right)\right]_c$	$C_{N_{\alpha f}} = C'_{N_{\alpha f}} \left(\frac{\lambda_{cpf}}{l_{ref}}\right)$

AMCP 706-280

TABLE 8-1. COMPUTATIONAL TABLE (cont)

Ref Data		Subsonic and Sonic Computation					
		Ring Tail - Force and Moment Characteristics					
1 Mach No.	41 leading edge diameter (led)	42 chord length (cl)	43 ring te location	44 $\Delta C_{N_{\alpha rt}}$	45 $\Delta C_{N_{\alpha rt}}$	46 $X_{cp rt}$	47 $\Delta C_{N_{\alpha rt}}$
0							
.5							
1.0							
1.5							
2.0							
2.5							
3.5							
4.5							
	$led \frac{d_{le}}{d_c}$, entry for Fig. 8-17	$cl \frac{c}{d_c}$, entry for Fig. 8-17	location of ring trailing edge with respect to base of body	from Fig. 8-17, (assume constant below Mach No = 0.8); per deg; ref area A_{rrf}	$C_{N_{\alpha rt}} = 57.3 (C_{N_{\alpha rt}}^{\circ})$ per rad; ref area A_{rrf}	$X_{cp rt} = l_{nose} - l_{at} + [l_{rt}]$ 0.75c measured from nose tip; assumes fin trailing edge is flush with body base. [] indicates term could or could not be in the equation, depending upon configuration being analyzed.	$V_{N_{\alpha rt}} = C_{N_{\alpha rt}} \left(\frac{X_{cp rt}}{r_{rt}} \right)$ per rad; ref area = A_{rrf} ; ref length = l_{ref} ; with respect to nose tip

TABLE 8-1. COMPUTATIONAL TABLE (cont)

Ref Data	Subsonic and Sonic Computation						
	Interference Effects			Complete Configuration - Force and Moment Characteristics			
1	48	49	50	51	52	53	54
Mach No.	$K_{f(b)}$	$K_{b(f)}$	K_t	$C_{N_{\alpha \text{ body}}}$	$(C_{N_{\alpha f}})_{IF}$	$C_{N_{\alpha f}}$	$C_{N_{\alpha \text{ total}}}$
0	1.32	.58	1.90	1.90	3.93	7.44	9.34
.5	1.32	.58	1.90	1.90	4.09	7.76	9.66
1.0	1.32	.58	1.90	1.90	4.61	8.75	10.65
1.5							
2.0							
2.5							
3.5							
4.5							
	from Fig. 8-18, invariant with Mach No.	from Fig. 8-18, invariant with Mach No.	$K_t, K_{f(b)}, K_{b(f)}$	from column 13 with incremental terms as applicable, per rad; ref area A_{ref}	interference-free fin from applicable column (29 or 37) (Note: Interference effects included in ring tail data) per rad; ref area A_{ref}	$C_{N_{\alpha f}} = K_t (C_{N_{\alpha f}})_{IF}$ per rad; ref area = A_{ref}	$C_{N_{\alpha \text{ total}}} = C_{N_{\alpha \text{ body}}} + C_{N_{\alpha f}}$ per rad; ref area A_{ref}

*Interference Free

AMCP 706-280

TABLE 8-1. COMPUTATIONAL TABLE (cont)

Data	Subsonic and Sonic Computation				
	Complete Configuration - Force and Moment Characteristics				
1	55	56	57	58	59
Mach No.	$C_{D\alpha}$	$(C_{D\alpha})_{IF}$	$C_{M\alpha f}$	$C_{M\alpha total}$	$\left(\frac{X_{cp}}{l_{ref}}\right)_{total}$
0	5.06	43.4	82.5	87.56	9.38
.5	5.06	45.1	85.6	90.66	9.38
1.0	5.06	50.9	96.5	101.56	9.52
1.5					
2.0					
2.5					
3.5					
4.5					
	from column 20 with incremental terms as applicable, per rad; ref area A_{ref} ; ref length l_{ref} ; with respect to nose tip	interference-free fin from applicable column (31 or 40) (Note: Interference effects included in ring tail data); per rad; ref area A_{ref} ; ref length l_{ref} ; with respect to nose tip	$C_{M\alpha f} = h_t (C_{M\alpha f})_{IF}$ per rad; ref area A_{ref} ; ref length l_{ref} ; with respect to nose tip	$C_{M\alpha total} = C_{M\alpha h} + C_{M\alpha f}$ per rad; ref area A_{ref} ; ref length l_{ref} ; with respect to nose tip	$\left(\frac{X_{cp}}{l_{ref}}\right)_{total} = \frac{C_{M\alpha total}}{C_{N\alpha total}}$; measured from nose tip

*Interference Free

TABLE 8-1. COMPUTATIONAL TABLE (cont)

Ref Data	Supersonic Computations								
	Body - Force and Moment Characteristics								
1 Mach No.	60 β	61 $\frac{l_n}{d}$	62 $\frac{l_{ab}}{d}$	63 $\frac{\beta d}{i_n}$	64 $\frac{l_{ab}}{\beta d}$	65 $C_{N_{\alpha}} \beta$	66 $\left(\frac{X_{cp}}{l_n}\right)_{\beta}$	67 $X_{cp} \beta$	68 $C_{M_{\alpha}} \beta$
0									
.5									
1.0									
1.5	1.12	4.0	7.76	0.280	6.94	2.6	.53	31.8	5.51
2.0	1.73	4.0	7.76	0.434	4.49	3.0	.68	41.1	8.22
2.5	2.29	4.0	7.76	0.571	3.39	3.15	.72	43.2	9.07
3.5	3.36	4.0	7.76	0.841	2.31	3.25	.83	49.8	10.78
4.5	4.39	4.0	7.76	1.10	1.77	3.25	.88	52.9	11.45
	from column 2	nondimensional nose length	nondimensional afterbody length	variable for entry in Fig. 8-2	variable for entry in Fig. 8-2	from Fig. 8-2 (tangent-ogive cylinder) or Fig. 8-4 (cone-cylinder). See also Figs. 8-6 and 8-7 for specific configuration. Per rad; ref. area A_{ref}	from Fig. 8-3 (tangent-ogive cylinder) or Fig. 8-5 (cone-cylinder)	measured from nose tip. See also Figs. 8-6 and 8-7 for specific configuration.	$C_{M_{\alpha}} \beta$ per rad; ref area A_{ref} ; ref length l_{ref} ; with respect to nose tip

AMCP 706-200

TABLE 8-1. COMPUTATIONAL TABLE (cont)

Supersonic Computations									
Ref Data	Boattail - Force and Moment Characteristics								
1	69	70	71	72	73	74	75	76	77
Mach No.	l_{bt}	d_{bt}	d_c	$\frac{l_{bt}}{d_c \beta}$	$C_{N_{\alpha} bt}$ $1 - \left(\frac{d_{bt}}{d_c}\right)^2$	$\Delta C_{N_{\alpha} bt}$	$\frac{X_{cp}}{l_{bt}}$	$X_{cp} l_{bt}$	$\Delta C_{N_{\alpha} bt}$
0									
.5					::	::			::
1.0					::	::			::
1.5					::	::			::
2.0					::	::			::
2.5					::	::			::
3.5					::	::			::
4.5					::	::			::
	length of boattail	small diameter of boattail	cylinder diameter (large diameter of boattail)	abscissa entry for Fig. 8-8	from Fig. 8-8	$C_{N_{\alpha} bt} \left[\frac{\left(\frac{d_{bt}}{d_c}\right)^2}{1 - \left(\frac{d_{bt}}{d_c}\right)^2} \right]$, per rad; ref area = A_{ref}	from Fig. 8-9	$X_{cp} l_{bt} = l_n + l_{ab} + \left(\frac{l_{cp}}{l_{bt}}\right) l_{bt}$, measured from nose tip	per rad; ref area = A_{ref} ; ref length = l_{ref} ; with respect to nose tip
									$\Delta C_{N_{\alpha} bt} = (C_{N_{\alpha} bt}) \left(\frac{l_{cp}}{l_{ref}}\right)$

TABLE 8-1. COMPUTATIONAL TABLE (cont)

Ref Data	Supersonic Computations						
	Flare - Force and Moment Characteristics						
1	78	79	80	81	82	83	84
Mach No.	d_{fl}	d_c	θ	$\Delta C_{N_{\alpha fl}}$	$\Delta C'_{N_{\alpha fl}}$	$X_{cp fl}$	$\Delta C_{y_{\alpha fl}}$
0 .5 1.0 1.5 2.0 2.5 3.5 4.5	flare diameter (maximum diameter of flare)	from column 71 (minimum diameter of flare)	flare half angle, see Fig. 8-24	from Fig. 8-10 at appropriate Mach number	per rad; ref area = A_{ref} ; $S_{fl} = \frac{\pi d_{fl}^2}{4}$	$X_{cp fl} = l_n + l_{ab} + 0.6l_{fl}$, measured from nose tip	per rad; ref area = A_{ref} ; ref length = l_{ref} ; with respect to nose tip
					$\Delta C'_{N_{\alpha fl}} = (\Delta C_{N_{\alpha fl}}) \left(\frac{S_{fl}}{A_{ref}} \right)$		$\Delta C_{y_{\alpha fl}} = (\Delta C'_{N_{\alpha fl}}) \left(\frac{X_{cp fl}}{l_{ref}} \right)$

AMCP 708-200

Ref Data		Supersonic Computations				
		Total Body		Fin - Force and Moment Characteristics		
Mach No.	85	86	87	88	89	90
	$C_{N_{\alpha b}}$	$C_{N_{\alpha b}}$	λ	$\tan \Lambda_{le}$	$\frac{\beta}{\tan \Lambda_{le}}$	$\frac{\tan \Lambda_{le}}{\beta}$
0						
.5						
1.0						
1.5	2.6	5.51	0	1.732	.646	
2.0	3.0	8.22	0	1.732	1.00	1.00
2.5	3.15	9.07	0	1.732		.756
3.5	3.25	10.78	0	1.732		.516
4.5	3.25	11.45	0	1.732		.395
	$C_{N_{\alpha b}} = C_{N_{\alpha fb}} + N_{N_{\alpha ft}} + N_{N_{\alpha ft}} + N_{N_{\alpha ft}}$ per rad; ref area A_{ref} ; with incremental terms added as applicable	$C_{N_{\alpha b}} = C_{N_{\alpha fb}} + N_{N_{\alpha bt}} + N_{N_{\alpha ft}}$ per rad; ref area A_{ref} ; ref length l_{ref} ; with respect to nose tip	taper ratio (from fin geometry (see Fig. 8-23))	tangent of leading edge sweep angle	abscissa entry for Fig. 8-13	abscissa entry for Fig. 8-13

TABLE 8-1. COMPUTATIONAL TABLE (cont)

Ref Data	Supersonic Computations								
	Fin - Force and Moment Characteristics								
1	91	92	or 93	94	95	96	97	98	
Mach No.	$AR \tan \Lambda_{lc}$	$\tan \Lambda_{lc}$	$C_{N\alpha}$	$\beta C_{N\alpha}$	$C_{N\alpha f}$	ΔY	ΔY_{\perp}	δ_{\perp}	$\frac{\beta}{\tan \Lambda_{lc}}$
0									
.5									
1.0									
1.5	4.0	4.75			2.74	.397	.112	≈ 0	.646
2.0	4.0	4.0	4.0	4.0	2.31	.097	.112	≈ 0	1.0
2.5	4.0		4.0	4.0	1.75	.097	.112	≈ 0	
3.5	4.0		4.0	4.0	1.19	.097	.112	≈ 0	
4.5	4.0		4.0	4.0	0.913	.097	.112	≈ 0	
	variable for entry, Fig. 8-13	from Fig. 8-13, for $\beta/\tan \Lambda_{lc}$ entry, at appropriate taper ratio (Λ)	from Fig. 8-13, for $\tan \Lambda_{lc}/\beta$ entry, at appropriate taper ratio (Λ)	$C_{N\alpha f} = (\tan \Lambda_{lc} C_{N\alpha}) \left(\frac{1}{\tan \Lambda_{lc}} \right) \text{ or } = \beta C_{N\alpha} \left(\frac{1}{\beta} \right)$ per rad; ref area = planform area, S_f	$\Delta Y = Y_{.15c} - Y_{0.06c}$, difference between upper fin surface coordinates at 15 and 6 percent chord stations	$\Delta Y_{\perp} = \frac{\Delta Y}{\cos \Lambda_{lc}}$	$\delta_{\perp} = \tan^{-1} \frac{\Delta Y_{\perp}}{5.85}$	Note: in deg; for wedge leading edge only.	abscissa for Fig. 8-15

AMCP 708-280

TABLE 8-1. COMPUTATIONAL TABLE (cont)

Supersonic Computations						
Ref Data	Fin - Force and Moment Characteristics					
1 Mach No.	99 $\frac{\tan \Lambda_{te}}{\beta}$	100 $\frac{C_{N\alpha f}}{(C_{N\alpha f})_{theory}}$	101 $C_{N\alpha f}$	102 $\frac{X_{cp}}{C_{rf}}$	103 $X_{cp f}$	104 $C_{N\alpha f}$
0						
.5						
1.0						
1.5		1.0	4.21	0.68	169.4	47.5
2.0	1.0	1.0	3.55	0.68	169.4	40.1
2.5	.756	1.0	2.69	0.68	169.4	30.4
3.5	.716	1.0	1.83	0.68	169.4	20.6
4.5	.395	1.0	1.402	0.68	169.4	15.85

abscissa for Fig. 8-15

from Fig. 8-15

$$C_{N\alpha fin} = \left(\frac{C_{N\alpha f}}{C_{N\alpha theory}} \right) (C_{N\alpha theory}) (S_f/A_{ref})$$

NOTE: $C_{N\alpha theory}$ from column 94; per rad; ref area = A_{ref}

from Fig. 8-14, at appropriate taper ratio (λ)

$$X_{cp f} = l_n + l_{ob} + [l_{tr}] - \left[1 - \left(\frac{X_{cp}}{C_r} \right)_f \right]$$

measured from nose tip; assume fin trailing edge is flush with body base. [] indicates term could or could not be in the equation, depending upon configuration being analyzed.

$$C_{N\alpha f} = C_{N\alpha f} \left(\frac{X_{cp f}}{L_{ref}} \right) \text{ per rad; ref area} = A_{ref}; \text{ ref length} = l_{ref}; \text{ with respect to nose tip}$$

TABLE 8-1. COMPUTATIONAL TABLE (cont)

Ref Data	Supersonic Computations					
	Rectangular Fin - Force and Moment Characteristics					
1	105	106	107	108	109	110
Mach No.	$\frac{1}{\beta AR}$	$\beta C_{N\alpha}$	$C_{N\alpha f}$	$C'_{N\alpha f}$	$\frac{X_{cp}}{c}$	$X_{cp f}$
0						
.5						
1.0						
1.5						
2.0						
2.5						
3.5						
4.5						
	variable for abscissa entry, Fig. 8-16 (Note: $\beta AR \geq 0.5$ for data to apply)	from Fig. 8-16	$\frac{(10)}{(9)} / \frac{(5)}{(4)}$ $C_{N\alpha f} = (\beta C_{N\alpha}) \frac{1}{\beta}$, per rad; ref area = S_f	$C'_{N\alpha f} = (C_{N\alpha f}) \left(\frac{S_f}{A_{ref}} \right)$ per rad; ref area = A_{ref}	from Fig. 8-16, (Note: c = chord length)	$X_{cp f} = l_n + l_{ab} + [l_{bc}] - \left(1 - \frac{l_{cp}}{c} \right) c$ measured from nose tip; assumes fin trailing edge is flush with body base. [] indicates term could or could not be in the equation, depending upon configuration being analyzed.

AMCP 706-280

TABLE 8-1. COMPUTATIONAL TABLE (cont)

Ref Data	Supersonic Computations				
	Rectangular in - Force and Moment Characteristics	112	113	114	115
1	111	112	113	114	115
Mach No.	$C_{N\alpha f}$	Leading Edge Dia (led)	Chord Length (cl)	Ring Trailing Edge (rte) Location	$\Delta C_{N\alpha rt}$
0 .5 1.0 1.5 2.0 2.5 3.5 4.5	$C_{N\alpha f} = C_{N\alpha f}^0 \left(\frac{X_{epf}}{l_{ref}} \right)$ per rad; ref area = A_{ref} ; ref length = l_{ref} ; with respect to nose tip	$\frac{d_{te}}{d_c}$, entry for Fig. 8-17	$\frac{c}{d_c}$, entry for Fig. 8-17	location of ring trailing edge (rte) with respect to base of body; values aft of body base are positive	from Fig. 8-17, per deg, ref area = A_{ref}

TABLE 8-1. COMPUTATIONAL TABLE (cont)

Ref Data	Supersonic Computations		
	Ring Tail - Force and Moment Characteristics		
1	116	117	118
Mach No.	$\Delta C_{N_{\alpha rt}}$	$X_{cp rt}$	$\Delta C_{N_{\alpha rt}}$
0			
.5			
1.0			
1.5			
2.0			
2.5			
3.5			
4.5			
	<p>(116) $\Delta C_{N_{\alpha rt}} = 57.3 \Delta C_{N_{\alpha rt}}$ per rad; ref area = A_{ref}</p>	<p>(117) [] indicates term could or could not be in the equation, depending upon configuration being analyzed.</p> <p>$X_{cp rt} = l_n + l_{ab} + [l_{bt}] + (rte - 0.5c)$</p>	<p>(118) $\Delta C_{N_{\alpha rt}} = \Delta C_{N_{\alpha rt}} \left(\frac{X_{cp rt}}{l_{ref}} \right)$ per rad; ref area = A_{ref}; ref length = l_{ref}; with respect to nose tip</p>

AMCP 706-280

TABLE 8-1. COMPUTATIONAL TABLE (cont)

Ref Data	Supersonic Computations				
	Rectangular Fin - Force and Moment Characteristics		Ring Tail - Force and Moment Characteristics		
1	111	112	113	114	115
Mach No.	$C_{M_{\alpha f}}$	Leading Edge Dia (led)	Chord Length (cl)	Ring Trailing Edge (rte) Location	$\Delta C_{N_{\alpha rt}}$
0					
.5					
1.0					
1.5					
2.0					
2.5					
3.5					
4.5					
	$C_{M_{\alpha f}} = C_{M_{\alpha f}} \left(\frac{X_{epf}}{l_{rnf}} \right)$ per rad; ref area = A_{ref} ; ref length = l_{ref} ; with respect to nose tip	$led = \frac{d_{te}}{d_c}$, entry for Fig. 8-17	$cl = \frac{c}{d_c}$, entry for Fig. 8-17	location of ring trailing edge (rte) with respect to base of body; values aft of body base are positive	from Fig. 8-17, per deg, ref area = A_{ref}

TABLE 8-1. COMPUTATIONAL TABLE (cont)

Ref Data	Supersonic Computations		
	Ring Tail - Force and Moment Characteristics		
1	116	117	118
Mach No.	$\Delta C_{N_{\alpha rt}}$	$X_{cp rt}$	$-\Delta C_{M_{\alpha rt}}$
0			
.5			
1.0			
1.5			
2.0			
2.5			
3.5			
4.5			
	<p>(116) $\Delta C_{N_{\alpha rt}} = 57.3 \Delta C_{N_{\alpha rt}}$ per rad; ref area = A_{ref}</p>	<p>(117) [] indicates term could or could not be in the equation, depending upon configuration being analyzed.</p> <p>$X_{cp rt} = l_n + l_{ab} + [l_{bt}] + (rtc - 0.5c)$</p>	<p>(118) $\Delta C_{M_{\alpha rt}} \left(\frac{X_{cp rt}}{l_{ref}} \right)$ per rad; ref area = A_{ref}; ref length = l_{ref}; with respect to nose tip</p>

AMCP 706-200

TABLE 8-1. COMPUTATIONAL TABLE (cont)

Ref Data	Supersonic Computations						
	Interference Effects (Method 1)						
1	119	120	121	122	123	124	125
Mach No.	d/b	$K_{f(b)}$	$\beta \cot \Lambda_{te}$	$\frac{\beta d^*}{c_{re}}$	H_1^*	$K_{b(f)}$	K_t
0 .5 1.0 1.5 2.0 2.5 3.5 4.5	ratio of body diameter to fin span	from Fig. 8-18	parametric variable for Fig. 8-20	abscissa variable for Fig. 8-20	$H_1 = K_{b(f)} \beta (C_{N_{\alpha f}}) (\Lambda_c + 1) \left(\frac{b}{d} - 1 \right)$ <p>Note: If afterbody extends beyond fin te use Fig. 8-20(A). If body base plane and fin te are flush use Fig. 8-20(B).</p>	$K_{b(f)} = H_1 \left[\frac{1}{\beta (C_{N_{\alpha f}}) (\Lambda_c + 1) \left(\frac{b}{d} - 1 \right)} \right]$	$K_t = K_{f(b)} + K_{b(f)}$
<p>Note: See Fig. 8-23 for explanation of geometrical terms; also subscript e signifies exposed (or values based on exposed surface).</p>							

TABLE 8-1. COMPUTATIONAL TABLE (cont)

Ref Data	Supersonic Computations			
	Interference Effects (Method 2)			
1	126	127	128	129
Mach No.	d/b	α_i	α_i/m	K_i
0				
.5				
1.0				
1.5	.375	.646	1.0	1.82
2.0	.375	1.000	1.0	1.74
2.5	.375	1.322	1.0	1.68
3.5	.375	1.940	1.0	1.59
4.5	.375	2.530	1.0	1.55
	abscissa entry for Fig. 8-21	$\alpha_i = \beta \tan \omega$; parametric variable for Fig. 8-21	variable describing fin geometry (governs choice of Figs. 8-21(A) through 8-21(F), where $m = \beta \tan \epsilon$)	from Fig. 8-21.

AMCP 706-280

TABLE 8-1. COMPUTATIONAL TABLE (cont)

Ref Data	Supersonic Computations				
	Complete Configuration - Force and Moment Characteristics				
1	130	131	132	133	134
Mach No.	$C_{N_{\alpha}} \text{ body}$	$(C_{N_{\alpha f}})_{IF}$	$C_{N_{\alpha f}}$	$C_{N_{\alpha total}}$	$C_{N_{\alpha b}}$
0					
.5					
1.0					
1.5	2.6	4.21	7.66	10.26	5.51
2.0	3.0	3.55	6.18	9.18	8.22
2.5	3.15	2.69	4.51	7.66	9.07
3.5	3.25	1.83	2.91	6.16	10.78
4.5	3.25	1.402	2.18	5.43	11.45
	from column 85 with incremental terms as applicable; per rad; ref area = A_{ref}	interference-free fin from applicable column (101 or 108 or 116) (Note: interference effects included in ring tail data.) Per rad; ref area = A_{ref}	$C_{N_{\alpha f}} = K_t (C_{N_{\alpha f}})_{IF}$. Note: K_t from column 125 or 129 as applicable per rad; ref area = A_{ref}	$C_{N_{\alpha total}} = C_{N_{\alpha body}} + C_{N_{\alpha f}}$ per rad; ref area = A_{ref}	from column 86 with incremental terms as applicable; per rad; ref area = A_{ref} ; ref length = l_{ref} ; with respect to nose tip
*Interference Free					

TABLE 8-1. COMPUTATIONAL TABLE (cont)

Ref Data	Supersonic Computations			
	Complete Configuration			
1	135	136	137	138
Mach No.	$(C_{M\alpha f})_{IF}^*$	$C_{M\alpha f}$	$C_{M\alpha total}$	$\left(\frac{X_{cp}}{l_{ref}}\right)_{total}$
0				
.5				
1.0				
1.5	47.5	86.5	92.01	8.97
2.0	40.1	69.8	78.02	8.50
2.5	30.4	51.1	60.17	7.85
3.5	20.6	32.8	43.58	7.07
4.5	15.9	24.6	36.05	6.65
	interference free fin from applicable column (104, 111 or 118) (Note: interference effects included in ring tail data); per rad; ref area = A_{ref} ; ref length = l_{ref} ; with respect to nose tip	(135) per rad; ref area = A_{ref} ; ref length = l_{ref} ; with respect to nose tip	(136) per rad; ref area = A_{ref} ; ref length = l_{ref} ; with respect to nose tip	(137) measured from nose tip
		$C_{M\alpha f} = K_t (C_{M\alpha f})_{IF}^*$	$C_{M\alpha total} = C_{M\alpha body} + C_{M\alpha f}$	$\left(\frac{X_{cp}}{l_{ref}}\right)_{total} = \frac{(C_{M\alpha})_{total}}{(C_{M\alpha})_{total}}$

* Interference Free

AMCR 708-200

TABLE 8-2. DRAG FORCE CALCULATION SHEET

General Data							
1	2	3	4	5	6	7	8
Mach No. M_∞	β	Altitude, Ft	Reference Area (A_{ref}), Ft ²	Reynolds No. Per Ft $\times 10^{-6}$ of Length	V_∞ Ft/Sec	$\rho_\infty \times 10^{-3}$, Slug/Ft ³	$P_\infty \times 10^{-3}$, Lb/Ft ²
0	1.0	0	1.225	0	0	2.378	2.116
.49	.871	75	1.225	3.46	546	2.372	2.110
.75	.661	171	1.225	5.28	834	2.366	2.103
.88	.474	234	1.225	6.21	982	2.362	2.098
1.02	.200	308	1.225	7.16	1134	2.357	2.093
1.15	.565	392	1.225	8.11	1288	2.351	2.086
1.30	.835	487	1.225	9.08	1445	2.344	2.020
1.59	1.24	711	1.225	11.06	1769	2.329	2.062
1.90	1.61	981	1.225	13.12	2109	2.310	2.042
2.05	1.79	1135	1.225	14.13	2285	2.300	2.031

arbitrarily selected
 $\beta = \sqrt{M_\infty^2 - 1}$ $M_\infty > 1$
 $\beta = \sqrt{1 - M_\infty^2}$ $M_\infty < 1$
 flight altitude at corresponding Mach number
 arbitrarily selected (usually cross sectional area of body cylindrical section, $\frac{\pi d_c^2}{4}$)
 from Fig. 8-40 (function of column ① and ②)
 rocket velocity
 atmospheric density (0.002378 slug/ft³ at sea level, std.)
 free stream total pressure (2116 lb/ft² at sea level, std.)

TABLE 8-2. DRAG FORCE CALCULATION SHEET (cont)

Ref Data	Body Geometry and Related Information						
1	9	10	11	12	13	14	15
Mech No. M_∞	f_n	$\frac{S_w}{A_{ref}}$	$\frac{d_c}{d_B}$	$\left(\frac{V}{a^*}\right)_j$	C_F	$\frac{l_{bt}}{d_c}$	$\frac{S_B - S_j}{A_{ref}}$
0	4.0	39.0	1.0	2.36	$C_F = \frac{\text{Rocket thrust}}{\text{Rocket jet chamber pressure} \times \text{jet throat area}}$	0	.359
.49	4.0	39.0	1.0	2.36		0	.359
.75	4.0	39.0	1.0	2.36		0	.359
.88	4.0	39.0	1.0	2.36		0	.359
1.02	4.0	39.0	1.0	2.36		0	.359
1.15	4.0	39.0	1.0	2.36		0	.359
1.30	4.0	39.0	1.0	2.36		0	.359
1.59	4.0	39.0	1.0	2.36		0	.359
1.90	4.0	39.0	1.0	2.36		0	.359
2.05	4.0	39.0	1.0	2.36		0	.359
	nose fineness ratio = $f_n = \frac{l_n}{d_c}$	ratio of body surface wetted area to reference area	ratio of body cylinder diameter to base diameter (flares or boattails)	$\left(\frac{V}{a^*}\right)_j = \sqrt{\frac{\gamma_j + 1}{2}} M_j^2 \left[1 + \left(\frac{\gamma_j - 1}{2}\right) M_j^2 \right]^{-1}$ (subscript j refers to rocket jet)			ratio of boattail length to cylinder diameter

AMCP 706-260

TABLE 8-2. DRAG-FORCE CALCULATION SHEET (cont)

Ref Data	Fin Geometry				
1 Mach No. M_∞	16 b Ft	17 S_f Ft ²	18 AR	19 $\tan \Lambda_{1/2}$	20 t Ft
0	2.08	1.882	2.31	.866	.18
.49	2.08	1.882	2.31	.866	.18
.75	2.08	1.882	2.31	.866	.18
.88	2.08	1.882	2.31	.866	.18
1.02	2.08	1.882	2.31	.866	.18
1.15	2.08	1.882	2.31	.866	.18
1.30	2.08	1.882	2.31	.866	.18
1.59	2.08	1.882	2.31	.866	.18
1.90	2.08	1.882	2.31	.866	.18
2.05	2.08	1.882	2.31	.866	.18
	fin span (see Fig. 8-23)	fin area (see Fig. 8-23)	Aspect Ratio $AR = b^2/S_f$	tangent of fin mid-chord sweep angle	fin thickness (see Fig. 8-23)

TABLE 8-2. DRAG FORCE CALCULATION SHEET (cont)

Ref Data		Fin Geometry				
1 Mach No. M_∞	21 c Ft	22 t/c	23 $\frac{h_{fin\ base}}{c}$	24 $\frac{S_w}{A_{ref}}$	25 $\frac{S_{fin\ base}}{A_{ref}}$	26 d_{rt} Ft
0	1.8	.1	.1	6.14	.306	0
.49	1.8	.1	.1	6.14	.306	0
.75	1.8	.1	.1	6.14	.306	0
.88	1.8	.1	.1	6.14	.306	0
1.02	1.8	.1	.1	6.14	.306	0
1.15	1.8	.1	.1	6.14	.306	0
1.30	1.8	.1	.1	6.14	.306	0
1.59	1.8	.1	.1	6.14	.306	0
1.90	1.8	.1	.1	6.14	.306	0
2.05	1.8	.1	.1	6.14	.306	0
	fin chord length	fin thickness to chord ratio	fin base thickness to chord ratio	ratio of fin wetted area to reference area	ratio of fin base area to reference area	diameter of ring tail

AMCP 706-280

TABLE 8-2. DRAG FORCE CALCULATION SHEET (cont)

Ref Data	Subsonic Computations							
	Body Drag Force							
1	27	28	29	30	31	32	33	34
Mach No. M_∞	$\frac{l_n}{d_c}$	$\left(\frac{R}{J_n}\right)^2$	$(Rf_n)^2$	$C_{D_n \text{ nose}}$	$C_{D_n \text{ bt}}$	Reynolds Number $\times 10^{-6}$	$\frac{S_w}{Ft^2}$	C_f
0	4.0	.063	16	0	0	0	39.0	
.49	4.0	.048	12.2	0	0	50.9	39.0	.0022
.75	4.0	.027	7.04	0	0	77.6	39.0	.00204
.88	4.0	.014	3.62	.0025	0	91.2	39.0	.00195
1.02	4.0	.003	.64	.0469	0	105.2	39.0	.00186
1.15								
1.30								
1.59								
1.90								
2.05								
	from column ①, abscissa entry for Fig. 8-26	[column ② / column ③] ² , abscissa entry for Fig. 8-27	abscissa entry for Fig. 8-28	from Fig. 8-26 (general nose shapes), Fig. 8-27 (optimum secant ogive), Fig. 8-28 (slender ogives), ref area A_{ref}	extrapolate supersonic data using Fig. 8-32 as a guide; ref area A_{ref}	Reynolds number based on total rocket length (column ⑤ $\times l_T$) (abscissa entry for Fig. 8-39)	ratio of wetted area of rocket surface to reference area i. e., cylindrical section would be $\frac{\pi d_c l_c}{(\pi d_c^2) / 4}$, column ⑧	from Fig. 8-39, ref area S_{ref}

TABLE 8-2. DRAG FORCE CALCULATION SHEET (cont)

Ref Data	Subsonic Computations			
	Body Drag Force			
1 Mach No. M_∞	35 C_{Df}	36 $C_{DB\ cyl}$ (Jet Off)	37 $C_{DB\ cyl}$ (Jet On)	38 P_B/P_∞
0				
.49	.0986	.131	.128	.94
.75	.0915	.135	.100	.89
.88	.0874	.145	.099	.85
1.02	.0834	.215	.133	.73
1.15				
1.30				
1.59				
1.90				
2.05				
	$C_{Df} = 1.15 (C_f) \frac{S_{sect}}{A_{ref}}$, ref area = A_{ref}	$C_{DB} = -C_{p_B}, C_{p_B}$ from Fig. 8-41; ref area = A_{ref}	$C_{DB} = \left[\frac{1 - P_B/P_\infty}{(\gamma/2) M_\infty^2} \right] \left(\frac{S_B - S_j}{A_{ref}} \right) \frac{P_B}{P_\infty}$ from Fig. 8-44 (as function of column 13) ref area = A_{ref}	from Fig. 8-44

AMCP 708-200

TABLE 8-2. DRAG FORCE CALCULATION SHEET (cont)

Ref Data	Subsonic Computations			
	Body Drag Force			
1	39	40	41	42
Mach No. M _∞	$\frac{P_{B_{bt \text{ or } fl}}}{P_{cyl}}$	$C_{D_{B_{fl \text{ or } bt}}}$ (Jet Off)	$C_{D_{B_{fl \text{ or } bt}}}$ (Jet On)	$C_{D_b \text{ total}}$ (Jet On/Jet Off)
0				
.49				.2296/.2266
.75				.2265/.1915
.88				.2349/.1889
1.02				.3453/.2633
1.15				
1.30				
1.59				
1.90				
2.05				
	from Fig. 8-43	$C_{D_B} = -C_{p_B} \left(\frac{A_{fl \text{ or } A_{bt}}}{A_{ref}} \right)$; C_{p_B} from Fig. 8-41; ref area = A_{ref}	$C_{D_B} = \left(1 - \frac{P_{B_{bt \text{ or } fl}}}{P_{\infty}} \right) \left(\frac{S_B - S_J}{A_{ref}} \right)$ $\frac{P_{B_{bt \text{ or } fl}}}{P_{\infty}} = \frac{P_B}{P_{\infty}} \left(\frac{P_{B_{bt \text{ or } fl}}}{P_{B_{cyl}}} \right)$, ref area = A_{ref}	$C_{D_{total}} = C_{D_{nose}} + [C_{D_{bt}}] + C_{D_{fl}} + C_{D_B}$ or (3) or (4) or (5) or (6) or (7) or (8) or (9)

[] indicates term could or could not be in the equation, depending upon configuration being analyzed.

TABLE 8-2. DRAG FORCE CALCULATION SHEET (cont)

Ref Data	Subsonic Computations			
	Fin Drag Force			
1	43	44	45	46
Mach No. M_∞	$AR \left(\frac{t}{c} \right)^{1/3}$	$\frac{M^2 - 1}{(t/c)^{2/3}}$	$\frac{C_{D_e}}{(t/c)^{5/3}}$	C_{D_e}
0	1.08	-4.63	0	0
.49	1.08	-3.51	0	0
.75	1.08	-2.02	0	0
.88	1.08	-1.04	.55	.023
1.02	1.08	.185	2.35	.0949
1.15				
1.30				
1.59				
1.90				
2.05				
	variable for Fig. 8-36 or 8-37 = $(18) \times \left[\frac{(22)}{AR} \right]^{1/3}$	variable for Fig. 8-36 or 8-37, $\frac{M^2 - 1}{\left[\frac{(22)}{AR} \right]^{2/3}}$	from Fig. 8-36 (rectangular fin) from Fig. 8-37 (delta fin) (for other planforms interpolate between above) ref area = S_f	$C_{D_e} \left[\frac{(t/c)^{5/3}}{(t/c)^{5/3}} \right]^{5/3} \left(\frac{2S_f}{A_{ref}} \right)$ ref area A_{ref}

AMCP 708-280

TABLE 8-2. DRAG FORCE CALCULATION SHEET (cont)

Ref Data	Subsonic Computations			
	Fin Drag Force			
1	47	48	49	50
Mach No. M_∞	$\frac{M^2 - 1}{\left(M^2 \frac{t}{c}\right)^{2/3}}$	$C_{D_w} \left(\frac{M}{t/c}\right)^{2/3}$	$C_{D_w, rt}$	C_f
0				
.47				.00294
.75				.00275
.88				.00268
1.02				.00260
1.15				
1.30				
1.57				
1.90				
2.05				
	variable for Fig. 8-38	from Fig. 8-38; ref area = S_f	<p>for double wedge section. For other sections multiply by modifying factor from Fig. 8-35; ref area = A_{ref} according to procedure in par. 8-3.1.5</p> $C_{D_w, 2D} = \frac{C_{D_w} \left(\frac{M}{t/c}\right)^{2/3}}{\left(\frac{M}{t/c}\right)^{2/3}}$ $\left(\frac{S_f}{A_{ref}}\right)$	from Fig. 8-39 with Reynolds Number based on fin mean chord length (or \bar{c}); ref area = S_f

TABLE 8-2. DRAG FORCE CALCULATION SHEET (cont)

Ref Data	Subsonic Computations			
	Fin Drag Force			
1 Mach No. M_∞	51 C_{D_f}	52 C'_{D_B}	53 C_{D_B}	54 $(C_{D_{fin}})_{total}$
0				
.49	.0181	.125	.0382	.0563
.75	.0169	.125	.0382	.0551
.88	.0165	.125	.0382	.0547
1.02	.0160	.185	.0566	.0726
1.15				
1.30				
1.59				
1.90				
2.05				

$C_{D_f} = C_f \left(\frac{S_f}{A_{ref}} \right) \text{ ref area} = A_{ref}$	$C'_{D_B} = -C_{p_B} \text{ from Figs. 8-45 and 8-46,} \\ \text{ref area} = \text{fin base area}$	$C_{D_B} = C'_{D_B} \left(\frac{\text{fin base area}}{A_{ref}} \right)$	$(C_{D_{fin}})_{total} = (C_{D_{fin}})_{ref} + C_{D_f} + C_{D_B}$ $\text{ref area} = A_{ref}$
---	---	--	--

AMCP 766-280

TABLE 3-2. DRAG FORCE CALCULATION SHEET (cont)

Ref Data	Supersonic Computations				
	Body Drag Force				
1	55	56	57	58	59
Mach No. M_∞	$C_{D_v \text{ nose}}$	$C_{D_v \text{ bt}}$	$C_{D_v \text{ fl}}$	$C_{D_B \text{ cyl}}$ (Jet Off)	$C_{D_B \text{ cyl}}$ (Jet On)
0					
.49					
.75					
.88					
1.02					
1.15	.0669			.216	.271
1.30	.0705			.206	.212
1.59	.0590			.179	.142
1.90	.0581			.154	.099
2.05	.0546			.142	.085
	from Fig. 8-26 or 8-29	from Fig. 8-30 (conical) or 8-31 (parabolic). Note that ordinate is $\frac{1}{4} C_{D_p} (l_{bt}/d_c)^2$ so that $C_{D_p} = (\text{ordinate value}) / \left[\frac{1}{4} (l_{bt}/d_c)^2 \right]$; ref area = A_{ref}	from Fig. 8-33 at appropriate Mach number, ref area = A_{ref}	$C_{D_B} = -C_{D_p}$; C_{D_B} from Fig. 8-41 ref area = A_{ref}	$C_{D_B} = \frac{1 - P_B/P_\infty \left(\frac{S_B - S_J}{A_{ref}} \right)}{(y/2) M_\infty^2} \frac{P_B}{P_\infty} - \frac{C_f^{1/3}}{(V/a^*)}$; or Fig. 8-42; ref area = A_{ref}

TABLE 8-2. DRAG FORCE CALCULATION SHEET (cont)

Ref Data	Supersonic Computations				
	Body Drag Force				
1	60	61	62	63	64
Mach No. M_∞	C_{f_b}	$C_{D_f b}$	C_{D_B} ft or bt (Jet Off)	C_{D_B} ft or bt (Jet On)	$(C_{D_{body}})_{total}$ Jet Off/Jet On
0					
.49					
.75					
.88					
1.02					
1.15	.00182	.0815			.3644/.4194
1.30	.00172	.0770			.3535/.3595
1.59	.00165	.0739			.3119/.2749
1.90	.00150	.0672			.2793/.2243
2.05	.00146	.0654			.2620/.2050
	from Fig. 8-39 with Reynolds Number based on body length or $(S) \times l_T$; ref area = S_b	$C_{D_f} = 1.15 (C_f) \left(\frac{S_b}{A_{ref}} \right)$; ref area = A_{ref}	$C_{D_B} = -C_{p_B} \left(\frac{A_{ft} \text{ or } A_{bt}}{A_{ref}} \right)$ C_{p_B} from Fig 8-41; ref area = A_{ref}	$C_{D_B} = \frac{(1 - P_B/P_\infty) (S_B - S_J)}{(\gamma/2 M_\infty^2) A_{ref}} \left(\frac{P_R}{P_\infty} \right) \frac{P_R}{P_\infty} = \frac{3}{5} C_f^{1/3} \left(\frac{P_{B_{bt}} \text{ or } f_l}{P_{B_{cyl}}} \right)$ ref area = A_{ref} from Fig. 8-43	$(C_{D_{body}})_{total} = C_{D_{nose}} \times C_{D_f} + [C_{D_{bt}} \text{ or } f_l]$ or (55) or (57) or (59) or (61) or (63) + C_{D_B} ref area = A_{ref}

[] indicates term could or could not be in the equation, depending upon configuration being analyzed.

AMCP 706-280

TABLE 8-2. DRAG FORCE CALCULATION SHEET (cont)

Ref Data	Supersonic Computations				
	Fin Drag Force				
1 Mach No. M_∞	65 βAR	66 $AR \tan \Lambda_{1/2}$	67 $\frac{C_{D_e}}{AR \left(\frac{L}{c}\right)^2}$	68 C_{D_e}	69 $C_{D_{ref}}$
0					
.49					
.75					
.88					
1.02					
1.15	1.305	2.00	1.61	.1205	
1.30	1.93	2.00	1.90	.1422	
1.59	2.87	2.00	1.50	.1122	
1.90	3.72	2.00	1.25	.0935	
2.05	4.14	2.00	1.20	.0897	
	abscissa entry for Fig. 8-34	parametric variable in Fig. 8-34	from Fig. 8-34 (at appropriate planform) ref area = S_f	$C_{D_e} = \frac{C_{D_e}}{AR \left(\frac{L}{c}\right)^2} \left[\frac{S_f}{A_{ref}} \right]$ ref area = A_{ref}	from Fig. 8-35 according to procedure presented in par. 8-3.1.5

For sections not shown, multiply the value obtained from Fig. 8-34 by a ratio obtained from Fig. 8-35. This ratio is section coefficient for new section to old section.

TABLE 8-2. DRAG FORCE CALCULATION SHEET (cont)

Ref Data xxxx	Supersonic Computations			
	Fin Drag Force			
1 Mach No. M_∞	70 C_f	71 C_{D_f}	72 C_{D_B}	73 $(C_{D_{fin}})_{total}$
0				
.49				
.75				
.88				
1.02				
1.15	.0025	.0077	.0952	.2259
1.30	.0024	.0074	.0925	.2445
1.59	.00228	.0070	.0898	.2113
1.90	.00205	.0063	.0792	.1811
2.05	.00200	.0061	.0766	.1724

from Fig. 8-39 with Reynolds Number based on fin mean chord length (or $\bar{c} \times c$), ref area = S_f

$$C_{D_f} = C_f \left(\frac{S_f}{A_{ref}} \right); \text{ ref area} = A_{ref}$$

$$C_{D_B} = -C_{p_B} \left(\frac{\text{fin base area}}{A_{ref}} \right); C_{p_B} \text{ from Fig. 8-45; } C_{p_B} \text{ ref area} = A_{ref}$$

$$(C_{D_{fin}})_{total} = C_{D_B} \text{ or } C_{D_{B,rt}} + C_{D_f} + C_{D_B}$$

AMCP 708-280

TABLE 8-2. DRAG FORCE CALCULATION SHEET (cont)

Ref Data	Supersonic Computations	
	Interference	Total
1	74	75
Mach No. M_∞	ΔC_{D_B}	$C_{D_{total}}$ Jet On/Jet Off
0		
.49		.2859/.2829
.75		.2816/.2466
.88		.2896/.2436
1.02		.4179/.3359
1.15		.5878/.6453
1.30		.5956/.6040
1.59		.5209/.4862
1.90		.4583/.4054
2.05		.4344/.3774

Interference due to fins on body base drag
(fin flush with base)

$$\Delta C_{D_B} = \frac{t}{c} \left(\frac{0.825}{M_\infty^2} - \frac{0.05}{M_\infty} \right) (n) \left(\frac{S_B - S_f}{A_{ref}} \right)$$

Note: $M_\infty = 2.0$, ref area = A_{ref}

(Subsonic) (42) (51) (74)

(Supersonic) (64) (73)

$$C_{D_{total}} = (C_{D_{body}})_{total} + (C_{D_{fin}})_{total} + \Delta C_{D_B}$$

INDEX

(Paragraph Numbers in Roman Figures; Page Numbers in **Bold Figures**.)

- A**
- Absorptivity, 6-6.1.2, 6-21
 - Accuracy - Rocket System, 7-1, 7-2
 - Actuating Device, 3-5.2.1, 3-9
 - Aerodynamic Friction Heating, 6-6.4, 6-22
 - Aerodynamic Stability, 7-3.2.1, 7-3
 - Aerodynamic Testing, 3-10.4, 3-18; 8-4, 8-67
 - Angular Errors, 7-3, 7-2; 7-5, 7-8
 - Angular Dispersion, 7-3.2.1, 7-3
 - Autospin, 3-4.5.1, 3-6
 - Auxiliary Devices, 3-7.7, 3-15
 - Axial Load Component, 6-3.2, 6-11
 - Axis of Inertia, 7-6.3, 7-14
- B**
- Ballistic Coefficient, 4-2.3, 4-3; 7-8.3.3.3, 7-31
 - Ballistic Phase Errors, 7-2, 7-2; 7-8, 7-25
 - Base Drag, 8-3.3, 8-51
 - Beams, 6-4.1, 6-13
 - Bearing Stress, 6-4.5, 6-18
 - Bending Load Components, 6-3.2, 6-11
 - Boattail Wave Drag, 8-3.1.2, 8-45
 - Body Drag Force Calculation Sheet, 8-3.4.2, 8-66
 - Body Geometry, Figure 8-24, 8-43
 - Body in Presence of Fin, 8-2.4.2, 8-34
 - Body-of-Revolution Base Drag
 - Rocket Jet Off, 8-3.3.1, 8-51
 - Rocket Jet On, 8-3.3.2, 8-63
 - Boost/Sustain System, 4-4.2, 4-9
 - Boost System, 4-5.2, 4-14
 - Booster Mass Ratio, 4-3.2.1, 4-5
 - Burning Phase Error, 7-2, 7-2
 - Burning Rate, 5-3.1.3, 5-11
- C**
- Center of Gravity, 6-2.1, 6-2
 - Circular Probable Error, 7-9, 7-31; 7-10.3, 7-35
 - Columns, 6-4.2, 6-15
 - Combustion Chamber Heating, 6-6.2, 6-22
 - Combustion Chamber Pressure, 5-4, 5-13
 - Composite Propellants, 5-3.1.1, 5-10
 - Computational Table, 8-3.4.2, 8-66
 - Conical Divergent Section, 5-2.2, 5-7
 - Constant Spin Acceleration, 7-7.2.2, 7-20
 - Constraints, Weapons, 3-6.2, 3-14
 - Cost Effectiveness, 3-11, 3-18
 - Cruciform, 5-3.1.2, 5-10
- D**
- Deflection Probable Error, 7-10.2, 7-35
 - De Laval Nozzle, 3-5.2.2, 3-10
 - Density Model
 - Annual, 2-2.4, 2-2
 - Seasonal, 2-2.4, 2-2
 - Design Data, Figure 8-25, 8-43
 - Design Optimization, 3-8, 3-16
 - Direct Fire Rockets, 4-3.1.2, 4-3
 - Discharge Correction Factor, 5-2.1.2, 5-7,
 - Dispersion
 - At Warhead Event, 7-8.3, 7-27
 - Due to Wind, 7-3.2.2, 7-3
 - Reduction, 7-3.2.5, 7-7; 7-7.2, 7-18
 - Double-Base Propellants, 5-3.1.1, 5-10
 - Drag Form Factor, 4-4.2e, 4-8
 - Drag, Free Range Equation, 4-3.1.1, 4-3
 - Ductility, 6-1, 6-2
 - Dynamic Unbalance, 7-8.2.6, 7-27
 - Dynamic Unbalance Effect, 7-6.3, 7-14
- E**
- Elastic Limit, 6-1, 6-2
 - Emissivity, 6-6.1.2, 6-21
 - Energy-Management Techniques, 4-2, 4-2; 4-4.1.2, 4-8; 4-5.1.2, 4-12; 4-6.1.2, 4-15; 4-7.1.2, 4-16
 - Environmental Testing, 3-10.5, 3-18
 - Erosion, 5-3.1.4, 5-12
 - Exhaust Plume Heating, 6-6.3, 6-22
- F**
- Fin Base Drag, 8-3.3.3, 8-65
 - Fin Geometry, Figure 8-23, 8-42
 - Fin in Presence of Body, 8-2.4.2, 8-34
 - Fin Wave Drag, 8-3.1.4, 8-48
 - Fin Body Interferences, 8-2.4.2, 8-34
 - Fins
 - Coplanar, 8-2.2, 8-19
 - Cruciform, 8-2.4.3, 8-37
 - Low Aspect Ratio, 8-2.2, 8-20
 - Rectangular Planform, 8-2.2, 8-20
 - Ring Tail, 8-2.3, 8-22

AMCP 706-280

Swept, 8-2.2, 8-20
 Unswept, 8-2.2, 8-20
 Flare Wave Drag, 8-3.1.3, 8-46
 Flight Testing, 3-10.2, 3-17
 Friction Drag, 8-3.2, 8-51
 Fuze, 3-5.2.1, 3-9
 Fuzing Errors, 7-8.2.8, 7-27

G

Grain, 5-3.1, 5-7
 Grain Composition, 3-5.2.2, 3-9
 Growth Factor, 4-2.3, 4-3; 4-3.2.3, 4-5; 4-3.3, 4-5

H

Hardness, 6-1, 6-2
 Heat Transfer, 6-6.1, 6-19

I

Ideal Flow, 5-2.1.1, 5-4
 Ideal Velocity Equation, 4-3.2.1, 4-5
 Ignition, 5-3.2, 5-12
 Impulse Variation, 7-8.3.2.3, 7-30
 Indirect Fire Systems, 4-3.1.1, 4-3
 Insulating Materials, 3-5.2.2, 3-10
 Internal Combustion Engine, 5-1, 5-2
 Internal Cylindrical Surfaces, 5-3.1.2, 5-10
 Internal Star Design, 5-3.1.2, 5-10

J

Joints, 6-4.5, 6-15

L

Launch Phase Errors, 7-6, 7-10
 Launcher Length, 7-7.2.1, 7-18
 Launcher Rail, 3-5.3, 3-13
 Law of Proportionality of Stress to Strain, 6-1, 6-2
 Linearized Flow Theory, Fins, 8-2.2, 8-22
 Linearized Slender Wing Theory, Fins, 8-2.2, 8-20
 Linearized Supersonic Wing Theory, Fins, 8-2.2, 8-22
 Lifting Line Theory, Fins, 8-2.2, 8-20
 Loads, 6-3, 6-10

M

Mallaunch, 7-8.3.1.2, 7-29
 Margin of Safety, 6-5, 6-19
 Mass, 6-2.1, 6-2
 Flow Rate, 5-2.1.2, 5-7
 Material Modulus of Elasticity, 6-4.2, 6-15
 Methods of Rocket Transport, 3-4.6, 3-7
 Military Rocket Systems, 3-2.1, 3-1
 Modulus of Elasticity, 6-1, 6-2
 Motor
 Combustion Chamber, 3-5.2.2, 3-10
 Exit Orifice, 3-5.2.2, 3-10
 Thrust Level, 5-5, 5-13
 Multi-Fin Configuration, 8-2.4.3, 8-37

Malaim, 7-8.3.1.1, 7-28
 Malalignment of Fins, 7-8.2.4, 7-27

Mallaunch, 7-8.3.1.2, 7-29
 Margin of Safety, 6-5, 6-19
 Mass, 6-2.1, 6-2
 Flow Rate, 5-2.1.2, 5-7
 Material Modulus of Elasticity, 6-4.2, 6-15
 Methods of Rocket Transport, 3-4.6, 3-7
 Military Rocket Systems, 3-2.1, 3-1
 Modulus of Elasticity, 6-1, 6-2
 Motor
 Combustion Chamber, 3-5.2.2, 3-10
 Exit Orifice, 3-5.2.2, 3-10
 Thrust Level, 5-5, 5-13
 Multi-Fin Configuration, 8-2.4.3, 8-37

N

Nose Wave Drag, 8-3.1.1, 8-44
 Nozzle
 Closure, 3-5.2.2, 3-11
 Contours, 5-2.2, 5-7
 Erosion, 5-2.3, 5-7
 Exhaust Velocity, 5-2.1.1, 5-4
 Numerical Example, 4-8, 4-19

O

Ogive Nose, 6-2.1, 6-2
 Operational Modes, 3-3, 3-3
 Oversize Head Configuration, 8-2.1.4, 8-16

P

Parabolic Section, 5-2.2, 5-7
 Parametric Performance, 4-2, 4-2; 4-4, 4-8; 4-5.2, 4-13; 4-6.2, 4-15; 4-7, 4-16; 4-7.2, 4-18
 Parametrics, 3-6.3, 3-14
 Payload, 3-7.1, 3-15
 Performance Estimates, 3-7.6, 3-15
 Plates, 6-4.4, 6-15
 Plug Nozzle, 3-5.2.2, 3-10
 Prelaunch Errors, 7-4, 7-7
 Preliminary Design, 3-7, 3-14
 Prespin Automatic Dynamic Alignment (PADA), 7-7.2.5, 7-24
 Launcher, 3-4.5.2, 3-7
 Pressure Vessels, 3-4.3, 6-15
 Propellant
 Charge or Grain, 3-5.2.2, 3-9; 5-3.1, 5-7
 Weight Fraction, 4-3.2.2, 4-5
 Proportional Limit, 6-1, 6-2
 Propulsion Phase Error, 7-7, 7-14

1-2

R

Range Probable Error, 7-10.1, 7-35
 Real Flow, 5-2.1.2, 5-7
 Recovery Temperature, 6-6.4, 6-23
 Requirements, Weapons, 3-6.1, 3-13
 Research Rocket Systems, 3-2.2, 3-2
 Ring Tail Wave Drag, 8-3.1.5, 8-48
 Rocket
 Launchers, 3-4.1, 3-4
 Motor, 3-5.2.2, 3-9
 Motor Requirement, 4-3.2, 4-5
 Nozzle, 5-2, 5-3
 Pitch Inertia, 6-2.2, 6-2
 Roll Inertia, 6-2.3, 6-7
 Rod and Tube, 5-3.1.2, 5-10

S

Sample Calculation Sheet, 8-2.4.4, 8-42
 Shearing Stress, 6-4.5, 6-17
 Six Degree of Freedom Equations, 7-5, 7-8
 Slender Body Theory
 Boattail, 8-2.1.2, 8-5
 Conical Flare Afterbody, 8-2.1.3, 8-5
 Nose Cylinder, 8-2.1.1, 8-4
 Slowly Uniformly Decreasing
 Spin (SUDS), 7-7.2.3, 7-20
 Solid Propellant Motor, 5-1, 5-2
 Sonic Velocity, 5-2.1.1, 5-6
 Sounding Rockets, 4-3.1.3, 4-5; 4-6, 4-15
 Specific Impulse, 4-3.2.1, 4-5
 Speed Change Errors, 7-3.1, 7-2
 Spin, 7-3.2.4, 7-5
 Spin Buck, 7-7.2.4, 7-20
 Spin-On-Straight Rail (SOSR), 3-4.5.3, 3-7
 Squib, 3-5.2.2, 3-11
 Standard Atmospheric Model, 2-2.1, 2-1
 Static Testing, 3-10.1, 3-17
 Static Unbalance, 7-8.2.5, 7-27
 Stress, 6-4, 6-13
 Structural Testing, 3-10.3, 3-17
 Synthetic Wind Profile, 2-2.2, 2-1
 System Elements, 3-5, 3-8
 System Integration, 3-9, 3-16

T

Temperature Profile, 2-2.4, 2-3; Table 2-4, 2-14
 Testing, 5-6, 5-15; 6-7, 6-24
 Thickness Effect, Fins, 8-2.2, 8-22
 Thrust Correction Factor, 5-2.1.2, 5-7
 Thrust Malalignment, 7-3.2.3, 7-3
 Total Drag, 8-3, 8-44
 Total Error, 7-2, 7-2
 Total Moment of Inertia, 6-2.2, 6-7
 Trajectory Profile, 4-4.1.1, 4-8; 4-5.1.1, 4-12; 4-6.1.1, 4-15; 4-7.1.1, 4-16
 Twin Fins, 8-2.4.3, 8-37

U

Ultimate Strength, 6-1, 6-2

V

Variable Acceleration Technique, 7-7.2.6, 7-24
 Velocity
 Correction Factor, 5-2.1.2, 5-7
 Requirement, 4-3.1, 4-3
 Vertical Ascent, 4-6.1.1, 4-15

W

Warhead, 3-5.2.1, 3-8
 Wave Drag, 8-3.1, 8-44
 Winds
 Lower Level, 2-2.3, 2-2
 Upper Level, 2-2.2, 2-1

Y

Yaw Oscillation Distance, 7-3.2.1, 7-3
 Yield Point, 6-1, 6-2